VERSLAGEN EN VERHANDELINGEN

REPORTS AND TRANSACTIONS

NATIONAAL LUCHTVAARTLABORATORIUM

NATIONAL AERONAUTICAL RESEARCH INSTITUTE

AMSTERDAM

XIX — 1954

[illegible]

[illegible]

[illegible]

[illegible]

[illegible]

[illegible]

Contents

Thirty-fifth Annual Report

of the

National Aeronautical Research Institute

N.L.L.

1954

A. Board and Organization.

By order of the Minister of Transport and "Waterstaat", the Minister of War and of the Navy, the Minister of Overseas Territories, the Minister of Education, Arts and Sciences, the Minister of Economic Affairs and the Minister of the Interior on 29th March 1954, the Statutes of the Institute have been drawn up in a modified version.

Under these statutes the Minister of Finance has appointed Mr. O. W. Vos as a member of the Board of the Institute. In the course of the year the Royal Netherlands Aircraft Factories Fokker and the Aviolanda Aircraft Company, Inc. joined the Institute as participants and were, therefore, entitled to appoint a member of the Board.

On 31 December 1954 the Board consisted of the following members:

Prof. Dr. Ir. H. J. van der Maas, President,	Technical University, Delft Ministry of Education, Arts and Sciences.
J. W. F. Backer, Vice-President	Dir. Gen. Dept. of Civil Aviation. Ministry of Transport and "Waterstaat".
Dr. L. Neher	former Postmaster General.
Prof. Ir. D. Dresden	President National Council for Industrial Research T. N. O.
Maj. Gen. J. A. Bach	Director of Ordnance and Supplies, Royal Dutch Air Force.
Commander J. Lugtenburg	Director Air Materiel Division, Royal Dutch Navy.
Dr. J. W. de Stoppelaar	Director of Economic Affairs, Ministry of Overseas Territories.
Drs. H. P. Jongsma	Director for Financial Participations, Ministry of Economic Affairs.
Mr. O. W. Vos	Dep. Director for Financial Participations, Ministry of Finance.
P. A. van de Velde	Director Aviolanda Aircraft Company Inc.
Ir. H. C. van Meerten	Chief Designer and Ass. Manager, Royal Netherlands Aircraft Factories Fokker.
C. Wijdooge	Head Techn. Sales Dept., Royal Dutch Airlines, K. L. M.
Prof. Dr. W. J. D. van Dijck	Scient. Advisor Royal Dutch Shell, for the Royal Dutch Aeronautical Association.

The executive committee consisted of president and vice-president. Mr. G. C. Klapwijk continued to be Secretary-treasurer of the Institute.

The Advisory Scientific Committee underwent no changes since 1953. Prof. Dr. A. van der Neut and Prof. Dr. R. Timman were Scientific Advisors to the Laboratory appointed by the Board.

The completion of the new transonic and supersonic windtunnels took much time.

With the Association Internationale des Constructeurs de Matériel Aéronautique (AICMA) agreement could be attained about a contract concerning part-time use of the transonic tunnel by the AICMA.

Much work was involved in the organisation of the 4th General Assembly of the NATO-Advisory Group for Aeronautical Research and Development (AGARD), which took place in The Hague. H. R. H. Prince Bernhard has been found willing to open this meeting. The President of the Board has been appointed member of the Executive Committee of AGARD.

B. The Laboratory.

1 *General.*

1.1 *Staff.*

The management consisted of:

Prof. Dr. C. Zwikker	Director
Ir. A. Boelen	Dep. Director
Section Aerodynamics (A):	Ir. J. F. Hengeveld Ir. J. A. Landstra
Section Combustion (C):	Ir. A. J. Marx Drs. W. J. Basting
Section Flutter and Theoretical Aerodynamics (F):	Dr. Ir. A. I. van de Vooren
Section Helicopters:	Ir. A. J. Marx Ir. L. R. Lucassen
Section Materials and Structures (S and M):	Dr. Ir. F. J. Plantema
Section Flying Models (O):	Ir. A. J. Marx Ir. G. Y. Fokkinga
Section Flight Testing (V):	Ir. A. J. Marx Ir. T. van Oosterom
Windtunnel Construction Bureau:	Ir. J. Boel
Documentation and Library:	Dra. G. Scherpenhuijsen Rom
Administration:	Drs. J. de Koning.

The staff of the laboratory has been extended to 55 scientists (engineers, mathematicians and physicists), 29 graduates of Technical Colleges, 96 technicians, 34 clerical staff and 19 other employees, 234 in total. 8 members of the staff, among whom 4 engineers, were in military service.

1.2 *Windtunnels and equipment.*

The Pilottunnel has been delivered at the end of the year. During tests with empty test-section (1.4×1.83 ft^2) an airspeed comparable with Ma $= 1$ could be reached. Straingauge balances and schlieren system were not yet ready.

The construction of the High-Speed Tunnel could begin in the course of the year.

The design of the Supersonic Tunnel is being studied further. A visit of AGARD-specialists in July gave the occasion to discuss the plans with American experts. As a result an intermittant, blow down type of tunnel was preferred to the originally designed continuous tunnel.

A linear analog-computer, comprising 18 function units and 36 scaling units, has been ordered. A study has been made of digital computers of Dutch design.

A 6-tons Schenk horizontal resonance-machine with slow mechanical drive has been put into use for fatigue testing.

A rotating test-stand for the testing of helicopter ram-jets has been installed and was in operation during the year.

1.3 *Research contracts.*

The greater part of the research was contracted by the Netherlands Aircraft Development Board (NIV). It was related to the development of prototypes on the one side, on the other side to more fundamental research and future development.

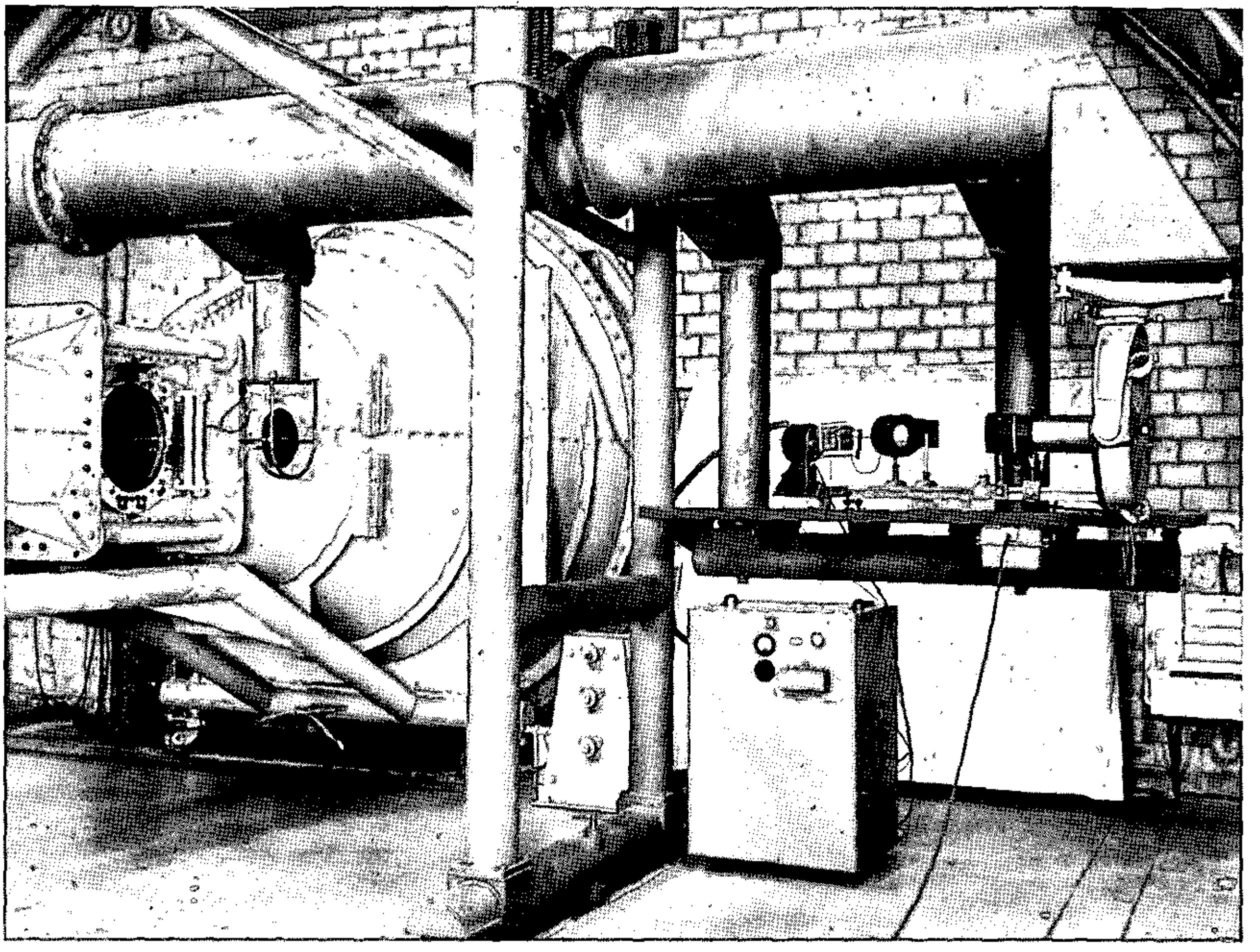

Test section and schlieren-apparatus of 1.4 $\times$ 1.83 ft. Pilot-tunnel.

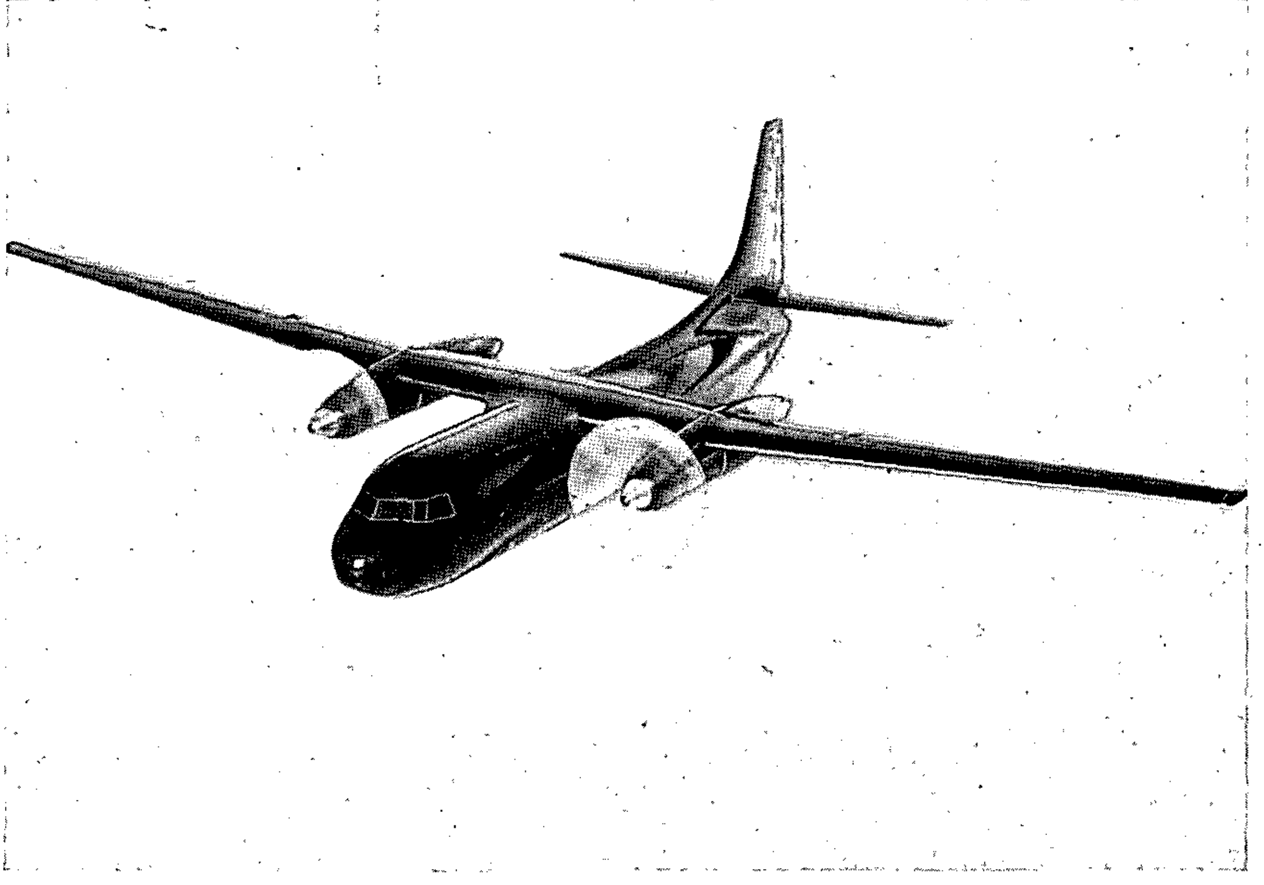

The model of the F-27.

A diversity of contracts were given by the Royal Dutch Air Force and the Royal Dutch Airlines K. L. M. Cooperation with the Department of Civil Aviation covered mainly study of Air Regulations and assistance in the testing of aircraft.

A number of small orders from industry, including testing and calibration of apparatus and windtunnel measurements on ship-models, etc. have been carried out.

The cooperation in the Advisory Group for Aeronautical Research and Development (AGARD) of the NATO resulted in a most important exchange of opinions with experts in the various fields. The N. L. L. provided also a contribution in the form of reports and papers on methods applied and instruments developed at the N. L. L.

2 *Aerodynamics Section.*

The larger part of the windtunnel-research was devoted to the development of prototypes under contract with the N. I. V. Because of a continuous lack of staff only little time could be spent on pure research. The following subjects, however, were tackled:

Comparison of windtunnel measurements with flight tests.

Reasonable agreement was found in various aspects (c.q. stick-fixed stability), but pertinent differences were found in stick-free stability, which will be investigated further (A 1292).

The influence on the stability of the open or closed wheel-well with extended landing-gear has been investigated (V 1741).

Tunnelwall influence.

The tunnelwall influence on three-dimensional flow around an aérofoil with a very high lift-coefficient has been analyzed assuming a certain circulation-distribution along the span.

Experiments have been made on a swept wing with fuselage, in the configurations high-wing, mid-wing and low-wing (A 1370).

Various subjects.

A new type of sting-mounting has been designed and constructed, also a new angle-of-attack-meter and control-surface deflection indicator.

For the construction of models a copying-lathe machine has been ordered. New applications of plastics in the construction, mounting and modifying of models have been found.

3 *Flutter and theoretical Aerodynamics Section.*

Boundary layer theory.

The three-dimensional boundary layer about a flat, yawed ellipsoïd under zero angle of incidence was calculated along 5 different streamlines up to the line of separation (F. 165). The differential equations governing the displacement thicknesses referred to the velocity profiles in the direction of the local potential flow and perpendicular to it, were numerically solved, partly at the NLL Computing Office and partly at the Mathematical Centre, where the ARRA electronic calculating machine was used. A paper referring to this investigation has been contributed to the memorial book "50 Jahre Grenzschichtforschung".

Load distribution of wings in steady flow.

The generalized Prandtl equation, derived in report F. 121, was used to calculate the load distribution for a twisted swept wing of aspect ratio 6 at two angles of incidence (report F 156). It may be concluded that for aspect ratios larger than 6 this method will be more accurate than that of Weissinger, but for aspect ratios smaller than 6 the reverse holds. Comparison was made by aid of Multhopp's method using two chordwise pivotal points.

The increase in induced drag due to a perturbation in the spanwise load distribution has been investigated. A series of diagrams permitting a rapid determination of this increase by aid of a number of schematized cases has been designed (F. 154).

Transonic flow.

By extension of the method of the integral equations, originating from Oswatitsch and Gullstrand, general integral equations for profiles at incidence or at zero incidence have been derived, which are valid both in the low transonic ($M_0 < 1$) and in the high transonic ($M_0 < 1$) region (F. 163).

A study was made of slender-body and slender-wing theory (F. 170).

Oscillating aerofoils.

The aerodynamic coefficients for an oscillating wing-flap system in two-dimensional subsonic flow have been interpolated with respect to the ratio of wing to flap chord (F. 155).

A method has been presented (F. 157), which gives an asymptotic solution of the boundary value problem corresponding to the oscillating aerofoil in two-dimensional subsonic flow. The solution is asymptotic in the parameter, which occurs in the wave equation and which is large if either the frequency is high or if the Mach number approaches 1. The method yields an exact solution for the aerodynamic forces at $M = 1$ and it is hoped to obtain useful approximations in a certain range of Mach numbers below $M = 1$.

The strip theory for the calculation of the aerodynamic forces on an oscillating swept wing of large aspect ratio was extended to the case of compressible, subsonic flow (F. 159). This leads to a generalization of Possio's equation.

Aeroelasticity; Flutter.

The influence of the chord ratios between wing, flap and tab upon binary flap-tab flutter has been investigated (F.166). The results were brought in the form of general criteria for the stability against flutter of such systems.

Mathematical methods for the calculation of the divergence speed, aileron reversal speed and of the aileron effectiveness have been presented under very general assumptions in report F. 160.

4 *Materials and structures Section.*

Theoretical structures work.

The stress and deflection analysis of swept wings was continued by applying the previously developed approximate methods to an infinitely long swept box beam and by extending the work for infinite and semi-infinite clamped root box beams in order to improve the accuracy of the results. Also vibrations of swept box beams were analyzed.

A theory of plastic flow for anisotropic hardening in plastic deformation of an initially isotropic material was published (Report S. 410).

An exploratory investigation of the Heal tensioned-skin method of construction was started.

A report on minimizing a quadratic function with additional conditions was completed (Report S. 437).

Static testing of structural components.

Plastic buckling tests were carried out on plates and square seamless tubes.

The report on the shear tests of webs with lightening holes, also containing a comparison with recent Swedish tests, was completed (Report S. 446). Likewise, a report on the second series of tests to determine the effective width of 24 S-T flat plates in the plastic range was issued (Report S. 438) and a summary on both test-series was prepared for publication.

A third test series with other aluminium alloys is being carried out.

Compression tests on open-section thin-walled stiffeners and a compression test on a stiffened panel to determine its fixity coefficient in the 150-tons compression machine (Report S. 442) were evaluated in final form.

Fatigue.

Various investigations running at the beginning of the year were completed, viz. those concerning fatigue of bonded spar booms (Report M. 1936), effect of tolerance of pin-hole joints on their fatigue strength (Report M. 1946), comparison of various types of riveted joints in repeated tensile loading (Report M. 1943). New investigations were started to determine the practically important part of the fatigue (Goodman) diagram of riveted joints and lugs, and the fatigue strength of redux-bonded simple lap joints in 75 S-T clad sheet loaded in repeated tension (Report M. 1969).

The cumulative-damage research on simple notched and unnotched 24 S-T alclad strips is nearing its completion and similar tests with riveted joints were started.

Dynamic calibrations of various fatigue machines were carried out.

Adhesives and plastics.

An investigation concerning the strength of adhesive-bonded joints at low temperatures was carried out (Report M. 1973).

The tests to determine the mechanical properties of glassfiber polyester laminates were continued. Some preliminary tests were made with foamed-in-place araldite.

Miscellaneous work.

Some experience has now been gained in ultrasonic testing to determine material defects, cracks in machine components etc.

Rapid-loading tests were made on simple frame structures.

Model analysis by means of plastic and electrical models of structural components is being studied.

Structural and material problems caused by aerodynamic heating in high-speed flight are the subject of preliminary studies.

5 *Flight testing Section.*

Stability and Control.

In the course of an investigation of the dynamic behaviour of an aeroplane by means of response measurements, frequency response curves were calculated based on data from steady flight. Some orientating flight-tests by means of transient response techniques gave satisfactory results.

The influence of elastic deformations on the stability and its method of analysis were studied. A numerical analysis for a hypothetical aeroplane with slender swept wings has been carried out.

For the calculation of the liftdistribution a well-known approximation has been chosen, which gave good agreement with an exact method developed by the flutter section.

Performance Reduction Methods.

A study has been performed of the measuring technique and performance reduction to standard conditions of the take-off groundrun for aeroplanes with constant-speed propellers as well as with jet propulsion (V. 1711). A survey has been given of the basic principles of performance testing in take-off and landing, as a contribution to the AGARD Flight Test Manual.

Flight tests.

The flight-testing of prototypes took up most of the time.

In connection with the "Triton" accident flight tests have been carried out in order to compare true and indicated values of heights, airspeed and rate-of-climb during take-off and initial climb, to check position-error correction data and the influence of sideslip on pitot-static pressures for a Lockheed Super-Constellation.

Next to the fore-mentioned response measurements with the Siebel laboratory aeroplane, measurements were made of the influence on stability and drag of open or closed nacelle during extension of landing gear. Comparative measurements on stickforce per g in turns and symmetrical climbs have been made.

A quantitative appreciation of the performance and control of two newly-built sailplanes has been given.

Instrumentation.

For the AGARD Flight Test Manual a complete list of instruments used at the N. L. L. for flight tests, with a short survey of their characteristics, has been drafted and will be kept up.

Various new instruments have been developed, incl. an accurate attitude-gyro and a recording control-position indicator.

6 *Helicopter Section.*

A study has been made of amendments to be incorporated in the draft airworthiness-requirements for helicopters in case of application of tip-ramjets.

A rotor with tip-ramjets has been tested extensively on the rotating test-stand.

Performance, stability and control of ramjet-helicopters are being studied.

A report has been delivered on ground-resonance effects and its theoretical background.

7 *Free-flying models.*

A series of RM-10 models were launched and measurements were made in a very simplified way.

Determination of the dragcoefficient for Mach numbers of 0.9—1.5 yielded a satisfactory agreement with the values mentioned in literature.

An electronically timed flashlight was developed as an alternative to the synchronized shutters of the ballistic cameras used in these tests.

8 *Combustion Section.*

The relation between airspeed, fuel consumption and thrust of a specific type of ramjets has been measured. An orientating investigation has been made into the nature of the combustion and the pressure distribution within the ramjet.

9 *Documentation and Publications.*

Catalogue of Aerodynamic Measurements (CAM).

A questionnaire has been sent to subscribers to obtain information on their experiences with the card system. As a result some of the participating institutes made an extensive investigation into the probability of retrieval with this system. At a combined meeting of the AGARD-Windtunnel Panel and Documentation Committee these results have been discussed.

The system has been adapted to Hollerith-cards also.

Central Aeronautical Abstracting Service (C. L. D.).

The by-laws of the Supervisory Committee have been altered to bring them into line with present practice. The resulting change of name has been approved of.

The General Assembly of AGARD in The Hague resulted in fruitful discussions of the members of the AGARD-Documentation Committee with Dutch observers and representatives of NIDER and FID.

Publications.

In 1954 160 reports were completed, of which the following were published:

a) *Multigraphed and ozalided reports:*

A. 1292	Landstra, J. A.	Siebel (Symmetrical gliding flight). Comparison of Flight-Test Results and Windtunnel Measurements (in Dutch).
A. 1328	Landstra, J. A. Thomas, C.	Investigation of Tunnelwall Influence on the Half-Model of a Swept Wing (in Dutch).
F. 130	Zaat, J. A.	Calculation of the Temperature Field for Incompressible Laminar Boundary layer Flow with and without Pressure Gradient.
F. 132	Zaat, J. A.	An Approximate Method for the Calculation of Turbulent Boundary-layers in Compressible Twodimensional and Rotationally-Symmetrical Threedimensional Flows (in Dutch).
F. 140	De Jager, E. M.	The Aerodynamic Forces and Moments on an Oscillating Aerofoil with Control-Surface between Two Parallel Walls.
F. 142	Van Spiegel, E. Van de Vooren, A. I.	On the Theory of the Oscillating Wing in Two-Dimensional Subsonic Flow.
F. 143	De Kock, A. C.	Manual for Users of the N. L. L. Card Catalogue.
F. 146	Van de Vooren, A. I. Eckhaus, W.	Strip Theory for Oscillating Swept Wings on Incompressible Flow.
F. 147	IJff, J. Bosschaart, A. C. A. Van de Vooren, A. I.	Influence of Compressibility on the Flutterspeed of a Family of Rectangular Cantilever Wings with Aileron.
F. 153	Eckhaus, W.	On the Theory of Oscillating Airfoils of Finite Span in Subsonic Flow.
F. 154	Eckhaus, W.	The Induced Drag due to Disturbances in the Lift Distribution.
F. 155	De Jager, E. M.	Tables of the Aerodynamic Aileron-Coefficients for an Oscillating Wing-Aileron System in a Subsonic, Compressible Flow.
M. 1923	Hartman, A.	Informative Investigation to check the Cumulative Damage Hypthesis $\sum \frac{n}{N} = 1$ on Riveted Single Lap Joints. 1953 (in Dutch).
M. 1931	Hartman, A.	Some Tests to Determine the Influence of some Factors on the Scatter in Endurance Tests on Extruded 24 ST and Rolled 24 ST Alclad.
M. 1952	Schijve, J.	The Fatigue Strength of Riveted Lap Joints and Pin Hole Joints.
M. 1932	Hartman, A.	Comparative Investigation at Fluctuating Tension ($R = 0$) on Dural Lugs of Different Design.
M. 1940	Hartman, A.	The Peeling Tests of Redux Bonded Light Alloy Sheet. II. 1954. (In Dutch.)

M. 1946	Hartman, A.	The Effect of Various Fits on the Fatigue Strength of Pin Hole Joints.
M. 1949	Schijve, J.	The Possibilities of Internal Friction Measurements for Material Testing, in Particular for Fatigue Testing. 1954. (In Dutch.)
S. 410	Besseling, J. F.	A Theory of Plastic Flow for Anisotropic Hardening in Plastic Deformation of an Initially Isotropic Material.
S. 415	Benthem, J. P. Kruithof, R.	Investigation on the Strength of 24-S-T Alclad Riveted and Bolted Lap Joints at Rapid Applied Loads.
S. 423	Benthem, J. P.	On the Buckling of Rods and Plates in the Plastic Region. II. 1954. (In Dutch.)
S. 428	Floor, W. K. G.	The Effective Rolling Radius of Pneumatic-Tyred Wheels.
S. 437	Benthem, J. P.	Note on Minimizing a Quadratic Function with Additional Linear Conditions by Matrix Methods, with Application to Stress Analysis.
S. 438	Botman, M.	The Experimental Determination of the Effective Width of Flat Plates in the Elastic and the Plastic Range. Part II. 1954. (In Dutch.)
V. 1670	Pool, A.	Method for Determining the Lag Correction for Pitot-Static Systems in Non-Steady Flight.
V. 1698	De Boer, I. Greebe, F. W.	Report of Flight Tests with the Aircraft PH-NLL, type Siebel 204 D-1. Determination of Longitudinal Stability and Control Characteristics in Gliding Flight with both Airscrews Feathered. 1953. (In Dutch.)
V. 1711	Douwes Dekker, E.	The Measurement and Evaluation of the Groundrun of Landplanes.
V. 1717	Kalkman, C. M.	The Influence of Transonic Airspeeds on Static Longitudinal Stability and Control of Aircraft.
V. 1739	Kalkman, C. M.	Methods for Determining Stick Forces per g. Comparison of Stick Forces per g in Symmetrical turning Flight of a Siebel 204 D-1 Aircraft.
V. 1748	Lucassen, L. R.	Helicopter Ground Resonance in Theory and Experiment.

b) *Miscellaneous Publications:*

MP. 93	—	List of Journals. Classified at N. L. L., 1953.
MP. 94	Zwikker, C.	Mechanisations in Research. Polytechnical Weekly Magazine.
MP. 95	Burgerhout, Th. J.	On the Numerical Solution of Partial Differential Equations of the Elliptic Type Part. I. Appl. Sci. Res. Section B Vol. 4, 1954. p. 161.
MP. 96	Van der Linden, J. C.	Resistance thermometers.
MP. 97	Timman, R.	Linearized Theory of the Oscillating Airfoil in Compressible Subsonic Flow. J. Aero. Sci. Vol. 21, nr. 4, April 1954. p. 230.
MP. 98	Scherpenhuijsen Rom, G.	Report on Subject Classification Systems. AGARD. May 1954.
MP. 100	Van de Vooren, A. I.	Measurements of Aerodynamic Forces on Oscillating Aerofoils. AGARD May 1954.
MP. 103	Plantema, F. J.	Structural Problems Arising from Heating of Supersonic Aircraft. De Ingenieur, no. 31. 1954. Luchtv. Tech. 5.
MP. 104	Van de Vooren, A. I.	Practical Difficulties Encountered in Establishing the N. L. L. Card Catalogue of Aerodynamic Measurements. NIDER-AGARD Meeting 30-4-1954.
MP. 105	Timman, R.	Methods and Results of Non-Stationary Airfoil Theory. AGARD Mei 1954.
MP. 107	Van Oosterom, T.	Performance Testing of Sailplanes. OSTIV 31 July 1954.

MP. 108	Timman, R.	Zum Reziprozitätssatz der Tragflächentheorie bei beliebiger instationärer Bewegung. Zeitschr. Flugw. 1953, Heft 6.
MP. 111	Scherpenhuijsen Rom, G.	Report on Standardisation of Documentation in the International Organisation for Standardisation (ISO) Nov. 1954.
MP. 112	Van de Vooren, A. I. De Kock, A. C.	Recent Experience with the N. L. L. Card Catalogue for Aerodynamic Measurements. AGARD Nov. 1954.
MP. 113	Zwikker, C.	Shocktubes. De Ingenieur, Vol. 67, nr. 13, 1-IV-'55.
MP. 114	Landstra, J. A.	Experiments at the Nationaal Luchtvaartlaboratorium, Amsterdam, Concerning Boundary-Layer, Interference of a Wing-Wall Junction. De Ingenieur, Vol. 66 No. 50, 10 Dec. 1954 L 43. (Lezing voor Ned. Ver. v. Luchtvaart-techniek.)
MP. 117	Zwikker, C.	The Physical Causes of the Sound Barrier.

C.C.L. Class. D 050: D 055: D 153

REPORT F. 141.

A One-Parameter Method for the Calculation of Laminar Compressible Boundary-Layer Flow with a Pressure Gradient

by

J. A. ZAAT.

Summary.

Based on the momentum equation of VON KÀRMÀN and the integrated heat equation suppositions are made for the analysis of the velocity and temperature profiles in laminar compressible boundary layer flow. The method is set up by means of the asymptotic behaviour of the boundary layer profiles and takes into account as many boundary conditions at the wall as possible. In connection with these boundary conditions the flow with and without heat transfer at the wall is dealt with.

Contents.

This investigation has been sponsored by the Netherlands Aircraft Development Board.

1 Introduction.

Contrary to the incompressible laminar boundary layer flow where the velocity field is independent of the temperature field, there appears to be a mutual influence of velocity and temperature boundary layers for compressible flow. This is caused by the fact that it is not allowed to neglect friction and compression heat at large velocities, and that the physical values (e. g. viscosity coefficient) appearing in the analysis, have to be considered not as constants, but as functions of the temperature as a result of the large differences in temperature. The analysis, of course, becomes more complicated by this mutual influence of velocity and temperature field. In general it appears to be impossible to obtain exact solutions of the boundary layer equations.

Hence, it is the more important to dispose of methods, which guarantee a sufficiently accurate approximation of the solutions of the boundary layer equations.

Like the method for incompressible boundary layer flow described in report F. 127 (ref. 1) a similar method is developed for compressible flow, which uses the principle of POHLHAUSEN and SCHLICHTING with the aid of the momentum equation of VON KÀRMÀN and the integrated heat equation.

This method is based on the asymptotic behaviour of the solutions of the boundary layer equations at the outer edge of the boundary layer flow so that all boundary conditions at the outer edge are satisfied automatically.

In choosing the number of boundary conditions which is taken into account, a compromise must be found between the accuracy of the approximation at the one side and the required computational work at the other side.

The two cases of flow with and without heat transfer at the wall will be dealt in this report.

Application of the method to rotationally symmetric flow gives no difficulty.

2 Symbols.

x, y	coordinates along and perpendicular to the wall.
U	velocity at the outer edge of the boundary layer.
U_∞	velocity of undisturbed flow.
u, v	velocity components within the boundary layer.
T	absolute temperature.
ρ	density.
μ	absolute coefficient of viscosity.
$\nu = \frac{\mu}{\rho}$	kinematic coefficient of viscosity.
τ	shear stress.
λ	coefficient of heat conduction.
$R = c_p - c_v$	gas constant.
c_p	specific heat at constant pressure.
c_v	specific heat at constant volume.
$k = c_p/c_v$	($k = 1.405$ for air).
$\sigma = \frac{c_p \mu}{\lambda}$	Prandtl number.

$$\gamma = \frac{T_u + C}{\overline{T} + C}\left(\frac{\overline{T}}{T_u}\right)^{1/2}, \quad \overline{T} = \frac{T_u + 3\,T_w}{4}$$

$$\beta = \frac{3}{2} - \frac{T_u}{T_u + C}, \quad C = 110°\mathrm{K}.$$

c	speed of sound.
c^*	critical speed of sound.
$M = \frac{U}{c}$	local Mach number.
δ	boundary layer thickness.
$H = \frac{\delta_1}{\delta_2}$	form parameter.
$\delta_1 = \int_0^\delta \left(1 - \frac{\rho u}{\rho_u U}\right) dy$	displacement thickness.
$\delta_2 = \int_0^\delta \frac{\rho u}{\rho_u U}\left(1 - \frac{u}{U}\right) dy$	*momentum thickness.*
$\delta_3 = -\int_0^\delta \frac{\rho u}{\rho_u U}\left(1 - \frac{T}{T_u}\right) dy$	loss of enthalpy thickness.
$\delta_4 = \int_0^\delta \frac{\mu}{\mu_u}\left(\frac{\partial u/U}{\partial y/\delta_2}\right)^2 dy$	dissipation function.
$\delta_5 = \int_0^\delta \frac{\rho u}{\rho_u U}\left(1 - \frac{u^2}{U^2}\right) dy$	kinetic energy function.
$Re_L = \frac{UL}{\nu_u}$	Reynolds number.
$\theta = \frac{U\delta_2^2}{\nu_u}, \ \theta_1 = \frac{U\delta_3^2}{\nu_u}, \ \theta_2 = \frac{U\delta_5^2}{\nu_u}$	integration quantities.
$\overline{u} = \frac{u}{U}$	dimensionless velocity.
$t = \frac{T}{T_u}$	dimensionless temperature.
ξ, ξ_0	coordinates.
$\alpha, \alpha_0, \Omega = \frac{\alpha}{\alpha_0}$	functions of x.
$a, b, \ldots f_0$; $p_0, q_0 \ldots t_0$	coefficients (functions of x).
Δ_1, p_1, γ_1	quantities introduced in section 6.
$p, q, \Delta, \Delta_0, Q, P$	quantities introduced in section 8.
$q(x) = -\lambda\left(\frac{\partial T}{\partial y}\right)_w$	heat transfer at the wall.

Subscripts

u and T	denoting outer flow.
w	denoting the wall.
x, y, ξ, ξ_0	denoting derivatives to x, y, ξ, ξ_0.
t, n	denoting tangential, normal direction.

3 Basic equations for the analysis of the laminar compressible boundary layers.

The laminar compressible boundary layer flow can be described by the following equations:

(i) The equation of motion

$$\rho u\, u_x + \rho v\, u_y = \rho_u\, U U_x + (\mu u_y)_y. \tag{3.1}$$

This equation is a result of simplifying the NAVIER-STOKES equation according to the usual boundary layer generalizations. It governs the equilibrium between the inertia force (left-hand term), the pressure (first term of right-hand side) and the frictional force (second term of right-hand side) acting on an element of fluid in the boundary layer flow.

(ii) The equation of continuity

$$(\rho u)_x + (\rho v)_y = 0 \tag{3.2}$$

denotes the conservation of mass of the element.

(iii) The energy equation

$$\rho c_p (u\, T_x + v\, T_y) = -\rho_u u\, U U_x + (\lambda T_y)_y + \mu u_y^2 \tag{3.3}$$

gives the variation of the heat content of the element per unit time (left-hand side) caused by the compression energy (first term right-hand side), the heat conduction or convection (second term) and the frictional energy (third term).

(iv) The equation of state for the ideal gas

$$p = R\rho T. \tag{3.4}$$

(v) The formula of SUTHERLAND, yielding an approximate relation between viscosity and temperature

$$\frac{\mu}{\mu_\infty} = \frac{T_\infty + C}{T + C}\left(\frac{T}{T_\infty}\right)^{3/2} \tag{3.5}$$

In the case of air C will have the value 110°K (ref. 2.3). In general, the formula of SUTHERLAND can be used up to the hypersonic range, excluding very low temperatures.

To simplify the calculations the linear relation

$$\frac{\mu}{\mu_u} = \frac{T_u + C}{\overline{T} + C}\left(\frac{\overline{T}}{T_u}\right)^{1/2}\frac{T}{T_u} = \gamma\left(\frac{T}{T_u}\right) \tag{3.6}$$

for the distribution $\frac{\mu}{\mu_u}$ across the boundary layer (in y-direction) will be introduced besides the relation (3.5).

In formula (3.6) $\overline{T}$ is an average temperature $\overline{T} = \frac{\alpha_1 T_u + \alpha_2 T_w}{\alpha_1 + \alpha_2}$, thus introducing a weighting factor α_1 for the outer temperature T_u and a weighting factor α_2 for the wall temperature T_w.

For $T = \overline{T}$ (3.6) satisfies the formula of SUTHERLAND. For $\alpha_1 = 0$ (3.6) changes into a formula

$$\frac{\mu}{\mu_u} = \frac{T_u + C}{T_w + C} \sqrt{\frac{T_w}{T_u}} \left(\frac{T}{T_u}\right),$$

which has been used by several authors (ref. 4, 5, 6 and 7).

For $\alpha_2 = 0$ (3.6) changes into

$$\frac{\mu}{\mu_u} = \frac{T}{T_u},$$

a particular form of the usual relation between temperature and viscosity

$$\frac{\mu}{\mu_u} = \left(\frac{T}{T_u}\right)^n,$$

(ref. 3, 9, 10, 11). At first sight one might choose for $\overline{T}$ the arithmetic average value $\overline{T} = \frac{T_u + T_w}{2}$, since this makes within the boundary layer the *maximum deviations in positive and negative direction* from the formula of SUTHERLAND about equally large.

However, the calculations of drag for flow along a heat-insulated flat plate at a PRANDTL number $\sigma = 1$ show that the value

$$\overline{T} = \frac{T_u + 3\,T_w}{4} \tag{3.7}$$

in formula (3.6) leads to about the same results as the formula of SUTHERLAND. For laminar compressible boundary layers without heat transfer at the wall the viscosity-relation of SUTHERLAND can be applied also within the boundary layer at a PRANDTL number $\sigma = 1$ without making the computations too laborious (Sec 5). This application has the advantage that it yields more accurate data which can be used in determining $\overline{T}$ in (3.6). From the calculations for flow along a flat plate it is evident that the relation (3.7) must be preferred to the arithmetic average $\overline{T} = \frac{T_u + T_w}{2}$ and the value $\overline{T} = T_w$, so that the relation (3.7) will also be applied to further calculations.

In the calculation the specific heat is assumed to be constant. The same holds for the number of PRANDTL, introduced in the calculation

$$\sigma = \frac{\mu c_p}{\lambda}.$$

The solutions of the above-mentioned equations, which describe the temperature field and the velocity field of the laminar boundary layer in compressible flow, have to satisfy the following boundary conditions.

$$\text{For} \quad y = 0;\ u = v = 0;\ \frac{\partial u}{\partial y} = \frac{\tau_w}{\mu_w}; \tag{3.8}$$

for a wall with prescribed temperature $T = T_w$

for a completely heat-insulated wall $\frac{\partial T}{\partial y} = 0$

$$y = \delta_u \quad u = U;\ \frac{\partial u}{\partial y} = \frac{\partial^2 u}{\partial y^2} = \frac{\partial^3 u}{\partial y^3} = \ldots = 0 \tag{3.9}$$

$$y = \delta_T \quad T = T_u;\ \frac{\partial T}{\partial y} = \frac{\partial^2 T}{\partial y^2} = \frac{\partial^3 T}{\partial y^3} = \ldots = 0 \tag{3.10}$$

δ_u is the thickness of the velocity boundary layer (in y-direction) and δ_T the thickness of the temperature boundary layer. In general δ_u and δ_T will be unequal.

If the shock waves will be left out of consideration, then the relation

$$c^2 = kR\,T_0 - \frac{k-1}{2} U^2 = k(c_p - c_v) T_0 - \\ - \frac{k-1}{2} U^2, \tag{3.11}$$

or

$$\frac{c^2}{U^2} = \frac{1}{M^2} = (k-1)\left[\frac{c_p T_0}{U^2} - \frac{1}{2}\right]$$

holds for adiabatic flow and, hence, for the flow outside the boundary layer (the subscript 0 denotes the undisturbed condition).

From the energy equation the relation

$$\frac{U^2}{2} + c_p(T_u - T_0) = 0 \tag{3.12}$$

follows for the outer flow. Hence, in connection with equation (3.11)

$$\frac{U^2}{c_p T_u} = M^2(k-1). \tag{3.13}$$

Furthermore

$$\frac{T_w}{T_u} = \frac{T_w\,c_p(k-1)}{c^2} = \frac{T_w}{T_0}(1 + \tfrac{1}{2}(k-1)M^2). \tag{3.14}$$

From the definition of the speed of sound $\frac{dp}{d\rho_u} = c^2$ and with the aid of the equation of BERNOULLI $U dU = -\frac{1}{\rho_u} dp = -c^2 \frac{d\rho_u}{\rho_u}$ the relation

$$M^2 = -\frac{U}{U_x} \frac{\rho_{u_x}}{\rho_u} \tag{3.15}$$

follows.

As the pressure across the boundary layer can be assumed to be constant, it follows from the ideal gas equation that

$$\frac{\rho_u}{\rho} = \frac{T}{T_u}. \tag{3.16}$$

From the relations for adiabatic flow outside the boundary layer $c^2 = \frac{kp}{\rho_u}$ and $c^2 = c_0 - \frac{k-1}{2} U^2$ follows

$$\frac{T_u}{T_0}=\left(\frac{\rho_u}{\rho_0}\right)^{k-1}=\frac{1}{1+\frac{k-1}{2}M^2}=1-\frac{\frac{k-1}{2}M^2_\infty}{1+\frac{k-1}{2}M^2_\infty}\frac{U^2}{U^2_\infty}. \tag{3.17}$$

The right-hand side of equation (3.17) holds only if no shock wave is present. If this occurs, the ensuing entropy variation will have to be taken into account.

The description of the laminar boundary layer flow in the compressible flow field will be carried out with the aid of the momentum equation of VON KÀRMÀN, the integrated heat equation and as far as necessary of the kinetic energy equation of WIEGHARDT.

Integration of the equation of motion in y-direction gives with the aid of the equation of continuity the momentum equation

$$\frac{d\delta_2}{dx}+\delta_2\frac{U_x}{U}[H+2-M^2]=\frac{\tau_w}{\rho_u U^2}=\frac{[\mu\, u_y]_w}{\rho_u U^2}=Re_{\delta_2}^{-1}\left[\frac{\partial u/U}{\partial y/\delta_2}\right]_v\frac{\mu_w}{\mu_u}, \tag{3.18}$$

where $H=\frac{\delta_1}{\delta_2}$,

$$\delta_1=\int_0^\delta\left(1-\frac{\rho}{\rho_u}\frac{u}{U}\right)dy \qquad \text{the displacement thickness} \tag{3.19}$$

$$\delta_2=\int_0^\delta\frac{\rho u}{\rho_u U}\left(1-\frac{u}{U}\right)dy \qquad \text{the momentum-loss thickness} \tag{3.20}$$

and

$$Re_{\delta_2}=\frac{\rho_u U\delta_2}{\mu_u}=\frac{U\delta_2}{\nu_u} \tag{3.21}$$

the REYNOLDS number with relation to the momentum-loss thickness.

Substituting $\theta=\delta_2 Re_{\delta_2}$ and taking into account the following relations

$$\frac{\rho_{u_x}}{\rho_u}=-\frac{U_x}{U}M^2;\ \frac{T_{u_x}}{T_u}=(k-1)\frac{\rho_{u_x}}{\rho_u};\ \frac{\mu_{u_x}}{\mu_u}=\left(\frac{3}{2}-\frac{T_u}{T_u+C}\right)\frac{T_{u_x}}{T_u}=\beta\frac{T_{u_x}}{T_u} \tag{3.22}$$

and

$$\frac{d\theta}{dx}=2\frac{d\delta_2}{dx}Re_{\delta_2}+\left(\frac{\rho_{u_x}}{\rho_u}-\frac{\mu_{u_x}}{\mu_u}+\frac{U_x}{U}\right)\theta=2\frac{d\delta_2}{dx}Re_{\delta_2}+[1-\{1-\beta(k-1)\}M^2]\frac{U_x}{U}\theta.$$

The momentum equation (3.18) changes into

$$\frac{d\theta}{dx}+\frac{U_x}{U}\theta\,[2H+3-\{1+\beta(k-1)\}M^2]\doteq 2\frac{\mu_w}{\mu_u}\left(\frac{\partial u/U}{\partial y/\delta_2}\right)_w=2\gamma\frac{T_w}{T_u}\left(\frac{\partial u/U}{\partial y/\delta_2}\right)_w. \tag{3.23}$$

The integrated heat equation will be obtained by multiplying the equation of continuity with c_pT and adding this to the energy equation (3.3)), which gives

$$(c_p\rho uT)_x+(c_p\rho vT)_y=-\rho_u u\,UU_x+(\lambda T_y)_y+uu_y^2$$

and then integrating this equation to y between $y=0$ and $y=\delta$. This gives together with the equation of continuity (3.2)

$$\frac{d}{dx}\int_0^\delta c_p\rho uT dy-T_u\frac{d}{dx}\int_0^\delta c_p\rho u dy=-\int_0^\delta\rho_u u\,UU_x dy-(\lambda T_y)_w+\int_0^\delta\mu u_y^2dy. \tag{3.24}$$

In connection with the adiabatic relation for the undisturbed flow (3.12), $\frac{U^2}{2}+c_pT_u=\text{const.}$, equation (3.24) changes into

$$\frac{d}{dx}c_p\int_0^\delta\rho u(T-T_u)dy=-UU_x\int_0^\delta u(\rho_u-\rho)dy-\lambda_w(T_y)_w+\int_0^\delta\mu u_y^2\,dy. \tag{3.25}$$

Introducing the enthalpy-loss thickness

$$\delta_3 = -\int_0^\delta \frac{\rho u}{\rho_u U}\left(1 - \frac{T}{T_u}\right) dy, \tag{3.26}$$

the dissipation function

$$\delta_4 = \int_0^\delta \frac{\mu}{\mu_u}\left(\frac{\partial u/U}{\partial y/\delta_2}\right)^2 dy \tag{3.27}$$

and the PRANDTL number $\sigma = \frac{\mu c_p}{\lambda}$, the equation (3.25) changes into

$$\frac{d}{dx}(\rho_u U T_u \delta_3) = -\frac{1}{c_p} U^2 U_x \rho_u \delta_3 - \frac{\mu_w}{\sigma}(T_y)_w + \frac{\mu_u U^2}{c_p} \frac{\delta_4}{\delta_2^2}. \tag{3.28}$$

With the aid of relation (3.13), by substituting the REYNOLDS number

$$Re_{\delta_3} = \frac{\rho_u U \delta_3}{\mu_u}$$

and differentiating in the following way

$$\frac{1}{\mu_u T_u}\frac{d}{dx}\left(\frac{\rho_u U \delta_3}{\mu_u}\mu_u T_u\right) = \left(\frac{\mu_{u_x}}{\mu} + \frac{T_{u_x}}{T_u}\right) Re_{\delta_3} + \frac{d\,Re_{\delta_3}}{dx} = -(\beta+1)(k-1)\frac{U_x}{U} M^2 Re_{\delta_3} + \frac{d\,Re_{\delta_3}}{dx}$$

equation (3.28) changes into

$$\frac{d\,Re_{\delta_3}}{dx} - \beta(k-1)\frac{U_x}{U} M^2 Re_{\delta_3} + \frac{\mu_w}{\mu_u}\frac{1}{\sigma}\frac{(T_y)_w}{T_u} - (k-1)M^2\frac{\delta_4}{\delta_2^2} = 0. \tag{3.29}$$

Substituting

$$\theta_1 = \delta_3 Re_{\delta_3} = \frac{\rho_u U \delta_3^2}{\mu_u}$$

and its differential quotient

$$\frac{d\theta_1}{dx} = \left(\frac{\rho_{u_x}}{\rho_u} - \frac{\mu_{u_x}}{\mu_u} + \frac{U_x}{U}\right)\theta_1 + 2\frac{d\delta_3}{dx} Re_{\delta_3} = \frac{d\delta_3}{dx} Re_{\delta_3} + \delta_3 \frac{d\,Re_{\delta_3}}{dx}$$

or

$$\delta_3 \frac{d\,Re_{\delta_3}}{dx} = \frac{d\delta_3}{dx} Re_{\delta_3} + [1 - \{1 - \beta(k-1)\}M^2]\frac{U_x}{U}\theta_1 = \tfrac{1}{2}\frac{d\theta_1}{dx} + \tfrac{1}{2}[1 - \{1 - \beta(k-1)\}M^2]\frac{U_x}{U}\theta_1,$$

into eq. (3.29) the integrated energy equation becomes

$$\frac{d\theta_1}{dx} + \frac{U_x}{U}\theta_1[1 - \{1 + \beta(k-1)\}M^2] + \frac{2}{\sigma}\frac{\mu_w}{\mu_u}\left(\frac{\partial \frac{T}{T_u}}{\partial y/\delta_3}\right)_w - 2(k-1)M^2\frac{\delta_4\delta_3}{\delta_2^2} = 0. \tag{3.30}$$

The kinetic energy equation of WIEGHARDT.

Multiplying the equation of continuity by $\frac{u^2}{2}$ and the equation of motion by u and adding these together, the result is

$$\left(\rho u \frac{u^2}{2}\right)_x + \left(\rho v \frac{u^2}{2}\right)_y = \rho_u u U U_x + u(\mu u_y)_y.$$

Integration to y between 0 and δ gives

$$\frac{d}{dx}\int_0^\delta \rho u \frac{u^2}{2} dy - \frac{U^2}{2}\frac{d}{dx}\int_0^\delta \rho u\, dy = U U_x \int_0^\delta \rho_u u\, dy - \int_0^\delta \mu u_y^2\, dy$$

or (3.31)

$$\frac{d}{dx}\int_0^\delta \rho u\left(\frac{U^2}{2} - \frac{u^2}{2}\right) dy + U U_x \int_0^\delta u(\rho_u - \rho)dy = \int_0^\delta \mu u_y^2\, dy.$$

Introducing the kinetic energy function

$$\delta_5 = \int_0^\delta \frac{\rho u}{\rho_u U}\left(1 - \frac{u^2}{U^2}\right) dy \tag{3.32}$$

and substituting

$$Re_{\delta_5} = \frac{\rho_u U \delta_5}{\mu_u}$$

changes equation (3.31) into

$$\frac{d\,Re_{\delta_5}}{dx} + \left\{2 + 2\frac{\delta_3}{\delta_5} - \beta(k-1)M^2\right\}\frac{U_x}{U}\,Re_{\delta_5} = 2\,\frac{\delta_4}{\delta_2{}^2}. \tag{3.34}$$

Multiplying with $2\,\delta_5$ and substituting

$$\theta_2 = \delta_5\,Re_{\delta_5} = \frac{\rho_u U \delta_5{}^2}{\mu_u} \tag{3.35}$$

changes equation (3.34) into

$$\frac{d\theta_2}{dx} + \frac{U_x}{U}\,\theta_2\left[5 + 4\frac{\delta_3}{\delta_5} - \{1 + \beta(k-1)\}\,M^2\right] = 4\,\frac{\delta_4\delta_5}{\delta_2{}^2}. \tag{3.36}$$

A relation between the kinetic and heat energy can be obtained by adding the equation of motion (3.1) multiplied by u to the energy equation (3.3)

$$\rho u\,\frac{\partial}{\partial x}\left(\frac{u^2}{2} + c_pT\right) + \rho v\,\frac{\partial}{\partial y}\left(\frac{u^2}{2} + c_pT\right) = \frac{\partial}{\partial y}\left\{\mu\,\frac{\partial}{\partial y}\left(\frac{u^2}{2} + c_pT\right)\right\} + \left(\frac{1}{\sigma} - 1\right)c_p\,\frac{\partial}{\partial y}\left(\mu\,\frac{\partial T}{\partial y}\right). \tag{3.37}$$

By integrating over y from 0 up to δ and applying the equation of continuity the relation

$$\frac{d}{dx}\int_0^\delta \rho u\left[\frac{U^2}{2} - \frac{u^2}{2} + c_p\,T_u - c_pT\right] dy = \frac{\mu_w c_p}{\sigma}\,(T_y)_w \tag{3.38}$$

is obtained. In connection with (3.13), (3.26) and (3.32), (3.38) can be transformed into the equation

$$\frac{d}{dx}\left\{\rho_u U\,T_u\left(\frac{k-1}{2}\,M^2\delta_5 - \delta_3\right)\right\} = \frac{\mu_w}{\sigma}\,(T_y)_w\,. \tag{3.39}$$

If no heat transfer to the wall takes place, $\left(\frac{\partial T}{\partial y}\right)_w = 0$, then (3.39) changers into

$$\rho_u U\,T_u\left(\frac{k-1}{2}\,M^2\delta_5 - \delta_3\right) = \text{constant} = 0. \tag{3.40}$$

The constant value of the right hand side vanishes since the left-hand side of (3.40) becomes equal to zero in the stagnation point. In that case the relation

$$\delta_3 = \frac{M^2}{2}\,(k-1)\,\delta_5, \tag{3.42}$$

exists and the energy equation of WIEGHARDT changes into

$$\frac{d\theta_2}{dx} + \frac{U_x}{U}\,\theta_2\,[5 + \{(2-\beta)(k-1) - 1\}\,M^2] = \frac{4\,\delta_4\delta_5}{\delta_2{}^2}. \tag{3.42}$$

For a PRANDTL *number* $\sigma = 1$ *and in the case that no heat transfer to the wall occurs,* $\left(\frac{\partial T}{\partial y}\right)_w = 0$, the calculations of the boundary layer can be simplified, because the solution

$$\frac{u^2}{2} + c_pT = \text{constant}$$

satisfies the differential equation (3.37). The adiabatic flow condition still exists in this case within the boundary layer, so that for $\sigma = 1$ the following temperature-velocity relations holds

$$\frac{T}{T_u} = 1 + \frac{k-1}{2}\,M^2\left(1 - \frac{u^2}{U^2}\right) \text{ for } \sigma = 1 \text{ and } \left(\frac{\partial T}{\partial y}\right)_w = 0. \tag{3.43}$$

When for flow along a flat plate without pressure gradient a constant wall temperature is prescribed, then the relation

$$\frac{u^2}{2} + c_p T = c_p T_w + \frac{u}{U}\left[\frac{U^2}{2} + c_p(T_u - T_w)\right], \tag{3.44}$$

satisfies (3.37) for $\sigma = 1$, as follows immediately by aid of (3.1).

In both cases only the equation of motion or the momentum equation of VON KÀRMÀN is necessary for the solution of the boundary layer flow.

4 The asymptotic behaviour of the solutions of the boundary layer equations.

The equation of continuity (3.2) yields the existence of a stream function $\psi(x, y)$, for which the velocity components in the boundary layer satisfy the following relations

$$\rho u = \frac{\partial \psi}{\partial y}, \tag{4.1}$$

$$\rho v = -\frac{\partial \psi}{\partial x}. \tag{4.2}$$

When introducing a new parameter

$$\varphi = \int_0^x \rho_u U(s)\, ds$$

which is connected with the undisturbed flow velocity outside the boundary layer, the quantities φ and ψ can be considered as new independent variables. Then

$$\frac{\partial}{\partial x} = \frac{\partial \varphi}{\partial x}\frac{\partial}{\partial \varphi} + \frac{\partial \psi}{\partial x}\frac{\partial}{\partial \psi} = \rho_u U \frac{\partial}{\partial \varphi} - \rho v \frac{\partial}{\partial \psi}$$

$$\frac{\partial}{\partial y} = \frac{\partial \psi}{\partial y}\frac{\partial}{\partial \psi} = \rho u \frac{\partial}{\partial \psi}.$$

Hence, the equations (3.1) and (3.3) become

$$U u \frac{\partial u}{\partial \varphi} = \frac{\rho_u}{\rho} U^2 \frac{dU}{d\varphi} + u \frac{\partial}{\partial \psi}\left(\mu \frac{\rho}{\rho_u} u \frac{\partial u}{\partial \psi}\right), \tag{4.3}$$

$$c_p U \frac{\partial T}{\partial \varphi} = -\frac{\rho_u}{\rho} U^2 \frac{dU}{d\varphi} + \frac{\partial}{\partial \psi}\left(\frac{\rho}{\rho_u} u \lambda \frac{\partial T}{\partial \psi}\right) + \mu u \frac{\rho}{\rho_u}\left(\frac{\partial u}{\partial \psi}\right)^2. \tag{4.4}$$

The relation (3.12) for the adiabatic flow condition outside the boundary layer yields

$$c_p \frac{\partial T_u}{\partial \varphi} + U \frac{\partial U}{\partial \varphi} = 0 \qquad \frac{\partial T_u}{\partial \psi} = 0. \tag{4.5}$$

This changes equations (4.3) and (4.4) into

$$U \frac{\partial (u^2 - U^2)}{\partial \varphi} = \left(\frac{\rho_u}{\rho} - 1\right) U \frac{\partial U^2}{\partial \varphi} + u \frac{\partial}{\partial \psi}\left(\mu \frac{\rho}{\rho_u} \frac{\partial}{\partial \psi}(u^2 - U^2)\right) \tag{4.6}$$

$$c_p U \frac{\partial (T - T_u)}{\partial \varphi} = \tfrac{1}{2}\left(1 - \frac{\rho_u}{\rho}\right) U \frac{dU^2}{d\varphi} + \frac{\partial}{\partial \psi}\left(\frac{\rho}{\rho_u} u \lambda \frac{\partial (T - T_u)}{\partial \psi}\right) + \mu u \frac{\rho}{\rho_u}\left(\frac{\partial (u - U)}{\partial \psi}\right)^2. \tag{4.7}$$

For the determination of the asymptotic behaviour at the outer edge of the boundary layer the quantities

$$\Delta T = T_u - T$$
$$\Delta u = U - u \tag{4.8}$$

will be introduced. As ΔT and Δu will be assumed to be small, their squares or products will be neglected. In relation with (3.16), (3.6) and (4.8) one has

$$\frac{\rho_u}{\rho} = \frac{T}{T_u} \approx 1 - \frac{\Delta T}{T} \qquad \frac{\mu}{\mu_u} = \gamma\left(\frac{T}{T_u}\right) \approx \gamma\left(1 - \frac{\Delta T}{T}\right). \tag{4.9}$$

Concerning the order of magnitude the following relations exist

$$\varphi = 0(1) \gg \psi = 0(\delta),\ \mu_u \approx 0(\delta^2),\ \lambda = \frac{c_p}{\sigma}\mu \approx 0(\delta^2).$$

After neglecting all terms of second and higher order in δ the boundary layer equations (4.6) and (4.7) change into

$$\gamma\,\mu_u \frac{\partial^2 \Delta u U}{\partial \psi^2} - \frac{\partial \Delta u U}{\partial \varphi} + \tfrac{1}{2} \frac{\Delta T}{T_u} \frac{dU^2}{d\varphi} = 0, \quad (4.10)$$

$$\frac{c_p}{\sigma} \gamma\,\mu_u \frac{\partial^2 \Delta T}{\partial \psi^2} - c_p \frac{\partial \Delta T}{\partial \varphi} - \tfrac{1}{2} \frac{\Delta T}{T_u} \frac{dU^2}{d\varphi} = 0, \quad (4.11)$$

where U and μ_u are functions of φ only. After substitution of

$$\psi = \sqrt{\gamma\,\mu_u}\,\Psi,\ \varphi = \phi \qquad (4.12)$$

where Ψ and ϕ are of order $0(1)$, the equations (4.10) and (4.11) become

$$U \frac{\partial^2 \Delta u}{\partial \Psi^2} - \frac{\partial \Delta u U}{\partial \phi} + \tfrac{1}{2} \frac{\Delta T}{T_u} \frac{dU^2}{d\phi} = 0, \quad (4.10a)$$

$$\frac{\partial^2 \Delta T}{\partial \Psi^2} - \frac{\partial \Delta T}{\partial \phi} + \frac{1}{2\,c_p} \frac{\Delta T}{T_u} \frac{dU^2}{d\phi} = 0. \quad (4.11a)$$

In order to consider the asymptotic behaviour of $\frac{T}{T_u}$ and $\frac{u}{U}$, i. e. the behaviour of $\frac{T}{T_u}$ and $\frac{u}{U}$, for large values of Ψ the following transformation are introduced:

$$\Psi = \delta\,\overline{\Psi} \ \text{ and } \ \phi - \phi_1 = \delta^2\,\overline{\phi} \qquad (4.12a)$$

where δ refers to the boundary layer thickness and $\varphi = \phi_1$ denotes a fixed value.

$\frac{T_w}{T_u}$ and U being regular functions of ϕ, the following TAYLOR expansions exist

$$\frac{T_w}{T_u}(\phi) = \frac{T_w}{T_u}(\phi_1) + (\phi - \phi_1)\left(\frac{d}{d\phi}\,\frac{T_w}{T_u}\right)_{\phi=\phi_1} + \\ + \ldots = \frac{T_w}{T_u}(\phi_1) + \delta^2\overline{\phi}\,0(1)$$

$$U(\phi) = U(\phi_1) + (\phi - \phi_1)\left(\frac{dU}{d\phi}\right)_{\phi=\phi_1} + \\ + \ldots = U(\phi_1) + \delta^2\overline{\phi}\,0(1).$$

Hence near $\overline{\phi} = 0 \left| \frac{T_w}{T_u} \right. ((\overline{\phi})$ and $U(\overline{\phi})$ may be considered as constants. The differential equations (4.10a) and (4.11a) become after substitution of eq. (4.12)

$$\frac{\partial^2 \Delta u}{\partial \overline{\Psi}^2} - \frac{\partial \Delta u}{\partial \overline{\phi}} = 0 \qquad (4.13)$$

$$\frac{1}{\sigma} \frac{\partial^2 \Delta T}{\partial \overline{\Psi}^2} - \frac{\partial \Delta T}{\partial \overline{\phi}} = 0. \qquad (4.14)$$

The pertaining bounday conditions are

$$\Delta T = \Delta u = 0 \qquad \text{for } \overline{\Psi} = \infty \qquad (4.15)$$
$$\Delta T = T_u - T_w \quad \Delta u = U \ \text{ for } \overline{\Psi} = 0.$$

The equations (4.13) and (4.14) with the boundary conditions (4.15) are satisfied by the solutions

$$\Delta u = U - u = \frac{2}{\sqrt{\pi}}\,U \int_{\varepsilon}^{\infty} e^{-\alpha^2}\, d\alpha \qquad (4.16)$$

$$\Delta T = T_u - T = \\ = \frac{2}{\sqrt{\pi}}(T_u - T_w) \int_{\varepsilon\sqrt{\sigma}}^{\infty} e^{-\alpha^2}\, d\alpha, \qquad (4.17)$$

where $\varepsilon = \dfrac{\overline{\Psi}}{2\sqrt{\overline{\phi}}}$.

The asymptotic behaviour of the velocity profile at the outer edge of the velocity boundary layer will then be given by

$$\frac{u}{U} = 1 - \frac{2}{\sqrt{\pi}} \int_{\varepsilon}^{\infty} e^{-\alpha^2}\, d\alpha, \qquad (4.18)$$

where $\varepsilon = \dfrac{\psi}{2\sqrt{\mu_u \gamma (\varphi - \varphi_1)}}$,

taking into account (4.12) and (4.12a).

The asymptotic behaviour of the temperature profile at the outer edge of the temperature boundary layer will be given by

$$\frac{T}{T_u} = 1 - \frac{2}{\sqrt{\pi}}\left(1 - \frac{T_w}{T_u}\right) \int_{\varepsilon\sqrt{\sigma}}^{\infty} e^{-\alpha^2}\, d\alpha. \quad (4.19)$$

For larger values of y is

$$\frac{\psi}{\sqrt{\varphi - \varphi_1}} = \frac{\int_0^y \rho u\, dy}{\sqrt{\varphi - \varphi_1}} \approx \frac{\rho_u\, U y}{\sqrt{\varphi - \varphi_1}},$$

sothat for the ψ- as well as for the y-coordinates the same asymptotic behaviour holds.

From the equations (4.18) and (4.19) follows that the asymptotic behaviour of $\frac{U - u}{U}$ changes into that of $\frac{T_u - T}{T_u - T_w}$ by substituting $\psi = \psi_1 \sqrt{\sigma}$.

Hence the velocity and temperature profiles show the same asymptotic behaviour at the outer edge of the boundary layer apart from a stress factor $\sqrt{\sigma}$. As a consequence the temperature boundary layer will in general have to be thicker for PRANDTL number $\sigma < 1$ and thinner for PRANDTL numbers $\sigma > 1$ than the velocity boundary layers, which agrees with the experiments.

5 Approximative functions for the velocity and temperature profiles of the laminar compressible boundary layer flow with pertaining boundary conditions.

When introducing besides the dimensionless velocities and temperatures

$$\frac{u}{U}=\bar{u},\ \frac{T}{T_u}=t, \tag{5.1}$$

the new coordinates

$$d\xi=\frac{\alpha}{t}dy;\ \ d\xi_0=\frac{\alpha_0}{t}dy, \tag{5.2}$$

where $\xi=\frac{\alpha}{\alpha_0}\xi_0=\Omega\xi_0$ and α, α_0 are functions of x, then the velocity and temperature profiles can be described approximately by the following functions

$$\bar{u}=1-(a+b\,\xi+c\xi^2+\dots)e^{-\xi^2}-f\int\limits_{\xi}^{\infty}e^{-\eta^2}d\eta \tag{5.4}$$

$$t=1-(1-t_w)\left[a_0+b_0\xi_0+c_0\xi_0^{\,2}+d_0\xi_0^{\,3}+\dots)e^{-\xi_0^2}+f_0\int\limits_{\xi_0}^{\infty}e^{-\eta^2}d\eta\right]. \tag{5.5}$$

The boundary conditions at the outer edge of the velocity and temperature boundary layers change into

$$\begin{array}{lll} \xi=\infty & \bar{u}=1 & \dfrac{\partial\bar{u}}{\partial\xi}=\dfrac{\partial^2\bar{u}}{\partial\xi^2}=\dots=0 \\[2ex] \xi_0=\infty & t=1 & \dfrac{\partial t}{\partial\xi_0}=\dfrac{\partial^2 t}{\partial\xi_0^{\,2}}=\dots=0. \end{array} \tag{5.6}$$

As these boundary conditions are satisfied by the functions (5.4) and (5.5), the coefficients a, b, c, $f\dots\dots f_0$, which are functions of x, can be determined by the boundary conditions at the wall. These boundary conditions, which follow from the differential equations (3.1), (3.2) and (3.3) in relation with (3.8) for $y=0$, are

$$\begin{aligned} & u=0;\ u_y=\frac{\tau_w}{\mu_w};\ (\mu\,u_y)_y=-\rho_u U U_x;\ (\mu\,u_y)_{yy}=0 \\ & 2(\rho u)_y\,u_{xy}-(\rho u)_{xy}\,u_y=(\mu\,u_y)_{yyy};\ \dots \\ & T=T_w\ \text{ or }\ \left(\frac{\partial T}{\partial y}\right)_w=0;\frac{c_p}{\sigma}(\mu T_y)_y+\mu u_y^{\,2}=0; \\ & c_p(\rho u)_y\,T_x=-\rho_u\,u_y U U_x+\frac{c_p}{\sigma}(\mu\,T_y)_{yy}+(\mu u_y^{\,2})_y; \\ & c_p[(\rho u)_{yy}\,T_x+2(\rho u)_y\,T_{xy}-(\rho u)_{xy}\,T_y]=-\rho_u u_{yy} U U_x+\frac{c_p}{\sigma}(\mu T_y)_{yyy}+(\mu u_y^{\,2})_{yy}. \end{aligned} \tag{5.7}$$

After substitution of (5.2), (5.3), (3.6) and (3.13) the first four boundary conditions at the wall for the equation of motion and the equation of energy change into

$$\bar{u}=u;\ \bar{u}_\xi=\frac{\tau_w t_w}{\alpha\mu_w U};\ \bar{u}_{\xi\xi}=-\frac{U_x}{\nu_u}\,\frac{1}{\gamma}\,\frac{t_w}{\alpha^2};\ \bar{u}_{\xi\xi\xi}=-\frac{1}{\Omega}\,\frac{t_{\xi_0}}{t_w}\,\bar{u}_{\xi\xi} \tag{5.8}$$

$$t=t_w;\ t_{\xi_0}=(t_{\xi_0})_w;\ t_{\xi_0\xi_0}+\sigma\,\Omega^2(k-1)M^2\,\bar{u}_\xi^{\,2}=0; \tag{5.9}$$

$$\bar{u}_\xi\bar{u}_{\xi\xi}\frac{t_x}{t}+2(k-1)M^2\frac{U_x}{U}\,\bar{u}_\xi\,\bar{u}_{\xi\xi}+\frac{1}{\sigma}\,\frac{1}{\Omega^3}\,\frac{U_x}{U}\,t_{\xi_0\xi_0\xi_0}=0. \tag{5.10}$$

In the separation point, $(\mu\,u_y)_{yyy}=0$ the following relation holds

$$\bar{u}_{\xi\xi\xi\xi}=\frac{3}{\Omega}\,\frac{t_{\xi_0}}{t_w}\,\bar{u}_{\xi\xi\xi}+\frac{3}{\Omega^2}\left(\frac{t_{\xi_0}}{t_w}\right)^2\bar{u}_{\xi\xi}=6\frac{(\bar{u}_{\xi\xi\xi})^2}{\bar{u}_{\xi\xi}}. \tag{5.11}$$

For the calculation of the boundary layer without heat transfer at the wall, hence for $(t_{\xi_0})_w=0$, another boundary condition can be taken into account without difficulty. The fifth boundary condition at the wall, which follows from the energy equation (3.3), yields the relation

$$c_p(\rho u)_{yy} T_x = -\rho_u u_{yy} U U_x + \frac{c_p}{\sigma}(\mu T_y)_{yyy} + (\mu u_y^2)_{yy}$$

or

$$(\bar{u}_{\xi\xi})^2 \frac{t_x}{t} + 2(k-1)M^2 \frac{U_x}{U}(\bar{u}_{\xi\xi})^2 + \frac{1}{\sigma\Omega^4} \frac{U_x}{U} t_{\xi_0\xi_0\xi_0\xi_0} = 0. \tag{5.12}$$

This last relation can be simplified by means of (5.10) to

$$\Omega\, \bar{u}_{\xi\xi}\, t_{\xi_0\xi_0\xi_0} = \bar{u}_\xi\, t_{\xi_0\xi_0\xi_0\xi_0}. \tag{5.13}$$

Starting from (5.4) and (5.5) one has for $\xi = \xi_0 = 0$

$$\begin{aligned}
&\bar{u} = 1 - a - \tfrac{1}{2}\sqrt{\pi} f & &1 = a_0 + \tfrac{1}{2}\sqrt{\pi} f_0\\
&\bar{u}_\xi = f - b & &t_{\xi_0} = (1-t_w)(f_0 - b_0)\\
&\bar{u}_{\xi\xi}\, 2(a-c) & &t_{\xi_0\xi_0} = (1-t_w)2(a_0 - c_0)\\
&\bar{u}_{\xi\xi\xi} = 2(3b - f) & &t_{\xi_0\xi_0\xi_0} = (1-t_w)2(3b_0 - f_0)\\
&\bar{u}_{\xi\xi\xi\xi} = 12(2c - a) & &t_{\xi_0\xi_0\xi_0\xi_0} = (1-t_w)12(2c_0 - a_0).
\end{aligned} \tag{5.14}$$

In relation with (5.14) the boundary conditions at the wall change into

$$\begin{gathered}
1 - a - \tfrac{1}{2}\sqrt{\pi} f = 0\\
f - b = \frac{\tau_w t_w}{\alpha\mu_w U}\\
2(a-c) = -\frac{U_x t_w}{\nu_u \gamma \alpha^2}\\
(3b - f) = \frac{1}{\Omega}\, \frac{1-t_w}{t_w}(f_0 - b_0)(a-c)\\
1 = a_0 + \tfrac{1}{2}\sqrt{\pi} f_0\\
(t_{\xi_0})_w = (1-t_w)(f_0 - b_0)\\
2(1-t_w)(a_0 - c_0) + \sigma\,\Omega^2(k-1)M^2(f-b)^2 = 0\\
(f-b)(a-c)\frac{(t_w)_x}{t_w} + 2(k-1)M^2\frac{U_x}{U}(f-b)(a-c) + \frac{1}{\sigma}\,\frac{1}{\Omega^3}\,\frac{U_x}{U}(3b_0 - f_0)(1-t_w) = 0.
\end{gathered} \tag{5.15}$$

In the separation point the following relation holds

$$(2c - a)(a - c) = (3b - f)^2. \tag{5.16}$$

When no heat transfer at the wall occurs, then

$$(t_{\xi_0})_w = 0 \quad \text{and} \quad f_0 = b_0$$

and the relation

$$\tfrac{2}{3}\Omega(a-c)b_0 = (f-b)(2c_0 - a_0) \tag{5.17}$$

follows from (4.13).

The quantities δ_1, δ_2, δ_3, δ_4 and δ_5 appearing in the differential equations of section 3 become, expressed in the new variables ξ and ξ_0

$$\delta_1 = \int_0^\delta \left(1 - \frac{\rho}{\rho_u}\frac{u}{U}\right) dy = \int_0^\delta \left(1 - \frac{\bar{u}}{t}\right) dy = \frac{1}{\alpha}\int_0^\infty (1-\bar{u})\,d\xi - \frac{1}{\alpha_0}\int_0^\infty (1-t)\,d\xi_0$$

$$\delta_2 = \int_0^\delta \frac{\rho u}{\rho_u U}\left(1 - \frac{u}{U}\right) dy = \int_0^\delta \frac{\bar{u}}{t}(1-\bar{u})\,dy = \frac{1}{\alpha}\int_0^\infty \bar{u}(1-\bar{u})\,d\xi$$

$$\delta_3 = -\int_0^\delta \frac{\rho u}{\rho_u U}\left(1 - \frac{T}{T_u}\right) dy = -\int_0^\delta \frac{\bar{u}}{t}(1-t)\,dy = -\frac{1}{\alpha}\int_0^\infty \bar{u}(1-t)\,d\xi$$

$$\delta_4 = \int_0^\delta \frac{\mu}{\mu_u}\left(\frac{\partial u/U}{\partial y/\delta_2}\right)^2 dy = \alpha\delta_2^2\gamma\int_0^\infty \bar{u}_\xi^2\,d\xi$$

$$\delta_5 = \int_0^\delta \frac{\rho u}{\rho_u U}\left(1 - \frac{u^2}{U^2}\right) dy = \int_0^\delta \frac{\bar{u}}{t}(1-\bar{u}^2)\,dy = \frac{1}{\alpha}\int_0^\infty \bar{u}(1-\bar{u}^2)\,d\xi.$$

With the aid of the equations (5.4) and (5.5) the quantities δ_1, δ_2, δ_3, δ_4, δ_5 can be expressed into the coefficients a, b, ... f, ... f_0 (see appendix)

$$\alpha\,\delta_1 = \tfrac{1}{2}\sqrt{\pi}(a + \tfrac{1}{2}c) + \tfrac{1}{2}(b + f) - \tfrac{1}{2}\sqrt{\pi}\,\Omega(1 - t_w)(a_0 + \tfrac{1}{2}c_0) - \tfrac{1}{2}\Omega(1 - t_w)(b_0 + f_0) \qquad (5.18)$$

$$\alpha\,\delta_2 = \tfrac{1}{2}\sqrt{\pi}\left[a + \tfrac{1}{2}c - \frac{\sqrt{2}}{2}a^2 - \frac{\sqrt{2}}{8}b^2 - \frac{3\sqrt{2}}{32}c^2 - \left(1 - \frac{\sqrt{2}}{2}\right)(f^2 + bf) - \frac{\sqrt{2}}{4}ac\right] +$$
$$+ \tfrac{1}{2}\left[b + f - ab - \frac{\pi}{2}af - \tfrac{1}{2}bc - \left(\frac{\pi}{4} - \tfrac{1}{2}\right)cf\right] \qquad (5.19)$$

$$\frac{\delta_4}{\alpha\delta_2^{\,2}}\,\frac{1}{\gamma} = \frac{\sqrt{2\pi}}{4}(a^2 + \tfrac{3}{4}b^2 + \tfrac{7}{16}c^2 + f^2 - fb - \tfrac{1}{2}ac) + af - \tfrac{1}{2}fc + \tfrac{1}{2}bc \qquad (5.20)$$

$$\alpha\delta_5 = \alpha\delta_2 + \frac{\sqrt{\pi}}{2\sqrt{3}}\left[a^3 + \tfrac{1}{2}a^2c + \tfrac{1}{2}ab^2 + \tfrac{1}{4}ac^2 + \left(\frac{3\sqrt{3}}{2} - \frac{3}{2}\right)(abf - \tfrac{1}{2}cf^2) + \tfrac{1}{4}b^2c +\right.$$
$$\left. + \left(\frac{3\sqrt{3}}{4} - 1\right)bcf + \tfrac{5}{72}c^3\right] + \frac{3}{2\sqrt{2}}bg\,tg\,\sqrt{2}\,(a^2f + \tfrac{1}{2}acf + \tfrac{1}{4}b^2f - bf^2 + \tfrac{3}{16}c^2f - f^3) + \tfrac{1}{2}a^2b +$$
$$+ \tfrac{1}{3}abc - \tfrac{1}{4}acf + \tfrac{1}{18}b^3 - \tfrac{1}{8}b^2f + \tfrac{1}{9}bc^2 - \tfrac{13}{96}c^2f + \frac{3\pi}{8}(bf^2 + f^3) + \tfrac{1}{8}\pi^{3/2}(af^2 + \tfrac{1}{2}cf^2) +$$
$$+ \tfrac{1}{2}\sqrt{\pi}(a + \tfrac{1}{2}c) + \tfrac{1}{2}(b + f) - \sqrt{\frac{\pi}{2}}\,[a^2 + \tfrac{1}{4}b^2 + \tfrac{3}{16}c^2 + (\sqrt{2} - 1)(f^2 + bf) + \tfrac{1}{2}ac] -$$
$$-(ac + \tfrac{1}{2}bc - \tfrac{1}{2}cf) - \frac{\pi}{4}(af + \tfrac{1}{2}cf). \qquad (5.21)$$

The quantity δ_3 appears to assume a very complicated form. For $\alpha\delta_3$ a good approximation can be obtained, when introducing for $\bar{u}$ the function

$$\bar{u} = 1 - (p_0 + q_0\xi_0 + r_0\xi_0^{\,2} + s_0\xi_0^{\,3})e^{-\xi_0^2} - t_0\int_{\xi_0}^{\infty} e^{-\eta^2}d\eta. \qquad (5.22)$$

The coefficients p_0, q_0, r_0, s_0 and t_0 are determined from the value of the function and its first three derivatives at the wall and from the constantness of the values $\alpha\delta_1$. Along the wall the following relations hold:

$$\begin{aligned}
\bar{u} &= 1 - p_0 - \tfrac{1}{2}\sqrt{\pi}\,t_0 = 1 - a - \tfrac{1}{2}\sqrt{\pi}\,f = 0\\
\bar{u}_\xi &= \frac{1}{\Omega}\,\bar{u}_{\xi_0} = \frac{1}{\Omega}(t_0 - q_0) = f - b\\
\bar{u}_{\xi\xi} &= \frac{1}{\Omega^2}\,\bar{u}_{\xi_0\xi_0} = \frac{2}{\Omega^2}(p_0 - r_0) = 2(a - c)\\
\bar{u}_{\xi\xi\xi} &= \frac{1}{\Omega^3}\,\bar{u}_{\xi_0\xi_0\xi_0} = \frac{2}{\Omega^3}(3\,q_0 - 3\,s_0 - t_0) = 2\,(3b - f).
\end{aligned} \qquad (5.23)$$

If $\alpha\delta_1$ remains unchanged, one has

$$\frac{1}{\Omega}\,[\tfrac{1}{2}\sqrt{\pi}(a + \tfrac{1}{2}c) + \tfrac{1}{2}(b + f)] = \tfrac{1}{2}\sqrt{\pi}(p_0 + \tfrac{1}{2}r_0) + \tfrac{1}{2}(q_0 + s_0 + t_0). \qquad (5.24)$$

By means of (5.22) and (5.5) $\alpha\delta_3$ can be approximated by

$$\alpha\delta_3 = \int_0^\infty \bar{u}(t - 1)d\xi = \Omega\int_0^\infty \bar{u}(1 - t)d\xi_0 =$$
$$= \Omega(t_w - 1)\int_0^\infty \left[1 - (p_0 + \ldots)e^{-\xi_0^2} - t_0\int_{\xi_0}^\infty e^{-\eta^2}d\eta\right]\left[(a_0 + b_0\xi_0 + c_0\xi_0^{\,2})e^{-\xi_0^2} + f_0\int_{\xi_0}^\infty e^{-\eta^2}d\eta\right]d\xi_0,$$

or

$$\frac{\alpha\delta_3}{t_w - 1} = A_{01}(a + \tfrac{1}{2}c) + A_{02}(b + f) + A_1\Omega + A_2(f - b)\,\Omega^2 + A_3(a - c)\,\Omega^3 + A_4(3\,b - f)\,\Omega^4, \qquad (5.25)$$

where

$$\begin{aligned}
A_{01} &= -0.18172\,a_0 - 0.18523\,b_0 - 0.20959\,c_0 - 0.07082\,f_0 \\
A_{02} &= -0.10253\,a_0 - 0.10451\,b_0 - 0.11825\,c_0 - 0.03995\,f_0 \\
A_1 &= +0.37549\,a_0 + 0.40285\,b_0 + 0.48333\,c_0 + 0.14218\,f_0 \\
A_2 &= 0.16994\,a_0 + 0.06515\,b_0 + 0.01350\,c_0 + 0.10133\,f_0 \\
A_3 &= 0.06580\,a_0 + 0.03238\,b_0 + 0.01270\,c_0 + 0.03594\,f_0 \\
A_4 &= 0.00749\,a_0 + 0.00433\,b_0 + 0.00225\,c_0 + 0.00383\,f_0 .
\end{aligned} \tag{5.26}$$

Previous to entering into details of the general method to approximate the velocity and temperature profiles in laminar compressible boundary layer flow, the particular case of no heat transfer at the wall with a PRANDTL number $\sigma = 1$ will be dealt with.

6 Calculation of the velocity and temperature profiles of the laminar compressible boundary layer without heat transfer at the wall for the Prandtl number $\sigma = 1$.

When no heat transfer at the wall occurs $\left(\frac{\partial T}{\partial y} = 0 \text{ for } y = 0\right)$ and the PRANDTL number is $\sigma = 1$, the simple temperature-velocity relation (3.43) exists

$$t = 1 + \frac{k-1}{2} M^2 (1 - \bar{u}^2). \tag{6.1}$$

Without making the computational work too laborious, the temperature-viscosity relation of SUTHERLAND

$$\frac{\mu}{\mu_u} = \frac{T_u + C}{T + C} \left(\frac{T}{T_u}\right)^{3/2} \tag{6.2}$$

can be used in this case for the description of the laminar boundary layer flow.

The boundary conditions at the wall

$$u = 0;\; u_y = \frac{\tau_w}{\mu_w};\; (\mu u_y)_y = -\rho_u U U_x;\; (\mu u_y)_{yy} = 0 \tag{6.3}$$

change into

$$\begin{gathered}
\bar{u} = 0;\; \bar{u}_\xi = \frac{\tau_w t_w}{\mu_w U \alpha};\; \frac{T_u + C}{t_w T_u + C}\, t_w^{-1/2}\, \bar{u}_{\xi\xi} = -\frac{U_x}{\nu_u \alpha^2} \\
\bar{u}_{\xi\xi\xi} = (k-1) M^2 \left(\frac{1}{2\,t_w} - \frac{T_u}{t_w T_u + C}\right) \bar{u}_\xi^{\,3}
\end{gathered} \tag{6.4}$$

by means of (6.1), (6.2) and (5.2).

In the separation point $\bar{u}_\xi = 0$ and therefore, also $\bar{u}_{\xi\xi\xi} = 0$. With the aid of (5.14), (6.1) and (6.2), eq. (6.4) yields the relations

$$a + \tfrac{1}{2}\sqrt{\pi}\, f = 1;\; f - b = \frac{\tau_w}{\mu_u \alpha U}\, \frac{t_w T_u + C}{T_u + C}\, t_w^{-1/2} \tag{6.5}$$

$$2(a - c) = -\frac{U_x}{\nu_u \alpha^2}\, \frac{t_w T_u + C}{T_u + C}\, t_w^{1/2};\; 2(3\,b - f) = \frac{t_w - 1}{t_w}\, \frac{C - t_w T_u}{C + t_w T_u} (f - b)^3. \tag{6.6}$$

As in the separation point $c = \frac{1}{2} a$, it may be assumed, like in the method of TIMMAN (ref. 12) that for the accelerated flow c is equal to 0, while for decelerated flow c will be taken equal to $\frac{1}{2} a$. The accelerated and decelerated flow are then described by separate solutions which join in the point $a = c = 0$ $(U_x = 0)$.

In connection with the relation (6.1) $\alpha\delta_1$ changes into

$$\begin{aligned}
\alpha\delta_1 &= \int_0^\infty (t - \bar{u})\, d\xi = \int_0^\infty (1 - \bar{u})\, d\xi + \int_0^\infty (t - 1)\, d\xi = \int_0^\infty (1 - \bar{u})\, d\xi + \frac{k-1}{2} M^2 \int_0^\infty (1 - \bar{u}^2)\, d\xi = \\
&= \left(1 + \frac{k-1}{2} M^2\right) \left[\tfrac{1}{2}\sqrt{\pi}(a + \tfrac{1}{2} c) + \tfrac{1}{2}(b + f)\right] + \frac{k-1}{2} M^2 \alpha\delta_2 .
\end{aligned} \tag{6.7}$$

$\alpha\delta_2$ is calculated with formula (5.19). The momentum equation of VON KÀRMÀN can be written by means of (6.1) and (6.2) in the following form:

$$\frac{d\theta}{dx}+\frac{U_x}{U}\theta\left[2H+3-\{1+\beta(k-1)\}M^2\right]=2\frac{\mu_w}{\mu_u}\frac{\alpha\delta_2}{t_w}\bar{u}_\xi=2\frac{T_u+C}{t_wT_u+C}\sqrt{t_w}\,\alpha\delta_2(f-b), \quad (6.8)$$

where

$$\theta=\frac{\rho_uU\delta_2^2}{\mu_u}=\frac{U}{\nu_u\alpha^2}(\alpha\delta_2)^2;\quad \beta=\tfrac{3}{2}-\frac{T_u}{T_u+C}. \quad (6.9)$$

Assuming

$$f-b=\Lambda_1;\quad \frac{t_w}{t_w-1}\,\frac{C+t_wT_u}{C-t_wT_u}=p_1;\quad \frac{T_u+C}{t_wT_w+C}\sqrt{t_w}=\gamma_1, \quad (6.10)$$

eqs. (6.5) and (6.6) yield the relations

$$\begin{aligned}
f&=\tfrac{3}{2}\Lambda_1+\frac{1}{4p_1}\Lambda_1^3\\
b&=\tfrac{1}{2}\Lambda_1+\frac{1}{4p_1}\Lambda_1^3\\
a&=1-\tfrac{1}{2}\sqrt{\pi}\left(\tfrac{3}{2}\Lambda_1+\frac{1}{4p_1}\Lambda_1^3\right)\\
2(a-c)&=-\frac{U_x}{\nu_u\alpha^2}\,\frac{t_w}{\gamma_1}\\
\frac{\tau_w}{\mu_u\alpha U}&=\Lambda_1\gamma_1.
\end{aligned} \quad (6.11)$$

For the accelerated flow is $c=0$, for the decelerated flow $c=\frac{1}{2}a$. By numerical integration of the momentum equation of VON KÀRMÀN (6.8) and applying formula (6.1), the whole temperature and velocity field of the compressible laminar boundary layer can be calculated.

In the stagnation point the momentum equation of VON KÀRMÀN (3.18) yields after multiplication by $Re_{\delta_2}=\frac{U\delta_2}{\nu_u}$, the relation $2a(\alpha\delta_1+2\alpha\delta_2)=f-b$ if the conditions $t_w(0)=1$, $p_1(0)=\infty$, $\gamma_1(0)=1$ are taken into account.

Like for incompressible flow this is satisfied by the usable value $a=-0.41502$ (ref. 12), sothat the initial value of Λ_1 in the stagnation point becomes $\Lambda_1=1.06445$.

Replacement of the formula of SUTHERLAND by the temperature-viscosity relation (3.6), leads to the following relations:

$$f=3b=\frac{2}{\sqrt{\pi}}(1-a);\ f-b=\frac{\tau_w}{\mu_u\alpha U\gamma};\ 2(a-c)=-\frac{U_x}{\nu_u\alpha^2}\,\frac{t_w}{\gamma}, \quad (6.12)$$

$$\frac{d\theta}{dx}+\frac{U_x}{U}\theta\left[2H+3-\{1+\beta(k-1)\}M^2\right]=2\gamma\alpha\delta_2\bar{u}_\xi=2\gamma\alpha\delta_2(f-b). \quad (6.13)$$

With the help of a simple example the influence of the various temperature-viscosity relations will be investigated. For that purpose flow along a flat plate will be considered without pressure gradient for a MACH number $M=2.5$ and with a prescribed temperature T_u of the undisturbed flow.

For flow along a flat plate without pressure gradient is $U_x=0$ and, therefore, $a=c=0$. The linear temperature-viscosity relation (3.6) leads with (6.12) and (6.13) to the relations:

$$\begin{gathered}
f=3b=\frac{2}{\sqrt{\pi}};\ \alpha\sqrt{\frac{\nu_ux}{U}}=\sqrt{\frac{\alpha\delta_2}{2\gamma(f-b)}}=\sqrt{\frac{3\sqrt{\pi}}{8}\,\frac{\alpha\delta_2}{\gamma}}\\
\frac{\tau_w}{\frac{1}{2}\rho_uU}\sqrt{\frac{Ux}{\nu_u}}=\sqrt{\frac{8}{3\sqrt{\pi}}\alpha\delta_2\gamma}.
\end{gathered} \quad (6.14)$$

The temperature-viscosity relation of SUTHERLAND gives for $a=c=0$ from (6.11) and (6.8) the relations

$$\begin{gathered}
f=\frac{2}{\sqrt{\pi}};\ b=f-\Lambda_1;\ \Lambda_1^3+6p_1\Lambda_1-\frac{8}{\sqrt{\pi}}p_1=0\\
\alpha\sqrt{\frac{\nu_ux}{U}}=\sqrt{\frac{\alpha\delta_2}{2\Lambda_1\gamma_1}};\ \frac{\tau_w}{\frac{1}{2}\rho_uU^2}\sqrt{\frac{Ux}{\nu_u}}=\sqrt{2\Lambda_1\gamma_1\alpha\delta_2}.
\end{gathered} \quad (6.15)$$

When carrying out the calculations with the values $k=1.4$, $M=2.5$, $C=110°$ K, with prescribed temperatures $T_u=220°$ K and $T_u=330°$K, the pertaining quantities of the boundary layer are given in table 1 for various temperature-viscosity relations across the boundary layer.

TABLE 1.

for $M=2.5$	$\frac{\mu}{\mu_u}=\frac{T_u+C}{\overline{T}+C}\left(\frac{\overline{T}}{T_u}\right)^{1/2}\left(\frac{T}{T_u}\right)$								
	$\overline{T}=T_u$	$\overline{T}=\frac{T_u+T_w}{2}$		$\overline{T}=T_w$		$\overline{T}=\frac{T_u+3\,T_w}{4}$		$\overline{T}=T$ Sutherland	
$T_u=$	220°K; 330°K	220°K	330°K	220°K	330°K	220°K	330°K	220°K	330°K
$\alpha\sqrt{\frac{\nu_u x}{U}}$	0.4386	0.4624	0.4708	0.4849	0.4985	0.4739	0.4852	0.4741	0.4853
$\frac{\delta_2}{x}\sqrt{\frac{Ux}{\nu_u}}$	0.660	0.626	0.615	0.597	0.581	0.610	0.596	0.605	0.590
$\frac{\delta_1}{x}\sqrt{\frac{Ux}{\nu_u}}$	4.684	4.443	4.364	4.237	4.121	4.335	4.234	4.333	4.149
$\frac{\tau_w}{\frac{1}{2}\rho_u U^2}\sqrt{\frac{Ux}{\nu_u}}$	0.660	0.626	0.615	0.597	0.581	0.610	0.596	0.605	0.590
b	0.376	0.376	0.376	0.376	0.376	0.376	0.376	0.3484	0.3432
f	1.128	1.128	1.128	1.128	1.128	1.128	1.128	1.128	1.128

The pertaining velocity profiles are given by the equation

$$\bar{u} = 1 - b\xi e^{-\xi^2} - f \int_{\xi}^{\infty} e^{-\eta^2} d\eta \qquad (6.16)$$

where

$$y \sqrt{\frac{U}{\nu_u x}} = \frac{1}{\alpha} \sqrt{\frac{U}{\nu_u x}} \int_0^{\xi} t d\xi =$$

$$= \frac{1}{\alpha} \sqrt{\frac{U}{\nu_u x}} \int_0^{\xi} \left[1 + \frac{k-1}{2} M^2 (1 - \bar{u}^2)\right] d\xi.$$

In fig. 1 the velocity and temperature profiles

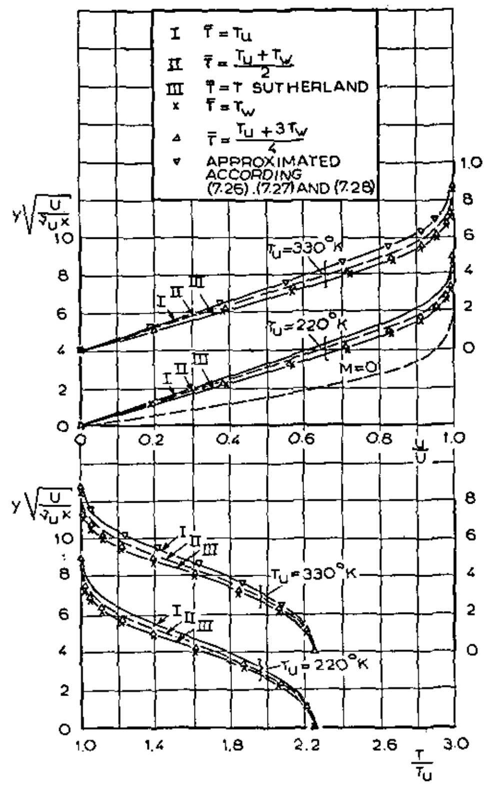

Fig. 1.

The velocity and temperature profiles of the boundary layer flow along the heat-insulated flat plate for $\sigma = 1$, $M = 2.5$, $T_u = 220°$ and $330°$K and various temperature viscosity relations

$$\frac{\mu}{\mu_u} = \frac{T_u + C}{\bar{T} + C} \left(\frac{\bar{T}}{T_u}\right)^{1/2} \left(\frac{T}{T_u}\right).$$

(The thermometer problem).

are drawn for $M = 2.5$ for various cases mentioned in table 1. The standardized velocity and temperature profiles $\frac{u}{U}$ and $\frac{T}{T_u}$ appear to be independent of the prescribed temperature of the undisturbed flow for the temperature-viscosity relation $\frac{\mu}{\mu_u} = \frac{T}{T_u}$ (in y-direction within the boundary layer). For the other above-mentioned temperature-viscosity relations the standardized velocity and temperature profiles $\frac{u}{U}$ and $\frac{T}{T_u}$ are, moreover, dependent upon the Mach number and also slightly upon the undisturbed flow temperature.

In fig. 2 the calculated drag coefficient $c_D \sqrt{Re} = \frac{\tau_w}{\frac{1}{2}\rho_u U} \sqrt{\frac{Ux}{\nu_u}}$ of the heat-insulated flat plate are plotted for various temperature-viscosity relations ($\bar{T} = \bar{T}_u$; $\bar{T} = \bar{T}_w$; $T = \frac{T_u + T_w}{2}$; $\bar{T} = T$) as a function of Mach number for $T_u = 220°$ and $330°$ K and $\sigma = 1$.

For $\frac{\mu}{\mu_u} = \frac{T}{T_u}$ the drag coefficient $c_D \sqrt{Re}$ appears to remain unchanged. For the other temperature-viscosity relations $c_D \sqrt{Re}$ is dependent not only upon the Mach number but also upon the temperature.

Figure 2 contains also some results taken from other authors (ref. 8, 9, 10, 11) who used the basic temperature-viscosity relation $\frac{\mu}{\mu_u} = \left(\frac{T}{T_u}\right)^n$. These curves appear to be independent of the outer flow temperature for a constant value of n.

Introducing, as in ref. 4, 5, 6 and 7, the temperature-viscosity relation as a linear relation $\frac{\mu}{\mu_\infty} = c \frac{T}{T_\infty}$, where c is determined in such a way that the SUTHERLAND formula is satisfied at the wall, which means that $c = \frac{T_\infty + C}{T_w + C} \sqrt{\frac{T_w}{T_\infty}}$, it is seen that this corresponds to $\bar{T} = T_w$ for flow along a flat plate. The drag coefficients $c_D \sqrt{Re}$ appear to be also in this case dependent upon the outer flow temperature (see fig. 2).

It appears from the form of the various drag curves in fig. 2, that weighting factors α_1 and α_2 can be added to T_u and T_w, such that for $\bar{T} = \frac{\alpha_1 T_u + \alpha_2 T_w}{\alpha_1 + \alpha_2}$ the same drag curves are obtained with formula (3.6) and with the formula of SUTHERLAND.

A good approximation will be obtained already, if in formula (3.6) $\bar{T}$ will be chosen as

$$\bar{T} = \frac{T_u + 3\,T_w}{4}. \qquad (6.17)$$

The relation (6.17) will be used as long as no better approximation is available for compressible laminar boundary layer calculations with and without heat transfer at the wall.

7 Calculation of the velocity and temperature profiles of the laminar compressible boundary layer flow without heat transfer at the wall for a Prandtl number $\sigma \neq 1$.

If the PRANDTL number σ differs from 1, the temperature and velocity distributions within the boundary layer will no longer satisfy the adiabatic flow condition (6.1). The boundary layer quantities will be approximated in this case as follows.

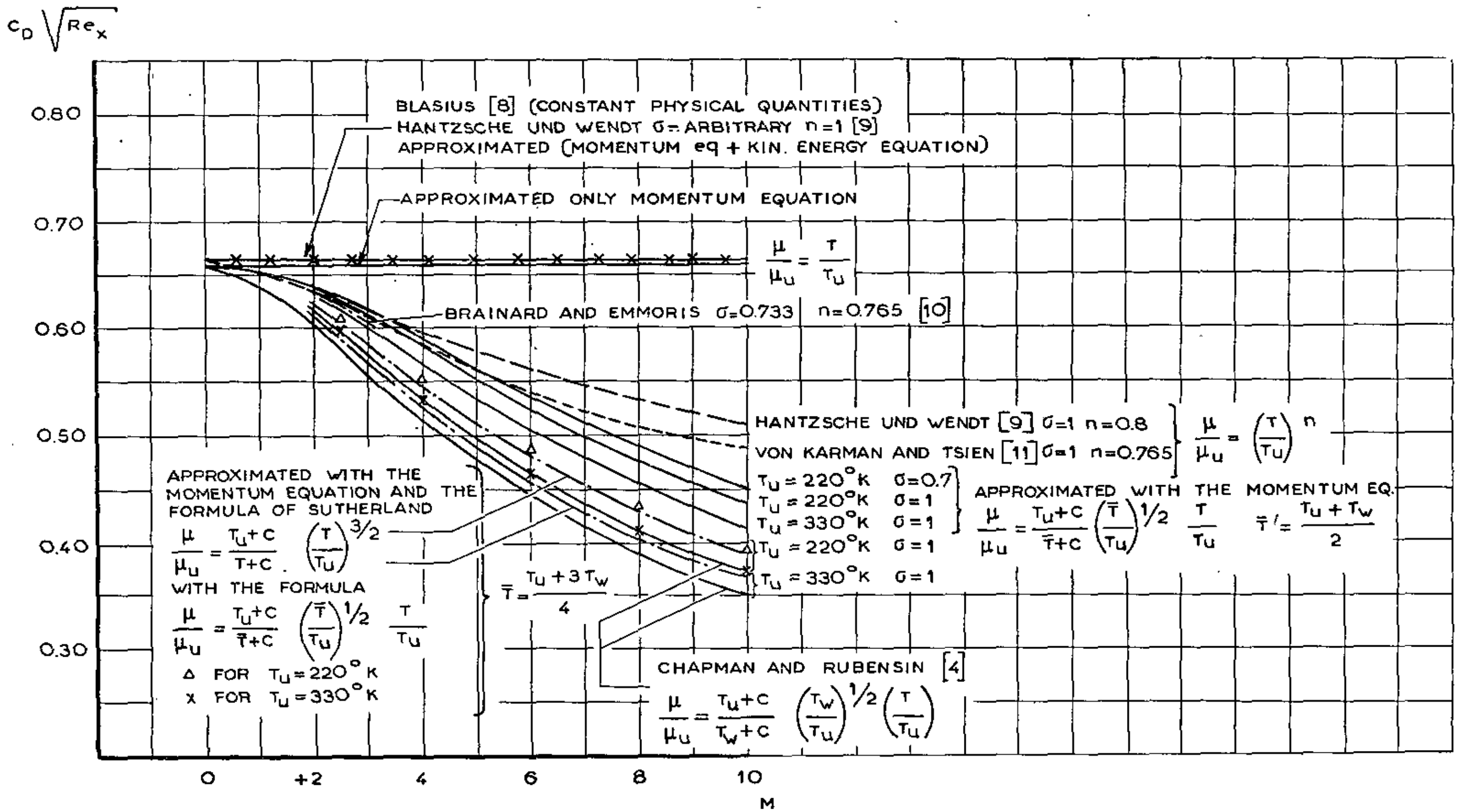

Fig. 2.

The calculated drag coefficient

$$c_D \sqrt{Re_x} = \frac{\tau_w}{\frac{1}{2}\rho_u U}\sqrt{\frac{Ux}{\nu_u}}$$

of the heat insulated flat plate for various temperature-viscosity relations. (The thermometer problem).

The boundary conditions at the wall (5.10) and (5.17) yield the following relations

$$f = 3\,b = \frac{2}{\sqrt{\pi}}(1-a) \tag{7.1}$$

$$f_0 = b_0 = \frac{2}{\sqrt{\pi}}(1-a_0) \tag{7.2}$$

$$2(a-c) = \frac{U_x t_w}{\nu_u \gamma \alpha^2} \tag{7.3}$$

$$(t_w-1)(a_0-c_0) = \frac{8}{9\pi}\sigma\Omega^2(k-1)M^2(1-a)^2 \tag{7.4}$$

$$\frac{(t_w)_x}{t_w} + 2(k-1)M^2\frac{U_x}{U} - \frac{3}{\sigma}\,\frac{1}{\Omega^3}\,\frac{(1-a_0)(t_w-1)}{(a-c)(1-a)}\,\frac{U_x}{U} = 0 \tag{7.5}$$

$$\frac{\tau_w t_w}{\alpha\mu_w U} = \frac{4}{3\sqrt{\pi}}(1-a). \tag{7.6}$$

$$\Omega(a-c)(1-a_0) = (1-a)(2\,c_0-a_0). \tag{7.7}$$

In the separation point one has by means of eq. (5.16) and $\tau_w = 0$

$$c = \tfrac{1}{2}\,a = 1/2. \tag{7.8}$$

The pertaining boundary layers for the accelerated and decelerated flow can be described by separate solutions just as with the method of TIMMAN (12). When choosing for the solution of the accelerated flow ($U_x > 0$) the relation $c = 0$ and for the solution of the decelerated flow ($U_x < 0$) the relation $c = \frac{1}{2}a$, then both solutions join in $U_x = 0$ for $c = a = 0$.

In connection with

$$\frac{U_x}{U} = \frac{M_x}{M}\,\frac{1}{1+\dfrac{k-1}{2}M^2}$$

eq. (7.5) changes into

$$t_{w_x} = \frac{3}{\sigma}\,\frac{1}{\Omega^3}\,\frac{(1-a_0)(t_w-1)}{(1-a)(a-c)}\,\frac{M_x}{M}\,\frac{t_w}{1+\dfrac{k-1}{2}M^2} - 2(k-1)\frac{M_x M}{1+\dfrac{k-1}{2}M^2}\,t_w. \tag{7.9}$$

The velocity field and the temperature field of the compressible laminar boundary layer flow without heat transfer at the wall can be described by means of the energy equation of WIEGHARDT

$$\frac{d\theta_2}{dx} + \frac{U_x}{U}\theta_2\,[5 + \{(2-\beta)(k-1)-1\}M^2] = 4\,\frac{\delta_4\delta_5}{\delta_2{}^2}, \tag{7.10}$$

where by aid of eq. (7.3) θ_2 is equal to

$$\theta_2 = \frac{U\delta_5{}^2}{\nu_u} = \frac{U}{\nu_u\alpha^2}(\alpha\delta_5)^2 = -\frac{2(a-c)\gamma}{t_w}\,\frac{U}{U_x}(\alpha\delta_5)^2, \tag{7.11}$$

and by aid of the relation (3.41)

$$\alpha\delta_3 = \frac{M^2}{2}(k-1)\alpha\delta_5. \tag{7.12}$$

The differential equation (7.10) depends not only on the known velocity distribution and temperature distribution of the outer flow but also on the quantities a and t_w. It is, therefore, necessary to compute the solution by means of an iterative method. For the PRANDTL number $\sigma = 1$ the following relation exists according to section 6

$$t = 1 + \frac{k-1}{2}M^2(1-\bar{u}^2).$$

With $\sigma \neq 1$ the relation

$$t_w = 1 + \frac{k-1}{2}M^2\sqrt{\sigma} \tag{7.13}$$

will be assumed to hold for the first iterationstep. The differential equation (7.10) can then be transformed with the aid of (7.11) and (5.21) into a differential equation for "a" with x as independent variable. This equation is numerically solved and yields the relation $a = a(x)$. In the stagnation point $(U = 0)$ the value a will be obtained from the relation

$$\frac{3\,a\gamma}{t_w}(\alpha\delta_5) + \frac{\delta_4}{\alpha\delta_2^{\,2}} = 0 \quad \text{for } t_w = \gamma = 1, \tag{7.14}$$

which follows from (7.10) for $U = 0$.

(7.4), (7.7) and (7.12) yield for $t_w = 1 + \dfrac{k-1}{2}\,q\,M^2$ the relations

$$a_0 - c_0 = \frac{16}{9\,\pi}\,\frac{\sigma}{q}\,\Omega^2(1-a)^2 = \lambda_1;\quad \frac{\Omega\,(a-c)}{1-a} = \frac{2\,c_0 - a_0}{1-a_0} = \lambda_2 \tag{7.15}$$

$$\frac{\alpha\delta_3}{t_w - 1} = \frac{\alpha\delta_5}{q}\,. \tag{7.16}$$

Hence

$$a_0 = \frac{2\,\lambda_1 + \lambda_2}{1 + \lambda_2};\; c_0 = \frac{\lambda_1 + \lambda_2 - \lambda_1\lambda_2}{1 + \lambda_2};\; b_0 = f_0 = \frac{2}{\sqrt{\pi}}\,\frac{1 - 2\,\lambda_1}{1 + \lambda_2} \tag{7.17}$$

From (7.16) Ω can be calculated as a function of $a = a(x)$ with the aid of (5.21), (5.25), (5.26) and (7.17). The pertaining values a_0 and c_0 are then also known.

The derivative t_{w_x} follows from (7.9) with the aid of (7.15) and the ensuing values a_0 and Ω. Numerical integration of t_{w_x} yields the second approximation of t_w, which again can be written in the form

$$t_w = 1 + \frac{k-1}{2}\,q(x)\,M^2$$

where $q(x)$ is a known function.

This process has to be repeated as long as t_w does not vary anymore. Usually two steps will be sufficient to obtain a good approximation.

Remarks.

1. As the momentum equation of VON KÀRMÀN depends not only upon the quantities a and t_w, but also upon Ω, while the kinetic energy equation of WIEGHARDT depends only upon t_w and a, it is preferable to use for the calculation of the boundary layer with pressure gradient and without heat transfer at the wall the equation of WIEGHARDT.
2. When besides the energy equation of WIEGHARDT also the momentum equation of VON KÀRMÀN is used, it is possible to calculate the function relation between the coefficients a and c. However, the computational work will probably become too laborious to instify the improved accuracy.
3. As it may be expected that for a given PRANDTL number the function Ω will not vary too much, it will be advisable to perform the calculation of Ω from formula (7.16) as follows. One chooses as a starting value the value $\Omega = \Omega_0 + \Delta\Omega$, where Ω_0 is the value of Ω pertaining to flow along a flat plate. After neglecting all terms of higher than the first order in $\Delta\Omega$, $\Delta\Omega$ can be solved at once as a function of a from (7.16). By means of an iteration process it is possible to calculate the function Ω very quickly.
4. The equation of WIEGHARDT can be solved in a simple way by writing it in the following form

$$\theta_2 = \int_0^x \left\{ \frac{2(a-c)\gamma}{t_w}(\alpha\delta_5)^2\,[5 + \{(2-\beta)(k-1) - 1\}M^2] + 4\,\frac{\delta_4}{\alpha\delta_2^{\,2}}\,\alpha\delta_5 \right\} dx \tag{7.18}$$

Starting from the value $a = a(0)$ at the stagnation point $x = x_0 = 0$, the pertaining values of the right-hand side of (7.18) can be calculated in a point, where x_1 is small, by aid of two estimated values $a = a_{11}$ and $a = a_{12}$. The left-hand side yields then the corresponding values a'_{11} and a'_{12}. Plotting the values a' against a, the value $a = a_{13}$ lying on the bisector can be assumed as a new approximate value by rectilinear interpolation (see fig. 3).

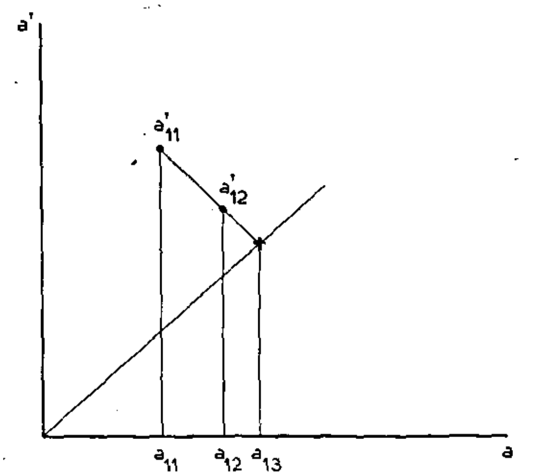

Fig. 3.

This gives the pertaining value of a'_{13}. This process can be repeated until a_1 will not vary anymore. Usually two steps are sufficient to obtain a good approximation.

Particular case.

For flow along a flat plate the boundary conditions (7.1) through (7.8) yield the following relations (using the fact that the wall temperature is constant):

$$a_0 = 1;\ c_0 = \tfrac{1}{2};\ f_0 = b_0 = 0;\ a = c = 0;$$

$$f = 3\,b = \frac{2}{\sqrt{\pi}}. \qquad (7.19)$$

$$t_w = 1 + \frac{16}{9\,\pi}\,\sigma\,\Omega^2(k-1)M^2, \frac{\tau_w t_w}{\alpha\mu_w U} = \frac{4}{3\sqrt{\pi}} \qquad (7.20)$$

The relation (7.12) changes into

$$\frac{\alpha\delta_3}{t_w - 1} = \frac{9\,\pi}{32}\,\frac{1}{\sigma\,\Omega^2}\,\alpha\delta_5 \qquad (7.21)$$

in connection with (7.20) and yields the equation

$$0.132916\,\Omega^4 + 0.617150\,\Omega^3 - $$

$$- 0.243204\,\Omega^2 = 0.402226\,\frac{1}{\sigma}. \qquad (7.22)$$

In table 2 the pertaining values of Ω and $\dfrac{t_w - 1}{\dfrac{k-1}{2}M^2}$ are given for various values of the Prandtl number,

TABLE 2.

σ	Ω	$\dfrac{t_w-1}{\frac{k-1}{2}M^2}$	$\sqrt{\sigma}$
0.6	1.07817	0.78937	0.7746
0.7	1.03421	0.84737	0.8367
0.8	0.99784	0.90152	0.8944
0.9	0.96704	0.95255	0.9487
1.0	0.94046	1.00102	1.0000
1.1	0.91720	1.04731	1.0488
1.5	0.84636	1.21608	1.2247

from which it is seen that approximately

$$\frac{t_w - 1}{\dfrac{k-1}{2}M^2} \approx \sqrt{\sigma}. \qquad (7.23)$$

Integration of the differential equation of Wieghardt (7.10) yields the relation

$$\frac{1}{\alpha} = 2\sqrt{\frac{\delta_4}{\alpha\delta_2{}^2}\,\frac{1}{\alpha\delta_5}}\sqrt{\frac{\nu_u x}{U}} = 2.29297\,\sqrt{\gamma}\sqrt{\frac{\nu_u x}{U}}. \qquad (7.24)$$

In connection with (5.18), (5.19), (7.19) and (7.20) one has

$$\delta_2\sqrt{\frac{U}{\nu_u x}} = 0.664\sqrt{\gamma};\ \delta_1\sqrt{\frac{U}{\nu_u x}} = 1.725(1 + \tfrac{5}{6}\,(k-1)\sigma\Omega^3 M^2)\sqrt{\gamma} \qquad (7.25)$$

$$\frac{\tau_w}{\frac{1}{2}\,\rho_u U^2}\sqrt{\frac{xU}{\nu_u}} = 0.656\,\sqrt{\gamma}.$$

The velocity and temperature profiles can be described by the equations

$$\bar{u} = 1 - b\,\xi\,e^{-\xi^2} - f\int_\xi^\infty e^{-\eta^2}\,d\eta \qquad (7.26)$$

$$t = 1 - (1 - t_w)(a_0 + c_0\xi_0{}^2)e^{-\xi_0{}^2}, \qquad (7.27)$$

where

$$y\sqrt{\frac{U}{\nu_u x}} = \frac{1}{\alpha}\sqrt{\frac{U}{\nu_u x}}\,\Omega\int_0^{\xi_0} t\,d\xi_0 =$$

$$= \frac{1}{x}\sqrt{\frac{U}{\nu_u x}}\,\Omega\left[\xi_0 + (t_w - 1)\left\{(a_0 + \tfrac{1}{2}\,c_0)\int_0^{\xi_0} e^{-\eta^2}\,d\eta - \frac{c_0}{2}\,\xi_0\,e^{-\xi_0{}^2}\right\}\right]. \qquad (7.28)$$

To verify how far these profiles agree with the profiles calculated in section 6, for a Prandtl number $\sigma = 1$, it is sufficient (in connection with the same linear factor $\sqrt{\gamma}$ appearing in both methods of analysis), if one compares only the profiles for $\gamma = 1$. For $\sigma = 1$, $M = 2.5$ and $\gamma = 1$ the velocity and temperature profiles (7.26) and (7.27) appear to coincide with the profiles calculated in section 6 (see fig. 1).

Use of the momentum equation of von Kàrmàn instead of the energy equation of Wieghardt, yields after integration the relation

$$\frac{1}{\alpha}\sqrt{\frac{U}{\nu_u x}} = \sqrt{\frac{8}{3\sqrt{\pi}}\,\gamma\,\frac{1}{\alpha\delta_2}} = 2.27995\,\sqrt{\gamma}, \qquad (7.29)$$

and hence

$$\frac{\tau_w}{\frac{1}{2}\rho_u U^2}\sqrt{\frac{Ux}{\nu_u}} = 0.660\sqrt{\gamma}. \qquad (7.30)$$

For $\sigma = 1$ and $\frac{\mu}{\mu_u} = \gamma\left(\frac{T}{T_u}\right)$ the solutions appear to be identical with the solutions obtained in section 6.

Application of the energy equation of WIEGHARDT as well as the momentum equation of VON KÀRMÀN yields the relation

$$\frac{4}{3\sqrt{\pi}}\gamma(1-a)\frac{1}{\alpha\delta_2} = 2\frac{\delta_4}{\alpha\delta_2{}^2}\alpha\delta_5 .$$

This is satisfied by the values $a = c = -0.046255$. From (7.24) it follows that

$$\frac{1}{\alpha}\sqrt{\frac{U}{\nu_u x}} = 2\sqrt{\frac{\delta_4}{\alpha\delta_2{}^2}\frac{1}{\alpha\delta_5}} = 2.366801\sqrt{\gamma},$$

and hence

$$\frac{\tau_w}{\frac{1}{2}\rho_u U^2}\sqrt{\frac{Ux}{\nu_u}} = 0.664\sqrt{\gamma}.$$

This value agrees for $\gamma = 1$ with the exact value calculated by BLASIUS (ref. 8) for constant material quantities.

In fig. 2 the drag coefficients $c_D\sqrt{Re_x} = \frac{\tau_w}{\frac{1}{2}\rho_u U}\sqrt{\frac{Ux}{\nu_u}}$ of the heat insulated flat plate are plotted as functions of MACH number for $\sigma = 1$, $T_u = 220°$ K, $T_u = 330°$ K and for $\sigma = 0.7$, $T_u = 220°$ K. Here formula (7.30) is used. The drag coefficients appear to be dependent on the MACH number and to a less extent also on the temperature of the undisturbed flow and the PRANDTL number.

8 Calculation of the velocity and temperature profiles of the laminar compressible boundary layer flow with heat transfer at the wall and prescribed wall temperature.

When dealing with the compressible laminar boundary layer flow with heat transfer at the wall one can start from a prescribed constant wall temperature as well as from a wall temperature variable in x-direction. The approximate method described below will use, besides the momentum equation of VON KÀRMÀN and the integrated heat equation, eight boundary conditions at the wall, viz. the first four boundary conditions ensuing from the equation of motion and the first four boundary conditions ensuing from the heat energy equation. These eight boundary conditions yielding the relations in (5.15) contain besides the coefficients a, b ... f_0 of the standardized velocity and temperature profiles (5.4) and (5.5) and the given quantities t_w, $(t_w)_x$, U, U_x, M, σ and $k = \frac{c_p}{c_v} = 1.4$ also the unknown quantities Ω, α, τ_w and $(t_{\xi_0})_w$. These unknown quantities and the six coefficients a, b, f, a_0, b_0, f_0 can be calculated from the eight boundary conditions and the two differential equations (3.23) and (3.30). The shear stress, the heat transfer at the wall and the temperature and velocity profiles of the boundary layer are then known.

In the separation point the relation (5.16) holds

$$(2c-a)(a-c) = (3b-f)^2. \qquad (8.1)$$

Assuming that the relation (8.1) will hold for the whole decelerated flow, one can describe the accelerated and decelerated flow by two separate solutions. When for the accelerated flow $c = 0$ and for the decelerated flow $c = p(x)a$, both solutions will join for $c = a = 0$ in $U_x = 0$.

With $c = pa$, (8.1) can be written in the following form

$$(3b-f)^2 = (2p-1)(1-p)a^2 = \frac{4}{\pi}q^2a^2. \qquad (8.2)$$

Hence, the relations (5.15) change into

$$c = pa;\; 3b-f = \frac{2}{\sqrt{\pi}}qa;\; f = \frac{2}{\sqrt{\pi}}(1-a)$$

$$\frac{2}{\sqrt{\pi}}qa = \frac{1}{\Omega}\frac{1-t_w}{t_w}(f_0-b_0)(1-p)a;$$

$$f_0 = \frac{2}{\sqrt{\pi}}(1-a_0) \qquad (8.3)$$

$$a_0 = -\frac{\sigma\Omega^2}{1-t_w}\frac{k-1}{2}M^2(f-b)^2;\; f-b = \frac{\tau_w t_w}{\alpha\mu_w U}$$

$$2(1-p)a = \frac{-U_x t_w}{\nu_u\gamma\alpha^2};\; (t_{\xi_0})_w = (1-t_w)(f_0-b_0) \qquad (8.3)$$

$$(f-b)(1-p)a\frac{(t_w)_x}{t_w} + 2(k-1)M^2\frac{U_x}{U}(1-p)a(f-b) + \frac{1}{\sigma}\frac{1}{\Omega^3}\frac{U_x}{U}(3b_0-f_0)(1-t_w) = 0.$$

Assuming

$$f-b = \frac{2}{\sqrt{\pi}}\Lambda;\; f_0-b_0 = \frac{2}{\sqrt{\pi}}\Lambda_0;\; \frac{q}{1-p}\frac{t_w}{1-t_w} = Q;\; -\frac{4}{\pi}\frac{\sigma}{1-t_w}\frac{k-1}{2}M^3 = P$$

the relations (8.3) can be simplified to

$$a = \frac{2-3\Lambda}{2+q};\; a_0 = P\Omega^2\Lambda^2;\; \frac{\tau_w t_w}{\alpha\mu_w U} = \frac{2}{\sqrt{\pi}}\Lambda,$$

$$f = \frac{2}{\sqrt{\pi}}\frac{q+3\Lambda}{2+q};\; f_0 = \frac{2}{\sqrt{\pi}}(1-P\Omega^2\Lambda^2);\; 2(1-p)\frac{2-3\Lambda}{2+q} = -\frac{U_x t_w}{\nu_u\gamma\alpha^2}, \qquad (8.4)$$

$$b = \frac{2}{\sqrt{\pi}} \frac{q + (1-q)\Lambda}{2+q}\,;\; b_0 = \frac{2}{\sqrt{\pi}}(1 - P\Omega^2\Lambda^2 - \Omega Q)\,;$$

$$c = p\,\frac{2-3\Lambda}{2+q}\,;\; \Lambda_0 = \Omega Q\,;\; (t_{\xi_0})_w = \frac{2}{\sqrt{\pi}}\Omega Q(1-t_w),$$

$$\frac{\sigma\Omega^3(1-p)\Lambda a}{1-t_w}\,\frac{(t_w)_x}{t_w} - \pi P\Omega^3(1-p)\Lambda a\,\frac{U_x}{U} + (2 - 2P\Omega^2\Lambda^2 - 3\Omega Q)\frac{U_x}{U} = 0. \tag{8.5}$$

For the accelerated flow is $p = 0$.
For the decelerated flow is $p \neq 0$

$$(2p-1)(1-p) = \frac{4}{\pi}q^2 \text{ or } \frac{q^2}{\left(\sqrt{\frac{\pi}{32}}\right)^2} + \frac{(p-\frac{3}{4})^2}{(\frac{1}{4})^2} = 1.$$

When the temperature distribution along the wall T_w is prescribed and the velocity distribution $\frac{U}{U_\infty}$ of the outer flow is known (this can be described by the local Mach number) the quantities necessary for the description of the compressible laminar boundary layer flow can be calculated by numerical integration with the aid of the momentum equation of von Kàrmàn (3.23), the integrated heat equation (3.30) and the relations (8.4) and (8.5).

With the momentum equation of von Kàrmàn

$$\frac{d\theta}{dx} + \frac{U_x}{U}\theta\,[2H + 3 - \{1 + \beta(k-1)\}M^2] = 2\gamma\bar{u}_\xi\alpha\delta_2 \tag{8.6}$$

and the integrated heat equation

$$\frac{d\theta_1}{dx} + \frac{U_x}{U}\theta_1\,[1 - \{1 + \beta(k-1)\}M^2] = -\frac{2}{\sigma}\,\frac{\gamma}{\Omega}\,t_{\xi_0}\alpha\delta_3 + 2(k-1)M^2\,\frac{\delta_4\delta_3}{\delta_2^2} \tag{8.7}$$

the following equations can be established:

$\frac{1}{\theta}$ times eq. (8.6) $-\frac{1}{\theta_1}$ times eq. (8.7) gives in connection with

$$\theta = \frac{U\delta_2^2}{\nu_u} = \frac{U(\alpha\delta_2)^2}{\nu_u\alpha^2} = -\frac{U}{U_x}\,\frac{\gamma}{t_w}(\alpha\delta_2)^2\,2\,(1-p)a$$

$$\theta_1 = \frac{U\delta_3^2}{\nu_u} = \frac{U(\alpha\delta_3)^2}{\nu_u\alpha^2} = -\frac{U}{U_x}\,\frac{\gamma}{t_w}(\alpha\delta_3)^2\,2\,(1-p)a$$

$$\frac{d}{dx}\ln\frac{\theta}{\theta_1} = -\frac{U_x}{U}\left[2H + 2 + \frac{t_w}{2(1-p)a}\left\{\frac{2\bar{u}_\xi}{\alpha\delta_2} + \frac{2}{\sigma}\,\frac{t_{\xi_0}}{\Omega}\,\frac{1}{\alpha\delta_3} - \frac{2(k-1)M^2}{\alpha\delta_3}\,\frac{1}{\gamma}\,\frac{\delta_4}{\alpha\delta_2^2}\right\}\right] = \pi(x). \tag{8.8}$$

This equation has the solution

$$\frac{\theta}{\theta_1}(x) = \frac{\theta}{\theta_1}(0)\,e^{\int_0^x \pi(x)dx}. \tag{8.9}$$

The differential equation

$$\frac{d\theta_1}{dx} + \theta_1\left[\frac{U_x}{U} + \frac{\rho_{u_x}}{\rho_u} + \frac{\mu_{u_x}}{\mu_u}\right] = -\frac{2}{\sigma}\,\frac{\gamma}{\Omega}\,t_{\xi_0}\alpha\delta_3 + 2(k-1)M^2\,\frac{\delta_4\delta_3}{\delta_2^2} = s(x) \tag{8.10}$$

follows from (8.7) in connection with (3.22).

This equation has the following solution

$$\theta_1 = \frac{1}{U\rho_u\mu_u(x)}\int_0^x s(x)U\rho_u\mu_u dx. \tag{8.11}$$

With the aid of (8.9) and (8.11) the computational process can be simplified in the following way. If for the points $x_0 = 0$, x_1, $x_2 \ldots$, x_{n-1} the pertaining values

$$q_0, q_1, \ldots q_{n-1};\; \Omega_0, \Omega_1 \ldots \Omega_{n-1};\; \Lambda_0, \Lambda_1, \ldots \Lambda_{n-1} \tag{8.12}$$

have been calculated, then for x_n the quantities q_{n_1} and Ω_{n_1} can be estimated with the aid of a difference scheme. The pertaining value Λ_{n_1} can be calculated from (8.5). Using the values (8.12) as well as the values for q_{n_1}, Ω_{n_1} and Λ_{n_1}, the quantities $\frac{\theta}{\theta_1}(x_n)$ and $\theta_1(x_n)$ can be obtained in first approximation by aid of (8.9) and (8.11). The second approximation q_{n_2} follows from $\theta(x_n)$ and Λ_{n_1}. The second approximation Ω_{n_2} follows from $\theta_1(x_n)$, Λ_{n_1} and q_{n_2}. Finally eq. (8.5) yields the second approximation Λ_{n_2}, when using q_{n_2} and Ω_{n_2}. This process will be repeated until Λ_n, q_n and Ω_n vary no longer.

Apart from the neighbourhood of the stagnation point and near the point where $U_x = 0$, it is to be expected that this process will converge very quickly sothat in general two steps will be sufficient to obtain the accuracy required. Near the stagnation point and near the point where $U_x = 0$ (the function p shows a discontinuity when passing from accelerated flow to decelerated flow) it is useful to start from a system of two values $q_{n_{11}}$, $\Omega_{n_{11}}$; $q_{n_{12}}$, $\Omega_{n_{12}}$ and to calculate with (8.5) the pertaining values $\Lambda_{n_{11}}$ and $\Lambda_{n_{12}}$.*)

Afterwards the values $q_{n_{21}}$, $\Omega_{n_{21}}$ and $q_{n_{22}}$, $\Omega_{n_{22}}$ can be calculated from θ and θ_1 with the above-mentioned method.

$$(t_{\xi_0})_w = \frac{2}{\sqrt{\pi}}\,\Omega\,\frac{q}{1-p}\,t_w \qquad (8.14)$$

varies continuously from accelerated to decelerated flow.

For the accelerated flow (8.14) takes in the point $U_x = 0$ the value

$$(t_{\xi_0})_w = \frac{2}{\sqrt{\pi}}\,\Omega\,q_1 t_w$$

and for the decelerated flow the value

$$(t_{\xi_0})_w = \frac{2}{\sqrt{\pi}}\,\Omega\,\frac{q}{1-p}\,t_w\,.$$

Equalizing these two values yields the relation

$$\frac{q}{1-p} = q_1$$

and in relation with (8.13)

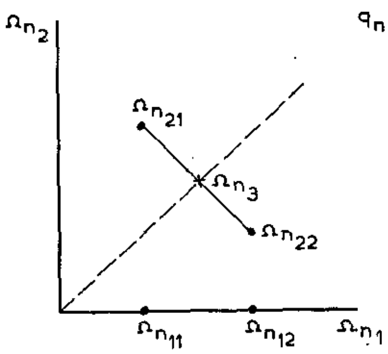

Fig. 4.

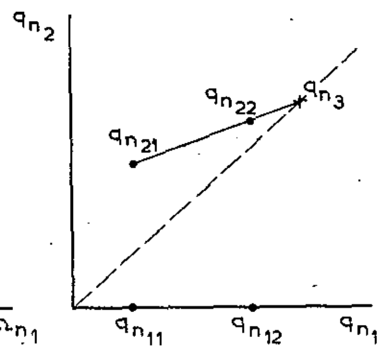

Fig. 5.

When plotting the calculated values Ω_{n_2} and q_{n_2} as functions of Ω_{n_1} and q_{n_1} resp., the points Ω_{n_3} and q_{n_3} lying on the bisector can be obtained rectilinear interpolation and be assumed as new approximated values. With the aid of these values Ω_{n_3} and q_{n_3} the pertaining value Λ_{n_3} can be calculated from (8.5). This iteration process has to be repeated until Ω_n and q_n will not vary anymore.

As the relation

$$\frac{q^2}{\left(\sqrt{\frac{\pi}{32}}\right)^2} + \frac{\left(p-\frac{3}{4}\right)^2}{\left(\frac{1}{4}\right)^2} = 1$$

or

$$(2p-1)(1-p) = \frac{4}{\pi}q^2 \qquad (8.13)$$

is ambiguous, it is necessary to make an additional assumption in order to fix the initial values p and q in the point $U_x = 0$ for the decelerated flow unambiguously. The assumption made is that the function of heat transfer

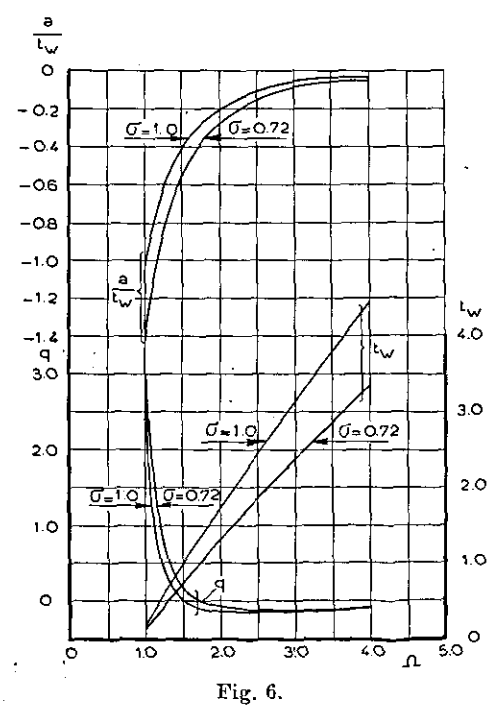

Fig. 6.

The values of t_w, q and $\frac{a}{t_w}$ at the stagnation point plotted as functions of Ω for laminar compressible boundary layer flow with heat transfer at the wall, for $\sigma = 0.72$ and $\sigma = 1.0$.

*) Near the stagnation point it is advisible to choose the values $\Omega_{1_{11}}$ and $\Omega_{1_{12}}$ as well as $q_{1_{11}}$ and $q_{1_{12}}$ at both sides of the values Ω_0 and q_0 obtained for the stagnation point. When passing $U_x = 0$ it is important to pay attention to the relation (8.15).

$$p = \frac{\frac{4}{\pi} q_1^2 + 1}{\frac{4}{\pi} q_1^2 + 2} \qquad q = \frac{q_1}{\frac{4}{\pi} q_1^2 + 2} \qquad (8.15)$$

which fixes unambiguously the initial values p and q at the beginning ($U_x = 0$) of the decelerated flow. At this point $\Lambda = \frac{2}{3}$.

The functions Ω and Λ are continuous at the point $U_x = 0$, while the functions p and q are discontinuous in that point. The same method of calculation will be applied at the beginning of the decelerated flow as near the stagnation point.

Since $P = 0$ and $\Omega Q = \frac{2}{3}$ (from (8.5)) at the stagnation point, eq. (8.4) yields

$$a_0 = 0,\ f_0 = 3\, b_0 = \frac{2}{\sqrt{\pi}},\ a = \frac{2 - 3\Lambda}{2 + q},$$

$$f = \frac{2}{\sqrt{\pi}}(1 - a),$$

$$b = \frac{2}{\sqrt{\pi}}(1 - a - \Lambda)\, q \frac{t_w}{1 - t_w} = \frac{2}{3} \frac{1}{\Omega}. \quad (8.16)$$

The momentum equation of von Kàrmàn and the integrated heat equation change in the stagnation point into

$$a\, \alpha \delta_2 (H + 2) + \frac{1}{\sqrt{\pi}} \Lambda\, t_w = 0 \qquad (8.17)$$

$$a\, \alpha \delta_3 = \frac{2}{3\sqrt{\pi}} \frac{1}{\sigma\Omega} t_w (1 - t_w). \qquad (8.18)$$

For the Prandtl numbers $\sigma = 0.72$ and $\sigma = 1$ the values of t_w, q and $\frac{a}{t_w}$ at the stagnation point are plotted as functions of Ω in fig. 6, sothat the initial values can be taken from the diagram. For other values of σ, Ω and q can be calculated, after estimation, by iteration from the equations (8.17) and (8.18).

9 The flow along a flat plate without pressure gradient with constant and variable wall temperature.

For flow along a flat plate $U_x = 0$. This changes the relations (8.4) and (8.5) derived in section 8 into

$$\Lambda = \tfrac{2}{3};\ a = c = 0;\ f = 3\, b = \frac{2}{\sqrt{\pi}};\ a_0 = \tfrac{4}{9}\, \Omega^2 P = -\frac{16}{9\pi} \frac{\sigma}{1 - t_w} \frac{k - 1}{2} M^2 \Omega^2$$

$$f_0 = \frac{2}{\sqrt{\pi}}(1 - a_0);\ b_0 = \frac{2}{\sqrt{\pi}}\left(1 - a_0 - q \frac{t_w}{1 - t_w} \Omega\right); \qquad (9.1)$$

$$\sigma \Omega^3 \frac{(t_w)_x}{1 - t_w} = \left(2 - 2\, a_0 - 3\,\Omega\, q \frac{t_w}{1 - t_w}\right) \frac{3\, \nu_u \gamma \alpha^2}{U}; \qquad (9.2)$$

$$\frac{\tau_w t_w}{\alpha \mu_w U} = \frac{4}{3\sqrt{\pi}};\ (t_{\xi_0})_w = \frac{2}{\sqrt{\pi}} \Omega\, q\, t_w. \qquad (9.3)$$

The momentum equation of von Kàrmàn (3.18)

$$\frac{d\delta_2}{dx} = \alpha \delta_2 \frac{d}{dx}\left(\frac{1}{\alpha}\right) = \frac{\tau_w}{\rho_u U^2} = \frac{4}{3\sqrt{\pi}} \frac{\alpha \nu_u \gamma}{U}$$

yields the relation

$$\left(\frac{1}{\alpha}\right)^2 = \frac{8}{3\sqrt{\pi}} \frac{1}{\alpha \delta_2} \frac{\nu_u}{U} \int_0^x \gamma dx. \qquad (9.4)$$

The integrated heat equation (3.28) can be written for flow along a flat plate without pressure gradient in the following form:

$$\frac{d\delta_3}{dx} = -\frac{\nu_u \gamma}{\sigma U} \frac{\alpha}{\Omega} t_{\xi_0} + \frac{\alpha \nu_u}{U}(k - 1) M^2 \frac{\delta_4}{\alpha \delta_2^2}. \qquad (9.5)$$

In connection with (9.4) is

$$\frac{d\delta_3}{dx} = \frac{d}{dx}\left(\frac{\alpha \delta_3}{\alpha}\right) = \frac{1}{\alpha} \frac{1}{\sqrt{\int_0^x \gamma\, dx}} \frac{d}{dx}\left(\alpha \delta_3 \sqrt{\int_0^x \gamma\, dx}\right)$$

which changes (9.5) into

$$\frac{d}{dx}\left(\alpha\delta_3\sqrt{\int_0^x \gamma dx}\right)=\frac{3\sqrt{\pi}}{8}\frac{\alpha\delta_2}{\sqrt{\int_0^x \gamma dx}}\left(-\frac{2}{\sqrt{\pi}}\frac{\gamma}{\sigma}qt_w+(k-1)M^2\frac{\delta_4}{\alpha\delta_2{}^2}\right) \tag{9.6}$$

with the solution

$$\alpha\delta_3\sqrt{\int_0^x \gamma dx}=-\frac{3}{4}\frac{\alpha\delta_2}{\sigma}\int_0^x\frac{\gamma q t_w}{\sqrt{\int_0^x \gamma dx}}dx+\frac{3\sqrt{\pi}}{4}(k-1)M^2\frac{\alpha\delta_2}{\gamma}\frac{\delta_4}{\alpha\delta_2{}^2}\sqrt{\int_0^x \gamma dx}. \tag{9.7}$$

For the case that no heat transfer takes place one has $q=0$ which simplifies the solution (9.7) into

$$\alpha\delta_3=\frac{3\sqrt{\pi}}{4}(k-1)M^2\frac{\alpha\delta_2}{\gamma}\frac{\delta_4}{\alpha\delta_2{}^2}. \tag{9.8}$$

Using again the result that the eigentemperature for a flat plate without heat transfer is constant, it follows from (9.2) that $a_0=1$ and from (9.1) that

$$t_w-1=\frac{16}{9\pi}\sigma\frac{k-1}{2}M^2\Omega^2.$$

This approximation is less accurate than that from section 7, as in section 7 one more boundary condition is taken into account.

For a prescribed constant wall temperature $t_w=$ const. there exists a solution $q=$ const., $\Omega=$ const. The equations (9.7) and (9.2) then change into

$$\alpha\delta_3=-\frac{3}{2}\frac{\alpha\delta_2}{\sigma}q\,t_w+\frac{3\sqrt{\pi}}{4}(k-1)M^2\frac{\alpha\delta_2}{\gamma}\frac{\delta_4}{\alpha\delta_2{}^2} \tag{9.9}$$

$$q\,t_w=\frac{2}{3\,\Omega}(1-t_w)+\frac{32}{27\,\pi}\Omega\,\sigma\frac{k-1}{2}M^2. \tag{9.10}$$

In the general case of a variable wall temperature, (9.2) changes in connection with (9.4) into

$$q\,t_w=\frac{1}{3\,\Omega}\left[2(1-t_w)+\frac{32}{9\,\pi}\Omega^2\sigma\frac{k-1}{2}M^2-\frac{8}{9\sqrt{\pi}}\frac{\sigma\Omega^3}{\alpha\delta_2}(t_w)_x\frac{\int_0^x\gamma dx}{\gamma}\right] \tag{9.11}$$

The calculations of the boundary layer can be carried out according to the method described in section 8.

To simplify the computational work the equations (9.11) and (9.7) are written in the following form. Assuming

$$m=\int_0^x\gamma dx;\quad s_1=\tfrac{2}{3}(1-t_w)\frac{\gamma}{\sqrt{m}}$$

$$s_2=\frac{32}{27\,\pi}\sigma\frac{k-1}{2}M^2\frac{\gamma}{\sqrt{m}};\quad s_3=-\frac{8}{27\sqrt{\pi}}\frac{\sigma}{\alpha\delta_2}(t_w)_x\sqrt{m}$$

and

$$y=\int_0^x\frac{\gamma q t_w}{\sqrt{\int_0^x\gamma\,dx}}dx, \tag{9.12}$$

one has

$$\frac{dy}{dx}=\frac{\gamma q t_w}{\sqrt{\int_0^x\gamma\,dx}}=\frac{s_1}{\Omega}+s_2\Omega+s_3\Omega^2,. \tag{9.13}$$

$$\frac{\alpha\delta_3}{t_w - 1} = -\frac{3}{4}\frac{\alpha\delta_2}{\sigma(t_w - 1)\sqrt{m}}\, y + \frac{3\sqrt{\pi}}{4}(k-1)M^2 \frac{\alpha\delta_2}{\gamma(t_w - 1)}\frac{\delta_4}{\alpha\delta_2^{\,2}}. \tag{9.14}$$

The following quantities appear during the computation

$$\alpha\delta_2 = 0.289430;\ \frac{\delta_4}{\alpha\delta_2^{\,2}} = 0.598413;\ k = 1.4.$$

In (9.14) is

$$\frac{\alpha\delta_3}{t_w - 1} = -0.126962 + 0.311955\,\Omega + (0.104446 - 0.012131\,P)\Omega^2 + (0.028238\,P - 0.102475\,R)\Omega^3 + \\ + (0.010397\,P + 0.262546\,R)\Omega^4 + 0.031941\,R\Omega^5 \tag{9.15}$$

where

$$P = -\frac{4}{\pi}\frac{\sigma}{1 - t_w}\frac{k-1}{2}M^2;\ R = \sigma\frac{(t_w)_x}{1 - t_w}\frac{m}{\gamma}.$$

The following temperature-viscosity relation will be used in the calculation

$$\frac{\mu}{\mu_u} = \gamma\frac{T}{T_u},\ \text{where}\ \gamma = \frac{T_u + C}{\frac{1 + 3\,t_w}{4}T_u + C}\left(\frac{1 + 3\,t_w}{4}\right)^{1/2}.$$

In the starting point $x = 0$ the equations (9.11) and (9.7) change into

$$q\,t_w = \frac{1}{3\,\Omega}\left[2(1 - t_w) + \frac{32}{9\,\pi}\Omega^2\sigma\frac{k-1}{2}M^2\right] \tag{9.16}$$

$$\alpha\delta_3 = -\frac{3}{2}\frac{\alpha\delta_2}{\sigma}q\,t_w + \frac{3\sqrt{\pi}}{4}(k-1)M^2\frac{\alpha\delta_2}{\gamma}\frac{\delta_4}{\alpha\delta_2^{\,2}}. \tag{9.17}$$

From these equations the values $\Omega = \Omega_0$ and $(q\,t_w)_0$ can be calculated. Near the starting point $x = 0$ one has

$$y \approx 2\sqrt{\gamma}\,(q\,t_w)_0\sqrt{x}. \tag{9.18}$$

The general solution of the boundary layer equations (9.13) and (9.14) is found as follows. After having calculated for the points of equal intervals $x_0 = 0,\ x_1,\ x_2,\ \ldots\ x_{n-1}$ the pertaining values Ω_0, $\ldots\ \Omega_{n-1}$, it is possible to calculate in the point $x = x_n$ for the value $\Omega = \Omega_{n_0}$ (estimated by means of a difference scheme) the pertaining value $\frac{dy}{dx}$ from (9.13) and with that also the value y (by integration of the curve $\frac{dy}{dx}$). The relation (9.14) yields with the obtained value $y = y(x_n)$ the corrected value $\Omega = \Omega_{n_1}$ in the point $x = x_n$. After this the values $\frac{dy}{dx}$ and y can be calculated again with the aid of $\Omega = \Omega_{n_1}$ and the value Ω can be corrected by means of (9.14). This process has to be repeated until the value $\Omega = \Omega_n$ does not vary anymore within the boundaries of the prescribed accuracy.

In general this process will converge very quickly. If Δx is sufficiently small, the relation

$$y = 2\sqrt{\gamma}\,(q\,t_w)_0\sqrt{x}$$

holds within the boundaries of the prescribed accuracy. By aid of this relation the initial scheme for the solution of the diff. eq. can be obtained in a simple way.

For that purpose

$$\frac{dy}{dx} = \frac{\sqrt{\gamma}\,(q\,y_w)_0}{\sqrt{x}}$$

is plotted in a graph between the points $x = 0$ and $x = x_1$.

Starting from the value $\Omega_{1_0} = \Omega_0$ in the point $x = x_1$, the value $\frac{dy}{dx}$ (formula 9.13) in the point $x = x_1$ can be corrected with the aid of the value Ω obtained from (9.14). By fairing again the curve $\frac{dy}{dx}$ from the point Δx until $x = x_1$ the pertaining value $y = y(x_1)$ can be determined (e.g. by means of a planimeter). This process has to be repeated until the value Ω will not vary anymore within the boundaries of the prescribed accuracy. The initial scheme will be more accurate if the initial intervals are chosen smaller. A better fairing of the curve $\frac{dy}{dx}$ can be obtained if the calculation is carried out for more points within the interval $< \Delta x, x_1 >$.

The calculation has been carried out for flow along a flat plate with the variable wall temperature

$$t_w - 1 = 0.5\,(1 - \tfrac{3}{2}\,\zeta) \tag{9.19}$$

and the quantities

$$T_u = 220°\text{K},\ C = 110°\text{K},\ \sigma = 0.72,\ M = 1.3.$$

$\zeta = \frac{x}{l}$ is the dimensionless length of the plate.

Expressing all results in terms of a, one obtains

TABLE 3.

Calculated values for flow along a flat plate without pressure gradient and with variable wall-temperature.

$$T_w = 1.5\, T_u \left(1 - \tfrac{1}{2}\, \frac{x}{L}\right) = 1.5\, T_u (1 - \tfrac{1}{2}\, \zeta)$$

ζ	γ	$\sqrt{m}$	P	R	S_1	S_2	$\frac{1}{3} S_3 \frac{\gamma}{\sqrt{m}}$	$\frac{dy}{d\zeta}$	y
0	0.93808	0	+ 0.61971	0	∞	∞	0	— ∞	0
0.05	0.94258	0.21683	0.66996	+ 0.05824	+ 1.34037	0.39911	0.06763	— 0.42150	— 0.05615
0.1	0.94711	0.30701	0.72907	0.12645	0.87406	0.28322	0.09575	— 0.18397	— 0.07049
0.2	0.95626	0.43523	0.88530	0.30562	0.51267	0.20172	0.13574	+ 0.03536	— 0.07685
0.3	0.96553	0.53434	1.12675	0.58066	0.33128	0.16590	0.16665	0.16594	— 0.06685
0.4	0.97489	0.61849	1.54928	1.05943	0.21017	0.14471	0.19290	0.26343	— 0.04547
0.5	0.98431	0.69318	2.47884	2.10884	0.11833	0.13037	0.21619	0.34366	— 0.01522
0.6	0.99373	0.76118	+ 6.19711	+ 6.29696	+ 0.04352	0.11986	0.23740	0.41332	+ 0.02253
0.7	1.00312	0.82416	— 12.3942	— 14.6259	— 0.02029	0.11174	0.25704	0.47569	0.06690
0.8	1.01239	0.88319	— 3.09856	— 4.16055	— 0.07642	0.10524	0.27546	0.53291	0.11740
0.9	1.02144	0.93899	— 1.77060	— 2.66358	— 0.12691	0.09987	0.29286	0.58591	0.17328
1.0	1.03016	0.99212	— 1.23942	— 2.06383	— 0.17306	0.09533	0.30943	+ 0.63571	+ 0.23428

ζ	Ω	qt_w	$\frac{1}{\alpha}\sqrt{\frac{U}{\nu_u x}}$	$(t_\xi)_w$	$\frac{\tau_w}{\rho_0 U^2}\sqrt{\frac{Ux}{\nu_u}}$	a_0	b_0	f_0	$\frac{lq_w(x)}{\lambda T_u \sqrt{Re_x}}$
0	1.298	— 0.13764	2.2082	— 0.20159	0.31957	+ 0.46404	+ 0.20159	+ 0.60477	∞
0.05	1.283	— 0.09696	2.2108	— 0.14036	0.32072	0.49005	0.27193	0.57542	+ 0.15133
0.1	1.261	— 0.05964	2.2135	— 0.08484	0.32187	0.51508	0.34755	0.54717	+ 0.06746
0.2	1.229	+ 0.01609	2.2188	+ 0.02231	0.32421	0.59394	0.52194	0.45819	— 0.01356
0.3	1.204	0.09183	2.2242	0.12473	0.32656	0.72558	0.76320	0.30965	— 0.06671
0.4	1.183	0.16712	2.2296	0.22307	0.32892	0.96351	1.1565	+ 0.04118	— 0.11144
0.5	1.165	0.24202	2.2350	0.31812	0.33130	1.4950	1.9864	— 0.55855	— 0.15360
0.6	1.149	0.31660	2.2405	0.41051	0.33365	+ 3.6367	+ 5.2351	— 2.9752	— 0.19605
0.7	1.135	0.39082	2.2459	0.50044	0.33599	— 7.0939	— 10.884	+ 9.1330	— 0.24071
0.8	1.122	0.46490	2.2513	0.58853	0.33828	— 1.7334	— 2.8010	3.0843	— 0.28946
0.9	1.110	0.53862	2.2566	0.67450	0.34051	— 0.96926	— 1.6322	2.2221	— 0.34411
1.0	1.099	0.61223	2.2620	+ 0.75894	0.34259	— 0.66482	— 1.1573	+ 1.8785	— 0.40721

$$\gamma = \frac{T_u + C}{\frac{1+3\,t_w}{4} T_u + C} \left(\frac{1+3\,t_w}{4}\right)^{1/2} =$$

$$= \frac{1}{1 + \frac{1}{4}(1 - \frac{3}{2}\zeta)} \left(1 + \tfrac{3}{8}(1 - \tfrac{3}{2}\zeta)\right)^{1/2}$$

$$m = \int_0^{\xi} \gamma d\zeta = -$$

$$- \frac{16}{3}\left[z - \sqrt{\frac{1}{2}}\; by\, tg\, z\sqrt{2}\right]_{z=\sqrt{\frac{11}{8}}}^{\sqrt{\frac{11}{8}-\frac{9}{16}\zeta}} .$$

In table 3 the calculated values of γ, $\sqrt{m}$, P, R, s_1, s_2, s_3 are given for $\zeta = 0$, 0.05, 0.1, 0.2 ..., 1.0. For $\zeta = 0$ (9.16) and (9.17) yield the values $\Omega = 1.29800$ $(q\,t_w)_0 = -1.13764$.

Near $y = 0$ the relation

$$\frac{dy}{d\zeta} = -\frac{0.13331}{\sqrt{\zeta}}$$

holds.

It is assumed that this relation holds until the point $\zeta = 0.01$. The values $\frac{dy}{d\zeta}$, y, Ω and $q\,t_w$ are calculated according to the above-described method with the aid of (9.12), (9.13) and (9.14). After that also the quantities a_0, b_0, f_0, $\frac{1}{\alpha}\sqrt{\frac{\mu}{\nu_u x}}$, $(t_{\xi_0})_w$ and $\frac{\tau_w}{\rho_u U^2}\sqrt{\frac{Ux}{\nu_u}}$ are calculated from (9.1), (9.3) and (9.4) (see table 3).

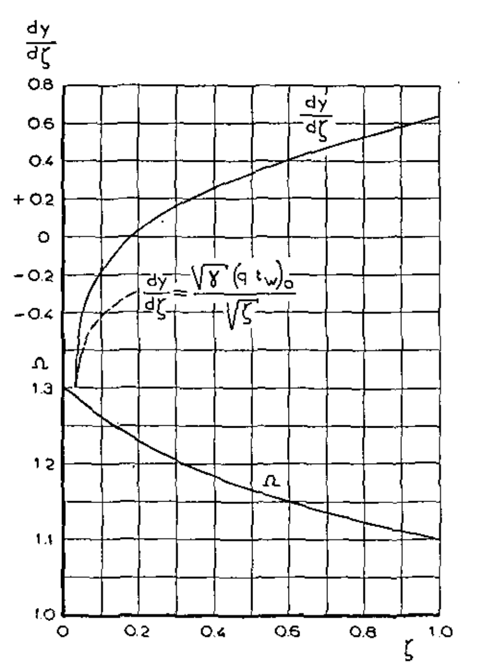

Fig. 7.

The boundary layer quantities $\frac{dy}{d\zeta} = \frac{\gamma q t_w}{\sqrt{\int_0^{\zeta} \gamma dx}}$ and Ω plotted as functions of ζ for flow along a flat plate with the variable wall temperature $T_w = \frac{3}{2}\,T_u\left(1 - \frac{1}{2}\zeta\right)$ $\left(\zeta = \frac{x}{L}\right)$.

In fig. 7 and 8 the quantities Ω, $\frac{dy}{d\zeta}$ and y are plotted as functions of ζ.

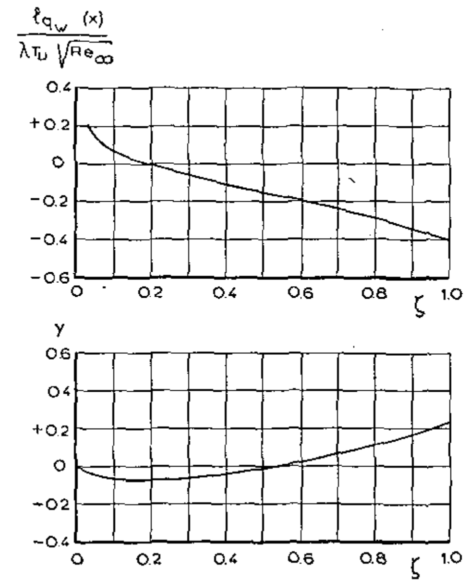

Fig. 8.

The dimensionless quantity for the heat transfer at the wall

$$\frac{l\,q_w}{\lambda\,T_u\sqrt{Re_\infty}}$$

and the quantity y for flow along a flat plate with the variable wall temperature $T_w = 1.5\,T_u\,(1 - \frac{1}{2}\zeta)$.

The velocity and temperature profiles are described by the functions

$$\bar{u} = 1 - \frac{2}{3\sqrt{\pi}}\,\xi\, e^{-\xi^2} - \frac{2}{\sqrt{\pi}} \int_{\xi}^{\infty} e^{-\eta^2} d\eta \quad (9.20)$$

$$t = 1 + (t_w - 1)\,(a_0\, e^{-\xi_0^2} + b_0 \xi_0 e^{-\xi_0^2} + f_0 \int_{\xi_0}^{\infty} e^{-\eta^2} d\eta) \quad (9.21)$$

where

$$y = \frac{\Omega}{\alpha} \int_0^{\xi_0} t\, d\xi_0 .$$

They are plotted for the points $\frac{x}{l} = 0$, 0.1, 0.3, 0.5, 2/3, 0.8 and 1.0 in figure 9 and 10. Fig. 10 contains also the field of isotherms $t =$ constant plotted against $y\sqrt{\frac{u}{\nu_u L}}$.

For the particular point $\zeta = 2/3$ is $t_w = 1$. By transition to the limit, (9.14) yields with $y = 0.05153$ the pertaining value $\Omega = 1.1393$.

Hence in connection with (9.11) the value $q\,t_w\Omega = 0.41705$ is obtained and according to (9.1) $(t_w - 1)a_0 = 0.17875$, $(t_w - 1)f_0 = -0.20170$ and $(t_w - 1)b_0 = 0.26889$.

The velocity profiles show a point of inflexion (see fig. 9) at the frontside of the plate, where the wall temperature is maximal. This indicates the unstable character of the boundary flow in that region. Together with the decreasing of the wall temperature backwards along the plate, the boundary layer flow becomes obviously ever more stable agreeing with the fact that the point of inflexion disappears.

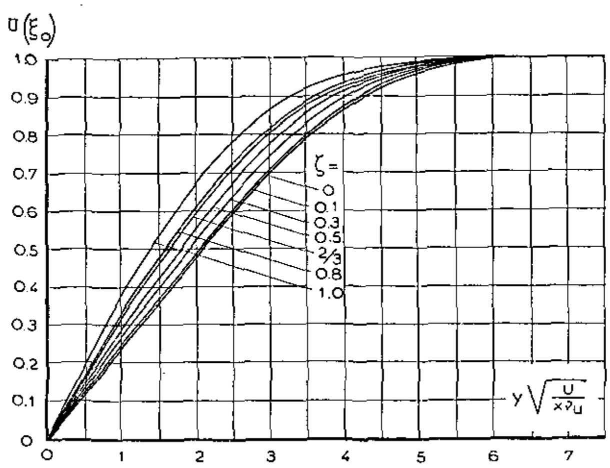

Fig. 9.

The velocity distribution within the boundary layer flow along a flat plate with the variable wall temperature $T_w = 1.5\, T_u (1 - \frac{1}{2}\zeta)$, for $M = 1.3$; $\sigma = 0.72$; $T_u = 220°$K.

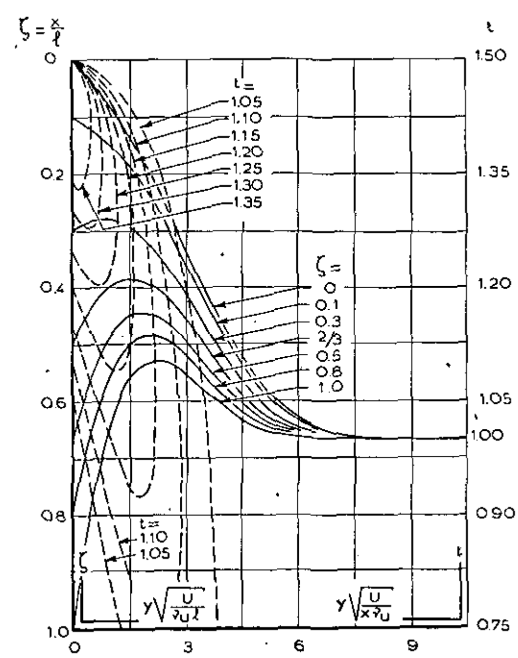

Fig. 10.

The temperature distribution in the boundary layer flow along a flat plate with variable wall temperature

$T_w = \frac{3}{2} T_u (1 - \frac{1}{2}\zeta)$

and the pertaining field of isotherms for

$M = 1.3$, $\sigma = 0.72$, $T_u = 220°$K.

The heat transfer at the wall can be calculated by means of the formula

$$q_w(x) = -\lambda \left(\frac{\partial T}{\partial y}\right)_w .$$

In dimensionless form this formula changes into

$$\frac{l q_w(x)}{\lambda T_u \sqrt{Re_\infty}} = -\sqrt{\frac{3\,\alpha\delta_2}{2\sqrt{\pi\, m}}}\ \frac{q\, t_w}{t_w}$$

(see fig. 8).

Fig. 8 shows that heat will be transferred from the wall to the outer flow until the point $\zeta = 0.179$, beyond that point heat transfer takes place in the opposite direction. The heat transfer from the outer flow to the wall takes place before the eigentemperature of the wall is reached, which will happen in the point $\zeta = 0.284$, according to formula $(t_w - 1) / \frac{k-1}{2} M^2 = \sqrt{\sigma}$.

10 Application of the method to a rotationally symmetric case.

The boundary layer calculations (velocity and temperature distributions) for a rotationally-symmetric body can be reduced to calculations for a two-dimensional profile by means of a simple transformation, described by Mangler (ref. 14).

When s is the arc length of the meridian section of the body of revolution, r_0 the distance of a point of the surface to the axis of symmetry, such that the contour is given by $r = r_0(s)$, n the length of the perpendicular of a point of the fluid to the wall, L the unit of length, $\bar{x}$ and $\bar{y}$ the arc lengths along and perpendicular to the two-dimensional image plane, then the following transformation has to be carried out in order to obtain two-dimensional flow.

$$\begin{aligned} \bar{x} &= \int_0^s \frac{r_0^2(s)}{L^2}\, ds & \bar{p}(\bar{x},\bar{y}) &= p(s,n) \\ & & \bar{T}(\bar{x},\bar{y}) &= T(s,n) \\ \bar{y} &= \frac{r_0(s)}{L}\, n & \bar{\rho}(\bar{x},\bar{y}) &= \rho(s,n) \\ \bar{\psi}(\bar{x},\bar{y}) &= \frac{1}{L}\,\psi(s,n) & \bar{\mu}(\bar{x},\bar{y}) &= \mu(s,n). \end{aligned} \tag{10.1}$$

The laminar boundary layer flow of the body of revolution is determined by the pressure distribution $p(s)$ and the contour $r_0(s)$. It is obtained by calculating firstly the two-dimensional boundary layer with the pressure distribution and the arc length

$$\bar{p}(\bar{x}) = p(s) \qquad \bar{x} = \int_0^s \frac{r_0^2(s)}{L^2}\, ds \tag{10.2}$$

and transforming afterwards the obtained results by means of (10.1) in three-dimensional quantities.

When the free flow along the body of revolution is known, the free flow for the two-dimensional case is also known and the boundary layer calculations can be carried out.

Introducing the dimensionless quantities

$$\tau_w{}^* = \frac{\tau_w}{\rho_u U^2} Re \qquad \overline{\tau_w}{}^* = \frac{\overline{\tau_w}}{\rho_u \overline{U}^2} \overline{Re}$$

$$\delta_1{}^* = \frac{\delta_1}{s} Re \qquad \overline{\delta_1}{}^* = \frac{\overline{\delta_1}}{x} \overline{Re}$$

$$\delta_2{}^* = \frac{\delta_2}{s} Re \qquad \overline{\delta_2}{}^* = \frac{\overline{\delta_2}}{x} \overline{Re}$$

where

$$Re = \sqrt{\frac{sU}{\nu_u}} \qquad \overline{Re} = \sqrt{\frac{\overline{xU}}{\nu_u}}$$

yields the following relations

$$\frac{\tau_w{}^*}{\overline{\tau_w}{}^*} = \frac{\overline{\delta_1}{}^*}{\delta_1{}^*} = \frac{\overline{\delta_2}{}^*}{\delta_2{}^*} = \sqrt{\frac{s\, r_0{}^2(s)}{\int_0^s r_0{}^2(s)\, ds}} \tag{10.3}$$

where τ_w, $\overline{\tau_w}$ are shear stresses at the wall, δ_1, $\overline{\delta_1}$ the displacement thicknesses and δ_2, $\overline{\delta_2}$ the momentum loss thicknesses of the rotationally symmetric boundary layer flow and the boundary layer frow of the two-dimensional image.

The potential flow along a body of revolution can be calculated for supersonic flow by means of the method of characteristics of PRANDTL and BUSEMANN (ref. 13) or the methods of TOLLMIEN and SCHÄFER (ref. 15 and 16).

11 Literature.

1. ZAAT, J. A., A One-Parameter Method for the Calculation of the Temperature Profile of Laminar Incompressible Boundary Layer Flow with a Pressure Gradient. N.L.L. Report F. 127 (1953).
2. TRIBUS, M., and BOELTER, L. M. K., Investigation of Aircraft Heaters. II — Properties of Gases. NACA A.R.R., October 1942.
3. YOUNG, A. D., Skin Friction in the Laminar Boundary Layer in Compressible Flow. Aero. Quart. Vol. 1, Aug. 1949, p. 137—164.
4. CHAPMAN, D. R., and ROBESIN, M. W., Temperature and Velocity Profiles in the Compressible Laminar Boundary Layer with Arbitrary Distribution of Surface Temperature. J. Aero. Sci. Vol. 16, No. 9, Sept. 1949, pp. 547—565.
5. CHAPMAN, D. R., Laminar Mixing of a Compressible Fluid. NACA Rep. 958, 1950.
6. LIBBY, P. A., MORDUCHOW, M. and BLOOM, M., A Critical Study of Integral Methods in Compressible Laminar Boundary Layers. NACA T.N. 2655, 1952.
7. MORDUCHOW, M. and CLARKE, J. H., Method for Calculation of Compressible Laminar Boundary Layer Characteristic in Axial Pressure Gradient with Zero Heat Transfer. NACA T.N. 2784, 1952,
8. GOLDSTEIN, S., Modern Developments in Fluid Dynamics. Vol. 1, Oxford Clarendon Press., 1938, p. 136, 157.
9. HANTZSCHE, W. und WENDT, M., Die laminare Grenzschicht der ebenen Platte mit und ohne Wärmeübergang. Jahrb. der Deutsrhen Luftfahrtforschrng, 1942 I, pp. 40—50.
10. BRAINERD, J. G. and EMMONS, H. W., Effect of Variable Viscosity on Boundary Layers with a Discussion of Drag Measurements. J. Appl. Mech., Trans. ASME, Vol. 64, 1942.
11. KÁRMÁN, T. VON and TSIEN, H. S., Boundary Layer in Compressible Fluids. J. Aer. Sci. Vol. 5, 1938, pp. 227—232.
12. TIMMAN, R., A One-Parameter Method for the Calculation of Laminar Boundary Layers. N.L.L. Report F. 35 (1949).
13. SAUER, S., Theoretische Einführung in die Gasdynamik. Springer, Berlin (1943).
14. MANGLER, W., Zusammenhang zwischen ebenen und rotationssymmetrischen Grenzschichten in kompressiblen Flüssigkeiten. Z.A.M.M. Bd. 28, nr. 4 (1948), S. 97.
15. SCHÄFER, M., Charakteristikenverfahren und Verdichtungsstösze. A.V.A.-Monographie C. 4. I.
16. TOLLMIEN, W. und SCHÄFER, M., Rotationssymetrische Überschallströmungen. L.G.L.-Bericht 139 II. T. (1941) S. 5.

APPENDIX.

The calculation of some integrals.

Putting

$$\int_\xi^\infty e^{-y^2} dy = A \qquad \xi^u e^{-\xi^2} = B_u$$

gives

$$E_u = \int_0^\infty B_u d\xi = \begin{cases} \frac{1}{2}\,(n!) & u = 2n+1 \\ \frac{1}{2}\sqrt{\pi}\,\frac{1.3.5\ldots.(2n-1)}{2^n} & \text{for } u = 2n > 0 \\ \frac{1}{2}\sqrt{\pi} & u = 0 \end{cases}$$

$$E_{u,v} = \int_0^\infty B_u B_v d\xi = \left(\frac{1}{\sqrt{2}}\right)^{u+v+1} \int_0^\infty B_{u+v}\, d\xi = \left(\frac{1}{\sqrt{2}}\right)^{u+v+1} E_{u+v}$$

$$E_{u,v,w} = \int_0^\infty B_u B_v B_w d\xi = \left(\frac{1}{\sqrt{3}}\right)^{u+v+w+1} \int_0^\infty B_{u+v+w}\, d\xi = \left(\frac{1}{\sqrt{3}}\right)^{u+v+w+1} E_{u+v+w}$$

$$I_1 = \int_0^\infty A d\xi = \tfrac{1}{2}$$

$$I_2 = \int_0^\infty A^2 d\xi = 2\int_0^\infty \xi\, e^{-\xi^2} A d\xi = -\left[e^{-\xi^2} A\right]_0^\infty - \int_0^\infty e^{-2\xi^2}\, d\xi = \tfrac{1}{2}\sqrt{\pi}\,(1-\tfrac{1}{2}\sqrt{2})$$

$$I_3 = \int_0^\infty A^3 d\xi = 3\int_0^\infty \xi\, e^{-\xi^2} A^2 d\xi = -\left[\tfrac{3}{2}A^2\right]_0^\infty - 3\int_0^\infty e^{-2\xi^2} A d\xi =$$

$$= \frac{3\pi}{8} - \frac{3}{\sqrt{2}}\int_0^\infty e^{-\xi^2} d\xi \int_{\xi/\sqrt{2}}^\infty e^{-y^2}\, dy \,{}^{*)} = \frac{3\pi}{8} - \frac{3}{\sqrt{2}}\int_{r=0}^{\infty}\int_{\theta=0}^{\operatorname{arc\,tg}\sqrt{2}} e^{-r^2}\, r dr d\theta = \frac{3\pi}{8} - \frac{3\operatorname{arc\,tg}\sqrt{2}}{2\sqrt{2}}$$

$$I_{1,u} = \int_0^\infty A B_u d\xi \,{}^{*)} = \int_{r=0}^{\infty}\int_{\theta=0}^{\frac{\pi}{4}} e^{-r^2} r^{u+1} \sin^u \theta\, dr\, d\theta = E_{u+1}\int_0^{\frac{\pi}{4}} \sin^u \theta d\theta$$

$$I_{2,u} = \int_0^\infty A^2 B_u d\xi = \frac{u-1}{2}\, I_{2,\,u-2} - \int_0^\infty \xi^{u-1}\, e^{-2\xi^2} A d\xi \,{}^{*)} =$$

$$= \frac{u-1}{2}\, I_{2,\,u-2} - \left(\frac{1}{\sqrt{2}}\right)^u \int_{r=0}^{\infty}\int_{\theta=0}^{\operatorname{arc\,tg}\sqrt{2}} e^{-r^2} r^u \sin^{u-1}\theta\, dr\, d\theta =$$

$$= \frac{u-1}{2}\, I_{2,\,u-2} - \left(\frac{1}{\sqrt{2}}\right)^u E_u \int_{\theta=0}^{\operatorname{arc\,tg}\sqrt{2}} \sin^{u-1}\theta d\theta.$$

$$I_{2,1} = \int_0^\infty A^2 B_1 d\xi = \tfrac{1}{3} I_3 = \frac{\pi}{8} - \frac{\operatorname{arc\,tg}\sqrt{2}}{2\sqrt{2}}.$$

$$I_{2,0} = \int_0^\infty A^2 B_0 d\xi = \int_0^\infty e^{-\xi^2} d\xi \int_\xi^\infty e^{-y^2}\, dy \int_\xi^\infty e^{-z^2}\, dz \,{}^{**)} = 2\int_{r=0}^{\infty}\int_{\psi=0}^{\frac{\pi}{4}}\int_{\theta=0}^{\operatorname{arc\,tg}\sin\psi} e^{-r^2}\, r^2 \cos\theta\, dr d\theta\, d\psi =$$

$$= \frac{\sqrt{\pi}}{2}\int_{\psi=0}^{\frac{\pi}{4}} \frac{\sin\psi}{\sqrt{1+\sin^2\psi}}\, d\psi = \frac{1}{24}\,\pi^{3/2}.$$

$$I_{1,u,v} = \int_0^\infty A B_u B_v d\xi = \int_0^\infty e^{-2\xi^2}\, \xi^{u+v} A d\xi = \left(\frac{1}{\sqrt{2}}\right)^{u+v+1} E_{u+v+1}\int_{\theta=0}^{\operatorname{arc\,tg}\sqrt{2}} \sin^{u+v}\, \theta d\theta.$$

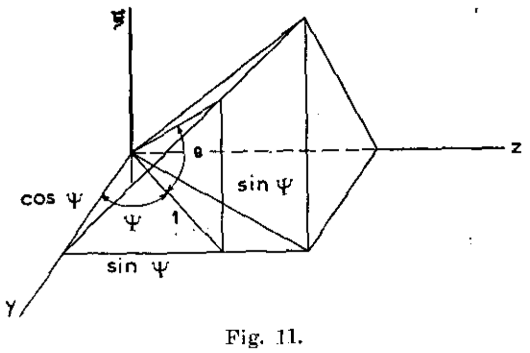

Fig. 11.

---

*) Introducing polar coordinates $\xi = r\sin\theta$, $y = r\cos\theta$.

**) Introducing sphero-coordinates
$y = r\cos\theta\cos\psi$
$z = r\cos\theta\sin\psi$
$\xi = r\sin\theta$.

Putting,

$$E_u = E'_u\,,\ E_{u,v} = E''_{u+v}\,,\ E_{u,v,w} = E'''_{u+v+w}\,,\ I_{1,u,v} = I'_{1,\,u+v}$$

gives in particular

$$E'_0 = \frac{\sqrt{\pi}}{2}\ ;\ E'_1 = \tfrac{1}{2};\ E'_2 = \frac{\sqrt{\pi}}{4};\ E'_3 = \tfrac{1}{2};\ E'_4 = \frac{3\sqrt{\pi}}{8}\ ;\ E'_5 = 1;\ E'_6 = \frac{15\sqrt{\pi}}{16}\ ;\ E'_7 = 3.$$

$$E''_0 = \frac{\sqrt{2\pi}}{4}\,;\ E''_1 = \tfrac{1}{4};\ E''_2 = \frac{\sqrt{2\pi}}{16}\ ;\ E''_3 = \tfrac{1}{8};\ E''_4 = \frac{3\sqrt{2\pi}}{64}\ ;\ E''_5 = \tfrac{1}{8};\ E''_6 = \frac{15\sqrt{2\pi}}{256}.$$

$$E'''_0 = \frac{\sqrt{3\pi}}{6};\ E'''_1 = \tfrac{1}{6};\ E'''_2 = \frac{\sqrt{3\pi}}{36};\ E'''_3 = \tfrac{1}{18};\ E'''_4 = \frac{\sqrt{3\pi}}{72};\ E'''_5 = \tfrac{1}{27};\ E'''_6 = \frac{5\sqrt{3\pi}}{432}.$$

$$I_1 = \tfrac{1}{2};\ I_2 = \frac{\sqrt{\pi}}{2}\left(1 - \frac{\sqrt{2}}{2}\right)\ ;\ I_3 = \frac{3\pi}{8} - \frac{3\operatorname{arc\,tg}\sqrt{2}}{2\sqrt{2}}.$$

$$I_{1,0} = \frac{\pi}{8};\ I_{1,1} = \frac{\sqrt{\pi}}{4}\left(1 - \frac{\sqrt{2}}{2}\right)\ ;\ I_{1,2} = \frac{\pi}{16} - \tfrac{1}{8}\ ;\ I_{1,3} = \frac{\sqrt{\pi}}{4}\left(1 - \frac{5\sqrt{2}}{8}\right).$$

$$I_{2,0} = \tfrac{1}{24}\,\pi^{3/2}\ ;\ I_{2,1} = \frac{\pi}{8} - \frac{\operatorname{arc\,tg}\sqrt{2}}{2\sqrt{2}};\ I_{2,2} = \tfrac{1}{48}\,\pi^{3/2} - \frac{\sqrt{\pi}}{8}\left(1 - \frac{\sqrt{3}}{3}\right)\ ;$$

$$I_{2,3} = \frac{\pi}{8} - \frac{5\sqrt{2}}{16}\operatorname{arc\,tg}\sqrt{2} + \frac{1}{24}\,;$$

$$I'_{1,0} = \frac{\sqrt{2}\operatorname{arc\,tg}\sqrt{2}}{4}\ ;\ I'_{1,1} = \frac{\sqrt{\pi}}{8}\left(1 - \frac{\sqrt{3}}{3}\right)\ ;\ I'_{1,2} = \frac{\sqrt{2}\operatorname{arc\,tg}\sqrt{2}}{16} - \tfrac{1}{24}\ ;\ I'_{1,3} = \frac{\sqrt{\pi}}{16}\left(1 - \frac{4\sqrt{3}}{9}\right);$$

$$I'_{1,4} = \frac{3\sqrt{2}\operatorname{arc\,tg}\sqrt{2}}{64} - \frac{13}{288};\ I'_{1,5} = \frac{\sqrt{\pi}}{16}\left(1 - \frac{\sqrt{3}}{2}\right);\ I'_{1,6} = \frac{15\sqrt{2}\operatorname{arc\,tg}\sqrt{2}}{256} - \frac{227}{3456}.$$

F 32

C. C. L. Class. D 410

REPORT F. 151

Tables of Aerodynamic Coefficients for an Oscillating Wing-Flap System in a Subsonic Compressible Flow.

Summary.

This report contains the numerical results for the aerodynamic coefficients of an oscillating wing-flap system, where the flap hinge axis coincides with the flap nose. The complete set of 9 complex coefficients is given for the Mach numbers $\beta = 0.35$, 0.5, 0.6, 0.7, 0.8. *The ratio of flap to wing chord is* 0.1, 0.2, 0.3. *Exact calculations have been made for 9 or 10 values of the reduced frequency* ω *in case of the wing coefficients and for 7 or 8* ω*-values in case of the flap coefficients. Interpolated values are presented for* $\omega = 0$ (0.02), 0.90 *if* $\beta = 0.8$ *and for* $\omega = 0$ (0.02), 1 *for all other* β*-values.*

Contents.

This investigation has been performed by order of the Netherlands Aircraft Development Board (N. I. V.).

1 Introduction.

The numerical results presented in this report have been obtained by aid of an analytical method originally developed by TIMMAN in his thesis and described in full detail in N.L.L.-Report F. 54 by TIMMAN and VAN DE VOOREN. The numerical computations of the basic points of which the results are presented in tables 1 through 4 have been carried out at the Mathematical Centre under the direction of VAN WIJNGAARDEN and with the assistance first of SCHEEN and later of BERGHUIS. The interpolated results of tables 5 through 28 have been calculated for the greater part at the N.L.L. under the direction of BURGERHOUT and WOUTERS by Miss GRAVESTEIN and Miss PIJL and for a small part at the Mathematical Centre.

The interpolation has been carried out in view of flutter calculations to be made for tapered wings. In such case it is usual practice at the N.L.L. to introduce TAYLOR expansions for the aerodynamic coefficients toward the reduced frequency. When using the GALERKIN method, the generalized aerodynamic forces assume the form

$$\nu^2 e^{i\nu t} \int_0^b m_L z^2 \frac{k_a}{\omega^2} \, l^2 dy \qquad (1.1)$$

where $m_L = \pi \rho l^2$ denotes the mass of air in the surrounding cylinder and zl the amplitude of translation at the elastic axis. The integration is over the span. Similar expressions are obtained in connection with the other coefficients.

Let now l_0 be the semi-chord in the reference section and ω_0 a value of the reduced frequency in that section. Then

$$\frac{l}{\omega} = \frac{l_0}{\omega_0}$$

is constant along the span.

For the aerodynamic coefficients the following expansions are used:

$$k_a(\omega) = k_a(\omega_0) + \\ + (\omega - \omega_0) \frac{dk_a}{d\omega}(\omega_0) + \tfrac{1}{2}(\omega - \omega_0)^2 \frac{d^2k_a}{d\omega^2}(\omega_0) + \ldots\ldots$$

The calculation of the expression (1.1) then can be separated into the calculation of, for instance, 3 terms, viz.

$$\nu^2 \frac{l_0^2}{\omega_0^2} k_a(\omega_0) \int_0^b m_L z^2 dy,$$

$$\nu^2 \frac{l_0^2}{\omega_0} \frac{dk_a}{d\omega} (\omega_0) \int_0^b m_L z^2 \xi \, dy,$$

$$\tfrac{1}{2} \nu^2 l_0^2 \frac{d^2 k_a}{d\omega^2} (\omega_0) \int_0^b m_L z^2 \xi^2 \, dy,$$

where $\xi = \frac{\omega - \omega_0}{\omega_0} = \frac{l - l_0}{l_0}$.

The advantage of this method is that all integrals become independent of the reduced frequency.

The values of the derivatives $\frac{dk_a}{d\omega}$ and $\frac{d^2k_a}{d\omega^2}$ are easily obtained from the tables 5 through 28 by aid of the formulae

$$\frac{dk_a}{d\omega} (\omega_0) = 25 \{ k_a(\omega_0 + 0.02) - k_a(\omega_0 - 0.02) \},$$

$$\frac{d^2k_a}{d\omega^2} (\omega_0) = 2500 \{ k_a(\omega_0 + 0.02) - 2\, k_a(\omega_0) + k_a(\omega_0 - 0.02) \}.$$

Completed May 1954.

TA

Table of aerodynamic coefficients for an oscillating wi

	ω	k_a'	k_a''	m_a'	m_a''	k_b'
$\beta = 0.35$	0.12536	— 0.03780	— 0.20708	0.02805	0.10310	— 1.68001
	0.25071	— 0.04504	— 0.35479	0.05835	0.17531	— 1.47348
	0.37607	— 0.00721	— 0.48870	0.08358	0.23923	— 1.38307
	0.50143	+ 0.07066	— 0.62280	0.10669	0.30135	— 1.34873
	0.62679	0.18513	— 0.76311	0.13000	0.36391	— 1.34751
	0.75214	0.33416	— 0.91357	0.15526	0.42783	— 1.36988
	1.00286	0.73149	— 1.25889	0.21672	0.56101	— 1.47202
	1.25357	1.25435	— 1.68831	0.30040	0.70093	— 1.64720
	1.88036	2.98984	— 3.35837	0.66249	1.04848	— 2.44851
	3.25929	5.65269	— 10.76088	2.26230	0.94136	— 5.56393
$\beta = 0.50$	0.150	— 0.05383	— 0.24597	0.04232	0.12124	— 1.68214
	0.300	— 0.05380	— 0.41753	0.08578	0.20097	— 1.47756
	0.450	+ 0.00624	— 0.58574	0.12756	0.27335	— 1.42920
	0.600	0.11518	— 0.76998	0.17467	0.34475	— 1.45797
	0.750	0.26531	— 0.98147	0.23215	0.41567	— 1.54078
	0.900	0.44865	— 1.22993	0.30397	0.48419	— 1.67055
	1.125	0.76270	— 1.69025	0.44459	0.57369	— 1.94698
	1.650	1.40780	— 3.20087	0.91373	+ 0.61429	— 2.85365
	3.000	1.59994	— 6.94061	1.45510	— 0.56677	— 3.76865
$\beta = 0.60$	0.10667	— 0.04943	— 0.19575	0.03421	0.09633	— 1.86936
	0.21333	— 0.07629	— 0.32752	0.07321	0.15689	— 1.60844
	0.32000	— 0.06854	— 0.44809	0.11022	0.20770	— 1.51052
	0.42667	— 0.03375	— 0.57275	0.14944	0.25486	— 1.49181
	0.53333	+ 0.02225	— 0.70847	0.19407	0.29938	— 1.52246
	0.64000	0.09424	— 0.85986	0.24636	0.34027	— 1.58989
	0.80000	0.22008	— 1.12305	0.34174	0.38986	— 1.74558
	0.96000	0.34792	— 1.43253	0.45668	0.41609	— 1.94892
	1.17333	0.48458	— 1.90226	0.62640	0.39739	— 2.24764
	1.70667	0.60559	— 3.05676	0.92567	+ 0.08932	— 2.71678
	3.20000	1.39471	— 6.71096	0.66588	— 0.47911	— 2.76302
$\beta = 0.70$	0.10929	— 0.06374	— 0.20732	0.04436	0.10039	— 1.94140
	0.21857	— 0.09728	— 0.34027	0.09261	0.15628	— 1.64938
	0.36429	— 0.09030	— 0.50905	0.15803	0.21277	— 1.55542
	0.54643	— 0.03728	— 0.74653	0.25654	0.26037	— 1.62288
	0.65571	+ 0.00165	— 0.90813	0.32502	0.27047	— 1.71004
	0.80143	0.04668	— 1.13908	0.41820	0.25499	— 1.83952
	0.94714	0.07896	— 1.37216	0.49782	0.20710	— 1.94657
	1.16571	0.12721	— 1.69741	0.56441	+ 0.10281	— 2.02057
	1.74857	0.49529	— 2.64753	0.54909	— 0.06614	— 2.06328
$\beta = 0.80$	0.1125	— 0.08660	— 0.21965	0.06102	0.10194	— 2.01344
	0.2250	— 0.12970	— 0.35128	0.12165	0.14414	— 1.68292
	0.3375	— 0.14245	— 0.47812	0.18204	0.16501	— 1.59870
	0.4950	— 0.14150	— 0.66100	0.26228	0.15755	— 1.59763
	0.5850	— 0.13596	— 0.76387	0.29605	0.13686	— 1.60182
	0.7200	— 0.11381	— 0.91241	0.32198	0.10109	— 1.58923
	0.9000	— 0.04437	— 1.12005	0.33094	0.07604	— 1.57545
	1.0800	+ 0.04905	— 1.37509	0.35439	+ 0.07442	— 1.62762
	1.8000	0.31751	— 2.51642	0.43858	— 0.09528	— 1.83661

1.

ithout control surface in a subsonic compressible flow.

k_b''	m_b'	m_b''
0.19841	0.83864	— 0.23938
— 0.00434	0.73659	— 0.28036
— 0.22005	0.69553	— 0.30712
— 0.44226	0.68462	— 0.33724
— 0.65928	0.69158	— 0.37303
— 0.87210	0.71078	— 0.41456
— 1.29041	0.77549	— 0.51389
— 1.70144	0.86627	— 0.63481
— 2.63852	1.16267	— 1.04038
— 2.67570	1.74483	— 2.33709
— 0.23763	0.83270	— 0.30922
— 0.02165	0.72370	— 0.36423
— 0.28722	0.69241	— 0.42089
— 0.53672	0.69439	— 0.49342
— 0.76941	0.71295	— 0.58283
— 0.98266	0.73908	— 0.68912
— 1.25161	0.77776	— 0.87868
— 1.46749	0.77221	— 1.40931
+ 0.03345	0.36345	— 2.24191
0.36713	0.92205	— 0.34021
0.20071	0.77758	— 0.40274
+ 0.00648	0.71360	— 0.45219
— 0.17577	0.68429	— 0.51160
— 0.34110	0.67083	— 0.58393
— 0.48751	0.66319	— 0.66899
— 0.66495	0.64819	— 0.81726
— 0.77849	0.61444	— 0.98228
— 0.81037	0.52431	— 1.20300
— 0.44410	0.15748	— 1.55086
+ 0.04326	0.14946	— 1.68445
0.48289	0.94266	— 0.43431
0.28887	0.76434	— 0.50798
+ 0.03511	0.65995	— 0.60981
— 0.19215	0.56929	— 0.78017
— 0.27299	0.50157	— 0.89374
— 0.31322	0.38165	— 1.03431
— 0.29046	0.23596	— 1.13722
— 0.21190	+ 0.02337	— 1.19746
— 0.21709	— 0.16975	— 1.12835
0.66787	0.93719	— 0.59020
0.43232	0.69110	— 0.67578
0.25706	0.53640	— 0.77544
0.12830	0.31465	— 0.90164
0.09553	0.18194	— 0.93528
+ 0.05702	+ 0.01564	— 0.92375
— 0.02672	— 0.09456	— 0.86194
— 0.11982	— 0.11059	— 0.84291
— 0.08111	— 0.20169	— 0.97367

Definition coefficients:

$$K = \pi \rho_0 l v^2 e^{i\nu t} \; (A k_a + B k_b)$$

$$M = \pi \rho_0 l^2 v^2 e^{i\nu t} \; (A m_a + B m_b)$$

K aerodynamic force, positive downward.

M ,, moment about mid-chord point, positive tailheavy.

ρ_0 air density (in undisturbed state).

l semi-chord.

v speed of flight.

β Mach number, v/c

ν frequency of the vibration.

ω reduced frequency, $\nu l/v$

t time.

Al amplitude of translation in mid-chord point, positive downward.

B amplitude of rotation, positive if trailing edge downward.

k_a', k_a'', real and imaginary part of k_a, etc.

All data contained in the table should be accurate within a few units of the last digit.

Table of aerodynamic coefficients for an oscillating wi

	ω	k_c'	k_c''	m_c'	m_c''	n_a'	n_a''	n_b'
$\beta = 0.35$	0	−0.84509	0	+0.05556	0	0	0	−0.00234
	0.12536	−0.65388	0.15852	−0.04159	−0.09192	0.00002	−0.00023	−0.00183
	0.25071	−0.55949	0.15062	−0.09101	−0.09911	0.00017	−0.00040	−0.00152
	0.37607	−0.51137	0.12812	−0.11758	−0.09839	0.00049	−0.00056	−0.00126
	0.50143	−0.48473	0.10652	−0.13373	−0.09774	0.00096	−0.00072	−0.00100
	0.62679	−0.46940	0.08800	−0.14462	−0.09832	0.00159	−0.00089	−0.00072
	0.75214	−0.46069	0.07251	−0.15262	−0.10008	0.00237	−0.00108	−0.00041
	1.00286	−0.45447	0.04928	−0.16435	−0.10639	0.00444	−0.00156	+0.00032
$\beta = 0.50$	0	−0.91410	0	+0.06010	0	0	0	−0.00254
	0.15	−0.64459	0.19958	−0.07994	−0.11410	0.00004	−0.00028	−0.00184
	0.3	−0.53841	0.18379	−0.13999	−0.11524	0.00031	−0.00049	−0.00149
	0.45	−0.49080	0.16329	−0.17155	−0.11161	0.00083	−0.00071	−0.00121
	0.6	−0.46593	0.14992	−0.19262	−0.10938	0.00160	−0.00096	−0.00092
	0.75	−0.45103	0.14365	−0.20933	−0.10830	0.00262	−0.00127	−0.00062
	0.9	−0.44012	0.14342	−0.22424	−0.10748	0.00389	−0.00168	−0.00034
	1.125	−0.42389	0.15176	−0.24523	−0.10502	0.00629	−0.00258	+0.00001
$\beta = 0.60$	0	−0.98955	0	+0.06506	0	0	0	−0.00274
	0.10667	−0.71879	0.23408	−0.07681	−0.12732	0.00001	−0.00022	−0.00209
	0.21333	−0.58977	0.23677	−0.14969	−0.13186	0.00014	−0.00039	−0.00177
	0.32	−0.52336	0.22335	−0.19134	−0.12502	0.00041	−0.00055	−0.00155
	0.42667	−0.48358	0.21294	−0.21974	−0.11699	0.00081	−0.00073	−0.00137
	0.53333	−0.45599	0.20770	−0.24176	−0.10882	0.00136	−0.00094	−0.00120
	0.64	−0.43370	0.20697	−0.26032	−0.10007	0.00204	−0.00119	−0.00105
	0.8	−0.40228	0.21148	−0.28381	−0.08457	0.00331	−0.00169	−0.00090
	0.96	−0.36757	0.21774	−0.30224	−0.06504	0.00486	−0.00240	−0.00085
	1.17333	−0.31346	0.21848	−0.31639	−0.03330	0.00724	−0.00377	−0.00096
$\beta = 0.70$	0	−1.10851	0	+0.07288	0	0	0	−0.00308
	0.10929	−0.73556	0.29229	−0.12682	−0.15284	0.00001	−0.00024	−0.00223
	0.21857	−0.57539	0.29435	−0.22160	−0.14482	0.00018	−0.00043	−0.00190
	0.36429	−0.47408	0.27785	−0.28768	−0.11266	0.00066	−0.00070	−0.00166
	0.54643	−0.39290	0.26941	−0.33477	−0.06316	0.00165	−0.00115	−0.00151
	0.65571	−0.34831	0.26452	−0.34942	−0.02870	0.00244	−0.00153	−0.00153
	0.80143	−0.28996	0.24883	−0.35166	+0.01937	0.00368	−0.00221	−0.00166
	0.94714	−0.23901	0.21771	−0.33419	+0.06219	0.00507	−0.00309	−0.00188
	1.16571	−0.19503	0.14962	−0.28311	0.10071	0.00734	−0.00476	−0.00211
$\beta = 0.80$	0	−1.31940	0	+0.08674	0	0	0	−0.00366
	0.1125	−0.72595	0.39872	−0.24003	−0.18730	0.00002	−0.00028	−0.00247
	0.225	−0.52026	0.37259	−0.36216	−0.12208	0.00026	−0.00052	−0.00218
	0.3375	−0.40548	0.34238	−0.41409	−0.03760	0.00069	−0.00079	−0.00210
	0.495	−0.29169	0.28780	−0.40561	+0.08224	0.00159	−0.00133	−0.00225
	0.585	−0.24837	0.24459	−0.36545	0.13235	0.00223	−0.00173	−0.00243
	0.72	−0.22134	0.17679	−0.28556	0.16120	0.00331	−0.00246	−0.00270
	0.9	−0.23772	0.12153	−0.20540	0.12798	0.00501	−0.00365	−0.00292

2.

eron system ($\tau = 0.1$) in a subsonic compressible flow.

n_b''	n_c'	n_c''
0	— 0.00601	0
— 0.00065	— 0.00581	— 0.00021
— 0.00172	— 0.00571	— 0.00058
— 0.00283	— 0.00566	— 0.00098
— 0.00395	— 0.00564	— 0.00137
— 0.00508	— 0.00562	— 0.00176
— 0.00622	— 0.00561	— 0.00214
— 0.00857	— 0.00561	— 0.00291
0	— 0.00650	0
— 0.00092	— 0.00623	— 0.00030
— 0.00236	— 0.00615	— 0.00080
— 0.00383	— 0.00613	— 0.00130
— 0.00533	— 0.00615	— 0.00179
— 0.00688	— 0.00618	— 0.00228
— 0.00848	— 0.00622	— 0.00274
— 0.01092	— 0.00629	— 0.00344
0	— 0.00704	0
— 0.00057	— 0.00678	— 0.00017
— 0.00167	— 0.00668	— 0.00055
— 0.00281	— 0.00667	— 0.00094
— 0.00396	— 0.00667	— 0.00132
— 0.00514	— 0.00670	— 0.00168
— 0.00635	— 0.00675	— 0.00204
— 0.00820	— 0.00681	— 0.00255
— 0.01004	— 0.00689	— 0.00305
— 0.01233	— 0.00696	— 0.00372
0	— 0.00788	0
— 0.00068	— 0.00755	— 0.00020
— 0.00199	— 0.00748	— 0.00064
— 0.00378	— 0.00751	— 0.00121
— 0.00608	— 0.00761	— 0.00186
— 0.00747	— 0.00769	— 0.00221
— 0.00925	— 0.00774	— 0.00269
— 0.01085	— 0.00778	— 0.00321
— 0.01291	— 0.00785	— 0.00414
0	— 0.00938	0
— 0.00091	— 0.00893	— 0.00026
— 0.00259	— 0.00893	— 0.00079
— 0.00427	— 0.00904	— 0.00123
— 0.00659	— 0.00915	— 0.00177
— 0.00781	— 0.00916	— 0.00210
— 0.00948	— 0.00916	— 0.00271
— 0.01156	— 0.00924	— 0.00376

Definition coefficients:

$$K = \pi \rho_0 l v^2 e^{i\nu t} \, (A k_a + B k_b + C k_c)$$

$$M = \pi \rho_0 l^2 v^2 e^{i\nu t} \, (A m_a + B m_b + C m_c)$$

$$N = \pi \rho_0 l^2 v^2 e^{i\nu t} \, (A n_a + B n_b + C n_c)$$

K aerodynamic force of wing + aileron, positive downward.

M aerodynamic moment of wing + aileron about mid-chord point, positive tailheavy.

N aerodynamic moment of aileron about hinge axis (= nose), positive tailhavy.

ρ_0 air density (in undisturbed state).

l semi-chord.

v speed of flight.

β Mach number, v/c

ν frequency of the vibration.

ω reduced frequency, $\nu l/v$

τ ratio between aileron chord and total chord.

t time.

Al amplitude of translation in mid-chord point, positive downward.

B amplitude of wing rotation, positive if trailing edge is downward.

C amplitude of aileron rotation, positive if trailing edge is downward.

k_c', k_c'', real and imaginary part of k_c, etc.

All data contained in the table should be accurate within a few units of the last digit.

Table of aerodynamic coefficients for an oscillating wi

	ω	k_c'	k_c''	m_c'	m_c''	n_a'	n_a''	n_b'
$\beta = 0.35$	0	— 1.17388	0	+ 0.15199	0	0	0	— 0.01358
	0.12536	— 0.91297	0.19450	+ 0.01964	— 0.13136	0.00007	— 0.00133	— 0.01061
	0.25071	— 0.78637	0.16296	— 0.04614	— 0.14780	0.00092	— 0.00231	— 0.00888
	0.37607	— 0.72308	0.11245	— 0.08034	— 0.15417	0.00266	— 0.00322	— 0.00756
	0.50143	*— 0.68919*	*0.06340*	*— 0.10009*	*— 0.16109*	*0.00525*	*— 0.00416*	*— 0.00627*
	0.62679	— 0.67082	+ 0.01843	— 0.11248	— 0.17000	0.00871	— 0.00517	— 0.00489
	0.75214	— 0.66178	— 0.02265	— 0.12070	— 0.18089	0.01304	— 0.00631	— 0.00339
	1.00286	— 0.66089	— 0.09518	— 0.13054	— 0.20755	0.02441	— 0.00915	— 0.00001
$\beta = 0.50$	0	— 1.26974	0	+ 0.16440	0	0	0	— 0.01468
	0.15	— 0.90334	0.24476	— 0.02588	— 0.16578	0.00018	— 0.00161	— 0.01071
	0.3	— 0.76430	0.19812	— 0.10488	— 0.17933	0.00166	— 0.00283	— 0.00886
	0.45	— 0.70658	0.14644	— 0.14490	— 0.18807	0.00450	— 0.00411	— 0.00747
	0.6	*— 0.68191*	*0.10509*	*— 0.17071*	*— 0.20014*	*0.00871*	*— 0.00560*	*— 0.00619*
	0.75	— 0.67338	0.07430	— 0.19108	— 0.21525	0.01431	— 0.00749	— 0.00498
	0.9	— 0.67346	0.05335	— 0.20980	— 0.23233	0.02133	— 0.00997	— 0.00395
	1.125	— 0.67958	0.03909	— 0.23892	— 0.25898	0.03442	— 0.01541	— 0.00304
$\beta = 0.60$	0	— 1.37454	0	+ 0.17797	0	0	0	— 0.01590
	0.10667	— 1.00597	0.29841	— 0.01526	— 0.18338	0.00001	— 0.00129	— 0.01211
	0.21333	— 0.83551	0.28301	— 0.11249	— 0.20078	0.00071	— 0.00225	— 0.01035
	0.32	— 0.75206	0.24748	— 0.16727	— 0.20431	0.00218	— 0.00321	— 0.00927
	0.42667	*— 0.70658*	*0.21742*	*— 0.20458*	*— 0.20768*	*0.00440*	*— 0.00426*	*— 0.00847*
	0.53333	— 0.67957	0.19578	— 0.23423	— 0.21212	0.00736	— 0.00550	— 0.00783
	0.64	— 0.66178	0.18223	— 0.26059	— 0.21698	0.01108	— 0.00702	— 0.00741
	0.8	— 0.64111	0.17471	— 0.29800	— 0.22263	0.01802	— 0.01008	— 0.00729
	0.96	— 0.61786	0.17823	— 0.33434	— 0.22319	0.02641	— 0.01444	— 0.00798
	1.17333	— 0.57117	0.19047	— 0.37858	— 0.21300	0.03917	— 0.02283	— 0.01014
$\beta = 0.70$	0	— 1.53979	0	+ 0.19937	0	0	0	— 0.01781
	0.10929	— 1.02974	0.38328	— 0.07450	— 0.22748	0.00002	— 0.00141	— 0.01293
	0.21857	*— 0.82444*	*0.35948*	*— 0.19994*	*— 0.23139*	*0.00092*	*— 0.00250*	— 0.01119
	0.36429	— 0.70298	0.31773	— 0.29161	— 0.21685	0.00350	— 0.00410	— 0.01017
	0.54643	— 0.61825	0.29363	— 0.36910	— 0.18960	0.00886	— 0.00686	— 0.01016
	0.65571	— 0.57309	0.28747	— 0.40492	— 0.16533	0.01311	— 0.00920	— 0.01090
	0.80143	— 0.50821	0.27632	— 0.43791	— 0.12286	0.01970	— 0.01340	— 0.01277
	0.94714	— 0.44021	0.24976	— 0.44924	— 0.07423	0.02695	*— 0.01892*	*— 0.01526*
	1.16571	— 0.35636	0.17148	— 0.42562	— 0.01100	0.03844	— 0.02929	— 0.01868
$\beta = 0.80$	0	— 1.83272	0	+ 0.23730	0	0	0	— 0.02120
	0.1125	*— 1.02975*	*0.51868*	*— 0.20837*	*— 0.28527*	*0.00008*	*— 0.00161*	— 0.01436
	0.225	— 0.76584	0.46939	— 0.38050	— 0.23361	0.00132	— 0.00299	— 0.01296
	0.3375	— 0.62644	0.42561	— 0.47214	— 0.15676	0.00362	— 0.00467	— 0.01305
	0.495	— 0.48374	0.36409	— 0.51612	— 0.02671	0.00835	— 0.00799	— 0.01506
	0.585	— 0.41958	0.31487	— 0.49731	+ 0.04277	0.01161	— 0.01053	— 0.01694
	0.72	— 0.36088	0.22362	— 0.42597	0.10888	0.01702	— 0.01513	— 0.01996
	0.9	— 0.36070	0.11472	— 0.31688	0.10739	0.02524	— 0.02271	— 0.02347

E 3.

leron system ($\tau = 0.2$) in a subsonic compressible flow.

n_b''	n_c'	n_c''
0	— 0.02509	0
— 0.00347	— 0.02346	— 0.00161
— 0.00936	— 0.02265	— 0.00459
— 0.01547	— 0.02219	— 0.00768
— 0.02164	— 0.02187	— 0.01075
— 0.02787	— 0.02161	— 0.01381
— 0.03419	— 0.02136	— 0.01686
— 0.04718	— 0.02087	— 0.02293
0	— 0.02714	0
— 0.00492	— 0.02498	— 0.00230
— 0.01283	— 0.02426	— 0.00627
— 0.02094	— 0.02401	— 0.01023
— 0.02925	— 0.02395	— 0.01411
— 0.03781	— 0.02401	— 0.01792
— 0.04662	— 0.02414	— 0.02165
— 0.06015	— 0.02442	— 0.02709
0	— 0.02938	0
— 0.00297	— 0.02729	— 0.00128
— 0.00899	— 0.02651	— 0.00429
— 0.01525	— 0.02627	— 0.00735
— 0.02163	— 0.02628	— 0.01033
— 0.02813	— 0.02644	— 0.01322
— 0.03479	— 0.02670	— 0.01601
— 0.04495	— 0.02719	— 0.02001
— 0.05505	— 0.02771	— 0.02376
— 0.06755	— 0.02821	— 0.02843
0	— 0.03291	0
— 0.00349	— 0.03024	— 0.00149
— 0.01067	— 0.02960	— 0.00500
— 0.02051	— 0.02980	— 0.00946
— 0.03313	— 0.03063	— 0.01444
— 0.04070	— 0.03122	— 0.01711
— 0.05029	— 0.03184	— 0.02038
— 0.05881	— 0.03216	— 0.02355
— 0.06942	— 0.03223	— 0.02873
0	— 0.03917	0
— 0.00465	— 0.03550	— 0.00194
— 0.01382	— 0.03545	— 0.00609
— 0.02300	— 0.03628	— 0.00954
— 0.03540	— 0.03749	— 0.01329
— 0.04183	— 0.03786	— 0.01521
— 0.05034	— 0.03805	— 0.01842
— 0.06060	— 0.03871	— 0.02359

Definition coefficients:

$$K = \pi\rho_0 l v^2 e^{i\nu t}\ (Ak_a + Bk_b + Ck_c)$$

$$M = \pi\rho_0 l^2 v^2 e^{i\nu t}\ (Am_a + Bm_b + Cm_c)$$

$$N = \pi\rho_0 l^2 v^2 e^{i\nu t}\ (An_a + Bn_b + Cn_c)$$

K aerodynamic force of wing + aileron, positive downward.

M aerodynamic moment of wing + aileron about mid-chord point, positive tailheavy.

N aerodynamic moment of aileron about hinge axis (= nose), positive tailhavy.

ρ_0 air density (in undisturbed state).

l semi-chord.

v speed of flight.

β Mach number, v/c

ν frequency of the vibration.

ω reduced frequency, $\nu l/v$

τ ratio between aileron chord and total chord.

t time.

Al amplitude of translation in mid-chord point, positive downward.

B amplitude of wing rotation, positive if trailing edge is downward.

C amplitude of aileron rotation, positive if trailing edge is downward.

k_c', k_c'', real and imaginary part of k_c, etc.

All data contained in the table should be accurate within a few units of the last digit.

TA

Table of aerodynamic coefficients for an oscillating wi

	ω	k_c'	k_c''	m_c'	m_c''	n_a'	n_a''	n_b'
$\beta = 0.35$	0	−1.41072	0	+0.26935	0	0	0	−0.03838
	0.12536	−1.10247	0.20299	0.11347	−0.15888	0.00013	−0.00376	−0.03004
	0.25071	−0.95503	0.14051	0.03821	−0.18298	0.00238	−0.00652	−0.02539
	0.37607	−0.88205	+0.05669	+0.00089	−0.19604	0.00700	−0.00910	−0.02202
	0.50143	−0.84304	−0.02528	−0.01894	−0.21024	0.01394	−0.01177	−0.01891
	0.62679	−0.82205	−0.10269	−0.02953	−0.22721	0.02319	−0.01467	−0.01570
	0.75214	−0.81193	−0.17603	−0.03469	−0.24686	0.03479	−0.01792	−0.01229
	1.00286	−0.81230	−0.31355	−0.03553	−0.29307	0.06527	−0.02610	−0.00486
$\beta = 0.50$	0	−1.52593	0	+0.29135	0	0	0	−0.04151
	0.15	−1.09464	0.25527	+0.06798	−0.20313	0.00041	−0.00455	−0.03038
	0.3	−0.93624	0.16944	−0.02081	−0.22891	0.00431	−0.00801	−0.02554
	0.45	−0.87452	0.07888	−0.06281	−0.25096	0.01187	−0.01165	−0.02234
	0.6	−0.85327	+0.00050	−0.08746	−0.27859	0.02309	−0.01596	−0.01970
	0.75	−0.85359	−0.06534	−0.10529	−0.31170	0.03802	−0.02143	−0.01758
	0.9	−0.86731	−0.11910	−0.12118	−0.34918	0.05670	−0.02869	−0.01626
	1.125	−0.90296	−0.17617	−0.14726	−0.41083	0.09145	−0.04456	−0.01659
$\beta = 0.60$	0	−1.65186	0	+0.31539	0	0	0	−0.04494
	0.10667	−1.21755	0.32660	+0.08795	−0.22415	−0.00004	−0.00364	−0.03427
	0.21333	−1.02213	0.28490	−0.02341	−0.25415	+0.00179	−0.00636	−0.02952
	0.32	−0.93093	0.22147	−0.08418	−0.26987	0.00566	−0.00908	−0.02694
	0.42667	−0.88587	0.16546	−0.12444	−0.28707	0.01153	−0.01211	−0.02532
	0.53333	−0.86453	0.12040	−0.15611	−0.30731	0.01938	−0.01570	−0.02440
	0.64	−0.85639	0.08624	−0.18472	−0.32973	0.02921	−0.02015	−0.02424
	0.8	−0.85583	0.05446	−0.22797	−0.36446	0.04752	−0.02915	−0.02586
	0.96	−0.85658	0.04392	−0.27514	−0.39582	0.06949	−0.04199	−0.03017
	1.17333	−0.84309	0.05376	−0.34250	−0.42380	0.10237	−0.06653	−0.03994
$\beta = 0.70$	0	−1.85046	0	+0.35331	0	0	0	−0.05034
	0.10929	−1.25074	0.42392	+0.03119	−0.28162	−0.00002	−0.00397	−0.03658
	0.21857	−1.01876	0.37196	−0.11278	−0.30331	+0.00229	−0.00706	−0.03201
	0.36429	−0.89334	0.29671	−0.21802	−0.31487	0.00906	−0.01166	−0.03016
	0.54643	−0.82270	0.24619	−0.31509	−0.32559	0.02307	−0.01974	−0.03216
	0.65571	−0.78898	0.23401	−0.36850	−0.32389	0.03409	−0.02667	−0.03586
	0.80143	−0.73532	0.22603	−0.43260	−0.30577	0.05091	−0.03910	−0.04365
	0.94714	−0.66649	0.21065	−0.48036	−0.26971	0.06893	−0.05533	−0.05350
	1.16571	−0.55390	0.14366	−0.50633	−0.20019	0.09640	−0.08557	−0.06774
$\beta = 0.80$	0	−2.20249	0	+0.42053	0	0	0	−0.05991
	0.1125	−1.26172	0.58058	−0.10379	−0.36426	0.00009	−0.00454	−0.04059
	0.225	−0.96898	0.50308	−0.30773	−0.34078	0.00325	−0.00844	−0.03735
	0.3375	−0.82540	0.44331	−0.43049	−0.29256	0.00917	−0.01330	−0.03892
	0.495	−0.67893	0.37983	−0.53301	−0.18696	0.02107	−0.02309	−0.04728
	0.585	−0.60462	0.33409	−0.54970	−0.11474	0.02904	−0.03058	−0.05440
	0.72	−0.51665	0.23725	−0.51754	−0.02180	0.04177	−0.04412	−0.06582
	0.9	−0.48031	0.08675	−0.41466	+0.02476	0.06012	−0.06609	−0.07977

4.

eron system ($\tau = 0.3$) in a subsonic compressible flow.

n_b''	n_c'	n_c''
0	— 0.05905	0
— 0.00890	— 0.05355	— 0.00528
— 0.02468	— 0.05070	— 0.01516
— 0.04107	— 0.04891	— 0.02540
— 0.05762	— 0.04746	— 0.03564
— 0.07434	— 0.04609	— 0.04586
— 0.09130	— 0.04469	— 0.05609
— 0.12622	— 0.04164	— 0.07668
0	— 0.06387	0
— 0.01269	— 0.05657	— 0.00755
— 0.03385	— 0.05390	— 0.02069
— 0.05560	— 0.05269	— 0.03391
— 0.07786	— 0.05204	— 0.04701
— 0.10081	— 0.05171	— 0.06002
— 0.12442	— 0.05164	— 0.07295
— 0.16062	— 0.05201	— 0.09205
0	— 0.06914	0
— 0.00737	— 0.06208	— 0.00414
— 0.02346	— 0.05931	— 0.01410
— 0.04021	— 0.05830	— 0.02426
— 0.05725	— 0.05811	— 0.03429
— 0.07464	— 0.05841	— 0.04410
— 0.09240	— 0.05908	— 0.05370
— 0.11945	— 0.06063	— 0.06761
— 0.14613	— 0.06260	— 0.08074
— 0.17867	— 0.06526	— 0.09682
0	— 0.07746	0
— 0.00861	— 0.06837	— 0.00474
— 0.02774	— 0.06606	— 0.01639
— 0.05396	— 0.06644	— 0.03141
— 0.08740	— 0.06929	— 0.04854
— 0.10724	— 0.07160	— 0.05778
— 0.13198	— 0.07462	— 0.06884
— 0.15334	— 0.07685	— 0.07890
— 0.17864	— 0.07816	— 0.09407
0	— 0.09219	0
— 0.01138	— 0.07963	— 0.00610
— 0.03568	— 0.07919	— 0.01999
— 0.05980	— 0.08200	— 0.03184
— 0.09167	— 0.08711	— 0.04468
— 0.10756	— 0.08933	— 0.05065
— 0.12765	— 0.09108	— 0.05966
— 0.15037	— 0.09313	— 0.07388

Definition coefficients:

$$K = \pi\rho_0 l v^2 e^{i\nu t}\ (Ak_a + Bk_b + Ck_c)$$

$$M = \pi\rho_0 l^2 v^2 e^{i\nu t}\ (Am_a + Bm_b + Cm_c)$$

$$N = \pi\rho_0 l^2 v^2 e^{i\nu t}\ (An_a + Bn_b + Cn_c)$$

K aerodynamic force of wing + aileron, positive downward.

M aerodynamic moment of wing + aileron about mid-chord point, positive tailheavy.

N aerodynamic moment of aileron about hinge axis (= nose), positive tailhavy.

ρ_0 air density (in undisturbed state).

l semi-chord.

v speed of flight.

β Mach number, v/c

ν frequency of the vibration.

ω reduced frequency, $\nu l/v$

τ ratio between aileron chord and total chord.

t time.

Al amplitude of translation in mid-chord point, positive downward.

B amplitude of wing rotation, positive if trailing edge is downward.

C amplitude of aileron rotation, positive if trailing edge is downward.

k_c', k_c'', real and imaginary part of k_c, etc.

All data contained in the table should be accurate within a few units of the last digit.

TABLE 5.

Wing coefficients for $\beta = 0$.

ω	k_a'	k_a''	m_a'	m_a''	k_b'	k_b''	m_b'	m_b''
0	0	0	0	0	— 2.0	0	+ 1.0	0
0.02	— 0.0026	— 0.0385	+ 0.0015	+ 0.0193	— 1.9290	+ 0.1112	0.9645	— 0.0756
0.04	— 0.0077	— 0.0741	0.0046	0.0371	— 1.8580	0.1549	0.9292	— 0.1175
0.06	— 0.0135	— 0.1071	0.0086	0.0535	— 1.7926	0.1717	0.8968	— 0.1458
0.08	— 0.0193	— 0.1377	0.0128	0.0688	— 1.7337	0.1720	0.8677	— 0.1660
0.10	— 0.0245	— 0.1664	0.0172	0.0832	— 1.6811	0.1614	0.8418	— 0.1807
0.12	— 0.0288	— 0.1935	0.0216	0.0968	— 1.6343	0.1434	0.8189	— 0.1917
0.14	— 0.0322	— 0.2193	0.0259	0.1097	— 1.5926	0.1201	0.7988	— 0.2001
0.16	— 0.0344	— 0.2441	0.0300	0.1220	— 1.5556	0.0931	0.7810	— 0.2065
0.18	— 0.0355	— 0.2679	0.0340	0.1339	— 1.5225	0.0634	0.7653	— 0.2117
0.20	— 0.0355	— 0.2910	0.0377	0.1455	— 1.4929	+ 0.0317	0.7514	— 0.2159
0.22	— 0.0342	— 0.3135	0.0413	0.1568	— 1.4663	— 0.0013	0.7392	— 0.2194
0.24	— 0.0318	— 0.3355	0.0447	0.1678	— 1.4425	— 0.0353	0.7284	— 0.2223
0.26	— 0.0282	— 0.3570	0.0479	0.1785	— 1.4209	— 0.0701	0.7189	— 0.2250
0.28	— 0.0235	— 0.3781	0.0509	0.1891	— 1.4014	— 0.1054	0.7105	— 0.2274
0.30	— 0.0176	— 0.3990	0.0538	0.1995	— 1.3837	— 0.1409	0.7031	— 0.2296
0.32	— 0.0106	— 0.4196	0.0565	0.2098	— 1.3677	— 0.1766	0.6966	— 0.2317
0.34	— 0.0026	— 0.4399	0.0591	0.2200	— 1.3530	— 0.2124	0.6909	— 0.2338
0.36	+ 0.0066	— 0.4601	0.0615	0.2301	— 1.3396	— 0.2483	0.6860	— 0.2358
0.38	0.0168	— 0.4801	0.0638	0.2401	— 1.3273	— 0.2842	0.6817	— 0.2379
0.40	0.0280	— 0.5000	0.0660	0.2500	— 1.3160	— 0.3200	0.6780	— 0.2400
0.42	0.0403	— 0.5197	0.0681	0.2599	— 1.3055	— 0.3558	0.6748	— 0.2421
0.44	0.0535	— 0.5394	0.0700	0.2697	— 1.2959	— 0.3914	0.6722	— 0.2443
0.46	0.0678	— 0.5590	0.0719	0.2795	— 1.2871	— 0.4269	0.6700	— 0.2465
0.48	0.0831	— 0.5785	0.0737	0.2892	— 1.2788	— 0.4623	0.6682	— 0.2488
0.50	0.0993	— 0.5979	0.0754	0.2990	— 1.2712	— 0.4976	0.6669	— 0.2512
0.52	0.1165	— 0.6173	0.0770	0.3087	— 1.2641	— 0.5327	0.6659	— 0.2537
0.54	0.1346	— 0.6367	0.0785	0.3183	— 1.2575	— 0.5676	0.6652	— 0.2562
0.56	0.1537	— 0.6560	0.0799	0.3280	— 1.2514	— 0.6025	0.6649	— 0.2588
0.58	0.1737	— 0.6753	0.0813	0.3377	— 1.2456	— 0.6372	0.6649	— 0.2614
0.60	0.1947	— 0.6946	0.0827	0.3473	— 1.2402	— 0.6717	0.6652	— 0.2641
0.62	0.2165	— 0.7138	0.0840	0.3569	— 1.2352	— 0.7061	0.6657	— 0.2669
0.64	0.2393	— 0.7330	0.0852	0.3665	— 1.2305	— 0.7404	0.6665	— 0.2698
0.66	0.2630	— 0.7523	0.0863	0.3761	— 1.2261	— 0.7746	0.6675	— 0.2727
0.68	0.2875	— 0.7715	0.0874	0.3857	— 1.2219	— 0.8086	0.6688	— 0.2757
0.70	0.3130	— 0.7907	0.0885	0.3953	— 1.2180	— 0.8425	0.6703	— 0.2788
0.72	0.3394	— 0.8099	0.0895	0.4049	— 1.2143	— 0.8763	0.6720	— 0.2819
0.74	0.3666	— 0.8291	0.0905	0.4145	— 1.2108	— 0.9100	0.6739	— 0.2850
0.76	0.3947	— 0.8482	0.0914	0.4241	— 1.2075	— 0.9435	0.6760	— 0.2882
0.78	0.4237	— 0.8674	0.0923	0.4337	— 1.2044	— 0.9770	0.6783	— 0.2915
0.80	0.4536	— 0.8866	0.0932	0.4433	— 1.2015	— 1.0103	0.6808	— 0.2949
0.82	0.4843	— 0.9058	0.0940	0.4529	— 1.1987	— 1.0436	0.6834	— 0.2982
0.84	0.5159	— 0.9250	0.0948	0.4625	— 1.1961	— 1.0767	0.6862	— 0.3016
0.86	0.5484	— 0.9442	0.0956	0.4721	— 1.1936	— 1.1098	0.6892	— 0.3051
0.88	0.5817	— 0.9635	0.0964	0.4817	— 1.1912	— 1.1427	0.6924	— 0.3086
0.90	0.6159	— 0.9827	0.0971	0.4913	— 1.1889	— 1.1756	0.6957	— 0.3122
0.92	0.6509	— 1.0019	0.0978	0.5010	— 1.1868	— 1.2084	0.6992	— 0.3158
0.94	0.6868	— 1.0211	0.0985	0.5106	— 1.1847	— 1.2412	0.7028	— 0.3194
0.96	0.7235	— 1.0404	0.0991	0.5202	— 1.1828	— 1.2738	0.7066	— 0.3231
0.98	0.7611	— 1.0596	0.0997	0.5298	— 1.1809	— 1.3064	0.7105	— 0.3268
1.00	0.7995	— 1.0789	0.1003	0.5395	— 1.1792	— 1.3390	0.7146	— 0.3305

TABLE 6.

Wing coefficients for $\beta = 0.35$.

ω	k_a'	k_a''	m_a'	m_a''	k_b'	k_b''	m_b'	m_b''
0	0	0	0	0	— 2.135	0	+ 1.068	0
0.02	— 0.0031	— 0.0409	+ 0.0018	+ 0.0204	— 2.048	+ 0.143	1.029	— 0.098
0.04	— 0.0101	— 0.0782	0.0057	0.0391	— 1.960	0.203	0.983	— 0.151
0.06	— 0.0172	— 0.1122	0.0106	0.0560	— 1.881	0.231	0.940	— 0.185
0.08	— 0.0244	— 0.1435	0.0158	0.0716	— 1.810	0.234	0.902	— 0.207
0.10	— 0.0311	— 0.1727	0.0212	0.0861	— 1.748	0.224	0.870	— 0.224
0.12	— 0.0365	— 0.2000	0.0266	0.0995	— 1.693	0.205	0.843	— 0.237
0.14	— 0.0408	— 0.2260	0.0319	0.1124	— 1.646	0.179	0.820	— 0.247
0.16	— 0.0440	— 0.2508	0.0370	0.1246	— 1.605	0.151	0.800	— 0.255
0.18	— 0.0464	— 0.2748	0.0420	0.1364	— 1.568	0.121	0.782	— 0.262
0.20	— 0.0476	— 0.2980	0.0468	0.1478	— 1.537	0.090	0.766	— 0.268
0.22	— 0.0477	— 0.3208	0.0514	0.1589	— 1.5095	0.0580	0.7534	— 0.2733
0.24	— 0.0463	— 0.3431	0.0559	0.1696	— 1.4853	+ 0.0235	0.7420	— 0.2780
0.26	— 0.0436	— 0.3649	0.0603	0.1802	— 1.4639	— 0.0124	0.7323	— 0.2822
0.28	— 0.0398	— 0.3866	0.0645	0.1906	— 1.4452	— 0.0484	0.7235	— 0.2863
0.30	— 0.0350	— 0.4081	0.0686	0.2009	— 1.4288	— 0.0842	0.7159	— 0.2905
0.32	— 0.0292	— 0.4293	0.0727	0.2111	— 1.4144	— 0.1199	0.7092	— 0.2948
0.34	— 0.0223	— 0.4505	0.0767	0.2211	— 1.4018	— 0.1555	0.7034	— 0.2993
0.36	— 0.0144	— 0.4717	0.0805	0.2312	— 1.3908	— 0.1913	0.6986	— 0.3036
0.38	— 0.0054	— 0.4929	0.0843	0.2412	— 1.3814	— 0.2270	0.6948	— 0.3080
0.40	+ 0.0047	— 0.5141	0.0880	0.2511	— 1.3733	— 0.2628	0.6917	— 0.3126
0.42	0.0158	— 0.5353	0.0918	0.2610	— 1.3663	— 0.2985	0.6893	— 0.3170
0.44	0.0278	— 0.5566	0.0955	0.2710	— 1.3605	— 0.3341	0.6873	— 0.3218
0.46	0.0408	— 0.5780	0.0991	0.2808	— 1.3557	— 0.3695	0.6859	— 0.3266
0.48	0.0548	— 0.5996	0.1028	0.2907	— 1.3519	— 0.4048	0.6851	— 0.3315
0.50	0.0696	— 0.6213	0.1064	0.3007	— 1.3489	— 0.4398	0.6848	— 0.3369
0.52	0.0854	— 0.6431	0.1101	0.3105	— 1.3469	— 0.4747	0.6848	— 0.3422
0.54	0.1021	— 0.6651	0.1138	0.3205	— 1.3455	— 0.5095	0.6853	— 0.3477
0.56	0.1198	— 0.6873	0.1175	0.3304	— 1.3448	— 0.5443	0.6861	— 0.3533
0.58	0.1383	— 0.7097	0.1212	0.3404	— 1.3448	— 0.5789	0.6874	— 0.3591
0.60	0.1577	— 0.7324	0.1249	0.3505	— 1.3457	— 0.6134	0.6890	— 0.3650
0.62	0.1781	— 0.7553	0.1287	0.3605	— 1.3470	— 0.6478	0.6909	— 0.3709
0.64	0.1993	— 0.7785	0.1325	0.3706	— 1.3489	— 0.6820	0.6931	— 0.3771
0.66	0.2213	— 0.8019	0.1364	0.3807	— 1.3514	— 0.7160	0.6957	— 0.3835
0.68	0.2443	— 0.8257	0.1403	0.3908	— 1.3545	— 0.7501	0.6985	— 0.3900
0.70	0.2680	— 0.8495	0.1444	0.4011	— 1.3580	— 0.7840	0.7015	— 0.3966
0.72	0.2928	— 0.8739	0.1485	0.4113	— 1.3623	— 0.8180	0.7049	— 0.4034
0.74	0.3183	— 0.8985	0.1527	0.4215	— 1.3669	— 0.8517	0.7085	— 0.4103
0.76	0.3446	— 0.9234	0.1570	0.4319	— 1.3720	— 0.8853	0.7124	— 0.4174
0.78	0.3717	— 0.9488	0.1613	0.4423	— 1.3777	— 0.9189	0.7164	— 0.4246
0.80	0.3998	— 0.9745	0.1657	0.4527	— 1.3838	— 0.9524	0.7208	— 0.4321
0.82	0.4285	— 1.0006	0.1702	0.4632	— 1.3904	— 0.9858	0.7253	— 0.4396
0.84	0.4582	— 1.0270	0.1749	0.4737	— 1.3975	— 1.0192	0.7300	— 0.4472
0.86	0.4887	— 1.0538	0.1797	0.4842	— 1.4050	— 1.0525	0.7349	— 0.4550
0.88	0.5202	— 1.0809	0.1844	0.4947	— 1.4127	— 1.0858	0.7401	— 0.4628
0.90	0.5524	— 1.1086	0.1892	0.5053	— 1.4210	— 1.1191	0.7455	— 0.4709
0.92	0.5856	— 1.1367	0.1943	0.5159	— 1.4298	— 1.1524	0.7511	— 0.4789
0.94	0.6195	— 1.1654	0.1994	0.5266	— 1.4392	— 1.1856	0.7568	— 0.4873
0.96	0.6543	— 1.1945	0.2047	0.5374	— 1.4490	— 1.2190	0.7626	— 0.4957
0.98	0.6899	— 1.2242	0.2102	0.5483	— 1.4594	— 1.2523	0.7686	— 0.5038
1.00	0.7259	— 1.2544	0.2159	0.5597	— 1.4703	— 1.2856	0.7747	— 0.5122

TABLE 7.

Wing coefficients for $\beta = 0.50$.

ω	k_a'	k_a''	m_a'	m_a''	k_b'	k_b''	m_b'	m_b''
0	0	0	0	0	— 2.309	0	+ 1.155	0
0.02	— 0.0042	— 0.0439	+ 0.0024	+ 0.0219	— 2.196	+ 0.189	1.104	— 0.127
0.04	— 0.0124	— 0.0832	0.0071	0.0414	— 2.086	0.286	1.042	— 0.192
0.06	— 0.0218	— 0.1185	0.0129	0.0589	— 1.988	0.305	0.988	— 0.231
0.08	— 0.0311	— 0.1506	0.0193	0.0747	— 1.901	0.314	0.943	— 0.258
0.10	— 0.0395	— 0.1801	0.0259	0.0892	— 1.826	0.306	0.905	— 0.277
0.12	— 0.0464	— 0.2075	0.0326	0.1026	— 1.762	0.284	0.873	— 0.292
0.14	— 0.0518	— 0.2335	0.0391	0.1152	— 1.707	0.255	0.846	— 0.304
0.16	— 0.0555	— 0.2582	0.0454	0.1272	— 1.659	0.220	0.822	— 0.313
0.18	— 0.0580	— 0.2821	0.0517	0.1386	— 1.619	0.184	0.801	— 0.321
0.20	— 0.0597	— 0.3055	0.0576	0.1496	— 1.585	0.149	0.783	— 0.321
0.22	— 0.0607	— 0.3284	0.0635	0.1603	— 1.5560	0.1157	0.7656	— 0.3342
0.24	— 0.0610	— 0.3509	0.0691	0.1708	— 1.5312	0.0833	0.7519	— 0.3426
0.26	— 0.0601	— 0.3732	0.0748	0.1810	— 1.5103	0.0500	0.7405	— 0.3506
0.28	— 0.0577	— 0.3954	0.0803	0.1911	— 1.4926	+ 0.0150	0.7311	— 0.3577
0.30	— 0.0538	— 0.4175	0.0858	0.2010	— 1.4776	— 0.0217	0.7237	— 0.3642
0.32	— 0.0487	— 0.4396	0.0913	0.2108	— 1.4649	— 0.0585	0.7174	— 0.3707
0.34	— 0.0427	— 0.4616	0.0967	0.2205	— 1.4543	— 0.0949	0.7118	— 0.3775
0.36	— 0.0359	— 0.4837	0.1022	0.2302	— 1.4458	— 0.1306	0.7066	— 0.3846
0.38	— 0.0280	— 0.5059	0.1078	0.2398	— 1.4391	— 0.1660	0.7020	— 0.3922
0.40	— 0.0194	— 0.5284	0.1133	0.2494	— 1.4344	— 0.2010	0.6980	— 0.4000
0.42	— 0.0098	— 0.5512	0.1190	0.2590	— 1.4313	— 0.2356	0.6950	— 0.4082
0.44	+ 0.0007	— 0.5741	0.1247	0.2686	— 1.4295	— 0.2702	0.6931	— 0.4166
0.46	0.0120	— 0.5974	0.1305	0.2781	— 1.4291	— 0.3042	0.6919	— 0.4253
0.48	0.0242	— 0.6209	0.1363	0.2877	— 1.4299	— 0.3382	0.6911	— 0.4341
0.50	0.0374	— 0.6448	0.1424	0.2972	— 1.4319	— 0.3720	0.6907	— 0.4433
0.52	0.0514	— 0.6690	0.1486	0.3067	— 1.4351	— 0.4056	0.6907	— 0.4527
0.54	0.0662	— 0.6936	0.1548	0.3162	— 1.4393	— 0.4388	0.6911	— 0.4624
0.56	0.0819	— 0.7186	0.1612	0.3257	— 1.4445	— 0.4719	0.6918	— 0.4725
0.58	0.0982	— 0.7441	0.1679	0.3352	— 1.4507	— 0.5045	0.6930	— 0.4828
0.60	0.1152	— 0.7700	0.1747	0.3448	— 1.4580	— 0.5367	0.6944	— 0.4934
0.62	0.1330	— 0.7965	0.1817	0.3543	— 1.4661	— 0.5688	0.6962	— 0.5044
0.64	0.1515	— 0.8234	0.1888	0.3638	— 1.4753	— 0.6005	0.6982	— 0.5156
0.66	0.1707	— 0.8508	0.1962	0.3732	— 1.4853	— 0.6318	0.7004	— 0.5272
0.68	0.1906	— 0.8788	0.2037	0.3827	— 1.4961	— 0.6630	0.7030	— 0.5390
0.70	0.2111	— 0.9074	0.2115	0.3922	— 1.5078	— 0.6938	0.7056	— 0.5512
0.72	0.2323	— 0.9365	0.2197	0.4016	— 1.5204	— 0.7243	0.7084	— 0.5636
0.74	0.2542	— 0.9663	0.2279	0.4110	— 1.5337	— 0.7545	0.7114	— 0.5763
0.76	0.2766	— 0.9968	0.2364	0.4203	— 1.5480	— 0.7842	0.7145	— 0.5894
0.78	0.2996	— 1.0279	0.2453	0.4297	— 1.5631	— 0.8138	0.7178	— 0.6028
0.80	0.3232	— 0.0597	0.2544	0.4389	— 1.5790	— 0.8429	0.7212	— 0.6164
0.82	0.3473	— 1.0922	0.2638	0.4481	— 1.5957	— 0.8717	0.7246	— 0.6304
0.84	0.3720	— 1.1254	0.2734	0.4572	— 1.6132	— 0.9001	0.7282	— 0.6446
0.86	0.3971	— 1.1594	0.2833	0.4663	— 1.6316	— 0.9281	0.7318	— 0.6592
0.88	0.4227	— 1.1943	0.2935	0.4753	— 1.6507	— 0.9556	0.7354	— 0.6740
0.90	0.4487	— 1.2300	0.3040	0.4842	— 1.6706	— 0.9827	0.7391	— 0.6891
0.92	0.4750	— 1.2666	0.3148	0.4930	— 1.6914	— 1.0092	0.7427	— 0.7046
0.94	0.5016	— 1.3039	0.3259	0.5016	— 1.7130	— 1.0352	0.7464	— 0.7204
0.96	0.5286	— 1.3420	0.3374	0.5101	— 1.7352	— 1.0607	0.7500	— 0.7364
0.98	0.5560	— 1.3807	0.3491	0.5185	— 1.7583	— 1.0858	0.7536	— 0.7528
1.00	0.5837	— 1.4199	0.3612	0.5267	— 1.7811	— 1.1104	0.7571	— 0.7693

TABLE 8.

Wing coefficients for $\beta = 0.60$.

ω	k_a'	k_a''	m_a'	m_a''	k_b'	k_b''	m_b'	m_b''
0	0	0	0	0	− 2.500	0	+ 1.250	0
0.02	− 0.0053	− 0.0470	+ 0.0030	+ 0.0235	− 2.354	+ 0.241	1.176	− 0.154
0.04	− 0.0154	− 0.0882	0.0087	0.0439	− 2.214	0.340	1.100	− 0.232
0.06	− 0.0266	− 0.1245	0.0159	0.0617	− 2.090	0.382	1.035	− 0.280
0.08	− 0.0373	− 0.1569	0.0238	0.0775	− 1.985	0.389	0.981	− 0.311
0.10	− 0.0467	− 0.1864	0.0316	0.0919	− 1.896	0.375	0.936	− 0.333
0.12	− 0.0545	− 0.2138	0.0393	0.1050	− 1.821	0.349	0.896	− 0.350
0.14	− 0.0612	− 0.2397	0.0469	0.1172	− 1.759	0.320	0.863	− 0.363
0.16	− 0.0671	− 0.2646	0.0543	0.1287	− 1.708	0.291	0.834	− 0.375
0.18	− 0.0719	− 0.2887	0.0614	0.1396	− 1.665	0.260	0.809	− 0.386
0.20	− 0.0751	− 0.3122	0.0685	0.1501	− 1.629	0.226	0.789	− 0.397
0.22	− 0.0767	− 0.3351	0.0755	0.1603	− 1.5989	0.1882	0.7723	− 0.4056
0.24	− 0.0770	− 0.3578	0.0825	0.1702	− 1.5735	0.1506	0.7574	− 0.4140
0.26	− 0.0763	− 0.3804	0.0894	0.1798	− 1.5524	0.1138	0.7441	− 0.4231
0.28	− 0.0748	− 0.4029	0.0963	0.1893	− 1.5352	0.0778	0.7321	− 0.4325
0.30	− 0.0722	− 0.4255	0.1032	0.1985	− 1.5215	0.0421	0.7219	− 0.4423
0.32	− 0.0685	− 0.4481	0.1102	0.2077	− 1.5105	+ 0.0065	0.7136	− 0.4522
0.34	− 0.0639	− 0.4709	0.1173	0.2168	− 1.5024	− 0.0288	0.7065	− 0.4624
0.36	− 0.0584	− 0.4939	0.1245	0.2257	− 1.4964	− 0.0636	0.7001	− 0.4731
0.38	− 0.0519	− 0.5172	0.1317	0.2345	− 1.4928	− 0.0980	0.6945	− 0.4841
0.40	− 0.0447	− 0.5407	0.1392	0.2434	− 1.4910	− 0.1317	0.6897	− 0.4956
0.42	− 0.0366	− 0.5646	0.1469	0.2520	− 1.4913	− 0.1649	0.6856	− 0.5075
0.44	− 0.0279	− 0.5889	0.1547	0.2607	− 1.4931	− 0.1973	0.6820	− 0.5200
0.46	− 0.0183	− 0.6136	0.1627	0.2691	− 1.4966	− 0.2293	0.6790	− 0.5329
0.48	− 0.0081	− 0.6388	0.1709	0.2775	− 1.5018	− 0.2607	0.6763	− 0.5461
0.50	+ 0.0028	− 0.6645	0.1794	0.2858	− 1.5084	− 0.2915	0.6740	− 0.5599
0.52	0.0143	− 0.6907	0.1881	0.2940	− 1.5164	− 0.3215	0.6720	− 0.5741
0.54	0.0264	− 0.7174	0.1971	0.3021	− 1.5256	− 0.3509	0.6703	− 0.5889
0.56	0.0390	− 0.7447	0.2064	0.3100	− 1.5363	− 0.3797	0.6686	− 0.6040
0.58	0.0521	− 0.7726	0.2160	0.3178	− 1.5481	− 0.4077	0.6673	− 0.6196
0.60	0.0658	− 0.8011	0.2257	0.3254	− 1.5610	− 0.4350	0.6659	− 0.6356
0.62	0.0799	− 0.8302	0.2359	0.3329	− 1.5750	− 0.4616	0.6646	− 0.6521
0.64	0.0942	− 0.8599	0.2464	0.3403	− 1.5899	− 0.4875	0.6632	− 0.6690
0.66	0.1093	− 0.8903	0.2572	0.3474	− 1.6060	− 0.5127	0.6618	− 0.6863
0.68	0.1245	− 0.9214	0.2683	0.3543	− 1.6232	− 0.5370	0.6604	− 0.7039
0.70	0.1395	− 0.9532	0.2797	0.3609	− 1.6414	− 0.5605	0.6588	− 0.7220
0.72	0.1555	− 0.9857	0.2915	0.3673	− 1.6604	− 0.5832	0.6571	− 0.7404
0.74	0.1714	− 1.0189	0.3035	0.3734	− 1.6805	− 0.6050	0.6552	− 0.7591
0.76	0.1875	− 1.0529	0.3160	0.3792	− 1.7014	− 0.6260	0.6531	− 0.7782
0.78	0.2037	− 1.0876	0.3287	0.3847	− 1.7231	− 0.6459	0.6508	− 0.7976
0.80	0.2201	− 1.1231	0.3417	0.3899	− 1.7456	− 0.6650	0.6482	− 0.8173
0.82	0.2364	− 1.1593	0.3551	0.3947	− 1.7689	− 0.6830	0.6453	− 0.8372
0.84	0.2528	− 1.1962	0.3688	0.3991	− 1.7929	− 0.7000	0.6421	− 0.8574
0.86	0.2691	− 1.2339	0.3828	0.4030	− 1.8175	− 0.7159	0.6385	− 0.8778
0.88	0.2852	− 1.2722	0.3971	0.4066	− 1.8428	− 0.7307	0.6345	− 0.8984
0.90	0.3012	− 1.3113	0.4116	0.4097	− 1.8687	− 0.7444	0.6302	− 0.9192
0.92	0.3170	− 1.3511	0.4264	0.4123	− 1.8950	− 0.7569	0.6254	− 0.9401
0.94	0.3326	− 1.3915	0.4414	0.4145	− 1.9218	− 0.7683	0.6201	− 0.9612
0.96	0.3479	− 1.4325	0.4567	0.4161	− 1.9489	− 0.7785	0.6144	− 0.9823
0.98	0.3628	− 1.4742	0.4722	0.4172	− 1.9764	− 0.7874	0.6083	− 1.0035
1.00	0.3773	− 1.5164	0.4878	0.4177	− 2.0042	− 0.7950	0.6016	− 1.0246

TABLE 9.

Wing coefficients for $\beta = 0.70$.

ω	k_a'	k_a''	m_a'	m_a''	k_b'	k_b''	m_b'	m_b''
0	0	0	0	0	— 2.801	0	+ 1.400	0
0.02	— 0.0072	— 0.0516	+ 0.0044	+ 0.0257	— 2.582	+ 0.334	1.289	— 0.207
0.04	— 0.0199	— 0.0949	0.0123	0.0473	— 2.385	0.451	1.182	— 0.307
0.06	— 0.0339	— 0.1321	0.0213	0.0655	— 2.223	0.500	1.095	— 0.365
0.08	— 0.0470	— 0.1649	0.0306	0.0809	— 2.092	0.506	1.022	— 0.400
0.10	— 0.0588	— 0.1944	0.0401	0.0945	— 1.984	0.493	0.965	— 0.426
0.12	— 0.0688	— 0.2217	0.0493	0.1066	— 1.897	0.467	0.917	— 0.441
0.14	— 0.0771	— 0.2473	0.0583	0.1180	— 1.825	0.433	0.878	— 0.457
0.16	— 0.0842	— 0.2719	0.0672	0.1286	— 1.766	0.398	0.841	— 0.469
0.18	— 0.0901	— 0.2956	0.0760	0.1386	— 1.718	0.362	0.812	— 0.482
0.20	— 0.0945	— 0.3189	0.0846	0.1480	— 1.679	0.325	0.785	— 0.497
0.22	— 0.0975	— 0.3419	0.0932	0.1568	— 1.6473	0.2863	0.7623	— 0.5088
0.24	— 0.0993	— 0.3648	0.1018	0.1655	— 1.6216	0.2484	0.7434	— 0.5210
0.26	— 0.1001	— 0.3875	0.1105	0.1739	— 1.6010	0.2111	0.7266	— 0.5337
0.28	— 0.0999	— 0.4104	0.1193	0.1819	— 1.5850	0.1749	0.7113	— 0.5470
0.30	— 0.0989	— 0.4334	0.1282	0.1896	— 1.5729	0.1402	0.6974	— 0.5609
0.32	— 0.0970	— 0.4566	0.1373	0.1972	— 1.5642	0.1060	0.6847	— 0.5754
0.34	— 0.0944	— 0.4801	0.1465	0.2044	— 1.5586	0.0732	0.6734	— 0.5905
0.36	— 0.0910	— 0.5039	0.1560	0.2113	— 1.5557	0.0415	0.6627	— 0.6063
0.38	— 0.0871	— 0.5280	0.1657	0.2179	— 1.5553	+ 0.0112	0.6518	— 0.6228
0.40	— 0.0826	— 0.5526	0.1756	0.2245	— 1.5571	— 0.0180	0.6418	— 0.6398
0.42	— 0.0775	— 0.5776	0.1858	0.2306	— 1.5610	— 0.0461	0.6321	— 0.6575
0.44	— 0.0719	— 0.6030	0.1963	0.2364	— 1.5668	— 0.0730	0.6225	— 0.6757
0.46	— 0.0659	— 0.6289	0.2071	0.2417	— 1.5742	— 0.0984	0.6130	— 0.6944
0.48	— 0.0596	— 0.6553	0.2181	0.2466	— 1.5833	— 0.1224	0.6034	— 0.7136
0.50	— 0.0531	— 0.6822	0.2293	0.2512	— 1.5938	— 0.1451	0.5935	— 0.7332
0.52	— 0.0462	— 0.7096	0.2409	0.2554	— 1.6055	— 0.1665	0.5834	— 0.7532
0.54	— 0.0393	— 0.7375	0.2527	0.2592	— 1.6185	— 0.1864	0.5728	— 0.7736
0.56	— 0.0324	— 0.7659	0.2647	0.2626	— 1.6325	— 0.2048	0.5619	— 0.7941
0.58	— 0.0254	— 0.7948	0.2770	0.2654	— 1.6474	— 0.2217	0.5504	— 0.8149
0.60	— 0.0183	— 0.8242	0.2895	0.2675	— 1.6631	— 0.2375	0.5383	— 0.8357
0.62	— 0.0111	— 0.8540	0.3021	0.2692	— 1.6795	— 0.2515	0.5257	— 0.8566
0.64	— 0.0040	— 0.8842	0.3149	0.2702	— 1.6964	— 0.2643	0.5124	— 0.8775
0.66	+ 0.0030	— 0.9148	0.3278	0.2706	— 1.7138	— 0.2752	0.4985	— 0.8982
0.68	0.0099	— 0.9457	0.3407	0.2703	— 1.7315	— 0.2849	0.4840	— 0.9187
0.70	0.0166	— 0.9770	0.3537	0.2695	— 1.7494	— 0.2932	0.4687	— 0.9389
0.72	0.0230	— 1.0085	0.3667	0.2680	— 1.7674	— 0.2999	0.4528	— 0.9588
0.74	0.0292	— 1.0404	0.3795	0.2657	— 1.7855	— 0.3052	0.4363	— 0.9782
0.76	0.0353	— 1.0724	0.3923	0.2627	— 1.8033	— 0.3091	0.4191	— 0.9971
0.78	0.0410	— 1.1046	0.4049	0.2592	— 1.8210	— 0.3118	0.4013	— 1.0154
0.80	0.0465	— 1.1368	0.4173	0.2552	— 1.8383	— 0.3133	0.3830	— 1.0331
0.82	0.0517	— 1.1691	0.4295	0.2505	— 1.8552	— 0.3136	0.3641	— 1.0500
0.84	0.0566	— 1.2014	0.4413	0.2451	— 1.8715	— 0.3125	0.3447	— 1.0662
0.86	0.0613	— 1.2337	0.4528	0.2392	— 1.8873	— 0.3105	0.3249	— 1.0815
0.88	0.0656	— 1.2658	0.4639	0.2328	— 1.9023	— 0.3074	0.3048	— 1.0959
0.90	0.0698	— 1.2978	0.4745	0.2258	— 1.9165	— 0.3034	0.2844	— 1.1094
0.92	0.0739	— 1.3296	0.4847	0.2183	— 1.9299	— 0.2986	0.2639	— 1.1219
0.94	0.0777	— 1.3610	0.4945	0.2102	— 1.9424	— 0.2929	0.2433	— 1.1334
0.96	0.0814	— 1.3921	0.5037	0.2015	— 1.9539	— 0.2863	0.2227	— 1.1438
0.98	0.0851	— 1.4229	0.5124	0.1926	— 1.9643	— 0.2794	0.2020	— 1.1533
1.00	0.0883	— 1.4533	0.5205	0.1836	— 1.9738	— 0.2719	0.1815	— 1.1617

TABLE 10.

Wing coefficients for $\beta = 0.80$.

ω	k_a'	k_a''	m_a'	m_a''	k_b'	k_b''	m_b'	m_b''
0	0	0	0	0	— 3.33	0	+ 1.667	0
0.02	— 0.0101	— 0.0594	+ 0.0058	+ 0.0297	— 2.98	+ 0.54	1.472	— 0.335
0.04	— 0.0272	— 0.1057	0.0165	0.0520	— 2.67	0.69	1.281	— 0.464
0.06	— 0.0454	— 0.1431	0.0287	0.0694	— 2.43	0.73	1.140	— 0.525
0.08	— 0.0629	— 0.1748	0.0412	0.0835	— 2.24	0.73	1.045	— 0.557
0.10	— 0.0784	— 0.2031	0.0536	0.0954	— 2.095	0.699	0.974	— 0.580
0.12	— 0.0914	— 0.2292	0.0654	0.1057	— 1.966	0.656	0.916	— 0.595
0.14	— 0.1020	— 0.2539	0.0767	0.1148	— 1.867	0.604	0.865	— 0.608
0.16	— 0.1107	— 0.2775	0.0875	0.1230	— 1.795	0.549	0.815	— 0.623
0.18	— 0.1178	— 0.3006	0.0980	0.1304	— 1.751	0.511	0.767	— 0.641
0.20	— 0.1236	— 0.3234	0.1085	0.1369	— 1.721	0.479	0.729	— 0.658
0.22	— 0.1286	— 0.3458	0.1191	0.1428	— 1.690	0.442	0.702	— 0.672
0.24	— 0.1327	— 0.3682	0.1297	0.1480	— 1.663	0.405	0.673	— 0.687
0.26	— 0.1359	— 0.3906	0.1404	0.1527	— 1.642	0.369	0.644	— 0.705
0.28	— 0.1384	— 0.4130	0.1511	0.1569	— 1.626	0.336	0.618	— 0.723
0.30	— 0.1402	— 0.4356	0.1618	0.1604	— 1.613	0.305	0.590	— 0.742
0.32	— 0.1415	— 0.4582	0.1725	0.1632	— 1.604	0.278	0.559	— 0.759
0.34	— 0.1425	— 0.4810	0.1833	0.1652	— 1.598	0.254	0.533	— 0.778
0.36	— 0.1432	— 0.5039	0.1941	0.1665	— 1.595	0.231	0.508	— 0.797
0.38	— 0.1435	— 0.5270	0.2049	0.1671	— 1.593	0.210	0.481	— 0.815
0.40	— 0.1435	— 0.5502	0.2155	0.1671	— 1.5929	0.1912	0.453	— 0.832
0.42	— 0.1434	— 0.5735	0.2259	0.1663	— 1.5931	0.1746	0.4243	— 0.8483
0.44	— 0.1431	— 0.5968	0.2361	0.1649	— 1.5938	0.1601	0.5956	— 0.8642
0.46	— 0.1426	— 0.6202	0.2459	0.1628	— 1.5950	0.1472	0.3664	— 0.8790
0.48	— 0.1420	— 0.6435	0.2554	0.1600	— 1.5965	0.1358	0.3369	— 0.8925
0.50	— 0.1413	— 0.6668	0.2645	0.1567	— 1.5980	0.1259	0.3072	— 0.9044
0.52	— 0.1404	— 0.6899	0.2729	0.1528	— 1.5994	0.1172	0.2774	— 0.9146
0.54	— 0.1393	— 0.7129	0.2807	0.1484	— 1.6006	0.1095	0.2476	— 0.9230
0.56	— 0.1380	— 0.7357	0.2879	0.1435	— 1.6014	0.1028	0.2182	— 0.9297
0.58	— 0.1364	— 0.7583	0.2944	0.1383	— 1.6018	0.0967	0.1892	— 0.9345
0.60	— 0.1345	— 0.7807	0.3003	0.1329	— 1.6016	0.0912	0.1609	— 0.9375
0.62	— 0.1323	— 0.8029	0.3055	0.1274	— 1.6007	0.0858	0.1335	— 0.9387
0.64	— 0.1296	— 0.8249	0.3099	0.1219	— 1.5992	0.0804	0.1072	— 0.9382
0.66	— 0.1265	— 0.8468	0.3138	0.1164	— 1.5971	0.0750	0.0821	— 0.9363
0.68	— 0.1228	— 0.8687	0.3170	0.1111	— 1.5945	0.0694	0.0584	— 0.9331
0.70	— 0.1186	— 0.8905	0.3197	0.1060	— 1.5918	0.0635	0.0362	— 0.9288
0.72	— 0.1138	— 0.9124	0.3220	0.1011	— 1.5892	0.0570	+ 0.0156	— 0.9238
0.74	— 0.1082	— 0.9343	0.3238	0.0968	— 1.5864	0.0497	— 0.0030	— 0.9178
0.76	— 0.1021	— 0.9564	0.3252	0.0928	— 1.5837	0.0418	— 0.0200	— 0.9114
0.78	— 0.0954	— 0.9787	0.3263	0.0893	— 1.5812	0.0334	— 0.0353	— 0.9044
0.80	— 0.0881	— 1.0012	0.3272	0.0862	— 1.5789	0.0244	— 0.0490	— 0.8972
0.82	— 0.0803	— 1.0241	0.3280	0.0834	— 1.5770	0.0150	— 0.0611	— 0.8898
0.84	— 0.0720	— 1.0473	0.3286	0.0810	— 1.5757	+ 0.0051	— 0.0715	— 0.8826
0.86	— 0.0632	— 1.0710	0.3293	0.0790	— 1.5749	— 0.0052	— 0.0806	— 0.8752
0.88	— 0.0540	— 1.0952	0.3300	0.0774	— 1.5747	— 0.0158	— 0.0882	— 0.8683
0.90	— 0.0444	— 1.1201	0.3309	0.0760	— 1.5755	— 0.0267	— 0.0946	— 0.8619

TABLE 11.
Flap coefficients for $\tau = 0.1$ and $\beta = 0$.

ω	k_c'	k_c''	m_c'	m_c''	n_a'	n_a''	n_b'	n_b''	n_c'	n_c''
0	−0.7916	0	+0.0520	0	0	0	−0.00220	0	−0.00563	0
0.02	−0.7631	+0.0564	0.0378	−0.0302	0	−0.00004	−0.00212	0	−0.00560	+0.00001
0.04	−0.7341	0.0858	0.0233	−0.0468	0	−0.00008	−0.00204	−0.00008	−0.00557	−0.00001
0.06	−0.7071	0.1041	+0.0098	−0.0579	0	−0.00012	−0.00196	−0.00018	−0.00554	−0.00005
0.08	−0.6825	0.1155	−0.0025	−0.0656	0	−0.00015	−0.00189	−0.00031	−0.00551	−0.00009
0.10	−0.6604	0.1224	−0.0135	−0.0710	0	−0.00018	−0.00183	−0.00045	−0.00548	−0.00014
0.12	−0.6406	0.1260	−0.0234	−0.0748	+0.00001	−0.00021	−0.00177	−0.00059	−0.00546	−0.00019
0.14	−0.6228	0.1274	−0.0323	−0.0775	0.00003	−0.00024	−0.00171	−0.00074	−0.00544	−0.00024
0.16	−0.6069	0.1272	−0.0402	−0.0793	0.00004	−0.00027	−0.00166	−0.00089	−0.00542	−0.00029
0.18	−0.5926	0.1258	−0.0473	−0.0805	0.00006	−0.00029	−0.00161	−0.00105	−0.00541	−0.00035
0.20	−0.5798	0.1235	−0.0537	−0.0813	0.00009	−0.00032	−0.00156	−0.00121	−0.00539	−0.00041
0.22	−0.5683	0.1205	−0.0595	−0.0818	0.00011	−0.00034	−0.00152	−0.00137	−0.00538	−0.00046
0.24	−0.5578	0.1171	−0.0647	−0.0820	0.00014	−0.00037	−0.00147	−0.00153	−0.00536	−0.00052
0.26	−0.5483	0.1133	−0.0693	−0.0821	0.00018	−0.00039	−0.00143	−0.00169	−0.00535	−0.00058
0.28	−0.5396	0.1093	−0.0736	−0.0821	0.00022	−0.00042	−0.00139	−0.00185	−0.00534	−0.00064
0.30	−0.5318	0.1051	−0.0775	−0.0819	0.00026	−0.00044	−0.00135	−0.00202	−0.00533	−0.00070
0.32	−0.5246	0.1008	−0.0811	−0.0817	0.00031	−0.00046	−0.00130	−0.00218	−0.00532	−0.00075
0.34	−0.5180	0.0965	−0.0843	−0.0815	0.00036	−0.00048	−0.00126	−0.00234	−0.00531	−0.00081
0.36	−0.5119	0.0921	−0.0873	−0.0813	0.00041	−0.00051	−0.00122	−0.00251	−0.00530	−0.00087
0.38	−0.5063	0.0876	−0.0901	−0.0810	0.00047	−0.00053	−0.00118	−0.00267	−0.00530	−0.00093
0.40	−0.5011	0.0832	−0.0926	−0.0807	0.00053	−0.00055	−0.00113	−0.00283	−0.00529	−0.00099
0.42	−0.4963	0.0788	−0.0949	−0.0805	0.00059	−0.00057	−0.00109	−0.00300	−0.00528	−0.00105
0.44	−0.4919	0.0744	−0.0970	−0.0803	0.00066	−0.00059	−0.00105	−0.00316	−0.00527	−0.00111
0.46	−0.4878	0.0701	−0.0990	−0.0801	0.00073	−0.00061	−0.00101	−0.00332	−0.00527	−0.00117
0.48	−0.4839	0.0658	−0.1009	−0.0799	0.00081	−0.00064	−0.00096	−0.00349	−0.00526	−0.00123
0.50	−0.4803	0.0615	−0.1026	−0.0797	0.00089	−0.00066	−0.00092	−0.00365	−0.00525	−0.00129
0.52	−0.4770	0.0573	−0.1042	−0.0795	0.00097	−0.00068	−0.00087	−0.00381	−0.00525	−0.00135
0.54	−0.4738	0.0531	−0.1057	−0.0794	0.00105	−0.00070	−0.00082	−0.00398	−0.00524	−0.00140
0.56	−0.4708	0.0490	−0.1071	−0.0793	0.00114	−0.00072	−0.00077	−0.00414	−0.00523	−0.00146
0.58	−0.4681	0.0450	−0.1084	−0.0792	0.00123	−0.00074	−0.00072	−0.00430	−0.00523	−0.00152
0.60	−0.4655	0.0410	−0.1096	−0.0792	0.00133	−0.00076	−0.00067	−0.00446	−0.00522	−0.00158
0.62	−0.4630	0.0370	−0.1107	−0.0792	0.00143	−0.00078	−0.00062	−0.00462	−0.00522	−0.00164
0.64	−0.4607	0.0331	−0.1118	−0.0792	0.00153	−0.00081	−0.00056	−0.00479	−0.00521	−0.00170
0.66	−0.4585	0.0292	−0.1128	−0.0792	0.00164	−0.00083	−0.00051	−0.00495	−0.00520	−0.00176
0.68	−0.4564	0.0254	−0.1137	−0.0793	0.00175	−0.00085	−0.00045	−0.00511	−0.00520	−0.00181
0.70	−0.4544	0.0216	−0.1146	−0.0794	0.00186	−0.00087	−0.00040	−0.00527	−0.00519	−0.00187
0.72	−0.4525	0.0179	−0.1154	−0.0794	0.00198	−0.00089	−0.00034	−0.00543	−0.00519	−0.00193
0.74	−0.4508	0.0142	−0.1162	−0.0795	0.00210	−0.00091	−0.00028	−0.00559	−0.00518	−0.00199
0.76	−0.4491	0.0106	−0.1169	−0.0797	0.00222	−0.00093	−0.00022	−0.00575	−0.00517	−0.00205
0.78	−0.4475	0.0070	−0.1176	−0.0799	0.00235	−0.00095	−0.00015	−0.00591	−0.00517	−0.00210
0.80	−0.4459	+0.0035	−0.1183	−0.0800	0.00248	−0.00097	−0.00009	−0.00608	−0.00516	−0.00216
0.82	−0.4444	0	−0.1189	−0.0802	0.00262	−0.00099	−0.00002	−0.00624	−0.00516	−0.00222
0.84	−0.4430	−0.0035	−0.1195	−0.0804	0.00276	−0.00102	+0.00004	−0.00640	−0.00515	−0.00228
0.86	−0.4417	−0.0069	−0.1200	−0.0807	0.00290	−0.00104	0.00011	−0.00656	−0.00514	−0.00234
0.88	−0.4404	−0.0103	−0.1205	−0.0810	0.00304	−0.00106	0.00018	−0.00672	−0.00514	−0.00239
0.90	−0.4391	−0.0137	−0.1210	−0.0813	0.00319	−0.00108	0.00025	−0.00688	−0.00513	−0.00245
0.92	−0.4379	−0.0170	−0.1215	−0.0816	0.00334	−0.00110	0.00032	−0.00704	−0.00512	−0.00251
0.94	−0.4367	−0.0203	−0.1219	−0.0819	0.00349	−0.00112	0.00040	−0.00720	−0.00512	−0.00257
0.96	−0.4356	−0.0236	−0.1223	−0.0822	0.00365	−0.00114	0.00047	−0.00736	−0.00511	−0.00263
0.98	−0.4345	−0.0268	−0.1227	−0.0825	0.00381	−0.00116	0.00055	−0.00752	−0.00511	−0.00268
1.00	−0.4335	−0.0300	−0.1230	−0.0829	0.00398	−0.00118	0.00062	−0.00768	−0.00510	−0.00274

TABLE 12.

Flap coefficients for $\tau = 0.1$ and $\beta = 0.35$.

ω	k_c'	k_c''	m_c'	m_c''	n_a'	n_a''	n_b'	n_b''	n_c'	n_c''
0	— 0.8451	0	+ 0.0556	0	0	0	— 0.00234	0	— 0.00601	0
0.02	— 0.8098	+ 0.0710	0.0379	— 0.0377	0	— 0.00005	— 0.00224	— 0.00001	— 0.00597	+ 0.00002
0.04	— 0.7739	0.1073	0.0198	— 0.0580	0	— 0.00009	— 0.00215	— 0.00007	— 0.00593	— 0.00001
0.06	— 0.7406	0.1304	+ 0.0030	— 0.0715	0	— 0.00013	— 0.00207	— 0.00017	— 0.00590	— 0.00004
0.08	— 0.7105	0.1446	— 0.0124	— 0.0806	0	— 0.00016	— 0.00199	— 0.00031	— 0.00587	— 0.00008
0.10	— 0.6835	0.1530	— 0.0262	— 0.0868	+ 0.00001	— 0.00019	— 0.00192	— 0.00045	— 0.00584	— 0.00013
0.12	— 0.6598	0.1577	— 0.0386	— 0.0911	0.00001	— 0.00022	— 0.00185	— 0.00061	— 0.00582	— 0.00019
0.14	— 0.6388	0.1599	— 0.0494	— 0.0941	0.00002	— 0.00025	— 0.00179	— 0.00077	— 0.00580	— 0.00025
0.16	— 0.6202	0.1603	— 0.0589	— 0.0961	0.00004	— 0.00028	— 0.00174	— 0.00094	— 0.00578	— 0.00031
0.18	— 0.6040	0.1593	— 0.0674	— 0.0974	0.00006	— 0.00030	— 0.00169	— 0.00111	— 0.00576	— 0.00037
0.20	— 0.5896	0.1576	— 0.0749	— 0.0983	0.00009	— 0.00033	— 0.00164	— 0.00128	— 0.00575	— 0.00043
0.22	— 0.5767	0.1552	— 0.0818	— 0.0989	0.00012	— 0.00036	— 0.00159	— 0.00145	— 0.00573	— 0.00049
0.24	— 0.5652	0.1523	— 0.0879	— 0.0991	0.00015	— 0.00038	— 0.00154	— 0.00162	— 0.00572	— 0.00055
0.26	— 0.5547	0.1490	— 0.0935	— 0.0992	0.00019	— 0.00041	— 0.00150	— 0.00179	— 0.00571	— 0.00061
0.28	— 0.5454	0.1456	— 0.0986	— 0.0992	0.00023	— 0.00044	— 0.00146	— 0.00197	— 0.00570	— 0.00067
0.30	— 0.5370	0.1420	— 0.1032	— 0.0990	0.00028	— 0.00047	— 0.00142	— 0.00215	— 0.00569	— 0.00073
0.32	— 0.5293	0.1385	— 0.1075	— 0.0988	0.00033	— 0.00050	— 0.00138	— 0.00233	— 0.00568	— 0.00080
0.34	— 0.5224	0.1348	— 0.1113	— 0.0986	0.00038	— 0.00052	— 0.00134	— 0.00251	— 0.00568	— 0.00087
0.36	— 0.5160	0.1311	— 0.1149	— 0.0985	0.00044	— 0.00055	— 0.00130	— 0.00269	— 0.00567	— 0.00093
0.38	— 0.5103	0.1273	— 0.1182	— 0.0984	0.00050	— 0.00057	— 0.00126	— 0.00287	— 0.00566	— 0.00099
0.40	— 0.5051	0.1237	— 0.1213	— 0.0982	0.00057	— 0.00059	— 0.00122	— 0.00304	— 0.00566	— 0.00105
0.42	— 0.5003	0.1201	— 0.1241	— 0.0981	0.00064	— 0.00061	— 0.00118	— 0.00322	— 0.00565	— 0.00112
0.44	— 0.4959	0.1167	— 0.1267	— 0.0980	0.00071	— 0.00064	— 0.00114	— 0.00340	— 0.00565	— 0.00118
0.46	— 0.4920	0.1133	— 0.1292	— 0.0979	0.00079	— 0.00066	— 0.00109	— 0.00358	— 0.00564	— 0.00124
0.48	— 0.4884	0.1099	— 0.1314	— 0.0978	0.00087	— 0.00069	— 0.00105	— 0.00376	— 0.00564	— 0.00130
0.50	— 0.4851	0.1067	— 0.1336	— 0.0977	0.00095	— 0.00072	— 0.00101	— 0.00394	— 0.00564	— 0.00137
0.52	— 0.4820	0.1035	— 0.1356	— 0.0977	0.00104	— 0.00074	— 0.00096	— 0.00412	— 0.00563	— 0.00143
0.54	— 0.4792	0.1005	— 0.1375	— 0.0978	0.00114	— 0.00077	— 0.00092	— 0.00430	— 0.00563	— 0.00149
0.56	— 0.4766	0.0975	— 0.1393	— 0.0978	0.00124	— 0.00080	— 0.00087	— 0.00448	— 0.00563	— 0.00155
0.58	— 0.4742	0.0945	— 0.1410	— 0.0979	0.00134	— 0.00083	— 0.00083	— 0.00466	— 0.00563	— 0.00161
0.60	— 0.4720	0.0917	— 0.1426	— 0.0981	0.00145	— 0.00085	— 0.00078	— 0.00484	— 0.00562	— 0.00168
0.62	— 0.4700	0.0889	— 0.1441	— 0.0983	0.00156	— 0.00088	— 0.00074	— 0.00502	— 0.00562	— 0.00174
0.64	— 0.4682	0.0862	— 0.1455	— 0.0985	0.00167	— 0.00091	— 0.00069	— 0.00520	— 0.00562	— 0.00180
0.66	— 0.4666	0.0836	— 0.1469	— 0.0987	0.00179	— 0.00094	— 0.00064	— 0.00538	— 0.00562	— 0.00186
0.68	— 0.4651	0.0811	— 0.1483	— 0.0989	0.00191	— 0.00097	— 0.00059	— 0.00556	— 0.00562	— 0.00192
0.70	— 0.4637	0.0786	— 0.1495	— 0.0992	0.00203	— 0.00100	— 0.00054	— 0.00575	— 0.00562	— 0.00198
0.72	— 0.4624	0.0762	— 0.1507	— 0.0995	0.00216	— 0.00103	— 0.00049	— 0.00593	— 0.00562	— 0.00204
0.74	— 0.4612	0.0739	— 0.1519	— 0.0998	0.00229	— 0.00106	— 0.00044	— 0.00611	— 0.00562	— 0.00210
0.76	— 0.4602	0.0716	— 0.1530	— 0.1002	0.00243	— 0.00109	— 0.00039	— 0.00629	— 0.00561	— 0.00216
0.78	— 0.4593	0.0694	— 0.1541	— 0.1006	0.00258	— 0.00112	— 0.00033	— 0.00648	— 0.00561	— 0.00222
0.80	— 0.4585	0.0673	— 0.1552	— 0.1010	0.00273	— 0.00115	— 0.00028	— 0.00667	— 0.00561	— 0.00229
0.82	— 0.4578	0.0653	— 0.1562	— 0.1014	0.00288	— 0.00118	— 0.00022	— 0.00686	— 0.00561	— 0.00235
0.84	— 0.4572	0.0633	— 0.1572	— 0.1019	0.00304	— 0.00122	— 0.00016	— 0.00704	— 0.00561	— 0.00241
0.86	— 0.4566	0.0614	— 0.1582	— 0.1024	0.00320	— 0.00126	— 0.00011	— 0.00723	— 0.00561	— 0.00247
0.88	— 0.4560	0.0595	— 0.1591	— 0.1029	0.00336	— 0.00130	— 0.00005	— 0.00742	— 0.00561	— 0.00253
0.90	— 0.4555	0.0577	— 0.1600	— 0.1034	0.00352	— 0.00134	+ 0.00001	— 0.00761	— 0.00561	— 0.00259
0.92	— 0.4551	0.0559	— 0.1609	— 0.1039	0.00369	— 0.00138	0.00007	— 0.00779	— 0.00561	— 0.00265
0.94	— 0.4548	0.0543	— 0.1618	— 0.1045	0.00387	— 0.00142	0.00013	— 0.00798	— 0.00561	— 0.00271
0.96	— 0.4546	0.0526	— 0.1626	— 0.1051	0.00405	— 0.00146	0.00019	— 0.00817	— 0.00561	— 0.00278
0.98	— 0.4545	0.0510	— 0.1634	— 0.1057	0.00423	— 0.00150	0.00025	— 0.00836	— 0.00561	— 0.00284
1.00	— 0.4545	0.0495	— 0.1641	— 0.1063	0.00441	— 0.00155	0.00032	— 0.00854	— 0.00561	— 0.00290

TABLE 13.

Flap coefficients for $\tau = 0.1$ and $\beta = 0.50$.

ω	k_c'	k_c''	m_c'	m_c''	n_a'	n_a''	n_b'	n_b''	n_c'	n_c''
0	−0.9141	0	+0.0601	0	0	0	−0.00254	0	−0.00650	0
0.02	−0.8689	+0.0910	+0.0372	−0.0480	0	−0.00005	−0.00241	+0.00003	−0.00645	+0.00003
0.04	−0.8232	0.1368	+0.0140	−0.0733	0	−0.00009	−0.00230	−0.00005	−0.00640	+0.00001
0.06	−0.7814	0.1650	−0.0076	−0.0894	0	−0.00013	−0.00219	−0.00017	−0.00636	−0.00003
0.08	−0.7439	0.1818	−0.0271	−0.0998	0	−0.00017	−0.00210	−0.00032	−0.00633	−0.00008
0.10	−0.7107	0.1915	−0.0446	−0.1063	+0.00001	−0.00020	−0.00201	−0.00048	−0.00630	−0.00014
0.12	−0.6816	0.1967	−0.0601	−0.1105	0.00001	−0.00023	−0.00194	−0.00065	−0.00627	−0.00020
0.14	−0.6561	0.1991	−0.0738	−0.1132	0.00003	−0.00026	−0.00187	−0.00083	−0.00624	−0.00027
0.16	−0.6338	0.1996	−0.0859	−0.1149	0.00005	−0.00029	−0.00181	−0.00101	−0.00622	−0.00033
0.18	−0.6143	0.1988	−0.0964	−0.1158	0.00008	−0.00032	−0.00176	−0.00120	−0.00621	−0.00040
0.20	−0.5974	0.1972	−0.1058	−0.1163	0.00011	−0.00035	−0.00171	−0.00140	−0.00620	−0.00047
0.22	−0.5827	0.1951	−0.1141	−0.1166	0.00014	−0.00038	−0.00166	−0.00159	−0.00618	−0.00053
0.24	−0.5697	0.1926	−0.1215	−0.1164	0.00017	−0.00041	−0.00161	−0.00178	−0.00617	−0.00060
0.26	−0.5582	0.1899	−0.1282	−0.1161	0.00021	−0.00044	−0.00157	−0.00198	−0.00617	−0.00067
0.28	−0.5478	0.1869	−0.1343	−0.1157	0.00026	−0.00046	−0.00153	−0.00217	−0.00616	−0.00073
0.30	−0.5384	0.1838	−0.1400	−0.1152	0.00031	−0.00049	−0.00149	−0.00236	−0.00615	−0.00080
0.32	−0.5300	0.1807	−0.1452	−0.1146	0.00037	−0.00052	−0.00145	−0.00256	−0.00615	−0.00087
0.34	−0.5222	0.1777	−0.1501	−0.1141	0.00044	−0.00055	−0.00141	−0.00275	−0.00614	−0.00094
0.36	−0.5153	0.1748	−0.1546	−0.1136	0.00050	−0.00058	−0.00138	−0.00295	−0.00614	−0.00100
0.38	−0.5090	0.1720	−0.1588	−0.1130	0.00057	−0.00061	−0.00134	−0.00314	−0.00614	−0.00107
0.40	−0.5032	0.1694	−0.1626	−0.1124	0.00064	−0.00064	−0.00130	−0.00334	−0.00613	−0.00113
0.42	−0.4979	0.1668	−0.1664	−0.1119	0.00071	−0.00067	−0.00127	−0.00354	−0.00613	−0.00120
0.44	−0.4931	0.1643	−0.1698	−0.1115	0.00079	−0.00070	−0.00123	−0.00373	−0.00613	−0.00127
0.46	−0.4886	0.1620	−0.1731	−0.1112	0.00088	−0.00073	−0.00119	−0.00393	−0.00613	−0.00134
0.48	−0.4845	0.1598	−0.1763	−0.1109	0.00098	−0.00076	−0.00115	−0.00413	−0.00613	−0.00140
0.50	−0.4808	0.1578	−0.1793	−0.1106	0.00107	−0.00079	−0.00111	−0.00433	−0.00613	−0.00146
0.52	−0.4773	0.1559	−0.1821	−0.1103	0.00117	−0.00083	−0.00107	−0.00453	−0.00614	−0.00153
0.54	−0.4741	0.1542	−0.1849	−0.1101	0.00127	−0.00086	−0.00103	−0.00473	−0.00614	−0.00160
0.56	−0.4712	0.1526	−0.1875	−0.1098	0.00138	−0.00089	−0.00100	−0.00493	−0.00614	−0.00166
0.58	−0.4684	0.1512	−0.1901	−0.1096	0.00149	−0.00093	−0.00096	−0.00513	−0.00615	−0.00172
0.60	−0.4659	0.1499	−0.1926	−0.1094	0.00160	−0.00096	−0.00092	−0.00533	−0.00615	−0.00179
0.62	−0.4635	0.1487	−0.1949	−0.1092	0.00173	−0.00100	−0.00088	−0.00554	−0.00615	−0.00186
0.64	−0.4613	0.1476	−0.1973	−0.1090	0.00185	−0.00104	−0.00084	−0.00574	−0.00616	−0.00192
0.66	−0.4592	0.1466	−0.1996	−0.1089	0.00198	−0.00108	−0.00080	−0.00595	−0.00616	−0.00199
0.68	−0.4572	0.1458	−0.2017	−0.1087	0.00212	−0.00112	−0.00076	−0.00616	−0.00617	−0.00206
0.70	−0.4553	0.1450	−0.2039	−0.1086	0.00225	−0.00116	−0.00072	−0.00636	−0.00617	−0.00212
0.72	−0.4536	0.1444	−0.2061	−0.1085	0.00240	−0.00120	−0.00068	−0.00657	−0.00617	−0.00218
0.74	−0.4519	0.1438	−0.2082	−0.1084	0.00255	−0.00125	−0.00064	−0.00678	−0.00618	−0.00225
0.76	−0.4503	0.1434	−0.2103	−0.1082	0.00270	−0.00130	−0.00060	−0.00699	−0.00618	−0.00231
0.78	−0.4488	0.1431	−0.2124	−0.1081	0.00286	−0.00135	−0.00056	−0.00720	−0.00619	−0.00237
0.80	−0.4474	0.1429	−0.2145	−0.1080	0.00302	−0.00140	−0.00052	−0.00741	−0.00619	−0.00244
0.82	−0.4459	0.1428	−0.2164	−0.1079	0.00319	−0.00145	−0.00049	−0.00763	−0.00620	−0.00250
0.84	−0.4445	0.1428	−0.2184	−0.1078	0.00335	−0.00150	−0.00045	−0.00784	−0.00620	−0.00256
0.86	−0.4430	0.1429	−0.2204	−0.1077	0.00353	−0.00156	−0.00041	−0.00805	−0.00621	−0.00262
0.88	−0.4416	0.1431	−0.2223	−0.1076	0.00371	−0.00162	−0.00037	−0.00827	−0.00621	−0.00268
0.90	−0.4401	0.1434	−0.2243	−0.1075	0.00389	−0.00168	−0.00034	−0.00848	−0.00622	−0.00274
0.92	−0.4387	0.1438	−0.2262	−0.1074	0.00408	−0.00174	−0.00031	−0.00870	−0.00622	−0.00280
0.94	−0.4372	0.1442	−0.2280	−0.1073	0.00426	−0.00181	−0.00027	−0.00891	−0.00623	−0.00287
0.96	−0.4358	0.1448	−0.2299	−0.1072	0.00445	−0.00188	−0.00024	−0.00913	−0.00624	−0.00293
0.98	−0.4344	0.1454	−0.2318	−0.1071	0.00466	−0.00195	−0.00021	−0.00935	−0.00624	−0.00299
1.00	−0.4329	0.1461	−0.2337	−0.1070	0.00487	−0.00203	−0.00017	−0.00956	−0.00625	−0.00305

TABLE 14.

Flap coefficients for $\tau = 0.1$ and $\beta = 0.60$.

ω	k_c'	k_c''	m_c'	m_c''	n_a'	n_a''	n_b'	n_b''	n_c'	n_c''
0	— 0.9896	0	+ 0.0651	0	0	0	— 0.00274	0	— 0.00704	0
0.02	— 0.9310	+ 0.1149	+ 0.0354	— 0.0604	0	— 0.00005	— 0.00259	+ 0.00005	— 0.00698	+ 0.00004
0.04	— 0.8722	0.1708	+ 0.0051	— 0.0907	0	— 0.00009	— 0.00244	— 0.00003	— 0.00692	+ 0.00002
0.06	— 0.8187	0.2030	— 0.0229	— 0.1087	0	— 0.00014	— 0.00232	— 0.00016	— 0.00687	— 0.00003
0.08	— 0.7717	0.2213	— 0.0481	— 0.1193	0	— 0.00018	— 0.00221	— 0.00032	— 0.00683	— 0.00009
0.10	— 0.7310	0.2317	— 0.0701	— 0.1257	+ 0.00001	— 0.00021	— 0.00211	— 0.00051	— 0.00679	— 0.00015
0.12	— 0.6963	0.2374	— 0.0891	— 0.1296	0.00002	— 0.00025	— 0.00203	— 0.00070	— 0.00676	— 0.00021
0.14	— 0.6667	0.2400	— 0.1055	— 0.1317	0.00003	— 0.00028	— 0.00196	— 0.00090	— 0.00673	— 0.00028
0.16	— 0.6416	0.2406	— 0.1196	— 0.1326	0.00005	— 0.00031	— 0.00191	— 0.00111	— 0.00671	— 0.00035
0.18	— 0.6203	0.2399	— 0.1319	— 0.1328	0.00008	— 0.00034	— 0.00185	— 0.00132	— 0.00670	— 0.00042
0.20	— 0.6013	0.2382	— 0.1430	— 0.1324	0.00011	— 0.00037	— 0.00180	— 0.00153	— 0.00669	— 0.00050
0.22	— 0.5844	0.2360	— 0.1530	— 0.1315	0.00015	— 0.00040	— 0.00175	— 0.00174	— 0.00668	— 0.00058
0.24	— 0.5693	0.2335	— 0.1620	— 0.1304	0.00020	— 0.00043	— 0.00171	— 0.00196	— 0.00668	— 0.00065
0.26	— 0.5559	0.2309	— 0.1703	— 0.1291	0.00025	— 0.00046	— 0.00167	— 0.00217	— 0.00667	— 0.00072
0.28	— 0.5440	0.2283	— 0.1779	— 0.1279	0.00030	— 0.00049	— 0.00163	— 0.00238	— 0.00667	— 0.00080
0.30	— 0.5332	0.2258	— 0.1848	— 0.1265	0.00035	— 0.00052	— 0.00159	— 0.00260	— 0.00667	— 0.00087
0.32	— 0.5234	0.2233	— 0.1913	— 0.1250	0.00041	— 0.00055	— 0.00155	— 0.00281	— 0.00667	— 0.00094
0.34	— 0.5145	0.2209	— 0.1974	— 0.1235	0.00047	— 0.00058	— 0.00151	— 0.00303	— 0.00667	— 0.00101
0.36	— 0.5064	0.2188	— 0.2030	— 0.1220	0.00054	— 0.00061	— 0.00148	— 0.00324	— 0.00667	— 0.00108
0.38	— 0.4989	0.2169	— 0.2083	— 0.1205	0.00061	— 0.00064	— 0.00145	— 0.00346	— 0.00667	— 0.00115
0.40	— 0.4920	0.2151	— 0.2134	— 0.1190	0.00069	— 0.00068	— 0.00141	— 0.00367	— 0.00667	— 0.00122
0.42	— 0.4856	0.2134	— 0.2182	— 0.1175	0.00078	— 0.00072	— 0.00138	— 0.00389	— 0.00667	— 0.00129
0.44	— 0.4796	0.2119	— 0.2227	— 0.1160	0.00087	— 0.00075	— 0.00135	— 0.00411	— 0.00667	— 0.00136
0.46	— 0.4741	0.2107	— 0.2271	— 0.1145	0.00097	— 0.00079	— 0.00132	— 0.00433	— 0.00668	— 0.00143
0.48	— 0.4688	0.2097	— 0.2313	— 0.1129	0.00107	— 0.00083	— 0.00128	— 0.00455	— 0.00668	— 0.00150
0.50	— 0.4638	0.2088	— 0.2353	— 0.1113	0.00118	— 0.00087	— 0.00125	— 0.00477	— 0.00669	— 0.00157
0.52	— 0.4590	0.2081	— 0.2392	— 0.1098	0.00129	— 0.00091	— 0.00122	— 0.00499	— 0.00670	— 0.00164
0.54	— 0.4545	0.2076	— 0.2430	— 0.1083	0.00141	— 0.00095	— 0.00119	— 0.00522	— 0.00670	— 0.00170
0.56	— 0.4501	0.2072	— 0.2466	— 0.1067	0.00153	— 0.00099	— 0.00116	— 0.00544	— 0.00671	— 0.00177
0.58	— 0.4459	0.2070	— 0.2501	— 0.1051	0.00165	— 0.00104	— 0.00113	— 0.00567	— 0.00672	— 0.00184
0.60	— 0.4417	0.2069	— 0.2536	— 0.1035	0.00178	— 0.00109	— 0.00110	— 0.00590	— 0.00673	— 0.00191
0.62	— 0.4377	0.2069	— 0.2570	— 0.1018	0.00191	— 0.00114	— 0.00108	— 0.00612	— 0.00674	— 0.00198
0.64	— 0.4337	0.2071	— 0.2603	— 0.1001	0.00204	— 0.00119	— 0.00105	— 0.00635	— 0.00675	— 0.00204
0.66	— 0.4297	0.2074	— 0.2635	— 0.0983	0.00218	— 0.00124	— 0.00103	— 0.00658	— 0.00676	— 0.00211
0.68	— 0.4257	0.2077	— 0.2666	— 0.0965	0.00232	— 0.00130	— 0.00100	— 0.00681	— 0.00676	— 0.00217
0.70	— 0.4217	0.2082	— 0.2697	— 0.0947	0.00247	— 0.00136	— 0.00098	— 0.00704	— 0.00677	— 0.00224
0.72	— 0.4178	0.2087	— 0.2727	— 0.0928	0.00263	— 0.00142	— 0.00096	— 0.00728	— 0.00678	— 0.00230
0.74	— 0.4139	0.2093	— 0.2756	— 0.0908	0.00280	— 0.00148	— 0.00095	— 0.00751	— 0.00679	— 0.00236
0.76	— 0.4100	0.2099	— 0.2784	— 0.0888	0.00297	— 0.00155	— 0.00093	— 0.00774	— 0.00680	— 0.00242
0.78	— 0.4061	0.2107	— 0.2811	— 0.0867	0.00314	— 0.00162	— 0.00091	— 0.00797	— 0.00680	— 0.00249
0.80	— 0.4023	0.2115	— 0.2838	— 0.0846	0.00332	— 0.00169	— 0.00090	— 0.00820	— 0.00681	— 0.00255
0.82	— 0.3984	0.2122	— 0.2864	— 0.0824	0.00350	— 0.00177	— 0.00089	— 0.00843	— 0.00682	— 0.00261
0.84	— 0.3944	0.2130	— 0.2890	— 0.0801	0.00368	— 0.00185	— 0.00088	— 0.00866	— 0.00683	— 0.00268
0.86	— 0.3903	0.2138	— 0.2914	— 0.0778	0.00387	— 0.00193	— 0.00087	— 0.00889	— 0.00684	— 0.00274
0.88	— 0.3861	0.2146	— 0.2937	— 0.0754	0.00406	— 0.00202	— 0.00086	— 0.00912	— 0.00685	— 0.00280
0.90	— 0.3817	0.2154	— 0.2960	— 0.0729	0.00425	— 0.00211	— 0.00086	— 0.00935	— 0.00686	— 0.00286
0.92	— 0.3771	0.2162	— 0.2982	— 0.0704	0.00445	— 0.00220	— 0.00085	— 0.00958	— 0.00687	— 0.00292
0.94	— 0.3724	0.2169	— 0.3002	— 0.0678	0.00465	— 0.00230	— 0.00085	— 0.00981	— 0.00688	— 0.00299
0.96	— 0.3676	0.2176	— 0.3022	— 0.0651	0.00486	— 0.00240	— 0.00085	— 0.01004	— 0.00689	— 0.00305
0.98	— 0.3626	0.2183	— 0.3041	— 0.0623	0.00507	— 0.00251	— 0.00085	— 0.01026	— 0.00690	— 0.00311
1.00	— 0.3576	0.2190	— 0.3059	— 0.0595	0.00529	— 0.00262	— 0.00085	— 0.01047	— 0.00691	— 0.00318

TABLE 15.

Flap coefficients for $\tau = 0.1$ and $\beta = 0.70$.

ω	k_c'	k_c''	m_c'	m_c''	n_a'	n_a''	n_b'	n_b''	n_c'	n_c''
0	— 1.1085	0	+ 0.0729	0	0	0	— 0.00308	0	— 0.00788	0
0.02	— 1.0246	+ 0.1531	+ 0.0300	— 0.0821	0	— 0.00006	— 0.00285	+ 0.00009	— 0.00777	+ 0.00005
0.04	— 0.9429	0.2170	— 0.0129	— 0.1201	0	— 0.00011	— 0.00267	— 0.00001	— 0.00770	+ 0.00004
0.06	— 0.8712	0.2558	— 0.0514	— 0.1393	0	— 0.00015	— 0.00252	— 0.00016	— 0.00764	— 0.00002
0.08	— 0.8095	0.2783	— 0.0854	— 0.1483	0	— 0.00019	— 0.00238	— 0.00036	— 0.00760	— 0.00008
0.10	— 0.7571	0.2888	— 0.1146	— 0.1520	+ 0.00001	— 0.00022	— 0.00227	— 0.00058	— 0.00756	— 0.00016
0.12	— 0.7129	0.2952	— 0.1396	— 0.1530	0.00003	— 0.00026	— 0.00219	— 0.00081	— 0.00754	— 0.00024
0.14	— 0.6757	0.2983	— 0.1611	— 0.1527	0.00005	— 0.00029	— 0.00212	— 0.00105	— 0.00752	— 0.00033
0.16	— 0.6446	0.2989	— 0.1794	— 0.1518	0.00007	— 0.00033	— 0.00205	— 0.00129	— 0.00750	— 0.00042
0.18	— 0.6182	0.2978	— 0.1952	— 0.1502	0.00010	— 0.00036	— 0.00200	— 0.00153	— 0.00749	— 0.00050
0.20	— 0.5950	0.2961	— 0.2094	— 0.1477	0.00014	— 0.00040	— 0.00194	— 0.00177	— 0.00748	— 0.00058
0.22	— 0.5740	0.2943	— 0.2224	— 0.1445	0.00019	— 0.00044	— 0.00190	— 0.00201	— 0.00748	— 0.00066
0.24	— 0.5552	0.2919	— 0.2344	— 0.1408	0.00023	— 0.00047	— 0.00186	— 0.00225	— 0.00748	— 0.00074
0.26	— 0.5385	0.2894	— 0.2450	— 0.1367	0.00028	— 0.00050	— 0.00182	— 0.00250	— 0.00748	— 0.00082
0.28	— 0.5236	0.2869	— 0.2546	— 0.1324	0.00034	— 0.00054	— 0.00178	— 0.00274	— 0.00748	— 0.00090
0.30	— 0.5104	0.2844	— 0.2634	— 0.1279	0.00041	— 0.00058	— 0.00175	— 0.00299	— 0.00749	— 0.00097
0.32	— 0.4981	0.2821	— 0.2715	— 0.1234	0.00048	— 0.00061	— 0.00172	— 0.00324	— 0.00749	— 0.00105
0.34	— 0.4869	0.2801	— 0.2791	— 0.1186	0.00056	— 0.00066	— 0.00168	— 0.00348	— 0.00750	— 0.00112
0.36	— 0.4763	0.2782	— 0.2863	— 0.1137	0.00065	— 0.00070	— 0.00166	— 0.00373	— 0.00751	— 0.00120
0.38	— 0.4662	0.2765	— 0.2931	— 0.1087	0.00074	— 0.00074	— 0.00164	— 0.00398	— 0.00752	— 0.00127
0.40	— 0.4565	0.2750	— 0.2994	— 0.1036	0.00083	— 0.00078	— 0.00161	— 0.00423	— 0.00753	— 0.00134
0.42	— 0.4471	0.2738	— 0.3054	— 0.0984	0.00093	— 0.00083	— 0.00159	— 0.00448	— 0.00754	— 0.00142
0.44	— 0.4380	0.2729	— 0.3110	— 0.0932	0.00103	— 0.00087	— 0.00157	— 0.00474	— 0.00755	— 0.00149
0.46	— 0.4291	0.2721	— 0.3162	— 0.0878	0.00114	— 0.00092	— 0.00156	— 0.00499	— 0.00756	— 0.00156
0.48	— 0.4204	0.2714	— 0.3210	— 0.0823	0.00125	— 0.00097	— 0.00154	— 0.00524	— 0.00757	— 0.00163
0.50	— 0.4120	0.2708	— 0.3255	— 0.0767	0.00136	— 0.00102	— 0.00153	— 0.00549	— 0.00758	— 0.00170
0.52	— 0.4038	0.2702	— 0.3297	— 0.0709	0.00149	— 0.00108	— 0.00152	— 0.00575	— 0.00760	— 0.00177
0.54	— 0.3955	0.2696	— 0.3336	— 0.0650	0.00161	— 0.00113	— 0.00151	— 0.00600	— 0.00761	— 0.00184
0.56	— 0.3873	0.2690	— 0.3371	— 0.0590	0.00174	— 0.00119	— 0.00151	— 0.00625	— 0.00762	— 0.00190
0.58	— 0.3792	0.2683	— 0.3403	— 0.0529	0.00188	— 0.00125	— 0.00151	— 0.00651	— 0.00764	— 0.00197
0.60	— 0.3710	0.2675	— 0.3432	— 0.0466	0.00201	— 0.00132	— 0.00151	— 0.00676	— 0.00765	— 0.00203
0.62	— 0.3629	0.2666	— 0.3457	— 0.0403	0.00216	— 0.00139	— 0.00152	— 0.00702	— 0.00767	— 0.00210
0.64	— 0.3547	0.2655	— 0.3479	— 0.0338	0.00232	— 0.00147	— 0.00152	— 0.00727	— 0.00768	— 0.00216
0.66	— 0.3466	0.2642	— 0.3498	— 0.0273	0.00248	— 0.00155	— 0.00153	— 0.00752	— 0.00769	— 0.00222
0.68	— 0.3384	0.2628	— 0.3512	— 0.0207	0.00263	— 0.00163	— 0.00154	— 0.00777	— 0.00770	— 0.00229
0.70	— 0.3303	0.2611	— 0.3523	— 0.0141	0.00280	— 0.00171	— 0.00156	— 0.00801	— 0.00771	— 0.00235
0.72	— 0.3222	0.2591	— 0.3530	— 0.0076	0.00297	— 0.00181	— 0.00157	— 0.00826	— 0.00772	— 0.00242
0.74	— 0.3142	0.2569	— 0.3532	— 0.0008	0.00313	— 0.00190	— 0.00159	— 0.00850	— 0.00772	— 0.00248
0.76	— 0.3062	0.2545	— 0.3532	+ 0.0058	0.00330	— 0.00200	— 0.00161	— 0.00874	— 0.00773	— 0.00255
0.78	— 0.2983	0.2519	— 0.3526	0.0124	0.00349	— 0.00211	— 0.00163	— 0.00899	— 0.00774	— 0.00262
0.80	— 0.2905	0.2490	— 0.3517	0.0189	0.00366	— 0.00220	— 0.00166	— 0.00923	— 0.00774	— 0.00268
0.82	— 0.2829	0.2457	— 0.3505	0.0253	0.00385	— 0.00232	— 0.00168	— 0.00945	— 0.00774	— 0.00275
0.84	— 0.2754	0.2421	— 0.3489	0.0315	0.00404	— 0.00243	— 0.00171	— 0.00967	— 0.00775	— 0.00282
0.86	— 0.2681	0.2382	— 0.3469	0.0376	0.00423	— 0.00254	— 0.00174	— 0.00989	— 0.00776	— 0.00289
0.88	— 0.2610	0.2340	— 0.3445	0.0436	0.00442	— 0.00266	— 0.00177	— 0.01011	— 0.00776	— 0.00296
0.90	— 0.2541	0.2295	— 0.3418	0.0494	0.00462	— 0.00278	— 0.00181	— 0.01033	— 0.00777	— 0.00304
0.92	— 0.2475	0.2247	— 0.3388	0.0550	0.00482	— 0.00291	— 0.00184	— 0.01055	— 0.00778	— 0.00311
0.94	— 0.2412	0.2197	— 0.3355	0.0603	0.00502	— 0.00304	— 0.00187	— 0.01077	— 0.00778	— 0.00318
0.96	— 0.2352	0.2143	— 0.3318	0.0654	0.00522	— 0.00318	— 0.00190	— 0.01097	— 0.00779	— 0.00326
0.98	— 0.2295	0.2087	— 0.3279	0.0703	0.00542	— 0.00332	— 0.00193	— 0.01116	— 0.00779	— 0.00334
1.00	— 0.2242	0.2028	— 0.3237	0.0750	0.00562	— 0.00346	— 0.00195	— 0.01135	— 0.00780	— 0.00342

TABLE 16.

Flap coefficienas for $\tau = 0.1$ and $\beta = 0.80$.

ω	k_c'	k_c''	m_c'	m_c''	n_a'	n_a''	n_b'	n_b''	n_c'	n_c''
0	— 1.3194	0	+ 0.0867	0	0	0	— 0.00366	0	— 0.00938	0
0.02	— 1.166	+ 0.2471	+ 0.0135	— 0.1279	0	— 0.00006	— 0.00331	+ 0.00018	— 0.00926	+ 0.00011
0.04	— 1.034	0.3448	— 0.0567	— 0.1777	0	— 0.00012	— 0.00303	+ 0.00005	— 0.00916	+ 0.00008
0.06	— 0.925	0.3856	— 0.1180	— 0.1959	0	— 0.00017	— 0.00282	— 0.00018	— 0.00907	0
0.08	— 0.835	0.3986	— 0.1712	— 0.1976	0	— 0.00021	— 0.00266	— 0.00044	— 0.00900	— 0.00009
0.10	— 0.7588	0.3999	— 0.2162	— 0.1921	+ 0.00001	— 0.00025	— 0.00253	— 0.00073	— 0.00896	— 0.00020
0.12	— 0.7074	0.3970	— 0.2531	— 0.1838	0.00003	— 0.00030	— 0.00244	— 0.00102	— 0.00892	— 0.00030
0.14	— 0.6618	0.3927	— 0.2833	— 0.1736	0.00006	— 0.00035	— 0.00237	— 0.00132	— 0.00890	— 0.00040
0.16	— 0.6215	0.3884	— 0.3073	— 0.1628	0.00010	— 0.00040	— 0.00231	— 0.00162	— 0.00890	— 0.00050
0.18	— 0.5859	0.3844	— 0.3264	— 0.1516	0.00014	— 0.00044	— 0.00226	— 0.00192	— 0.00890	— 0.00059
0.20	— 0.5545	0.3799	— 0.3431	— 0.1392	0.00019	— 0.00048	— 0.00222	— 0.00222	— 0.00891	— 0.00068
0.22	— 0.5267	0.3743	— 0.3585	— 0.1256	0.00024	— 0.00052	— 0.00219	— 0.00252	— 0.00892	— 0.00077
0.24	— 0.5019	0.3681	— 0.3723	— 0.1112	0.00030	— 0.00056	— 0.00216	— 0.00281	— 0.00894	— 0.00086
0.26	— 0.4794	0.3625	— 0.3841	— 0.0966	0.00037	— 0.00060	— 0.00214	— 0.00311	— 0.00896	— 0.00094
0.28	— 0.4585	0.3573	— 0.3942	— 0.0817	0.00044	— 0.00065	— 0.00212	— 0.00341	— 0.00898	— 0.00102
0.30	— 0.4391	0.3524	— 0.4026	— 0.0666	0.00052	— 0.00069	— 0.00211	— 0.00371	— 0.00900	— 0.00109
0.32	— 0.4203	0.3472	— 0.4094	— 0.0512	0.00061	— 0.00074	— 0.00210	— 0.00401	— 0.00902	— 0.00117
0.34	— 0.4033	0.3417	— 0.4147	— 0.0356	0.00070	— 0.00080	— 0.00210	— 0.00431	— 0.00904	— 0.00124
0.36	— 0.3867	0.3359	— 0.4184	— 0.0198	0.00080	— 0.00086	— 0.00211	— 0.00460	— 0.00906	— 0.00131
0.38	— 0.3707	0.3301	— 0.4207	— 0.0039	0.00090	— 0.00092	— 0.00212	— 0.00490	— 0.00908	— 0.00138
0.40	— 0.3554	0.3242	— 0.4214	+ 0.0118	0.00101	— 0.00098	— 0.00213	— 0.00519	— 0.00910	— 0.00145
0.42	— 0.3407	0.3174	— 0.4207	0.0276	0.00112	— 0.00105	— 0.00215	— 0.00549	— 0.00911	— 0.00152
0.44	— 0.3267	0.3102	— 0.4185	0.0429	0.00124	— 0.00112	— 0.00217	— 0.00578	— 0.00913	— 0.00159
0.46	— 0.3133	0.3025	— 0.4150	0.0577	0.00136	— 0.00119	— 0.00220	— 0.00607	— 0.00914	— 0.00166
0.48	— 0.3007	0.2943	— 0.4101	0.0719	0.00149	— 0.00127	— 0.00223	— 0.00637	— 0.00914	— 0.00172
0.50	— 0.2888	0.2856	— 0.4039	0.0855	0.00162	— 0.00135	— 0.00226	— 0.00666	— 0.00915	— 0.00179
0.52	— 0.2778	0.2765	— 0.3965	0.0981	0.00176	— 0.00143	— 0.00230	— 0.00693	— 0.00915	— 0.00186
0.54	— 0.2676	0.2671	— 0.3880	0.1098	0.00190	— 0.00152	— 0.00234	— 0.00720	— 0.00916	— 0.00193
0.56	— 0.2585	0.2573	— 0.3785	0.1205	0.00205	— 0.00161	— 0.00238	— 0.00747	— 0.00916	— 0.00200
0.58	— 0.2503	0.2472	— 0.3682	0.1300	0.00220	— 0.00170	— 0.00242	— 0.00774	— 0.00916	— 0.00208
0.60	— 0.2431	0.2370	— 0.3571	0.1384	0.00235	— 0.00180	— 0.00246	— 0.00800	— 0.00916	— 0.00216
0.62	— 0.2369	0.2267	— 0.3455	0.1454	0.00250	— 0.00190	— 0.00251	— 0.00824	— 0.00916	— 0.00224
0.64	— 0.2318	0.2165	— 0.3335	0.1511	0.00265	— 0.00201	— 0.00255	— 0.00849	— 0.00916	— 0.00233
0.66	— 0.2278	0.2062	— 0.3214	0.1555	0.00281	— 0.00212	— 0.00259	— 0.00874	— 0.00916	— 0.00242
0.68	— 0.2247	0.1962	— 0.3092	0.1586	0.00298	— 0.00223	— 0.00263	— 0.00899	— 0.00916	— 0.00251
0.70	— 0.2226	0.1863	— 0.2972	0.1605	0.00314	— 0.00235	— 0.00267	— 0.00923	— 0.00916	— 0.00260
0.72	— 0.2213	0.1768	— 0.2856	0.1612	0.00330	— 0.00247	— 0.00270	— 0.00948	— 0.00916	— 0.00271
0.74	— 0.2209	0.1676	— 0.2744	0.1607	0.00348	— 0.00259	— 0.00273	— 0.00971	— 0.00916	— 0.00282
0.76	— 0.2213	0.1590	— 0.2638	0.1591	0.00365	— 0.00271	— 0.00276	— 0.00994	— 0.00917	— 0.00293
0.78	— 0.2223	0.1509	— 0.2538	0.1565	0.00384	— 0.00283	— 0.00279	— 0.01017	— 0.00917	— 0.00304
0.80	— 0.2239	0.1436	— 0.2446	0.1531	0.00402	— 0.00295	— 0.00282	— 0.01040	— 0.00918	— 0.00315
0.82	— 0.2260	0.1375	— 0.2360	0.1489	0.00421	— 0.00309	— 0.00284	— 0.01064	— 0.00919	— 0.00327
0.84	— 0.2285	0.1323	— 0.2281	0.1442	0.00441	— 0.00323	— 0.00287	— 0.01087	— 0.00920	— 0.00339
0.86	— 0.2313	0.1279	— 0.2205	0.1390	0.00460	— 0.00336	— 0.00289	— 0.01110	— 0.00921	— 0.00352
0.88	— 0.2344	0.1243	— 0.2129	0.1335	0.00481	— 0.00350	— 0.00290	— 0.01133	— 0.00922	— 0.00364
0.90	— 0.2377	0.1215	— 0.2054	0.1280	0.00501	— 0.00365	— 0.00292	— 0.01156	— 0.00924	— 0.00376

TABLE 17.

Flap coefficients for $\tau = 0.2$ and $\beta = 0$.

ω	k_c'	k_c''	m_c'	m_c''	n_a'	n_a''	n_b'	n_b''	n_c'	n_c''
0	− 1.0996	0	+ 0.1424	0	0	0	− 0.01272	0	− 0.02350	0
0.02	− 1.0602	+ 0.0741	0.1227	− 0.0421	− 0.00001	− 0.00025	− 0.01226	+ 0.00003	− 0.02325	+ 0.00007
0.04	− 1.0204	0.1108	0.1028	− 0.0655	− 0.00002	− 0.00047	− 0.01180	− 0.00036	− 0.02299	− 0.00011
0.06	− 0.9834	0.1323	0.0843	− 0.0812	− 0.00003	− 0.00068	− 0.01136	− 0.00093	− 0.02275	− 0.00037
0.08	− 0.9498	0.1445	0.0676	− 0.0923	− 0.00001	− 0.00088	− 0.01096	− 0.00160	− 0.02254	− 0.00070
0.10	− 0.9197	0.1505	0.0526	− 0.1003	+ 0.00001	− 0.00106	− 0.01059	− 0.00235	− 0.02234	− 0.00107
0.12	− 0.8928	0.1522	0.0392	− 0.1062	0.00006	− 0.00123	− 0.01025	− 0.00314	− 0.02216	− 0.00146
0.14	− 0.8687	0.1508	0.0273	− 0.1106	0.00013	− 0.00139	− 0.00994	− 0.00396	− 0.02199	− 0.00188
0.16	− 0.8471	0.1472	0.0166	− 0.1138	0.00021	− 0.00155	− 0.00964	− 0.00480	− 0.02184	− 0.00231
0.18	− 0.8278	0.1420	+ 0.0071	− 0.1162	0.00032	− 0.00170	− 0.00937	− 0.00567	− 0.02171	− 0.00275
0.20	− 0.8104	0.1357	− 0.0014	− 0.1180	0.00045	− 0.00185	− 0.00911	− 0.00655	− 0.02158	− 0.00319
0.22	− 0.7947	0.1285	− 0.0091	− 0.1194	0.00060	− 0.00199	− 0.00886	− 0.00743	− 0.02146	− 0.00364
0.24	− 0.7805	0.1207	− 0.0160	− 0.1206	0.00077	− 0.00213	− 0.00862	− 0.00832	− 0.02135	− 0.00410
0.26	− 0.7676	0.1124	− 0.0222	− 0.1215	0.00096	− 0.00227	− 0.00838	− 0.00922	− 0.02125	− 0.00456
0.28	− 0.7558	0.1038	− 0.0279	− 0.1222	0.00117	− 0.00240	− 0.00815	− 0.01011	− 0.02115	− 0.00502
0.30	− 0.7451	0.0951	− 0.0330	− 0.1229	0.00141	− 0.00254	− 0.00793	− 0.01101	− 0.02106	− 0.00548
0.32	− 0.7353	0.0862	− 0.0376	− 0.1235	0.00166	− 0.00267	− 0.00771	− 0.01192	− 0.02097	− 0.00594
0.34	− 0.7263	0.0772	− 0.0418	− 0.1240	0.00193	− 0.00280	− 0.00749	− 0.01282	− 0.02089	− 0.00640
0.36	− 0.7180	0.0682	− 0.0457	− 0.1245	0.00223	− 0.00293	− 0.00727	− 0.01372	− 0.02081	− 0.00686
0.38	− 0.7103	0.0591	− 0.0492	− 0.1250	0.00254	− 0.00305	− 0.00705	− 0.01462	− 0.02073	− 0.00733
0.40	− 0.7032	0.0501	− 0.0524	− 0.1255	0.00288	− 0.00318	− 0.00683	− 0.01553	− 0.02065	− 0.00779
0.42	− 0.6966	0.0411	− 0.0554	− 0.1260	0.00323	− 0.00330	− 0.00660	− 0.01643	− 0.02057	− 0.00825
0.44	− 0.6904	0.0321	− 0.0581	− 0.1265	0.00361	− 0.00343	− 0.00637	− 0.01733	− 0.02050	− 0.00872
0.46	− 0.6846	0.0232	− 0.0606	− 0.1271	0.00400	− 0.00355	− 0.00614	− 0.01823	− 0.02042	− 0.00918
0.48	− 0.6792	0.0144	− 0.0629	− 0.1277	0.00441	− 0.00368	− 0.00591	− 0.01913	− 0.02035	− 0.00964
0.50	− 0.6741	+ 0.0056	− 0.0650	− 0.1283	0.00485	− 0.00380	− 0.00567	− 0.02003	− 0.02028	− 0.01010
0.52	− 0.6693	− 0.0031	− 0.0670	− 0.1290	0.00530	− 0.00393	− 0.00543	− 0.02093	− 0.02020	− 0.01056
0.54	− 0.6648	− 0.0117	− 0.0688	− 0.1297	0.00577	− 0.00405	− 0.00518	− 0.02182	− 0.02013	− 0.01102
0.56	− 0.6606	− 0.0203	− 0.0705	− 0.1304	0.00627	− 0.00417	− 0.00493	− 0.02272	− 0.02006	− 0.01148
0.58	− 0.6566	− 0.0288	− 0.0720	− 0.1312	0.00678	− 0.00429	− 0.00467	− 0.02361	− 0.01998	− 0.01194
0.60	− 0.6527	− 0.0372	− 0.0734	− 0.1320	0.00731	− 0.00442	− 0.00441	− 0.02451	− 0.01991	− 0.01240
0.62	− 0.6491	− 0.0456	− 0.0747	− 0.1329	0.00786	− 0.00454	− 0.00415	− 0.02540	− 0.01984	− 0.01286
0.64	− 0.6456	− 0.0538	− 0.0759	− 0.1338	0.00843	− 0.00466	− 0.00387	− 0.02629	− 0.01976	− 0.01332
0.66	− 0.6422	− 0.0620	− 0.0771	− 0.1347	0.00902	− 0.00478	− 0.00359	− 0.02719	− 0.01969	− 0.01377
0.68	− 0.6390	− 0.0702	− 0.0781	− 0.1356	0.00963	− 0.00491	− 0.00331	− 0.02808	− 0.01961	− 0.01423
0.70	− 0.6360	− 0.0783	− 0.0790	− 0.1366	0.01025	− 0.00503	− 0.00302	− 0.02897	− 0.01953	− 0.01469
0.72	− 0.6330	− 0.0863	− 0.0799	− 0.1376	0.01090	− 0.00515	− 0.00272	− 0.02986	− 0.01946	− 0.01514
0.74	− 0.6302	− 0.0942	− 0.0807	− 0.1387	0.01157	− 0.00527	− 0.00242	− 0.03075	− 0.01938	− 0.01560
0.76	− 0.6275	− 0.1021	− 0.0814	− 0.1398	0.01225	− 0.00539	− 0.00210	− 0.03163	− 0.01930	− 0.01606
0.78	− 0.6248	− 0.1099	− 0.0821	− 0.1409	0.01295	− 0.00552	− 0.00179	− 0.03252	− 0.01922	− 0.01651
0.80	− 0.6222	− 0.1177	− 0.0827	− 0.1420	0.01368	− 0.00564	− 0.00146	− 0.03341	− 0.01913	− 0.01697
0.82	− 0.6197	− 0.1254	− 0.0833	− 0.1431	0.01442	− 0.00576	− 0.00113	− 0.03429	− 0.01905	− 0.01742
0.84	− 0.6173	− 0.1330	− 0.0838	− 0.1443	0.01518	− 0.00588	− 0.00080	− 0.03518	− 0.01897	− 0.01787
0.86	− 0.6149	− 0.1406	− 0.0843	− 0.1455	0.01596	− 0.00600	− 0.00045	− 0.03606	− 0.01888	− 0.01833
0.88	− 0.6126	− 0.1482	− 0.0847	− 0.1468	0.01676	− 0.00613	− 0.00010	− 0.03695	− 0.01880	− 0.01878
0.90	− 0.6104	− 0.1557	− 0.0850	− 0.1481	0.01758	− 0.00625	+ 0.00026	− 0.03783	− 0.01871	− 0.01924
0.92	− 0.6082	− 0.1632	− 0.0853	− 0.1494	0.01841	− 0.00637	0.00062	− 0.03871	− 0.01862	− 0.01969
0.94	− 0.6060	− 0.1706	− 0.0856	− 0.1507	0.01927	− 0.00649	0.00099	− 0.03960	− 0.01852	− 0.02014
0.96	− 0.6039	− 0.1780	− 0.0859	− 0.1520	0.02014	− 0.00662	0.00137	− 0.04048	− 0.01843	− 0.02059
0.98	− 0.6018	− 0.1853	− 0.0861	− 0.1533	0.02104	− 0.00674	0.00176	− 0.04136	− 0.01834	− 0.02104
1.00	− 0.5998	− 0.1926	− 0.0863	− 0.1547	0.02195	− 0.00686	0.00216	− 0.04224	− 0.01824	− 0.02150

TABLE 18.

Flap coefficients for $\tau = 0.2$ and $\beta = 0.35$.

ω	k_c'	k_c''	m_c'	m_c''	n_a'	n_a''	n_b'	n_b''	n_c'	n_c''
0	−1.1739	0	+0.1520	0	0	0	−0.01358	0	−0.02509	0
0.02	−1.1252	+0.0939	0.1276	−0.0526	−0.00001	−0.00026	−0.01302	+0.00011	−0.02478	+0.00012
0.04	−1.0760	0.1400	0.1027	−0.0813	−0.00002	−0.00050	−0.01247	−0.00029	−0.02447	−0.00004
0.06	−1.0305	0.1675	0.0797	−0.1007	−0.00003	−0.00071	−0.01195	−0.00089	−0.02418	−0.00033
0.08	−0.9896	0.1832	0.0589	−0.1138	−0.00002	−0.00091	−0.01150	−0.00161	−0.02393	−0.00068
0.10	−0.9531	0.1913	0.0402	−0.1230	0	−0.00110	−0.01109	−0.00240	−0.02371	−0.00107
0.12	−0.9209	0.1943	0.0237	−0.1298	+0.00005	−0.00128	−0.01071	−0.00324	−0.02351	−0.00150
0.14	−0.8926	0.1938	+0.0091	−0.1349	0.00012	−0.00146	−0.01037	−0.00412	−0.02333	−0.00195
0.16	−0.8677	0.1910	−0.0037	−0.1387	0.00021	−0.00162	−0.01006	−0.00504	−0.02318	−0.00241
0.18	−0.8458	0.1865	−0.0150	−0.1416	0.00033	−0.00178	−0.00977	−0.00598	−0.02304	−0.00288
0.20	−0.8265	0.1808	−0.0250	−0.1439	0.00047	−0.00193	−0.00949	−0.00693	−0.02292	−0.00336
0.22	−0.8093	0.1742	−0.0339	−0.1457	0.00063	−0.00208	−0.00924	−0.00789	−0.02281	−0.00385
0.24	−0.7939	0.1670	−0.0420	−0.1471	0.00081	−0.00223	−0.00900	−0.00885	−0.02270	−0.00434
0.26	−0.7801	0.1594	−0.0494	−0.1484	0.00101	−0.00238	−0.00878	−0.00981	−0.02260	−0.00482
0.28	−0.7677	0.1515	−0.0560	−0.1495	0.00124	−0.00252	−0.00856	−0.01078	−0.02252	−0.00531
0.30	−0.7565	0.1434	−0.0620	−0.1505	0.00150	−0.00267	−0.00834	−0.01175	−0.02244	−0.00580
0.32	−0.7464	0.1352	−0.0674	−0.1514	0.00178	−0.00281	−0.00814	−0.01272	−0.02237	−0.00630
0.34	−0.7374	0.1271	−0.0723	−0.1524	0.00207	−0.00296	−0.00793	−0.01370	−0.02231	−0.00679
0.36	−0.7292	0.1189	−0.0768	−0.1534	0.00239	−0.00311	−0.00773	−0.01468	−0.02224	−0.00728
0.38	−0.7217	0.1108	−0.0810	−0.1544	0.00274	−0.00325	−0.00752	−0.01566	−0.02218	−0.00778
0.40	−0.7149	0.1027	−0.0848	−0.1554	0.00311	−0.00340	−0.00731	−0.01665	−0.02212	−0.00827
0.42	−0.7087	0.0947	−0.0884	−0.1564	0.00349	−0.00355	−0.00710	−0.01763	−0.02207	−0.00876
0.44	−0.7032	0.0869	−0.0916	−0.1575	0.00388	−0.00370	−0.00690	−0.01861	−0.02202	−0.00925
0.46	−0.6982	0.0791	−0.0946	−0.1586	0.00430	−0.00385	−0.00670	−0.01960	−0.02197	−0.00973
0.48	−0.6936	0.0714	−0.0973	−0.1598	0.00475	−0.00400	−0.00650	−0.02059	−0.02192	−0.01022
0.50	−0.6895	0.0639	−0.0999	−0.1610	0.00522	−0.00415	−0.00629	−0.02158	−0.02187	−0.01072
0.52	−0.6857	0.0564	−0.1023	−0.1623	0.00571	−0.00430	−0.00607	−0.02257	−0.02183	−0.01121
0.54	−0.6822	0.0491	−0.1045	−0.1636	0.00622	−0.00446	−0.00585	−0.02355	−0.02179	−0.01169
0.56	−0.6791	0.0419	−0.1065	−0.1649	0.00675	−0.00462	−0.00565	−0.02454	−0.02175	−0.01218
0.58	−0.6763	0.0347	−0.1084	−0.1664	0.00731	−0.00478	−0.00543	−0.02553	−0.02171	−0.01267
0.60	−0.6738	0.0277	−0.1102	−0.1679	0.00789	−0.00494	−0.00520	−0.02653	−0.02167	−0.01315
0.62	−0.6715	0.0208	−0.1119	−0.1694	0.00849	−0.00510	−0.00497	−0.02753	−0.02163	−0.01364
0.64	−0.6695	0.0139	−0.1134	−0.1710	0.00911	−0.00527	−0.00474	−0.02853	−0.02159	−0.01413
0.66	−0.6677	0.0072	−0.1149	−0.1727	0.00975	−0.00544	−0.00450	−0.02953	−0.02155	−0.01462
0.68	−0.6661	+0.0005	−0.1163	−0.1744	0.01043	−0.00562	−0.00426	−0.03054	−0.02151	−0.01511
0.70	−0.6647	−0.0060	−0.1176	−0.1761	0.01113	−0.00580	−0.00402	−0.03155	−0.02147	−0.01559
0.72	−0.6635	−0.0125	−0.1188	−0.1779	0.01185	−0.00599	−0.00378	−0.03256	−0.02143	−0.01608
0.74	−0.6625	−0.0188	−0.1200	−0.1797	0.01259	−0.00618	−0.00354	−0.03357	−0.02139	−0.01656
0.76	−0.6616	−0.0251	−0.1211	−0.1816	0.01334	−0.00638	−0.00329	−0.03459	−0.02135	−0.01705
0.78	−0.6608	−0.0313	−0.1221	−0.1835	0.01413	−0.00658	−0.00304	−0.03561	−0.02131	−0.01754
0.80	−0.6602	−0.0374	−0.1231	−0.1855	0.01494	−0.00678	−0.00278	−0.03663	−0.02127	−0.01802
0.82	−0.6597	−0.0435	−0.1240	−0.1875	0.01578	−0.00699	−0.00252	−0.03765	−0.02123	−0.01850
0.84	−0.6594	−0.0494	−0.1248	−0.1896	0.01662	−0.00720	−0.00226	−0.03868	−0.02119	−0.01899
0.86	−0.6592	−0.0553	−0.1256	−0.1917	0.01749	−0.00742	−0.00201	−0.03971	−0.02115	−0.01948
0.88	−0.6592	−0.0612	−0.1264	−0.1938	0.01838	−0.00765	−0.00174	−0.04075	−0.02111	−0.01996
0.90	−0.6593	−0.0669	−0.1272	−0.1960	0.01929	−0.00788	−0.00146	−0.04179	−0.02107	−0.02045
0.92	−0.6594	−0.0726	−0.1279	−0.1982	0.02023	−0.00812	−0.00118	−0.04283	−0.02103	−0.02093
0.94	−0.6596	−0.0781	−0.1286	−0.2004	0.02120	−0.00836	−0.00090	−0.04387	−0.02099	−0.02142
0.96	−0.6599	−0.0836	−0.1292	−0.2027	0.02219	−0.00860	−0.00062	−0.04492	−0.02095	−0.02190
0.98	−0.6603	−0.0891	−0.1298	−0.2049	0.02321	−0.00885	−0.00034	−0.04597	−0.02092	−0.02238
1.00	−0.6608	−0.0944	−0.1303	−0.2072	0.02426	−0.00911	−0.00005	−0.04703	−0.02088	−0.02286

TABLE 19.

Flap coefficients for $\tau = 0.2$ and $\beta = 0.50$.

ω	k_c'	k_c''	m_c'	m_c''	n_a'	n_a''	n_b'	n_b''	n_c'	n_c''
0	— 1.2697	0	+ 0.1644	0	0	0	— 0.01468	0	— 0.02714	0
0.02	— 1.2072	+ 0.1210	0.1329	— 0.0671	— 0.00001	— 0.00028	— 0.01398	+ 0.00022	— 0.02675	+ 0.00020
0.04	— 1.1446	0.1796	0.1010	— 0.1027	— 0.00003	— 0.00052	— 0.01329	— 0.00018	— 0.02637	+ 0.00006
0.06	— 1.0876	0.2142	0.0717	— 0.1259	— 0.00005	— 0.00075	— 0.01268	— 0.00081	— 0.02602	— 0.00024
0.08	— 1.0369	0.2334	0.0452	— 0.1412	— 0.00003	— 0.00096	— 0.01215	— 0.00161	— 0.02572	— 0.00063
0.10	— 0.9920	0.2428	0.0216	— 0.1514	0	— 0.00115	— 0.01167	— 0.00249	— 0.02547	— 0.00107
0.12	— 0.9528	0.2462	+ 0.0008	— 0.1586	+ 0.00006	— 0.00134	— 0.01125	— 0.00344	— 0.02525	— 0.00155
0.14	— 0.9187	0.2459	— 0.0175	— 0.1643	0.00013	— 0.00152	— 0.01088	— 0.00442	— 0.02506	— 0.00205
0.16	— 0.8889	0.2431	— 0.0336	— 0.1675	0.00023	— 0.00169	— 0.01055	— 0.00543	— 0.02490	— 0.00256
0.18	— 0.8632	0.2386	— 0.0478	— 0.1704	0.00036	— 0.00186	— 0.01026	— 0.00646	— 0.02476	— 0.00308
0.20	— 0.8407	0.2329	— 0.0602	— 0.1726	0.00053	— 0.00203	— 0.00999	— 0.00750	— 0.02464	— 0.00361
0.22	— 0.8213	0.2266	— 0.0712	— 0.1745	0.00070	— 0.00219	— 0.00974	— 0.00856	— 0.02454	— 0.00414
0.24	— 0.8046	0.2199	— 0.0808	— 0.1760	0.00090	— 0.00235	— 0.00950	— 0.00962	— 0.02446	— 0.00467
0.26	— 0.7896	0.2129	— 0.0895	— 0.1768	0.00113	— 0.00251	— 0.00928	— 0.01069	— 0.02438	— 0.00520
0.28	— 0.7763	0.2056	— 0.0974	— 0.1780	0.00139	— 0.00267	— 0.00907	— 0.01176	— 0.02432	— 0.00574
0.30	— 0.7643	0.1981	— 0.1049	— 0.1793	0.00166	— 0.00283	— 0.00886	— 0.01283	— 0.02426	— 0.00627
0.32	— 0.7536	0.1907	— 0.1117	— 0.1804	0.00196	— 0.00299	— 0.00866	— 0.01390	— 0.02421	— 0.00680
0.34	— 0.7440	0.1834	— 0.1178	— 0.1815	0.00229	— 0.00316	— 0.00846	— 0.01497	— 0.02417	— 0.00733
0.36	— 0.7354	0.1763	— 0.1236	— 0.1825	0.00263	— 0.00332	— 0.00828	— 0.01606	— 0.02413	— 0.00786
0.38	— 0.7278	0.1694	— 0.1289	— 0.1836	0.00300	— 0.00349	— 0.00809	— 0.01715	— 0.02409	— 0.00839
0.40	— 0.7208	0.1626	— 0.1339	— 0.1848	0.00340	— 0.00367	— 0.00792	— 0.01823	— 0.02406	— 0.00892
0.42	— 0.7147	0.1560	— 0.1384	— 0.1860	0.00382	— 0.00384	— 0.00773	— 0.01931	— 0.02404	— 0.00945
0.44	— 0.7092	0.1496	— 0.1427	— 0.1873	0.00427	— 0.00402	— 0.00756	— 0.02040	— 0.02402	— 0.00997
0.46	— 0.7042	0.1433	— 0.1468	— 0.1887	0.00474	— 0.00420	— 0.00738	— 0.02149	— 0.02400	— 0.01049
0.48	— 0.6997	0.1372	— 0.1508	— 0.1901	0.00523	— 0.00438	— 0.00721	— 0.02258	— 0.02399	— 0.01101
0.50	— 0.6958	0.1313	— 0.1545	— 0.1916	0.00575	— 0.00456	— 0.00704	— 0.02367	— 0.02398	— 0.01153
0.52	— 0.6923	0.1257	— 0.1579	— 0.1932	0.00629	— 0.00475	— 0.00687	— 0.02478	— 0.02397	— 0.01205
0.54	— 0.6891	0.1202	— 0.1614	— 0.1948	0.00686	— 0.00495	— 0.00670	— 0.02589	— 0.02396	— 0.01256
0.56	— 0.6864	0.1150	— 0.1646	— 0.1965	0.00745	— 0.00516	— 0.00653	— 0.02701	— 0.02396	— 0.01308
0.58	— 0.6840	0.1099	— 0.1677	— 0.1983	0.00807	— 0.00538	— 0.00636	— 0.02813	— 0.02395	— 0.01359
0.60	— 0.6819	0.1051	— 0.1707	— 0.2001	0.00871	— 0.00560	— 0.00619	— 0.02925	— 0.02395	— 0.01411
0.62	— 0.6800	0.1004	— 0.1737	— 0.2020	0.00938	— 0.00582	— 0.00602	— 0.03038	— 0.02395	— 0.01462
0.64	— 0.6784	0.0959	— 0.1765	— 0.2039	0.01006	— 0.00604	— 0.00585	— 0.03151	— 0.02395	— 0.01513
0.66	— 0.6770	0.0916	— 0.1793	— 0.2058	0.01078	— 0.00627	— 0.00569	— 0.03264	— 0.02396	— 0.01564
0.68	— 0.6759	0.0875	— 0.1819	— 0.2078	0.01153	— 0.00651	— 0.00553	— 0.03377	— 0.02397	— 0.01615
0.70	— 0.6750	0.0835	— 0.1846	— 0.2099	0.01229	— 0.00677	— 0.00537	— 0.03492	— 0.02398	— 0.01665
0.72	— 0.6742	0.0797	— 0.1872	— 0.2120	0.01308	— 0.00704	— 0.00521	— 0.03607	— 0.02399	— 0.01716
0.74	— 0.6736	0.0761	— 0.1898	— 0.2141	0.01390	— 0.00733	— 0.00505	— 0.03723	— 0.02400	— 0.01767
0.76	— 0.6732	0.0727	— 0.1924	— 0.2163	0.01474	— 0.00762	— 0.00490	— 0.03839	— 0.02402	— 0.01817
0.78	— 0.6728	0.0694	— 0.1944	— 0.2186	0.01560	— 0.00792	— 0.00475	— 0.03956	— 0.02403	— 0.01867
0.80	— 0.6726	0.0663	— 0.1975	— 0.2208	0.01649	— 0.00823	— 0.00461	— 0.04073	— 0.02405	— 0.01917
0.82	— 0.6726	0.0634	— 0.1999	— 0.2231	0.01741	— 0.00856	— 0.00447	— 0.04190	— 0.02406	— 0.01967
0.84	— 0.6727	0.0606	— 0.2025	— 0.2253	0.01835	— 0.00890	— 0.00433	— 0.04308	— 0.02408	— 0.02016
0.86	— 0.6729	0.0580	— 0.2049	— 0.2276	0.01932	— 0.00924	— 0.00420	— 0.04426	— 0.02410	— 0.02066
0.88	— 0.6731	0.0556	— 0.2074	— 0.2300	0.02031	— 0.00960	— 0.00407	— 0.04544	— 0.02412	— 0.02116
0.90	— 0.6734	0.0534	— 0.2098	— 0.2323	0.02133	— 0.00997	— 0.00395	— 0.04662	— 0.02414	— 0.02165
0.92	— 0.6738	0.0513	— 0.2123	— 0.2346	0.02237	— 0.01036	— 0.00383	— 0.04781	— 0.02416	— 0.02214
0.94	— 0.6742	0.0494	— 0.2147	— 0.2370	0.02344	— 0.01076	— 0.00372	— 0.04900	— 0.02418	— 0.02262
0.96	— 0.6747	0.0476	— 0.2170	— 0.2394	0.02453	— 0.01118	— 0.00362	— 0.05020	— 0.02421	— 0.02311
0.98	— 0.6752	0.0460	— 0.2194	— 0.2418	0.02565	— 0.01162	— 0.00352	— 0.05140	— 0.02423	— 0.02360
1.00	— 0.6757	0.0446	— 0.2218	— 0.2442	0.02679	— 0.01208	— 0.00342	— 0.05260	— 0.02426	— 0.02409

TABLE 20.

Flap coefficients for $\tau = 0.2$ and $\beta = 0.60$.

ω	k_c'	k_c''	m_c'	m_c''	n_a'	n_a''	n_b'	n_b''	n_c'	n_c''
0	— 1.3745	0	+ 0.1780	0	0	0	— 0.01590	0	— 0.02938	0
0.02	— 1.2938	+ 0.1534	0.1369	— 0.0844	— 0.00002	— 0.00030	— 0.01500	+ 0.00036	— 0.02888	+ 0.00032
0.04	— 1.2132	0.2254	0.0954	— 0.1276	— 0.00004	— 0.00057	— 0.01415	— 0.00003	— 0.02841	+ 0.00018
0.06	— 1.1406	0.2651	0.0573	— 0.1536	— 0.00005	— 0.00080	— 0.01341	— 0.00074	— 0.02801	— 0.00017
0.08	— 1.0770	0.2862	+ 0.0233	— 0.1700	— 0.00005	— 0.00102	— 0.01279	— 0.00162	— 0.02767	— 0.00061
0.10	— 1.0223	0.2966	— 0.0063	— 0.1806	— 0.00001	— 0.00123	— 0.01226	— 0.00261	— 0.02738	— 0.00111
0.12	— 0.9758	0.3005	— 0.0317	— 0.1879	+ 0.00006	— 0.00142	— 0.01182	— 0.00369	— 0.02714	— 0.00164
0.14	— 0.9365	0.3003	— 0.0536	— 0.1927	0.00015	— 0.00160	— 0.01144	— 0.00480	— 0.02695	— 0.00220
0.16	— 0.9034	0.2975	— 0.0723	— 0.1961	0.00027	— 0.00178	— 0.01109	— 0.00593	— 0.02680	— 0.00276
0.18	— 0.8752	0.2930	— 0.0887	— 0.1984	0.00042	— 0.00196	— 0.01078	— 0.00707	— 0.02667	— 0.00333
0.20	— 0.8505	0.2873	— 0.1034	— 0.2001	0.00059	— 0.00213	— 0.01051	— 0.00823	— 0.02656	— 0.00390
0.22	— 0.8286	0.2808	— 0.1168	— 0.2011	0.00078	— 0.00230	— 0.01027	— 0.00939	— 0.02648	— 0.00448
0.24	— 0.8093	0.2740	— 0.1289	— 0.2019	0.00101	— 0.00248	— 0.01005	— 0.01055	— 0.02642	— 0.00506
0.26	— 0.7923	0.2673	— 0.1397	— 0.2026	0.00127	— 0.00266	— 0.00985	— 0.01171	— 0.02637	— 0.00564
0.28	— 0.7773	0.2607	— 0.1496	— 0.2032	0.00155	— 0.00284	— 0.00965	— 0.01288	— 0.02633	— 0.00621
0.30	— 0.7641	0.2541	— 0.1588	— 0.2037	0.00186	— 0.00302	— 0.00946	— 0.01406	— 0.02630	— 0.00678
0.32	— 0.7522	0.2476	— 0.1673	— 0.2043	0.00219	— 0.00321	— 0.00928	— 0.01525	— 0.02627	— 0.00735
0.34	— 0.7415	0.2414	— 0.1752	— 0.2048	0.00255	— 0.00340	— 0.00911	— 0.01644	— 0.02625	— 0.00791
0.36	— 0.7320	0.2354	— 0.1826	— 0.2053	0.00293	— 0.00359	— 0.00895	— 0.01763	— 0.02624	— 0.00847
0.38	— 0.7234	0.2296	— 0.1895	— 0.2060	0.00334	— 0.00378	— 0.00880	— 0.01883	— 0.02625	— 0.00903
0.40	— 0.7157	0.2242	— 0.1962	— 0.2068	0.00377	— 0.00398	— 0.00866	— 0.02003	— 0.02626	— 0.00959
0.42	— 0.7088	0.2191	— 0.2026	— 0.2075	0.00423	— 0.00419	— 0.00852	— 0.02124	— 0.02627	— 0.01014
0.44	— 0.7025	0.2143	— 0.2086	— 0.2082	0.00473	— 0.00440	— 0.00838	— 0.02245	— 0.02629	— 0.01069
0.46	— 0.6967	0.2098	— 0.2144	— 0.2090	0.00525	— 0.00462	— 0.00826	— 0.02366	— 0.02632	— 0.01124
0.48	— 0.6915	0.2055	— 0.2200	— 0.2098	0.00579	— 0.00484	— 0.00814	— 0.02488	— 0.02635	— 0.01179
0.50	— 0.6868	0.2016	— 0.2254	— 0.2106	0.00636	— 0.00508	— 0.00802	— 0.02610	— 0.02638	— 0.01233
0.52	— 0.6824	0.1980	— 0.2307	— 0.2115	0.00696	— 0.00533	— 0.00790	— 0.02732	— 0.02642	— 0.01286
0.54	— 0.6783	0.1946	— 0.2359	— 0.2124	0.00758	— 0.00559	— 0.00780	— 0.02855	— 0.02646	— 0.01339
0.56	— 0.6745	0.1916	— 0.2409	— 0.2133	0.00823	— 0.00585	— 0.00770	— 0.02978	— 0.02650	— 0.01392
0.58	— 0.6710	0.1889	— 0.2459	— 0.2143	0.00891	— 0.00612	— 0.00761	— 0.03102	— 0.02655	— 0.01445
0.60	— 0.6677	0.1864	— 0.2509	— 0.2152	0.00961	— 0.00640	— 0.00753	— 0.03227	— 0.02660	— 0.01497
0.62	— 0.6647	0.1841	— 0.2558	— 0.2161	0.01033	— 0.00670	— 0.00747	— 0.03353	— 0.02665	— 0.01549
0.64	— 0.6618	0.182[illegible]	— 0.2606	— 0.2170	0.01108	— 0.00702	— 0.00741	— 0.03479	— 0.02670	— 0.01601
0.66	— 0.6590	0.1804	— 0.2654	— 0.2179	0.01186	— 0.00735	— 0.00735	— 0.03605	— 0.02675	— 0.01652
0.68	— 0.6564	0.1789	— 0.2701	— 0.2187	0.01267	— 0.00769	— 0.00730	— 0.03732	— 0.02681	— 0.01703
0.70	— 0.6538	0.1777	— 0.2748	— 0.2195	0.01350	— 0.00804	— 0.00727	— 0.03859	— 0.02687	— 0.01754
0.72	— 0.6512	0.1766	— 0.2795	— 0.2202	0.01436	— 0.00841	— 0.00725	— 0.03986	— 0.02693	— 0.01804
0.74	— 0.6487	0.1758	— 0.2841	— 0.2209	0.01524	— 0.00880	— 0.00724	— 0.04113	— 0.02700	— 0.01854
0.76	— 0.6462	0.1752	— 0.2888	— 0.2216	0.01614	— 0.00921	— 0.00724	— 0.04240	— 0.02706	— 0.01903
0.78	— 0.6437	0.1748	— 0.2934	— 0.2221	0.01707	— 0.00964	— 0.00726	— 0.04368	— 0.02712	— 0.01952
0.80	— 0.6411	0.1747	— 0.2980	— 0.2226	0.01802	— 0.01008	— 0.00729	— 0.04495	— 0.02719	— 0.02001
0.82	— 0.6385	0.1746	— 0.3026	— 0.2230	0.01900	— 0.01054	— 0.00733	— 0.04622	— 0.02726	— 0.02049
0.84	— 0.6359	0.1747	— 0.3072	— 0.2233	0.02000	— 0.01103	— 0.00738	— 0.04749	— 0.02733	— 0.02097
0.86	— 0.6332	0.1750	— 0.3117	— 0.2235	0.02102	— 0.01154	— 0.00745	— 0.04876	— 0.02740	— 0.02144
0.88	— 0.6303	0.1754	— 0.3163	— 0.2237	0.02206	— 0.01207	— 0.00753	— 0.05003	— 0.02746	— 0.02190
0.90	— 0.6274	0.1760	— 0.3208	— 0.2237	0.02312	— 0.01263	— 0.00762	— 0.05129	— 0.02753	— 0.02236
0.92	— 0.6244	0.1766	— 0.3254	— 0.2236	0.02420	— 0.01321	— 0.00773	— 0.05255	— 0.02759	— 0.02282
0.94	— 0.6212	0.1773	— 0.3299	— 0.2235	0.02530	— 0.01381	— 0.00785	— 0.05380	— 0.02765	— 0.02329
0.96	— 0.6179	0.1781	— 0.3343	— 0.2232	0.02641	— 0.01444	— 0.00798	— 0.05505	— 0.02771	— 0.02376
0.98	— 0.6144	0.1791	— 0.3387	— 0.2228	0.02754	— 0.01509	— 0.00812	— 0.05630	— 0.02777	— 0.02422
1.00	— 0.6108	0.1801	— 0.3430	— 0.2223	0.02870	— 0.01578	— 0.00828	— 0.05754	— 0.02782	— 0.02467

TABLE 21.

Flap coefficients for $\tau = 0.2$ and $\beta = 0.70$.

ω	k_c'	k_c''	m_c'	m_c''	n_a'	n_a''	n_b'	n_b''	n_c'	n_c''
0	— 1.5398	0	+ 0.1994	0	0	0	— 0.01781	0	— 0.03291	0
0.02	— 1.4239	+ 0.2111	0.1402	— 0.1151	— 0.00002	— 0.00033	— 0.01656	+ 0.00070	— 0.03220	+ 0.00052
0.04	— 1.3116	0.3047	0.0815	— 0.1700	— 0.00006	— 0.00062	— 0.01543	+ 0.00025	— 0.03157	+ 0.00035
0.06	— 1.2134	0.3516	+ 0.0285	— 0.1999	— 0.00006	— 0.00087	— 0.01451	— 0.00062	— 0.03107	— 0.00004
0.08	— 1.1291	0.3733	— 0.0179	— 0.2160	— 0.00006	— 0.00109	— 0.01377	— 0.00171	— 0.03067	— 0.00060
0.10	— 1.0583	0.3818	— 0.0579	— 0.2248	— 0.00001	— 0.00131	— 0.01317	— 0.00291	— 0.03036	— 0.00120
0.12	— 0.9996	0.3836	— 0.0920	— 0.2298	+ 0.00007	— 0.00152	— 0.01269	— 0.00418	— 0.03012	— 0.00183
0.14	— 0.9511	0.3814	— 0.1207	— 0.2322	0.00019	— 0.00172	— 0.01228	— 0.00546	— 0.02994	— 0.00247
0.16	— 0.9112	0.3774	— 0.1448	— 0.2333	0.00033	— 0.00192	— 0.01193	— 0.00677	— 0.02980	— 0.00311
0.18	— 0.8779	0.3722	— 0.1655	— 0.2335	0.00051	— 0.00212	— 0.01165	— 0.00809	— 0.02970	— 0.00376
0.20	— 0.8488	0.3660	— 0.1840	— 0.2327	0.00071	— 0.00232	— 0.01140	— 0.00942	— 0.02964	— 0.00440
0.22	— 0.8227	0.3590	— 0.2010	— 0.2313	0.00094	— 0.00252	— 0.01117	— 0.01076	— 0.02960	— 0.00504
0.24	— 0.7996	0.3518	— 0.2166	— 0.2293	0.00120	— 0.00271	— 0.01097	— 0.01211	— 0.02958	— 0.00568
0.26	— 0.7792	0.3449	— 0.2310	— 0.2274	0.00149	— 0.00291	— 0.01079	— 0.01345	— 0.02957	— 0.00630
0.28	— 0.7614	0.3387	— 0.2442	— 0.2256	0.00182	— 0.00313	— 0.01064	— 0.01480	— 0.02959	— 0.00692
0.30	— 0.7455	0.3332	— 0.2565	— 0.2236	0.00217	— 0.00336	— 0.01050	— 0.01615	— 0.02962	— 0.00753
0.32	— 0.7311	0.3281	— 0.2681	— 0.2217	0.00255	— 0.00358	— 0.01038	— 0.01751	— 0.02967	— 0.00814
0.34	— 0.7179	0.3232	— 0.2790	— 0.2196	0.00296	— 0.00381	— 0.01029	— 0.01887	— 0.02973	— 0.00874
0.36	— 0.7055	0.3186	— 0.2894	— 0.2173	0.00341	— 0.00405	— 0.01020	— 0.02022	— 0.02979	— 0.00933
0.38	— 0.6940	0.3144	— 0.2993	— 0.2149	0.00387	— 0.00429	— 0.01013	— 0.02158	— 0.02986	— 0.00991
0.40	— 0.6834	0.3106	— 0.3089	— 0.2124	0.00437	— 0.00454	— 0.01007	— 0.02295	— 0.02994	— 0.01048
0.42	— 0.6734	0.3072	— 0.3181	— 0.2098	0.00490	— 0.00482	— 0.01004	— 0.02433	— 0.03002	— 0.01105
0.44	— 0.6640	0.3042	— 0.3269	— 0.2071	0.00545	— 0.00511	— 0.01001	— 0.02573	— 0.03010	— 0.01161
0.46	— 0.6549	0.3015	— 0.3355	— 0.2042	0.00603	— 0.00540	— 0.01000	— 0.02711	— 0.03020	— 0.01216
0.48	— 0.6461	0.2992	— 0.3437	— 0.2011	0.00665	— 0.00571	— 0.01001	— 0.02850	— 0.03029	— 0.01271
0.50	— 0.6375	0.2972	— 0.3517	— 0.1979	0.00728	— 0.00603	— 0.01003	— 0.02988	— 0.03039	— 0.01324
0.52	— 0.6291	0.2954	— 0.3594	— 0.1944	0.00795	— 0.00637	— 0.01006	— 0.03129	— 0.03049	— 0.01376
0.54	— 0.6209	0.2938	— 0.3668	— 0.1908	0.00864	— 0.00672	— 0.01013	— 0.03268	— 0.03060	— 0.01428
0.56	— 0.6127	0.2924	— 0.3740	— 0.1869	0.00936	— 0.00710	— 0.01022	— 0.03407	— 0.03070	— 0.01479
0.58	— 0.6045	0.2913	— 0.3809	— 0.1828	0.01010	— 0.00750	— 0.01032	— 0.03546	— 0.03082	— 0.01529
0.60	— 0.5963	0.2904	— 0.3876	— 0.1785	0.01086	— 0.00792	— 0.01045	— 0.03685	— 0.03093	— 0.01578
0.62	— 0.5881	0.2894	— 0.3941	— 0.1740	0.01164	— 0.00836	— 0.01060	— 0.03824	— 0.03104	— 0.01626
0.64	— 0.5797	0.2883	— 0.4003	— 0.1692	0.01245	— 0.00882	— 0.01076	— 0.03962	— 0.03114	— 0.01674
0.66	— 0.5713	0.2873	— 0.4062	— 0.1642	0.01328	— 0.00930	— 0.01094	— 0.04099	— 0.03124	— 0.01721
0.68	— 0.5627	0.2862	— 0.4117	— 0.1589	0.01414	— 0.00981	— 0.01115	— 0.04237	— 0.03134	— 0.01767
0.70	— 0.5540	0.2850	— 0.4170	— 0.1535	0.01502	— 0.01034	— 0.01137	— 0.04372	— 0.03143	— 0.01813
0.72	— 0.5452	0.2837	— 0.4220	— 0.1478	0.01591	— 0.01089	— 0.01161	— 0.04505	— 0.03152	— 0.01858
0.74	— 0.5363	0.2822	— 0.4265	— 0.1420	0.01682	— 0.01147	— 0.01187	— 0.04636	— 0.03161	— 0.01903
0.76	— 0.5273	0.2806	— 0.4306	— 0.1359	0.01774	— 0.01207	— 0.01215	— 0.04766	— 0.03169	— 0.01947
0.78	— 0.5181	0.2787	— 0.4344	— 0.1297	0.01868	— 0.01270	— 0.01244	— 0.04894	— 0.03176	— 0.01991
0.80	— 0.5089	0.2765	— 0.4377	— 0.1233	0.01963	— 0.01335	— 0.01275	— 0.05020	— 0.03183	— 0.02035
0.82	— 0.4996	0.2739	— 0.4406	— 0.1168	0.02059	— 0.01403	— 0.01306	— 0.05143	— 0.03190	— 0.02079
0.84	— 0.4902	0.2710	— 0.4431	— 0.1103	0.02156	— 0.01474	— 0.01339	— 0.05265	— 0.03196	— 0.02123
0.86	— 0.4808	0.2678	— 0.4452	— 0.1036	0.02254	— 0.01547	— 0.01373	— 0.05385	— 0.03201	— 0.02166
0.88	— 0.4714	0.2644	— 0.4468	— 0.0969	0.02353	— 0.01622	— 0.01407	— 0.05502	— 0.03206	— 0.02209
0.90	— 0.4620	0.2606	— 0.4481	— 0.0901	0.02453	— 0.01700	— 0.01443	— 0.05617	— 0.03210	— 0.02252
0.92	— 0.4527	0.2562	— 0.4489	— 0.0833	0.02554	— 0.01780	— 0.01478	— 0.05731	— 0.03213	— 0.02295
0.94	— 0.4435	0.2515	— 0.4492	— 0.0764	0.02657	— 0.01862	— 0.01513	— 0.05842	— 0.03215	— 0.02339
0.96	— 0.4344	0.2464	— 0.4492	— 0.0695	0.02761	— 0.01947	— 0.01548	— 0.05951	— 0.03217	— 0.02383
0.98	— 0.4254	0.2408	— 0.4487	— 0.0626	0.02866	— 0.02034	— 0.01583	— 0.06058	— 0.03219	— 0.02428
1.00	— 0.4167	0.2349	— 0.4478	— 0.0557	0.02972	— 0.02123	— 0.01617	— 0.06163	— 0.03220	— 0.02473

TABLE 22.

Flap coefficients for $\tau = 0.2$ and $\beta = 0.80$.

ω	k_c'	k_c''	m_c'	m_c''	n_a'	n_a''	n_b'	n_b''	n_c'	n_c''
0	−1.8327	0	+0.2373	0	0	0	−0.02120	0	−0.03917	0
0.02	−1.651	+0.3330	0.1347	−0.1800	−0.00004	−0.00038	−0.01913	+0.00127	−0.03801	+0.00092
0.04	−1.446	0.4617	+0.0383	−0.2524	−0.00007	−0.00068	−0.01748	+0.00063	−0.03709	0.00066
0.06	−1.263	0.5114	−0.0453	−0.2822	−0.00010	−0.00096	−0.01623	−0.00076	−0.03643	+0.00006
0.08	−1.141	0.5247	−0.1160	−0.2901	−0.00006	−0.00122	−0.01534	−0.00207	−0.03595	−0.00066
0.10	−1.0645	0.5227	−0.1761	−0.2882	+0.00001	−0.00146	−0.01467	−0.00365	−0.03564	−0.00145
0.12	−1.0090	0.5153	−0.2262	−0.2828	0.00013	−0.00170	−0.01420	−0.00525	−0.03544	−0.00223
0.14	−0.9550	0.5063	−0.2676	−0.2752	0.00028	−0.00194	−0.01380	−0.00688	−0.03534	−0.00301
0.16	−0.9036	0.4976	−0.3010	−0.2669	0.00047	−0.00218	−0.01351	−0.00850	−0.03529	−0.00376
0.18	−0.8557	0.4894	−0.3284	−0.2584	0.00069	−0.00241	−0.01328	−0.01014	−0.03530	−0.00451
0.20	−0.8123	0.4810	−0.3526	−0.2484	0.00095	−0.00266	−0.01311	−0.01177	−0.03535	−0.00522
0.22	−0.7744	0.4719	−0.3751	−0.2368	0.00124	−0.00293	−0.01298	−0.01340	−0.03543	−0.00591
0.24	−0.7420	0.4622	−0.3961	−0.2240	0.00157	−0.00318	−0.01290	−0.01504	−0.03553	−0.00659
0.26	−0.7138	0.4535	−0.4150	−0.2111	0.00192	−0.00346	−0.01286	−0.01667	−0.03566	−0.00725
0.28	−0.6887	0.4459	−0.4321	−0.1978	0.00231	−0.00375	−0.01286	−0.01831	−0.03580	−0.00787
0.30	−0.6658	0.4388	−0.4475	−0.1842	0.00273	−0.00406	−0.01289	−0.01995	−0.03596	−0.00847
0.32	−0.6444	0.4318	−0.4613	−0.1700	0.00319	−0.00438	−0.01296	−0.02157	−0.03613	−0.00905
0.34	−0.6239	0.4247	−0.4736	−0.1549	0.00368	−0.00471	−0.01307	−0.02320	−0.03630	−0.00961
0.36	−0.6039	0.4175	−0.4844	−0.1392	0.00419	−0.00506	−0.01321	−0.02483	−0.03648	−0.01014
0.38	−0.5845	0.4101	−0.4938	−0.1231	0.00474	−0.00543	−0.01339	−0.02644	−0.03665	−0.01065
0.40	−0.5658	0.4026	−0.5013	−0.1067	0.00531	−0.00582	−0.01360	−0.02804	−0.03682	−0.01114
0.42	−0.5476	0.3951	−0.5074	−0.0900	0.00591	−0.00624	−0.01385	−0.02963	−0.03698	−0.01162
0.44	−0.5298	0.3874	−0.5120	−0.0732	0.00653	−0.00667	−0.01414	−0.03120	−0.03713	−0.01208
0.46	−0.5126	0.3793	−0.5149	−0.0562	0.00718	−0.00713	−0.01445	−0.03275	−0.03727	−0.01253
0.48	−0.4959	0.3708	−0.5162	−0.0393	0.00784	−0.00761	−0.01479	−0.03427	−0.03740	−0.01297
0.50	−0.4798	0.3617	−0.5159	−0.0226	0.00852	−0.00812	−0.01515	−0.03577	−0.03752	−0.01340
0.52	−0.4643	0.3518	−0.5140	−0.0063	0.00922	−0.00865	−0.01554	−0.03724	−0.03762	−0.01383
0.54	−0.4496	0.3412	−0.5105	+0.0095	0.00994	−0.00920	−0.01596	−0.03869	−0.03771	−0.01425
0.56	−0.4357	0.3300	−0.5055	0.0247	0.01067	−0.00978	−0.01639	−0.04011	−0.03779	−0.01467
0.58	−0.4227	0.3181	−0.4991	0.0391	0.01142	−0.01038	−0.01683	−0.04149	−0.03785	−0.01510
0.60	−0.4106	0.3056	−0.4914	0.0527	0.01218	−0.01100	−0.01728	−0.04284	−0.03790	−0.01554
0.62	−0.3996	0.2927	−0.4825	0.0651	0.01296	−0.01164	−0.01774	−0.04416	−0.03794	−0.01598
0.64	−0.3896	0.2795	−0.4726	0.0763	0.01375	−0.01230	−0.01820	−0.04545	−0.03797	−0.01644
0.66	−0.3807	0.2658	−0.4619	0.0864	0.01455	−0.01298	−0.01865	−0.04671	−0.03799	−0.01691
0.68	−0.3730	0.2519	−0.4504	0.0952	0.01536	−0.01368	−0.01909	−0.04795	−0.03801	−0.01740
0.70	−0.3663	0.2378	−0.4383	0.1027	0.01618	−0.01440	−0.01953	−0.04916	−0.03803	−0.01790
0.72	−0.3609	0.2236	−0.4260	0.1089	0.01702	−0.01513	−0.01996	−0.05034	−0.03805	−0.01842
0.74	−0.3566	0.2095	−0.4134	0.1138	0.01787	−0.01588	−0.02037	−0.05150	−0.03807	−0.01896
0.76	−0.3534	0.1955	−0.4009	0.1173	0.01873	−0.01665	−0.02077	−0.05265	−0.03810	−0.01951
0.78	−0.3513	0.1818	−0.3883	0.1196	0.01961	−0.01744	−0.02115	−0.05379	−0.03814	−0.02008
0.80	−0.3503	0.1685	−0.3761	0.1205	0.02051	−0.01825	−0.02152	−0.05492	−0.03819	−0.02066
0.82	−0.3503	0.1558	−0.3640	0.1202	0.02142	−0.01908	−0.02189	−0.05604	−0.03825	−0.02125
0.84	−0.3513	0.1439	−0.3522	0.1186	0.02235	−0.01993	−0.02226	−0.05716	−0.03833	−0.02184
0.86	−0.3534	0.1330	−0.3405	0.1159	0.02329	−0.02082	−0.02264	−0.05829	−0.03843	−0.02243
0.88	−0.3565	0.1232	−0.3287	0.1122	0.02426	−0.02175	−0.02305	−0.05944	−0.03856	−0.02302
0.90	−0.3607	0.1147	−0.3169	0.1074	0.02524	−0.02271	−0.02347	−0.06060	−0.03871	−0.02359

TABLE 23.

Flap coefficients for $\tau = 0.3$ and $\beta = 0$.

ω	k_c'	k_c''	m_c'	m_c''	n_a'	n_a''	n_b'	n_b''	n_c'	n_c''
0	−1.3215	0	+0.2523	0	0	0	−0.03595	0	−0.05531	0
0.02	−1.2744	+0.0839	0.2288	−0.0503	−0.00003	−0.00069	−0.03466	+0.00022	−0.05446	+0.00024
0.04	−1.2270	0.1232	0.2052	−0.0782	−0.00007	−0.00133	−0.03336	−0.00077	−0.05360	−0.00033
0.06	−1.1832	0.1444	0.1834	−0.0971	−0.00008	−0.00192	−0.03213	−0.00225	−0.05279	−0.00123
0.08	−1.1436	0.1546	0.1637	−0.1105	−0.00006	−0.00247	−0.03101	−0.00402	−0.05205	−0.00231
0.10	−1.1081	0.1575	0.1462	−0.1203	+0.00001	−0.00299	−0.02999	−0.00599	−0.05138	−0.00353
0.12	−1.0764	0.1554	0.1305	−0.1276	0.00012	−0.00348	−0.02904	−0.00809	−0.05076	−0.00485
0.14	−1.0480	0.1497	0.1166	−0.1331	0.00029	−0.00394	−0.02817	−0.01029	−0.05020	−0.00622
0.16	−1.0226	0.1415	0.1043	−0.1373	0.00052	−0.00439	−0.02736	−0.01256	−0.04969	−0.00764
0.18	−0.9999	0.1315	0.0933	−0.1406	0.00080	−0.00482	−0.02661	−0.01487	−0.04921	−0.00910
0.20	−0.9794	0.1201	0.0834	−0.1432	0.00114	−0.00523	−0.02590	−0.01722	−0.04877	−0.01058
0.22	−0.9609	0.1078	0.0747	−0.1454	0.00154	−0.00563	−0.02522	−0.01959	−0.04835	−0.01207
0.24	−0.9441	0.0948	0.0669	−0.1472	0.00199	−0.00603	−0.02458	−0.02198	−0.04795	−0.01358
0.26	−0.9289	0.0813	0.0597	−0.1487	0.00250	−0.00642	−0.02396	−0.02439	−0.04758	−0.01509
0.28	−0.9150	0.0675	0.0533	−0.1501	0.00307	−0.00680	−0.02336	−0.02680	−0.04723	−0.01661
0.30	−0.9022	0.0534	0.0476	−0.1514	0.00369	−0.00717	−0.02277	−0.02922	−0.04688	−0.01814
0.32	−0.8905	0.0392	0.0424	−0.1526	0.00437	−0.00754	−0.02219	−0.03164	−0.04655	−0.01967
0.34	−0.8797	0.0249	0.0377	−0.1538	0.00510	−0.00791	−0.02162	−0.03406	−0.04622	−0.02120
0.36	−0.8696	+0.0106	0.0335	−0.1550	0.00588	−0.00827	−0.02105	−0.03648	−0.04590	−0.02273
0.38	−0.8603	−0.0037	0.0296	−0.1561	0.00672	−0.00863	−0.02048	−0.03891	−0.04559	−0.02426
0.40	−0.8516	−0.0180	0.0261	−0.1572	0.00762	−0.00899	−0.01991	−0.04133	−0.04528	−0.02579
0.42	−0.8434	−0.0323	0.0229	−0.1584	0.00857	−0.00934	−0.01934	−0.04375	−0.04497	−0.02732
0.44	−0.8358	−0.0465	0.0200	−0.1596	0.00957	−0.00969	−0.01877	−0.04617	−0.04466	−0.02885
0.46	−0.8286	−0.0606	0.0174	−0.1609	0.01063	−0.01005	−0.01819	−0.04859	−0.04435	−0.03038
0.48	−0.8218	−0.0747	0.0150	−0.1622	0.01174	−0.01040	−0.01760	−0.05100	−0.04404	−0.03190
0.50	−0.8153	−0.0886	0.0129	−0.1635	0.01290	−0.01075	−0.01700	−0.05342	−0.04373	−0.03343
0.52	−0.8091	−0.1025	0.0109	−0.1649	0.01412	−0.01110	−0.01640	−0.05583	−0.04341	−0.03495
0.54	−0.8033	−0.1163	0.0091	−0.1663	0.01539	−0.01144	−0.01579	−0.05823	−0.04310	−0.03647
0.56	−0.7977	−0.1299	0.0075	−0.1678	0.01671	−0.01179	−0.01516	−0.06064	−0.04278	−0.03799
0.58	−0.7923	−0.1435	0.0061	−0.1693	0.01808	−0.01214	−0.01453	−0.06304	−0.04245	−0.03950
0.60	−0.7871	−0.1570	0.0048	−0.1709	0.01951	−0.01249	−0.01388	−0.06544	−0.04212	−0.04102
0.62	−0.7821	−0.1705	0.0036	−0.1725	0.02099	−0.01283	−0.01322	−0.06784	−0.04179	−0.04253
0.64	−0.7773	−0.1838	0.0025	−0.1741	0.02252	−0.01318	−0.01254	−0.07023	−0.04146	−0.04405
0.66	−0.7726	−0.1970	0.0016	−0.1758	0.02410	−0.01352	−0.01186	−0.07263	−0.04111	−0.04556
0.68	−0.7680	−0.2102	0.0008	−0.1776	0.02573	−0.01387	−0.01116	−0.07502	−0.04076	−0.04707
0.70	−0.7635	−0.2233	+0.0001	−0.1794	0.02741	−0.01421	−0.01044	−0.07741	−0.04041	−0.04858
0.72	−0.7592	−0.2363	−0.0005	−0.1812	0.02915	−0.01456	−0.00971	−0.07979	−0.04005	−0.05008
0.74	−0.7550	−0.2492	−0.0010	−0.1830	0.03094	−0.01490	−0.00896	−0.08217	−0.03968	−0.05159
0.76	−0.7508	−0.2621	−0.0015	−0.1849	0.03278	−0.01525	−0.00820	−0.08456	−0.03931	−0.05309
0.78	−0.7467	−0.2748	−0.0019	−0.1868	0.03467	−0.01559	−0.00743	−0.08694	−0.03893	−0.05460
0.80	−0.7427	−0.2875	−0.0022	−0.1888	0.03662	−0.01594	−0.00664	−0.08932	−0.03854	−0.05610
0.82	−0.7388	−0.3002	−0.0024	−0.1908	0.03861	−0.01628	−0.00583	−0.09169	−0.03815	−0.05760
0.84	−0.7349	−0.3128	−0.0025	−0.1928	0.04065	−0.01663	−0.00501	−0.09406	−0.03775	−0.05910
0.86	−0.7310	−0.3253	−0.0026	−0.1948	0.04275	−0.01697	−0.00417	−0.09644	−0.03734	−0.06060
0.88	−0.7271	−0.3378	−0.0026	−0.1969	0.04489	−0.01732	−0.00331	−0.09881	−0.03693	−0.06209
0.90	−0.7233	−0.3502	−0.0026	−0.1990	0.04709	−0.01766	−0.00244	−0.10118	−0.03650	−0.06359
0.92	−0.7195	−0.3625	−0.0025	−0.2012	0.04934	−0.01801	−0.00155	−0.10355	−0.03607	−0.06509
0.94	−0.7158	−0.3748	−0.0023	−0.2034	0.05164	−0.01835	−0.00064	−0.10591	−0.03564	−0.06658
0.96	−0.7121	−0.3871	−0.0021	−0.2055	0.05399	−0.01870	+0.00028	−0.10828	−0.03519	−0.06807
0.98	−0.7083	−0.3993	−0.0018	−0.2077	0.05639	−0.01905	0.00122	−0.11064	−0.03474	−0.06957
1.00	−0.7046	−0.4114	−0.0015	−0.2100	0.05884	−0.01939	+0.00218	−0.11301	−0.03428	−0.07106

TABLE 24.

Flap coefficients for $\tau = 0.3$ and $\beta = 0.35$.

ω	k_c'	k_c''	m_c'	m_c''	n_a'	n_a''	n_b'	n_b''	n_c'	n_c''
0	−1.1407	0	+0.2694	0	0	0	−0.03838	0	−0.05905	0
0.02	−1.3526	+0.1071	0.2402	−0.0630	−0.00004	−0.00073	−0.03681	+0.00044	−0.05801	+0.00044
0.04	−1.2942	0.1562	0.2108	−0.0974	−0.00008	−0.00140	−0.03525	−0.00051	−0.05698	−0.00007
0.06	−1.2405	0.1850	0.1836	−0.1206	−0.00009	−0.00202	−0.03381	−0.00205	−0.05603	−0.00101
0.08	−1.1922	0.1997	0.1591	−0.1367	−0.00008	−0.00259	−0.03252	−0.00391	−0.05517	−0.00217
0.10	−1.1495	0.2049	0.1375	−0.1484	−0.00002	−0.00312	−0.03135	−0.00602	−0.05440	−0.00348
0.12	−1.1118	0.2041	0.1184	−0.1570	+0.00010	−0.00363	−0.03030	−0.00828	−0.05372	−0.00490
0.14	−1.0787	0.1993	0.1015	−0.1635	0.00028	−0.00411	−0.02936	−0.01065	−0.05312	−0.00638
0.16	−1.0497	0.1918	0.0866	−0.1685	0.00052	−0.00457	−0.02851	−0.01310	−0.05258	−0.00791
0.18	−1.0242	0.1824	0.0735	−0.1726	0.00082	−0.00501	−0.02772	−0.01561	−0.05209	−0.00948
0.20	−1.0017	0.1716	0.0621	−0.1762	0.00118	−0.00545	−0.02699	−0.01815	−0.05165	−0.01107
0.22	−0.9817	0.1598	0.0520	−0.1792	0.00160	−0.00588	−0.02633	−0.02071	−0.05125	−0.01268
0.24	−0.9638	0.1474	0.0429	−0.1817	0.00210	−0.00630	−0.02572	−0.02329	−0.05088	−0.01430
0.26	−0.9477	0.1345	0.0346	−0.1840	0.00264	−0.00671	−0.02512	−0.02588	−0.05054	−0.01592
0.28	−0.9333	0.1212	0.0272	−0.1861	0.00325	−0.00712	−0.02454	−0.02849	−0.05021	−0.01755
0.30	−0.9204	0.1078	0.0206	−0.1882	0.00392	−0.00754	−0.02399	−0.03110	−0.04990	−0.01918
0.32	−0.9090	0.0944	0.0147	−0.1903	0.00465	−0.00795	−0.02346	−0.03371	−0.04961	−0.02081
0.34	−0.8986	0.0809	0.0094	−0.1923	0.00544	−0.00836	−0.02294	−0.03633	−0.04934	−0.02245
0.36	−0.8891	0.0674	0.0046	−0.1944	0.00628	−0.00877	−0.02243	−0.03896	−0.04909	−0.02409
0.38	−0.8805	0.0540	+0.0002	−0.1965	0.00719	−0.00918	−0.02192	−0.04159	−0.04885	−0.02572
0.40	−0.8727	0.0408	−0.0038	−0.1986	0.00815	−0.00959	−0.02142	−0.04422	−0.04862	−0.02735
0.42	−0.8657	0.0276	−0.0074	−0.2008	0.00917	−0.01001	−0.02093	−0.04686	−0.04838	−0.02899
0.44	−0.8593	0.0145	−0.0107	−0.2030	0.01025	−0.01044	−0.02044	−0.04950	−0.04815	−0.03062
0.46	−0.8535	+0.0015	−0.0136	−0.2053	0.01139	−0.01087	−0.01994	−0.05215	−0.04792	−0.03226
0.48	−0.8482	−0.0115	−0.0163	−0.2077	0.01258	−0.01130	−0.01944	−0.05479	−0.04770	−0.03389
0.50	−0.8434	−0.0244	−0.0187	−0.2101	0.01385	−0.01173	−0.01894	−0.05744	−0.04748	−0.03552
0.52	−0.8391	−0.0371	−0.0209	−0.2126	0.01517	−0.01217	−0.01844	−0.06009	−0.04726	−0.03715
0.54	−0.8352	−0.0496	−0.0229	−0.2152	0.01654	−0.01262	−0.01794	−0.06274	−0.04704	−0.03879
0.56	−0.8316	−0.0620	−0.0247	−0.2179	0.01797	−0.01308	−0.01744	−0.06540	−0.04682	−0.04042
0.58	−0.8284	−0.0743	−0.0263	−0.2206	0.01946	−0.01354	−0.01693	−0.06807	−0.04660	−0.04205
0.60	−0.8255	−0.0865	−0.0278	−0.2234	0.02101	−0.01402	−0.01641	−0.07075	−0.04638	−0.04368
0.62	−0.8229	−0.0986	−0.0291	−0.2263	0.02262	−0.01451	−0.01588	−0.07343	−0.04616	−0.04531
0.64	−0.8206	−0.1106	−0.0303	−0.2292	0.02429	−0.01500	−0.01535	−0.07612	−0.04594	−0.04694
0.66	−0.8186	−0.1225	−0.0314	−0.2322	0.02603	−0.01549	−0.01482	−0.07881	−0.04572	−0.04857
0.68	−0.8167	−0.1343	−0.0323	−0.2353	0.02783	−0.01600	−0.01428	−0.08151	−0.04550	−0.05020
0.70	−0.8151	−0.1460	−0.0331	−0.2384	0.02968	−0.01652	−0.01374	−0.08422	−0.04528	−0.05184
0.72	−0.8137	−0.1576	−0.0338	−0.2416	0.03159	−0.01705	−0.01319	−0.08693	−0.04505	−0.05347
0.74	−0.8126	−0.1691	−0.0344	−0.2448	0.03356	−0.01759	−0.01263	−0.08965	−0.04483	−0.05510
0.76	−0.8116	−0.1805	−0.0350	−0.2482	0.03560	−0.01815	−0.01206	−0.09238	−0.04460	−0.05674
0.78	−0.8108	−0.1918	−0.0355	−0.2516	0.03770	−0.01872	−0.01148	−0.09512	−0.04437	−0.05837
0.80	−0.8102	−0.2031	−0.0359	−0.2550	0.03986	−0.01931	−0.01091	−0.09786	−0.04414	−0.06001
0.82	−0.8097	−0.2143	−0.0362	−0.2585	0.04209	−0.01992	−0.01033	−0.10062	−0.04390	−0.06164
0.84	−0.8095	−0.2254	−0.0363	−0.2621	0.04438	−0.02054	−0.00975	−0.10338	−0.04366	−0.06328
0.86	−0.8094	−0.2364	−0.0364	−0.2657	0.04673	−0.02117	−0.00916	−0.10615	−0.04343	−0.06492
0.88	−0.8095	−0.2474	−0.0365	−0.2694	0.04914	−0.02182	−0.00857	−0.10893	−0.04319	−0.06656
0.90	−0.8097	−0.2583	−0.0364	−0.2731	0.05161	−0.02248	−0.00798	−0.11172	−0.04295	−0.06820
0.92	−0.8100	−0.2692	−0.0364	−0.2769	0.05414	−0.02315	−0.00738	−0.11452	−0.04270	−0.06984
0.94	−0.8104	−0.2800	−0.0363	−0.2807	0.05673	−0.02384	−0.00678	−0.11733	−0.04245	−0.07149
0.96	−0.8109	−0.2907	−0.0361	−0.2846	0.05938	−0.02454	−0.00617	−0.12015	−0.04220	−0.07314
0.98	−0.8115	−0.3014	−0.0359	−0.2885	0.06209	−0.02526	−0.00556	−0.12298	−0.04194	−0.07479
1.00	−0.8122	−0.3121	−0.0356	−0.2925	0.06487	−0.02599	−0.00495	−0.12581	−0.04168	−0.07644

F 54

TABLE 25.

Flap coefficients for $\tau = 0.3$ and $\beta = 0.50$.

ω	k_c'	k_c''	m_c'	m_c''	n_a'	n_a''	n_b'	n_b''	n_c'	n_c''
0	− 1.5259	0	+ 0.2914	0	0	0	− 0.04151	0	− 0.06387	0
0.02	− 1.4513	+ 0.1389	0.2537	− 0.0805	− 0.00005	− 0.00078	− 0.03952	+ 0.00077	− 0.06256	+ 0.00073
0.04	− 1.3769	0.2034	0.2158	− 0.1234	− 0.00011	− 0.00150	− 0.03758	− 0.00014	− 0.06127	+ 0.00025
0.06	− 1.3098	0.2394	0.1812	− 0.1518	− 0.00014	− 0.00215	− 0.03584	− 0.00176	− 0.06012	− 0.00073
0.08	− 1.2500	0.2575	0.1503	− 0.1708	− 0.00013	− 0.00274	− 0.03435	− 0.00388	− 0.05913	− 0.00202
0.10	− 1.1978	0.2641	0.1229	− 0.1838	− 0.00006	− 0.00328	− 0.03303	− 0.00622	− 0.05827	− 0.00348
0.12	− 1.1520	0.2636	0.0987	− 0.1932	+ 0.00008	− 0.00380	− 0.03186	− 0.00872	− 0.05751	− 0.00506
0.14	− 1.1125	0.2587	0.0775	− 0.2002	0.00029	− 0.00430	− 0.03086	− 0.01134	− 0.05686	− 0.00671
0.16	− 1.0780	0.2510	0.0591	− 0.2057	0.00056	− 0.00479	− 0.02996	− 0.01406	− 0.05630	− 0.00840
0.18	− 1.0484	0.2415	0.0428	− 0.2102	0.00089	− 0.00527	− 0.02914	− 0.01682	− 0.05581	− 0.01013
0.20	− 1.0228	0.2307	0.0288	− 0.2141	0.00131	− 0.00573	− 0.02842	− 0.01961	− 0.05538	− 0.01188
0.22	− 1.0006	0.2192	0.0164	− 0.2175	0.00178	− 0.00619	− 0.02776	− 0.02242	− 0.05501	− 0.01363
0.24	− 0.9815	0.2072	+ 0.0056	− 0.2207	0.00230	− 0.00663	− 0.02715	− 0.02526	− 0.05469	− 0.01539
0.26	− 0.9646	0.1948	− 0.0040	− 0.2235	0.00291	− 0.00708	− 0.02658	− 0.02812	− 0.05440	− 0.01715
0.28	− 0.9496	0.1822	− 0.0127	− 0.2263	0.00358	− 0.00754	− 0.02604	− 0.03098	− 0.05414	− 0.01892
0.30	− 0.9362	0.1694	− 0.0208	− 0.2289	0.00431	− 0.00801	− 0.02554	− 0.03385	− 0.05390	− 0.02069
0.32	− 0.9243	0.1567	− 0.0281	− 0.2315	0.00511	− 0.00847	− 0.02506	− 0.03673	− 0.05369	− 0.02242
0.34	− 0.9137	0.1441	− 0.0348	− 0.2343	0.00597	− 0.00894	− 0.02460	− 0.03961	− 0.05350	− 0.02420
0.36	− 0.9044	0.1318	− 0.0409	− 0.2371	0.00689	− 0.00942	− 0.02415	− 0.04250	− 0.05332	− 0.02599
0.38	− 0.8962	0.1197	− 0.0464	− 0.2400	0.00789	− 0.00990	− 0.02373	− 0.04540	− 0.05316	− 0.02775
0.40	− 0.8891	0.1078	− 0.0515	− 0.2430	0.00895	− 0.01039	− 0.02332	− 0.04830	− 0.05301	− 0.02952
0.42	− 0.8828	0.0961	− 0.0563	− 0.2460	0.01007	− 0.01089	− 0.02292	− 0.05122	− 0.05287	− 0.03128
0.44	− 0.8771	0.0846	− 0.0607	− 0.2492	0.01126	− 0.01140	− 0.02253	− 0.05414	− 0.05275	− 0.03303
0.46	− 0.8722	0.0732	− 0.0648	− 0.2525	0.01251	− 0.01193	− 0.02215	− 0.05707	− 0.05264	− 0.03479
0.48	− 0.8679	0.0621	− 0.0686	− 0.2559	0.01382	− 0.01246	− 0.02178	− 0.06001	− 0.05253	− 0.03654
0.50	− 0.8643	0.0512	− 0.0721	− 0.2594	0.01521	− 0.01301	− 0.02141	− 0.06296	− 0.05243	− 0.03829
0.52	− 0.8611	0.0406	− 0.0755	− 0.2630	0.01666	− 0.01357	− 0.02105	− 0.06592	− 0.05234	− 0.04004
0.54	− 0.8585	0.0302	− 0.0787	− 0.2667	0.01817	− 0.01414	− 0.02070	− 0.06889	− 0.05225	− 0.04178
0.56	− 0.8564	0.0201	− 0.0818	− 0.2705	0.01975	− 0.01473	− 0.02036	− 0.07187	− 0.05218	− 0.04353
0.58	− 0.8546	0.0102	− 0.0847	− 0.2745	0.02139	− 0.01534	− 0.02003	− 0.07486	− 0.05211	− 0.04527
0.60	− 0.8533	+ 0.0005	− 0.0875	− 0.2786	0.02309	− 0.01596	− 0.01970	− 0.07786	− 0.05204	− 0.04701
0.62	− 0.8524	− 0.0090	− 0.0902	− 0.2827	0.02487	− 0.01661	− 0.01937	− 0.08088	− 0.05198	− 0.04875
0.64	− 0.8517	− 0.0182	− 0.0927	− 0.2869	0.02672	− 0.01728	− 0.01907	− 0.08391	− 0.05193	− 0.05048
0.66	− 0.8514	− 0.0273	− 0.0951	− 0.2912	0.02863	− 0.01798	− 0.01877	− 0.08695	− 0.05188	− 0.05222
0.68	− 0.8514	− 0.0361	− 0.0974	− 0.2956	0.03060	− 0.01870	− 0.01849	− 0.09000	− 0.05183	− 0.05396
0.70	− 0.8517	− 0.0447	− 0.0997	− 0.3001	0.03264	− 0.01944	− 0.01821	− 0.09308	− 0.05179	− 0.05568
0.72	− 0.8523	− 0.0531	− 0.1020	− 0.3047	0.03474	− 0.02022	− 0.01794	− 0.09617	− 0.05175	− 0.05742
0.74	− 0.8531	− 0.0613	− 0.1042	− 0.3093	0.03691	− 0.02102	− 0.01770	− 0.09927	− 0.05172	− 0.05915
0.76	− 0.8541	− 0.0693	− 0.1064	− 0.3141	0.03915	− 0.02185	− 0.01746	− 0.10237	− 0.05170	− 0.06089
0.78	− 0.8554	− 0.0770	− 0.1085	− 0.3189	0.04146	− 0.02272	− 0.01724	− 0.10549	− 0.05168	− 0.06262
0.80	− 0.8569	− 0.0846	− 0.1106	− 0.3238	0.04383	− 0.02362	− 0.01703	− 0.10862	− 0.05166	− 0.06434
0.82	− 0.8586	− 0.0919	− 0.1127	− 0.3288	0.04628	− 0.02456	− 0.01684	− 0.11176	− 0.05165	− 0.06607
0.84	− 0.8605	− 0.0990	− 0.1149	− 0.3338	0.04878	− 0.02553	− 0.01667	− 0.11491	− 0.05164	− 0.06779
0.86	− 0.8626	− 0.1059	− 0.1170	− 0.3389	0.05136	− 0.02654	− 0.01652	− 0.11807	− 0.05164	− 0.06951
0.88	− 0.8649	− 0.1126	− 0.1191	− 0.3440	0.05399	− 0.02759	− 0.01638	− 0.12124	− 0.05163	− 0.07123
0.90	− 0.8673	− 0.1191	− 0.1212	− 0.3492	0.05670	− 0.02869	− 0.01627	− 0.12442	− 0.05164	− 0.07295
0.92	− 0.8699	− 0.1254	− 0.1233	− 0.3545	0.05947	− 0.02983	− 0.01617	− 0.12761	− 0.05165	− 0.07466
0.94	− 0.8727	− 0.1314	− 0.1254	− 0.3598	0.06231	− 0.03102	− 0.01609	− 0.13081	− 0.05167	− 0.07638
0.96	− 0.8756	− 0.1372	− 0.1275	− 0.3651	0.06521	− 0.03226	− 0.01604	− 0.13401	− 0.05169	− 0.07809
0.98	− 0.8786	− 0.1428	− 0.1296	− 0.3705	0.06817	− 0.03355	− 0.01602	− 0.13722	− 0.05172	− 0.07980
1.00	− 0.8818	− 0.1482	− 0.1317	− 0.3760	0.07119	− 0.03488	− 0.01602	− 0.14043	− 0.05174	− 0.08150

TABLE 26.

Flap coefficients for $\tau = 0.3$ and $\beta = 0.60$.

ω	k_c'	k_c''	m_c'	m_c''	n_a'	n_a''	n_b'	n_b''	n_c'	n_c''
0	− 1.6519	0	+ 0.3154	0	0	0	− 0.04494	0	− 0.06914	0
0.02	− 1.5555	+ 0.1770	0.2665	− 0.1014	− 0.00006	− 0.00081	− 0.04240	+ 0.00124	− 0.06747	+ 0.00110
0.04	− 1.4600	0.2571	0.2172	− 0.1536	− 0.00015	− 0.00161	− 0.04000	+ 0.00035	− 0.06586	+ 0.00065
0.06	− 1.3747	0.2989	0.1725	− 0.1858	− 0.00020	− 0.00228	− 0.03793	− 0.00148	− 0.06448	− 0.00046
0.08	− 1.3002	0.3186	0.1327	− 0.2065	− 0.00018	− 0.00288	− 0.03618	− 0.00383	− 0.06332	− 0.00191
0.10	− 1.2365	0.3260	0.0983	− 0.2204	− 0.00009	− 0.00345	− 0.03471	− 0.00648	− 0.06237	− 0.00356
0.12	− 1.1826	0.3260	0.0687	− 0.2304	+ 0.00008	− 0.00400	− 0.03346	− 0.00929	− 0.06158	− 0.00532
0.14	− 1.1372	0.3212	0.0435	− 0.2378	0.00031	− 0.00453	− 0.03239	− 0.01221	− 0.06092	− 0.00715
0.16	− 1.0991	0.3134	0.0220	− 0.2436	0.00062	− 0.00503	− 0.03146	− 0.01524	− 0.06036	− 0.00902
0.18	− 1.0670	0.3037	+ 0.0033	− 0.2481	0.00100	− 0.00553	− 0.03066	− 0.01830	− 0.05990	− 0.01092
0.20	− 1.0390	0.2927	− 0.0132	− 0.2519	0.00145	− 0.00602	− 0.02995	− 0.02139	− 0.05952	− 0.01283
0.22	− 1.0143	0.2808	− 0.0281	− 0.2552	0.00198	− 0.00652	− 0.02932	− 0.02450	− 0.05921	− 0.01474
0.24	− 0.9928	0.2687	− 0.0417	− 0.2581	0.00258	− 0.00702	− 0.02875	− 0.02762	− 0.05896	− 0.01665
0.26	− 0.9742	0.2567	− 0.0539	− 0.2612	0.00324	− 0.00752	− 0.02824	− 0.03075	− 0.05875	− 0.01856
0.28	− 0.9579	0.2448	− 0.0648	− 0.2640	0.00397	− 0.00803	− 0.02777	− 0.03389	− 0.05858	− 0.02047
0.30	− 0.9435	0.2331	− 0.0748	− 0.2669	0.00478	− 0.00855	− 0.02734	− 0.03705	− 0.05843	− 0.02237
0.32	− 0.9309	0.2215	− 0.0842	− 0.2699	0.00566	− 0.00908	− 0.02695	− 0.04021	− 0.05830	− 0.02426
0.34	− 0.9199	0.2102	− 0.0928	− 0.2729	0.00661	− 0.00962	− 0.02659	− 0.04338	− 0.05820	− 0.02616
0.36	− 0.9103	0.1993	− 0.1009	− 0.2760	0.00763	− 0.01017	− 0.02625	− 0.04656	− 0.05814	− 0.02805
0.38	− 0.9018	0.1887	− 0.1084	− 0.2792	0.00872	− 0.01074	− 0.02594	− 0.04975	− 0.05810	− 0.02993
0.40	− 0.8944	0.1785	− 0.1155	− 0.2824	0.00988	− 0.01132	− 0.02566	− 0.05296	− 0.05808	− 0.03180
0.42	− 0.8879	0.1687	− 0.1222	− 0.2858	0.01110	− 0.01192	− 0.02541	− 0.05617	− 0.05809	− 0.03367
0.44	− 0.8823	0.1593	− 0.1287	− 0.2894	0.01240	− 0.01253	− 0.02518	− 0.05940	− 0.05812	− 0.03553
0.46	− 0.8774	0.1503	− 0.1349	− 0.2930	0.01377	− 0.01316	− 0.02496	− 0.06264	− 0.05816	− 0.03739
0.48	− 0.8731	0.1416	− 0.1409	− 0.2968	0.01521	− 0.01381	− 0.02476	− 0.06590	− 0.05822	− 0.03923
0.50	− 0.8694	0.1333	− 0.1467	− 0.3007	0.01672	− 0.01450	− 0.02458	− 0.06917	− 0.05829	− 0.04106
0.52	− 0.8663	0.1254	− 0.1524	− 0.3046	0.01830	− 0.01522	− 0.02444	− 0.07245	− 0.05837	− 0.04289
0.54	− 0.8637	0.1179	− 0.1579	− 0.3086	0.01995	− 0.01596	− 0.02434	− 0.07574	− 0.05846	− 0.04471
0.56	− 0.8615	0.1108	− 0.1633	− 0.3127	0.02166	− 0.01673	− 0.02426	− 0.07905	− 0.05856	− 0.04652
0.58	− 0.8597	0.1041	− 0.1687	− 0.3169	0.02344	− 0.01753	− 0.02422	− 0.08237	− 0.05867	− 0.04832
0.60	− 0.8583	0.0978	− 0.1741	− 0.3211	0.02529	− 0.01837	− 0.02421	− 0.08570	− 0.05879	− 0.05012
0.62	− 0.8572	0.0918	− 0.1795	− 0.3254	0.02722	− 0.01924	− 0.02421	− 0.07905	− 0.05893	− 0.05191
0.64	− 0.8564	0.0862	− 0.1848	− 0.3297	0.02921	− 0.02015	− 0.02424	− 0.09240	− 0.05908	− 0.05369
0.66	− 0.8558	0.0810	− 0.1901	− 0.3340	0.03127	− 0.02111	− 0.02431	− 0.09577	− 0.05924	− 0.05547
0.68	− 0.8555	0.0761	− 0.1954	− 0.3384	0.03340	− 0.02211	− 0.02442	− 0.09914	− 0.05942	− 0.05724
0.70	− 0.8553	0.0716	− 0.2008	− 0.3428	0.03560	− 0.02315	− 0.02456	− 0.10252	− 0.05960	− 0.05900
0.72	− 0.8552	0.0675	− 0.2063	− 0.3472	0.03786	− 0.02424	− 0.02474	− 0.10590	− 0.05979	− 0.06074
0.74	− 0.8553	0.0637	− 0.2117	− 0.3516	0.04018	− 0.02539	− 0.02496	− 0.10929	− 0.05999	− 0.06248
0.76	− 0.8554	0.0602	− 0.2171	− 0.3559	0.04257	− 0.02659	− 0.02522	− 0.11268	− 0.06020	− 0.06420
0.78	− 0.8556	0.0572	− 0.2225	− 0.3602	0.04501	− 0.02784	− 0.02552	− 0.11607	− 0.06041	− 0.06591
0.80	− 0.8558	0.0545	− 0.2279	− 0.3645	0.04752	− 0.02915	− 0.02586	− 0.11945	− 0.06063	− 0.06761
0.82	− 0.8561	0.0521	− 0.2334	− 0.3687	0.05009	− 0.03052	− 0.02624	− 0.12283	− 0.06086	− 0.06930
0.84	− 0.8564	0.0500	− 0.2390	− 0.3729	0.05271	− 0.03196	− 0.02667	− 0.12621	− 0.06110	− 0.07098
0.86	− 0.8566	0.0482	− 0.2448	− 0.3769	0.05538	− 0.03346	− 0.02715	− 0.12957	− 0.06134	− 0.07264
0.88	− 0.8567	0.0468	− 0.2507	− 0.3809	0.05811	− 0.03502	− 0.02766	− 0.13292	− 0.06158	− 0.07429
0.90	− 0.8568	0.0457	− 0.2567	− 0.3848	0.06089	− 0.03665	− 0.02822	− 0.13625	− 0.06183	− 0.07592
0.92	− 0.8569	0.0448	− 0.2628	− 0.3886	0.06371	− 0.03836	− 0.02883	− 0.13956	− 0.06209	− 0.07754
0.94	− 0.8567	0.0442	− 0.2689	− 0.3923	0.06658	− 0.04014	− 0.02948	− 0.14285	− 0.06234	− 0.07914
0.96	− 0.8565	0.0438	− 0.2751	− 0.3958	0.06949	− 0.04199	− 0.03017	− 0.14612	− 0.06260	− 0.08073
0.98	− 0.8562	0.0438	− 0.2813	− 0.3992	0.07244	− 0.04391	− 0.03090	− 0.14937	− 0.06286	− 0.08231
1.00	− 0.8558	0.0440	− 0.2876	− 0.4025	0.07543	− 0.04592	− 0.03169	− 0.15260	− 0.06312	− 0.08388

TABLE 27.

Flap coefficients for $\tau = 0.3$ and $\beta = 0.70$.

ω	k_c'	k_c''	m_c'	m_c''	n_a'	n_a''	n_b'	n_b''	n_c'	n_c''
0	—1.8505	0	+ 0.3533	0	0	0	—0.05034	0	—0.07746	0
0.02	—1.7121	+ 0.2447	0.2828	—0.1387	—0.00009	—0.00093	—0.04678	+ 0.00220	—0.07509	+ 0.00182
0.04	—1.5794	0.3494	0.2132	—0.2056	—0.00021	—0.00173	—0.04358	+ 0.00120	—0.07296	+ 0.00129
0.06	—1.4641	0.3991	0.1511	—0.2429	—0.00026	—0.00244	—0.04098	—0.00104	—0.07124	—0.00006
0.08	—1.3660	0.4193	0.0968	—0.2642	—0.00024	—0.00308	—0.03891	—0.00390	—0.06986	—0.00182
0.10	—1.2840	0.4245	0.0505	—0.2772	—0.00011	—0.00369	—0.03725	—0.00708	—0.06878	—0.00379
0.12	—1.2160	0.4217	+ 0.0111	—0.2857	+ 0.00008	—0.00427	—0.03590	—0.01042	—0.06795	—0.00586
0.14	—1.1602	0.4147	—0.0220	—0.2915	0.00036	—0.00485	—0.03479	—0.01387	—0.06732	—0.00799
0.16	—1.1148	0.4054	—0.0497	—0.2957	0.00073	—0.00541	—0.03389	—0.01736	—0.06684	—0.01013
0.18	—1.0774	0.3949	—0.0733	—0.2993	0.00119	—0.00597	—0.03314	—0.02088	—0.06648	—0.01227
0.20	—1.0452	0.3834	—0.0945	—0.3018	0.00172	—0.00653	—0.03252	—0.02443	—0.06622	—0.01441
0.22	—1.0169	0.3711	—0.1140	—0.3035	0.00234	—0.00710	—0.03199	—0.02800	—0.06605	—0.01654
0.24	—0.9920	0.3586	—0.1318	—0.3048	0.00303	—0.00767	—0.03153	—0.03158	—0.06594	—0.01866
0.26	—0.9703	0.3467	—0.1482	—0.3064	0.00380	—0.00827	—0.03114	—0.03516	—0.06590	—0.02076
0.28	—0.9515	0.3358	—0.1633	—0.3079	0.00464	—0.00888	—0.03082	—0.03875	—0.06591	—0.02285
0.30	—0.9349	0.3257	—0.1774	—0.3096	0.00556	—0.00951	—0.03058	—0.04235	—0.06597	—0.02491
0.32	—0.9204	0.3162	—0.1906	—0.3114	0.00656	—0.01015	—0.03039	—0.04595	—0.06608	—0.02696
0.34	—0.9074	0.3072	—0.2032	—0.3130	0.00764	—0.01082	—0.03025	—0.04956	—0.06623	—0.02898
0.36	—0.8957	0.2986	—0.2154	—0.3145	0.00880	—0.01152	—0.03018	—0.05319	—0.06641	—0.03098
0.38	—0.8852	0.2905	—0.2272	—0.3160	0.01003	—0.01224	—0.03016	—0.05684	—0.06662	—0.03296
0.40	—0.8756	0.2830	—0.2386	—0.3175	0.01134	—0.01299	—0.03020	—0.06049	—0.06686	—0.03492
0.42	—0.8669	0.2762	—0.2496	—0.3190	0.01273	—0.01377	—0.03030	—0.06414	—0.06712	—0.03686
0.44	—0.8588	0.2700	—0.2604	—0.3204	0.01418	—0.01458	—0.03045	—0.06780	—0.06741	—0.03878
0.46	—0.8512	0.2644	—0.2710	—0.3217	0.01570	—0.01544	—0.03064	—0.07148	—0.06772	—0.04066
0.48	—0.8441	0.2593	—0.2814	—0.3229	0.01729	—0.01635	—0.03089	—0.07516	—0.06806	—0.04252
0.50	—0.8374	0.2547	—0.2917	—0.3240	0.01895	—0.01732	—0.03120	—0.07885	—0.06841	—0.04436
0.52	—0.8309	0.2507	—0.3018	—0.3248	0.02068	—0.01833	—0.03157	—0.08253	—0.06877	—0.04618
0.54	—0.8247	0.2471	—0.3119	—0.3254	0.02248	—0.01939	—0.03201	—0.08621	—0.06916	—0.04797
0.56	—0.8186	0.2440	—0.3219	—0.3258	0.02434	—0.02050	—0.03251	—0.08989	—0.06956	—0.04973
0.58	—0.8125	0.2413	—0.3318	—0.3259	0.02627	—0.02167	—0.03308	—0.09355	—0.06998	—0.05147
0.60	—0.8064	0.2390	—0.3416	—0.3258	0.02826	—0.02290	—0.03372	—0.09720	—0.07040	—0.05318
0.62	—0.8003	0.2371	—0.3514	—0.3254	0.03031	—0.02419	—0.03443	—0.10083	—0.07083	—0.05485
0.64	—0.7940	0.2354	—0.3610	—0.3247	0.03240	—0.02555	—0.03521	—0.10443	—0.07126	—0.05650
0.66	—0.7876	0.2339	—0.3705	—0.3236	0.03455	—0.02698	—0.03605	—0.10800	—0.07170	—0.05812
0.68	—0.7810	0.2325	—0.3799	—0.3222	0.03675	—0.02848	—0.03695	—0.11154	—0.07213	—0.05972
0.70	—0.7742	0.2313	—0.3891	—0.3205	0.03900	—0.03004	—0.03792	—0.11504	—0.07256	—0.06128
0.72	—0.7671	0.2302	—0.3982	—0.3184	0.04128	—0.03168	—0.03894	—0.11849	—0.07299	—0.06282
0.74	—0.7597	0.2292	—0.4070	—0.3158	0.04360	—0.03339	—0.04002	—0.12189	—0.07340	—0.06433
0.76	—0.7521	0.2282	—0.4156	—0.3129	0.04595	—0.03518	—0.04115	—0.12523	—0.07381	—0.06582
0.78	—0.7442	0.2272	—0.4240	—0.3096	0.04833	—0.03703	—0.04233	—0.12852	—0.07421	—0.06729
0.80	—0.7359	0.2261	—0.4320	—0.3060	0.05074	—0.03896	—0.04356	—0.13175	—0.07459	—0.06874
0.82	—0.7274	0.2248	—0.4398	—0.3020	0.05317	—0.04096	—0.04483	—0.13491	—0.07496	—0.07016
0.84	—0.7185	0.2233	—0.4473	—0.2977	0.05562	—0.04304	—0.04613	—0.13801	—0.07531	—0.07157
0.86	—0.7094	0.2216	—0.4543	—0.2931	0.05808	—0.04518	—0.04746	—0.14103	—0.07564	—0.07296
0.88	—0.6999	0.2197	—0.4610	—0.2882	0.06056	—0.04739	—0.04882	—0.14398	—0.07596	—0.07434
0.90	—0.6902	0.2174	—0.4673	—0.2830	0.06305	—0.04968	—0.05020	—0.14686	—0.07625	—0.07571
0.92	—0.6803	0.2147	—0.4732	—0.2775	0.06554	—0.05203	—0.05159	—0.14966	—0.07652	—0.07707
0.94	—0.6702	0.2116	—0.4786	—0.2718	0.06804	—0.05445	—0.05299	—0.15238	—0.07677	—0.07842
0.96	—0.6599	0.2081	—0.4835	—0.2659	0.07054	—0.05693	—0.05440	—0.15503	—0.07699	—0.07976
0.98	—0.6494	0.2044	—0.4879	—0.2598	0.07304	—0.05948	—0.05581	—0.15761	—0.07719	—0.08111
1.00	—0.6388	0.2003	—0.4919	—0.2534	0.07555	—0.06209	—0.05721	—0.16011	—0.07738	—0.08246

TABLE 28.

Flap coefficients for $\tau = 0.3$ and $\beta = 0.80$.

ω	k_c'	k_c''	m_c'	m_c''	n_a'	n_a''	n_b'	n_b''	n_c'	n_c''
0	— 2.2025	0	+ 0.4205	0	0	0	— 0.05991	0	— 0.9219	0
0.02	— 1.925	+ 0.3878	0.2952	— 0.2173	— 0.00014	— 0.00107	— 0.0540	+ 0.0040	— 0.0883	+ 0.0032
0.04	— 1.711	0.5314	0.1819	— 0.3069	— 0.00028	— 0.00196	— 0.0493	+ 0.0025	— 0.0851	0.0024
0.06	— 1.545	0.5853	0.0855	— 0.3467	— 0.00033	— 0.00273	— 0.0459	— 0.0008	— 0.0829	+ 0.0005
0.08	— 1.417	0.5956	+ 0.0029	— 0.3609	— 0.00025	— 0.00343	— 0.0434	— 0.0048	— 0.0812	— 0.0019
0.10	— 1.3128	0.5882	— 0.0667	— 0.3642	— 0.00008	— 0.00412	— 0.0416	— 0.0088	— 0.0802	— 0.0045
0.12	— 1.2334	0.5748	— 0.1242	— 0.3636	+ 0.00022	— 0.00478	— 0.0401	— 0.0131	— 0.0793	— 0.0071
0.14	— 1.1655	0.5599	— 0.1721	— 0.3606	0.00060	— 0.00546	— 0.0392	— 0.0174	— 0.0790	— 0.0097
0.16	— 1.1074	0.5460	— 0.2111	— 0.3574	0.00109	— 0.00613	— 0.0385	— 0.0217	— 0.0787	— 0.0122
0.18	— 1.0576	0.5332	— 0.2437	— 0.3539	0.00164	— 0.00682	— 0.0379	— 0.0260	— 0.0787	— 0.0146
0.20	— 1.0147	0.5205	— 0.2731	— 0.3492	0.00231	— 0.00753	— 0.0376	— 0.0303	— 0.0788	— 0.0170
0.22	— 0.9775	0.5065	— 0.3010	— 0.3426	0.00305	— 0.00825	— 0.0373	— 0.0347	— 0.0791	— 0.0194
0.24	— 0.9449	0.4929	— 0.3271	— 0.3351	0.00389	— 0.00896	— 0.0374	— 0.0390	— 0.0794	— 0.0217
0.26	— 0.9160	0.4807	— 0.3512	— 0.3272	0.00481	— 0.00976	— 0.0375	— 0.0433	— 0.0798	— 0.0238
0.28	— 0.8899	0.4700	— 0.3736	— 0.3193	0.00582	— 0.01060	— 0.0377	— 0.0475	— 0.0804	— 0.0260
0.30	— 0.8660	0.4603	— 0.3946	— 0.3109	0.00691	— 0.01149	— 0.0380	— 0.0518	— 0.0809	— 0.0281
0.32	— 0.8438	0.4511	— 0.4143	— 0.3015	0.00808	— 0.01242	— 0.0385	— 0.0561	— 0.0814	— 0.0301
0.34	— 0.8228	0.4422	— 0.4327	— 0.2912	0.00933	— 0.01342	— 0.0390	— 0.0603	— 0.0821	— 0.0321
0.36	— 0.8028	0.4337	— 0.4500	— 0.2801	0.01065	— 0.01446	— 0.0397	— 0.0646	— 0.0828	— 0.0339
0.38	— 0.7834	0.4258	— 0.4661	— 0.2684	0.01203	— 0.01552	— 0.0405	— 0.0688	— 0.0834	— 0.0357
0.40	— 0.7645	0.4180	— 0.4810	— 0.2559	0.01348	— 0.01667	— 0.0415	— 0.0729	— 0.0841	— 0.0374
0.42	— 0.7460	0.4102	— 0.4946	— 0.2425	0.01499	— 0.01787	— 0.0425	— 0.0770	— 0.0847	— 0.0391
0.44	— 0.7278	0.4024	— 0.5069	— 0.2285	0.01655	— 0.01917	— 0.0436	— 0.0810	— 0.0854	— 0.0406
0.46	— 0.7098	0.3945	— 0.5177	— 0.2138	0.01815	— 0.02053	— 0.0449	— 0.0850	— 0.0861	— 0.0422
0.48	— 0.6921	0.3862	— 0.5270	— 0.1986	0.01980	— 0.02198	— 0.0462	— 0.0888	— 0.0867	— 0.0436
0.50	— 0.6746	0.3776	— 0.5348	— 0.1830	0.02149	— 0.02348	— 0.0476	— 0.0926	— 0.0873	— 0.0450
0.52	— 0.6575	0.3684	— 0.5410	— 0.1672	0.02322	— 0.02505	— 0.0491	— 0.0963	— 0.0878	— 0.0464
0.54	— 0.6407	0.3586	— 0.5455	— 0.1512	0.02498	— 0.02668	— 0.0507	— 0.0999	— 0.0883	— 0.0477
0.56	— 0.6244	0.3481	— 0.5484	— 0.1351	0.02677	— 0.02837	— 0.0523	— 0.1034	— 0.0888	— 0.0490
0.58	— 0.6085	0.3369	— 0.5496	— 0.1189	0.02858	— 0.03012	— 0.0540	— 0.1067	— 0.0892	— 0.0503
0.60	— 0.5932	0.3250	— 0.5492	— 0.1030	0.03042	— 0.03195	— 0.0557	— 0.1100	— 0.0896	— 0.0516
0.62	— 0.5785	0.3122	— 0.5473	— 0.0878	0.03227	— 0.03383	— 0.0574	— 0.1132	— 0.0900	— 0.0529
0.64	— 0.5645	0.2986	— 0.5439	— 0.0731	0.03414	— 0.03575	— 0.0591	— 0.1163	— 0.0903	— 0.0542
0.66	— 0.5513	0.2843	— 0.5391	— 0.0590	0.03603	— 0.03775	— 0.0608	— 0.1192	— 0.0905	— 0.0555
0.68	— 0.5389	0.2692	— 0.5330	— 0.0457	0.03793	— 0.03982	— 0.0625	— 0.1221	— 0.0907	— 0.0569
0.70	— 0.5273	0.2535	— 0.5258	— 0.0333	0.03984	— 0.04193	— 0.0642	— 0.1249	— 0.0909	— 0.0582
0.72	— 0.5167	0.2372	— 0.5175	— 0.0218	0.04177	— 0.04412	— 0.0658	— 0.1277	— 0.0911	— 0.0597
0.74	— 0.5070	0.2204	— 0.5084	— 0.0114	0.04371	— 0.04635	— 0.0674	— 0.1303	— 0.0912	— 0.0611
0.76	— 0.4985	0.2032	— 0.4985	— 0.0021	0.04567	— 0.04864	— 0.0690	— 0.1329	— 0.0913	— 0.0626
0.78	— 0.4911	0.1859	— 0.4879	+ 0.0060	0.04765	— 0.05099	— 0.0705	— 0.1355	— 0.0915	— 0.0642
0.80	— 0.4850	0.1684	— 0.4768	0.0129	0.04965	— 0.05340	— 0.0720	— 0.1380	— 0.0916	— 0.0658
0.82	— 0.4804	0.1510	— 0.4653	0.0183	0.05167	— 0.05585	— 0.0735	— 0.1405	— 0.0918	— 0.0674
0.84	— 0.4773	0.1340	— 0.4534	0.0223	0.05373	— 0.05835	— 0.0750	— 0.1430	— 0.0920	— 0.0690
0.86	— 0.4761	0.1174	— 0.4410	0.0247	0.05582	— 0.06089	— 0.0765	— 0.1454	— 0.0923	— 0.0707
0.88	— 0.4771	0.1016	— 0.4282	0.0256	0.05795	— 0.06348	— 0.0781	— 0.1479	— 0.0827	— 0.0723
0.90	— 0.4803	0.0868	— 0.4147	0.0248	0.06012	— 0.06609	— 0.0798	— 0.1504	— 0.0931	— 0.0739

F.58

REPORT F. 146

Strip Theory for Oscillating Swept Wings in Incompressible Flow

by

A. I. VAN DE VOOREN and W. ECKHAUS.

Summary.

It is shown that strip theory for a swept wing differs from that for a straight wing by the fact that a constant spanwise intensity of the trailing vortices gives a contribution to the downwash in the case of a swept wing, but not for a straight wing. This makes that two new terms should be added to the usual coefficients, the first of which corresponds to the varying amplitude in bending or torsion of the wing while the second corresponds to taper. These additional forces vanish if the angle of sweep φ is 0° and are maximal if $\varphi = 45°$.

Numerical results for the new coefficients are presented for $\omega = 0$, (0.1), 1.0; 1.2 and 1.5, where ω denotes the reduced frequency referred to semi-chord. In an appendix the case of a wing-flap system with constant chord ratio τ is considered and numerical results are presented for $\tau = 0.2$.

Contents.

This investigation has been sponsored by the Netherlands Aircraft Development Board (N.I.V.).

1 Introduction.

The aerodynamic forces used in flutter calculations for straight wings of not too small aspect ratio are usually derived from a two-dimensional approximation.

This approximation involves that the forces in a certain chordwise section are assumed to be equal to those forces which would arise if the section considered were part of an infinite wing with the same chord and oscillating with the same amplitudes in translation and rotation as the true wing in that particular section.

The reason that the two-dimensional approximation has proved to be so fruitful for straight wings is, besides its simplicity, the fact that a local linear variation in chord or deformation functions does not modify the aerodynamic forces. The linear variation in chord or deformation functions gives rise to a constant spanwise strength of the trailing vortices and since these vortices have equal distance to the section considered, the downwash remains the same and with it, the solution of the integral equation.

In the case of a swept wing two modifications arise:

1° the aerodynamic forces must be multiplied by the factor $\cos\varphi$, where φ is the angle of sweep,

2° the compensation for a local linear variation in chord or deformation functions is lacking due to the unequal distance to the section considered of the vortices arisen at the same moment.

In this report formulae and numerical results for the aerodynamic forces are presented, which take these two modifications into account. It is expected that these results allow the same accuracy for a swept wing as the two-dimensional approximation does in the case of a straight wing. An important practical advantage is that also for a swept wing the results only depend upon sectional quantities. No solution of an integral equation for the distribution of the circulation along the span is required. The general result assumes the form of the original two-dimensional approximation for a straight wing, multiplied by $\cos\varphi$, together with three correction terms, which are proportional to the local variations in chord, in bending deformation and in torsion deformation respectively and of which the proportionality constants depend on the reduced frequency ω only. These constants are given in numerical form as functions of ω. It is shown that the result like the two-dimensional approximation for straight wings, may be used if the reduced frequency, referred to the semispan, is larger than 1. For smaller values of the reduced frequency a correction, analogous to the REISSNER correction (ref. 5) for straight wings, should be added.

The method by which these results have been derived, is the same that also has been applied in the steady case for obtaining a generalization of the PRANDTL equation for swept wings (refs. 1, 2). This method makes use of an asymptotic expansion for the downwash, valid for large values of the aspect ratio. The term independent of the aspect ratio gives rise to the two-dimensional approximation. For a straight wing there occurs no term inversely proportional to the aspect ratio, but in the case of a swept wing such term exists. It is this term which is responsible for the corrections mentioned above.

2 List of symbols.

b	semi-span
l	semi-chord
$l(0)$	semi-chord at root section
p	pressure, positive downward
s	$\frac{1}{l}\frac{dl}{dy}$, eq. (6.10)
v	speed of the undisturbed flow
w	downwash
x	coordinate in flow direction, positive in direction of v
y	coordinate in direction perpendicular to x and in the plane of the wing, positive to starboard
x_0, y_0	x, y coordinates of the point where the downwash is calculated
k_g, m_g, i_g	aerodynamic derivatives in two-dimensional flow, defined by eq. (6.7)
A, A'	wing and wake region in x, y-plane
$\bar{A}, \bar{A}'$	wing and wake region in X, Y-plane
G	degree of freedom (Al = translation, B = rotation wing, C = relative rotation of flap)
K	force of wing section per unit span, positive downward
M	moment of wing section about mid-chord point per unit span, positive if tailheavy
N	moment of flap section about hinge point per unit span, positive if tailheavy
P	circulation function
X, Y	coordinates defined by eq. (3.3)
$\bar{X}, \bar{Y}$	coordinates defined by eq. (5.18)
$\vec{\gamma}$	vorticity vector
γ_x, γ_y	vorticity components when decomposed along x- and y-axes (see fig. 4.1)
γ_ξ, γ_η	vorticity components when decomposed along X- and Y-axes
φ	angle of sweep, positive for sweepback
ε	$\frac{l(0)}{b}$
ρ	air density
τ	ratio of flap chord to wing chord
ν	frequency of oscillation
ω	reduced frequency, $\frac{\nu l}{v}$
$\Gamma(Y)$	circulation about profile in section Y.

A superscript (2) denotes that the corresponding symbol refers to two-dimensional flow for a straight wing.

Δ denotes the difference in a quantity due to strip theory for a swept wing compared with strip theory for a straight wing.

3 General principle.

3.1 Starting from a general vorticity distribution on the wing and in the wake, the downwash in an arbitrary point x_0, y_0 of the wing is obtained by aid of BIOT and SAVART's law, which may be applied in incompressible flow, either steady or unsteady. This formula reads

$$4\pi w(x_0, y_0) = \\ = \iint_{A+A'} \frac{(y-y_0)\gamma_x - (x-x_0)\gamma_y}{r^3}\, dx\, dy, \quad (3.1)$$

where γ_x and γ_y are the vorticity components in x- and y-direction and w the downwash. The x-axis is parallel to the main stream and the y-axis per-

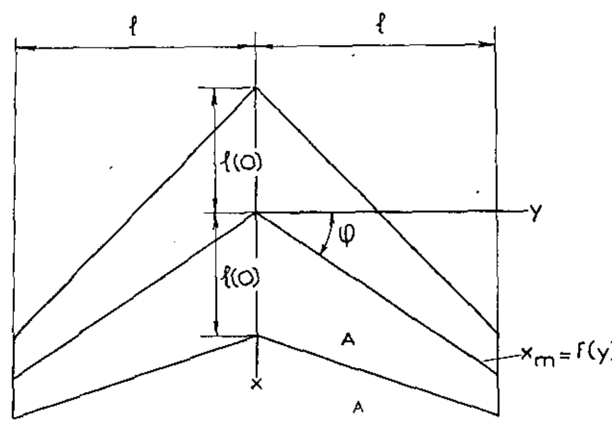

Fig. 3.1

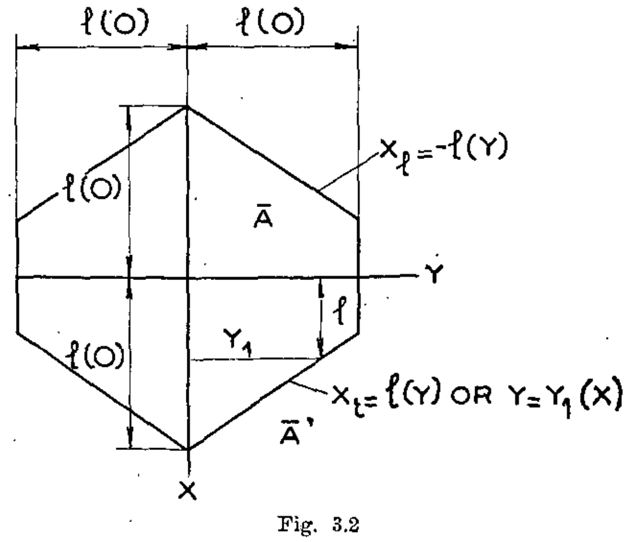

Fig. 3.2

pendicular to it in the plane of the wing. r denotes the distance between the points x_0, y_0 and x, y, i.e.:

$$r = \sqrt{(x - x_0)^2 + (y - y_0)^2}, \qquad (3.2)$$

A and A' denote the wing and the wake, respectively.

For most points of a wing of not too small aspect ratio the coordinate y will be large with respect to the coordinate $x - x_m$, where $x_m = f(y)$ is the x-coordinate of the mid-chord line. In order to express this fact mathematically, the transformation

$$x = f\left(\frac{Y}{\varepsilon}\right) + X, \qquad (3.3)$$
$$y = \frac{Y}{\varepsilon}$$

is introduced, where $\varepsilon = \frac{l(0)}{b}$ with $l(0)$ equal to the semi-chord in the section $y = 0$ and b equal to the semi-span. ε will be assumed small. It follows from eq. (3.3) that for the wing region $\bar{A}$ in the X, Y-plane both coordinates X and Y vary between $-l(0)$ and $+l(0)$ and are in general of the same order of magnitude (see figs. 3.1 and 3.2).

Considering a swept wing, the function f is given by

$$f(y) = f\left(\frac{Y}{\varepsilon}\right) = \frac{|Y|}{\varepsilon} \tan\varphi, \qquad (3.4)$$

where φ is the angle of sweep. Substitution of eqs. (3.3) and (3.4) into eq. (3.1) leads to

$$4\pi w(X_0, Y_0) = \varepsilon \int_0^{l(0)} \int_{-l}^{\infty} \frac{(Y - Y_0)\gamma_x - \{\varepsilon(X - X_0) + (Y - Y_0)\tan\varphi\}\gamma_y}{[\{\varepsilon(X - X_0) + (Y - Y_0)\tan\varphi\}^2 + (Y - Y_0)^2]^{3/2}}\, dX\, dY$$
$$+ \varepsilon \int_{-l(0)}^{0} \int_{-l}^{\infty} \frac{(Y - Y_0)\gamma_x - \{\varepsilon(X - X_0) - (Y + Y_0)\tan\varphi\}\gamma_y}{[\{\varepsilon(X - X_0) - (Y + Y_0)\tan\varphi\}^2 + (Y - Y_0)^2]^{3/2}}\, dX dY. \qquad (3.5)$$

It has been assumed that Y_0 is positive; the first term of the right hand side gives the downwash due to the right wing and the second term the downwash due to the left wing.

The right hand side of eq. (3.5) will now be expanded into a power series in ε, where ε^2 and higher powers of ε will be neglected. In order to obtain this expansion into a suitable form, use will be made of some fundamental concepts.

3.2 The equation of continuity for the vortex field reads

$$\frac{\partial \gamma_x}{\partial x} + \frac{\partial \gamma_y}{\partial y} = 0.$$

Transforming to X, Y-coordinates, it is found by aid of eqs. (3.3) and (3.4) that for the right semi-wing holds

$$\frac{\partial}{\partial x} = \frac{\partial}{\partial X}, \quad \frac{\partial}{\partial y} = -\tan\varphi \frac{\partial}{\partial X} + \varepsilon \frac{\partial}{\partial Y}.$$

Furthermore, when the vorticity vector is decomposed into an oblique system of axes (ξ, η), where the η-axis coincides with the mid-chord line of the wing and the ξ-axis with the x-axis (see fig. 3.3), the components γ_ξ and γ_η are given by

$$\gamma_\xi = \gamma_x - \gamma_y \tan\varphi, \ \gamma_\eta = \frac{\gamma_y}{\cos\varphi}. \qquad (3.6)$$

On the left semi-wing one has

$$\gamma_\xi = \gamma_x + \gamma_y \tan\varphi, \ \gamma_\eta = \frac{\gamma_y}{\cos\varphi}. \qquad (3.6a)$$

Hence, the continuity equation becomes

$$\frac{\partial \gamma_\xi}{\partial X} + \varepsilon \frac{\partial \gamma_y}{\partial Y} = 0, \qquad (3.7)$$

from which it follows that γ_ξ is of order ε.

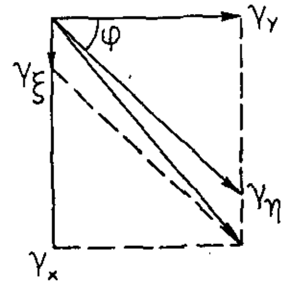

Fig. 3.3

3.3 The vortex distribution in the wake satisfies the relation:

$$\vec{\gamma}(X, Y) = \vec{\gamma}(l, Y) e^{-i\nu\frac{X-l}{v}}, \ X \geqq l \qquad (3.8)$$

if the wing performs an oscillation of frequency ν which may be either unstable ($Im\,\nu < 0$) or periodic ($Im\,\nu = 0$). The case of a damped oscillation ($Im\,\nu > 0$) will not be considered since the initial disturbance then plays an important role (ref. 3).

The component $\gamma_y(l, Y)$ follows from the condition that the pressure at the trailing edge is zero. Since

$$\frac{p(X, Y)}{\rho v} = -\gamma_y(X, Y) - i\,\frac{\nu}{v}\int\limits_{-l}^{X} \gamma_y(X, Y)\,dX, \tag{3.9}$$

where $p(X, Y)$ denotes the pressure difference between upper and lower side of the wing (positive downward), the condition of zero pressure at the trailing edge yields

$$\gamma_y(l, Y) = -i\,\frac{\nu}{v}\,\Gamma(Y), \tag{3.10}$$

where the circulation $\Gamma(Y)$ is given by

$$\Gamma(Y) = \int\limits_{-l}^{l} \gamma_y(X, Y)\,dX. \tag{3.11}$$

From the continuity equation (3.7) follows that

$$\gamma_\xi(l, Y) = -\varepsilon\left\{\frac{d\Gamma(Y)}{dY} - \gamma_y(l, Y)\,\frac{dl}{dy}\right\}. \tag{3.12}$$

Both γ_ξ and γ_y are continuous in the point $X = l$.

3.4 In order to reduce the double integrals in eq. (3.5) the functions γ_ξ and γ_y will be expanded into their Taylor series towards the variable Y, viz.

$$\begin{aligned}
\gamma_\xi(X, Y) &= \gamma_\xi(X, Y_0) + (Y - Y_0)\,\frac{\partial\gamma_\xi}{\partial Y}(X, Y_0) + \frac{(Y - Y_0)^2}{2}\,\frac{\partial^2\gamma_\xi}{\partial Y^2}(X, Y_0) + \ldots \\
\gamma_y(X, Y) &= \gamma_y(X, Y_0) + (Y - Y_0)\,\frac{\partial\gamma_y}{\partial Y}(X, Y_0) + \frac{(Y - Y_0)^2}{2}\,\frac{\partial^2\gamma_y}{\partial Y^2}(X, Y_0) + \ldots
\end{aligned} \tag{3.13}$$

The convergence of these series will be slower if Y or Y_0 approaches one of the wing tips or the middle section of a swept wing, while the series lose their meaning for Y or Y_0 equal to 0 or $\pm\, l(0)$. Near the tips γ_ξ and $\dfrac{\partial\gamma_y}{\partial Y}$ become infinitely large, while in the central section these functions are discontinuous in Y. Hence, the results of the present theory will apply with less accuracy in the regions near the tips or the central section. The assumption of large aspect ratio involves that a large part of the wing lies at some distance (e.g. more than a chord length) from these regions.

4 Derivation of the integral equation.

4.1 After the preparatory work of the preceding section, the reduction of eq. (3.5) may be continued. The first term of the right hand side of this equation may be written as

$$\varepsilon\int\limits_{0}^{l(0)}\int\limits_{-l}^{\infty} \frac{(Y - Y_0)\gamma_\xi - \varepsilon(X - X_0)\gamma_y}{[\{\varepsilon(X - X_0) + (Y - Y_0)\tan\varphi\}^2 + (Y - Y_0)^2]^{3/2}}\,dX\,dY.$$

By introduction of the expansions (3.13) the integration to Y may be performed. The term considered becomes equal to

$$\varepsilon\int\limits_{-l}^{\infty}\sum_{n=0}^{\infty}\frac{1}{n}\left\{\frac{\partial^n\gamma_\xi}{\partial Y^n}(X, Y_0)\,.\,I_{n+1} - \varepsilon(X - X_0)\,\frac{\partial^n\gamma_y}{\partial Y^n}(X, Y_0)\,.\,I_n\right\}dX, \tag{4.1}$$

where

$$I_n = \int\limits_{0}^{Y_1} \frac{(Y - Y_0)^n}{[\{\varepsilon(X - X_0) + (Y - Y_0)\tan\varphi\}^2 + (Y - Y_0)^2]^{3/2}}\,dY. \tag{4.2}$$

It follows by elementary integration (refs. 1, 2) that

$$I_0 = \left.\frac{\dfrac{Y - Y_0}{\cos^2\varphi} + \varepsilon(X - X_0)\tan\varphi}{\varepsilon^2(X - X_0)^2[\{\varepsilon(X - X_0) + (Y - Y_0)\tan\varphi\}^2 + (Y - Y_0)^2]^{1/2}}\right|_{0}^{Y_1} = 0\left(\frac{1}{\varepsilon^2}\right),$$

$$I_1 = -\left.\frac{(Y - Y_0)\tan\varphi + \varepsilon(X - X_0)}{\varepsilon(X - X_0)[\{\varepsilon(X - X_0) + (Y - Y_0)\tan\varphi\}^2 + (Y - Y_0)^2]^{1/2}}\right|_{0}^{Y_1} = 0\left(\frac{1}{\varepsilon}\right),$$

while I_2 turns out to be of order $\log \varepsilon$ and I_n if $n \geqslant 3$ of order 1 in ε. Since γ_ξ is of order ε, the expression (4.1) may be replaced by

$$\varepsilon \int_{-l}^{\infty} \left[I_1 \gamma_\xi (X, Y_0) - \varepsilon (X - X_0) \left\{ I_0 \gamma_y (X, X_0) + I_1 \frac{\partial \gamma_y}{\partial Y} (X, Y_0) \right\} + R_2(X, Y_0) \right] dX, \tag{4.3}$$

where the remainder $R_2(X, Y_0)$ is of order $\varepsilon \log \varepsilon$.

The function (4.3) is a function of ε, denoted by $F(\varepsilon)$ and its behaviour for small values of ε will be investigated by determining $F(0)$ and $\frac{\partial F}{\partial \varepsilon}(0)$. This will be done for the various terms separately.

4.2 The term

$$-\varepsilon^2 \int_{-l}^{\infty} (X - X_0) I_0 \, \gamma_y (X, Y_0) \, dX. \tag{4.4}$$

Substitution of the value for I_0 yields

$$-\int_{-l}^{\infty} \frac{\frac{Y - Y_0}{\cos^2 \varphi} + \varepsilon (X - X_0) \tan \varphi}{(X - X_0) [\{ \varepsilon (X - X_0) + (Y - Y_0) \tan \varphi \}^2 + (Y - Y_0)^2]^{1/2}} \Bigg|_0^{Y_1} \gamma_y (X, Y_0) dX. \tag{4.5}$$

If $\varepsilon = 0$, this becomes equal to

$$-\frac{2}{\cos \varphi} \int_{-l}^{\infty} \frac{\gamma_y (X, Y_0)}{X - X_0} dX, \tag{4.6}$$

since $0 < Y_0 < Y_1$ and hence $\frac{Y - Y_0}{|Y - Y_0|} = 1$ for $Y = Y_1$ and -1 for $Y = 0$. The infinite integrals in (4.5) and (4.6) are convergent, since for large values of X, $\gamma_y(X, Y_0)$ is given by eq. (3.8), where $Im\, \nu$ was assumed to be negative.

Performing formally the differentiation of (4.5) to ε under the integral sign, the result turns out to be

$$\int_{-l}^{\infty} \frac{\varepsilon (X - X_0)(Y - Y_0)}{[\{ \varepsilon (X - X_0) + (Y - Y_0) \tan \varphi \}^2 + (Y - Y_0)^2]^{3/2}} \Bigg|_0^{Y_1} \gamma_y (X, X_0) dX. \tag{4.7}$$

The integrand in (4.7) is a continuous function of both variables X and ε. Moreover, (4.7) converges uniformly in ε for small values of ε since the absolute value of the integrand is smaller than

$$\mu(X) = \frac{\varepsilon (X - X_0)}{(Y - Y_0)^2} \Bigg|_0^{Y_1} \gamma_y (l, Y_0) \, e^{Im \nu \, . \frac{X - l}{v}}.$$

Since $\int_N^\infty \mu(X) dX$ converges if $Im\, \nu$ is negative, (4.7) is uniformly convergent in ε and the differentiation of (4.5) to ε may be performed under the integral sign. (Compare ref. 4, Sec. 4.4).

Substitution of $\varepsilon = 0$ makes the expression (4.7) equal to zero. The second derivative to ε becomes for $\varepsilon = 0$ equal to

$$\int_{-l}^{\infty} \frac{(X - X_0) \cos^3 \varphi}{(Y - Y_0)^2} \Bigg|_0^{Y_1} \gamma_y (X, Y_0) dX.$$

The region $-l$ to $+l$ gives a finite contribution to this integral, while the contribution of the region $+l$ to ∞ is proportional to

$$\gamma_y (l, Y_0) \int_l^\infty (X - X_0) e^{-i\nu \frac{X - l}{v}} dX = \gamma_y (l, Y_0) \left\{ \frac{v (l - X_0)}{i\nu} - \frac{v^2}{\nu^2} \right\}.$$

Substituting eq. (3.10) it is seen that there appears a term, not explicitly dependent upon ν and a term inversely proportional to $\frac{\nu}{v}$. Hence, when (4.4) is replaced by (4.6) the error which is made consists of terms of order ε^2 or higher and of terms of order $\frac{\varepsilon^2}{\omega}$ or higher, where $\omega = \frac{\nu l}{v}$ is of the same order as $\frac{\nu}{v}$.

4.3 The term

$$\varepsilon \int_{-l}^{\infty} I_1 \left\{ \gamma_\xi (X, X_0) - \varepsilon (X - X_0) \frac{\partial \gamma_y}{\partial Y} (X, Y_0) \right\} dX. \tag{4.8}$$

Substitution of the value for I_1 leads to

$$-\int_{-l}^{\infty} \frac{(Y - Y_0) \tan \varphi + \varepsilon (X - X_0)}{(X - X_0) [\{ \varepsilon (X - X_0) + (Y - Y_0) \tan \varphi \}^2 + (Y - Y_0)^2]^{1/2}} \Bigg|_0^{Y_1} \Big\{ \gamma_\xi (X, Y_0) -$$

$$- \varepsilon (X - X_0) \frac{\partial \gamma_y}{\partial Y} (X, Y_0) \Big\} dX,$$

which, with the same reasoning as used in Sec. 4.2, is equal to

$$-2 \sin \varphi \int_{-l}^{\infty} \frac{\gamma_\xi (X, Y_0) - \varepsilon (X - X_0) \frac{\partial \gamma_y}{\partial Y} (X, Y_0)}{X - X_0} dX.$$

Since

$$\int_{-l}^{\infty} \frac{\varepsilon (X - X_0) \frac{\partial \gamma_y}{\partial Y} (X, Y_0)}{X - X_0} dX = - \int_{-l}^{\infty} \frac{\partial \gamma_\xi (X, Y_0)}{\partial X} dX = 0,$$

the final result is

$$-2 \sin \varphi \int_{-l}^{\infty} \frac{\gamma_\xi (X, Y_0)}{X - X_0} dX, \tag{4.9}$$

with an error again containing terms of order ε^2 and order $\dfrac{\varepsilon^2}{\omega}$.

4.4 The remainder

$$\varepsilon \int_{-l}^{\infty} R_2 (X, Y_0) dX$$

contains terms of order $\varepsilon^2 \log \varepsilon$ and $\dfrac{\varepsilon^2 \log \varepsilon}{\omega}$.

4.5 Consider now the second term of the right hand side of eq. (3.5). Since this term is due to the left semi-wing, eq. (3.6a) must be applied which yields

$$\varepsilon \int_{-l(0)}^{0} \int_{-l}^{\infty} \frac{(Y - Y_0) \gamma_\xi - \{ \varepsilon (X - X_0) + 2 Y_0 \tan \varphi \} \gamma_y}{[\{ \varepsilon (X - X_0) - (Y + Y_0) \tan \varphi \}^2 + (Y - Y_0)^2]^{3/2}} dX\, dY. \tag{4.10}$$

Since γ_ξ is of order ε and since the nominator is always of order 1 (the theory is not valid in the region near the central section, where $Y - Y_0$ may approach zero), this term is evidently of order ε^2 or $\dfrac{\varepsilon^2}{\omega}$, except possibly for the part

$$-2 \varepsilon Y_0 \tan \varphi \int_{-l(0)}^{0} \int_{-l}^{\infty} \frac{\gamma_y}{[\{ \varepsilon (X - X_0) - (Y + Y_0) \tan \varphi \}^2 + (Y - Y_0)^2]^{3/2}} dX\, dY,$$

which contains a contribution of order ε equal to

$$-2 \varepsilon Y_0 \tan \varphi \int_{-l(0)}^{0} \int_{-l}^{\infty} \frac{\gamma_y}{\{ (Y + Y_0)^2 \tan^2 \varphi + (Y - Y_0)^2 \}^{3/2}} dX\, dY.$$

The integration to X can be performed. However, it follows from eq. (3.9) that

$$-i \frac{\nu}{v} \int_{-l}^{\infty} \gamma_y \, dX = \left\{ \frac{p (X, Y)}{\rho v} + \gamma_y (X, Y) \right\}_{X = \infty}$$

and since both the pressure and the vorticity vanish for $X = \infty$, it is found that

$$\int_{-l}^{\infty} \gamma_y \, dX = 0.$$

Hence the whole expression (4.10) consists of terms which are at least either small of order ε^2 or of order $\frac{\varepsilon^2}{\omega}$.

4.6 Making use of the results of the preceding sections, it is seen that eq. (3.5) may be written as

$$4\pi w(X_0, Y_0) = -\frac{2}{\cos\varphi} \int_{-l}^{\infty} \frac{\gamma_y(X, Y_0)}{X - X_0}\, dX - 2\sin\varphi \int_{-l}^{\infty} \frac{\gamma_\xi(X, Y_0)}{X - X_0}\, dX + 0(\varepsilon^2 \log \varepsilon) + 0\left(\frac{\varepsilon^2 \log \varepsilon}{\omega}\right)$$

or

$$w(X_0, Y_0) = -\frac{1}{2\pi} \int_{-l}^{\infty} \frac{\gamma_\eta(X, Y_0)}{X - X_0}\, dX - \frac{\sin\varphi}{2\pi} \int_{-l}^{\infty} \frac{\gamma_\xi(X, Y_0)}{X - X_0}\, dX + 0(\varepsilon^2 \log \varepsilon) + 0\left(\frac{\varepsilon^2 \log \varepsilon}{\omega}\right). \tag{4.11}$$

Since $\gamma_t = \gamma_\eta + \gamma_\xi \sin\varphi$ denotes the tangential component of the vorticity when this is decomposed along the mid-chord line and perpendicular to it, this equation may also be written as

$$w(X_0, Y_0) = -\frac{1}{2\pi} \int_{-l}^{\infty} \frac{\gamma_t(X, Y_0)}{X - X_0}\, dX + 0(\varepsilon^2) + 0\left(\frac{\varepsilon^2}{\omega}\right), \tag{4.12}$$

although this form offers no advantage compared with (4.11) for further evaluation. This is due to the fact that the solution must satisfy the KUTTA condition, viz. (see eq. (3.9))

$$\gamma_y(l, Y) = -i\,\frac{\nu}{v} \int_{-l}^{l} \gamma_y(X, Y)\, dx,$$

where γ_y is not replaced by γ_t.

The second term of the right hand side of (4.11) is of order ε and hence disappears for a swept wing of infinite span. It is seen that for this case the solution for γ_η is independent of the angle of sweep. However, γ_y and the pressure then become proportional to $\cos\varphi$. Hence, the result is obtained that for a swept wing of infinite span all forces and moments are proportional to $\cos\varphi$. This is in agreement with the usual method of decomposing the velocity v into a component $v\cos\varphi$ perpendicular to the wing and a component $v\sin\varphi$ parallel to A. The first component leads also to forces proportional to $\cos\varphi$, while the second component produces no reactions.

The terms of order $\varepsilon^2 \log \varepsilon$ and $\frac{\varepsilon^2 \log \varepsilon}{\omega}$ in eq. (4.11) will be neglected. As far as the first term is concerned, this involves that the aspect ratio may not be too small. The neglect of terms of order $\frac{\varepsilon^2 \log \varepsilon}{\omega}$ involves the further limitation, that the reduced frequency neither may be small. In fact, it is known that for the steady case there exist additional terms of order ε containing spanwise integrations (see ref. 2).

It may be concluded that these terms may only be neglected if ω is larger than ε. Since $\omega = \frac{\nu l}{v}$ and $\varepsilon = \frac{l(0)}{b}$ this means that, neglecting the difference between l and $l(0)$ in these order considerations, the reduced frequency referred to the semi-span, viz. $\frac{\nu b}{v}$, should be larger than 1, for instance 3, in order that the present theory may be applied. This limitation is the same for straight and for swept wings.

Finally, it may be added that the aspect ratio corrections introduced by REISSNER (ref. 5) for straight wings are of order $\frac{\varepsilon^2 \log \varepsilon}{\omega}$ and hence represent for small ω the dominant terms. REISSNER finds his correction to become unimportant for larger ω-values.

4.7 That eq. (4.12) stands for the true two-dimensional approximation can be shown in the following way.

The vortex distribution in an arbitrary section Y_0 of the wing is determined by the components $\gamma_\xi(X, Y_0)$ and $\gamma_\eta(X, Y_0)$. If it is assumed that these components retain their same values also in all other sections, namely for $-\infty < y < \infty$, a two-dimensional flow is obtained. In this way the equation of continuity is violated, since γ_ξ would vanish if γ_η is constant. This is, however, an effect of smaller order (ε^2), as can be explained by remarking that the greatest contribution to the downwash at (X_0, Y_0) is caused by the vortices lying nearest to the point (X_0, Y_0). In this region the variation of γ_η is unimportant save for its causing a γ_ξ-component.

If γ_ξ and γ_η are assumed independent of Y, eq. (3.5) becomes by aid of eq. (3.6)

$$4\pi\, w(X_0, Y_0) = \varepsilon \int_{-\infty}^{\infty}\int_{-l}^{\infty} \frac{(Y-Y_0)\gamma_\xi(X, Y_0) - \varepsilon(X-X_0)\cos\varphi\,\gamma_\eta(X, Y_0)}{[\{\varepsilon(X-X_0)+(Y-Y_0)\tan\varphi\}^2+(Y-Y_0)^2]^{3/2}}\, dX\, dY.$$

It has been shown in Sec. 4.2 that if in the definition of I_n the limits of integration 0 and $l(0)$ are replaced by any other limits, provided Y_0 lies between them, the error which is introduced is of order ε^2. Hence, performing the integration to Y_0, one may write

$$4\pi\, w(X_0, Y_0) = \varepsilon \int_{-l}^{x} \{ I_1\gamma_\xi(X, Y_0) - \varepsilon(X-X_0)\cos\varphi\, I_0\gamma_\eta(X, Y_0) \}\, dX + 0(\varepsilon^2).$$

By substitution of the values for I_0 and I_1, eq. (4.12) is again obtained.

The fact that γ_ξ now enters into the two-dimensional approximation, is due to the unequal distance of the components γ_ξ at both sides of the section considered to that section. This is the effect mentioned already in the introduction.

4.8 A further point valuable to be mentioned is that, although the mid-chord line was used to define the angle of sweepback, any other line of constant chord fraction might have been used since this also introduces differences of order ε^2.

Since γ_ξ is of order ε and γ_η of order 1, the angle between the vector $\vec{\gamma}$ and the mid-chord line is also of order ε. This means that γ_t is equal to $|\gamma|$ with an error of order ε^2. Since the angle between all lines of constant chord fraction at the wing is small of order ε, one may take γ_t along any of these lines.

Thus eq. (4.12) remains invariant within the relevant accuracy for definitions of the angle of sweepback referring to lines between the leading and the trailing edge of the wing. This invariance does not, of course, exist for the components γ_ξ and γ_η. In particular, if φ would correspond to the angle of the trailing edge and hence γ_η would be parallel to the trailing edge, eq. (3.12) would simplify into

$$\gamma_\xi(l, Y) = -\varepsilon\, \frac{d\Gamma(Y)}{dY}.$$

It seems, however, probable on physical grounds that the approximation will be best if φ is referred to a line anywhere between the mid-chord line and the quarter-chord line.

5 The solution of the integral equation.

The integral equation (4.11) expressing the known downwash at the wing surface in terms of the unknown vortex distribution at the wing and in its wake, contains the two unknown functions γ_y and γ_ξ. These functions are related by the continuity equation for the vortex field

$$\gamma_\xi(X, Y) = -\varepsilon \frac{\partial}{\partial Y} \int_{-l}^{X} \gamma_y(X, Y)\, dX. \tag{5.1}$$

Since the solution γ_y of eq. (4.11) can be written as

$$\gamma_y = (\gamma_y^{(2)} + \Delta\gamma_y)\cos\varphi,$$

where $\gamma_y^{(2)}$ denotes the two-dimensional vortex distribution for a straight wing, eq. (5.1) may be replaced by

$$\gamma_\xi(X, Y) = -\varepsilon\cos\varphi \frac{\partial}{\partial Y} \int_{-l}^{X} \gamma_y^{(2)}(X, Y)\, dX + 0(\varepsilon^2). \tag{5.2}$$

Neglecting again the term $0(\varepsilon^2)$ means that $\gamma_\xi(X, Y)$ becomes a known function. The problem then becomes to find a solution for $\Delta\gamma_y$, satisfying the KUTTA condition and to determine the change in pressure given by

$$\frac{\Delta p(X, Y)}{\rho v} = -\Delta\gamma_y(X, Y) - i\,\frac{\nu}{v} \int_{-l}^{X} \Delta\gamma_y(X, Y)\, dX. \tag{5.3}$$

By aid of eqs. (3.8), (3.10) and (3.12), eq. (4.11) will now be written as

$$4\pi w(X_0, Y_0) = -\frac{2}{\cos\varphi} \oint_{-l}^{l} \frac{\gamma_y(X, Y_0)}{X - X_0} dX + \frac{2i\frac{\nu}{v}}{\cos\varphi} \Gamma(Y_0) e^{i\omega} \int_{l}^{\infty} \frac{e^{-i\nu\frac{X}{v}}}{X - X_0} dX -$$

$$-2\sin\varphi \oint_{-l}^{l} \frac{\gamma_\xi(X, Y_0)}{X - X_0} dX - 2\sin\varphi \cdot \gamma_\xi(l, Y_0) e^{-i\omega} \int_{l}^{\infty} \frac{e^{-i\nu\frac{X}{v}}}{X - X_0} dX. \tag{5.4}$$

Introducing

$$\begin{aligned} \gamma_y &= (\gamma_y^{(2)} + \Delta\gamma_y) \cos\varphi, \\ \Gamma &= (\Gamma^{(2)} + \Delta\Gamma) \cos\varphi, \\ p &= (p^{(2)} + \Delta p) \cos\varphi, \end{aligned} \tag{5.5}$$

where the two-dimensional quantities are determined by

$$4\pi w(X_0, Y_0) = -2 \oint_{-l}^{l} \frac{\gamma_y^{(2)}(X, Y_0)}{X - X_0} dX + 2i\frac{\nu}{v} \Gamma^{(2)}(Y_0) e^{i\omega} \int_{l}^{\infty} \frac{e^{-i\nu\frac{X}{v}}}{X - X_0} dX \tag{5.6}$$

and subtracting eq. (5.6) from eq. (5.4), the result is

$$0 = -2 \oint_{-l}^{l} \frac{\Delta\gamma_y(X, Y_0)}{X - X_0} dX + 2i\frac{\nu}{v} \Delta\Gamma(Y_0) e^{i\omega} \int_{l}^{\infty} \frac{e^{-i\nu\frac{X}{v}}}{X - X_0} dX -$$

$$-2\sin\varphi \oint_{-l}^{l} \frac{\gamma_\xi(X, Y_0)}{X - X_0} dX - 2\sin\varphi \cdot \gamma_\xi(l, Y_0) e^{i\omega} \int_{l}^{\infty} \frac{e^{-i\nu\frac{X}{v}}}{X - X_0} dX. \tag{5.7}$$

This equation can be solved in two different ways. Either the sum of the second and fourth terms will be put equal to $-4\pi\Delta w(X_0, Y_0)$ and the solution of the equation

$$4\pi\Delta w(X_0, Y_0) = -2 \oint_{-l}^{l} \frac{\Delta\gamma_y(X, Y_0) + \sin\varphi \cdot \gamma_\xi(X, Y_0)}{X - X_0} dX, \tag{5.8}$$

well-known from the steady case, will be used or the sum of the third and fourth terms will be put equal to $-4\pi\Delta w(X_0, Y_0)$ and use will be made of the solution of the equation

$$4\pi\Delta w(X_0, Y_0) = -2 \oint_{-l}^{l} \frac{\Delta\gamma_y(X, Y_0)}{X - X_0} dX + 2i\frac{\nu}{v} \Delta\Gamma(Y_0) e^{i\omega} \int_{l}^{\infty} \frac{e^{-i\nu\frac{X}{v}}}{X - X_0} dX, \tag{5.9}$$

which is known from the unsteady case.

The first method appears to lead to quicker results and will be presented hereunder, while the second method has been elaborated in Appendix 1. The first method has been used by SCHWARZ (ref. 6) for the straight wing of infinite span.

The solution of eq. (5.8) for which $\Delta\gamma_y(l, Y)$ is finite, as it should be according to the KUTTA condition, is

$$\Delta\gamma_y(X, Y_0) + \sin\varphi \cdot \gamma_\xi(X, Y_0) = \frac{2}{\pi} \sqrt{\frac{l - X}{l + X}} \oint_{-l}^{l} \Delta w(X_0, Y_0) \sqrt{\frac{l + X_0}{l - X_0}} \frac{dX_0}{X_0 - X}. \tag{5.10}$$

Substituting for $-4\pi\Delta w(X_0, Y_0)$ the second and fourth term of eq. (5.7) the following double integral appears

$$\oint_{-l}^{l} \frac{l + X_0}{l - X_0} \left\{ \int_{l}^{\infty} \frac{e^{-i\nu\frac{\eta}{v}}}{\eta - X_0} d\eta \right\} \frac{dX_0}{X_0 - X}.$$

It has been shown by SCHWARZ that the order of integration may be interchanged. The integration to X_0 can then be performed and according to eq. (A 2.7) the result is

$$\pi \int_{l}^{\infty} \frac{e^{-i\nu\frac{\eta}{v}}}{\eta - X} \sqrt{\frac{\eta + l}{\eta - l}} d\eta.$$

Hence, if the parameter Y_0 is omitted, the solution (5.10) may be written as

$$\Delta\gamma_y(X) = -\frac{1}{\pi}\left\{ i\frac{\nu}{v}\Delta\Gamma - \sin\varphi\,.\,\gamma_\xi(l)\right\} e^{i\omega}\sqrt{\frac{l-X}{l+X}}\int_l^\infty \frac{e^{-i\frac{\nu}{v}\eta}}{\eta-X}\sqrt{\frac{\eta+l}{\eta-l}}\,d\eta - \sin\varphi\,.\,\gamma_\xi(X). \tag{5.11}$$

Since

$$\Delta\Gamma = \int_{-l}^{l}\Delta\gamma_y dX$$

integration of (5.11) leads by aid of the integral (A 2.4) to the result

$$\Delta\Gamma = -\left\{ i\frac{\nu}{v}\Delta\Gamma - \sin\varphi\,.\,\gamma_\xi(l)\right\} e^{i\omega}\int_l^\infty\left\{\sqrt{\frac{\eta+l}{\eta-l}}-1\right\} e^{-i\frac{\nu}{v}\eta}\,d\eta - \sin\varphi\,.\int_{-l}^{l}\gamma_\xi(X)dX.$$

By using the integral (A 2.10) this becomes equal to

$$\Delta\Gamma = \left[\frac{\pi l}{2}e^{i\omega}\left\{ iH_0^{(2)}(\omega) + H_1^{(2)}(\omega)\right\} - \frac{i}{\omega}l\right]\left\{ i\frac{\nu}{v}\Delta\Gamma - \sin\varphi\,.\,\gamma_\xi(l)\right\} - \sin\varphi\int_{-l}^{l}\gamma_\xi(X)dX$$

or

$$\Delta\Gamma = \left\{\frac{il}{\omega} + \frac{2l}{\pi\omega^2}\,\frac{e^{-i\omega}}{iH_0^{(2)}(\omega)+H_1^{(2)}(\omega)}\right\}\sin\varphi\,.\,\gamma_\xi(l) - \frac{2i\sin\varphi}{\pi\omega}\,\frac{e^{-i\omega}}{iH_0^{(2)}(\omega)+H_1^{(2)}(\omega)}\int_{-l}^{l}\gamma_\xi(X)dX. \tag{5.12}$$

Finally, this is substituted into eq. (5.11), leading to

$$\Delta\gamma_y(X) = \frac{2}{\pi^2}\,\frac{\sin\varphi}{iH_0^{(2)}(\omega)+H_1^{(2)}(\omega)}\left\{\frac{i}{\omega}\gamma_\xi(l) - \frac{1}{l}\int_{-l}^{l}\gamma_\xi(X)dX\right\}\sqrt{\frac{l-X}{l+X}}\int_l^\infty\frac{e^{-i\frac{\nu}{v}\eta}}{\eta-X}\sqrt{\frac{\eta+l}{\eta-l}}\,d\eta -$$

$$- \sin\varphi\,.\,\gamma_\xi(X). \tag{5.13}$$

The pressure difference follows by application of eq. (5.3). In the evaluation the following expression occurs

$$\frac{2}{\pi}\left[\sqrt{\frac{l-X}{l+X}}\int_l^\infty\frac{e^{-i\frac{\nu}{v}\eta}}{\eta-X}\sqrt{\frac{\eta+l}{\eta-l}}\,d\eta + i\frac{\nu}{v}\int_{-l}^{X}\sqrt{\frac{l-X}{l+X}}\left\{\int_l^\infty\frac{e^{-i\frac{\nu}{v}\eta}}{\eta-X}\sqrt{\frac{\eta+l}{\eta-l}}\,d\eta\right\}dX\right].$$

It has been shown by SCHWARZ and, moreover, the derivation is presented in Appendix 2, that this expression is equal to

$$-i\omega\left\{ iH_0^{(2)}(\omega) + H_1^{(2)}(\omega)\right\}\left(\frac{\pi}{2} + \sin^{-1}\frac{X}{l}\right) - iH_0^{(2)}(\omega)\sqrt{\frac{l-X}{l+X}}.$$

The pressure difference then turns out to be

$$\frac{\Delta p(X)}{\rho v} = \frac{\sin\varphi}{\pi}\left\{\frac{i}{\omega}\gamma_\xi(l) - \frac{1}{l}\int_{-l}^{l}\gamma_\xi(X)dX\right\}\left\{ i\omega\left(\frac{\pi}{2}+\sin^{-1}\frac{X}{l}\right) + \right.$$

$$\left. + \frac{iH_0^{(2)}(\omega)}{iH_0^{(2)}(\omega)+H_1^{(2)}(\omega)}\sqrt{\frac{l-X}{l+X}}\right\} + \sin\varphi\left\{\gamma_\xi(X) + i\frac{\nu}{v}\int_{-l}^{X}\gamma_\xi(X)dX\right\}. \tag{5.14}$$

In order to express the right hand side into two-dimensional quantities, use will be made of eq. (5.2). Then

$$\gamma_\xi(X) + i\frac{\nu}{v}\int_{-l}^{X}\gamma_\xi(X)dX = -\varepsilon\cos\varphi\,\frac{\partial}{\partial Y}\left\{\int_{-l}^{X}\gamma_y^{(2)}(X,Y)dX + i\frac{\nu}{v}\int_{-l}^{X}\left\{\int_{-l}^{X}\gamma_y^{(2)}(X,Y)dX\right\}dX\right.$$

$$= \frac{\varepsilon}{\rho v}\cos\varphi\,\frac{\partial}{\partial Y}\int_{-l}^{X}p^{(2)}(X,Y)dX, \tag{5.15}$$

where the relation between $p^{(2)}(X,Y)$ and $\gamma_y^{(2)}(X,Y)$ is analogous to that between Δp and $\Delta\gamma_y$ as given by eq. (5.3).

In particular

$$\gamma_\xi(l) + i\frac{\nu}{v}\int_{-l}^{l}\gamma_\xi(X)dX = \frac{\varepsilon}{\rho v}\cos\varphi\,\frac{dK^{(2)}}{dY}, \tag{5.16}$$

where $K^{(2)}$ is the two-dimensional force on the wing.

Introducing

$$P(\omega) = \frac{H_1^{(2)}(\omega)}{iH_0^{(2)}(\omega) + H_1^{(2)}(\omega)}$$

and using eqs. (5.15) and (5.16), the pressure differences become finally

$$\Delta p(X.Y) = -\frac{\varepsilon\sin\varphi\cos\varphi}{\pi}\left\{\frac{\pi}{2} + \sin^{-1}\frac{X}{l} + \frac{1-P(\omega)}{i\omega}\sqrt{\frac{l-X}{l+X}}\right\}\frac{dK^{(2)}}{dY} +$$

$$+\varepsilon\sin\varphi\cos\varphi\frac{\partial}{\partial Y}\int_{-l}^{X}p^{(2)}(X,Y)dX. \tag{5.17}$$

In this formula, differentiation to Y must be performed at a constant value of X, i.e. it gives the rate of change in the direction parallel to the mid-chord line. By introducing dimensionless coordinates

$$\overline{X} = \frac{X}{l} \text{ and } \overline{Y} = \frac{Y}{l(0)} = \frac{y}{b} \tag{5.18}$$

one obtains

$$\frac{\partial}{\partial Y} = \frac{1}{l(0)}\left\{\frac{\partial}{\partial\overline{Y}} - \overline{X}s\,\frac{\partial}{\partial\overline{X}}\right\}$$

where $s = \frac{1}{l}\,\frac{dl}{d\overline{Y}}$.

Differentiation to $\overline{Y}$ is performed by keeping $\overline{X}$ constant, i.e. it gives the rate of change in the direction of a constant fraction of the chord.

Eq. (5.17) now can be written as

$$\Delta p(\overline{X},\overline{Y}) = -\frac{\sin\varphi\cos\varphi}{\pi}\left(\frac{\pi}{2} + \sin^{-1}\overline{X} + \frac{1-P(\omega)}{i\omega}\sqrt{\frac{1-\overline{X}}{1+\overline{X}}}\right)\frac{1}{b}\,\frac{dK^{(2)}}{d\overline{Y}} +$$

$$+\sin\varphi\cos\varphi\;\frac{1}{b}\left\{\frac{\partial}{\partial\overline{Y}}\,l\int_{-1}^{\overline{X}}p^{(2)}(\overline{X},\overline{Y})d\overline{X} - l\overline{X}s\,p^{(2)}(\overline{X},\overline{Y})\right\}, \tag{5.19}$$

where $-1 \leqslant \overline{X} \leqslant 1$ and $-1 \leqslant \overline{Y} \leqslant 1$.

6 Calculation of force and moment.

6.1 If, in analogy to eqs. (5.5), the total force and moment per unit span are defined by

$$\begin{aligned} K &= (K^{(2)} + \Delta K)\cos\varphi, \\ M &= (M^{(2)} + \Delta M)\cos\varphi, \end{aligned} \tag{6.1}$$

where M is the moment about the mid-chord point (with vector in the direction of the positive Y-axis), the quantities ΔK and ΔM are given by

$$\Delta K = l\int_{-1}^{1}\Delta p\,d\overline{X} \text{ and } \Delta M = l^2\int_{-1}^{1}\Delta p\,.\,\overline{X}\,d\overline{X} \tag{6.2}$$

while

$$K^{(2)} = l\int_{-1}^{1}p^{(2)}\,d\overline{X} \text{ and } M^{(2)} = l^2\int_{-1}^{1}p^{(2)}\,.\,\overline{X}\,d\overline{X}. \tag{6.3}$$

Substituting eq. (5.17) into the formula for ΔK, the following reductions can be made:

$$\int_{-1}^{1} \left\{ \frac{\pi}{2} + \sin^{-1} \overline{X} + \frac{1-P(\omega)}{i\omega} \sqrt{\frac{1-\overline{X}}{1+\overline{X}}} \right\} d\overline{X} = \pi \left(1 + \frac{1-P}{i\omega} \right),$$

$$\int_{-1}^{1} \left\{ \frac{\partial}{\partial \overline{Y}} \, l \int_{-1}^{\overline{X}} p^{(2)} (\overline{X}, \overline{Y}) d\overline{X} \right\} d\overline{X} - \int_{-1}^{1} l \, \overline{X} \, s \, p^{(2)} (\overline{X}, \overline{Y}) d\overline{X} =$$

$$\frac{d}{d\overline{Y}} \, l \int_{-1}^{1} \left\{ \int_{-1}^{\overline{X}} p^{(2)}(\overline{X}, \overline{Y}) d\overline{X} \right\} d\overline{X} - \frac{s}{l} M^{(2)} = \frac{d}{d\overline{Y}} \left\{ K^{(2)} - \frac{M^{(2)}}{l} \right\} - \frac{s}{l} M^{(2)} = \frac{dK^{(2)}}{d\overline{Y}} - \frac{1}{l} \frac{dM^{(2)}}{d\overline{Y}}.$$

Hence

$$\Delta K(\overline{Y}) = - \frac{l \sin\varphi \cos\varphi}{b} \left\{ \frac{1-P}{i\omega} \frac{dK^{(2)}}{d\overline{Y}} + \frac{1}{l} \frac{dM^{(2)}}{d\overline{Y}} \right\}. \tag{6.4}$$

When calculating ΔM, one has

$$\int_{-1}^{1} \overline{X} \left\{ \frac{\pi}{2} + \sin^{-1} \overline{X} + \frac{1-P(\omega)}{i\omega} \sqrt{\frac{1-\overline{X}}{1+\overline{X}}} \right\} d\overline{X} = \frac{1}{4} \pi \left(1 - 2 \frac{1-P}{i\omega} \right),$$

$$\int_{-1}^{1} \overline{X} \left\{ \frac{\partial}{\partial \overline{Y}} \, l \int_{-1}^{\overline{X}} p^{(2)}(\overline{X}, \overline{Y}) d\overline{X} \right\} d\overline{X} - \int_{-1}^{1} l \, \overline{X}^2 \, s \, p^{(2)} (\overline{X}, \overline{Y}) d\overline{X} =$$

$$\frac{d}{d\overline{Y}} \, l \int_{-1}^{1} \left\{ \int_{-1}^{\overline{X}} p^{(2)} (\overline{X}, \overline{Y}) d\overline{X} \right\} d \, \frac{1}{2} \overline{X}^2 - \frac{s}{l^2} I^{(2)} =$$

$$\frac{d}{d\overline{Y}} \left\{ \frac{1}{2} K^{(2)} - \frac{1}{2} \frac{I^{(2)}}{l^2} \right\} - \frac{s}{l^2} I^{(2)} = \frac{1}{2} \left\{ \frac{dK^{(2)}}{d\overline{Y}} - \frac{1}{l^2} \frac{dI^{(2)}}{d\overline{Y}} \right\},$$

where

$$I^{(2)} = l^3 \int_{-1}^{1} p^{(2)} \overline{X}^2 \, d\overline{X}. \tag{6.5}$$

Hence

$$\Delta M(\overline{Y}) = \frac{l \sin\varphi \cos\varphi}{4\,b} \left[\left(1 + 2 \frac{1-P}{i\omega} \right) l \frac{dK^{(2)}}{d\overline{Y}} - \frac{2}{l} \frac{dI^{(2)}}{d\overline{Y}} \right]. \tag{6.6}$$

Introducing dimensionless coefficients by putting

$$\begin{aligned} K^{(2)} &= \pi \rho \, l \, v^2 e^{ivt} G \, k_g , \\ M^{(2)} &= \pi \rho \, l^2 v^2 e^{ivt} G \, m_g , \\ I^{(2)} &= \pi \rho \, l^3 v^2 e^{ivt} G \, i_g , \end{aligned} \tag{6.7}$$

where G denotes any degree of freedom ($Al =$ translation, $B =$ rotation, etc.), one may write

$$\begin{aligned} \frac{dK^{(2)}}{d\overline{Y}} &= \pi \rho \, v^2 e^{ivt} \frac{d}{d\overline{Y}} (lG \, k_g) = \pi \rho \, l v^2 e^{ivt} \left(s \, G \, k_g + k_g \frac{dG}{d\overline{Y}} + \omega s \, G \frac{dk_g}{d\omega} \right) \\ \frac{dM^{(2)}}{d\overline{Y}} &= \pi \rho \, l^2 v^2 e^{ivt} \left(2 \, s \, G \, m_g + m_g \frac{dG}{d\overline{Y}} + \omega s \, G \frac{dm_g}{d\omega} \right) \\ \frac{dI^{(2)}}{d\overline{Y}} &= \pi \rho \, l^3 v^2 e^{ivt} \left(3 \, s \, G \, i_g + i_g \frac{dG}{d\overline{Y}} + \omega s \, G \frac{di_g}{d\omega} \right). \end{aligned} \tag{6.8}$$

Important: It should be noted that if $z(\overline{Y})$ denotes the bending deformation, A is equal to $\frac{z}{l}$.

It is now seen that the changes ΔK and ΔM are partly due to the change of the amplitude along the span $\left(\frac{dG}{d\overline{Y}} \right)$ and partly to wing taper. Both effects make that the circulation varies along the span. Consequently there will be written

$$\Delta K = \pi\rho \frac{l^2}{b} v^2 e^{ivt} \left(k_{g_1} \frac{dG}{d\overline{Y}} + k_{g_2} G s \right) \sin\varphi \cos\varphi$$

$$\Delta M = \pi\rho \frac{l^3}{b} v^2 e^{ivt} \left(m_{g_1} \frac{dG}{d\overline{Y}} + m_{g_2} G s \right) \sin\varphi \cos\varphi, \tag{6.9}$$

where again

$$s = \frac{1}{l} \frac{dl}{d\overline{Y}}. \tag{6.10}$$

Hence

$$k_{g_1} = - \left\{ \frac{1-P}{i\omega} k_g + m_g \right\}$$

$$k_{g_2} = - \left\{ \frac{1-P}{i\omega} \left(k_g + \omega \frac{dk_g}{d\omega} \right) + \left(2\, m_g + \omega \frac{dm_g}{d\omega} \right) \right.$$

$$m_{g_1} = \frac{1}{4} \left\{ \left(1 + 2\, \frac{1-P}{i\omega} \right) k_g - 2\, i_g \right\} \tag{6.11}$$

$$m_{g_2} = \frac{1}{4} \left\{ \left(1 + 2\, \frac{1-P}{i\omega} \right) \left(k_g + \omega \frac{dk_g}{d\omega} \right) - 2 \left(3\, i_g + \omega \frac{di_g}{d\omega} \right) \right\}.$$

The final conclusion is, that in order to obtain the aerodynamic forces acting on a strip of a swept wing, the original formulae (6.7) may be used provided the coefficient k_g are replaced by

$$\left\{ k_g + \frac{l \sin\varphi \cos\varphi}{b} \left(k_{g_1} \frac{1}{G} \frac{dG}{d\overline{Y}} + k_{g_2} \frac{1}{l} \frac{dl}{d\overline{Y}} \right) \right\} \cos\varphi \tag{6.12}$$

with a similar modification for the coefficient m_g.

For the degrees of freedom translation (A) and rotation (B) of the whole wing, the following coefficients should be substituted in the right hand side of eqs. (6.11) and in eq. (6.12)

$$\begin{aligned} k_a &= \omega^2 - 2\,P\,.\,i\omega \\ m_a &= P\,.\,i\omega \\ k_b &= -2\,P\,(1 + \tfrac{1}{2} i\omega) - i\omega \\ m_b &= P\,(1 + \tfrac{1}{2} i\omega) - \tfrac{1}{2}\, i\omega + \tfrac{1}{8}\,\omega^2. \end{aligned} \tag{6.13}$$

The coefficients i_a and i_b are calculated by aid of the expressions for the pressure difference given in ref. 7.

Taking the pressure differences again positive in downward direction, one has

$$p_a^{(2)} = \rho v^2 e^{ivt} A \left[2\,\omega^2 \sin\theta - 2\,P\,.\,i\omega \cot\frac{\theta}{2} \right].$$

Using eqs. (6.5) and (6.7), while $\overline{X} = -\cos\theta$, it is found that

$$i_a = \tfrac{1}{4}\,\omega^2 - P\,.\,i\omega. \tag{6.14}$$

In the same way

$$p_b^{(2)} = \rho v^2 e^{ivt} B \left[-\omega^2 \sin\theta \cos\theta + i\omega \left(\cot\frac{\theta}{2} - 4 \sin\theta \right) - 2\,P\,.\,(1 + \tfrac{1}{2} i\omega) \cot\frac{\theta}{2} \right] \tag{6.15}$$

and $\quad i_b = -P\,(1 + \tfrac{1}{2} i\omega).$

Corresponding formulae for a flap hinging about its leading edge and with a chord which is equal to a constant fraction of the wing chord are presented in Appendix III.

6.2 A certain complication arises at the tip section, where in the two-dimensional approximation the circulation and the force are suddenly reduced to zero. Actually this reduction is spread over some distance inward from the tip, but the difference between these two cases will be neglected. Hence, in the formulae of Section 6 special care must be taken of the tip section since otherwise the vortices γ_ξ which are due to the decreasing circulation at the tip would be neglected completely. At the tip eq. (5.1) should be replaced by:

$$\gamma_\xi (X, Y) = \varepsilon \int_{-l}^{X} \gamma_y(X, Y) dX \cdot \delta \{ Y - l(0) \}, \tag{6.16}$$

where $\delta \{ Y - l(0) \}$ denotes the Dirac function. This means that at the tip section $Y = l(0)$, γ_ξ is infinitely large in such a way that

$$\int_{l(0)-\Delta l}^{l(0)+\Delta l} \gamma_\xi(X, Y) dY = \varepsilon \int_{-l}^{X} \gamma_y(X, Y) dX.$$

Moreover at the tip section the integral equation (4.12) should be replaced by

$$w \{ X_0, l(0) \} = - \frac{1}{4\pi} \int_{-l}^{\infty} \frac{\gamma_t \{ X, l(0) \}}{X - X_0} \, dX,$$

since the vortices γ_t exist only inward, but not outward of the tip section.

Consequently, in the formulae (5.15) through (5.18), (6.4) and (6.6), the additional tip forces are obtained by replacing the operator

$$\frac{d}{dY} \text{ by } -\tfrac{1}{2} \delta \{ Y - l(0) \} \text{ or } \frac{d}{d\overline{Y}} \text{ by } -\tfrac{1}{2} \delta \{ \overline{Y} - 1 \}.$$

Substituting eqs (6.7), the additional tip force and moment are

$$\Delta K(1) = \frac{l \sin\varphi \cos\varphi}{2 b} \left\{ \frac{1 - P}{i\omega} G \, l \, k_g + G \, l \, m_g \right\} \delta(\overline{Y} - 1),$$

$$\Delta M(1) = - \frac{l \sin\varphi \cos\varphi}{8 b} \left\{ \left(1 + 2 \frac{1 - P}{i\omega} \right) G \, l^2 \, k_g - 2 \, G \, l^2 \, i_g \right\} \delta(\overline{Y} - 1).$$

Hence, a concentrated aerodynamic force of magnitude

$$- \frac{l \sin\varphi \cos^2\varphi}{b} \, k_{g_1} \frac{G(1)}{2} \, \pi \rho \, l \, v^2 \, e^{i\nu t} \tag{6.17}$$

as well as a concentrated aerodynamic moment of magnitude

$$- \frac{l \sin\varphi \cos^2\varphi}{b} \, m_{g_1} \frac{G(1)}{2} \, \pi \rho \, l^2 \, v^2 \, e^{i\nu t} \tag{6.18}$$

should be added at the tip section.

Although the accuracy of the two-dimensional approximation decreases near the tip, it is consequent to include the aerodynamic reactions (6.17) and (6.18). It may be expected that their inclusion will improve the approximation.

7 Results.

The coefficients k_{a_1}, k_{a_2}, k_{b_1}, k_{b_2}, m_{a_1}, m_{a_2}, m_{b_1} and m_{b_2} have been computed by aid of the formulae of the preceding section. They are given in table 1 for a number of ω-values and are plotted in figs. 7.1—7.4.

It is seen that the real parts of the coefficients with subscript b become infinitely large if ω ap-

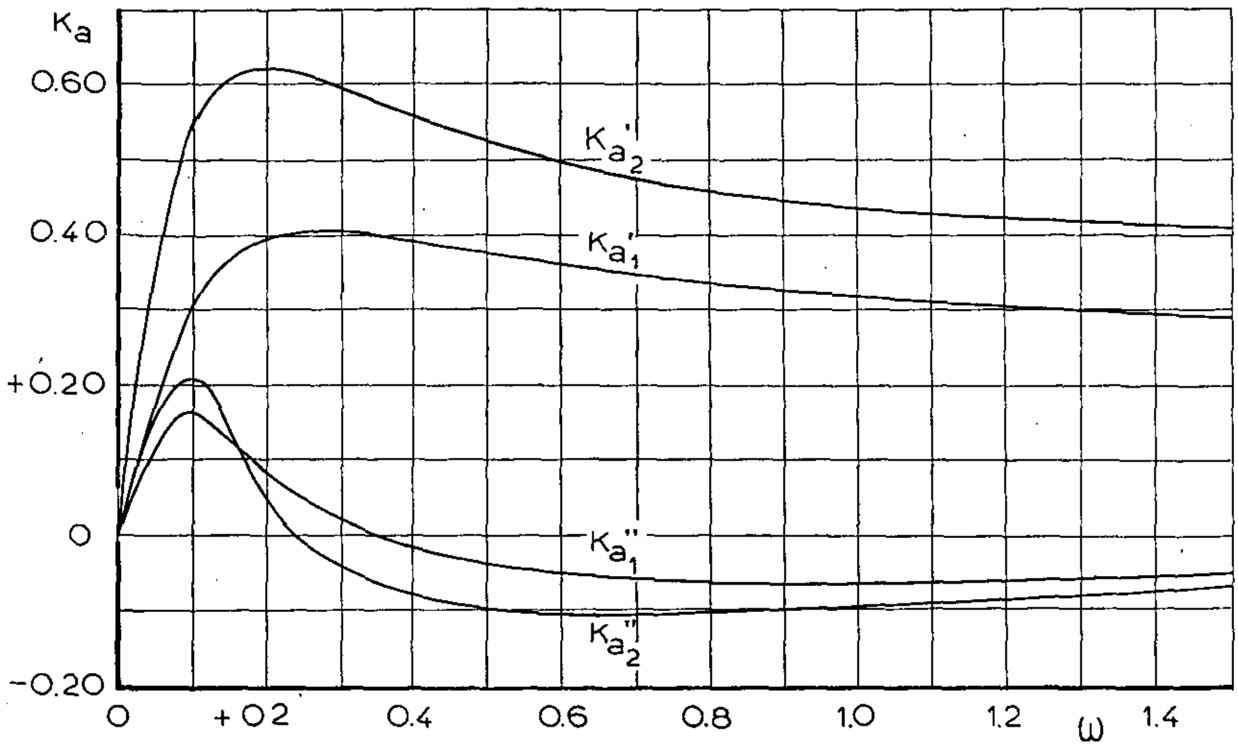

Fig. 7.1. Coefficient k_a as a function of ω ($k_a = k_a' + i\,k_a''$).

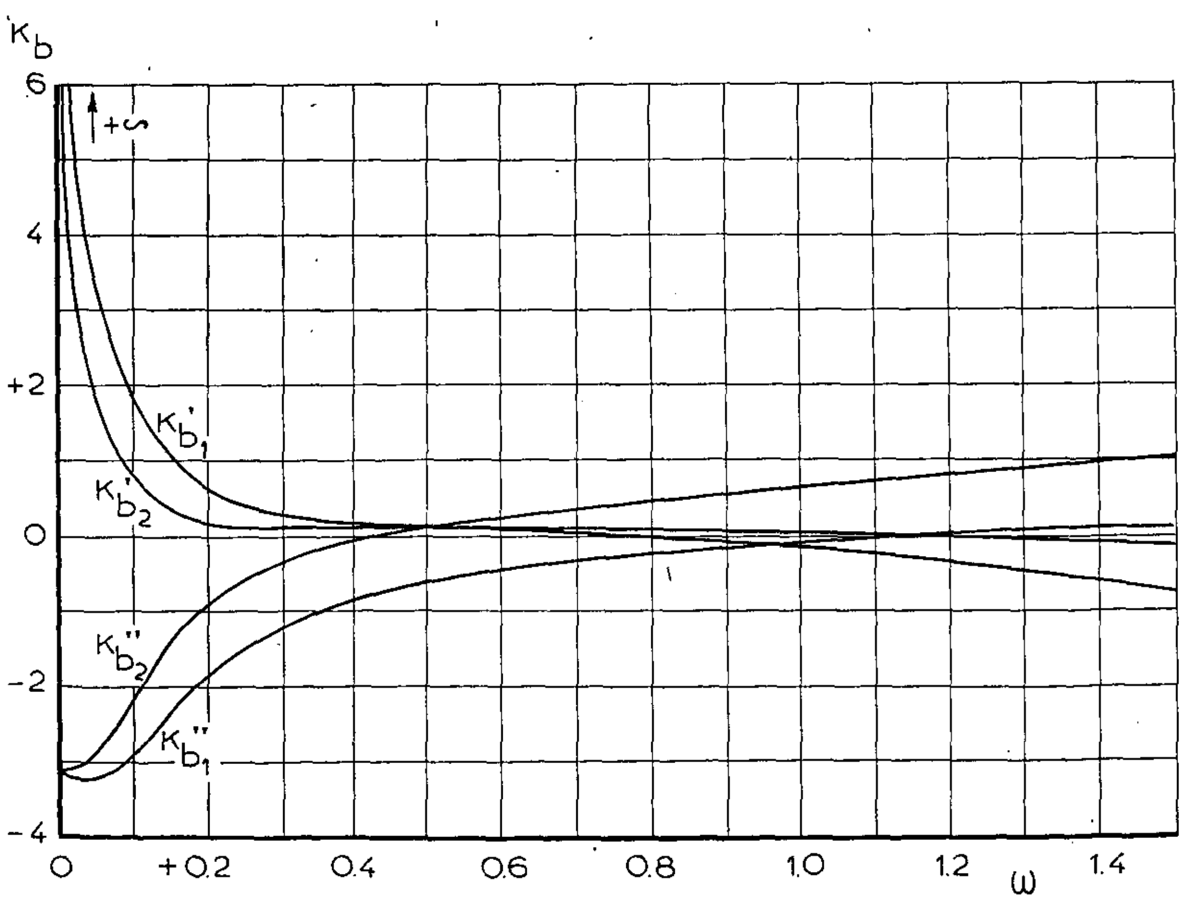

Fig. 7.2. Coefficient k_b as a function of ω ($k_b = k_b' + i\,k_b''$).

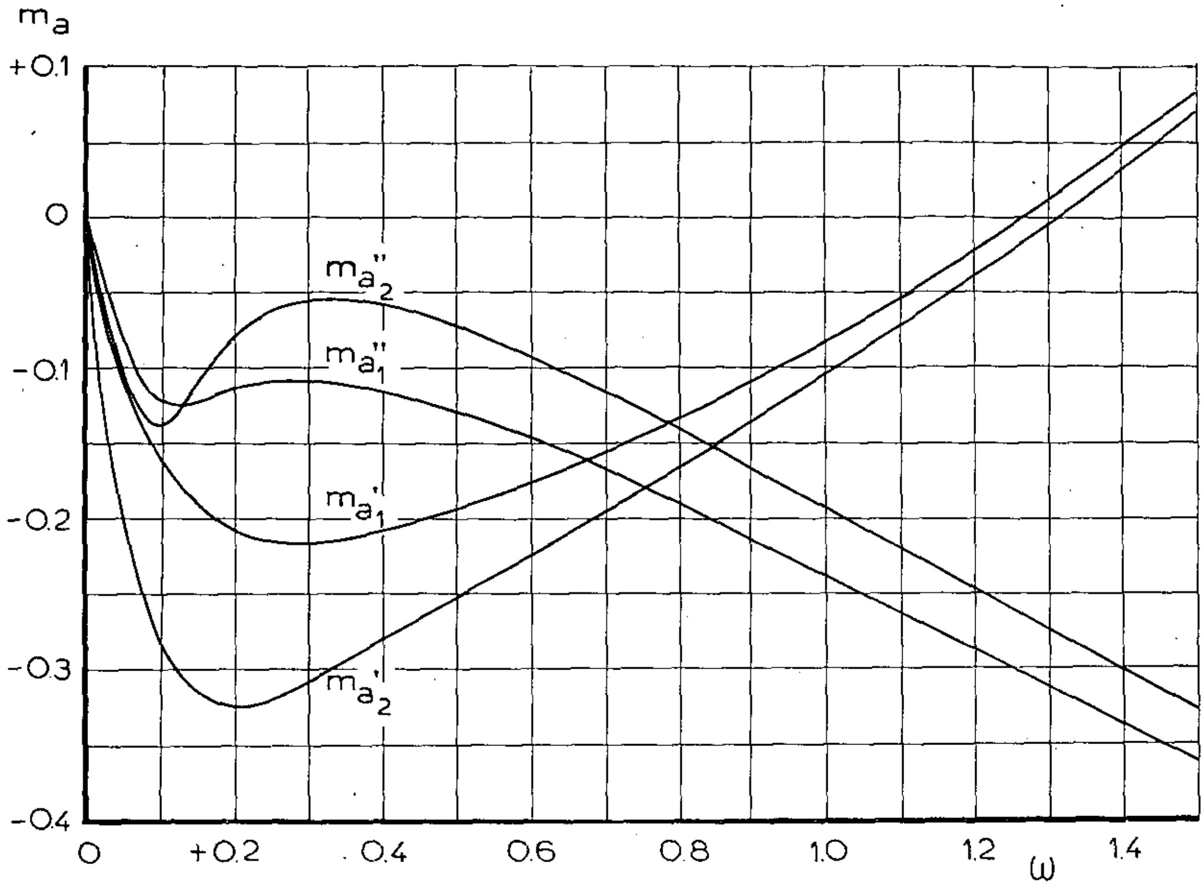

Fig. 7.3. Coefficient m_a as a function of ω ($m_a = m_a' + i\,m_a''$).

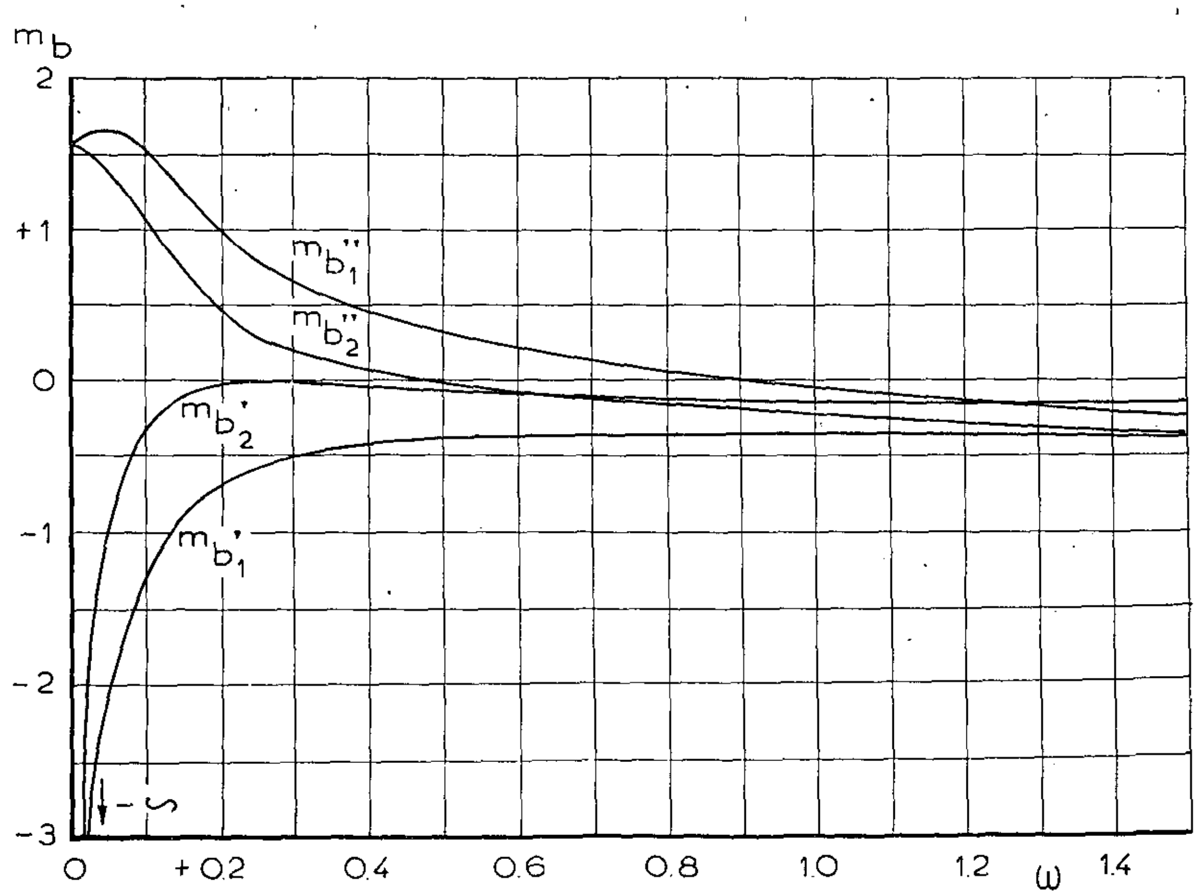

Fig. 7.4. Coefficient m_b as a function of ω ($m_b = m_b' + i m_b''$).

proaches zero. This is due to the factor $\frac{1-P}{i\omega}$ in the formulae (6.11). For small values of ω, the P-function may be expanded as

$$P = 1 + i\omega \log \omega + 0(\omega^2)$$

and hence $\frac{1-P}{i\omega}$ becomes logarithmically infinite for 0. Since $k_b = -2$ for $\omega \to 0$, the coefficients k_{b_1}, k_{b_2}, m_{b_1}, and m_{b_2} become also logarithmically infinite.

However, this does not mean that infinitely large aerodynamic forces are ever introduced in the calculation. It should be remembered that the present theory may only be applied if ω is at least equal to ε. Since it will be clear from eq. (6.12) that the new coefficients are multiplied by $\frac{l}{b}$, that is by a factor which is of order ε, it follows that the additional aerodynamic forces are determined by expressions of the type εk_{b_1} for $\omega > \varepsilon$. The real part of this force is plotted in fig. 7.5 for a series of ε-values, from which it is seen that *no infinitely large aerodynamic forces arise since for $\omega = \varepsilon$ the force is given by $\varepsilon k_{b_1} = \omega k_{b_1}$ which becomes zero in the limit $\omega \to 0$.*

general, of the same order of magnitude. In this transformation a small parameter ε, denoting for rectangular wings the inverse of the aspect ratio, occurs.

In the present theory all terms of order $\varepsilon^2 \log \varepsilon$ and $\frac{\varepsilon^2 \log \varepsilon}{\omega}$ are neglected, which means that its validity is restricted to wings of not too small aspect ratio, which are oscillating at not too small values of the reduced frequency. For straight wings there exists no term of order ε and the usual two-dimensional aerodynamic forces are obtained. For swept wings a term of order ε exists and the resulting expression for the downwash, which forms an integral equation for the vortex distribution, is given by eq. (4.12).

It is to be noted that this integral equation contains the spanwise coordinate as a parameter Y_0. This same integral equation arises if the wing would have infinite span and the vortex pattern of the section Y_0 would be repeated in all sections. This pattern contains also a vortex component γ_ξ in chordwise direction, which would be absent in the case of a real infinite wing. Hence, the approximation may be said to yield the correct strip theory for a swept wing. The difference with a straight wing is that γ_ξ now contributes to the downwash.

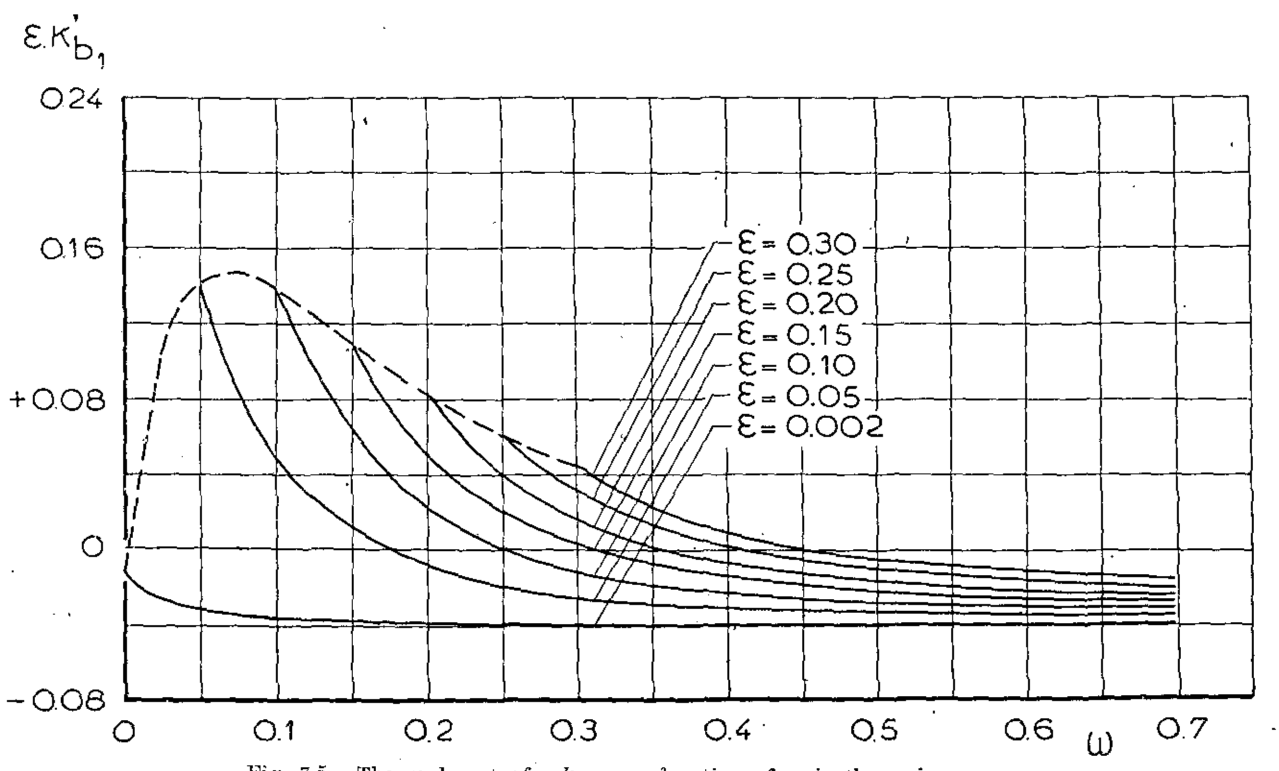

Fig. 7.5. The real part of εk_{b_1} as a function of ω in the region $\omega > \varepsilon$.

8 Recapitulation.

By application of Biot and Savart's law the downwash in an arbitrary point of the wing is expressed in terms of the vortex distribution at the wing and in the wake. The coordinates x and y are transformed by aid of eqs. (3.3) into new coordinates X and Y which at the wing are, in

The integral equation is solved by taking for γ_ξ a known function; viz. the approximation given by eq. (5.2), where $\gamma_y^{(2)}$ is obtained by aid of strip theory for a straight wing. Using either the solution of the integral equation for the two-dimensional steady case or for the unsteady case, the present equation can also be solved. The pressure distribution, as well as the forces and moments then can be calculated.

The final result is given by eq. (6.12). It is seen that the sweep of the wing gives rise to two additional terms of which the first corresponds to the varying amplitude of the degree of freedom considered and the second is due to taper. The effect of the additional terms is maximum for 45° sweep.

Numerical results for the new coefficients k_{g_1} and k_{g_2} are presented in table 1.

Like the orthodox strip theory for a straight wing, the present theory should preferably be used only if the reduced frequency ω is at least equal to ε, which means that the reduced frequency defined by aid of the semi-span $\left(\frac{\nu b}{v}\right)$ should be larger than 1. Otherwise finite span corrections (REISSNER) may become important.

9 List of references.

1. TIMMAN, R. et LEMAIGRE, B., "La ligne portante de forme arbitraire considérée comme cas limite d'une surface portante en fluide incompressible". N. L. L. Report F. 95 (1951).
2. VOOREN, A. I. VAN DE, "The Generalization of Prandtl's Equation for Yawed and Swept Wings". N.L.L. Report F. 121 (1952).
3. VOOREN, A. I. VAN DE, "Generalization of the Theodorsen Function to Stable Oscillations". J. of the Aero. Sc., Vol. 19, p. 209—211, March 1952.
4. WHITTAKER, E. T. and WATSON, G. N., "A Course of Modern Analysis". Cambridge, At the University Press, 1915.
5. REISSNER, E., "Effect of Finite Span on the Airload Distributions for Oscillating Wings". Part I, NACA Report No. 1194, 1947.
6. SCHWARZ, L., "Berechnung der Druckverteilung einer harmonisch sich verformenden Tragfläche in ebener Strömung". Luftfahrtforschung, Vol. 17, p. 379—386, 1940.
7. KÜSSNER, H. G. and SCHWARZ, L., "Der schwingende Flügel mit aerodynamisch ausgeglichenem Ruder". Luftfahrtforschung, Vol. 17, p. 337—354, 1940.
8. HOFSOMMER, D. J., "Systematic Representation of Aerodynamic Coefficients of an Oscillating Aerofoil in Two-dimensional Incompressible Flow". N.L.L. Report F. 61 (1950).
9. MUSKHELISHVILI, N. I., "Singular Integral Equations" (1946). Translated by J. R. M. Radok, Noordhoff, Groningen (1953).

APPENDIX 1.

Alternative method for solving the integral equation.

It is seen that eq. (5.9) is of the same type as eq. (5.6), which is the integral equation for the vortex distribution of an oscillating aerofoil in two-dimensional flow. The corresponding solution for the pressure distribution is in the form, first presented by HOFSOMMER (ref. 8), given by

$$\frac{p^{(2)}(X)}{\rho v} = -\frac{1}{\pi}\left[\frac{1}{l}\left\{T(\omega)\sqrt{\frac{l-X}{l+X}}+\sqrt{\frac{l+X}{l-X}}\right\}\int_{-l}^{l}\sqrt{\frac{l+X_0}{l-X_0}}\,w(X_0)dX_0 + \right.$$
$$\left. + 2\left(i\frac{\nu}{v}+\frac{\partial}{\partial X}\right)\int_{-l}^{l}\Lambda(X,X_0)w(X_0)dX_0\right], \qquad \text{(A 1.1)}$$

where

$$\Lambda(X,X_0) = \tfrac{1}{2}\log\frac{l^2-XX_0+\sqrt{l^2-X^2}\sqrt{l^2-X_0^2}}{l^2-XX_0-\sqrt{l^2-X^2}\sqrt{l^2-X_0^2}}.$$

When replacing $p^{(2)}$ by Δp and w by Δw, the solution corresponding to eq. (5.9) is obtained. According to eq. (5.7) Δw is equal to

$$\Delta w(X_0) = \frac{\sin\varphi}{2\pi}\left\{\oint_{-l}^{l}\frac{\gamma_\xi(X)}{X-X_0}dX + \gamma_\xi(l)\,e^{i\omega}\int_{l}^{\infty}\frac{e^{-i\nu\frac{X}{v}}}{X-X_0}\,dX\right\}. \qquad \text{(A 1.2)}$$

Substituting $\Delta w(X_0)$ into the first term of the right hand side of eq. (A 1.1), the order of integration may be interchanged and by using eqs. (A 2.1) and (A 2.2), the result is

$$\int_{-l}^{l}\sqrt{\frac{l+X_0}{l-X_0}}\,\Delta w(X_0)dX_0 = -\frac{\sin\varphi}{2}\left\{\int_{-l}^{l}\gamma_\xi(X)dX + \gamma_\xi(l)e^{i\omega}\int_{l}^{\infty}\left(1-\sqrt{\frac{\eta+l}{\eta-l}}\right)e^{-i\frac{\nu}{v}\eta}\,d\eta\right\}.$$

Using now eq. (A 2.10), one obtains

$$\int_{-l}^{l}\sqrt{\frac{l+X_0}{l-X_0}}\,\Delta w(X_0)dX_0 = -\frac{\sin\varphi}{2}\left\{\int_{-l}^{l}\gamma_\xi(X)dX - \left[\frac{i}{\omega}l - \frac{\pi l}{2}e^{i\omega}\left\{i\,H_0^{(2)}(\omega) + \right.\right.\right.$$
$$\left.\left.\left. + H_1^{(2)}(\omega)\right\}\right]\gamma_\xi(l)\right\}. \qquad \text{(A 1.3)}$$

For the reduction of the second term of eq. (A 1.1) use will be made of the following relation for $\Lambda(X, X_0)$, see eq. (A 2.1)

$$\Lambda(X, X_0) = \sqrt{\frac{l+X_0}{l-X_0}} \left\{ \oint_{-l}^{X} \sqrt{\frac{l-X}{l+X}} \frac{dX}{X_0 - X} - \frac{\pi}{2} - \sin^{-1} \frac{X}{l} \right\}. \qquad \text{(A 1.4)}$$

Substitution of the first term for $\Lambda(X, X_0)$ and of the first term for $\Delta w(X_0)$ into the second term of (A 1.1) yields

$$\frac{\sin\varphi}{2\pi} \int_{-l}^{l} \sqrt{\frac{l+X_0}{l-X_0}} \left\{ \oint_{-l}^{X} \sqrt{\frac{l-X'}{l+X'}} \frac{dX'}{X_0 - X'} \right\} \left\{ \oint_{-l}^{l} \frac{\gamma_\xi(X'')}{X'' - X_0} dX'' \right\} dX_0 .$$

The order of integration to X'' and X_0 may again be interchanged, thus obtaining

$$\frac{\sin\varphi}{2\pi} \int_{-l}^{l} \gamma_\xi(X'') \left[\oint_{-l}^{l} \sqrt{\frac{l+X_0}{l-X_0}} \cdot \frac{1}{X'' - X_0} \left\{ \oint_{-l}^{X} \sqrt{\frac{l-X'}{l+X'}} \frac{dX'}{X_0 - X'} \right\} dX_0 \right] dX''. \qquad \text{(A 1.5)}$$

Consider now the integrations to X' and X_0. If X would be equal to l, this would mean integration over the square. The dotted lines are the lines where the integrand is singular and where a Cauchy

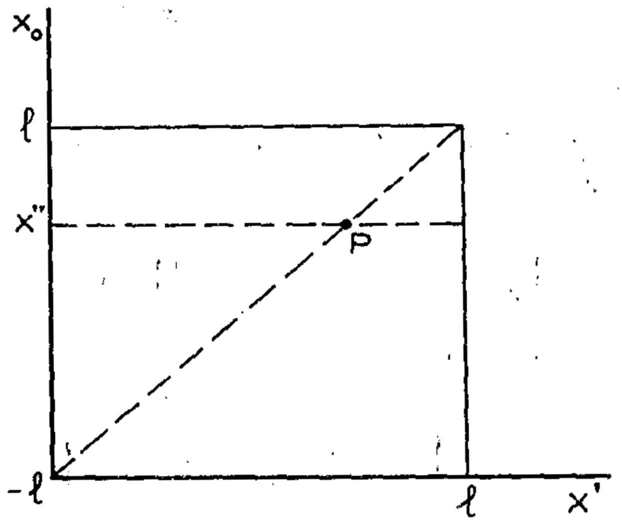

principal value must be taken. It is seen that if the integration to X' is performed first, there are no particular difficulties and the result is according to eqs. (A 2.2) and (A 2.3):

$$\oint_{-l}^{l} \sqrt{\frac{l+X_0}{l-X_0}} \frac{1}{X'' - X_0} \left\{ \int_{-l}^{l} \sqrt{\frac{l-X'}{l+X'}} \frac{dX'}{X_0 - X'} \right\} dX_0 = -\pi^2 .$$

If the upper boundary of the integration to X' is not l, but X, and if X is smaller than X'', the order of integration may be interchanged since the point P is not contained in the region of integration. By partial fraction and use of eq. (A 2.1) it is seen that

$$\oint_{-l}^{l} \sqrt{\frac{l+X_0}{l-X_0}} \frac{dX_0}{(X'' - X_0)(X_0 - X')} = 0.$$

If, however, X is larger than X'', one should write

$$\oint_{-l}^{l} \sqrt{\frac{l+X_0}{l-X_0}} \frac{1}{X'' - X_0} \left\{ \int_{-l}^{l} - \int_{X}^{l} \sqrt{\frac{l-X'}{l+X'}} \frac{dX'}{X_0 - X'} \right\} dX_0 ,$$

and this is equal to $-\pi^2$. Hence (A 1.5) becomes equal to

$$-\frac{\pi}{2} \sin\varphi \int_{-l}^{X} \gamma_\xi(X'') \, dX''.$$

The reduction of the double integral is known as the POINCARÉ-BERTRAND theorem and can be found in ref. 9.

If the second term of $\Delta w(X_0)$ in eq. (A 1.2) is substituted into the second term of eq. (A 1.1), it is seen that X is always smaller than X'' and therefore the change of the order of integration is allowed. The result is

$$\frac{\sin\varphi}{2\pi}\gamma_\xi(l)e^{i\omega}\int_l^\infty e^{-i\frac{\nu}{v}X''}\left[\int_{-l}^{X}\sqrt{\frac{l-X'}{l+X'}}\left\{\oint_{-l}^{l}\sqrt{\frac{l+X_0}{l-X_0}}\frac{dX_0}{(X''-X_0)(X_0-X')}\right\}dX'\right\}dX''=$$

$$=\frac{\sin\varphi}{2}\gamma_\xi(l)e^{i\omega}\int_l^\infty e^{-i\frac{\nu}{v}X''}\sqrt{\frac{X''+l}{X''-l}}\left\{\int_{-l}^{X}\sqrt{\frac{l-X'}{l+X'}}\frac{dX'}{X''-X'}\right\}dX''.$$

Finally, substitution of the remaining terms of eq. (A 1.4) into eq. (A 1.1) yields by application of (A 1.3)

$$\left(\frac{\pi}{2}+\sin^{-1}\frac{X}{l}\right)\frac{\sin\varphi}{2}\left\{\int_{-l}^{l}\gamma_\xi(X)dX-\left[\frac{il}{\omega}-\frac{\pi l}{2}e^{i\omega}\left\{iH_0^{(2)}(\omega)+H_1^{(2)}(\omega)\right\}\right]\gamma_\xi(l)\right\}.$$

Hence, it is obtained that

$$\int_{-l}^{l}\Lambda(X,X_0)w(X_0)dX_0=-\frac{\pi}{2}\sin\varphi\int_{-l}^{X}\gamma_\xi(X'')dX''+$$

$$+\frac{\sin\varphi}{2}\gamma_\xi(l)e^{i\omega}\int_l^\infty e^{-i\frac{\nu}{v}X''}\sqrt{\frac{X''+l}{X''-l}}\left\{\int_{-l}^{X}\sqrt{\frac{l-X'}{l+X'}}\frac{dX'}{X''-X'}\right\}dX''+$$

$$+\left(\frac{\pi}{2}+\sin^{-1}\frac{X}{l}\right)\frac{\sin\varphi}{2}\left\{\int_{-l}^{l}\gamma_\xi(X)dX-\left[\frac{il}{\omega}-\frac{\pi l}{2}e^{i\omega}\left\{iH_0^{(2)}(\omega)+H_1^{(2)}(\omega)\right\}\right]\gamma_\xi(l)\right\}. \quad \text{(A 1.6)}$$

Application of the operator $i\,\frac{\nu}{v}+\frac{\partial}{\partial X}$ to the first term of the right hand side yields

$$-\frac{\pi}{2}\sin\varphi\left\{\gamma_\xi(X)+i\,\frac{\nu}{v}\int_{-l}^{X}\gamma_\xi(X'')dX''\right\},$$

which according to eq. (5.15) is equal to

$$-\frac{\pi\varepsilon}{2\,\rho v}\sin\varphi\cos\varphi\,\frac{\partial}{\partial Y}\int_{-l}^{X}p^{(2)}(X,Y)dX. \quad \text{(A 1.7)}$$

Application of the same operator to the second term yields

$$\frac{\sin\varphi}{2}\gamma_\xi(l)e^{i\omega}\left[\sqrt{\frac{l-X}{l+X}}\int_l^\infty\frac{e^{-i\frac{\nu}{v}X''}}{X''-X}\sqrt{\frac{X''+l}{X''-l}}\,dX''\right.$$

$$\left.+\,i\,\frac{\nu}{v}\int_{-l}^{X}\sqrt{\frac{l-X'}{l+X'}}\left\{\int_l^\infty\frac{e^{-i\frac{\nu}{v}X''}}{X''-X}\sqrt{\frac{X''+l}{X''-l}}\,dX''\right\}dX\right],$$

which is according to eq. (A 2.10) equal to

$$\frac{\sin\varphi}{4}\pi\gamma_\xi(l)e^{i\omega}\left[-i\omega\left\{iH_0^{(2)}(\omega)+H_1^{(2)}(\omega)\right\}\left(\frac{\pi}{2}+\sin^{-1}\frac{X}{l}\right)-iH_0^{(2)}(\omega)\sqrt{\frac{l-X}{l+X}}\right]. \quad \text{(A 1.8)}$$

Finally,

$$\left(i\,\frac{\nu}{v}+\frac{\partial}{\partial X}\right)\left(\frac{\pi}{2}+\sin^{-1}\frac{X}{l}\right)=i\,\frac{\nu}{v}\left(\frac{\pi}{2}+\sin^{-1}\frac{X}{l}\right)+\frac{1}{\sqrt{l^2-X^2}}. \quad \text{(A 1.9)}$$

Using eqs. (A 1.7), (A 1.8) and (A 1.9), one has

$$2\left(i\frac{\nu}{v}+\frac{\partial}{\partial X}\right)\int_{-l}^{l}\Lambda(X,X_0)w(X_0)dX_0=-\frac{\pi\varepsilon}{\rho v}\sin\varphi\cos\varphi\frac{\partial}{\partial Y}\int_{-l}^{X}p^{(2)}(X,Y)dX-$$

$$-\frac{\sin\varphi}{2}\pi\gamma_\xi(l)e^{i\omega}i\,H_0^{(2)}(\omega)\sqrt{\frac{l-X}{l+X}}+\sin\varphi\left(\frac{\pi}{2}+\sin^{-1}\frac{X}{l}\right)\Big\{\gamma_\xi(l)+$$

$$+i\frac{\nu}{v}\int_{-l}^{l}\gamma_\xi(X)dX\Big\}+\frac{\sin\varphi}{\sqrt{l^2-X^2}}\Big\{\int_{-l}^{l}\gamma_\xi(X)dX-\left[\frac{il}{\omega}-\frac{\pi l}{2}e^{i\omega}\left\{i\,H_0^{(2)}(\omega)+H_1^{(2)}(\omega)\right\}\right]\gamma_\xi(l)\Big\}.$$

By application of eqs. (A 1.3) and (5.16), it follows that

$$\frac{\Delta p(X,Y)}{\rho v}=-\frac{i}{2\pi}\frac{\varepsilon}{\rho v}\frac{\sin\varphi\cos\varphi}{\omega}\left\{T(\omega)\sqrt{\frac{l-X}{l+X}}+\sqrt{\frac{l+X}{l-X}}\right\}\frac{\partial K^{(2)}}{\partial Y}-$$

$$-\frac{\varepsilon\sin\varphi\cos\varphi}{\pi\rho v}\left\{\frac{\pi}{2}+\sin^{-1}\frac{X}{l}-i\frac{l}{\omega}\frac{1}{\sqrt{l^2-X^2}}\right\}\frac{\partial K^{(2)}}{\partial Y}+$$

$$+\frac{\varepsilon}{\rho v}\sin\varphi\cos\varphi\frac{\partial}{\partial Y}\int_{-l}^{X}p^{(2)}(X,Y)dX+\frac{\sin\varphi}{4}\left\{T(\omega)\sqrt{\frac{l-X}{l+X}}+\right.$$

$$\left.+\sqrt{\frac{l+X}{l-X}}\right\}e^{i\omega}\left\{i\,H_0^{(2)}(\omega)+H_1^{(2)}(\omega)\right\}\gamma_\xi(l)+\frac{\sin\varphi}{2}\gamma_\xi(l)e^{i\omega}i\,H_0^{(2)}(\omega)\sqrt{\frac{l-X}{l+X}}-$$

$$-\frac{l\sin\varphi}{2\sqrt{l^2-X^2}}e^{i\omega}\left\{i\,H_0^{(2)}(\omega)+H_1^{(2)}(\omega)\right\}\gamma_\xi(l).$$

Since $-\frac{1}{2}\sqrt{\frac{l+X}{l-X}}+\frac{l}{\sqrt{l^2-X^2}}=\frac{1}{2}\sqrt{\frac{l-X}{l+X}}$, this can be written as

$$\frac{\Delta p(X,Y)}{\rho v}=-\frac{i}{2\pi}\frac{\varepsilon\sin\varphi\cos\varphi}{\rho v\omega}\left\{T(\omega)-1\right\}\sqrt{\frac{l-X}{l+X}}\frac{\partial K^{(2)}}{\partial Y}-$$

$$-\frac{\varepsilon\sin\varphi\cos\varphi}{\pi\rho v}\left\{\frac{\pi}{2}+\sin^{-1}\frac{X}{l}\right\}\frac{\partial K^{(2)}}{\partial Y}+\frac{\varepsilon\sin\varphi\cos\varphi}{\rho v}\frac{\partial}{\partial Y}\int_{-l}^{X}p^{(2)}(X,Y)dX+$$

$$+\frac{\sin\varphi}{4}\left\{T(\omega)-1\right\}\sqrt{\frac{l-X}{l+X}}e^{i\omega}\left\{i\,H_0^{(2)}(\omega)+H_1^{(2)}(\omega)\right\}\gamma_\xi(l)+$$

$$+\frac{\sin\varphi}{2}\sqrt{\frac{l-X}{l+X}}e^{i\omega}\,.\,i\,H_0^{(2)}(\omega)\,.\,\gamma_\xi(l).$$

With

$$T(\omega)-1=\frac{-i\,H_0^{(2)}(\omega)+H_1^{(2)}(\omega)}{i\,H_0^{(2)}(\omega)+H_1^{(2)}(\omega)}-1=\frac{-2\,i\,H_0^{(2)}(\omega)}{i\,H_0^{(2)}(\omega)+H_1^{(2)}(\omega)}=2\left\{P(\omega)-1\right\},$$

the final result is

$$\Delta p(X,Y)=-\frac{\varepsilon\sin\varphi\cos\varphi}{\pi}\left\{\frac{\pi}{2}+\sin^{-1}\frac{X}{l}+\frac{1-P(\omega)}{i\omega}\sqrt{\frac{l-X}{l+X}}\right\}\frac{\partial K^{(2)}}{\partial Y}+$$

$$+\varepsilon\sin\varphi\cos\varphi\frac{\partial}{\partial Y}\int_{-l}^{X}p^{(2)}(X,Y)dX,$$

which is identical to eq. (5.17).

APPENDIX 2.

Some integrals.

1°. By putting $\tan\frac{\psi}{2}=Z$, one has

$$\int_0^{\varphi}\frac{d\psi_0}{\cos\psi_0-\cos\psi}=\int_0^{\tan\frac{\varphi}{2}}\frac{dz}{\sin^2\frac{\psi}{2}\,z^2\cos^2\frac{\psi}{2}}=\frac{1}{\sin\psi}\log\left|\frac{z+\tan\frac{\psi}{2}}{z-\tan\frac{\psi}{2}}\right|_0^{\tan\frac{\varphi}{2}}=$$

$$=\frac{1}{\sin\psi}\log\left|\frac{\sin\frac{\psi+\varphi}{2}}{\sin\frac{\psi-\varphi}{2}}\right|=\frac{1}{\sin\psi}\,L(\varphi;\psi).$$

Hence

$$\int_0^{\varphi}\frac{1+\cos\psi_0}{\cos\psi_0-\cos\psi}\,d\psi_0=\int_0^{\varphi}d\psi_0+\int_0^{\varphi}\frac{1+\cos\psi}{\cos\psi_0-\cos\psi}\,d\psi_0=\varphi+\frac{1+\cos\psi}{\sin\psi}\,L(\varphi,\psi).$$

Substituting

$$\cos\varphi=-\frac{X}{l},\quad \cos\psi=-\frac{X_0}{l}$$

$$\int_{-l}^{X}\sqrt{\frac{l-X}{l+X}}\;\frac{dX}{X_0-X}=\frac{\pi}{2}+\sin^{-1}\frac{X}{l}+\sqrt{\frac{l-X_0}{l+X_0}}\,\Lambda(X,X_0),\tag{A 2.1}$$

where $\Lambda\ (X,X_0)$ is given in app. 1.
In particular, for $X=l$

$$\oint_{-l}^{l}\sqrt{\frac{l-X}{l+X}}\;\frac{dX}{X_0-X}=\pi\qquad\text{if}\quad -l<X_0<l,\tag{A 2.2}$$

since Λ vanishes if X or X_0 is either $-l$ or l.
By replacing X by $-X$ and X_0 by $-X_0$ in eq. (A 2.2)

$$\oint_{-l}^{l}\sqrt{\frac{l+X}{l-X}}\;\frac{dX}{X_0-X}=-\pi\qquad\text{if}\quad -l<X_0<l.\tag{A 2.3}$$

2°. By putting $\tan\frac{\psi}{2}=Z$, one has

$$\int_0^{\varphi}\frac{d\psi_0}{a+\cos\psi_0}=\frac{2}{\sqrt{a^2-1}}\tan^{-1}\left\{\sqrt{\frac{a-1}{a+1}}\tan\frac{\varphi}{2}\right\}\ \text{if}\quad a>1.$$

Also

$$\int_0^{\varphi}\frac{1+\cos\psi_0}{a+\cos\psi_0}\,d\psi_0=\int_0^{\varphi}d\psi_0-(a-1)\int_0^{\varphi}\frac{d\psi_0}{a+\cos\psi_0}=\varphi-2\sqrt{\frac{a-1}{a+1}}\tan^{-1}\left\{\sqrt{\frac{a-1}{a+1}}\tan\frac{\varphi}{2}\right\}.$$

Introducing again $\cos\varphi=-\frac{X}{l}$, $a=\frac{\eta}{l}$

$$\int_{-l}^{X}\sqrt{\frac{l-X}{l+X}}\;\frac{dX}{\eta-X}=\frac{\pi}{2}+\sin^{-1}\frac{X}{l}-2\sqrt{\frac{\eta-l}{\eta+l}}\tan^{-1}\left\{\sqrt{\frac{\eta-l}{\eta+l}\cdot\frac{l+X}{l-X}}\right\}.\tag{A 2.4}$$

In particulier if $X = l$

$$\int_{-l}^{l} \sqrt{\frac{l-X}{l+X}} \, \frac{dX}{\eta - X} = \pi \left\{ 1 - \sqrt{\frac{\eta - l}{\eta + l}} \right\} \tag{A 2.5}$$

and by replacing X by $-X$ and η by $-\eta$

$$\int_{-l}^{l} \sqrt{\frac{l+X}{l-X}} \, \frac{dX}{\eta - X} = -\pi \left\{ 1 - \sqrt{\frac{\eta + l}{\eta - l}} \right\}. \tag{A 2.6}$$

3°. By partial fraction and by using eqs. (A 2.3) and (A 2.6)

$$\oint_{-l}^{l} \sqrt{\frac{l+X}{l-X}} \, \frac{dX}{(\eta - X)(X - X_0)} = \frac{1}{\eta - X_0} \oint_{-l}^{l} \sqrt{\frac{l+X}{l-X}} \left\{ \frac{1}{\eta - X} + \frac{1}{X - X_0} \right\} dX =$$

$$\frac{\pi}{\eta - X_0} \sqrt{\frac{\eta + l}{\eta - l}}. \tag{A 2.7}$$

4°. Using HEINE's formula

$$\int_0^\infty e^{-i\omega \operatorname{Cosh} \xi} \operatorname{Cosh} n\xi \, d\xi = \frac{\pi}{2} \, i^{-n-1} H_n^{(2)}(\omega)$$

one finds by substituting $\eta = l \operatorname{Cosh} \xi$

$$\int_l^\infty \frac{e^{-i \frac{\nu}{v} \eta}}{\sqrt{\eta^2 - l^2}} \, d\eta = -\frac{\pi}{2} \, i \, H_0^{(2)}(\omega), \tag{A 2.8}$$

$$\frac{1}{l} \int_l^\infty \frac{\eta \, e^{-i \frac{\nu}{v} \eta}}{\sqrt{\eta^2 - l^2}} \, d\eta = -\frac{\pi}{2} \, H_1^{(2)}(\omega); \tag{A 2.9}$$

Hence

$$\frac{1}{l} \int_l^\infty \sqrt{\frac{\eta + l}{\eta - l}} \, e^{-i \frac{\nu}{v} \eta} \, d\eta = -\frac{\pi}{2} \left\{ i \, H_0^{(2)}(\omega) + H_1^{(2)}(\omega) \right\}. \tag{A 2.10}$$

5°. Let

$$F(X) = -\frac{2}{\pi} \sqrt{\frac{l-X}{l+X}} \int_l^\infty \frac{e^{-i \frac{\nu}{v} \eta}}{\eta - X} \sqrt{\frac{\eta + l}{\eta - l}} \, d\eta. \tag{A 2.11}$$

Then $i \dfrac{\nu}{v} \displaystyle\int_{-l}^{X} F(X) dX$ is, after change of order of integration, equal to

$$-\frac{2 i \nu}{\pi v} \int_l^\infty e^{-i \frac{\nu}{v} \eta} \sqrt{\frac{\eta + l}{\eta - l}} \left\{ \int_{-l}^{X} \sqrt{\frac{l-X}{l+X}} \, \frac{dX}{\eta - X} \right\} d\eta.$$

Using eqs. (A 2.4) and (A 2.10), this becomes

$$-\frac{2 i \nu}{\pi v} \int_l^\infty e^{-i \frac{\nu}{v} \eta} \sqrt{\frac{\eta + l}{\eta - l}} \left\{ \frac{\pi}{2} + \sin^{-1} \frac{X}{l} - 2 \sqrt{\frac{\eta - l}{\eta + l}} \tan^{-1} \sqrt{\frac{\eta - l}{\eta + l} \cdot \frac{l + X}{l - X}} \right\} d\eta =$$

$$= i\omega \left\{ i H_0^{(2)}(\omega) + H_1^{(2)}(\omega) \right\} \left(\frac{\pi}{2} + \sin^{-1} \frac{X}{l} \right) + \frac{4 i \nu}{\pi v} \int_l^\infty e^{-i \frac{\nu}{v}} \tan^{-1} \sqrt{\frac{\eta - l}{\eta + l} \cdot \frac{l + X}{l - X}} \, d\eta.$$

The last term is reduced by partial integration and thus becomes

$$-\frac{4}{\pi}\int_l^\infty \tan^{-1}\sqrt{\frac{\eta-l}{\eta+l}\,\frac{l+X}{l-X}}\,de^{-i\frac{\nu}{v}\eta}$$

$$=\frac{4}{\pi}\int_l^\infty e^{-i\frac{\nu}{v}\eta}\,\frac{1}{1+\frac{\eta-l}{\eta+l}\cdot\frac{l+X}{l-X}}\cdot\frac{1}{\sqrt{\frac{\eta-l}{\eta+l}}}\sqrt{\frac{l+X}{l-X}}\cdot\frac{2l}{(\eta+l)^2}\,d\eta$$

$$=\frac{4l}{\pi}\sqrt{\frac{l+X}{l-X}}\int_l^\infty e^{-i\frac{\nu}{v}\eta}\,\frac{1}{(\eta+l)+(\eta-l)\frac{l+X}{l-X}}\,\frac{d\eta}{\sqrt{\eta^2-l^2}}=$$

$$=\frac{2}{\pi}\sqrt{l^2-X^2}\int_l^\infty\frac{e^{-i\frac{\nu}{v}\eta}}{\eta-X}\,\frac{d\eta}{\sqrt{\eta^2-l^2}}.$$

Since

$$\sqrt{\frac{l^2-X^2}{\eta^2-l^2}}=\frac{l+X}{\eta+l}\sqrt{\frac{l-X}{l+X}\cdot\frac{\eta+l}{\eta-l}}=\left(1-\frac{\eta-X}{\eta+l}\right)\sqrt{\frac{l-X}{l+X}\cdot\frac{\eta+l}{\eta-l}}$$

this may be replaced by

$$-F(X)-\frac{2}{\pi}\sqrt{\frac{l-X}{l+X}}\int_l^\infty\frac{e^{-i\frac{\nu}{v}\eta}}{\sqrt{\eta^2-l^2}}\,d\eta=-F(X)+i\,H_0^{(2)}(\omega)\sqrt{\frac{l-X}{l+X}}.$$

Hence

$$F(X)+i\frac{\nu}{v}\int_{-l}^{X}F(X)dX=+\,i\omega\left\{i\,H_0^{(2)}(\omega)+H_1^{(2)}(\omega)\right\}\left(\frac{\pi}{2}+\sin^{-1}\frac{X}{l}\right)+i\,H_0^{(2)}(\omega)\sqrt{\frac{l-X}{l+X}}, \tag{A 2.12}$$

where $F(X)$ is given by eq. (A 2.11).

APPENDIX 3.

Forces and moments for a swept wing with flap.

In the case of a flap hinging about its leading edge the degree of freedom C = rotation of flap relative to wing should be added and the moment N of the flap about its hinge axis should be calculated also. It will be assumed that the flap chord is a constant fraction of the whole chord.

The new coefficients k_{c_1}, k_{c_2}, m_{c_1} and m_{c_2} are again defined by eqs. (6.11). At the right hand side of these equations one should substitute [1])

$$\begin{aligned}\pi k_c &= -2P\left(\Phi_1+\tfrac{1}{2}i\omega\Phi_2\right)-i\omega\Phi_3+\tfrac{1}{2}\omega^2\Phi_4,\\ \pi m_c &= P\left(\Phi_1+\tfrac{1}{2}i\omega\Phi_2\right)-\Phi_5+\tfrac{1}{2}i\omega\left(\Phi_3-\Phi_6\right)+\omega^2\left(\Phi_7-\Phi_4\right),\\ \pi i_c &= -P\left(\Phi_1+\tfrac{1}{2}i\omega\Phi_2\right)-\Phi_{41}+i\omega\Phi_{42}+\omega^2\Phi_{43}.\end{aligned} \tag{A 3.1}$$

The formula for πi_c has been calculated by aid of the pressure distribution $p_c^{(2)}$ as given in ref. 7.

Analogous to eq. (6.1), the flap moment N is equal to

$$N=(N^{(2)}+\Delta N)\cos\varphi. \tag{A 3.2}$$

If the flap leading edge is at $\overline{X}=\overline{X}_1=-\cos\varphi$, it follows that

$$\Delta N=l^2\int_{\overline{X}_1}^{1}\Delta p\,.\,(\overline{X}-\overline{X}_1)d\overline{X}. \tag{A 3.3}$$

---

[1]) Some of the Φ-functions have been defined and given in numerical form in ref. 7, while the others are defined in eq. (A 3.13).

Substituting formula (5.19) into this expression, the following integrals will be used in the evaluation

$$\int_{\overline{X}_1}^{1}\left(\frac{\pi}{2}+\sin^{-1}\overline{X}\right)(\overline{X}-\overline{X}_1)d\overline{X}=\tfrac{3}{8}\pi-\pi\overline{X}_1+\tfrac{1}{4}\pi\overline{X}_1^2+\left(\frac{\overline{X}_1^2}{2}+\tfrac{1}{4}\right)\sin^{-1}\overline{X}_1+\tfrac{3}{4}\overline{X}_1\sqrt{1-\overline{X}_1^2},$$

$$\int_{\overline{X}_1}^{1}\sqrt{\frac{1-\overline{X}}{1+\overline{X}}}(\overline{X}-\overline{X}_1)d\overline{X}=-\tfrac{1}{4}\pi-\tfrac{1}{2}\pi\overline{X}_1+(\tfrac{1}{2}+\overline{X}_1)\sin^{-1}\overline{X}_1+(1+\tfrac{1}{2}\overline{X}_1)\sqrt{1-\overline{X}_1^2},$$

$$\int_{\overline{X}_1}^{1}(\overline{X}-\overline{X}_1)\left\{\frac{\partial}{\partial\overline{Y}}\,l\int_{-1}^{\overline{X}}p^{(2)}(\overline{X},\overline{Y})d\overline{X}\right\}d\overline{X}-\int_{\overline{X}_1}^{1}l\,(\overline{X}-\overline{X}_1)\overline{X}\,s\,p^{(2)}(\overline{X},\overline{Y})d\overline{X}=$$

$$\frac{d}{d\overline{Y}}\,l\int_{\overline{X}_1}^{1}\left\{\int_{-1}^{\overline{X}}p^{(2)}(\overline{X},\overline{Y})d\overline{X}\right\}d\,(\tfrac{1}{2}\overline{X}^2-\overline{X}\overline{X}_1)-ls\int_{\overline{X}_1}^{1}p^{(2)}(\overline{X},\overline{Y}).(\overline{X}-\overline{X}_1)^2d\overline{X}-$$

$$-ls\overline{X}_1\int_{\overline{X}_1}^{1}p^{(2)}(\overline{X},\overline{Y}).(\overline{X}-\overline{X}_1)d\overline{X}=$$

$$(\tfrac{1}{2}-\overline{X}_1)\frac{dK^{(2)}}{d\overline{Y}}+\tfrac{1}{2}\overline{X}_1^2\left(\frac{dK^{(2)}}{d\overline{Y}}-\frac{dR^{(2)}}{d\overline{Y}}\right)-\tfrac{1}{2}\frac{d}{d\overline{Y}}\frac{J^{(2)}}{l^2}+\tfrac{1}{2}\overline{X}_1^2\frac{dR^{(2)}}{d\overline{Y}}-$$

$$-\frac{s}{l^2}J^{(2)}-\frac{s\overline{X}_1}{l}N^{(2)}=(\tfrac{1}{2}-\overline{X}_1+\tfrac{1}{2}\overline{X}_1^2)\frac{dK^{(2)}}{d\overline{Y}}-\frac{1}{2\,l^2}\frac{dJ^{(2)}}{d\overline{Y}}-\frac{s\overline{X}_1}{l}N^{(2)},$$

where

$$\begin{aligned}R^{(2)}&=l\int_{\overline{X}_1}^{1}p^{(2)}d\overline{X},\\ N^{(2)}&=l^2\int_{\overline{X}_1}^{1}p^{(2)}(\overline{X}-\overline{X}_1)d\overline{X},\\ J^{(2)}&=l^3\int_{\overline{X}_1}^{1}p^{(2)}(\overline{X}-\overline{X}_1)^2d\overline{X}.\end{aligned}\tag{A 3.4}$$

Hence

$$\Delta N=\frac{l\sin\varphi\cos\varphi}{b}\left[\left[\frac{1}{8}+\frac{1}{4}\overline{X}_1^2-\frac{1}{\pi}\left(\frac{1}{4}+\frac{1}{2}\overline{X}_1^2\right)\sin^{-1}\overline{X}_1-\right.\right.$$

$$-\frac{3}{4\pi}\overline{X}_1\sqrt{1-\overline{X}_1^2}+\frac{1-P}{i\omega}\left\{\frac{1}{4}+\frac{1}{2}\overline{X}_1-\frac{1}{\pi}\left(\frac{1}{2}+\overline{X}_1\right)\sin^{-1}\overline{X}_1-\right.$$

$$\left.\left.-\frac{1}{\pi}\left(1+\frac{1}{2}\overline{X}_1\right)\sqrt{1-\overline{X}_1^2}\right\}\right]l\frac{dK^{(2)}}{d\overline{Y}}-\frac{1}{2\,l}\frac{dJ^{(2)}}{d\overline{Y}}-s\overline{X}_1N^{(2)}\bigg].$$

Making use of the first equation (6.8) and of the forms

$$\begin{aligned}N^{(2)}&=\pi\rho\,l^2v^2e^{i\nu t}G\,n_g\\ \frac{dJ^{(2)}}{d\overline{Y}}&=\pi\rho\,l^3v^2e^{i\nu t}\left(3\,s\,G\,j_g+j_g\frac{dG}{d\overline{Y}}+\omega\,s\,G\frac{dj_g}{d\omega}\right)\end{aligned}\tag{A 3.5}$$

and introducing in analogy to eqs. (6.9) and (6.10)

$$\Delta N=\pi\rho\,\frac{l^3}{b}\,v^2e^{i\nu t}\left(n_{g_1}\frac{dG}{d\overline{Y}}+n_{g_2}Gs\right)\sin\varphi\cos\varphi\tag{A 3.6}$$

it follows that

$$n_{g_1}=\left\{f_1(\overline{X}_1)+\frac{1-P}{i\omega}f_2(\overline{X}_1)\right\}k_g-\frac{1}{2}j_g\tag{A 3.7}$$

$$n_{g_2} = \left\{ f_1(\overline{X}_1) + \frac{1-P}{i\omega} f_2(\overline{X}_1) \right\} \left(k_g + \omega \frac{dk_g}{d\omega} \right) - \tfrac{1}{2} \left(3\, j_g + \omega \frac{dj_g}{d\omega} \right) - \overline{X}_1\, n_g ,$$

where

$$f_1(\overline{X}_1) = \frac{1}{2} \left(\frac{1}{2} - \frac{1}{\pi} \sin^{-1} \overline{X}_1 \right) \left(\frac{1}{2} + \overline{X}_1^2 \right) - \frac{3}{4\pi}\, \overline{X}_1 \sqrt{1-\overline{X}_1^2} ,$$

$$f_2(\overline{X}_1) = \left(\frac{1}{2} - \frac{1}{\pi} \sin^{-1} \overline{X}_1 \right) \left(\frac{1}{2} + \overline{X}_1 \right) - \frac{1}{\pi} \left(1 + \frac{1}{2} \overline{X}_1 \right) \sqrt{1-\overline{X}_1^2}. \tag{A 3.8}$$

The coefficients k_a, k_b and k_c have been given in eqs. (6.13) and (A 3.1), while the remaining coefficients are equal to

$$\begin{aligned}
\pi\, n_a &= -P \,.\, i\omega\, \Phi_8 + \tfrac{1}{2}\, \omega^2\, \Phi_4 , \\
\pi\, n_b &= -P\, (1 + \tfrac{1}{2}\, i\omega)\, \Phi_8 - \tfrac{1}{2}\, i\omega\, \Phi_9 - \tfrac{1}{4}\, \omega^2\, (\Phi_4 - \Phi_7), \\
\pi^2\, n_c &= -P\, (\Phi_1 + \tfrac{1}{2}\, i\omega\, \Phi_2)\, \Phi_8 - \Phi_{10} - \tfrac{1}{2}\, i\omega\, \Phi_{11} + \tfrac{1}{4}\, \omega^2\, \Phi_{12} , \\
\pi\, j_a &= \quad P\, i\omega\, \Phi_{44} + \omega^2\, \Phi_{45} , \\
\pi\, j_b &= \quad P\, (1 + \tfrac{1}{2}\, i\omega) \Phi_{44} - i\omega\, (\tfrac{1}{2}\, \Phi_{44} + 2\, \Phi_{45}) + \omega^2\, \Phi_{46} , \\
\pi^2\, j_c &= \quad P\, (\Phi_1 + \tfrac{1}{2}\, i\omega\, \Phi_2)\, \Phi_{44} + \Phi_{47} + i\omega\, \Phi_{48} + \omega^2\, \Phi_{49} .
\end{aligned} \tag{A 3.9}$$

The coefficients k_{c_1}, k_{c_2}, m_{c_1}, m_{c_2}, n_{a_1}, n_{a_2}, n_{b_1}, n_{b_2}, n_{c_1} and n_{c_2} have been computed for a flap chord which is 20 % of the wing chord, i. e. $\overline{X}_1 = 0.6$ and $\tau = 0.2$. Results have been presented in table 2 and in figs. A 3.1 to A 3.5.

Similarly to the concentrated forces acting at the tip section, which have been considered in Sec. 6.2, there exist also concentrated forces at the inner end $\overline{Y}_i$ and the outer end $\overline{Y}_u$ of the flap.

The reactions at $\overline{Y} = \overline{Y}_u$ are given by the following expressions

1° a concentrated aerodynamic force of magnitude

$$-\frac{l \sin\varphi \cos^2\varphi}{b}\, k_{c_1}\, \frac{C(\overline{Y}_u)}{2}\, \pi\, \rho\, l\, v^2\, e^{i\nu t} , \tag{A 3.10}$$

2° a concentrated aerodynamic moment about the wing mid-chord point of magnitude

$$-\frac{l \sin\varphi \cos^2\varphi}{b}\, m_{c_1}\, \frac{C(\overline{Y}_u)}{2}\, \pi\, \rho\, l^2\, v^2\, e^{i\nu t} , \tag{A 3.11}$$

3° a concentrated aerodynamic moment about the flap leading edge of magnitude

$$-\frac{l \sin\varphi \cos^2\varphi}{b}\, n_{c_1}\, \frac{C(\overline{Y}_u)}{2}\, \pi\, \rho\, l^2\, v^2\, e^{i\nu t} . \tag{A 3.12}$$

The reactions at the inward end of the flap $\overline{Y}_i$ are obtained from eqs (A 3.10), (A 3.11) and (A 3.12) by changing the sign and replacing $C(\overline{Y}_u)$ by $C(\overline{Y}_i)$.

If $\overline{Y}_u = 1$, the concentrated moment (A 3.12) should be replaced by

$$-\sum_{g_1} \frac{l \sin\varphi \cos^2\varphi}{b}\, n_{g_1}\, \frac{G(1)}{2}\, \pi\, \rho\, l^2\, v^2\, e^{i\nu t} ,$$

where the summation should be performed over the degrees of freedom A, B and C.

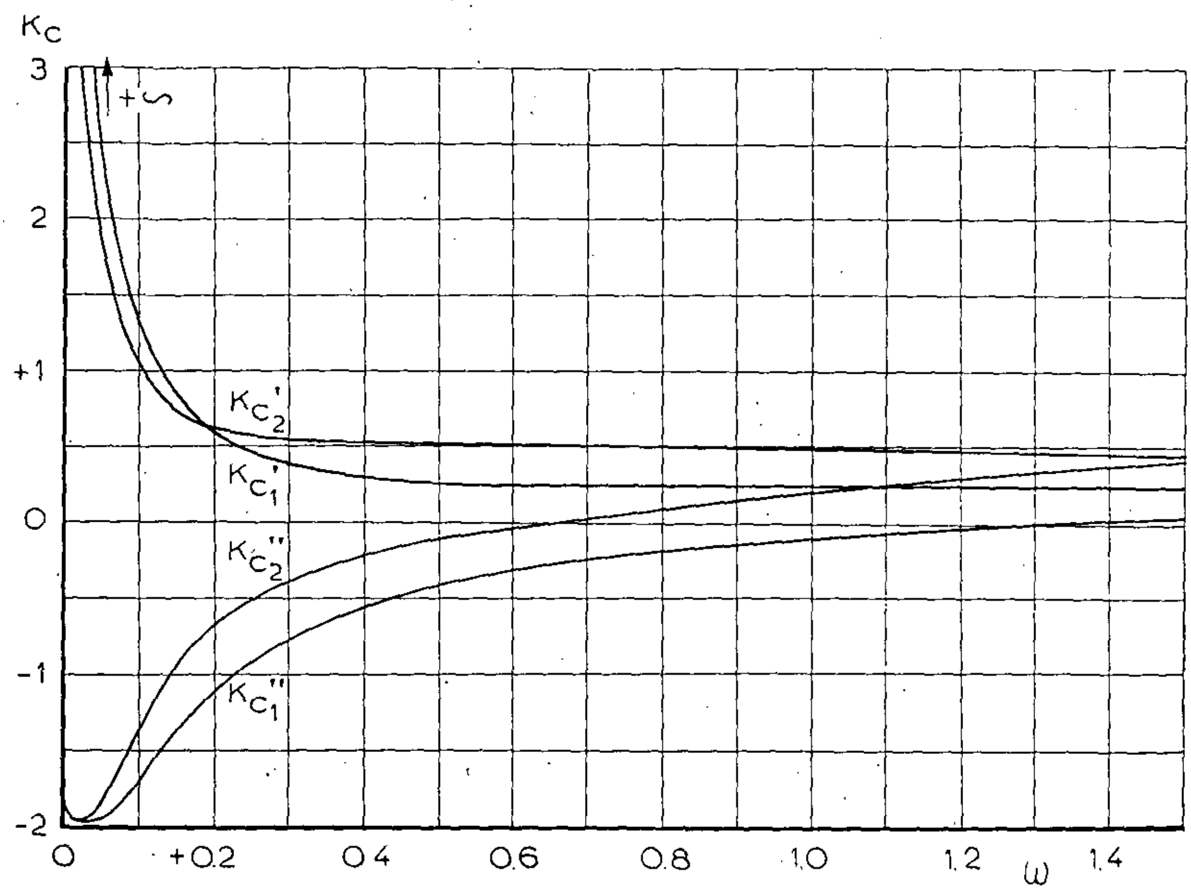

Fig. A 3.1. Coefficient k_c as a function of ω ($k_c = k_c' + i\,k_c''$)

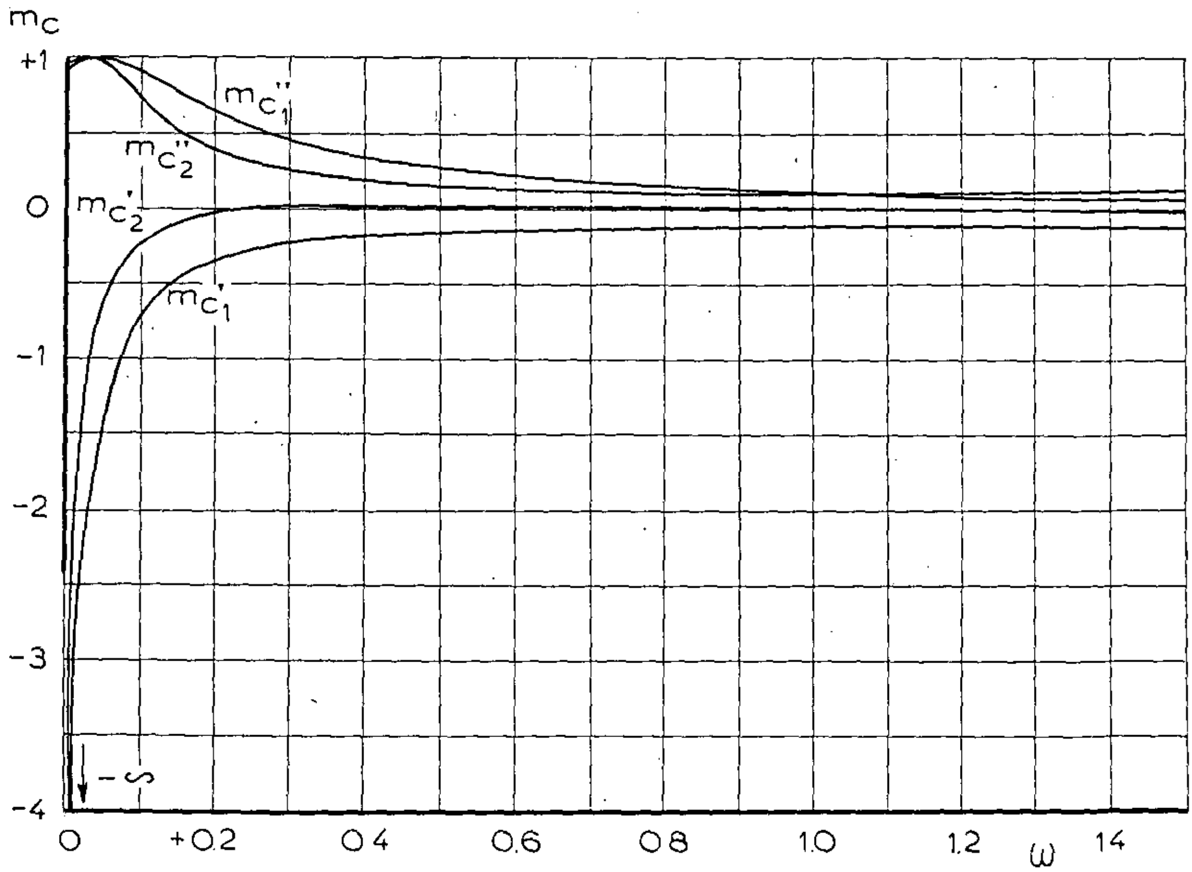

Fig. A. 3.2. Coefficient m_c as a function of ω ($m_c = m_c' + i\,m_c''$).

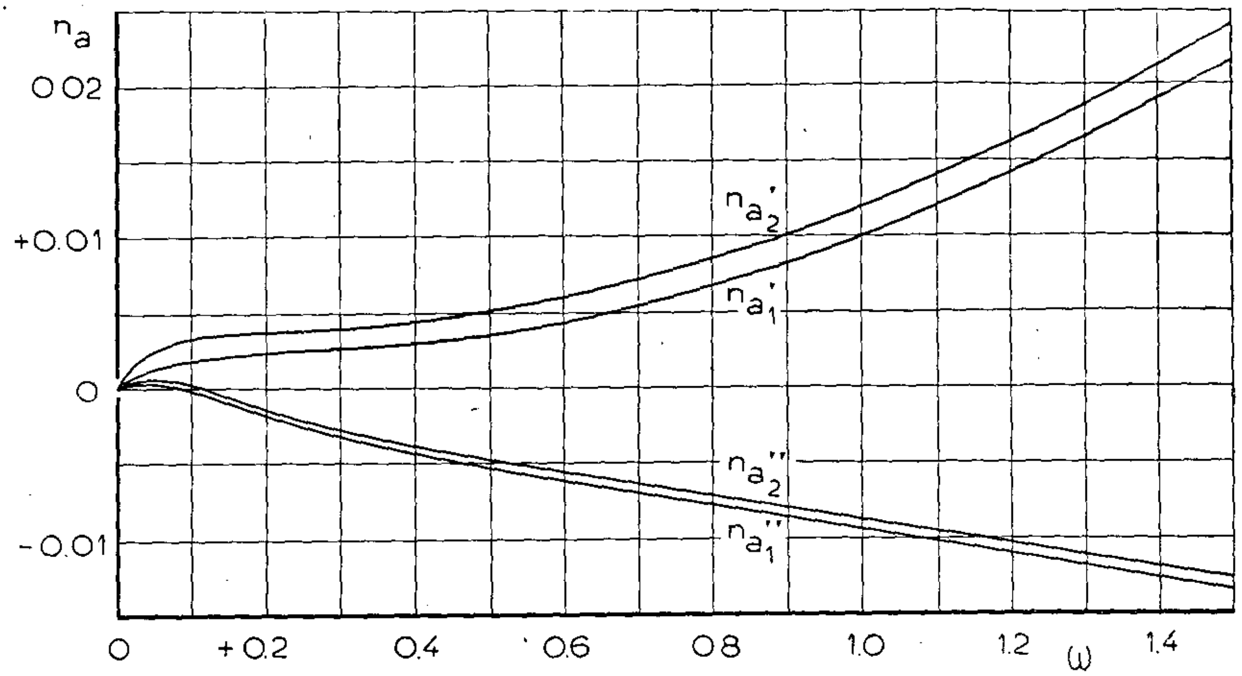

Fig. A. 3.3. Coefficient n_a as a function of ω ($n_a = n_a' + i\,n_a''$).

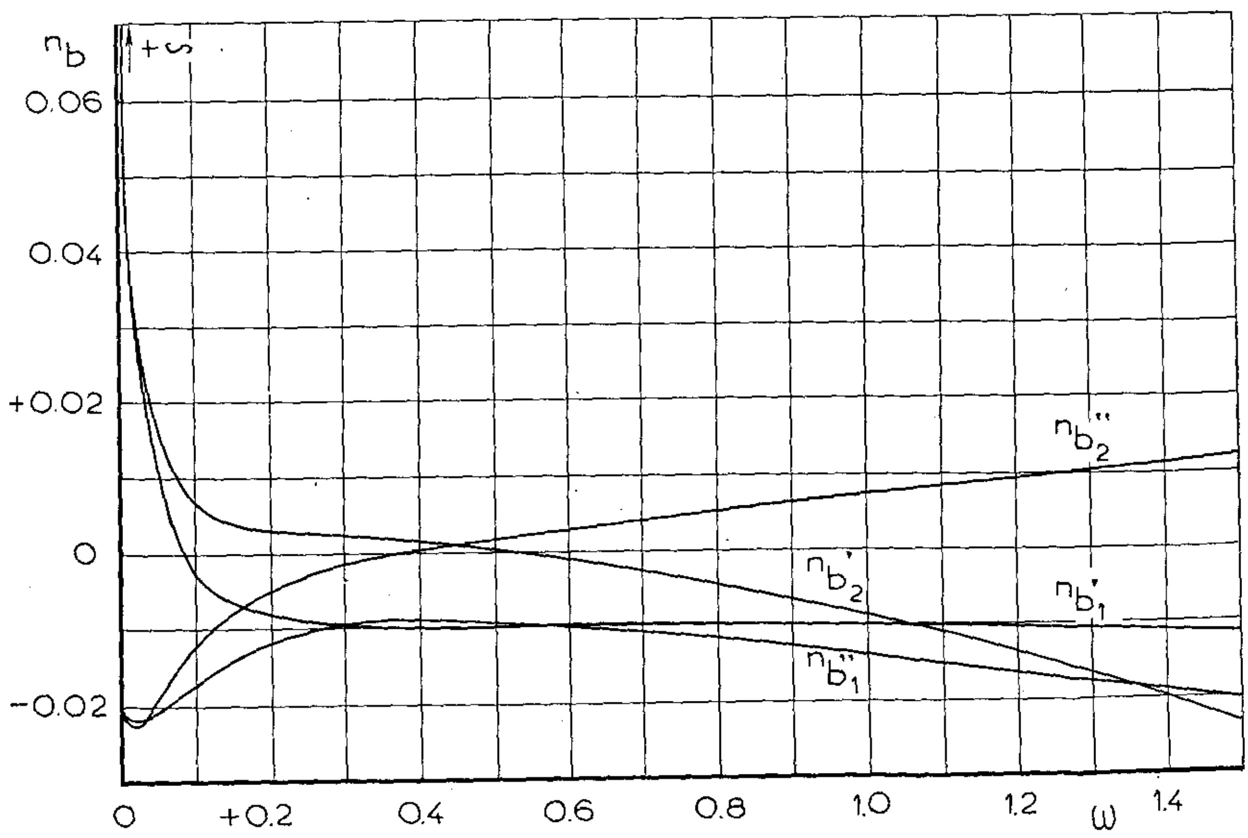

Fig. A. 3.4. Coefficient n_b as a function of ω ($n_b = n_b' + i\,n_b''$).

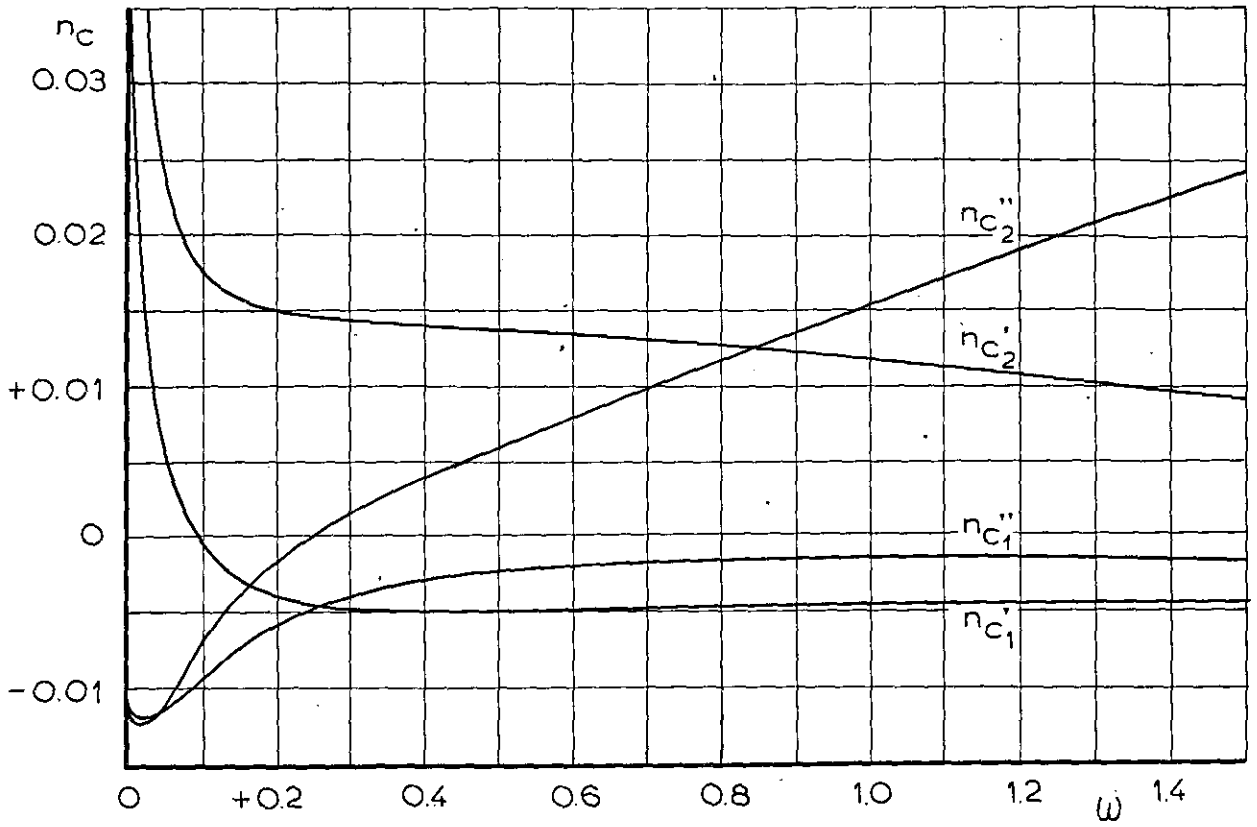

Fig. A. 3.5. Coefficient n_c as a function of ω ($n_c = n_c' + i n_c''$).

Definitions of new Φ-functions.

$$
\begin{aligned}
\Phi_{41}(\varphi) &= \tfrac{2}{3} \sin^3\varphi, \\
\Phi_{42}(\varphi) &= \tfrac{1}{3} \sin^3\varphi \cos\varphi, \\
\Phi_{43}(\varphi) &= \tfrac{1}{4} (\pi - \varphi) \cos\varphi + \tfrac{1}{60} \sin\varphi \, (12 + \cos^2\varphi + 2\cos^4\varphi), \\
\Phi_{44}(\varphi) &= -(\pi - \varphi)\,(1 - 2\cos\varphi + 2\cos^2\varphi) + \tfrac{1}{3} \sin\varphi \,(1 - 2\cos\varphi)\,(4 - \cos\varphi), \\
\Phi_{45}(\varphi) &= (\pi - \varphi)\,(\tfrac{1}{4} + \cos^2\varphi) + \tfrac{1}{12} \sin\varphi \cos\varphi \,(13 + 2\cos^2\varphi), \qquad \text{(A 3.13)} \\
\Phi_{46}(\varphi) &= \tfrac{1}{4} (\pi - \varphi) \cos\varphi + \tfrac{1}{60} \sin\varphi \,(8 + 9\cos^2\varphi - 2\cos^4\varphi), \\
\Phi_{47}(\varphi) &= \tfrac{2}{3} (\pi - \varphi) \sin\varphi \,(1 - \cos\varphi)(1 - 2\cos\varphi) - \tfrac{2}{3} (1 - \cos\varphi)^2 \,(1 + \cos\varphi)(2 - \cos\varphi), \\
\Phi_{48}(\varphi) &= -(\pi - \varphi)^2 \cos\varphi \,(1 + \cos\varphi) - \tfrac{2}{3}(\pi - \varphi) \sin\varphi \,(1 + \cos\varphi)^2 (2 + \cos\varphi) - \tfrac{1}{3} \sin^2\varphi \,(1 + \cos\varphi)(2 + \cos^2\varphi), \\
\Phi_{49}(\varphi) &= \tfrac{1}{2} (\pi - \varphi)^2 \cos\varphi \,(1 + 2\cos^2\varphi) + \tfrac{1}{3} (\pi - \varphi) \sin\varphi \,(1 + 7\cos^2\varphi + \cos^4\varphi) + \tfrac{1}{2} \sin^2\varphi \cos\varphi \,(2 + \cos^2\varphi).
\end{aligned}
$$

TABLE 1.

Aerodynamic coefficients for swept wing.

ω	k'_{a_1}	k''_{a_1}	k'_{b_1}	k''_{b_1}	k'_{a_2}	k''_{a_2}	k'_{b_2}	k''_{b_2}	m'_{a_1}	m''_{a_1}	m'_{b_1}	m''_{b_1}	m'_{a_2}	m''_{a_2}	m'_{b_2}	m''_{b_2}
0	0	0	+ ∞	— 3.14159	0	0	+ ∞	— 3.14159	0	0	— ∞	+ 1.57080	0	0	— ∞	+ 1.57080
0.1	+ 0.30456	+ 0.16238	+ 1.78345	— 2.92289	+ 0.54101	+ 0.20920	+ 0.75963	— 2.13512	— 0.15965	— 0.12279	— 1.31262	+ 1.52680	— 0.28027	— 0.13944	— 0.32030	+ 1.09914
0.2	+ 0.39212	+ 0.08067	+ 0.61330	— 1.84752	+ 0.62162	+ 0.04508	+ 0.16941	— 0.90663	— 0.20992	— 0.11310	— 0.68237	+ 0.98169	— 0.32415	— 0.07947	— 0.02471	+ 0.47226
0.3	+ 0.40228	+ 0.01934	+ 0.28128	— 1.23154	+ 0.59591	— 0.04225	+ 0.12834	— 0.36731	— 0.21679	— 0.10942	— 0.49220	+ 0.65555	— 0.30763	— 0.05652	— 0.02346	+ 0.19992
0.4	+ 0.39121	— 0.01750	+ 0.16484	— 0.86179	+ 0.55734	— 0.08186	+ 0.13679	— 0.08125	— 0.20860	— 0.11624	— 0.42141	+ 0.45089	— 0.27992	— 0.05815	— 0.05421	+ 0.06172
0.5	+ 0.37553	— 0.03889	+ 0.11640	— 0.62103	+ 0.52355	— 0.09839	+ 0.13082	+ 0.10321	— 0.19419	— 0.13004	— 0.39163	+ 0.31112	— 0.25110	— 0.07219	— 0.08199	— 0.02151
0.6	+ 0.36020	— 0.05113	+ 0.09122	— 0.45227	+ 0.49663	— 0.10385	+ 0.10445	+ 0.24163	— 0.17644	— 0.14807	— 0.37818	+ 0.20820	— 0.22280	— 0.09248	— 0.10325	— 0.07944
0.7	+ 0.34658	— 0.05791	+ 0.07355	— 0.32641	+ 0.47560	— 0.10391	+ 0.05986	+ 0.35675	— 0.15629	— 0.16871	— 0.37191	+ 0.12758	— 0.19479	— 0.11603	— 0.11915	— 0.12453
0.8	+ 0.33487	— 0.06140	+ 0.05728	— 0.22764	+ 0.45913	— 0.10136	— 0.00055	+ 0.45900	— 0.13404	— 0.19096	— 0.36902	+ 0.06124	— 0.16656	— 0.14129	— 0.13110	— 0.16250
0.9	+ 0.32491	— 0.06285	+ 0.03989	— 0.14677	+ 0.44611	— 0.09759	— 0.07491	+ 0.55356	— 0.10974	— 0.21424	— 0.36780	+ 0.00447	— 0.13761	— 0.16745	— 0.14024	— 0.19628
1.0	+ 0.31645	— 0.06305	+ 0.02031	— 0.07826	+ 0.43571	— 0.09327	— 0.16196	+ 0.64326	— 0.08336	— 0.23819	— 0.36744	— 0.04559	— 0.10751	— 0.19411	— 0.14737	— 0.22748
1.2	+ 0.30308	— 0.06138	— 0.02698	+ 0.03470	+ 0.42045	— 0.08462	— 0.37124	+ 0.81385	— 0.02417	— 0.28728	— 0.36780	— 0.13248	— 0.04287	— 0.24789	— 0.15756	— 0.28535
1.5	+ 0.28924	— 0.05685	— 0.11935	+ 0.16949	+ 0.40607	— 0.07299	— 0.76717	+ 1.05792	+ 0.08145	— 0.36233	— 0.36904	— 0.24334	+ 0.06800	— 0.32856	— 0.16688	— 0.36646

TABLE 2.

Additional aerodynamic coefficients for flap of swept wing ($\tau = 0.2$).

ω	k'_{c_1}	k''_{c_2}	k'_{c_1}	k''_{c_2}	m'_{c_1}	m''_{c_1}	m'_{c_2}	m''_{c_2}	n'_{a_1}	n''_{a_1}	n'_{b_1}	n''_{b_1}	n'_{c_1}	n''_{c_1}	n'_{a_2}	n''_{a_2}	n'_{b_2}	n''_{b_2}	n'_{c_2}	n''_{c_2}
0	+ ∞	— 1.72731	+ ∞	— 1.72731	— ∞	0.86365	— ∞	+ 0.86365	0	0	+ ∞	— 0.01997	+ ∞	— 0.01098	0	0	+ ∞	— 0.01997	+ ∞	— 0.01098
0.1	1.27912	— 1.70475	1.02194	— 1.36171	— 0.72019	0.90062	— 0.23127	0.71524	0.00174	— 0.00037	— 0.00284	— 0.01747	— 0.00049	— 0.00948	+ 0.00316	+ 0.00015	+ 0.00684	— 0.01251	+ 0.01758	— 0.00679
0.2	0.58090	— 1.11370	0.60014	— 0.69049	— 0.34403	0.61201	— 0.01581	0.38811	0.00224	— 0.00194	— 0.00870	— 0.01197	— 0.00401	— 0.00577	+ 0.00372	— 0.00163	0.00310	— 0.00513	0.01563	— 0.00153
0.3	0.37211	— 0.76613	0.53440	— 0.38327	— 0.22380	0.43871	+ 0.01240	0.2483	0.00252	— 0.00324	— 0.00991	— 0.00975	— 0.00479	— 0.00381	+ 0.00395	— 0.00289	0.00219	— 0.00179	0.01441	+ 0.00160
0.4	0.29550	— 0.55446	0.52240	— 0.21564	— 0.17566	0.33224	0.01172	0.18244	0.00292	— 0.00433	— 0.01011	— 0.00915	— 0.00494	— 0.00276	+ 0.00437	— 0.00386	0.00135	+ 0.00019	0.01406	0.00398
0.5	0.26375	— 0.41545	0.51842	— 0.10615	— 0.15338	0.26223	0.00683	0.14809	0.00353	— 0.00529	— 0.01007	— 0.00936	— 0.00490	— 0.00217	+ 0.00505	— 0.00472	+ 0.00027	0.00167	0.01372	0.00607
0.6	0.24945	— 0.31764	0.51444	— 0.02419	— 0.14191	0.21325	+ 0.00210	0.12884	0.00437	— 0.00618	— 0.01001	— 0.01000	— 0.00483	— 0.00182	+ 0.00597	— 0.00553	— 0.00106	0.00293	0.01338	0.00804
0.7	0.24254	— 0.24470	0.50923	+ 0.04315	— 0.13551	0.17714	— 0.00185	0.11765	0.00544	— 0.00704	— 0.00998	— 0.01088	— 0.00475	— 0.00162	+ 0.00714	— 0.00633	— 0.00263	0.00408	0.01302	0.00993
0.8	0.23891	— 0.18765	0.50279	0.10191	— 0.13168	0.14938	— 0.00511	0.11115	0.00673	— 0.00787	— 0.01000	— 0.01191	— 0.00468	— 0.00150	+ 0.00852	— 0.00712	— 0.00444	0.00518	0.01264	0.01178
0.9	0.23673	— 0.14122	0.49530	0.15525	— 0.12923	0.12728	— 0.00788	0.10759	0.00824	— 0.00869	— 0.01007	— 0.01304	— 0.00461	— 0.00144	+ 0.01012	— 0.00792	— 0.00647	0.00623	0.01223	0.01361
1.0	0.23512	— 0.10219	0.48692	0.20494	— 0.12758	0.10917	— 0.01033	0.10597	0.00997	— 0.00950	— 0.01018	— 0.01422	— 0.00456	— 0.00142	+ 0.01192	— 0.00871	— 0.00873	0.00726	0.01180	0.01542
1.2	0.23219	— 0.03873	0.46780	0.29721	— 0.12549	0.08093	— 0.01472	0.10642	0.01405	— 0.01112	— 0.01053	— 0.01670	— 0.00448	— 0.00144	+ 0.01614	— 0.01033	— 0.01394	0.00927	0.01085	0.01899
1.5	0.22660	+ 0.03513	0.43377	0.42512	— 0.12358	0.05047	— 0.02096	0.11230	0.02169	— 0.01354	— 0.01131	— 0.02057	— 0.00439	— 0.00157	+ 0.02395	— 0.01278	— 0.02345	0.01221	0.00918	0.02429

$$
\boxed{
\begin{aligned}
k_g &= k'_g + i\,k''_g \\
m_g &= m'_g + i\,m''_g \\
n_g &= n'_g + i\,n''_g
\end{aligned}
}
$$

C.C.L. Class. D 410

REPORT F. 155.

Tables of the Aerodynamic Aileron-Coefficients for an Oscillating Wing-Aileron System in a Subsonic, Compressible Flow

by

E. M. DE JAGER.

Summary.

This report presents numerical results for the aerodynamic aileron coefficients of an oscillating wing-aileron system, where the aileron hinge axis coincides with the nose of the aileron.

The complete set of the 5 complex coefficients is given for the Mach-numbers 0; 0.35; 0.50; 0.60; 0.70; 0.80; the reduced frequency being equal to 0 (0.1) 1.0 and the chord ratio equal to 0 (0.02) 0.1 (0.05) 0.3.

Contents.

This investigation has been sponsored by the Netherlands Aircraft Development Board (N.I.V.).

1 Introduction.

The purpose of this report is to furnish numerical data for the aileron coefficients k_c, m_c, n_a, n_b and n_c for various values of the ratio τ of aileron to total chord at 5 assigned values of the Mach-number and 10 values of the reduced frequency ω (for the definitions, see Sec. 2).

In NLL-report F. 151 numerical data have been presented for the aerodynamic coefficients including data for the aileron coefficients with $\tau = 0.1$; 0.2 and 0.3. These data were obtained by aid of the theoretical work of TIMMAN and VAN DE VOOREN and the numerical computations, performed at the Mathematical Centre and the N.L.L.

The results for $\tau = 0.1$; 0.2 and 0.3 with $\beta = 0$; 0.35; 0.50; 0.60; 0.70; 0.80 and $\omega = 0.(0.1).1.0$ have been used as a basic set for the interpolation toward τ; $\tau = 0.02.(0.02).0.1$ and $\tau = 0.15$; 0.25. Using the formulae of the NLL-report F. 54, k_c, m_c, n_a, n_b and n_c have been expanded for small values of τ. The results are:

$$k_c = \tau^{1/2}(a_0 + a_1\tau + a_2\tau^2 + \ldots)$$
$$m_c = \tau^{1/2}(b_0 + b_1\tau + b_2\tau^2 + \ldots)$$
$$n_a = \tau^{2\frac{1}{2}}(c_0 + c_1\tau + c_2\tau^2 + \ldots)$$
$$n_b = \tau^{2\frac{1}{2}}(d_0 + d_1\tau + d_2\tau^2 + \ldots)$$
$$n_c = \tau^2(e_0 + e_1\tau + e_2\tau^2 + \ldots),$$

where the coefficients a_0, a_1, b_0 etc. are rather complicated functions of β and ω. Only the coefficient e_0 is given by a fairly simple expression viz.

$$e_0 = -\frac{1}{3\pi^2\sqrt{1-\beta^2}}.$$

These expansions justify the interpolation of $\frac{k_c}{\tau^{1/2}}$, $\frac{m_c}{\tau^{1/2}}$, $\frac{n_a}{\tau^{2\frac{1}{2}}}$, $\frac{n_b}{\tau^{2\frac{1}{2}}}$ and $\frac{n_c}{\tau^2}$ by means of the method of the central differences. Because the derivatives are available for three values of τ, the second difference in the interpolation procedure must be kept constant.

This interpolation procedure has been carried out as a check for $\beta = 0$ and $\omega = 0.1$; 0.7 and the results appeared to be in excellent agreement (see table 1) with the exact values, calculated by means of the formulae given by KÜSSNER and SCHWARZ (see "Luftfahrtforschung" 1940 Vol. 17). Hence it seems certainly justified to use the above-mentioned interpolation procedure also for $\beta > 0$.

The numerical computations have been performed at the N.L.L. under the direction of Mr J. G. WOUTERS.

2 List of Symbols.

$K = \pi\rho_0 l v^2 e^{i\nu t}\ (A\,k_a + B\,k_b + C\,k_c)$

$M = \pi\rho_0 l^2 v^2 e^{i\nu t}\ (A\,m_a + B\,m_b + C\,m_c)$

$N = \pi\rho_0 l^2 v^2 e^{i\nu t}\ (A\,n_a + B\,n_b + C\,n_c)$

K = aerodynamic force of wing + aileron; positive downward

M = aerodynamic moment of wing + aileron about mid-chord point, positive tailheavy

N = aerodynamic moment of aileron about hinge axis (= nose), positive tailheavy

ρ_0 = air density (in undisturbed state)

l = semi-chord
v = speed of flight
β = Mach-number, $\frac{v}{c}$
ν = frequency of vibration
ω = reduced frequency, $\frac{\nu l}{v}$
τ = ratio between aileron chord and total chord
Al = amplitude of translation in midchord point, positive downward
B = amplitude of wing rotation, positive if trailing edge is downward
C = amplitude of aileron rotation, positive if trailing edge is downward
k_c' = real part of k_c
k_c'' = imaginary part of k_c etc.

Completed July 1954.

TABLE 1. Comparison between exact and interpolated values.

	τ	k_c'	k_c''	m_c'	m_c''	n_a'	n_a''	n_b'	n_b''	n_c'	n_c''
$\beta = 0,\ \omega = 0.1$ exact	0.02	-0.2988	0.0606	-0.0253	-0.0312	0	0	-0.00003	-0.00001	-0.00022	0
	0.04	-0.4213	0.0836	-0.0289	-0.0444	0	-0.00002	-0.00018	-0.00005	-0.00087	-0.00001
	0.06	-0.5145	0.0998	-0.0270	-0.0546	0	-0.00005	-0.00051	-0.00013	-0.00196	-0.00003
	0.08	-0.5924	0.1123	-0.0216	-0.0633	0	-0.00010	-0.00104	-0.00026	-0.00350	-0.00007
	0.15	-0.8027	0.1400	$+0.0150$	-0.0871	0.00001	-0.00051	-0.00510	-0.00118	-0.01245	-0.00046
	0.25	-1.0200	0.1559	0.0969	-0.1113	0.00001	-0.00187	-0.01875	-0.00395	-0.03527	-0.00207
interpolated	0.02	-0.2988	0.0606	-0.0253	-0.0313	0	0	-0.00003	-0.00001	-0.00022	0
	0.04	-0.4213	0.0836	-0.0288	-0.0445	0	-0.00002	-0.00018	-0.00005	-0.00087	-0.00001
	0.06	-0.5145	0.0999	-0.0269	-0.0547	0	-0.00005	-0.00051	-0.00013	-0.00196	-0.00003
	0.08	-0.5924	0.1124	-0.0215	-0.0634	0	-0.00010	-0.00104	-0.00026	-0.00350	-0.00007
	0.15	-0.8027	0.1400	$+0.0150$	-0.0871	0	-0.00051	-0.00510	-0.00119	-0.01244	-0.00046
	0.25	-1.0200	0.1559	0.0968	-0.1113	0.00002	-0.00188	-0.01874	-0.00395	-0.03528	-0.00206
$\beta = 0,\ \omega = 0.7$ exact	0.02	-0.2035	0.0383	-0.0729	-0.0257	0.00003	-0.00002	0	-0.00010	-0.00021	-0.00002
	0.04	-0.2879	0.0439	-0.0954	-0.0403	0.00019	-0.00009	-0.00003	-0.00054	-0.00085	-0.00012
	0.06	-0.3525	0.0413	-0.1074	-0.0537	0.00053	-0.00024	-0.00010	-0.00149	-0.00190	-0.00041
	0.08	-0.4068	$+0.0335$	-0.1132	-0.0667	0.00107	-0.00049	-0.00021	-0.00303	-0.00336	-0.00096
	0.15	-0.5543	-0.0211	-0.1040	-0.1094	0.00507	-0.00242	-0.00128	-0.01432	-0.01136	-0.00626
	0.25	-0.7048	-0.1463	-0.0435	-0.1602	0.01765	-0.00889	-0.00595	-0.04984	-0.02935	-0.02840
interpolated	0.02	-0.2035	0.0383	-0.0732	-0.0261	0.00003	-0.00002	-0.00001	-0.00010	-0.00021	-0.00001
	0.04	-0.2879	0.0439	-0.0956	-0.0406	0.00019	-0.00009	-0.00003	-0.00054	-0.00085	-0.00012
	0.06	-0.3525	0.0413	-0.1076	-0.0540	0.00052	-0.00024	-0.00010	-0.00149	-0.00190	-0.00041
	0.08	-0.4068	$+0.0335$	-0.1133	-0.0668	0.00107	-0.00050	-0.00021	-0.00303	-0.00335	-0.00096
	0.15	-0.5543	-0.0212	-0.1040	-0.1093	0.00506	-0.00242	-0.00129	-0.01432	-0.01136	-0.00626
	0.25	-0.7049	-0.1464	-0.0436	-0.1603	0.01765	-0.00889	-0.00594	-0.04985	-0.02936	-0.02841

TABLE 2. Coefficients for $\tau = 0.02$.

	ω	k_c'	k_c''	m_c'	m_c''	n_a'	n_a''	n_b'	n_b''	n_c'	n_c''
$\beta = 0$	0	− 0.3589	0	+ 0.0046	0	0	0	− 0.00004	0	− 0.00022	0
	0.1	− 0.2988	0.0606	− 0.0253	− 0.0313	0	0	− 0.00003	− 0.00001	− 0.00022	0
	0.2	− 0.2615	0.0654	− 0.0440	− 0.0347	0	− 0.00001	− 0.00003	− 0.00002	− 0.00022	0
	0.3	− 0.2393	0.0610	− 0.0551	− 0.0334	0	− 0.00001	− 0.00002	− 0.00004	− 0.00022	− 0.00001
	0.4	− 0.2249	0.0549	− 0.0624	− 0.0313	0.00001	− 0.00001	− 0.00002	− 0.00005	− 0.00022	− 0.00001
	0.5	− 0.2154	0.0489	− 0.0672	− 0.0293	0.00002	− 0.00001	− 0.00002	− 0.00007	− 0.00021	− 0.00001
	0.6	− 0.2086	0.0434	− 0.0706	− 0.0275	0.00002	− 0.00001	− 0.00001	− 0.00008	− 0.00021	− 0.00001
	0.7	− 0.2035	0.0383	− 0.0732	− 0.0261	0.00003	− 0.00002	− 0.00001	− 0.00010	− 0.00021	− 0.00001
	0.8	− 0.1999	0.0339	− 0.0752	− 0.0247	0.00005	− 0.00002	0	− 0.00011	− 0.00021	− 0.00002
	0.9	− 0.1970	0.0297	− 0.0766	− 0.0237	0.00006	− 0.00002	+ 0.00001	− 0.00013	− 0.00021	− 0.00002
	1.0	− 0.1947	0.0261	− 0.0778	− 0.0229	0.00007	− 0.00002	0.00001	− 0.00014	− 0.00022	− 0.00002
$\beta = 0.35$	0	− 0.3831	0	+ 0.0051	0	0	0	− 0.00004	0	− 0.00023	0
	0.1	− 0.3089	0.0750	− 0.0324	− 0.0383	0	0	− 0.00003	− 0.00001	− 0.00023	0
	0.2	− 0.2652	0.0814	− 0.0552	− 0.0416	0	− 0.00001	− 0.00003	− 0.00002	− 0.00023	0
	0.3	− 0.2404	0.0785	− 0.0686	− 0.0400	0.00001	− 0.00001	− 0.00002	− 0.00004	− 0.00023	− 0.00001
	0.4	− 0.2251	0.0742	− 0.0773	− 0.0375	0.00001	− 0.00001	− 0.00002	− 0.00006	− 0.00023	− 0.00001
	0.5	− 0.2151	0.0705	− 0.0833	− 0.0351	0.00002	− 0.00001	− 0.00002	− 0.00007	− 0.00023	− 0.00001
	0.6	− 0.2081	0.0676	− 0.0878	− 0.0332	0.00003	− 0.00001	− 0.00001	− 0.00009	− 0.00023	− 0.00001
	0.7	− 0.2033	0.0657	− 0.0913	− 0.0314	0.00004	− 0.00002	− 0.00001	− 0.00011	− 0.00023	− 0.00002
	0.8	− 0.1997	0.0646	− 0.0944	− 0.0298	0.00005	− 0.00002	0	− 0.00012	− 0.00023	− 0.00002
	0.9	− 0.1969	0.0644	− 0.0970	− 0.0285	0.00006	− 0.00002	0	− 0.00014	− 0.00023	− 0.00002
	1.0	− 0.1951	0.0646	− 0.0993	− 0.0274	0.00008	− 0.00003	+ 0.00001	− 0.00016	− 0.00023	− 0.00002
$\beta = 0.50$	0	− 0.4145	0	+ 0.0055	0	0	0	− 0.00004	0	− 0.00025	0
	0.1	− 0.3209	0.0929	− 0.0427	− 0.0467	0	0	− 0.00004	− 0.00001	− 0.00025	0
	0.2	− 0.2679	0.1002	− 0.0712	− 0.0486	0	− 0.00001	− 0.00003	− 0.00003	− 0.00025	0
	0.3	− 0.2394	0.0983	− 0.0873	− 0.0454	0.00001	− 0.00001	− 0.00003	− 0.00004	− 0.00025	− 0.00001
	0.4	− 0.2218	0.0958	− 0.0980	− 0.0409	0.00001	− 0.00001	− 0.00002	− 0.00006	− 0.00025	− 0.00001
	0.5	− 0.2097	0.0944	− 0.1060	− 0.0371	0.00002	− 0.00001	− 0.00002	− 0.00008	− 0.00025	− 0.00001
	0.6	− 0.2007	0.0946	− 0.1124	− 0.0333	0.00003	− 0.00002	− 0.00001	− 0.00010	− 0.00025	− 0.00001
	0.7	− 0.1933	0.0960	− 0.1176	− 0.0295	0.00004	− 0.00002	− 0.00001	− 0.00012	− 0.00025	− 0.00002
	0.8	− 0.1871	0.0984	− 0.1224	− 0.0255	0.00006	− 0.00002	0	− 0.00014	− 0.00025	− 0.00002
	0.9	− 0.1802	0.1016	− 0.1267	− 0.0215	0.00007	− 0.00003	0	− 0.00015	− 0.00025	− 0.00002
	1.0	− 0.1732	0.1055	− 0.1308	− 0.0175	0.00009	− 0.00003	0	− 0.00017	− 0.00025	− 0.00003

TABLE 2 (*continued*).

	ω	k_c'	k_c''	m_c'	m_c''	n_a'	n_a''	n_b'	n_b''	n_c'	n_c''
$\beta = 0.60$	0	— 0.4487	0	+ 0.0059	0	0	0	— 0.00005	0	— 0.00027	0
	0.1	— 0.3296	0.1116	— 0.0563	— 0.0547	0	0	— 0.00004	— 0.00001	— 0.00027	0
	0.2	— 0.2684	0.1194	— 0.0904	— 0.0543	0	— 0.00001	— 0.00003	— 0.00003	— 0.00027	0
	0.3	— 0.2351	0.1178	— 0.1097	— 0.0479	0.00001	— 0.00001	— 0.00003	— 0.00005	— 0.00027	— 0.00001
	0.4	— 0.2138	0.1168	— 0.1230	— 0.0401	0.00001	— 0.00001	— 0.00002	— 0.00007	— 0.00027	— 0.00001
	0.5	— 0.1978	0.1173	— 0.1328	— 0.0322	0.00002	— 0.00002	— 0.00002	— 0.00009	— 0.00027	— 0.00001
	0.6	— 0.1844	0.1193	— 0.1404	— 0.0239	0.00003	— 0.00002	— 0.00002	— 0.00011	— 0.00027	— 0.00002
	0.7	— 0.1711	0.1221	— 0.1466	— 0.0150	0.00005	— 0.00002	— 0.00001	— 0.00013	— 0.00027	— 0.00002
	0.8	— 0.1584	0.1247	— 0.1511	— 0.0054	0.00006	— 0.00003	— 0.00001	— 0.00015	— 0.00027	— 0.00003
	0.9	— 0.1450	0.1266	— 0.1541	+ 0.0048	0.00008	— 0.00004	— 0.00001	— 0.00017	— 0.00027	— 0.00003
	1.0	— 0.1294	0.1274	— 0.1553	0.0156	0.00010	— 0.00004	— 0.00001	— 0.00019	— 0.00028	— 0.00004
$\beta = 0.70$	0	— 0.5026	0	+ 0.0066	0	0	0	— 0.00005	0	— 0.00030	0
	0.1	— 0.3423	0.1339	— 0.0788	— 0.0636	0	0	— 0.00004	— 0.00001	— 0.00030	0
	0.2	— 0.2636	0.1457	— 0.1232	— 0.0577	0	— 0.00001	— 0.00003	— 0.00003	— 0.00030	— 0.00001
	0.3	— 0.2209	0.1450	— 0.1481	— 0.0433	0.00001	— 0.00001	— 0.00003	— 0.00006	— 0.00030	— 0.00001
	0.4	— 0.1932	0.1425	— 0.1630	— 0.0253	0.00002	— 0.00001	— 0.00003	— 0.00008	— 0.00030	— 0.00001
	0.5	— 0.1684	0.1420	— 0.1719	— 0.0065	0.00003	— 0.00002	— 0.00002	— 0.00010	— 0.00030	— 0.00002
	0.6	— 0.1456	0.1402	— 0.1757	+ 0.0134	0.00004	— 0.00002	— 0.00002	— 0.00012	— 0.00030	— 0.00002
	0.7	— 0.1237	0.1354	— 0.1740	0.0333	0.00005	— 0.00003	— 0.00002	— 0.00015	— 0.00031	— 0.00003
	0.8	— 0.1037	0.1268	— 0.1666	0.0518	0.00007	— 0.00004	— 0.00002	— 0.00017	— 0.00031	— 0.00003
	0.9	— 0.0874	0.1145	— 0.1547	0.0669	0.00009	— 0.00005	— 0.00002	— 0.00019	— 0.00031	— 0.00004
	1.0	— 0.0763	0.0994	— 0.1391	0.0769	0.00011	— 0.00006	— 0.00002	— 0.00021	— 0.00031	— 0.00005
$\beta = 0.80$	0	— 0.5982	0	+ 0.0078	0	0	0	— 0.00006	0	— 0.00036	0
	0.1	— 0.3452	0.1898	— 0.1313	— 0.0801	0	0	— 0.00004	— 0.00001	— 0.00036	0
	0.2	— 0.2382	0.1842	— 0.1877	— 0.0458	0	— 0.00001	— 0.00004	— 0.00004	— 0.00036	— 0.00001
	0.3	— 0.1842	0.1719	— 0.2101	— 0.0024	0.00001	— 0.00001	— 0.00004	— 0.00007	— 0.00036	— 0.00001
	0.4	— 0.1419	0.1579	— 0.2092	+ 0.0413	0.00002	— 0.00002	— 0.00003	— 0.00010	— 0.00036	— 0.00002
	0.5	— 0.1110	0.1359	— 0.1892	0.0783	0.00003	— 0.00002	— 0.00003	— 0.00012	— 0.00036	— 0.00002
	0.6	— 0.0934	0.1110	— 0.1565	0.0995	0.00004	— 0.00003	— 0.00003	— 0.00015	— 0.00036	— 0.00003
	0.7	— 0.0894	0.0886	— 0.1222	0.1019	0.00006	— 0.00004	— 0.00004	— 0.00017	— 0.00036	— 0.00005
	0.8	— 0.0944	0.0738	— 0.0978	0.0896	0.00008	— 0.00005	— 0.00003	— 0.00019	— 0.00036	— 0.00007
	0.9	— 0.1017	0.0718	— 0.0841	0.0728	0.00010	— 0.00006	— 0.00003	— 0.00022	— 0.00036	— 0.00009

TABLE 3. Coefficients for $\tau = 0.04$.

	ω	k_c'	k_c''	m_c'	m_c''	n_a'	n_a''	n_b'	n_b''	n_c'	n_c''
$\beta = 0$	0	−0.5058	0	+0.0133	0	0	0	−0.00022	0	−0.00088	0
	0.1	−0.4213	0.0836	−0.0288	−0.0445	0	−0.00002	−0.00018	−0.00005	−0.00087	−0.00001
	0.2	−0.3690	0.0888	−0.0550	−0.0497	0.00001	−0.00003	−0.00015	−0.00013	−0.00086	−0.00003
	0.3	−0.3379	0.0813	−0.0706	−0.0485	0.00003	−0.00004	−0.00013	−0.00021	−0.00086	−0.00005
	0.4	−0.3179	0.0713	−0.0807	−0.0462	0.00005	−0.00006	−0.00011	−0.00029	−0.00086	−0.00006
	0.5	−0.3044	0.0615	−0.0874	−0.0440	0.00009	−0.00007	−0.00009	−0.00038	−0.00085	−0.00008
	0.6	−0.2950	0.0524	−0.0921	−0.0421	0.00014	−0.00008	−0.00006	−0.00046	−0.00085	−0.00010
	0.7	−0.2879	0.0439	−0.0956	−0.0406	0.00019	−0.00009	−0.00003	−0.00054	−0.00085	−0.00012
	0.8	−0.2827	0.0363	−0.0983	−0.0393	0.00025	−0.00010	0	−0.00063	−0.00085	−0.00014
	0.9	−0.2786	0.0292	−0.1003	−0.0385	0.00033	−0.00011	+0.00004	−0.00071	−0.00085	−0.00016
	1.0	−0.2753	0.0228	−0.1019	−0.0379	0.00041	−0.00012	0.00008	−0.00079	−0.00085	−0.00018
$\beta = 0.35$	0	−0.5400	0	+0.0143	0	0	0	−0.00023	0	−0.00094	0
	0.1	−0.4357	0.1037	−0.0384	−0.0544	0	−0.00002	−0.00019	−0.00005	−0.00093	−0.00001
	0.2	−0.3746	0.1113	−0.0702	−0.0598	0.00001	−0.00003	−0.00016	−0.00013	−0.00092	−0.00003
	0.3	−0.3400	0.1057	−0.0889	−0.0582	0.00003	−0.00005	−0.00014	−0.00022	−0.00092	−0.00004
	0.4	−0.3187	0.0982	−0.1011	−0.0556	0.00006	−0.00006	−0.00012	−0.00031	−0.00092	−0.00007
	0.5	−0.3049	0.0915	−0.1093	−0.0530	0.00010	−0.00007	−0.00010	−0.00041	−0.00092	−0.00009
	0.6	−0.2955	0.0861	−0.1156	−0.0511	0.00015	−0.00008	−0.00007	−0.00050	−0.00091	−0.00011
	0.7	−0.2891	0.0820	−0.1204	−0.0494	0.00021	−0.00010	−0.00004	−0.00059	−0.00092	−0.00013
	0.8	−0.2846	0.0790	−0.1246	−0.0481	0.00028	−0.00011	−0.00002	−0.00069	−0.00092	−0.00015
	0.9	−0.2812	0.0773	−0.1281	−0.0471	0.00036	−0.00013	+0.00002	−0.00078	−0.00092	−0.00017
	1.0	−0.2792	0.0763	−0.1312	−0.0465	0.00045	−0.00015	0.00005	−0.00088	−0.00092	−0.00019
$\beta = 0.50$	0	−0.5841	0	+0.0154	0	0	0	−0.00025	0	−0.00101	0
	0.1	−0.4528	0.1288	−0.0522	−0.0664	0	−0.00002	−0.00020	−0.00005	−0.00100	−0.00001
	0.2	−0.3786	0.1374	−0.0921	−0.0701	0.00001	−0.00003	−0.00017	−0.00015	−0.00100	−0.00003
	0.3	−0.3391	0.1333	−0.1146	−0.0666	0.00003	−0.00005	−0.00015	−0.00024	−0.00099	−0.00005
	0.4	−0.3149	0.1283	−0.1295	−0.0615	0.00007	−0.00006	−0.00013	−0.00034	−0.00099	−0.00007
	0.5	−0.2985	0.1250	−0.1407	−0.0573	0.00011	−0.00008	−0.00010	−0.00045	−0.00099	−0.00009
	0.6	−0.2867	0.1240	−0.1496	−0.0531	0.00017	−0.00010	−0.00008	−0.00055	−0.00100	−0.00012
	0.7	−0.2773	0.1247	−0.1569	−0.0490	0.00023	−0.00012	−0.00006	−0.00065	−0.00100	−0.00014
	0.8	−0.2695	0.1269	−0.1638	−0.0448	0.00031	−0.00014	−0.00003	−0.00076	−0.00100	−0.00016
	0.9	−0.2612	0.1305	−0.1699	−0.0406	0.00040	−0.00016	−0.00001	−0.00087	−0.00100	−0.00018
	1.0	−0.2526	0.1351	−0.1758	−0.0363	0.00050	−0.00020	+0.00001	−0.00098	−0.00101	−0.00021

TABLE 3 (continued).

	ω	k_c'	k_c''	m_c'	m_c''	n_a'	n_a''	n_b'	n_b''	n_c'	n_c''
$\beta = 0.60$	0	−0.6324	0	+0.0167	0	0	0	−0.00027	0	−0.00110	0
	0.1	−0.4651	0.1550	−0.0706	−0.0780	0	−0.00002	−0.00021	−0.00005	−0.00108	−0.00001
	0.2	−0.3798	0.1642	−0.1183	−0.0787	0.00001	−0.00004	−0.00018	−0.00016	−0.00108	−0.00003
	0.3	−0.3337	0.1606	−0.1454	−0.0711	0.00004	−0.00005	−0.00016	−0.00027	−0.00108	−0.00006
	0.4	−0.3047	0.1578	−0.1641	−0.0618	0.00007	−0.00007	−0.00014	−0.00038	−0.00108	−0.00008
	0.5	−0.2834	0.1574	−0.1780	−0.0522	0.00012	−0.00009	−0.00012	−0.00049	−0.00108	−0.00010
	0.6	−0.2657	0.1593	−0.1891	−0.0423	0.00019	−0.00011	−0.00010	−0.00061	−0.00108	−0.00013
	0.7	−0.2485	0.1625	−0.1983	−0.0315	0.00025	−0.00013	−0.00008	−0.00072	−0.00108	−0.00015
	0.8	−0.2320	0.1659	−0.2054	−0.0199	0.00034	−0.00017	−0.00007	−0.00084	−0.00109	−0.00018
	0.9	−0.2146	0.1686	−0.2106	−0.0073	0.00044	−0.00021	−0.00006	−0.00096	−0.00109	−0.00020
	1.0	−0.1943	0.1702	−0.2135	+0.0063	0.00055	−0.00025	−0.00005	−0.00107	−0.00110	−0.00023
$\beta = 0.70$	0	−0.7083	0	+0.0187	0	0	0	−0.00031	0	−0.00123	0
	0.1	−0.4827	0.1880	−0.1015	−0.0917	0	−0.00002	−0.00023	−0.00006	−0.00121	−0.00001
	0.2	−0.3737	0.2014	−0.1637	−0.0849	0.00002	−0.00004	−0.00019	−0.00019	−0.00120	−0.00004
	0.3	−0.3152	0.1988	−0.1986	−0.0665	0.00004	−0.00006	−0.00017	−0.00031	−0.00121	−0.00007
	0.4	−0.2772	0.1947	−0.2202	−0.0438	0.00009	−0.00008	−0.00015	−0.00044	−0.00121	−0.00009
	0.5	−0.2440	0.1935	−0.2340	−0.0196	0.00014	−0.00010	−0.00014	−0.00057	−0.00121	−0.00012
	0.6	−0.2134	0.1912	−0.2409	+0.0061	0.00021	−0.00013	−0.00013	−0.00070	−0.00122	−0.00014
	0.7	−0.1837	0.1852	−0.2407	0.0324	0.00029	−0.00016	−0.00013	−0.00082	−0.00122	−0.00017
	0.8	−0.1561	0.1743	−0.2330	0.0573	0.00038	−0.00021	−0.00013	−0.00095	−0.00123	−0.00021
	0.9	−0.1329	0.1582	−0.2189	0.0782	0.00048	−0.00027	−0.00013	−0.00106	−0.00123	−0.00025
	1.0	−0.1162	0.1380	−0.1996	0.0931	0.00059	−0.00033	−0.00014	−0.00117	−0.00125	−0.00030
$\beta = 0.80$	0	−0.8431	0	+0.0222	0	0	0	−0.00037	0	−0.00146	0
	0.1	−0.4856	0.2645	−0.1732	−0.1155	0	−0.00002	−0.00025	−0.00008	−0.00144	−0.00002
	0.2	−0.3406	0.2554	−0.2532	−0.0710	0.00002	−0.00005	−0.00022	−0.00023	−0.00143	−0.00005
	0.3	−0.2649	0.2381	−0.2866	−0.0136	0.00005	−0.00007	−0.00020	−0.00039	−0.00144	−0.00007
	0.4	−0.2068	0.2189	−0.2889	+0.0451	0.00011	−0.00010	−0.00020	−0.00054	−0.00145	−0.00011
	0.5	−0.1634	0.1895	−0.2651	0.0962	0.00017	−0.00013	−0.00020	−0.00069	−0.00145	−0.00014
	0.6	−0.1373	0.1555	−0.2232	0.1272	0.00025	−0.00017	−0.00021	−0.00083	−0.00145	−0.00019
	0.7	−0.1297	0.1236	−0.1773	0.1337	0.00033	−0.00022	−0.00022	−0.00096	−0.00145	−0.00024
	0.8	−0.1352	0.1009	−0.1430	0.1196	0.00043	−0.00028	−0.00022	−0.00109	−0.00145	−0.00032
	0.9	−0.1452	0.0950	−0.1218	0.0978	0.00054	−0.00034	−0.00021	−0.00121	−0.00145	−0.00041

TABLE 4. Coefficients for $\tau = 0.06$.

	ω	k_c'	k_c''	m_c'	m_c''	n_a'	n_a''	n_b'	n_b''	n_c'	n_c''
$\beta = 0$	0	— 0.6174	0	+ 0.0244	0	0	0	— 0.00061	0	— 0.00199	0
	0.1	— 0.5145	0.0999	— 0.0269	— 0.0547	0	— 0.00005	— 0.00051	— 0.00013	— 0.00196	— 0.00003
	0.2	— 0.4510	0.1044	— 0.0587	— 0.0617	0.00003	— 0.00009	— 0.00043	— 0.00034	— 0.00194	— 0.00009
	0.3	— 0.4132	0.0934	— 0.0775	— 0.0609	0.00007	— 0.00012	— 0.00037	— 0.00057	— 0.00193	— 0.00015
	0.4	— 0.3890	0.0797	— 0.0897	— 0.0587	0.00015	— 0.00015	— 0.00031	— 0.00080	— 0.00192	— 0.00021
	0.5	— 0.3727	0.0660	— 0.0977	— 0.0567	0.00025	— 0.00018	— 0.00025	— 0.00103	— 0.00191	— 0.00028
	0.6	— 0.3611	0.0533	— 0.1034	— 0.0551	0.00037	— 0.00021	— 0.00017	— 0.00126	— 0.00191	— 0.00034
	0.7	— 0.3525	0.0413	— 0.1076	— 0.0540	0.00052	— 0.00024	— 0.00010	— 0.00149	— 0.00190	— 0.00041
	0.8	— 0.3461	0.0304	— 0.1107	— 0.0531	0.00070	— 0.00027	— 0.00001	— 0.00171	— 0.00190	— 0.00047
	0.9	— 0.3410	0.0202	— 0.1131	— 0.0528	0.00090	— 0.00030	+ 0.00009	— 0.00194	— 0.00189	— 0.00053
	1.0	— 0.3370	0.0107	— 0.1149	— 0.0528	0.00112	— 0.00033	0.00020	— 0.00217	— 0.00189	— 0.00060
$\beta = 0.35$	0	— 0.6591	0	+ 0.0262	0	0	0	— 0.00065	0	— 0.00213	0
	0.1	— 0.5322	0.1242	— 0.0380	— 0.0669	0	— 0.00005	— 0.00053	— 0.00013	— 0.00209	— 0.00003
	0.2	— 0.4581	0.1315	— 0.0765	— 0.0743	0.00003	— 0.00009	— 0.00045	— 0.00036	— 0.00208	— 0.00009
	0.3	— 0.4163	0.1229	— 0.0991	— 0.0733	0.00008	— 0.00013	— 0.00039	— 0.00061	— 0.00206	— 0.00016
	0.4	— 0.3907	0.1121	— 0.1137	— 0.0709	0.00016	— 0.00016	— 0.00033	— 0.00086	— 0.00206	— 0.00023
	0.5	— 0.3743	0.1022	— 0.1237	— 0.0688	0.00027	— 0.00020	— 0.00027	— 0.00111	— 0.00205	— 0.00030
	0.6	— 0.3633	0.0939	— 0.1311	— 0.0673	0.00041	— 0.00023	— 0.00020	— 0.00137	— 0.00205	— 0.00037
	0.7	— 0.3560	0.0872	— 0.1369	— 0.0663	0.00057	— 0.00028	— 0.00013	— 0.00162	— 0.00205	— 0.00043
	0.8	— 0.3510	0.0818	— 0.1417	— 0.0658	0.00077	— 0.00031	— 0.00005	— 0.00188	— 0.00205	— 0.00050
	0.9	— 0.3475	0.0779	— 0.1459	— 0.0657	0.00099	— 0.00036	+ 0.00003	— 0.00215	— 0.00205	— 0.00056
	1.0	— 0.3457	0.0750	— 0.1495	— 0.0660	0.00124	— 0.00043	0.00013	— 0.00241	— 0.00206	— 0.00063
$\beta = 0.50$	0	— 0.7130	0	+ 0.0283	0	0	0	— 0.00070	0	— 0.00230	0
	0.1	— 0.5532	0.1546	— 0.0540	— 0.0817	0	— 0.00006	— 0.00055	— 0.00014	— 0.00026	— 0.00003
	0.2	— 0.4634	0.1630	— 0.1024	— 0.0874	0.00003	— 0.00010	— 0.00047	— 0.00040	— 0.00224	— 0.00011
	0.3	— 0.4160	0.1562	— 0.1296	— 0.0843	0.00009	— 0.00014	— 0.00041	— 0.00067	— 0.00223	— 0.00017
	0.4	— 0.3871	0.1484	— 0.1476	— 0.0795	0.00018	— 0.00018	— 0.00035	— 0.00094	— 0.00222	— 0.00024
	0.5	— 0.3680	0.1427	— 0.1611	— 0.0757	0.00031	— 0.00022	— 0.00029	— 0.00122	— 0.00222	— 0.00032
	0.6	— 0.3546	0.1399	— 0.1718	— 0.0720	0.00045	— 0.00026	— 0.00024	— 0.00150	— 0.00223	— 0.00039
	0.7	— 0.3442	0.1392	— 0.1808	— 0.0685	0.00064	— 0.00032	— 0.00017	— 0.00179	— 0.00224	— 0.00047
	0.8	— 0.3358	0.1405	— 0.1891	— 0.0650	0.00085	— 0.00038	— 0.00011	— 0.00209	— 0.00224	— 0.00054
	0.9	— 0.3272	0.1436	— 0.1967	— 0.0615	0.00110	— 0.00046	— 0.00005	— 0.00239	— 0.00225	— 0.00060
	1.0	— 0.3185	0.1481	— 0.2040	— 0.0579	0.00137	— 0.00055	0	— 0.00269	— 0.00226	— 0.00068

TABLE 4 (continued).

	ω	k_c'	k_c''	m_c'	m_c''	n_a'	n_a''	n_b'	n_b''	n_c'	n_c''
$\beta = 0.60$	0	— 0.7719	0	+ 0.0306	0	0	0	— 0.00076	0	— 0.00249	0
	0.1	— 0.5685	0.1864	— 0.0756	— 0.0962	0	— 0.00006	— 0.00058	— 0.00015	— 0.00244	— 0.00003
	0.2	— 0.4654	0.1956	— 0.1334	— 0.0986	0.00003	— 0.00010	— 0.00050	— 0.00043	— 0.00242	— 0.00011
	0.3	— 0.4102	0.1894	— 0.1663	— 0.0909	0.00010	— 0.00014	— 0.00043	— 0.00074	— 0.00242	— 0.00019
	0.4	— 0.3759	0.1844	— 0.1890	— 0.0815	0.00019	— 0.00019	— 0.00038	— 0.00104	— 0.00242	— 0.00027
	0.5	— 0.3513	0.1824	— 0.2060	— 0.0718	0.00034	— 0.00024	— 0.00033	— 0.00135	— 0.00242	— 0.00034
	0.6	— 0.3312	0.1835	— 0.2199	— 0.0617	0.00051	— 0.00030	— 0.00028	— 0.00167	— 0.00243	— 0.00042
	0.7	— 0.3121	0.1865	— 0.2316	— 0.0507	0.00070	— 0.00037	— 0.00024	— 0.00199	— 0.00244	— 0.00050
	0.8	— 0.2936	0.1902	— 0.2412	— 0.0387	0.00094	— 0.00046	— 0.00021	— 0.00231	— 0.00245	— 0.00057
	0.9	— 0.2741	0.1935	— 0.2486	— 0.0254	0.00120	— 0.00057	— 0.00018	— 0.00264	— 0.00246	— 0.00065
	1.0	— 0.2513	0.1958	— 0.2537	— 0.0109	0.00150	— 0.00071	— 0.00017	— 0.00295	— 0.00248	— 0.00073
$\beta = 0.70$	0	— 0.8646	0	+ 0.0343	0	0	0	— 0.00085	0	— 0.00279	0
	0.1	— 0.5895	0.2282	— 0.1124	— 0.1143	0	— 0.00006	— 0.00063	— 0.00017	— 0.00272	— 0.00004
	0.2	— 0.4588	0.2409	— 0.1876	— 0.1076	0.00002	— 0.00011	— 0.00053	— 0.00051	— 0.00270	— 0.00013
	0.3	— 0.3893	0.2357	— 0.2301	— 0.0876	0.00012	— 0.00016	— 0.00048	— 0.00085	— 0.00271	— 0.00022
	0.4	— 0.3443	0.2300	— 0.2571	— 0.0629	0.00024	— 0.00022	— 0.00043	— 0.00120	— 0.00272	— 0.00030
	0.5	— 0.3058	0.2280	— 0.2752	— 0.0363	0.00039	— 0.00028	— 0.00040	— 0.00155	— 0.00272	— 0.00038
	0.6	— 0.2702	0.2253	— 0.2856	— 0.0076	0.00057	— 0.00036	— 0.00038	— 0.00191	— 0.00274	— 0.00046
	0.7	— 0.2355	0.2189	— 0.2879	+ 0.0222	0.00080	— 0.00046	— 0.00038	— 0.00226	— 0.00276	— 0.00054
	0.8	— 0.2026	0.2069	— 0.2816	0.0511	0.00104	— 0.00059	— 0.00039	— 0.00261	— 0.00277	— 0.00063
	0.9	— 0.1742	0.1888	— 0.2677	0.0762	0.00132	— 0.00075	— 0.00042	— 0.00292	— 0.00278	— 0.00074
	1.0	— 0.1526	0.1655	— 0.2474	0.0952	0.00160	— 0.00093	— 0.00043	— 0.00320	— 0.00280	— 0.00086
$\beta = 0.80$	0	— 1.0291	0	+ 0.0407	0	0	0	— 0.00101	0	— 0.00332	0
	0.1	— 0.5921	0.3192	— 0.1971	— 0.1440	0	— 0.00007	— 0.00070	— 0.00021	— 0.00324	— 0.00005
	0.2	— 0.4215	0.3066	— 0.2953	— 0.0943	0.00006	— 0.00014	— 0.00061	— 0.00063	— 0.00322	— 0.00015
	0.3	— 0.3298	0.2855	— 0.3380	— 0.0287	0.00015	— 0.00019	— 0.00057	— 0.00105	— 0.00324	— 0.00024
	0.4	— 0.2607	0.2625	— 0.3450	+ 0.0394	0.00029	— 0.00027	— 0.00056	— 0.00147	— 0.00326	— 0.00033
	0.5	— 0.2080	0.2287	— 0.3213	0.1002	0.00046	— 0.00037	— 0.00058	— 0.00189	— 0.00327	— 0.00043
	0.6	— 0.1747	0.1884	— 0.2751	0.1395	0.00068	— 0.00048	— 0.00061	— 0.00227	— 0.00327	— 0.00054
	0.7	— 0.1631	0.1491	— 0.2221	0.1507	0.00090	— 0.00063	— 0.00065	— 0.00262	— 0.00327	— 0.00068
	0.8	— 0.1679	0.1194	— 0.1802	0.1375	0.00116	— 0.00079	— 0.00066	— 0.00296	— 0.00328	— 0.00086
	0.9	— 0.1798	0.1087	— 0.1526	0.1132	0.00145	— 0.00097	— 0.00066	— 0.00330	— 0.00329	— 0.00106

TABLE 5. Coefficients for $\tau = 0.08$.

	ω	k_c'	k_c''	m_c'	m_c''	n_a'	n_a''	n_b'	n_b''	n_c'	n_c''
$\beta = 0$	0	−0.7105	0	+0.0374	0	0	0	−0.00125	0	−0.00357	0
	0.1	−0.5924	0.1124	−0.0215	−0.0634	0	−0.00010	−0.00104	−0.00026	−0.00350	−0.00007
	0.2	−0.5197	0.1155	−0.0578	−0.0720	0.00005	−0.00018	−0.00089	−0.00070	−0.00345	−0.00021
	0.3	−0.4764	0.1009	−0.0794	−0.0719	0.00015	−0.00025	−0.00077	−0.00116	−0.00342	−0.00036
	0.4	−0.4487	0.0832	−0.0931	−0.0701	0.00031	−0.00031	−0.00064	−0.00163	−0.00340	−0.00051
	0.5	−0.4300	0.0656	−0.1022	−0.0685	0.00051	−0.00038	−0.00052	−0.00210	−0.00338	−0.00066
	0.6	−0.4167	0.0490	−0.1087	−0.0674	0.00077	−0.00043	−0.00037	−0.00257	−0.00337	−0.00081
	0.7	−0.4068	0.0335	−0.1133	−0.0668	0.00107	−0.00050	−0.00021	−0.00303	−0.00335	−0.00096
	0.8	−0.3993	0.0191	−0.1168	−0.0666	0.00143	−0.00055	−0.00003	−0.00350	−0.00334	−0.00111
	0.9	−0.3934	+0.0055	−0.1194	−0.0671	0.00184	−0.00062	+0.00017	−0.00396	−0.00333	−0.00126
	1.0	−0.3885	−0.0073	−0.1213	−0.0678	0.00229	−0.00067	0.00038	−0.00442	−0.00332	−0.00141
$\beta = 0.35$	0	−0.7585	0	+0.0400	0	0	0	−0.00133	0	−0.00381	0
	0.1	−0.6129	0.1401	−0.0336	−0.0774	0.00001	−0.00011	−0.00110	−0.00026	−0.00373	−0.00006
	0.2	−0.5282	0.1464	−0.0776	−0.0869	0.00005	−0.00019	−0.00094	−0.00074	−0.00368	−0.00022
	0.3	−0.4805	0.1344	−0.1033	−0.0867	0.00016	−0.00027	−0.00081	−0.00124	−0.00365	−0.00037
	0.4	−0.4515	0.1200	−0.1198	−0.0850	0.00033	−0.00034	−0.00069	−0.00175	−0.00364	−0.00054
	0.5	−0.4331	0.1067	−0.1311	−0.0836	0.00055	−0.00041	−0.00057	−0.00227	−0.00363	−0.00071
	0.6	−0.4209	0.0952	−0.1394	−0.0829	0.00084	−0.00048	−0.00043	−0.00279	−0.00362	−0.00087
	0.7	−0.4130	0.0854	−0.1458	−0.0829	0.00117	−0.00057	−0.00029	−0.00331	−0.00362	−0.00102
	0.8	−0.4078	0.0773	−0.1512	−0.0834	0.00157	−0.00065	−0.00014	−0.00384	−0.00362	−0.00118
	0.9	−0.4045	0.0707	−0.1558	−0.0845	0.00203	−0.00076	+0.00004	−0.00438	−0.00362	−0.00133
	1.0	−0.4030	0.0654	−0.1597	−0.0860	0.00254	−0.00088	0.00022	−0.00491	−0.00363	−0.00149
$\beta = 0.50$	0	−0.8204	0	+0.0433	0	0	0	−0.00145	0	−0.00413	0
	0.1	−0.6372	0.1749	−0.0510	−0.0948	0.00001	−0.00011	−0.00114	−0.00028	−0.00403	−0.00007
	0.2	−0.5347	0.1823	−0.1064	−0.1025	0.00007	−0.00020	−0.00097	−0.00081	−0.00398	−0.00024
	0.3	−0.4810	0.1724	−0.1374	−0.1003	0.00018	−0.00028	−0.00084	−0.00136	−0.00395	−0.00041
	0.4	−0.4486	0.1614	−0.1579	−0.0963	0.00037	−0.00037	−0.00073	−0.00192	−0.00394	−0.00058
	0.5	−0.4276	0.1529	−0.1732	−0.0933	0.00062	−0.00045	−0.00062	−0.00250	−0.00394	−0.00075
	0.6	−0.4132	0.1478	−0.1853	−0.0907	0.00092	−0.00055	−0.00051	−0.00307	−0.00395	−0.00092
	0.7	−0.4025	0.1452	−0.1955	−0.0884	0.00130	−0.00066	−0.00039	−0.00366	−0.00397	−0.00109
	0.8	−0.3941	0.1450	−0.2051	−0.0861	0.00174	−0.00080	−0.00026	−0.00426	−0.00398	−0.00126
	0.9	−0.3859	0.1471	−0.2139	−0.0839	0.00224	−0.00095	−0.00015	−0.00488	−0.00400	−0.00141
	1.0	−0.3777	0.1509	−0.2223	−0.0817	0.00280	−0.00115	−0.00005	−0.00550	−0.00401	−0.00158

TABLE 5 (continued).

	ω	k_c'	k_c''	m_c'	m_c''	n_a'	n_a''	n_b'	n_b''	n_c'	n_c''
$\beta = 0.60$	0	— 0.8882	0	+ 0.0469	0	0	0	— 0.00156	0	— 0.00447	0
	0.1	— 0.6552	0.2112	— 0.0749	— 0.1118	0.00001	— 0.00012	— 0.00120	— 0.00030	— 0.00434	— 0.00008
	0.2	— 0.5376	0.2194	— 0.1409	— 0.1162	0.00006	— 0.00021	— 0.00102	— 0.00088	— 0.00429	— 0.00026
	0.3	— 0.4753	0.2103	— 0.1786	— 0.1092	0.00020	— 0.00030	— 0.00090	— 0.00150	— 0.00428	— 0.00045
	0.4	— 0.4371	0.2026	— 0.2045	— 0.1004	0.00040	— 0.00039	— 0.00079	— 0.00211	— 0.00428	— 0.00063
	0.5	— 0.4103	0.1987	— 0.2242	— 0.0914	0.00068	— 0.00050	— 0.00070	— 0.00275	— 0.00429	— 0.00081
	0.6	— 0.3888	0.1985	— 0.2404	— 0.0822	0.00103	— 0.00062	— 0.00060	— 0.00340	— 0.00431	— 0.00099
	0.7	— 0.3689	0.2008	— 0.2544	— 0.0720	0.00142	— 0.00077	— 0.00053	— 0.00405	— 0.00434	— 0.00116
	0.8	— 0.3496	0.2045	— 0.2662	— 0.0605	0.00192	— 0.00096	— 0.00047	— 0.00472	— 0.00436	— 0.00132
	0.9	— 0.3291	0.2082	— 0.2761	— 0.0477	0.00245	— 0.00119	— 0.00043	— 0.00538	— 0.00438	— 0.00149
	1.0	— 0.3052	0.2112	— 0.2835	— 0.0333	0.00305	— 0.00148	— 0.00041	— 0.00602	— 0.00442	— 0.00167
$\beta = 0.70$	0	— 0.9949	0	+ 0.0525	0	0	0	— 0.00176	0	— 0.00500	0
	0.1	— 0.6789	0.2610	— 0.1161	— 0.1341	0.00001	— 0.00012	— 0.00129	— 0.00034	— 0.00484	— 0.00008
	0.2	— 0.5310	0.2715	— 0.2019	— 0.1283	0.00008	— 0.00023	— 0.00110	— 0.00103	— 0.00480	— 0.00030
	0.3	— 0.4531	0.2632	— 0.2506	— 0.1080	0.00024	— 0.00033	— 0.00099	— 0.00173	— 0.00481	— 0.00050
	0.4	— 0.4030	0.2558	— 0.2823	— 0.0829	0.00048	— 0.00044	— 0.00090	— 0.00244	— 0.00482	— 0.00069
	0.5	— 0.3609	0.2528	— 0.3045	— 0.0556	0.00079	— 0.00058	— 0.00085	— 0.00317	— 0.00485	— 0.00088
	0.6	— 0.3220	0.2498	— 0.3185	— 0.0255	0.00116	— 0.00075	— 0.00082	— 0.00390	— 0.00489	— 0.00106
	0.7	— 0.2838	0.2433	— 0.3240	+ 0.0062	0.00162	— 0.00096	— 0.00084	— 0.00461	— 0.00492	— 0.00123
	0.8	— 0.2469	0.2310	— 0.3202	0.0377	0.00212	— 0.00124	— 0.00088	— 0.00532	— 0.00493	— 0.00142
	0.9	— 0.2142	0.2119	— 0.3078	0.0659	0.00268	— 0.00156	— 0.00095	— 0.00595	— 0.00495	— 0.00163
	1.0	— 0.1883	0.1865	— 0.2880	0.0883	0.00326	— 0.00194	— 0.00101	— 0.00654	— 0.00498	— 0.00185
$\beta = 0.80$	0	— 1.1842	0	+ 0.0624	0	0	0	— 0.00209	0	— 0.00595	0
	0.1	— 0.6810	0.3631	— 0.2104	— 0.1692	0.00001	— 0.00014	— 0.00144	— 0.00043	— 0.00574	— 0.00011
	0.2	— 0.4915	0.3469	— 0.3239	— 0.1169	0.00011	— 0.00028	— 0.00126	— 0.00129	— 0.00571	— 0.00035
	0.3	— 0.3868	0.3225	— 0.3752	— 0.0466	0.00030	— 0.00039	— 0.00119	— 0.00214	— 0.00576	— 0.00056
	0.4	— 0.3095	0.2966	— 0.3878	+ 0.0278	0.00059	— 0.00055	— 0.00119	— 0.00299	— 0.00581	— 0.00076
	0.5	— 0.2492	0.2599	— 0.3664	0.0959	0.00094	— 0.00076	— 0.00124	— 0.00385	— 0.00583	— 0.00095
	0.6	— 0.2095	0.2149	— 0.3189	0.1423	0.00137	— 0.00101	— 0.00133	— 0.00462	— 0.00583	— 0.00117
	0.7	— 0.1935	0.1695	— 0.2615	0.1588	0.00183	— 0.00132	— 0.00143	— 0.00534	— 0.00584	— 0.00143
	0.8	— 0.1969	0.1331	— 0.2137	0.1480	0.00234	— 0.00165	— 0.00149	— 0.00602	— 0.00585	— 0.00177
	0.9	— 0.2100	0.1169	— 0.1800	0.1228	0.00293	— 0.00204	— 0.00151	— 0.00670	— 0.00588	— 0.00215

TABLE 6. Coefficients for $\tau = 0.1$.

	ω	k_c'	k_c''	m_c'	m_c''	n_a'	n_a''	n_b'	n_b''	n_c'	n_c''
$\beta = 0$	0	−0.7916	0	+0.0520	0	0	0	−0.00220	0	−0.00563	0
	0.1	−0.6604	0.1224	−0.0135	−0.0710	0	−0.00018	−0.00183	−0.00045	−0.00548	−0.00014
	0.2	−0.5798	0.1235	−0.0537	−0.0813	0.00009	−0.00032	−0.00156	−0.00121	−0.00539	−0.00041
	0.3	−0.5318	0.1051	−0.0775	−0.0819	0.00026	−0.00044	−0.00135	−0.00202	−0.00533	−0.00070
	0.4	−0.5011	0.0832	−0.0926	−0.0807	0.00053	−0.00055	−0.00113	−0.00283	−0.00529	−0.00099
	0.5	−0.4803	0.0615	−0.1026	−0.0797	0.00089	−0.00066	−0.00092	−0.00365	−0.00525	−0.00129
	0.6	−0.4655	0.0410	−0.1096	−0.0792	0.00133	−0.00076	−0.00067	−0.00446	−0.00522	−0.00158
	0.7	−0.4544	0.0216	−0.1146	−0.0794	0.00186	−0.00087	−0.00040	−0.00527	−0.00519	−0.00187
	0.8	−0.4459	+0.0035	−0.1183	−0.0800	0.00248	−0.00097	−0.00009	−0.00608	−0.00516	−0.00216
	0.9	−0.4391	−0.0137	−0.1210	−0.0813	0.00319	−0.00108	+0.00025	−0.00688	−0.00513	−0.00245
	1.0	−0.4335	−0.0300	−0.1230	−0.0829	0.00398	−0.00118	0.00062	−0.00768	−0.00510	−0.00274
$\beta = 0.35$	0	−0.8451	0	+0.0556	0	0	0	−0.00234	0	−0.00601	0
	0.1	−0.6835	0.1530	−0.0262	−0.0868	0.00001	−0.00019	−0.00192	−0.00045	−0.00584	−0.00013
	0.2	−0.5896	0.1576	−0.0749	−0.0983	0.00009	−0.00033	−0.00164	−0.00128	−0.00575	−0.00043
	0.3	−0.5370	0.1420	−0.1032	−0.0990	0.00028	−0.00047	−0.00142	−0.00215	−0.00569	−0.00073
	0.4	−0.5051	0.1237	−0.1213	−0.0982	0.00057	−0.00059	−0.00122	−0.00304	−0.00566	−0.00105
	0.5	−0.4851	0.1067	−0.1336	−0.0977	0.00095	−0.00072	−0.00101	−0.00394	−0.00564	−0.00137
	0.6	−0.4720	0.0917	−0.1426	−0.0981	0.00145	−0.00085	−0.00078	−0.00484	−0.00562	−0.00168
	0.7	−0.4637	0.0786	−0.1495	−0.0992	0.00203	−0.00100	−0.00054	−0.00575	−0.00562	−0.00198
	0.8	−0.4585	0.0673	−0.1552	−0.1010	0.00273	−0.00115	−0.00028	−0.00667	−0.00561	−0.00229
	0.9	−0.4555	0.0577	−0.1600	−0.1034	0.00352	−0.00134	+0.00001	−0.00761	−0.00561	−0.00259
	1.0	−0.4545	0.0495	−0.1641	−0.1063	0.00441	−0.00155	0.00032	−0.00854	−0.00561	−0.00290
$\beta = 0.50$	0	−0.9141	0	+0.0601	0	0	0	−0.00254	0	−0.00650	0
	0.1	−0.7107	0.1915	−0.0446	−0.1063	0.00001	−0.00020	−0.00201	−0.00048	−0.00630	−0.00014
	0.2	−0.5974	0.1972	−0.1058	−0.1163	0.00011	−0.00035	−0.00171	−0.00140	−0.00620	−0.00047
	0.3	−0.5384	0.1838	−0.1400	−0.1152	0.00031	−0.00049	−0.00149	−0.00236	−0.00615	−0.00080
	0.4	−0.5032	0.1694	−0.1626	−0.1124	0.00064	−0.00064	−0.00130	−0.00334	−0.00613	−0.00113
	0.5	−0.4808	0.1578	−0.1793	−0.1106	0.00107	−0.00079	−0.00111	−0.00433	−0.00613	−0.00146
	0.6	−0.4659	0.1499	−0.1926	−0.1094	0.00160	−0.00096	−0.00092	−0.00533	−0.00615	−0.00179
	0.7	−0.4554	0.1450	−0.2039	−0.1086	0.00225	−0.00116	−0.00072	−0.00636	−0.00617	−0.00212
	0.8	−0.4474	0.1429	−0.2145	−0.1080	0.00302	−0.00140	−0.00052	−0.00741	−0.00619	−0.00244
	0.9	−0.4401	0.1434	−0.2243	−0.1075	0.00389	−0.00168	−0.00034	−0.00848	−0.00622	−0.00274
	1.0	−0.4329	0.1461	−0.2337	−0.1070	0.00487	−0.00203	−0.00017	−0.00956	−0.00625	−0.00305

TABLE 6 (continued).

	ω	k_c'	k_c''	m_c'	m_c''	n_a'	n_a''	n_b'	n_b''	n_c'	n_c''
$\beta = 0.60$	0	— 0.9896	0	+ 0.0651	0	0	0	— 0.00274	0	— 0.00704	0
	0.1	— 0.7310	0.2317	— 0.0701	— 0.1257	0.00001	— 0.00021	— 0.00211	— 0.00051	— 0.00679	— 0.00015
	0.2	— 0.6013	0.2382	— 0.1430	— 0.1324	0.00011	— 0.00037	— 0.00180	— 0.00153	— 0.00669	— 0.00050
	0.3	— 0.5332	0.2258	— 0.1848	— 0.1265	0.00035	— 0.00052	— 0.00159	— 0.00260	— 0.00667	— 0.00087
	0.4	— 0.4920	0.2151	— 0.2134	— 0.1190	0.00069	— 0.00068	— 0.00141	— 0.00367	— 0.00667	— 0.00122
	0.5	— 0.4638	0.2088	— 0.2353	— 0.1113	0.00118	— 0.00087	— 0.00125	— 0.00477	— 0.00669	— 0.00157
	0.6	— 0.4417	0.2069	— 0.2536	— 0.1035	0.00178	— 0.00109	— 0.00110	— 0.00590	— 0.00673	— 0.00191
	0.7	— 0.4217	0.2082	— 0.2697	— 0.0947	0.00247	— 0.00136	— 0.00098	— 0.00704	— 0.00677	— 0.00224
	0.8	— 0.4023	0.2115	— 0.2838	— 0.0846	0.00332	— 0.00169	— 0.00090	— 0.00820	— 0.00681	— 0.00255
	0.9	— 0.3817	0.2154	— 0.2960	— 0.0729	0.00425	— 0.00211	— 0.00086	— 0.00935	— 0.00686	— 0.00286
	1.0	— 0.3576	0.2190	— 0.3059	— 0.0595	0.00529	— 0.00262	— 0.00085	— 0.01047	— 0.00691	— 0.00318
$\beta = 0.70$	0	— 1.1085	0	+ 0.0729	0	0	0	— 0.00308	0	— 0.00788	0
	0.1	— 0.7571	0.2888	— 0.1146	— 0.1520	0.00001	— 0.00022	— 0.00227	— 0.00058	— 0.00756	— 0.00016
	0.2	— 0.5950	0.2961	— 0.2094	— 0.1477	0.00014	— 0.00040	— 0.00194	— 0.00177	— 0.00748	— 0.00058
	0.3	— 0.5104	0.2844	— 0.2634	— 0.1279	0.00041	— 0.00058	— 0.00175	— 0.00299	— 0.00749	— 0.00097
	0.4	— 0.4565	0.2750	— 0.2994	— 0.1036	0.00083	— 0.00078	— 0.00161	— 0.00423	— 0.00753	— 0.00134
	0.5	— 0.4120	0.2708	— 0.3255	— 0.0767	0.00136	— 0.00102	— 0.00153	— 0.00549	— 0.00758	— 0.00170
	0.6	— 0.3710	0.2675	— 0.3432	— 0.0466	0.00201	— 0.00132	— 0.00151	— 0.00676	— 0.00765	— 0.00203
	0.7	— 0.3303	0.2611	— 0.3523	— 0.0141	0.00280	— 0.00171	— 0.00156	— 0.00801	— 0.00771	— 0.00235
	0.8	— 0.2905	0.2490	— 0.3517	+ 0.0189	0.00366	— 0.00220	— 0.00166	— 0.00923	— 0.00774	— 0.00268
	0.9	— 0.2541	0.2295	— 0.3418	0.0494	0.00462	— 0.00278	— 0.00181	— 0.01033	— 0.00777	— 0.00304
	1.0	— 0.2242	0.2028	— 0.3237	0.0750	0.00562	— 0.00346	— 0.00195	— 0.01135	— 0.00780	— 0.00342
$\beta = 0.80$	0	— 1.3194	0	+ 0.0867	0	0	0	— 0.00366	0	— 0.00938	0
	0.1	— 0.7588	0.3999	— 0.2162	— 0.1921	0.00001	— 0.00025	— 0.00253	— 0.00073	— 0.00896	— 0.00020
	0.2	— 0.5545	0.3799	— 0.3431	— 0.1392	0.00019	— 0.00048	— 0.00222	— 0.00222	— 0.00891	— 0.00068
	0.3	— 0.4391	0.3524	— 0.4026	— 0.0666	0.00052	— 0.00069	— 0.00211	— 0.00371	— 0.00900	— 0.00109
	0.4	— 0.3554	0.3242	— 0.4214	+ 0.0118	0.00101	— 0.00098	— 0.00213	— 0.00519	— 0.00910	— 0.00145
	0.5	— 0.2888	0.2856	— 0.4039	0.0855	0.00162	— 0.00135	— 0.00226	— 0.00666	— 0.00915	— 0.00179
	0.6	— 0.2431	0.2370	— 0.3571	0.1384	0.00235	— 0.00180	— 0.00246	— 0.00800	— 0.00916	— 0.00216
	0.7	— 0.2226	0.1863	— 0.2972	0.1605	0.00314	— 0.00235	— 0.00267	— 0.00923	— 0.00916	— 0.00260
	0.8	— 0.2239	0.1436	— 0.2446	0.1531	0.00402	— 0.00295	— 0.00282	— 0.01040	— 0.00918	— 0.00315
	0.9	— 0.2377	0.1215	— 0.2054	0.1280	0.00501	— 0.00365	— 0.00292	— 0.01156	— 0.00924	— 0.00376

TABLE 7. Coefficients for $\tau = 0.15$.

	ω	k_c'	k_c''	m_c'	m_c''	n_a'	n_a''	n_b'	n_b''	n_c'	n_c''
$\beta = 0$	0	−0.9610	0	0.0941	0	0	0	−0.00613	0	−0.01294	0
	0.1	−0.8027	0.1400	+0.0150	−0.0871	0	−0.00051	−0.00510	−0.00119	−0.01244	−0.00046
	0.2	−0.7061	0.1342	−0.0329	−0.1013	0.00023	−0.00089	−0.00437	−0.00326	−0.01213	−0.00136
	0.3	−0.6485	0.1053	−0.0612	−0.1041	0.00075	−0.00122	−0.00379	−0.00546	−0.01192	−0.00234
	0.4	−0.6116	0.0723	−0.0789	−0.1047	0.00143	−0.00153	−0.00322	−0.00769	−0.01176	−0.00332
	0.5	−0.5864	0.0397	−0.0905	−0.1055	0.00241	−0.00183	−0.00265	−0.00991	−0.01162	−0.00430
	0.6	−0.5682	+0.0085	−0.0984	−0.1070	0.00361	−0.00212	−0.00200	−0.01212	−0.01149	−0.00528
	0.7	−0.5543	−0.0212	−0.1040	−0.1093	0.00506	−0.00242	−0.00129	−0.01432	−0.01136	−0.00626
	0.8	−0.5433	−0.0494	−0.1079	−0.1123	0.00675	−0.00271	−0.00048	−0.01652	−0.01122	−0.00723
	0.9	−0.5342	−0.0765	−0.1106	−0.1159	0.00868	−0.00301	+0.00041	−0.01870	−0.01108	−0.00820
	1.0	−0.5264	−0.1025	−0.1124	−0.1200	0.01083	−0.00330	0.00138	−0.02087	−0.01093	−0.00916
$\beta = 0.35$	0	−1.0259	0	0.1005	0	0	0	−0.00653	0	−0.01381	0
	0.1	−0.8314	0.1764	+0.0019	−0.1066	0.00001	−0.00053	−0.00534	−0.00121	−0.01323	−0.00045
	0.2	−0.7191	0.1746	−0.0561	−0.1230	0.00024	−0.00093	−0.00457	−0.00345	−0.01291	−0.00143
	0.3	−0.6566	0.1488	−0.0895	−0.1266	0.00075	−0.00129	−0.00398	−0.00583	−0.01271	−0.00246
	0.4	−0.6192	0.1199	−0.1105	−0.1285	0.00155	−0.00164	−0.00346	−0.00825	−0.01259	−0.00352
	0.5	−0.5961	0.0927	−0.1246	−0.1309	0.00258	−0.00200	−0.00292	−0.01069	−0.01250	−0.00457
	0.6	−0.5815	0.0678	−0.1346	−0.1344	0.00392	−0.00237	−0.00234	−0.01313	−0.01243	−0.00560
	0.7	−0.5727	0.0451	−0.1421	−0.1389	0.00551	−0.00279	−0.00172	−0.01561	−0.01238	−0.00663
	0.8	−0.5678	0.0246	−0.1481	−0.1443	0.00740	−0.00324	−0.00106	−0.01811	−0.01233	−0.00766
	0.9	−0.5659	+0.0059	−0.1529	−0.1507	0.00954	−0.00377	−0.00035	−0.02066	−0.01228	−0.00868
	1.0	−0.5662	−0.0110	−0.1569	−0.1576	0.01199	−0.00436	+0.00042	−0.02323	−0.01224	−0.00970
$\beta = 0.50$	0	−1.1097	0	+0.1086	0	0	0	−0.00707	0	−0.01494	0
	0.1	−0.8649	0.2223	−0.0173	−0.1309	0.00001	−0.00055	−0.00561	−0.00127	−0.01424	−0.00046
	0.2	−0.7300	0.2215	−0.0902	−0.1466	0.00028	−0.00098	−0.00479	−0.00375	−0.01390	−0.00155
	0.3	−0.6610	0.1981	−0.1306	−0.1491	0.00083	−0.00136	−0.00421	−0.00638	−0.01374	−0.00267
	0.4	−0.6207	0.1739	−0.1571	−0.1502	0.00171	−0.00177	−0.00372	−0.00904	−0.01367	−0.00379
	0.5	−0.5964	0.1532	−0.1763	−0.1523	0.00287	−0.00219	−0.00325	−0.01173	−0.01365	−0.00490
	0.6	−0.5815	0.1371	−0.1916	−0.1556	0.00433	−0.00269	−0.00278	−0.01447	−0.01367	−0.00599
	0.7	−0.5723	0.1248	−0.2047	−0.1597	0.00609	−0.00324	−0.00230	−0.01727	−0.01370	−0.00707
	0.8	−0.5666	0.1162	−0.2170	−0.1644	0.00818	−0.00393	−0.00185	−0.02014	−0.01375	−0.00814
	0.9	−0.5629	0.1111	−0.2286	−0.1694	0.01056	−0.00474	−0.00143	−0.02305	−0.01382	−0.00917
	1.0	−0.5598	0.1092	−0.2398	−0.1745	0.01325	−0.00574	−0.00107	−0.02599	−0.01389	−0.01019

TABLE 7 (continued).

	ω	k_c'	k_c''	m_c'	m_c''	n_a'	n_a''	n_b'	n_b''	n_c'	n_c''
$\beta = 0.60$	0	— 1.2013	0	+ 0.1176	0	0	0	— 0.00765	0	— 0.01617	0
	0.1	— 0.8905	0.2703	— 0.0450	— 0.1556	0.00001	— 0.00059	— 0.00589	— 0.00134	— 0.01533	— 0.00048
	0.2	— 0.7368	0.2701	— 0.1317	— 0.1685	0.00030	— 0.00103	— 0.00504	— 0.00412	— 0.01499	— 0.00167
	0.3	— 0.6578	0.2481	— 0.1814	— 0.1668	0.00094	— 0.00145	— 0.00450	— 0.00700	— 0.01490	— 0.00290
	0.4	— 0.6118	0.2286	— 0.2152	— 0.1640	0.00187	— 0.00191	— 0.00405	— 0.00994	— 0.01489	— 0.00408
	0.5	— 0.5823	0.2151	— 0.2415	— 0.1613	0.00317	— 0.00245	— 0.00368	— 0.01294	— 0.01495	— 0.00524
	0.6	— 0.5607	0.2075	— 0.2641	— 0.1589	0.00479	— 0.00306	— 0.00335	— 0.01599	— 0.01506	— 0.00636
	0.7	— 0.5427	0.2047	— 0.2846	— 0.1558	0.00670	— 0.00383	— 0.00313	— 0.01911	— 0.01519	— 0.00745
	0.8	— 0.5255	0.2058	— 0.3038	— 0.1512	0.00896	— 0.00479	— 0.00302	— 0.02226	— 0.01532	— 0.00848
	0.9	— 0.5071	0.2092	— 0.3216	— 0.1448	0.01149	— 0.00598	— 0.00305	— 0.02539	— 0.01547	— 0.00947
	1.0	— 0.4853	0.2137	— 0.3379	— 0.1361	0.01429	— 0.00746	— 0.00320	— 0.02847	— 0.01559	— 0.01047
$\beta = 0.70$	0	— 1.3457	0	+ 0.1318	0	0	0	— 0.00858	0	— 0.01811	0
	0.1	— 0.9216	0.3431	— 0.0947	— 0.1913	0.00001	— 0.00062	— 0.00633	— 0.00151	— 0.01704	— 0.00052
	0.2	— 0.7322	0.3398	— 0.2073	— 0.1923	0.00037	— 0.00112	— 0.00545	— 0.00473	— 0.01675	— 0.00190
	0.3	— 0.6360	0.3183	— 0.2719	— 0.1766	0.00109	— 0.00162	— 0.00497	— 0.00805	— 0.01675	— 0.00322
	0.4	— 0.5762	0.3030	— 0.3171	— 0.1575	0.00220	— 0.00218	— 0.00468	— 0.01142	— 0.01690	— 0.00446
	0.5	— 0.5293	0.2949	— 0.3522	— 0.1351	0.00365	— 0.00287	— 0.00456	— 0.01485	— 0.01708	— 0.00563
	0.6	— 0.4864	0.2904	— 0.3792	— 0.1085	0.00542	— 0.00375	— 0.00463	— 0.01830	— 0.01730	— 0.00671
	0.7	— 0.4431	0.2846	— 0.3983	— 0.0779	0.00752	— 0.00488	— 0.00493	— 0.02171	— 0.01750	— 0.00772
	0.8	— 0.3989	0.2740	— 0.4076	— 0.0444	0.00983	— 0.00629	— 0.00541	— 0.02497	— 0.01763	— 0.00870
	0.9	— 0.3558	0.2555	— 0.4067	— 0.0108	0.01234	— 0.00799	— 0.00603	— 0.02795	— 0.01772	— 0.00970
	1.0	— 0.3172	0.2280	— 0.3960	+ 0.0207	0.01500	— 0.00996	— 0.00666	— 0.03071	— 0.01775	— 0.01074
$\beta = 0.80$	0	— 1.6017	0	+ 0.1568	0	0	0	— 0.01020	0	— 0.02156	0
	0.1	— 0.9239	0.4712	— 0.2078	— 0.2432	0.00002	— 0.00070	— 0.00705	— 0.00189	— 0.02009	— 0.00064
	0.2	— 0.6926	0.4409	— 0.3625	— 0.1944	0.00049	— 0.00130	— 0.00625	— 0.00592	— 0.01997	— 0.00224
	0.3	— 0.5576	0.4062	— 0.4407	— 0.1228	0.00138	— 0.00194	— 0.00605	— 0.00998	— 0.02024	— 0.00361
	0.4	— 0.4632	0.3735	— 0.4766	— 0.0413	0.00269	— 0.00277	— 0.00625	— 0.01400	— 0.02058	— 0.00475
	0.5	— 0.3847	0.3327	— 0.4733	+ 0.0408	0.00431	— 0.00384	— 0.00682	— 0.01790	— 0.02082	— 0.00576
	0.6	— 0.3259	0.2786	— 0.4346	0.1069	0.00621	— 0.00517	— 0.00762	— 0.02149	— 0.02092	— 0.00677
	0.7	— 0.2936	0.2176	— 0.3747	0.1434	0.00828	— 0.00676	— 0.00848	— 0.02474	— 0.02093	— 0.00793
	0.8	— 0.2875	0.1605	— 0.3145	0.1474	0.01055	— 0.00854	— 0.00919	— 0.02776	— 0.02099	— 0.00932
	0.9	— 0.3010	0.1226	— 0.2635	0.1264	0.01307	— 0.01061	— 0.00983	— 0.03076	— 0.02122	— 0.01082

TABLE 8. Coefficients for $\tau = 0.2$.

	ω	k_c'	k_c''	m_c'	m_c''	n_a'	n_a''	n_b'	n_b''	n_c'	n_c''
$\beta = 0$	0	−1.0996	0	0.1424	0	0	0	−0.01272	0	−0.02350	0
	0.1	−0.9197	0.1505	+0.0526	−0.1003	0.00001	−0.00106	−0.01059	−0.00235	−0.02234	−0.00107
	0.2	−0.8104	0.1357	−0.0014	−0.1180	0.00045	−0.00185	−0.00911	−0.00655	−0.02158	−0.00319
	0.3	−0.7451	0.0951	−0.0330	−0.1229	0.00141	−0.00254	−0.00793	−0.01101	−0.02106	−0.00548
	0.4	−0.7032	0.0501	−0.0524	−0.1255	0.00288	−0.00318	−0.00683	−0.01553	−0.02065	−0.00779
	0.5	−0.6741	+0.0056	−0.0650	−0.1283	0.00485	−0.00380	−0.00567	−0.02003	−0.02028	−0.01010
	0.6	−0.6527	−0.0372	−0.0734	−0.1320	0.00731	−0.00442	−0.00441	−0.02451	−0.01991	−0.01240
	0.7	−0.6360	−0.0783	−0.0790	−0.1366	0.01025	−0.00503	−0.00302	−0.02897	−0.01953	−0.01469
	0.8	−0.6222	−0.1177	−0.0827	−0.1420	0.01368	−0.00564	−0.00146	−0.03341	−0.01913	−0.01697
	0.9	−0.6104	−0.1557	−0.0850	−0.1481	0.01758	−0.00625	+0.00026	−0.03783	−0.01871	−0.01924
	1.0	−0.5998	−0.1926	−0.0863	−0.1547	0.02195	−0.00686	0.00216	−0.04224	−0.01824	−0.02150
$\beta = 0.35$	0	−1.1739	0	0.1520	0	0	0	−0.01358	0	−0.02509	0
	0.1	−0.9631	0.1913	+0.0402	−0.1230	0	−0.00110	−0.01109	−0.00240	−0.02371	−0.00107
	0.2	−0.8265	0.1808	−0.0250	−0.1439	0.00047	−0.00193	−0.00949	−0.00693	−0.02292	−0.00336
	0.3	−0.7565	0.1434	−0.0620	−0.1505	0.00150	−0.00267	−0.00834	−0.01175	−0.02244	−0.00580
	0.4	−0.7149	0.1027	−0.0848	−0.1554	0.00311	−0.00340	−0.00731	−0.01665	−0.02212	−0.00827
	0.5	−0.6895	0.0639	−0.0999	−0.1610	0.00522	−0.00415	−0.00629	−0.02158	−0.02187	−0.01072
	0.6	−0.6738	+0.0277	−0.1102	−0.1679	0.00789	−0.00494	−0.00520	−0.02653	−0.02167	−0.01315
	0.7	−0.6647	−0.0060	−0.1176	−0.1761	0.01113	−0.00580	−0.00402	−0.03155	−0.02147	−0.01559
	0.8	−0.6602	−0.0374	−0.1231	−0.1855	0.01494	−0.00678	−0.00278	−0.03663	−0.02127	−0.01802
	0.9	−0.6593	−0.0669	−0.1272	−0.1960	0.01929	−0.00788	−0.00146	−0.04179	−0.02107	−0.02045
	1.0	−0.6608	−0.0944	−0.1303	−0.2072	0.02426	−0.00911	−0.00005	−0.04703	−0.02088	−0.02286
$\beta = 0.50$	0	−1.2697	0	0.1644	0	0	0	−0.01468	0	−0.02714	0
	0.1	−0.9920	0.2428	+0.0216	−0.1514	0	−0.00115	−0.01167	−0.00249	−0.02547	−0.00107
	0.2	−0.8407	0.2329	−0.0602	−0.1726	0.00053	−0.00203	−0.00999	−0.00750	−0.02464	−0.00361
	0.3	−0.7643	0.1981	−0.1049	−0.1793	0.00166	−0.00283	−0.00886	−0.01283	−0.02426	−0.00627
	0.4	−0.7208	0.1626	−0.1339	−0.1848	0.00340	−0.00367	−0.00792	−0.01823	−0.02406	−0.00892
	0.5	−0.6958	0.1313	−0.1545	−0.1916	0.00575	−0.00456	−0.00704	−0.02367	−0.02398	−0.01153
	0.6	−0.6819	0.1051	−0.1707	−0.2001	0.00871	−0.00560	−0.00619	−0.02925	−0.02395	−0.01411
	0.7	−0.6750	0.0835	−0.1846	−0.2099	0.01229	−0.00677	−0.00537	−0.03492	−0.02398	−0.01665
	0.8	−0.6726	0.0663	−0.1975	−0.2208	0.01649	−0.00823	−0.00461	−0.04073	−0.02405	−0.01917
	0.9	−0.6734	0.0534	−0.2098	−0.2323	0.02133	−0.00997	−0.00395	−0.04662	−0.02414	−0.02165
	1.0	−0.6757	0.0446	−0.2218	−0.2442	0.02679	−0.01208	−0.00342	−0.05260	−0.02426	−0.02409

TABLE 8 (continued).

	ω	k_c'	k_c''	m_c'	m_c''	n_a'	n_a''	n_b'	n_b''	n_c'	n_c''
$\beta = 0.60$	0	— 1.3745	0	+ 0.1780	0	0	0	— 0.01590	0	— 0.02938	0
	0.1	— 1.0223	0.2966	— 0.0063	— 0.1806	— 0.00001	— 0.00123	— 0.01226	— 0.00261	— 0.02738	— 0.00111
	0.2	— 0.8505	0.2873	— 0.1034	— 0.2001	+ 0.00059	— 0.00213	— 0.01051	— 0.00823	— 0.02656	— 0.00390
	0.3	— 0.7641	0.2541	— 0.1588	— 0.2037	0.00186	— 0.00302	— 0.00946	— 0.01406	— 0.02630	— 0.00678
	0.4	— 0.7157	0.2242	— 0.1952	— 0.2068	0.00377	— 0.00398	— 0.00866	— 0.02003	— 0.02626	— 0.00959
	0.5	— 0.6868	0.2016	— 0.2254	— 0.2106	0.00636	— 0.00508	— 0.00802	— 0.02610	— 0.02638	— 0.01233
	0.6	— 0.6677	0.1864	— 0.2509	— 0.2152	0.00961	— 0.00640	— 0.00753	— 0.03227	— 0.02660	— 0.01497
	0.7	— 0.6538	0.1777	— 0.2748	— 0.2195	0.01350	— 0.00804	— 0.00727	— 0.03859	— 0.02687	— 0.01754
	0.8	— 0.6411	0.1747	— 0.2980	— 0.2226	0.01802	— 0.01008	— 0.00729	— 0.04495	— 0.02719	— 0.02001
	0.9	— 0.6274	0.1760	— 0.3208	— 0.2237	0.02312	— 0.01263	— 0.00762	— 0.05129	— 0.02753	— 0.02236
	1.0	— 0.6108	0.1801	— 0.3430	— 0.2223	0.02870	— 0.01578	— 0.00828	— 0.05754	— 0.02782	— 0.02467
$\beta = 0.70$	0	— 1.5398	0	+ 0.1994	0	0	0	— 0.01781	0	— 0.03291	0
	0.1	— 1.0583	0.3818	— 0.0579	— 0.2248	— 0.00001	— 0.00131	— 0.01317	— 0.00291	— 0.03036	— 0.00120
	0.2	— 0.8488	0.3660	— 0.1840	— 0.2327	+ 0.00071	— 0.00232	— 0.01140	— 0.00942	— 0.02964	— 0.00440
	0.3	— 0.7455	0.3332	— 0.2565	— 0.2236	0.00217	— 0.00336	— 0.01050	— 0.01615	— 0.02962	— 0.00753
	0.4	— 0.6834	0.3106	— 0.3089	— 0.2124	0.00437	— 0.00454	— 0.01007	— 0.02295	— 0.02994	— 0.01048
	0.5	— 0.6375	0.2972	— 0.3517	— 0.1979	0.00728	— 0.00603	— 0.01003	— 0.02988	— 0.03039	— 0.01324
	0.6	— 0.5963	0.2904	— 0.3876	— 0.1785	0.01086	— 0.00792	— 0.01045	— 0.03685	— 0.03093	— 0.01578
	0.7	— 0.5540	0.2850	— 0.4170	— 0.1535	0.01502	— 0.01034	— 0.01137	— 0.04372	— 0.03143	— 0.01813
	0.8	— 0.5089	0.2765	— 0.4377	— 0.1233	0.01963	— 0.01335	— 0.01275	— 0.05020	— 0.03183	— 0.02035
	0.9	— 0.4620	0.2606	— 0.4481	— 0.0901	0.02453	— 0.01700	— 0.01443	— 0.05617	— 0.03210	— 0.02252
	1.0	— 0.4167	0.2349	— 0.4478	— 0.0557	0.02972	— 0.02123	— 0.01617	— 0.06163	— 0.03220	— 0.02473
$\beta = 0.80$	0	— 1.8327	0	+ 0.2373	0	0	0	— 0.02120	0	— 0.03917	0
	0.1	— 1.0645	0.5227	— 0.1761	— 0.2882	0.00001	— 0.00146	— 0.01467	— 0.00365	— 0.03564	— 0.00145
	0.2	— 0.8123	0.4810	— 0.3526	— 0.2484	0.00095	— 0.00266	— 0.01311	— 0.01177	— 0.03535	— 0.00522
	0.3	— 0.6658	0.4388	— 0.4475	— 0.1842	0.00273	— 0.00406	— 0.01289	— 0.01995	— 0.03596	— 0.00847
	0.4	— 0.5658	0.4026	— 0.5013	— 0.1067	0.00531	— 0.00582	— 0.01360	— 0.02804	— 0.03682	— 0.01114
	0.5	— 0.4798	0.3617	— 0.5159	— 0.0226	0.00852	— 0.00812	— 0.01515	— 0.03577	— 0.03752	— 0.01340
	0.6	— 0.4106	0.3056	— 0.4914	+ 0.0527	0.01218	— 0.01100	— 0.01728	— 0.04284	— 0.03790	— 0.01554
	0.7	— 0.3663	0.2378	— 0.4383	0.1027	0.01618	— 0.01440	— 0.01953	— 0.04916	— 0.03803	— 0.01790
	0.8	— 0.3503	0.1685	— 0.3761	0.1205	0.02051	— 0.01825	— 0.02152	— 0.05492	— 0.03819	— 0.02066
	0.9	— 0.3607	0.1147	— 0.3169	0.1074	0.02524	— 0.02271	— 0.02347	— 0.06060	— 0.03871	— 0.02359

TABLE 9. Coefficients for $\tau = 0.25$.

	ω	k_c'	k_c''	m_c'	m_c''	n_a'	n_a''	n_b'	n_b''	n_c'	n_c''
$\beta = 0$	0	− 1.2180	0	0.1955	0	0	0	− 0.02249	0	− 0.03755	0
	0.1	− 1.0200	0.1559	0.0968	− 0.1113	0.00002	− 0.00188	− 0.01874	− 0.00395	− 0.03528	− 0.00206
	0.2	− 0.9002	0.1305	0.0380	− 0.1319	0.00075	− 0.00327	− 0.01617	− 0.01118	− 0.03378	− 0.00617
	0.3	− 0.8285	0.0773	+ 0.0039	− 0.1387	0.00240	− 0.00449	− 0.01414	− 0.01888	− 0.03272	− 0.01060
	0.4	− 0.7821	+ 0.0194	− 0.0167	− 0.1431	0.00493	− 0.00562	− 0.01229	− 0.02668	− 0.03186	− 0.01507
	0.5	− 0.7494	− 0.0378	− 0.0298	− 0.1478	0.00832	− 0.00672	− 0.01033	− 0.03443	− 0.03105	− 0.01953
	0.6	− 0.7248	− 0.0930	− 0.0382	− 0.1535	0.01257	− 0.00782	− 0.00825	− 0.04216	− 0.03022	− 0.02398
	0.7	− 0.7049	− 0.1464	− 0.0436	− 0.1603	0.01765	− 0.00889	− 0.00594	− 0.04985	− 0.02936	− 0.02841
	0.8	− 0.6879	− 0.1978	− 0.0467	− 0.1679	0.02357	− 0.00998	− 0.00338	− 0.05750	− 0.02842	− 0.03281
	0.9	− 0.6727	− 0.2477	− 0.0483	− 0.1762	0.03029	− 0.01105	− 0.00055	− 0.06512	− 0.02742	− 0.03719
	1.0	− 0.6585	− 0.2964	− 0.0486	− 0.1852	0.03783	− 0.01214	+ 0.00258	− 0.07272	− 0.02632	− 0.04156
$\beta = 0.35$	0	− 1.3002	0	0.2087	0	0	0	− 0.02403	0	− 0.04009	0
	0.1	− 1.0576	0.2003	0.0860	− 0.1368	− 0.00002	− 0.00195	− 0.01961	− 0.00402	− 0.03739	− 0.00206
	0.2	− 0.9194	0.1792	+ 0.0151	− 0.1616	+ 0.00079	− 0.00342	− 0.01682	− 0.01181	− 0.03582	− 0.00648
	0.3	− 0.8433	0.1291	− 0.0245	− 0.1711	0.00255	− 0.00471	− 0.01488	− 0.02013	− 0.03485	− 0.01122
	0.4	− 0.7984	0.0756	− 0.0484	− 0.1789	0.00531	− 0.00601	− 0.01316	− 0.02857	− 0.03416	− 0.01599
	0.5	− 0.7710	+ 0.0241	− 0.0638	− 0.1876	0.00896	− 0.00734	− 0.01150	− 0.03706	− 0.03359	− 0.02074
	0.6	− 0.7543	− 0.0245	− 0.0737	− 0.1979	0.01354	− 0.00876	− 0.00975	− 0.04560	− 0.03308	− 0.02547
	0.7	− 0.7448	− 0.0705	− 0.0804	− 0.2097	0.01913	− 0.01029	− 0.00787	− 0.05426	− 0.03256	− 0.03022
	0.8	− 0.7403	− 0.1142	− 0.0848	− 0.2229	0.02568	− 0.01205	− 0.00589	− 0.06302	− 0.03204	− 0.03496
	0.9	− 0.7400	− 0.1559	− 0.0875	− 0.2374	0.03319	− 0.01401	− 0.00382	− 0.07191	− 0.03149	− 0.03970
	1.0	− 0.7423	− 0.1958	− 0.0890	− 0.2529	0.04176	− 0.01620	− 0.00164	− 0.08098	− 0.03094	− 0.0444[illegible]
$\beta = 0.50$	0	− 1.4064	0	0.2257	0	0	0	− 0.02596	0	− 0.04336	0
	0.1	− 1.1014	0.2562	+ 0.0690	− 0.1689	− 0.00003	− 0.00204	− 0.02066	− 0.00415	− 0.04010	− 0.00205
	0.2	− 0.9370	0.2353	− 0.0197	− 0.1950	+ 0.00087	− 0.00359	− 0.01773	− 0.01276	− 0.03845	− 0.00696
	0.3	− 0.8550	0.1878	− 0.0674	− 0.2059	0.00282	− 0.00501	− 0.01584	− 0.02194	− 0.03766	− 0.01211
	0.4	− 0.8093	0.1398	− 0.0978	− 0.2159	0.00579	− 0.00649	− 0.01431	− 0.03124	− 0.03721	− 0.01726
	0.5	− 0.7843	0.0964	− 0.1188	− 0.2276	0.00983	− 0.00809	− 0.01294	− 0.04063	− 0.03697	− 0.02234
	0.6	− 0.7718	0.0587	− 0.1350	− 0.2415	0.01492	− 0.00995	− 0.01166	− 0.05025	− 0.03681	− 0.02738
	0.7	− 0.7676	+ 0.0261	− 0.1486	− 0.2573	0.02108	− 0.01206	− 0.01048	− 0.06002	− 0.03677	− 0.03236
	0.8	− 0.7689	− 0.0016	− 0.1611	− 0.2746	0.02829	− 0.01467	− 0.00945	− 0.07003	− 0.03680	− 0.03731
	0.9	− 0.7746	− 0.0243	− 0.1731	− 0.2931	0.03662	− 0.01781	− 0.00862	− 0.08018	− 0.03688	− 0.04223
	1.0	− 0.7829	− 0.0422	− 0.1849	− 0.3123	0.04601	− 0.02161	− 0.00808	− 0.09049	− 0.03702	− 0.04707

F 106

TABLE 9 (continued).

	ω	k_c'	k_c''	m_c'	m_c''	n_a'	n_a''	n_b'	n_b''	n_c'	n_c''
$\beta = 0.60$	0	− 1.5225	0	0.2444	0	0	0	− 0.02813	0	− 0.04694	0
	0.1	− 1.1360	0.3145	+ 0.0422	− 0.2020	− 0.00005	− 0.00217	− 0.02171	− 0.00433	− 0.04302	− 0.00211
	0.2	− 0.9500	0.2940	− 0.0630	− 0.2279	+ 0.00098	− 0.00376	− 0.01867	− 0.01398	− 0.04140	− 0.00752
	0.3	− 0.8583	0.2482	− 0.1222	− 0.2372	0.00314	− 0.00535	− 0.01693	− 0.02402	− 0.04083	− 0.01309
	0.4	− 0.8091	0.2066	− 0.1619	− 0.2466	0.00644	− 0.00707	− 0.01570	− 0.03430	− 0.04069	− 0.01857
	0.5	− 0.7819	0.1734	− 0.1927	− 0.2575	0.01085	− 0.00903	− 0.01481	− 0.04475	− 0.04087	− 0.02392
	0.6	− 0.7664	0.1489	− 0.2199	− 0.2699	0.01640	− 0.01141	− 0.01426	− 0.05537	− 0.04122	− 0.02910
	0.7	− 0.7577	0.1324	− 0.2459	− 0.2827	0.02310	− 0.01436	− 0.01415	− 0.06624	− 0.04172	− 0.03417
	0.8	− 0.7510	0.1233	− 0.2718	− 0.2947	0.03081	− 0.01805	− 0.01459	− 0.07716	− 0.04233	− 0.03906
	0.9	− 0.7440	0.1207	− 0.2984	− 0.3049	0.03952	− 0.02265	− 0.01563	− 0.08804	− 0.04300	− 0.04374
	1.0	− 0.7345	0.1228	− 0.3256	− 0.3124	0.04900	− 0.02836	− 0.01733	− 0.09873	− 0.04364	− 0.04827
$\beta = 0.70$	0	− 1.7056	0	+ 0.2737	0	0	0	− 0.03150	0	− 0.05258	0
	0.1	− 1.1773	0.4084	− 0.0086	− 0.2534	− 0.00005	− 0.00232	− 0.02331	− 0.00478	− 0.04758	− 0.00227
	0.2	− 0.9520	0.3796	− 0.1453	− 0.2692	+ 0.00117	− 0.00410	− 0.02027	− 0.01596	− 0.04614	− 0.00846
	0.3	− 0.8443	0.3347	− 0.2238	− 0.2682	0.00366	− 0.00595	− 0.01887	− 0.02753	− 0.04604	− 0.01455
	0.4	− 0.7826	0.3030	− 0.2815	− 0.2663	0.00740	− 0.00807	− 0.01838	− 0.03922	− 0.04662	− 0.02033
	0.5	− 0.7398	0.2829	− 0.3304	− 0.2617	0.01236	− 0.01076	− 0.01867	− 0.05111	− 0.04751	− 0.02574
	0.6	− 0.7027	0.2725	− 0.3741	− 0.2520	0.01846	− 0.01419	− 0.01984	− 0.06304	− 0.04860	− 0.03076
	0.7	− 0.6643	0.2666	− 0.4132	− 0.2356	0.02549	− 0.01858	− 0.02198	− 0.07474	− 0.04971	− 0.03537
	0.8	− 0.6212	0.2600	− 0.4454	− 0.2119	0.03326	− 0.02404	− 0.02501	− 0.08569	− 0.05068	− 0.03966
	0.9	− 0.5735	0.2476	− 0.4682	− 0.1822	0.04142	− 0.03065	− 0.02860	− 0.09575	− 0.05140	− 0.04373
	1.0	− 0.5238	0.2255	− 0.4800	− 0.1483	0.04996	− 0.03830	− 0.03238	− 0.10479	− 0.05179	− 0.04778
$\beta = 0.80$	0	− 2.0300	0	+ 0.3258	0	0	0	− 0.03750	0	− 0.06258	0
	0.1	− 1.1921	0.5606	− 0.1278	− 0.3284	− 0.00002	− 0.00258	− 0.02598	− 0.00597	− 0.05565	− 0.00271
	0.2	− 0.9189	0.5064	− 0.3213	− 0.3003	+ 0.00156	− 0.00468	− 0.02337	− 0.01988	− 0.05499	− 0.01001
	0.3	− 0.7680	0.4559	− 0.4308	− 0.2477	0.00458	− 0.00720	− 0.02332	− 0.03387	− 0.05618	− 0.01639
	0.4	− 0.6659	0.4166	− 0.5017	− 0.1794	0.00891	− 0.01038	− 0.02505	− 0.04766	− 0.05794	− 0.02166
	0.5	− 0.5762	0.3761	− 0.5358	− 0.0985	0.01427	− 0.01455	− 0.02837	− 0.06065	− 0.05956	− 0.02602
	0.6	− 0.4993	0.3207	− 0.5295	− 0.0184	0.02029	− 0.01978	− 0.03284	− 0.07240	− 0.06069	− 0.02996
	0.7	− 0.4437	0.2494	− 0.4888	+ 0.0430	0.02679	− 0.02593	− 0.03755	− 0.08270	− 0.06108	− 0.03410
	0.8	− 0.4155	0.1706	− 0.4301	0.0752	0.03371	− 0.03296	− 0.04183	− 0.09192	− 0.06144	− 0.03889
	0.9	− 0.4199	0.1019	− 0.3671	0.0732	0.04117	− 0.04096	− 0.04611	− 0.10087	− 0.06239	− 0.04395

TABLE 10. Coefficients for $\tau = 0.3$.

	ω	k_c'	k_c''	m_c'	m_c''	n_a'	n_a''	n_b'	n_b''	n_c'	n_c''
$\beta = 0$	0	— 1.3215	0	0.2523	0	0	0	— 0.03595	0	— 0.05531	0
	0.1	— 1.1081	0.1575	0.1462	— 0.1203	0.00001	— 0.00299	— 0.02999	— 0.00599	— 0.05138	— 0.00353
	0.2	— 0.9794	0.1201	0.0834	— 0.1432	0.00114	— 0.00523	— 0.02590	— 0.01722	— 0.04877	— 0.01058
	0.3	— 0.9022	+ 0.0534	+ 0.0476	— 0.1514	0.00369	— 0.00717	— 0.02277	— 0.02922	— 0.04688	— 0.01814
	0.4	— 0.8516	— 0.0180	— 0.0261	— 0.1572	0.00762	— 0.00899	— 0.01991	— 0.04133	— 0.04528	— 0.02579
	0.5	— 0.8153	— 0.0886	+ 0.0129	— 0.1635	0.01290	— 0.01075	— 0.01700	— 0.05342	— 0.04373	— 0.03343
	0.6	— 0.7871	— 0.1570	+ 0.0048	— 0.1709	0.01951	— 0.01249	— 0.01388	— 0.06544	— 0.04212	— 0.04102
	0.7	— 0.7635	— 0.2233	+ 0.0001	— 0.1794	0.02741	— 0.01421	— 0.01044	— 0.07741	— 0.04041	— 0.04858
	0.8	— 0.7427	— 0.2875	— 0.0022	— 0.1888	0.03662	— 0.01594	— 0.00664	— 0.08932	— 0.03854	— 0.05610
	0.9	— 0.7233	— 0.3502	— 0.0026	— 0.1990	0.04709	— 0.01766	— 0.00244	— 0.10118	— 0.03650	— 0.06359
	1.0	— 0.7046	— 0.4114	— 0.0015	— 0.2100	0.05884	— 0.01939	+ 0.00218	— 0.11301	— 0.03428	— 0.07106
$\beta = 0.35$	0	— 1.1407	0	0.2694	0	0	0	— 0.03838	0	— 0.05905	0
	0.1	— 1.1495	0.2049	0.1375	— 0.1484	— 0.00002	— 0.00312	— 0.03135	— 0.00602	— 0.05440	— 0.00348
	0.2	— 1.0017	0.1716	0.0621	— 0.1762	+ 0.00118	— 0.00545	— 0.02699	— 0.01815	— 0.05165	— 0.01107
	0.3	— 0.9204	0.1078	+ 0.0206	— 0.1882	0.00392	— 0.00754	— 0.02399	— 0.03110	— 0.04990	— 0.01918
	0.4	— 0.8727	+ 0.0408	— 0.0038	— 0.1986	0.00815	— 0.00959	— 0.02142	— 0.04422	— 0.04862	— 0.02735
	0.5	— 0.8434	— 0.0244	— 0.0187	— 0.2101	0.01385	— 0.01173	— 0.01894	— 0.05744	— 0.04748	— 0.03552
	0.6	— 0.8255	— 0.0865	— 0.0278	— 0.2234	0.02101	— 0.01402	— 0.01641	— 0.07075	— 0.04638	— 0.04368
	0.7	— 0.8151	— 0.1460	— 0.0331	— 0.2384	0.02968	— 0.01652	— 0.01374	— 0.08422	— 0.04528	— 0.05184
	0.8	— 0.8102	— 0.2031	— 0.0359	— 0.2550	0.03986	— 0.01931	— 0.01091	— 0.09786	— 0.04414	— 0.06001
	0.9	— 0.8097	— 0.2583	— 0.0364	— 0.2731	0.05161	— 0.02248	— 0.00798	— 0.11172	— 0.04295	— 0.06820
	1.0	— 0.8122	— 0.3121	— 0.0356	— 0.2925	0.06487	— 0.02599	— 0.00495	— 0.12581	— 0.04168	— 0.07644
$\beta = 0.50$	0	— 1.5259	0	0.2914	0	0	0	— 0.04151	0	— 0.06387	0
	0.1	— 1.1978	0.2641	0.1229	— 0.1838	— 0.00006	— 0.00328	— 0.03303	— 0.00622	— 0.05827	— 0.00348
	0.2	— 1.0228	0.2307	+ 0.0288	— 0.2141	+ 0.00131	— 0.00573	— 0.02842	— 0.01961	— 0.05538	— 0.01188
	0.3	— 0.9362	0.1694	— 0.0208	— 0.2289	0.00431	— 0.00801	— 0.02554	— 0.03385	— 0.05390	— 0.02069
	0.4	— 0.8891	0.1078	— 0.0515	— 0.2430	0.00895	— 0.01039	— 0.02332	— 0.04830	— 0.05301	— 0.02952
	0.5	— 0.8643	0.0512	— 0.0721	— 0.2594	0.01521	— 0.01301	— 0.02141	— 0.06296	— 0.05243	— 0.03829
	0.6	— 0.8533	+ 0.0005	— 0.0875	— 0.2786	0.02309	— 0.01596	— 0.01970	— 0.07786	— 0.05204	— 0.04701
	0.7	— 0.8517	— 0.0447	— 0.0997	— 0.3001	0.03264	— 0.01944	— 0.01821	— 0.09308	— 0.05179	— 0.05568
	0.8	— 0.8569	— 0.0846	— 0.1106	— 0.3238	0.04383	— 0.02362	— 0.01703	— 0.10862	— 0.05166	— 0.06434
	0.9	— 0.8673	— 0.1191	— 0.1212	— 0.3492	0.05670	— 0.02869	— 0.01627	— 0.12442	— 0.05164	— 0.07295
	1.0	— 0.8818	— 0.1482	— 0.1317	— 0.3760	0.07119	— 0.03488	— 0.01602	— 0.14043	— 0.05174	— 0.08150

TABLE 10 (continued).

	ω	k_c'	k_c''	m_c'	m_c''	n_a'	n_a''	n_b'	n_b''	n_c'	n_c''
$\beta = 0.60$	0	— 1.6519	0	0.3154	0	0	0	— 0.04494	0	— 0.06914	0
	0.1	— 1.2365	0.3260	+ 0.0983	— 0.2204	— 0.00009	— 0.00345	— 0.03471	— 0.00648	— 0.06237	— 0.00356
	0.2	— 1.0390	0.2927	— 0.0132	— 0.2519	+ 0.00145	— 0.00602	— 0.02995	— 0.02139	— 0.05952	— 0.01283
	0.3	— 0.9435	0.2331	— 0.0748	— 0.2669	0.00478	— 0.00855	— 0.02734	— 0.03705	— 0.05843	— 0.02237
	0.4	— 0.8944	0.1785	— 0.1155	— 0.2824	0.00988	— 0.01132	— 0.02566	— 0.05296	— 0.05808	— 0.03180
	0.5	— 0.8694	0.1333	— 0.1467	— 0.3007	0.01672	— 0.01450	— 0.02458	— 0.06917	— 0.05829	— 0.04106
	0.6	— 0.8583	0.0978	— 0.1741	— 0.3211	0.02529	— 0.01837	— 0.02421	— 0.08570	— 0.05879	— 0.05012
	0.7	— 0.8553	0.0716	— 0.2008	— 0.3428	0.03560	— 0.02315	— 0.02456	— 0.10252	— 0.05960	— 0.05900
	0.8	— 0.8558	0.0545	— 0.2279	— 0.3645	0.04752	— 0.02915	— 0.02586	— 0.11945	— 0.06063	— 0.06761
	0.9	— 0.8568	0.0457	— 0.2567	— 0.3848	0.06089	— 0.03665	— 0.02822	— 0.13625	— 0.06183	— 0.07592
	1.0	— 0.8558	0.0440	— 0.2876	— 0.4025	0.07543	— 0.04592	— 0.03169	— 0.15260	— 0.06312	— 0.08388
$\beta = 0.70$	0	— 1.8505	0	0.3533	0	0	0	— 0.05034	0	— 0.07746	0
	0.1	— 1.2840	0.4245	+ 0.0505	— 0.2772	— 0.00011	— 0.00369	— 0.03725	— 0.00708	— 0.06878	— 0.00379
	0.2	— 1.0452	0.3834	— 0.0945	— 0.3018	+ 0.00172	— 0.00653	— 0.03252	— 0.02443	— 0.06622	— 0.01441
	0.3	— 0.9349	0.3257	— 0.1774	— 0.3096	0.00556	— 0.00951	— 0.03058	— 0.04235	— 0.06597	— 0.02491
	0.4	— 0.8756	0.2830	— 0.2386	— 0.3175	0.01134	— 0.01299	— 0.03020	— 0.06049	— 0.06686	— 0.03492
	0.5	— 0.8374	0.2547	— 0.2917	— 0.3240	0.01895	— 0.01732	— 0.03120	— 0.07885	— 0.06841	— 0.04436
	0.6	— 0.8064	0.2390	— 0.3416	— 0.3258	0.02826	— 0.02290	— 0.03372	— 0.09720	— 0.07040	— 0.05318
	0.7	— 0.7742	0.2313	— 0.3891	— 0.3205	0.03900	— 0.03004	— 0.03792	— 0.11504	— 0.07256	— 0.06128
	0.8	— 0.7359	0.2261	— 0.4320	— 0.3060	0.05074	— 0.03896	— 0.04356	— 0.13175	— 0.07459	— 0.06874
	0.9	— 0.6902	0.2174	— 0.4673	— 0.2830	0.06305	— 0.04968	— 0.05020	— 0.14686	— 0.07625	— 0.07571
	1.0	— 0.6388	0.2003	— 0.4919	— 0.2534	0.07555	— 0.06209	— 0.05721	— 0.16011	— 0.07738	— 0.08246
$\beta = 0.80$	0	— 2.2025	0	+ 0.4205	0	0	0	— 0.05991	0	— 0.09219	0
	0.1	— 1.3128	0.5882	— 0.0667	— 0.3642	— 0.00008	— 0.00412	— 0.04160	— 0.00880	— 0.08020	— 0.00450
	0.2	— 1.0147	0.5205	— 0.2731	— 0.3492	+ 0.00231	— 0.00753	— 0.03760	— 0.03030	— 0.07880	— 0.01700
	0.3	— 0.8660	0.4603	— 0.3946	— 0.3109	0.00691	— 0.01149	— 0.03800	— 0.05180	— 0.08090	— 0.02810
	0.4	— 0.7645	0.4180	— 0.4810	— 0.2559	0.01348	— 0.01667	— 0.04150	— 0.07290	— 0.08410	— 0.03740
	0.5	— 0.6746	0.3776	— 0.5348	— 0.1830	0.02149	— 0.02348	— 0.04760	— 0.09260	— 0.08730	— 0.04500
	0.6	— 0.5932	0.3250	— 0.5492	— 0.1030	0.03042	— 0.03195	— 0.05570	— 0.11000	— 0.08960	— 0.05160
	0.7	— 0.5273	0.2535	— 0.5258	— 0.0333	0.03984	— 0.04193	— 0.06420	— 0.12490	— 0.09090	— 0.05820
	0.8	— 0.4850	0.1684	— 0.4768	+ 0.0129	0.04965	— 0.05340	— 0.07200	— 0.13800	— 0.09160	— 0.06580
	0.9	— 0.4803	0.0868	— 0.4147	0.0248	0.06012	— 0.06609	— 0.07980	— 0.15040	— 0.09310	— 0.07390

F 110

C.C.L. Class: F 402

REPORT F. 147.

Influence of Compressibility on the Flutter speed of a Family of Rectangular Cantilever Wings with Aileron

by

J. IJFF, A. C. A. BOSSCHAART and A. I. VAN DE VOOREN.

Summary.

In this report diagrams are presented, showing for a family of rectangular wing-aileron systems the dimensionless flutter speed as function of the ratio between flexural and torsional resonance frequency.

The calculations have been performed for Mach numbers 0, 0.5 and 0.7. The relative mass parameter, the positions of the elastic and inertia axes, the aileron static balance, the control-cable stiffness and the structural damping have been varied systematically.

For binary wing-aileron flutter the allowed static unbalance of the aileron has been calculated.

Contents.

This investigation has been performed by order of the Netherlands Aircraft Development Board (N.I.V.).

1 Introduction.

This paper is to be considered as a continuation of report F. 118 (ref. 1), where the influence of compressibility on the flutter speed of a family of rectangular wings has been investigated. In the present report diagrams are presented showing the influence of compressibility on the flutter speed of the same family of rectangular wings, but this time provided with an aileron on the outer half of the span. For the greater part of the calculations the aileron has been assumed to be statically balanced and freely rotating, but a few calculations have also been made for an unbalanced aileron while some other calculations were performed for an aileron which was elastically restrained by the control cables. The unbalanced aileron has been investigated more completely for the cases of binary flutter, viz. wing bending-aileron and wing torsion-aileron.

The aerodynamic forces, which were used, have been obtained by aid of strip theory from the results of the two-dimensional subsonic flow theory for an oscillating aerofoil which has been published in ref. 2. The present calculations were started before it had been recognized that these results were subject to a small numerical error. This error does, however, not greatly affect the flutter calculations as has been checked by the computation of a single case with the improved numerical results.

2 List of symbols.

b — semispan.
c — wing chord.
l — semi-chord.
ξl — distance between midpoint of chord and elastic axis (positive if elastic axis is ahead).
σl — distance between elastic axis and inertia axis (positive if elastic axis is ahead).
$\sigma_r l$ — distance between aileron hinge axis and aileron inertia axis.
τ — ratio between aileron and wing-chord.
$\mu \pi \rho l^2$ — mass of wing with aileron per unit span.
$\mu_r \pi \rho l^2$ — mass of aileron with balance per unit span.
κ — radius of gyration of wing with aileron about inertia axis.
$\kappa_r l$ — radius of gyration aileron with balance about inertia axis.
zl — vertical movement of wing elastic axis due to bending.
φ — torsional movement of wing about elastic axis
γ — aileron deflection from horizontal level.
(subscript 1 for deformation functions)

ν — frequency (rad/sec).
ν_B — uncoupled frequency of wing bending in vacuum (rad/sec).
ν_T — uncoupled frequency of wing torsion about the elastic axis in vacuum (rad/sec).
ν_c — uncoupled frequency of aileron deflection in vacuum (rad/sec).
ρ — air density.
ω — reduced frequency $\frac{\nu l}{v}$
h — structural damping factor.

3 Procedure.

The calculations have been performed for a rectangular wing, rigidly fixed at the root and fitted with an aileron without aerodynamic balance and extending over the outer half of the wing.

Bending and torsion have been determined by one prescribed deformation function each, which is given in table 1. The displacement of the aileron has been determined by the assumption that it is torsionally rigid and hence makes an angle γ with its mean position which is the same for all sections. The bending of the aileron is such that wing and aileron have the same displacements at the hinge axis.

In this way results are obtained which have the physical meaning that for the chosen value of the reduced frequency ω those values of the ratio $\frac{\nu_B^2}{\nu_T^2}$ are determined for which the wing can perform a harmonic oscillation.

Mathematically, it is possible that a negative value of $\frac{\nu_B^2}{\nu_T^2}$ will be found, but it will be clear that no physical meaning can be ascribed to negative values of $\frac{\nu_B^2}{\nu_T^2}$. In actual wing constructions the values of $\frac{\nu_B^2}{\nu_T^2}$ will range from 0 to 1.

If the aileron is elastically restrained by control cables the unknowns which are solved from the flutter determinant are $\frac{\nu_c^2}{\nu_T^2}$ and $\frac{\nu^2}{\nu_c^2}$, where ν_c denotes the natural frequency of the aileron in vacuum. In this case the flexural stiffness has been neglected, but the deformation function for the fundamental mode of wing bending has been retained. Although the neglect of the flexural stiffness may give rise to small numerical differences, the qualitative influence of the control cable stiffness will be obtained in this way (see also ref. 4 where a comparison between the cases that the flexural stiffness has been retained and that it has been neglected, has been made for incompressible flow).

TABLE 1.

Deformation functions.

spar station $\frac{y}{b}$	0	$^1/_8$	$^2/_8$	$^3/_8$	$^1/_2$	$^5/_8$	$^6/_8$	$^7/_8$	1
wing bending z	0	0.0169	0.0682	0.1547	0.2752	0.4268	0.6039	0.7983	1
wing torsion φ	0	0.1490	0.3170	0.4890	0.6511	0.7921	0.9029	0.9745	1
aileron deflection γ	0	0	0	0	0/1	1	1	1	1

In the case of elastic control cables it is assumed that the control column is fixed. In the section $y = \frac{3}{4}\, b$ aileron and wing are then subject to equal but opposite elastic moments which are proportional to the relative deflection of the aileron with regard to the wing in that section, i.e. to $\gamma - \varphi$ ($\frac{3}{4}\, b$).

The equations of motion have been solved by aid of the Galerkin procedure. The weight functions have been taken equal to the deformation functions (Rayleigh-Ritz analysis). In this way the equation referring to the aileron expresses the equilibrium of moments about the aileron hinge axis.

The flutter determinant has been solved for several assumed values of the reduced frequency ω with $\frac{\nu_B^2}{\nu_T^2}$ and $\frac{\nu^2}{\nu_B^2}$ as unknown quantities if the aileron is free to deflect. ν_B and ν_T are the uncoupled frequencies of the wing for bending and torsion in vacuum. The non-dimensional flutter speed then follows from the formula

$$\frac{2\,v}{\nu_T C} = \frac{1}{\omega} \sqrt{\frac{\nu_B^2}{\nu_T^2} \cdot \frac{\nu^2}{\nu_B^2}}\,.$$

The results of the calculations are presented in diagrams where the non-dimensional flutter speed $\frac{2\,v}{\nu_T C}$ has been plotted versus the ratio of natural frequencies $\left(\frac{\nu_B}{\nu_T}\right)^2$ or, in the case of elastic control cables, versus $\left(\frac{\nu_c}{\nu_T}\right)^2$.

The divergence and aileron reversal speeds have also been added in the diagrams. They were also calculated by aid of strip theory.

For the binary systems, where the influence of static balance of the aileron has been investigated no flutter speeds were calculated. It has been investigated which combinations of dimensionless static moment and dimensionless moment of inertia about the hinge axis make flutter impossible. Diagrams with these two quantities as coordinates show the boundaries between the stable and unstable regions.

4 Numerical data.

The calculations have been performed for rectangular wings whose values of the relative density parameter (μ) as well as the positions of the elastic axis (E.A.) and the inertia axis (I.A.) are constant along the span. The following 27 combinations have been investigated.

TABLE II.

Values of parameters.

E.A. I.A. μ	0.2 c 0.3 c 5	0.3 c 0.4 c 15	0.4 c 0.5 c 30

The values of E.A. and I.A. denote the backward position of the axis with regard to the leading edge.

The radius of gyration of the wing including the aileron, has been assumed to be 0.3 c for all positions of the inertia axis. The aileron moment of inertia (about its inertia axis) is determined by $\mu_r \kappa_r^2 = 0.05$. The ratio between aileron and wing chord is given by $\tau = 0.2$. The aileron is not aerodynamically balanced and has its hinge axis at the nose. Three values of the Mach number, viz. 0, 0.5 and 0.7 have been considered. The air density has been taken equal to ⅛ kg m^{-4} sec^2, which is standard value at sea level.

For the calculations referring to a *wing with free aileron*, all 27 cases have been investigated. The aileron has been assumed here to be statically balanced. No structural damping was introduced.

Some special calculations have been made in order to investigate the influences of structural damping and aileron static unbalance. These calculations refer to the three cases where $\mu = 5$, 15 and 30, while the position of the elastic axis is at 0.3 c and that of the inertia axis at 0.4 c. For each of these three cases three calculations were made, the parameters of which are given in table III.

TABLE III.

Values of parameters.

Aileron non-dimensional static moment $\mu_r \sigma_r$	0	0	0.04
Structural damping h	0.05	0.15	0

Since the damping has been introduced as hysteresis damping by multiplying all stiffnesses by $1 + ih$, the same amount of damping exists for wing bending and wing torsion, while the motion of the aileron is not restricted by any direct damping due to the lack of control cable stiffness.

In the case of the unbalanced aileron, the aileron moment of inertia about its hinge axis is determined by $\mu_r(\kappa_r^2 + \sigma_r^2) = 0.5$, while some minor approximations have been introduced, which are mentioned in Appendix I.

The calculations for a *wing with an elastically restrained aileron* have been limited to the same three cases for which the influences of structural damping and aileron unbalance were investigated, viz. $\mu = 5$, 15, 30. E.A. at 0.3 c, I.A. at 0.4 c.

Structural damping was assumed zero, while the aileron was statically balanced. In order to simplify the calculations the flexural stiffness has been neglected, but the fundamental wing bending mode was still assumed to approximate the bending deformation adequately.

For the binary system *wing bending-aileron* the only parameters which occur are $\left(\frac{\nu_c}{\nu_B}\right)^2$ and μ (see Appendix 2). If the aileron is left free, $\left(\frac{\nu_c}{\nu_B}\right)^2 = 0$. The stability region (but not the flutter speed) even becomes independent of μ. This case has been calculated. Moreover, results are presented for $\left(\frac{\nu_c}{\nu_B}\right)^2 = 3$ and $\mu = 15$.

For the binary system *wing torsion-aileron* the determining parameters are $\left(\frac{\nu_c}{\nu_T}\right)^2$, the position of the elastic axis as well as the moment of inertia about the elastic axis. The case which has been investigated is $\left(\frac{\nu_c}{\nu_T}\right)^2 = 0$, E.A. $= 0.3$ c. The value of the moment of inertia does not influence the stability region if the aileron is left free.

5 Results.

5.1 *Calculations for ternary systems.*

The results of the flutter calculations for the wing with *statically balanced* and *elastically unrestrained* aileron have been presented in figs 1 to 27 (structural damping zero). In these figures the non-dimensional flutter speed $\frac{2v}{\nu_T c}$ has been given as function of the ratio $\frac{\nu_B^2}{\nu_T^2}$, while the numbers added to the calculated points refer to the reduced frequency ω.

It is seen from these diagrams that for Mach numbers 0 and 0.5 the flutter speed $\frac{2v}{\nu_T c}$ is nearly always between 1.0 and 1.5. Apart from some irregular behaviour in the range $\left(\frac{\nu_B}{\nu_T}\right)^2$ between 0 and 1, this flutter speed is nearly independent of $\left(\frac{\nu_B}{\nu_T}\right)^2$ and in particular the corresponding curve has a horizontal asymptote. This asymptote indicates that the system will also be unstable if the flexural stiffness is infinitely large and hence the corresponding instability consists chiefly of *wing torsion-aileron* flutter.

While the influence of the Mach number is small if $M \leqslant 0.5$, the results for $M = 0.7$ are different.

For this Mach number the horizontal asymptote has disappeared, indicating that the system is not liable to pure torsion-aileron flutter at higher Mach numbers. This has been confirmed by the separate results which will be presented for this binary system.

It is seen that the wing torsion-aileron instability disappears again at higher speeds if $\left(\frac{\nu_B}{\nu_T}\right)^2$ is larger than a certain value. For smaller values of $\left(\frac{\nu_B}{\nu_T}\right)^2$, including the range 0 to 1, the instability does not disappear but is changed into a bending torsion mode which agrees with that found for the wing alone (ref. 1). This can be verified especially in the case of large values of μ, where the bending torsion flutter speed is rather high (for instance, figs 6 and 9).

Some interaction between bending-torsion flutter and torsion-aileron flutter occurs for values of $\left(\frac{\nu_B}{\nu_T}\right)^2$ near 0.5 and is responsible for a sharp local increase of the flutter speed near this value of $\left(\frac{\nu_B}{\nu_T}\right)^2$. This local increase exists only for $M=0$ and 0.5.

Pure bending-aileron flutter does not exist for statically balanced ailerons. This type of flutter would make that the curve denoting the lower flutter speed would have a cusp in the origin (see figs 34, 36, 38).

While for small values of $\left(\frac{\nu_B}{\nu_T}\right)^2$, viz. near 0.1, μ has little influence if M is equal to 0 or 0.5, μ becomes a more important parameter if $M=0.7$. In this case there is an increase of flutter speed with μ, which is similar to the influence of μ found for the wing alone at all Mach numbers (ref. 1).

The positions of the elastic and inertia axes appear to be of minor importance in the present investigation, where the lower flutter speed is chiefly determined by the aileron. For the higher flutter speeds results are narrowly connected with those of ref. 1.

It has been shown in Appendix 1, that if $\omega \to 0$, one of the points which are found in this type of diagrams, approaches the point $\left(\frac{\nu_B}{\nu_T}\right)^2=0$, $\frac{2v}{\nu_T c}$ = divergence speed, while the other point approaches $\left(\frac{\nu_B}{\nu_T}\right)^2=0$ and a value of the speed which is higher than the divergence speed (see eq. (A 1.7)).

As shown in the figures (28) to (33), the influence of the *structural damping* consists mainly in a shrinking of the unstable region. It is seen that for incompressible flow pure wing torsion-aileron flutter disappears with less damping if μ is large than if μ is small.

Results for the *unbalanced aileron* are presented in figs 34 to 39. It is seen that pure wing torsion-aileron flutter is also possible at $M=0.7$ if the aileron is unbalanced. For $M=0$ there arises also pure wing bending-aileron flutter as is seen by the fact that the curve has a cusp at the origin.

These results are confirmed by the calculations for the binary cases, figs (43) to (45). It follows that if the unbalance of the aileron would still further be increased, bending aileron flutter would also become possible at $M=0.7$.

In the cases with elastically restrained aileron the results are presented in the figures (40) to (42) where the non-dimensional flutter speed $\frac{2v}{\nu_T c}$ has been given as function of the ratio $\frac{\nu_c^2}{\nu_T^2}$. The curve has a horizontal asymptote which indicates that wing bending-torsion flutter with $\nu_B=0$ occur, if the aileron is restrained infinitely. This agrees well with the results of ref. 1.

Moreover the points with $\nu_c=0$ correspond to the points $\nu_B=0$ of the foregoing calculations for elastically unrestrained aileron.

The deep minimum in the curve has been caused mainly by torsion-aileron flutter and will also exist if the bending stiffness would be infinitely large. The influence of the Mach number consists of a flattening-out of this minimum while the flutter speed increases with increasing Mach number.

This indicates again that torsion-aileron flutter will disappear at high Mach numbers. The curves for divergence speed and aileron reversal speed refer to $M=0$, but those for $M=0.5$ and $M=0.7$ can be easily obtained by multiplication of the speed by a factor $\sqrt{1-M^2}$.

5.2 *Calculations for binary systems.*

For the binary systems (figs 43 to 46) it has been investigated for a number of reduced frequencies which combinations of the static moment $\mu_r\sigma_r$ and the moment of inertia about the hinge axis $\mu_r(\varkappa_r^2+\tau_r^2)$ lead to harmonic oscillations. For each value of the reduced frequency a conic is obtained. The envelope of these curves divides the whole plane in a stable and an unstable region.

It is seen from fig. 43 and 44 that for *wing bending-aileron* flutter the allowed aileron static unbalance is nearly independent of the aileron moment of inertia provided the latter is larger than a certain limit depending upon the stiffness of the control cables.

Below this limit the allowed static unbalance of the aileron increases with decreasing moment of inertia (see fig. 45). This increase is even quicker for $M=0$ than for $M=0.7$.

Hence, while in general $M=0$ will limit the allowed unbalance, for small values of the aileron moment of inertia the opposite may occur. An example of this possibility has been given by WILLIAMS (ref. 3).

It has been shown in Appendix 2 that the conics in the diagrams of fig. 44—45 move parallel to the q-axis if the ratio ν_c/ν_B is changed. If this ratio is increased, the conics shift toward larger values of the moment of inertia.

The results are independent of μ if the aileron is unrestrained but depend upon μ for $\frac{\nu_c}{\nu_B}=0$. *This follows also from* Appendix 2.

The results for the binary system *wing torsion-aileron* are presented for $\frac{\nu_c}{\nu_T}=0$ only (fig. 46). In contrary with the wing bending-aileron case the allowed unbalance or required overbalance now depends upon the moment of inertia. It is a well-known fact that in the case of wing torsion-aileron the mass coupling is only eliminated by overbalancing the aileron and that this overbalance *must be larger if the aileron moment of inertia* becomes larger (the product of inertia of the aileron with regard to the elastic axis and the aileron hinge axis should vanish). In fig. 46 the compressibility appears to be favourable. However, for large values of ν_c/ν_T together with small values of the aileron moment of inertia the contrary effect will occur. This is in analogy to the wing bending-aileron results.

6 Conclusions.

1. The lowest flutter speed for a wing with statically *balanced aileron is nearly independent* of the Mach number if this remains smaller than or equal to 0.5. For $M=0.7$ an increase in flutter speed may occur. This is due to the fact that at higher values of the Mach number the aileron is less liable to flutter.
2. Flutter at $M=0.7$ is mainly wing flutter, while for $M=0$ and $M=0.5$ the aileron plays an important role unless the structural damping is large.
3. Concerning wing bending-aileron and wing torsion-aileron flutter it has been found that usually $M=0$ requires a more forward position of the aileron center of gravity than $M=0.7$. For large control cable stiffness and small aileron moment of inertia this position shifts especially for $M=0$ backward. This may result in giving $M=0.7$ the more critical conditions.

7 List of references.

1. IJFF, J. Influence of Compressibility on the Calculated Flexure-Torsion Flutterspeed of a Family of Rectangular Cantilever Wings. N.L.L. Report F. 118. 1953.
2. TIMMAN, R. and VOOREN, A. I. VAN DE. Theory of the Oscillating Wing with Aerodynamically Balanced Control Surface in a Two-Dimensional Subsonic, Compressible Flow. N.L.L. Report F. 54. 1949.
3. WILLIAMS, D. E. The Effect of Compressibility on Elevator Flutter. R.A.E. Techn. note Structures 142. 1953.
4. VOOREN, A. I. VAN DE. Diagrams of Flutter, Divergence and Aileron Reversal Speeds for Wings of Certain Standard Type. N.L.L. Report V. 1397. 1947.

APPENDIX 1.

The limiting case $\omega \to 0$.

It will be investigated in this Appendix which points of the curves in figs 1—39 are obtained if ω approaches 0.

The *Galerkin equations assume the following* form

$$\begin{gathered}q_1\left(U_{11}+L_{11}-\frac{1+ih}{\nu^2}E_{11}\right)+\\ +q_2(U_{12}+L_{12})+q_3(U_{13}+L_{13})=0\\[1ex] q_1(U_{12}+L_{21})+q_2\left(U_{22}+L_{22}-\frac{1+ih}{\nu^2}E_{22}\right)+\\ +q_3(U_{23}+L_{23})=0 \qquad \text{(A 1.1)}\\[1ex] q_1(U_{13}+L_{31})+q_2(U_{23}+L_{32})+\\ +q_3(U_{33}+L_{33})=0,\end{gathered}$$

where the first equation refers to wing bending, the second to wing torsion and the third equation to aileron rotation. In these equations the quantities U_{ik} denote the inertia terms, L_{ik} the aerodynamic terms and E_{ik} the elastic terms. Since the aileron is freely rotating, the elastic term E_{33} has been omitted. q_1, q_2 and q_3 are generalized coordinates corresponding to wing bending, wing torsion and aileron rotation respectively. The aerodynamic terms are given by

$$L_{11}=\frac{1}{\omega^2}\int_0^b k_a z_1^2\,dy$$

$$L_{12}=\frac{1}{\omega^2}\int_0^b \{k_a\xi+k_b-k_c\}\,z_1\varphi_1\,dy$$

$$L_{13}=\frac{1}{\omega^2}\int_0^b k_c z_1\gamma_1\,dy$$

$$L_{21}=\frac{1}{\omega^2}\int_0^b \{k_a\xi+m_a-n_a\}\,z_1\varphi_1\,dy$$

$$L_{22}=\frac{1}{\omega^2}\int_0^b \{k_a\xi^2+(m_a-n_a+k_b-k_c)\xi+ m_b-m_c-n_b+n_c\}\,\varphi_1^2 dy$$

$$L_{23}=\frac{1}{\omega^2}\int_0^b \{k_c\xi+m_c-n_c\}\,\varphi_1\gamma_1\,dy.$$

$$L_{31}=\frac{1}{\omega^2}\int_0^b n_a z_1\gamma_1\,dy$$

$$L_{32}=\frac{1}{\omega^2}\int_0^b \{n_a\xi+n_b-n_c\}\,\varphi_1\gamma_1\,dy$$

$$L_{33}=\frac{1}{\omega^2}\int_0^b n_c\gamma_1^2\,dy$$

where the aerodynamic coefficients are defined in accordance with Küssner, but with the mid-chord point as point of reference. ξl denotes the distance of the elastic axis ahead of the mid-chord axis.

Making use of the known formulae for the derivatives and performing the limit $\omega \to 0$, it is found that

$$\lim_{\omega \to 0} \frac{k_a'}{\omega^2}, \frac{m_a'}{\omega^2} \text{ and } \frac{n_a'}{\omega^2} = 0\,(ln\,\omega).$$

$$\lim_{\omega \to 0} \frac{k_a''}{\omega^2}, \frac{m_a''}{\omega^2} \text{ and } \frac{n_a''}{\omega^2} = 0\left(\frac{1}{\omega}\right)$$

$$\lim_{\omega \to 0} \frac{k_b'}{\omega^2}, \frac{m_b'}{\omega^2}, \frac{n_b'}{\omega^2}, \frac{k_c'}{\omega^2}, \frac{m_c'}{\omega^2} \text{ and } \frac{n_c'}{\omega^2} = 0\left(\frac{1}{\omega^2}\right)$$

$$\lim_{\omega \to 0} \frac{k_b''}{\omega^2}, \frac{m_b''}{\omega^2}, \frac{n_b''}{\omega^2}, \frac{k_c''}{\omega^2}, \frac{m_c''}{\omega^2} \text{ and } \frac{n_c''}{\omega^2} = 0\left(\frac{ln\,\omega}{\omega}\right).$$

In this way the order of all aerodynamic terms is known. In the evaluation of the determinant of the system (A 1.1)

$$\lambda = \frac{\nu_B^2}{\nu_T^2} \quad \text{and} \quad x = \frac{\nu^2}{\nu_B^2}$$

are taken as unknowns, where ν_B and ν_T are defined by

$$E_{11} = \nu_B^2 U_{11} \quad \text{and} \quad E_{22} = \nu_T^2 U_{22}.$$

Putting the complex flutter determinant equal to 0, two real equations are obtained. These equations can be written in the form

$$\left.\begin{aligned} &\{D'x^2 + (B' - hB'')x\}\lambda + \\ &+ \{(C' - hC'')x + (A' - 2hA'')\} = 0 \\ &\{D''x^2 + (B'' + hB')x\}\lambda + \\ &+ \{(C'' + hC')x + (A'' + 2hA')\} = 0 \end{aligned}\right\} \qquad (A\,1.2)$$

where the coefficients $A' \ldots D''$ depend upon the inertia and aerodynamic terms U_{ik} and L_{ik}. It can be shown that

$$\lim_{\omega \to 0} A' = 0\left(\frac{1}{\omega^2}\right) \qquad \lim_{\omega \to 0} A'' = 0\left(\frac{ln\,\omega}{\omega}\right)$$

$$\lim_{\omega \to 0} B' = 0\left(\frac{1}{\omega^4}\right) \qquad \lim_{\omega \to 0} B'' = 0\left(\frac{ln\,\omega}{\omega^3}\right)$$

$$\lim_{\omega \to 0} C' = \left(\frac{ln\,\omega}{\omega^2}\right) \qquad \lim_{\omega \to 0} C'' = 0\left(\frac{1}{\omega^3}\right)$$

$$\lim_{\omega \to 0} D' = 0\left(\frac{ln\,\omega}{\omega^4}\right) \qquad \lim_{\omega \to 0} D'' = 0\left(\frac{1}{\omega^5}\right).$$

Elimination of λ from the two equations (A 1.2) yields

$$ax^2 + bx + c = 0 \qquad (A\,1.3)$$

where

$$\begin{aligned} a &= C''D' - C'D'' + h(C'D' + C''D'') \\ b &= A''D' - A'D'' + 2h(A'D' + A''D'') - \\ &\quad - (1 + h^2)(B''C' - B'C'') \\ c &= -(1 + 2h^2)(A'B'' - A''B') + \\ &\quad + h(A'B' + A''B''). \end{aligned}$$

Two cases must now be distinguished, viz. $h = 0$ and $h \neq 0$. If $h = 0$, it follows that

$$\lim_{\omega \to 0} a = 0\left(\frac{ln\,\omega}{\omega^7}\right), \quad \lim_{\omega \to 0} b = 0\left(\frac{1}{\omega^7}\right)$$

and

$$\lim_{\omega \to 0} c = 0\left(\frac{ln\,\omega}{\omega^5}\right).$$

Since in this case $4ac$ is small with regard to b^2, the solution of eq. (A 1.3)

$$x = \frac{-b \pm \sqrt{b^2 - 4ac}}{2a}$$

may be simplified for $\omega \to 0$ to

$$x_1 = \frac{b}{a} = 0\left(\frac{1}{ln\,\omega}\right) \quad \text{and} \quad x_2 = -\frac{c}{b} = 0\,(\omega^2 ln\,\omega).$$

Once x is known, λ is determined by one of the equations (A 1.2) and it follows that

$$\lambda_1 = -\frac{C''}{D''x} = 0(\omega^2\,ln\,\omega)$$

and

$$\lambda_2 = -\frac{A'}{B'x} = 0\left(\frac{1}{ln\,\omega}\right).$$

It is seen that both values of λ approach 0 and hence the curves from the figs 1 to 39 end at both sides at a point of the vertical axis. The ordinates of these points are determined by

$$\frac{2v}{\nu_T c} = \frac{1}{\omega}\sqrt{\lambda x}, \qquad (A\,1.4)$$

which yield finite values.

If $h \neq 0$, it follows that

$$\lim_{\omega \to 0} a = 0\left(\frac{1}{\omega^8}\right), \quad \lim_{\omega \to 0} b = 0\left(\frac{1}{\omega^7}\right)$$

and

$$\lim_{\omega \to 0} c = 0\left(\frac{1}{\omega^6}\right).$$

In this case both roots are of order ω and the corresponding values of λ are given by

$$\lambda = -\frac{C''x + 2hA'}{D''x^2 + hB'x} = \frac{hC''x - A'}{B'x} = 0\,(\omega).$$

Again the values assumed by λ if $\omega \to 0$ are 0, while the ordinates are again given by eq. (A 1.4). After substitution of the values for λ and x into eq. (A 1.4), the result turns out to be

$$\frac{2v}{\nu_T c} = \frac{1}{\omega}\sqrt{\frac{-\{B'C''(1+h^2) + A'D''\} \pm \sqrt{\{B'C''(1+h^2) - A'D''\}^2 - 4h^2A'B'C''D''}}{2B'D''}} \qquad (A\,1.5)$$

This result is also valid for $h=0$.

It is seen from the foregoing that only A', B', C'' and D'' appear in the final results for $\omega=0$. In order to find the numerical values of the non-dimensional speeds $\frac{2v}{\nu_T c}$ which are approached for $\omega \to 0$, these quantities must be evaluated.

It follows again from the expansion of the flutter determinant that

$$\lim_{\omega\to 0} A' = \frac{1}{\omega^2} U_{11}U_{22}S_{33}'$$

$$\lim_{\omega\to 0} B' = -\frac{1}{\omega^4} U_{11}(S_{22}'S_{33}' - S_{23}'S_{32}')$$

$$\lim_{\omega\to 0} C'' = -\frac{1}{\omega^3} U_{22}(S_{11}''S_{33}' - S_{13}'S_{31}'')$$

$$\lim_{\omega\to 0} D'' = \frac{1}{\omega^5}\{ S_{11}''(S_{22}'S_{33}' - S_{23}'S_{32}') + S_{21}''(S_{13}'S_{32}' - S_{12}'S_{33}') + S_{31}''(S_{12}'S_{23}' - S_{13}'S_{22}')\} \qquad \text{(A 1.6)}$$

where

$$S_{ij}' = \lim_{\omega\to 0} \omega^2 A_{ij}' \qquad i=1,2,3 \qquad j=2,3$$

$$S_{i1}'' = \lim_{\omega\to 0} \omega A_{i1}'' \qquad i=1,2,3$$

and

$$A_{ik}' = U_{ik} + L_{ik}', \qquad A_{ik}'' = L_{ik}'' \qquad i,k=1,2,3.$$

The quantities S_{ij}' and S_{i1}'' are finite.

For $h=0$, one obtains

$$\left(\frac{2v}{\nu_T c}\right)_1 = \sqrt{\frac{U_{22}(S_{33}'S_{11}'' - S_{13}'S_{31}'')}{S_{11}''(S_{22}'S_{33}' - S_{23}'S_{32}') + S_{21}''(S_{13}'S_{32}' - S_{12}'S_{33}') + S_{31}''(S_{12}'S_{23}' - S_{13}'S_{22}')}}\,.$$

$$\left(\frac{2v}{\nu_T c}\right)_2 = \sqrt{\frac{U_{22}S_{33}'}{S_{22}'S_{33}' - S_{23}'S_{32}'}}$$

The last value is identical to the divergence speed.

APPENDIX 2.

Wing bending-aileron system.

In the case of wing bending-aileron flutter the torsional stiffness is assumed infinite. Hence in the flutter determinant as derived from eq. (A 1.1) the coefficient of E_{22} must be taken zero and this yields:

$$U_{11}U_{33}\frac{\nu_c^2\nu_B^2}{\nu^4} - \left(U_{11}A_{33} + \frac{\nu_c^2}{\nu_B^2}U_{33}A_{11}\right)\frac{\nu_B^2}{\nu^2} + A_{11}A_{33} - A_{13}A_{31} = 0 \qquad \text{(A 2.1)}$$

where:

$$A_{ij} = U_{ij} + L_{ij} = U_{ij} + L_{ij}' + iL_{ij}'' = A_{ij}' + iA_{ij}''.$$

As it is the intention to vary the unbalance factor $\mu_r\sigma_r$ the terms which are related to this factor will be written in the form:

$$\begin{aligned} A_{13}' &= L_{13}' + \mu_r\sigma_r\,.\,a = L_{13}' + pa \\ A_{31}' &= L_{31}' + \mu_r\sigma_r\,.\,a = L_{31}' + pa \qquad \text{(A 2.2)} \\ A_{33}' &= L_{33}' + \mu_r(\kappa_r^2 + \sigma_r^2)b = L_{33}' + q\,.\,b = x \end{aligned}$$

where a and b are constants.

Now eliminating the real value ν^2 from the two real equations which are identical to (A 2.1) and substituting (A. 2.2) the result is:

$$a_{11}(pa)^2 + 2a_{12}(pa)x + a_{22}x^2 + 2a_{13}(pa) + 2a_{23}x + a_{33} = 0. \qquad \text{(A 2.3)}$$

For a given value of pa, x is determined by:

$$x = \frac{-\{a_{12}(pa) + a_{23}\} \pm \sqrt{\{a_{12}(pa) + a_{23}\}^2 - a_{22}\{a_{11}(pa)^2 + 2a_{13}(pa) + a_{33}\}}}{a_{22}} \qquad \text{(A 2.4)}$$

At the vertical tangent (pa = constant) the discriminant of (A 2.4) will be zero, hence:

$$(pa)^2(a_{12}^2 - a_{11}a_{22}) + 2(pa)(a_{12}a_{23} - a_{13}a_{22}) + (a_{23}^2 - a_{22}a_{33}) = 0 \qquad \text{(A 2.5)}$$

where:

$$\begin{aligned} a_{12}^2 - a_{11}a_{22} &= U_{11}^2\left(U_{33}A_{11}''\frac{\nu_c^2}{\nu_B^2} + U_{11}A_{33}''\right)^2\{\tfrac14(A_{13}'' + A_{31}'')^2 - A_{11}''A_{33}''\}. \\ a_{12}a_{23} - a_{13}a_{22} &= \tfrac12 U_{11}^2\left(U_{33}A_{11}''\frac{\nu_c^2}{\nu_B^2} + U_{11}A_{33}''\right)^2\{\tfrac12(L_{13}'A_{31}'' + L_{31}'A_{13}'')\times \\ &\quad (A_{13}'' + A_{31}'') - A_{11}''A_{33}''(L_{13}' + L_{31}')\}. \qquad \text{(A 2.6)} \\ a_{23}^2 - a_{22}a_{33} &= U_{11}^2\left(U_{33}A_{11}''\frac{\nu_c^2}{\nu_B^2} + U_{11}A_{33}''\right)^2\{\tfrac14(L_{13}'A_{31}'' + L_{31}'A_{31}'')^2 - \\ &\quad - A_{11}''A_{33}''(A_{11}''A_{33}'' - A_{13}''A_{31}'' + L_{13}'L_{31}')\}. \end{aligned}$$

Hence, the absois $p = \mu_r\sigma_r$ of the vertical tangent of any conic is independent of the ratio ν_c/ν_B.

The shape of the conics is determined by the first equation (A 2.6), this yields:

$$\tfrac14(A_{13}'' + A_{31}'')^2 - A_{11}''A_{33}'' \begin{cases} > 0 & \text{hyperbolae} \\ = 0 & \text{parabolae} \\ < 0 & \text{ellipses} \end{cases}$$

As in the equation (A 2.3) the factors σ and ξ do not appear the conics are independent of the location of the elastic and inertia axes.

Moreover in the case $\nu_c = 0$ the wing mass density parameter will vanish.

Completed May 1954.

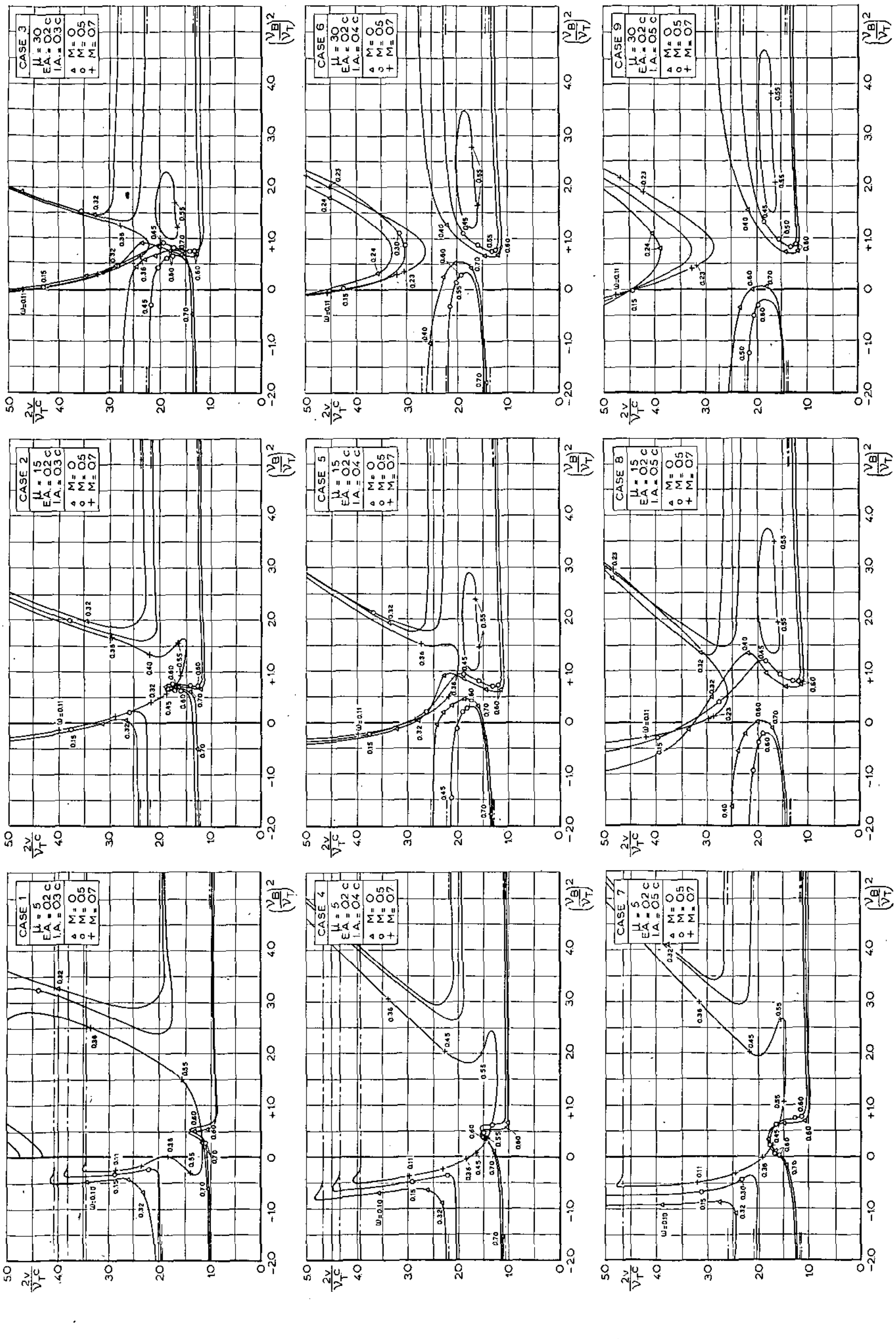

Figs. 1—9. Influence of Mach number on flutter speed.

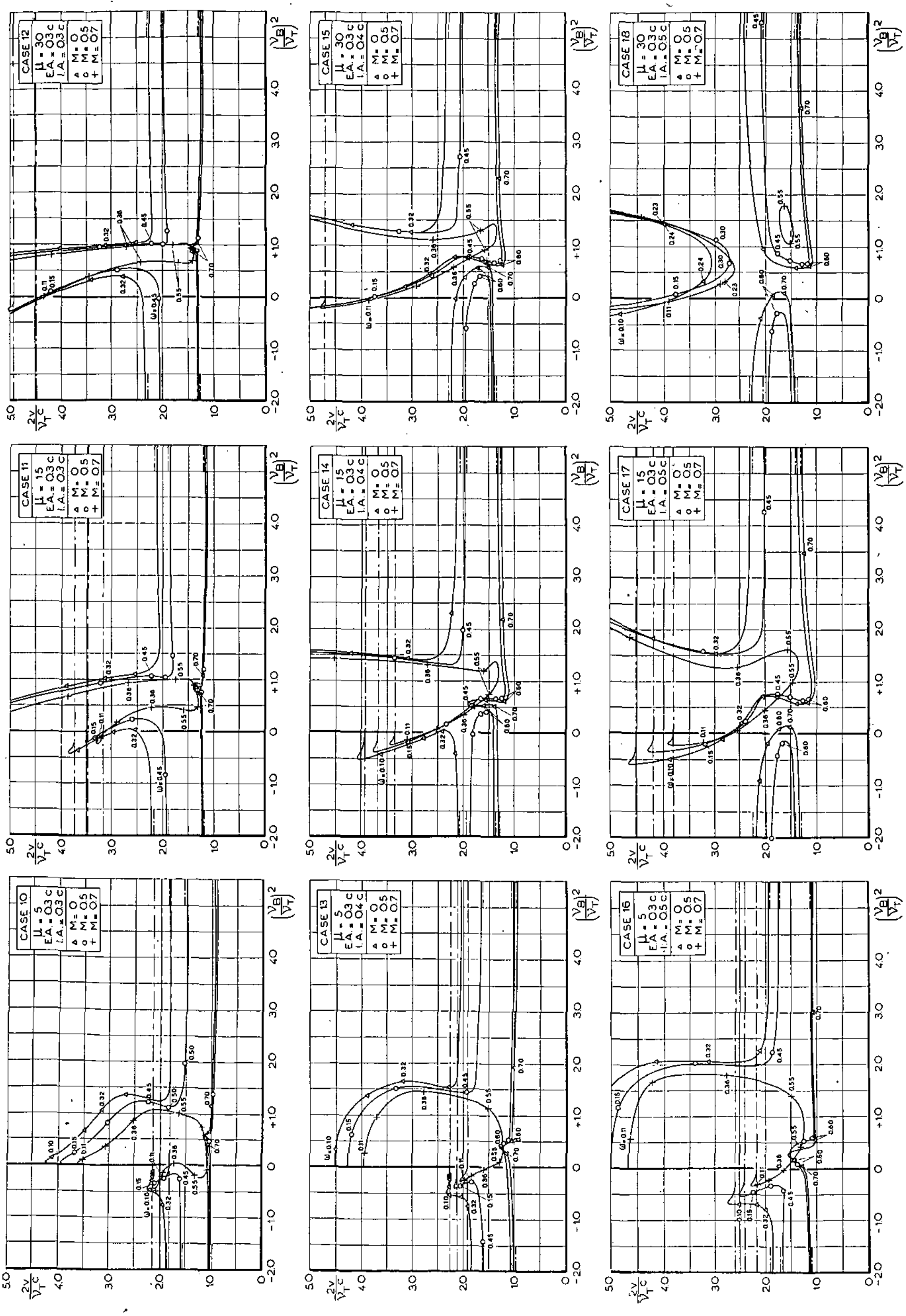

Figs. 10—18. Influence of Mach number on flutter speed.

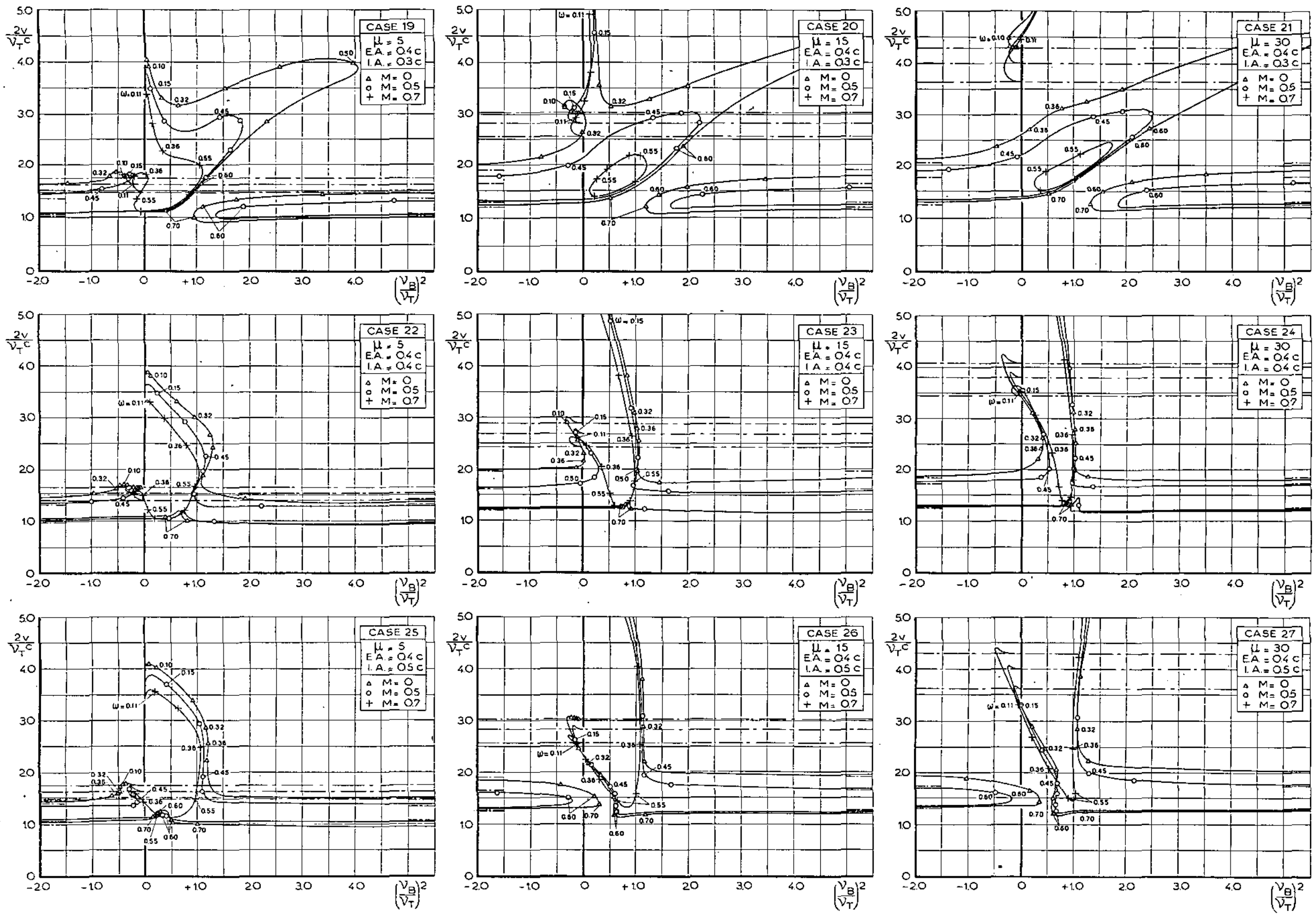

Figs. 19—27. Influence of Mach number on flutter speed.

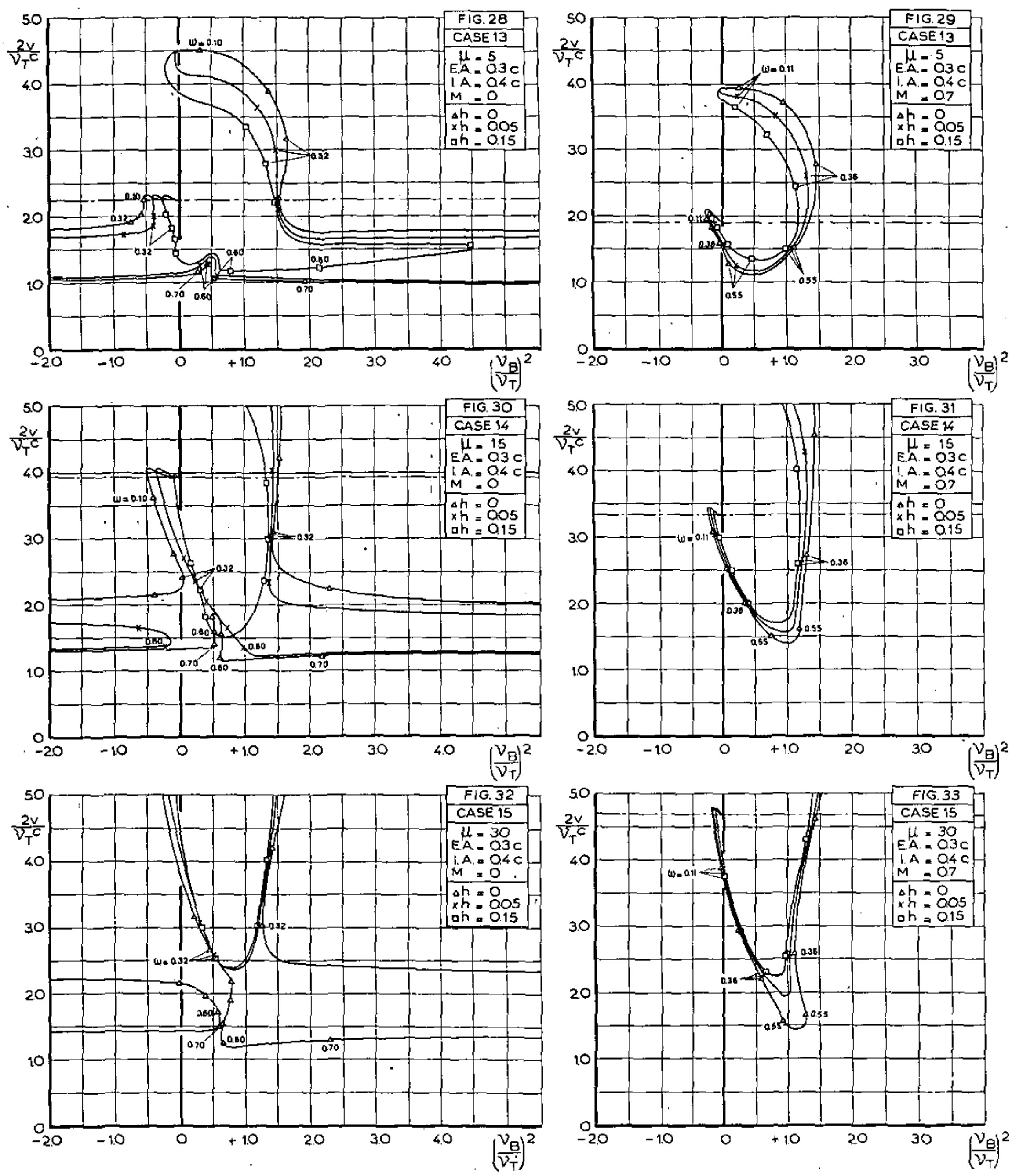

Figs. 28—33. Influence of structural damping on flutter speed.

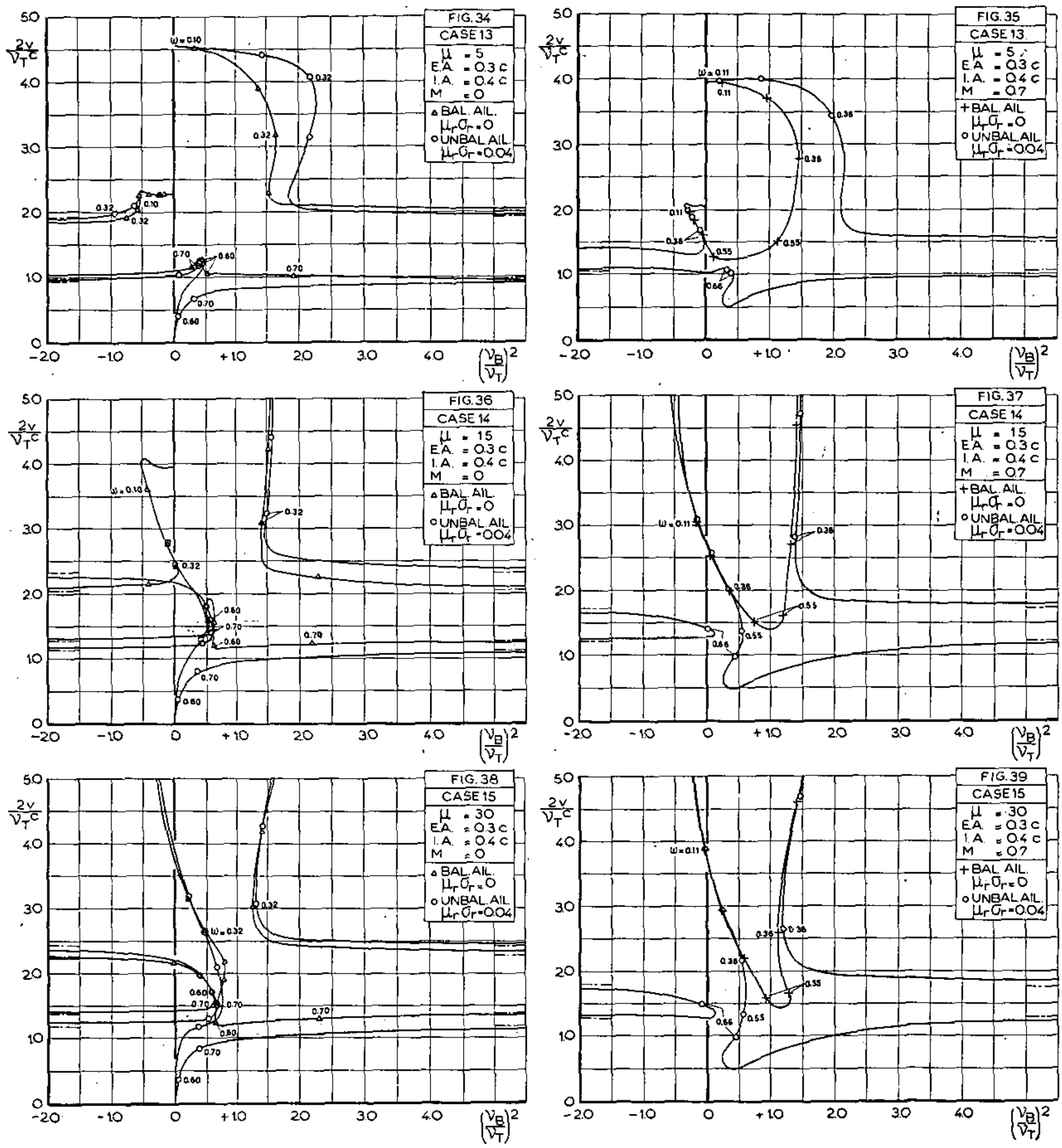

Figs. 34—39. Influence of static aileron balance on flutter speed.

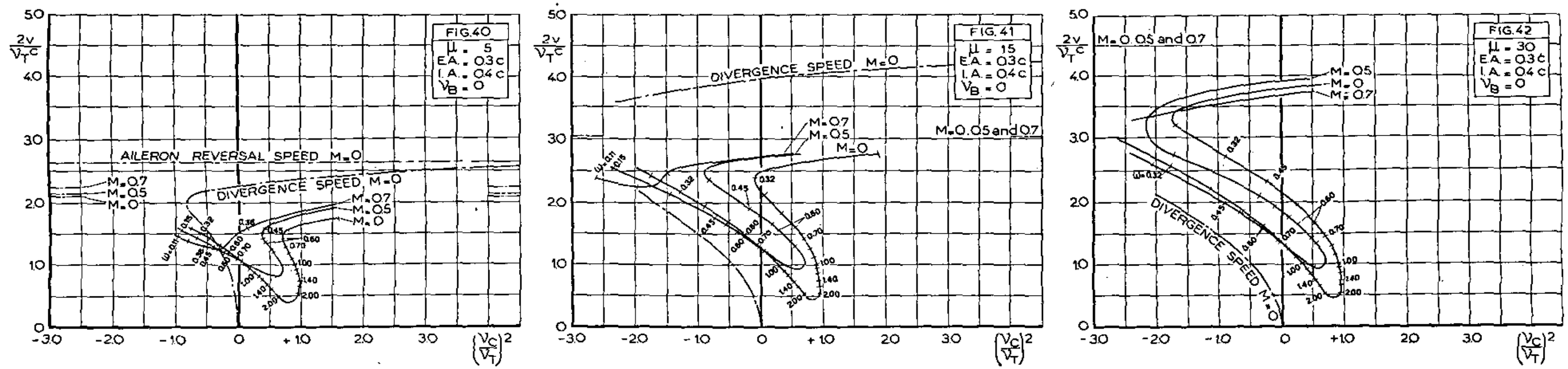

Figs. 40—42. Influence of control circuit stiffness on flutter speed.

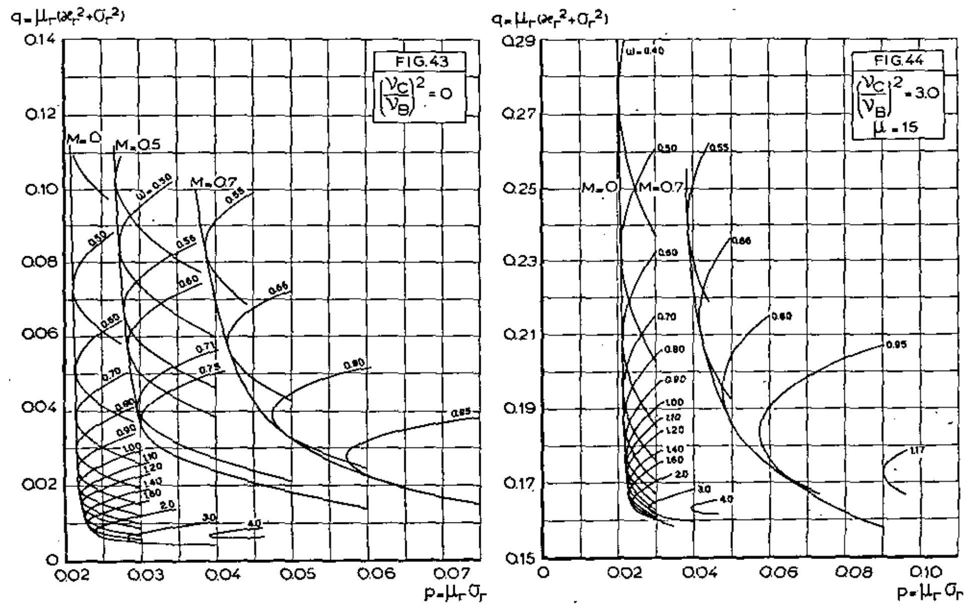

Figs. 43, 44. Influence of aileron static balance and aileron moment of inertia on stability of wing bending-aileron flutter.

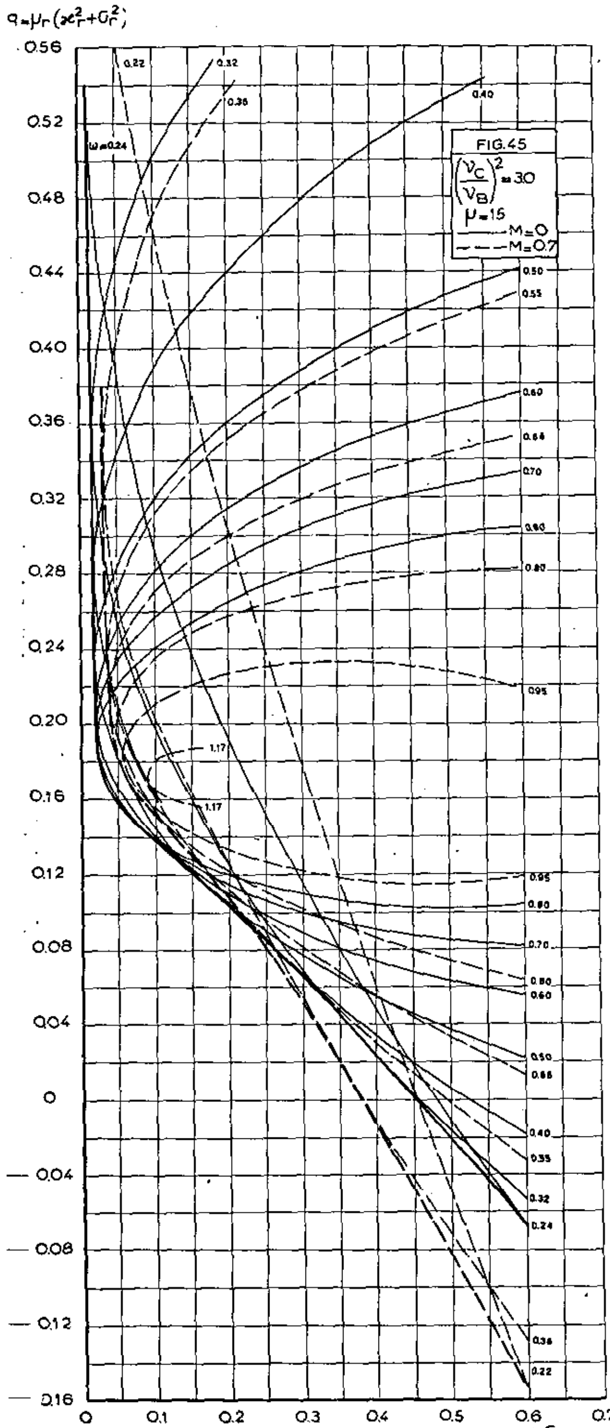

Fig. 45. Same as fig. 44, but other scale.

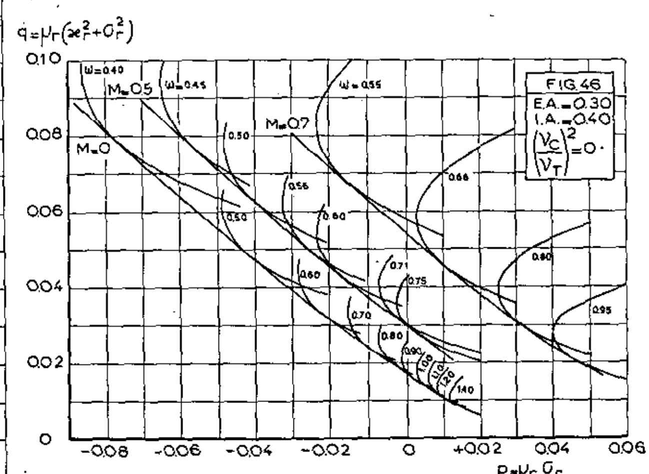

Fig. 46. Influence of aileron static balance and aileron moment of inertia on stability of wing torsion-aileron flutter.

REPORT F. 159.

Strip Theory for Oscillating Swept Wings in Compressible Subsonic Flow

by

W. ECKHAUS.

Summary.

By means of an asymptotic expansion, valid for high aspect ratio and a not too low frequency, a strip theory is derived, which can be expected to possess the same accuracy as the usual two-dimensional approximation for straight wings. It is shown, that according to this strip theory the pressure consists of the two-dimensional pressure, multiplied by a factor cos φ (φ being the sectional angle of sweep) plus an additional pressure, which follows from an equation of the Possio type, and which is only zero if φ is zero, or if the wing is infinitely long. In the limiting case of incompressible flow the theory is shown to lead to results identical with earlier results for that case. Methods of computing the pressure distribution from the integral equation of the strip theory are indicated and discussed.

Contents.

1 Introduction.

The aerodynamic forces on an oscillating lifting surface, the knowledge of which is necessary to perform flutter calculations are often derived by means of a two-dimensional approximation. The great advantage of this approximation is the simplicity of the results: the aerodynamic forces on a spanwise wing station are a function of the geometry and the reduced frequency of this station only. The accuracy of the approximation is satisfactory for straight wings of large aspect ratio, oscillating at a frequency which is not too low. In fact, it has been shown in ref. 1 that the two-dimensional approximation follows from the exact lifting surface equation by means of an asymptotic expansion, when the terms neglected are of the same order of magnitude, as the terms neglected in the steady problem, when one uses the wellknown Prandtl equation, again provided that the frequency of oscillation is not too low. However, the situation changes if the wing under consideration is not straight. In ref. 2 VAN DE VOOREN and the author considered the case of wings with simple sweep back in incompressible flow. The strip theory, presented in that reference, was again obtained by means of an asymptotic expansion, where the terms omitted are of the same order as in the case of the two-dimensional approximation for straight wings. The aerodynamic forces on a spanwise wing section, obtained by this strip theory appear to consist of the two-dimensional term multiplied by the factor cos φ (where φ is the angle of sweep), and an additional term, proportional to the variation of the deflection functions and the chord in spanwise direction. The theory of ref. 2 makes it possible to perform flutter calculations on swept wings with the same accuracy and the same simplicity, as the usual two-dimensional approximation in the case of straight wings.

In this report we shall consider the general case of a lifting surface of arbitrary shape, oscillating in compressible subsonic flow. We shall assume the aspect ratio and the frequency of oscillation not too small and derive a strip theory which, for that general case, will again possess the same accuracy as the two-dimensional approximation in the case of a straight wing, and from which the theory of ref. 2 will follow as a special case of Mach number equal to zero.

Acknowledgment: The author wishes to acknowledge valuable discussions with dr. ir. A. I. VAN DE VOOREN.

2 List of symbols.

X, X_0	coordinate in flight direction (positive backward)
Y, Y_0	coordinate in spanwise direction (positive to starboard)

z	coordinate in the direction perpendicular to the X–Y plane
w	downwash (positive downward)
U	velocity of flight
M	Mach number
ν	circular frequency
ρ	density of the air
b	semi span
$l(y)$	semi chord
φ	angle of sweep
ε	the ratio of root chord to wing span $\frac{l(0)}{b}$
p	pressure jump on the airfoil (positive downward)
$\frac{\nu l}{U} = \omega$	reduced frequency
$\beta = \sqrt{1-M^2}$	
$H_\nu^{(2)}$	Hankel fuction of second kind and order ν
$se_n(\eta)$	Odd Mathieu function.

3 Formulation of the problem.

In the linearised theory the problem of a harmonically oscillating airfoil in subsonic compressible flow can be formulated as an integral equation, which relates the unknown pressure distribution on the wing to the prescribed downwash. The derivation of this general equation will not be given here, — it can be found, for instance, in refs. 3 and 4.

The equation reads:

$$4\pi w(x_0, y_0) = -\frac{1}{\rho U} \lim_{z_0 \to 0} \frac{\partial^2}{\partial z_0^2} \iint_S p(x,y)\, e^{-i\frac{\nu}{U}(x_0-x)} \left\{ \int_{-\infty}^{x_0-x} e^{i\frac{\nu}{U}\frac{1}{\beta^2}[\lambda - MR]} \frac{d\lambda}{R} \right\} dx\,dy \qquad (3.1)$$

where:

$$R = \{ \lambda^2 + \beta^2 (y_0 - y)^2 + \beta^2 z_0^2 \}^{\frac{1}{2}} \qquad (3.2)$$

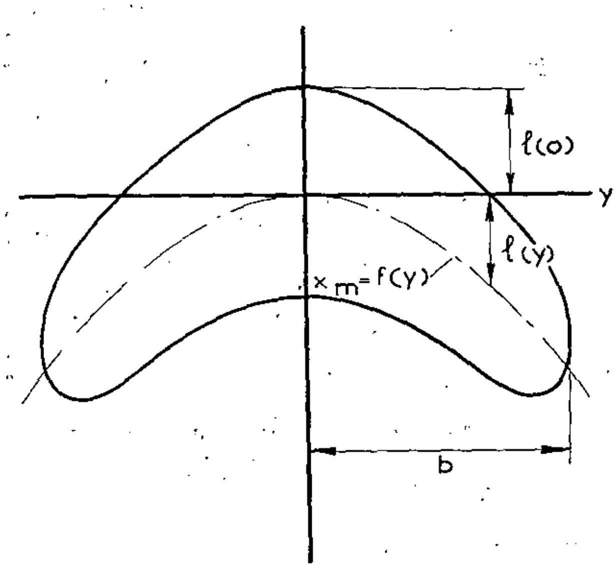

Fig. 3.1

Integration over S denotes the integration over the wing surface. The downwash $w(x_0, y_0)$ follows from the given wing deflection-function $z_m(x_0, y_0)$ if the condition of tangential flow at the wing surface is applied, viz.

$$w(x_0, y_0) = i\nu\, z_m(x_0 y_0) + U \frac{\partial z_m}{\partial x_0}(x_0 y_0) \qquad (3.3)$$

Our particular case is that of a wing of large aspect ratio oscillating at a frequency which is

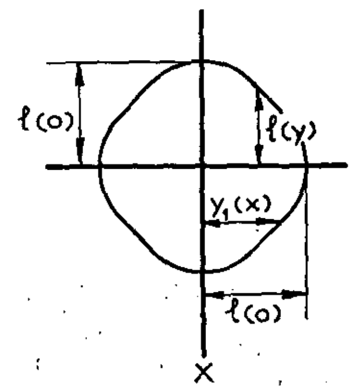

Fig. 3.2

not too low, and our problem to find an approximation of eq. (3.1) for that particular case.

The method of investigation, in this report, is inspired on the general method for treatment of wings of large aspect ratio, given by TIMMAN and LEMAIGRE in ref. 5. By means of this method we shall derive an approximate equation, equivalent to eq. (3.1), together with an estimate of the order of magnitude of the terms omitted. Before doing so, however, we shall transform eq. 3.1 into a more suitable form.

For a wing of large aspect ratio, for the most part of the wing $|y_0 - y| \gg |x_0 - x|$. To express this fact mathematically we introduce the coordinate transformation

$$\left. \begin{aligned} x &= f\left(\frac{Y}{\varepsilon}\right) + X \\ y &= \frac{1}{\varepsilon} Y \end{aligned} \right\} \qquad (3.4)$$

$$\varepsilon = \frac{l(0)}{b} \qquad (3.5)$$

$f(y)$ is the equation of the mid chord line, ε is a small parameter.

In the new coordinate system $|X - X_0|$ and $|Y - Y_0|$ are in general of the same order of magnitude (see fig. 3.1 and 3.2).

Substituting the transformation (3.4) into eq. (3.1) we obtain:

$$4\,\pi w(X_0, Y_0) = -\frac{1}{\rho U}\lim_{z_0 \to 0}\frac{\partial^2}{\partial z_0^2}\int_{-l(0)}^{l(0)}\int_{-l(y)}^{l(y)} p(X,Y)e^{-i\frac{\nu}{u}(X_0-X)}\left\{\int_{-\infty}^{X_0-X} e^{i\frac{\nu}{u}\frac{1}{\beta^2}\left[\lambda+M^2(f_0-f)-M\frac{1}{\varepsilon}R'\right]}\frac{d\lambda}{R'}\right\}dXdY \tag{3.6}$$

where:

$$R' = \{(\varepsilon\lambda + f_0 - f)^2 + \beta^2(Y_0 - Y)^2 + \varepsilon^2\beta^2 z_0^2\}^{\frac{1}{2}} \tag{3.7}$$

and:

$$\left.\begin{aligned} f_0 &= f\left(\frac{Y_0}{\varepsilon}\right) \\ f &= f\left(\frac{Y}{\varepsilon}\right) \end{aligned}\right\} \tag{3.8}$$

The actual aircraft wings are always symmetrical about the line $y = 0$, hence $f(y) = f(-y)$, with a possible discontinuity in its derivative at $y = 0$. Furthermore, the curvature of $f(y)$ is not large, and we assume therefore, that we can represent $f(y)$ with sufficient accuracy by the first two terms of its expansion in a Taylor series to y, viz.:

$$f(y) \cong f(y_0) + (y - y_0)\frac{df}{dy}(y_0) \tag{3.9}$$

if y and y_0 are both positive.
We also may write:

$$\frac{df}{dy}(y_0) = \tan\varphi$$

where φ is the angle of sweep at the section $y = y_0$.
Hence we find:

$$\left.\begin{aligned} &\text{for the right semi wing} \quad (Y > 0),\ f_0 - f = \frac{1}{\varepsilon}(Y_0 - Y)\tan\varphi \\ &\text{for the left semi wing} \quad (Y < 0),\ f_0 - f = \frac{1}{\varepsilon}(Y_0 + Y)\tan\varphi \end{aligned}\right\} \tag{3.10}$$

Let now

$$w(X_0, Y_0) = w_r(X_0, Y_0) + w_l(X_0, Y_0) \tag{3.11}$$

where w_r and w_l are the downwashes due to the right and the left semi wing respectively. Substituting eq. (3.10) into eq. (3.6) we obtain:

$$4\,\pi w_r(X_0, Y_0) = -$$
$$-\frac{1}{\rho U}\lim_{z_0 \to 0}\frac{\partial^2}{\partial z_0^2}\int_0^{l(0)}\int_{-l(y)}^{l(y)} p(X,Y)e^{-i\frac{\nu}{u}(X_0-X)}\left\{\int_{-\infty}^{X_0-X} e^{i\frac{\nu}{u}\frac{1}{\beta^2}\left[\lambda+M^2\frac{1}{\varepsilon}(Y_0-Y)\tan\varphi-M\frac{1}{\varepsilon}R'_r\right]}\frac{d\lambda}{R'_r}\right\}dXdY \tag{3.12}$$

$$4\,\pi w_l(X_0, Y_0) = -$$
$$-\frac{1}{\rho U}\lim_{z_0 \to 0}\frac{\partial^2}{\partial z_0^2}\int_{-l(0)}^{0}\int_{-l(y)}^{l(y)} p(X,Y)e^{-i\frac{\nu}{u}(X_0-X)}\left\{\int_{-\infty}^{X_0-X} e^{i\frac{\nu}{u}\frac{1}{\beta^2}\left[\lambda+M^2\frac{1}{\varepsilon}(Y_0+Y)\tan\varphi-M\frac{1}{\varepsilon}R'_l\right]}\frac{d\lambda}{R_l'}\right\}dXdY \tag{3.13}$$

where

$$R_r' = \{[\varepsilon\lambda + (Y_0 - Y)\tan\varphi]^2 + \beta^2(Y_0 - Y)^2 + \varepsilon^2\beta^2 z_0^2\}^{\frac{1}{2}} \tag{3.14}$$

$$R_l' = \{[\varepsilon\lambda + (Y_0 + Y)\tan\varphi]^2 + \beta^2(Y_0 - Y)^2 + \varepsilon^2\beta^2 z_0^2\}^{\frac{1}{2}} \tag{3.15}$$

Eq. (3.11), with eqs. (3.12), (3.13), (3.14) and (3.15) represents the final formulation of our problem; our goal will be to find an asymptotic expansion for the right hand side of eq. (3.11), valid for small ε.

4 Derivation of the approximate integral equation.

We assume that the section, in which the downwash will be calculated lies on the right semi wing, $Y_0 > 0$.
For the unknown pressure distribution $p(X, Y)$ we introduce the Taylor series expansion to Y, viz.:

$$\left.\begin{aligned} p(X,Y) &= p(X,Y_0) + (Y - Y_0)\frac{\partial p}{\partial Y}(X,Y_0) + \ldots\ldots \text{ on the right semi wing} \\ p(X,Y) &= p(X,Y_0) - (Y + Y_0)\frac{\partial p}{\partial Y}(X,Y_0) + \ldots\ldots \text{ on the left semi wing} \end{aligned}\right\} \tag{4.1}$$

Substituting eq. (4.1) into eq. (3.12) and (3.13), we obtain after interchanging the order of integration:

$$\left.\begin{aligned} 4\,\pi w_r(X_0, Y_0) &= -\frac{1}{\rho U}\int_{-l(Y_0)}^{l(Y_0)}\sum_{n=0}^{\infty}\frac{\partial^n p}{\partial Y^n}(X, Y_0)\,e^{-i\frac{\nu}{U}(X_0-X)}\,a_n^{(r)}I_n^{(r)}dX \\ 4\,\pi w_l(X_0, Y_0) &= -\frac{1}{\rho U}\int_{-l(Y_0)}^{l(Y_0)}\sum_{n=0}^{\infty}\frac{\partial^n p}{\partial Y^n}(X, Y_0)\,e^{-i\frac{\nu}{U}(X_0-X)}\,a_n^{(l)}I_n^{(l)}dX \end{aligned}\right\}\tag{4.2}$$

Where $a_n^{(r)}$ and $a_n^{(l)}$ are the coefficients of the Taylor expansion (4.1) and:

$$\left.\begin{aligned} I_n^{(r)} &= \lim_{z_0\to 0}\frac{\partial^2}{\partial z_0^2}\int_0^{Y_1}\int_{-\infty}^{X_0-X} e^{i\frac{\nu}{U}\frac{1}{\beta^2}\left[\lambda+\frac{M^2}{\varepsilon}(Y_0-Y)\tan\varphi - M\frac{1}{\varepsilon}R'_r\right]}\frac{(Y-Y_0)^n}{R'_r}\,d\lambda dY \\ I_n^{(l)} &= \lim_{z_0\to 0}\frac{\partial^2}{\partial z_0^2}\int_{-Y_1}^{0}\int_{-\infty}^{X_0-X} e^{i\frac{\nu}{U}\frac{1}{\beta^2}\left[\lambda+\frac{M^2}{\varepsilon}(Y_0+Y)\tan\varphi - M\frac{1}{\varepsilon}R'_l\right]}\frac{(Y+Y_0)^n}{R'_l}\,d\lambda dY \end{aligned}\right\}\tag{4.3}$$

The integrals $I_n^{(r)}$ and $I_n^{(l)}$ are investigated in appendix I.
The results are:

$$I_0^{(r)} = i\frac{\nu}{U}\pi\beta_1\frac{M_1}{\cos\varphi}\int_{-\infty}^{X_0-X} e^{i\frac{\nu}{u}\frac{1}{\beta_1^2}\lambda}\,H_1^{(2)}\left(\frac{\nu}{U}\frac{M_1}{\beta_1^2}|\lambda|\right)\frac{d\lambda}{|\lambda|} + 0\left(\frac{\varepsilon^2}{\nu}\right)\ldots\ldots\tag{4.4}$$

$$I_1^{(r)} = \varepsilon\sin\varphi\pi\,\frac{M_1}{\beta_1^3}\frac{\nu}{U}\int_{-\infty}^{X_0-X} e^{i\frac{\nu}{u}\frac{1}{\beta_1^2}\lambda}\left\{M_1H_0^{(2)}\left(\frac{\nu}{U}\frac{M_1}{\beta_1^2}|\lambda|\right)+i\frac{\lambda}{|\lambda|}H_1^{(2)}\left(\frac{\nu}{U}\frac{M_1}{\beta_1^2}|\lambda|\right)\right\}d\lambda + 0\left(\frac{\varepsilon^2}{\nu}\right).\tag{4.5}$$

where:

$$\left.\begin{aligned} M_1 &= M\cos\varphi \\ \beta_1 &= \sqrt{1-M_1^2} \end{aligned}\right\}\tag{4.6}$$

Furthermore:

$$\left.\begin{aligned} I_2^{(r)} &= 0\left(\frac{\varepsilon^2}{\nu}\right)\ \text{if}\ \nu\to 0 \\ I_2^{(r)} &= 0\left(\frac{\varepsilon^2}{\nu}\right)+0\left(\frac{\varepsilon^2 M}{\sqrt{\nu}}\right)\ \text{if}\ \nu\to\infty \end{aligned}\right\}\tag{4.7}$$

$$I_n^{(r)} = 0\left(\frac{\varepsilon^2}{\nu}\right)\ \text{for}\ n>2\tag{4.8}$$

$$I_n^{(l)} = 0\left(\frac{\varepsilon^2}{\nu}\right)\tag{4.9}$$

These results are derived under the assumption $M \neq 0$. The validity of the theory in the limiting case $M=0$ will be proved in section 5 of this report.

We must draw attention to the fact, that our expression for $I_0^{(r)}$, given in eq. (4.4), becomes meaningless if $X_0 - X > 0$, because of a non-integrable singularity in the integrand for $\lambda = 0$. In that case a different expression for $I_0^{(r)}$ must be used. However, in $I_0^{(r)}$, as it is given by eq. (4.4), we recognise the kernel function of Possio's equation, and hence, the different forms taken by that kernel function for $X_0 - X < 0$ and $X_0 - X > 0$ are known to us. They are given, for instance, in ref. 11. From the results of ref. 11 we can derive

if $X_0 - X > 0$

$$I_0^{(r)} = \left\{-2\frac{\nu}{U}\pi + i\frac{\nu}{U}\frac{M_1}{\beta_1}\pi\int_{X_0-X}^{\infty} e^{i\frac{\nu}{u}\frac{1}{\beta_1^2}\lambda}\,H_1^{(2)}\left(\frac{\nu}{U}\frac{M_1}{\beta_1^2}|\lambda|\right)\frac{d\lambda}{|\lambda|}\right\}\frac{1}{\cos\varphi}$$

In the subsequent parts of this report we shall use for $I_0^{(r)}$ the expression given by eq. (4.4) knowing however, that we must replace it by a different expression, if $X_0 - X > 0$.

Introducing the results of Appendix I into eq. (4.2) we obtain

$$4\,\rho U w(X_0, Y_0)\cos\varphi = -i\,\frac{\nu}{U}\,\frac{M_1}{\beta_1}\int_{-l}^{l} p(X, Y_0)\, e^{-i\frac{\nu}{u}(X_0-X)} \left\{ \int_{-\infty}^{X_0-X} e^{i\frac{\nu}{u}\frac{1}{\beta_1^2}\lambda} H_1^{(2)}\left(\frac{\nu}{U}\,\frac{M_1}{\beta_1^2}|\lambda|\right)\frac{d\lambda}{|\lambda|}\right\} dX -$$

$$-\,\varepsilon \sin\varphi\cos\varphi\,\frac{\nu}{U}\,\frac{M_1}{\beta_1^3}\int_{-l}^{l}\frac{\partial p}{\partial y}(X, Y_0)\, e^{-i\frac{\nu}{u}(X_0-X)} \left\{ \int_{-\infty}^{X_0-X} e^{i\frac{\nu}{u}\frac{1}{\beta_1^2}\lambda}\left[M_1 H_0^{(2)}\left(\frac{\nu}{U}\,\frac{M_1}{\beta_1^2}|\lambda|\right)+\right.\right.$$

$$\left.\left.+\,i\frac{\lambda}{|\lambda|}H_1^{(2)}\left(\frac{\nu}{U}\,\frac{M_1}{\beta_1^2}|\lambda|\right)\right]d\lambda\right\} dX + g(\varepsilon, \nu) \tag{4.10}$$

where:

$$g(\varepsilon,\nu) = 0\left(\frac{\varepsilon^2}{\nu}\right) \text{ if } \nu \to 0$$

and

$$g(\varepsilon,\nu) = 0\left(\frac{\varepsilon^2}{\nu}\right) + 0\left(\frac{\varepsilon^2 M}{\sqrt{\nu}}\right) \text{ if } \nu \to \infty \tag{4.11}$$

Eq. (4.10) is the final approximate integral equation of our theory. It can be expected to give a good approximation of the problem for wings of high aspect ratio, oscillating at a frequency which is not too low.

5 Some considerations on the approximate integral equation.

The first important property of eq. (4.10) is, that it does not contain the variable Y any more. The pressure at a section Y_0 is given by eq. (4.10) as a function of parameters of that section only. For this reason we may call the present theory a strip theory. Considering the eq. (4.10) we see, that its right-hand side consists of two terms, the first being of order 1, the second of order ε. For straight wings, $\varphi = 0$, the second term vanishes, and we obtain the wellknown Possio equation for two-dimensional flow. For an infinitely long wing, $\varepsilon = 0$, the second term again vanishes, and we obtain a modified Possio equation, in which, in comparison with the two-dimensional equation, the Mach number and the downwash are multiplied by the factor $\cos\varphi$. In the general case, where neither φ nor ε is equal to zero, the second term of the right hand side of the eq. (4.10) contributes to the pressure distribution. It is clear that this contribution will be of order ε, and that it represents a first approximation to the finite-span effect of the swept wing. Let us represent the pressure, which follows from eq. (4.10) by the following relation

$$p = (p^{(2)} + \Delta p)\cos\varphi \tag{5.1}$$

Δp is of order ε, $p^{(2)}$ follows from the Possio equation, in which the Mach number is multiplied by $\cos\varphi$, viz.

$$4\,\rho U w(X_0, Y_0) = -i\,\frac{\nu}{U}\,\frac{M_1}{\beta_1}\int_{-l(y_0)}^{l(y_0)} p^{(2)}(X, Y_0)\, e^{-i\frac{\nu}{u}(X_0-X)} \left\{ \int_{-\infty}^{X_0-X} e^{i\frac{\nu}{u}\frac{1}{\beta_1^2}\lambda} H_1^{(2)}\left(\frac{\nu}{U}\,\frac{M_1}{\beta_1^2}|\lambda|\right)\frac{d\lambda}{|\lambda|}\right\} dX \tag{5.2}$$

$p^{(2)}(X, Y_0)$ can be assumed to be known, as it can be evaluated by usual methods of solving the Possio equation. In fact, $p^{(2)}(X, Y_0)$ can directly be derived from the tabulated results of the Possio equation, by substituting for M the value of $M\cos\varphi$. Substituting eq. (5.1) into eq. (4.10) and using eq. (5.2), we obtain an integral equation for Δp, which we can write in the form

$$4\,\rho U w_1(X_0, Y_0) = -i\,\frac{\nu}{U}\,\frac{M_1}{\beta_1}\int_{-l}^{l}\Delta p(X, Y_0)\, e^{-i\frac{\nu}{u}(X_0-X)} \left\{ \int_{-\infty}^{X_0-X} e^{i\frac{\nu}{u}\frac{1}{\beta_1^2}\lambda} H_1^{(2)}\left(\frac{\nu}{U}\,\frac{M_1}{\beta_1^2}|\lambda|\right)\frac{d\lambda}{|\lambda|}\right\} dX \tag{5.3}$$

$$4\,\rho U w_1(X_0, Y_0) = \varepsilon\sin\varphi\,\frac{M_1}{\beta_1^3}\,\frac{\nu}{U}\int_{-l}^{l}\frac{\partial[p^{(2)}\cos\varphi]}{\partial Y}(X, Y_0)\, e^{-i\frac{\nu}{u}(X_0-X)} \left\{ \int_{-\infty}^{X_0-X} e^{i\frac{\nu}{u}\frac{1}{\beta_1^2}\lambda}\left[M_1 H_0^{(2)}\left(\frac{\nu}{U}\,\frac{M_1}{\beta_1^2}|\lambda|\right)+\right.\right.$$

$$\left.\left.+\,i\frac{\lambda}{|\lambda|}H_1^{(2)}\left(\frac{\nu}{U}\,\frac{M_1}{\beta_1^2}|\lambda|\right)\right]d\lambda\right\} dX. \tag{5.4}$$

Note, that instead of $\varepsilon\,\dfrac{\partial p}{\partial Y}$ we have written $\varepsilon\,\dfrac{\partial[p^{(2)}\cos\varphi]}{\partial Y}$. In view of relation (5.1) by this assumption an error of order ε^2 is introduced.

Eq. (5.3) is again an equation of the Possio-type. The prescribed downwash w_1 is known, as $p^{(2)}$ is known, and can be evaluated. Hence, our problem reduces to the problem of solving an equation of Possio-type.

The prescribed downwash w_1 is a function of $\dfrac{\partial[p^{(2)}\cos\varphi]}{\partial Y}$. By considering this factor we may draw some conclusions with respect to the behaviour of the unknown pressure Δp. $p^{(2)}$ is a function of the reduced frequency $\omega = \dfrac{\nu l}{U}$, and of the wing-deflection function z_a. Hence we may write:

$$\frac{\partial[p^{(2)}\cos\varphi]}{\partial Y} = \cos\varphi\left\{\frac{\partial p^{(2)}}{\partial\omega}\,\omega\cdot\frac{1}{l}\,\frac{dl}{dY} + \right.$$
$$\left. + \frac{\partial p^{(2)}}{\partial z_a}\,\frac{dz_a}{dY} - p^{(2)}\tan\varphi\,\frac{d\varphi}{dY}\right\}. \quad (5.5)$$

We may therefore expect, that the additional pressure Δp will consist of three terms, respectively proportional to:

a) The spanwise variation of the chord $\frac{dl}{dy}$.

b) The spanwise variation of the wing deflection function $\frac{dz_a}{dy}$.

c) The spanwise variation of the sectional angle of sweep $\frac{d\varphi}{dy}$.

It may be useful to point out, that $w_1(X_0, Y_0)$ can also be expressed in terms of generalized $He^{(2)}$ functions. The $He^{(2)}$ function of zero order was introduced by SCHWARZ in ref. 12. This function is defined by the relation:

$$He^{(2)}(\lambda, X) = \int_0^X e^{iU} H_0^{(2)}(\lambda U)\, dU.$$

If we now introduce the generalisation:

$$He_n^{(2)}(\lambda, X) = \int_0^X e^{iU} H_n^{(2)}(\lambda U)\, dU.$$

then it is easy to see that $w_1(X_0, Y_0)$ is given by a combination of $He_0^{(2)}$ and $He_1^{(2)}$. $He_0^{(2)}$ was tabulated by SCHWARZ in ref. 12.

Some remarks must be made on the order of magnitude of terms omitted in the integral equation. We have seen that if M tends to zero this order becomes $\frac{\varepsilon^2}{\nu}$. However, our derivation was valid under the assumption of $M \neq 0$, and in fact, in ref. 2, where the strip theory for swept wings in incompressible flow was presented, the order of magnitude of the terms omitted appeared to be $\frac{\varepsilon^2 \log\varepsilon}{\nu}$.

Let us consider the following simple case:

$$\int_0^a \frac{dt}{t + M + \varepsilon} = \log(a + M + \varepsilon) - \log(M + \varepsilon).$$

This integral is of order 1 if $M \neq 0$, but of order $\log\varepsilon$ if $M = 0$.

This example shows us a possible origin of the differences mentioned above. However, to prove that the present theory is valid up to $M = 0$, and hence is in accordance with the theory of ref. 2, we shall derive from the present theory the limiting case $M = 0$ and compare the results with results of ref. 2.

6 The case of incompressible flow.

According to the present theory, the pressure *distribution on a swept wing consists of two terms:* $p^{(2)}\cos\varphi$ and $\Delta p\cos\varphi$ (see eq. 5.1). We shall now consider Δp and the case $M = 0$. From the eq. (5.3) and (5.4) we obtain, after substituting series expansions for the Hankel-functions and taking $M = 0$:

$$2\pi\rho U w_1(X_0, Y_0) = \int_{-l}^{l} \Delta p(X, Y_0)\, e^{-i\frac{\nu}{U}(X_0 - X)} \left\{ \int_{-\infty}^{X_0 - X} e^{i\frac{\nu}{U}\lambda}\,\frac{d\lambda}{\lambda^2} \right\} dX \qquad (6.1)$$

$$2\pi\rho U w_1(X_0, Y_0) = -\varepsilon\sin\varphi \int_{-l}^{l} \frac{\partial(p^{(2)}\cos\varphi)}{\partial Y}\, e^{-i\frac{\nu}{U}(X_0 - X)} \left\{ \int_{-\infty}^{X_0 - X} e^{i\frac{\nu}{U}\lambda}\,\frac{d\lambda}{\lambda} \right\} dX \qquad (6.2)$$

Eq. (6.1) is the wellknown Birnbaum-equation. We shall now prove the eq. (6.1) together with w_1 given by eq. (6.2) to be identical with the integral equation derived in ref. 2. In this reference the problem was formulated in terms of vorticity distribution. Hence, we must introduce the vorticity distribution into our integral equation. Let the components of the vorticity in the X and Y direction be given by γ_X and γ_Y respectively, and let us define furthermore:

$$\gamma_\xi = \gamma_X - \gamma_Y \tan\varphi.$$

The equation of continuity of the vortexfield is then according to ref. 2:

$$\frac{\partial\gamma_\xi}{\partial X} + \varepsilon\,\frac{\partial\gamma_Y}{\partial Y} = 0 \qquad (6.3)$$

while the relation between the pressure jump on the airfoil and the vorticity is

$$p(X, Y) = -\rho U\left\{ \gamma_Y(X, Y) + i\frac{\nu}{U} \int_{-l(Y)}^{X} \gamma_Y(X', Y)\, dX' \right\}. \qquad (6.4)$$

Introducing eq. (6.4) into eqs. (6.1) and (6.2) we obtain:

$$2\pi w_1(X_0, Y_0) = -\int_{-l(Y_0)}^{l(Y_0)} \left\{ \Delta\gamma_Y(X, Y_0) + i\frac{\nu}{U}\int_{-l}^{X} \Delta\gamma_Y(X', Y_0)\, dX' \right\} e^{-i\frac{\nu}{u}(X_0 - X)} \int_{-\infty}^{X_0 - X} e^{i\frac{\nu}{u}\lambda}\,\frac{d\lambda}{\lambda^2}\, dX \qquad (6.5)$$

$$2\pi w_1(X_0, Y_0) = \varepsilon \sin\varphi \int\limits_{-l(Y_0)}^{l(Y_0)} \Big\{ \frac{\partial[\gamma_Y^{(2)}\cos\varphi]}{\partial Y}(X, Y_0) +$$

$$+ i\frac{\nu}{U}\frac{\partial\cos\varphi}{\partial Y}\int\limits_{-l(Y_0)}^{X}\gamma_Y^{(2)}(X', Y)dX' \Big\} e^{-i\frac{\nu}{u}(X_0-X)}\int\limits_{-\infty}^{X_0-X} e^{i\frac{\nu}{u}\lambda}\frac{d\lambda}{\lambda}dX. \tag{6.6}$$

Let us first consider the eq. (6.5). Partial integration with respect to λ yields:

$$2\pi w_1(X_0, Y_0) = -$$

$$-\int\limits_{-l(Y_0)}^{l(Y_0)}\{\Delta\gamma_Y(X, Y_0) + i\frac{\nu}{U}\int\limits_{-l(Y_0)}^{X}\Delta\gamma_Y(X', Y_0)dX'\}\Big\{-\frac{1}{X_0-X} + i\frac{\nu}{U}e^{-i\frac{\nu}{u}(X_0-X)}\int\limits_{-\infty}^{X_0-X}e^{i\frac{\nu}{u}\lambda}\frac{d\lambda}{\lambda}\Big\}dX \tag{6.7}$$

or:

$$2\pi w_1(X_0, Y_0) = -\int\limits_{-l(Y_0)}^{l(Y_0)}\frac{\Delta\gamma_Y(X, Y_0)}{X-X_0}dX - i\frac{\nu}{U}\int\limits_{-l(Y_0)}^{l(Y_0)}\Big\{\int\limits_{-l(Y)}^{X}\Delta\gamma_Y(X', Y_0)dX'\Big\}\frac{dX}{X-X_0} -$$

$$- i\frac{\nu}{U}\int\limits_{-l(Y_0)}^{l(Y_0)}\Delta\gamma_Y(X, Y_0)\Big\{\int\limits_{-\infty}^{X_0-X}e^{i\frac{\nu}{u}\lambda}\frac{d\lambda}{\lambda}\Big\}e^{-i\frac{\nu}{u}(X_0-X)}dX -$$

$$-\left(i\frac{\nu}{u}\right)^2\int\limits_{-l(Y_0)}^{l(Y_0)}\Big\{\int\limits_{-l(Y_0)}^{X}\Delta\gamma_X(X', Y_0)dX'\Big\}\Big\{\int\limits_{-\infty}^{X_0-X}e^{i\frac{\nu}{u}\lambda}\frac{d\lambda}{\lambda}\Big\}e^{-i\frac{\nu}{u}(X_0-X)}dX. \tag{6.8}$$

The last term on the right-hand side of eq. (6.8) will now partially be integrated with respect to X, viz.:

$$-\left(i\frac{\nu}{U}\right)^2\int\limits_{-l(Y_0)}^{l(Y_0)}\Big\{\int\limits_{-l(Y_0)}^{X}\Delta\gamma_X(X', Y_0)dX'\Big\}\Big\{\int\limits_{-\infty}^{X_0-X}e^{i\frac{\nu}{U}}\frac{d\lambda}{\lambda}\Big\}e^{-i\frac{\nu}{U}(X_0-X)}dX =$$

$$= -i\frac{\nu}{U}\int\limits_{-l(Y_0)}^{l(Y_0)}\Delta\gamma_X(X', Y_0)dX' \cdot e^{-i\frac{\nu}{U}(X_0-l)}\int\limits_{-\infty}^{X_0-l(Y_0)}e^{i\frac{\nu}{U}\lambda}\frac{d\lambda}{\lambda} +$$

$$+ i\frac{\nu}{U}\int\limits_{-l(Y_0)}^{l(Y_0)}\Delta\gamma_X(X, Y_0)e^{-i\frac{\nu}{U}(X_0-X)}\Big\{\int\limits_{-\infty}^{X_0-X}e^{i\frac{\nu}{U}\lambda}\frac{d\lambda}{\lambda}\Big\}dX + i\frac{\nu}{U}\int\limits_{-l(Y_0)}^{l(Y_0)}\Big\{\int\limits_{-l(Y_0)}^{X}\Delta\gamma_X(X', Y_0)dX'\Big\}\frac{dX}{X-X_0}. \tag{6.9}$$

Substitution of eq. (6.9) into eq. (6.8) yields:

$$2\pi w_1(X_0, Y_0) = -\int\limits_{-l(Y_0)}^{l(Y_0)}\frac{\Delta\gamma_Y(X, Y_0)}{X-X_0}dX - i\frac{\nu}{U}\int\limits_{-l(Y_0)}^{l(Y_0)}\Delta\gamma_Y(X', Y_0)dX' \cdot e^{-i\frac{\nu}{U}(X_0-l)}\int\limits_{-\infty}^{X_0-l}e^{i\frac{\nu}{U}\lambda}\frac{d\lambda}{\lambda} \tag{6.10}$$

Introduce now:

$$\Delta\Gamma(Y_0) = \int\limits_{-l(Y_0)}^{l(Y_0)}\Delta\gamma_Y(X', Y_0)dX' \tag{6.11}$$

and furthermore

$$\lambda = X_0 - t. \tag{6.12}$$

Eq. (6.10) then becomes:

$$2\pi w_1(X_0, Y_0) = -\int\limits_{-l(Y_0)}^{l(Y_0)}\frac{\Delta\gamma_Y(X, Y_0)}{X-X_0}dX + i\frac{\nu}{U}\Delta\Gamma(Y_0)e^{i\frac{\nu}{U}l}\int\limits_{l(Y_0)}^{\infty}e^{-i\frac{\nu}{U}t}\frac{dt}{t-X_0}. \tag{6.13}$$

Consider now the eq. (6.6). Analogous to the eq. (5.1) we have:

$$\gamma_Y = (\gamma_Y^{(2)} + \Delta\gamma)\cos\varphi$$

and hence from eq. (6.3) it follows:

$$\frac{\partial\gamma_\xi}{\partial X} = -\varepsilon\frac{\partial[\gamma_Y^{(2)}\cos\varphi]}{\partial Y} + 0(\varepsilon^2) \tag{6.14}$$

Introducing eq. (6.14) into (6.6) we obtain:

$$2\pi w_1(X_0, Y_0) = -\sin\varphi \int_{-l}^{l} \frac{\partial\gamma_\xi}{\partial X}(X, X_0) e^{-i\frac{\nu}{U}(X_0-X)} \int_{-\infty}^{X_0-X} e^{i\frac{\nu}{U}\lambda} \frac{d\lambda}{\lambda}\, dX -$$

$$- i\frac{\nu}{U}\sin\varphi \int_{-l}^{l} \gamma_\xi(X, Y_0)\, e^{-i\frac{\nu}{U}(X_0-X)} \int_{-\infty}^{X_0-X} e^{i\frac{\nu}{U}\lambda} \frac{d\lambda}{\lambda}\, dX. \tag{6.15}$$

Partial integration of the first term on the right hand side of eq. (6.15) yields:

$$2\pi w_1(X_0, Y_0) = -\sin\varphi \Big\{ \gamma_\xi(l, Y_0) e^{-i\frac{\nu}{U}(X_0-l)} \int_{-\infty}^{X_0-l} e^{i\frac{\nu}{U}\lambda} \frac{d\lambda}{\lambda} -$$

$$- \gamma_\xi(-l, Y_0) e^{-i\frac{\nu}{U}(X_0+l)} \int_{-\infty}^{X_0+l} e^{i\frac{\nu}{U}\lambda} \frac{d\lambda}{\lambda} \Big\} + \sin\varphi \int_{-l}^{l} \gamma_\zeta(X, Y_0) \frac{dX}{X - X_0}. \tag{6.16}$$

Due to the singularity on the leading edge of the airfoil, the term $\gamma_\zeta(-l, Y_0)$ is formally undetermined. However, from the physical point of view, the pressure jump on the leading edge, and hence also the vorticity, must be equal to zero. Making furthermore use of the relation (6.12) we obtain:

$$2\pi w_1(X_0, Y_0) = \sin\varphi \Big\{ \int_{-l}^{l} \frac{\gamma_\xi(X, Y_0)}{X - X_0} dX + \gamma_\xi(l, Y_0) e^{i\frac{\nu}{U}l} \int_{l}^{\infty} e^{-i\frac{\nu}{U}t} \frac{dt}{t - X_0} \Big\}. \tag{6.17}$$

Eq. (6.17), together with eq. (6.13) gives us finally the integral equation for incompressible flow, viz.:

$$\int_{-l}^{l'} \frac{\Delta\gamma_Y(X, Y_0)}{X - X_0} dX - i\frac{\nu}{U}\Delta\Gamma(Y_0) e^{i\frac{\nu}{U}l} \int_{l}^{\infty} e^{-i\frac{\nu}{U}t} \frac{dt}{t - X_0} + \sin\varphi \int_{-l}^{l} \gamma_\xi(X, Y_0) \frac{dX}{X - X_0} +$$

$$+ \sin\varphi\gamma_\xi(l, Y_0) e^{i\frac{\nu}{U}l} \int_{l}^{\infty} e^{-i\frac{\nu}{U}t} \frac{dt}{t - X_0} = 0 \tag{6.18}$$

Eq. (6.18) is identical with the integral equation given in section 6 of ref. 2. This equation is solved in ref. 2 for the case of φ being constant along the span (wing with a simple sweep).

7 On the solution of the approximate integral equation.

In section 5 we have shown, that according to our strip theory the additional pressure, which represents the effect of sectional sweep of the wing, follows from an integral equation of the Possio-type. The prescribed downwash, however, is given in an expression of somewhat complicated form, including integrals over the chordwise pressure distribution in two-dimensional flow.

It seems of great practical importance to solve this equation, as one would obtain tabulated values of the aerodynamic forces and moments, which would make it possible to perform the flutter calculations on wings of any shape in compressible flow, with the same accuracy and simplicity as in the case of straight wing. There are two possible ways of solution. In this report we shall only point them out, without going into a detailed discussion. To investigate these methods more closely and to arrive to a final computational procedure is a separate task which has as yet not been performed.

The first method is, to solve the eq. (5.3) by means of the usual procedure of numerical solution of the Possio equation. However, before doing so, an extensive preparatory work must be performed consisting of the evaluation and tabulation of $w_1(X_0, Y_0)$ given by eq. (5.4), where use must be made of the known tabulated results for the pressure distribution in two-dimensional flow.

The second method is based on the following reasoning: We know the solution of the Possio equation in the form of an infinite series in terms of Mathieu-functions. It is the solution of the two-dimensional problem of an oscillating airfoil in compressible flow given by TIMMAN and VAN DE VOOREN in ref. 10 and it was shown in ref. 11 that this solution indeed satisfies the Possio equation. Hence, we obtain a solution of our problem if we substitute w_1 given by eq. (5.4) into the solution given in ref. 10, and put for M the value $M_1 = M\cos\varphi$. The only terms which are a function of the downwash in TIMMAN and VAN DE VOOREN's solution, are the coefficients Q_n, given by:

$$Q_n = -\frac{2}{\pi\nu\beta} \int_0^{\pi} e^{-i\frac{M^2}{\beta^2}\omega\cos\eta} \Big\{ \frac{dw}{d\eta}(0, \eta) -$$

$$- i\omega\sin\eta\, w(0, \eta) \Big\}\; se_n(\eta)\, d\eta \tag{7.1}$$

where

$$X = l\cosh\xi\cos\eta. \tag{7.2}$$

Hence, what we have to do, is to substitute the values of w_1 from eq. (5.4) for w and M_1 for M and evaluate the new Q_n. When this is done, p can be computed using the same procedure which was used by TIMMAN and VAN DE VOOREN to obtain numerical results in the two-dimensional case.

It is at the present not yet possible to predict, which of the two methods requires less computational work.

8 References.

1. ECKHAUS, W. On the Theory of Oscillating Airfoils of Finite Span in Subsonic Flow. N.L.L. Report F. 153 (1954).
2. VAN DE VOOREN, A. I. and ECKHAUS, W. Strip Theory for Oscillating Swept Wings in Incompressible Flow. N.L.L. Report F. 146 (1954).
3. KÜSSNER, H .C. Allgemeine Tragflächentheorie. Luftfahrtforschung. Vol. 17, p. 370 (1940).
4. WATKINS, C. E., RUNYAN, H. L. and WOOLSTON, D. S. *On the Kernel Function of the Integral Equation Relating the Lift and Downwash Distribution of Oscillating Finite Wings in Subsonic Flow.* N.A.C.A. T. N. 3131 (1954).
5. TIMMAN, R. et LEMAIGRE, B. La ligne portante de forme arbitraire considérée comme cas limite d'une surface portante en fluide incompressible. N.L.L. Report F. 95 (1951).
6. GREIDANUS, J. H. and VAN HEEMERT, A. Theory of *the Oscillating Airfoil in Two-Dimensional Incompressible Flow.* N.L.L. Report F. 41 (1948).
7. WATSON, G. N. A Treatise on the Theory of Bessel Functions, Cambridge. At the University Press (1944).
8. SCHWARZ, L. Berechnung der Druckverteilung einer harmonisch sich verformenden Tragfläche in ebener Strömung. Luftfahrforschung, Vol. 17, p. 379 (1940).
9. MUSKHELISHVILI, N. I. Singular Integral Equations (1946). *Translated by I. R. M. Radok, Noordhoff,* Groningen (1953).
10. TIMMAN, R. and VAN DE VOOREN, A. I. Theory of the Oscillating Wing with Aerodynamically Balanced Control Surface in a Two-dimensional Subsonic Compressible Flow. N.L.L. Report F. 54 (1949).
11. VAN SPIEGEL, E. and VAN DE VOOREN, A. I. On the Theory of the Oscillating Wing in Two-Dimensional Subsonic Flow. N.L.L. Report F. 142 (1953).
12. SCHWARZ, L. Untersuchung einiger mit den Zylinderfunktionen nullter Ordnung verwandter Funktionen. Luftfahrtforschung, Vol. 20, p. 341 (1944).

APPENDIX A.

Calculation of the integrals I_n.

A.1. General considerations.

In this appendix we shall investigate the integrals $I_n{}^{(r)}$ and $I_n{}^{(l)}$, as defined by eq. (4.3), viz.

$$I_n{}^{(r)} = \lim_{z_0 \to 0} \frac{\partial^2}{\partial z_0{}^2} \int\limits_0^{Y_1(X)} \int\limits_{-\infty}^{X_0-X} e^{i\frac{\nu}{u}\frac{1}{\beta^2}\left[\lambda + \frac{M^2}{\varepsilon}(Y_0-Y)\tan\varphi - \frac{M}{\varepsilon}R'_r\right]} \frac{(Y-Y_0)^n}{R_r'}\, d\lambda\, dY$$

$$I_n{}^{(l)} = \lim_{z_0 \to 0} \frac{\partial^2}{\partial z_0{}^2} \int\limits_{-Y_1(X)}^{0} \int\limits_{-\infty}^{X_0-X} e^{i\frac{\nu}{u}\frac{1}{\beta^2}\left[\lambda + \frac{M^2}{\varepsilon}(Y_0+Y)\tan\varphi - \frac{M}{\varepsilon}R'_l\right]} \frac{(Y+Y_0)^n}{R_l'}\, d\lambda\, dY \tag{A.1}$$

where

$$R_r' = \{[\varepsilon\lambda + (Y_0 - Y)\tan\varphi]^2 + \beta^2(Y_0 - Y)^2 + \varepsilon^2\beta^2 z_0{}^2\}^{\frac{1}{2}}$$

$$R_l' = \{[\varepsilon\lambda + (Y_0 + Y)\tan\varphi]^2 + \beta^2(Y_0 - Y)^2 + \varepsilon^2\beta^2 z_0{}^2\}^{\frac{1}{2}} \tag{A.2}$$

The order of integration will be interchanged by writing

$$I_n = \lim_{z_0 \to 0} \frac{\partial^2}{\partial z_0{}^2} \int\limits_{-\infty}^{X_0-X} K_n\, d\lambda \tag{A.3}$$

where

$$K_n{}^{(r)} = \int\limits_0^{Y_1(X)} e^{i\frac{\nu}{U}\frac{1}{\beta^2}\left[\lambda + \frac{M^2}{\varepsilon}(Y_0-Y)\tan\varphi - \frac{M}{\varepsilon}R'_r\right]} \frac{(Y-Y_0)^n}{R_r'}\, dY$$

$$K_n{}^{(l)} = \int\limits_{-Y_1(X)}^{0} e^{i\frac{\nu}{U}\frac{1}{\beta^2}\left[\lambda + \frac{M^2}{\varepsilon}(Y_0+Y)\tan\varphi - \frac{M}{\varepsilon}R'_l\right]} \frac{(Y+Y_0)^n}{R_l'}\, dY. \tag{A.4}$$

The investigation will be performed under the assumption $M \neq 0$. Later we shall show the results to be valid also in the limiting case $M = 0$, by comparing them with the known solution for incompressible flow (see section 6).

A.2. Reduction of $K_n^{(r)}$.

Introduce

$$M_1 = M \cos\varphi, \quad \beta_1 = \sqrt{1 - M_1^2} \tag{A.5}$$

which represent the Mach-number and the β-value for the flow component perpendicular to the swept wing.

Introduce moreover

$$\begin{aligned} (Y_0 - Y)\,\frac{\beta_1^2}{\cos^2\varphi} + \varepsilon\lambda \tan\varphi &= \alpha \\ \lambda^2 + \frac{\beta_1^2}{\cos^2\varphi}\, z_0^2 &= r^2 \end{aligned} \tag{A.6}$$

where α denotes the new variable of integration.

It can be shown by a suitable reduction that

$$R_r'^2 = \frac{\cos^2\varphi}{\beta_1^2}\,(\alpha^2 + \varepsilon^2\beta^2 r^2) \tag{A.7}$$

while

$$Y - Y_0 = \frac{\cos^2\varphi}{\beta_1^2}\,(\varepsilon\lambda\tan\varphi - \alpha)\,. \tag{A.8}$$

Substituting this in eq. (A.4), one obtains

$$K_n^{(r)} = \frac{\cos^{2n+1}\varphi}{\beta_1^{2n+1}}\, e^{i\frac{\nu}{u}\frac{1}{\beta_1^2}\lambda} \int_{\alpha_1}^{\alpha_2} e^{i\frac{\nu}{U\beta^2}\frac{M_1}{\varepsilon\beta_1}\left(\frac{M_1}{\beta_1}\alpha\tan\varphi - \sqrt{\alpha^2+\varepsilon^2\beta^2 r^2}\right)} \frac{(\varepsilon\lambda\tan\varphi - \alpha)^n}{\sqrt{\alpha^2+\varepsilon^2\beta^2 r^2}}\, d\alpha \tag{A.9}$$

where the limits of integration are

$$\begin{aligned} \alpha_1 &= (Y_0 - Y_1)\,\frac{\beta_1^2}{\cos^2\varphi} + \varepsilon\lambda\tan\varphi \\ \alpha_2 &= Y_0\,\frac{\beta_1^2}{\cos^2\varphi} + \varepsilon\lambda\tan\varphi. \end{aligned} \tag{A.10}$$

Introduce again a new integration variable t by

$$\alpha = \varepsilon\beta\, r\, t \tag{A.11}$$

which makes $K_n^{(r)}$ equal to

$$K_n^{(r)} = \frac{\cos^{2n+1}\varphi}{\beta_1^{2n+1}}\,\varepsilon^n\, e^{i\frac{\nu}{U\beta_1^2}\lambda} \int_{t_1}^{t_2} e^{i\frac{\nu}{U\beta}\frac{M_1 r}{\beta_1}\left(\frac{M_1}{\beta_1}t\tan\varphi - \sqrt{t^2+1}\right)} \frac{(\lambda\tan\varphi - \beta r t)^n}{\sqrt{t^2+1}}\, dt \tag{A.12}$$

where

$$\begin{aligned} t_1 &= \frac{\lambda}{\beta r}\tan\varphi + \frac{(Y_0 - Y_1)}{\varepsilon}\,\frac{\beta_1^2}{\beta r\cos^2\varphi} \\ t_2 &= \frac{\lambda}{\beta r}\tan\varphi + \frac{Y_0}{\varepsilon}\,\frac{\beta_1^2}{\beta r\cos^2\varphi}. \end{aligned} \tag{A.13}$$

Let it first be assumed that $0 < Y_0 < Y_1$. Then, for $\varepsilon \to 0$, we have $t_1 \to -\infty$ and $t_2 \to +\infty$. The integral in (A.12) will then be replaced by

$$K_n^{(r)} = K_{n_1}^{(r)} - K_{n_2}^{(r)} - K_{n_3}^{(r)} \tag{A.14}$$

where the limits of integration of $K_{n_1}^{(r)}$, $K_{n_2}^{(r)}$, and $K_{n_3}^{(r)}$ are $-\infty$ and $+\infty$, $-\infty$ and t_1, t_2 and $+\infty$ respectively.

In order to reduce the first of these three integrals, the substitutions

$$t = \sinh\vartheta \tag{A.15}$$

$$\begin{aligned} \frac{M_1}{\beta_1}\tan\varphi &= \frac{\beta}{\beta_1}\sinh\theta \\ 1 &= \frac{\beta}{\beta_1}\cosh\theta \end{aligned} \tag{A.16}$$

will be made. (A.16) is allowed since

$$\frac{\beta_1^2}{\beta^2} - \frac{M_1^2\tan^2\varphi}{\beta^2} = 1.$$

Hence

$$K_{n_1}(r) = \varepsilon^n \left(\frac{\cos\varphi}{\beta_1}\right)^{2n+1} e^{i\frac{\nu}{U\beta_1^2}\lambda} \int_{-\infty}^{\infty} e^{-i\frac{\nu}{U}\frac{M_1}{\beta_1^2} r\cosh(\vartheta-\theta)} (\lambda\tan\varphi - \beta r\sinh\vartheta)^n \, d\vartheta. \qquad \text{(A.17)}$$

As will be shown in Sec. A.3, this formula leads to Hankel functions of the second kind. The convergence of the integral is ascertained by the usual assumption $Im\,\nu < 0$.

Consider now $K_{n_3}(r)$. Since the integration-variable t assumes large values in the whole interval, one has

$$\frac{M_1}{\beta_1} t\tan\varphi - \sqrt{t^2+1} = \left(\frac{M_1}{\beta_1}\tan\varphi - 1\right) t + 0\left(\frac{1}{t}\right)$$

and

$$\sqrt{t^2+1} = t + 0\left(\frac{1}{t}\right).$$

Neglecting for the moment the terms $0\left(\frac{1}{t}\right)$, K_{n_3} becomes equal to

$$K_{n_3}(r) = \frac{\cos^{2n+1}\varphi}{\beta_1^{2n+1}} \varepsilon^n e^{i\frac{\nu}{U\beta_1^2}\lambda} \int_{t_2}^{\infty} e^{i\frac{\nu}{U\beta}\frac{M_1 r}{\beta_1}\left(\frac{M_1}{\beta_1}\tan\varphi - 1\right)t} \frac{(\lambda\tan\varphi - \beta r t)^n}{t} dt.$$

Introducing rt as new variable, it is seen that the parameter r disappears completely, both from the integrand and from the limits of integration (using (A.13)). Hence, this approximation for $K_{n_3}(r)$ becomes independent of r and also of z_0 (see (A.6)). This means that in this approximation no contribution is made toward I_n (A.3).

Taking now into account the terms $0\left(\frac{1}{t}\right)$, it follows that $K_{n_3}(r)$ consists of terms proportional to

$$\left.\begin{array}{l} \varepsilon^n e^{i\frac{\nu}{u\beta_1^2}\lambda} \nu r^{k+1} \int_{t_2}^{\infty} e^{i\nu Brt} t^{k-2} dt \\ \text{from } 0(t) \text{ in the exponential)} \\ \varepsilon^n e^{i\frac{\nu}{u\beta_1^2}\lambda} r^k \int_{t_2}^{\infty} e^{i\nu Brt} t^{k-3} dt \\ \text{from } 0(t) \text{ in the denominator} \end{array}\right\} k = 0, 1, 2, n$$

where

$$B = \frac{M_1}{U\beta\beta_1}\left(\frac{M_1}{\beta_1}\tan\varphi - 1\right).$$

Since $t_2 = 0\left(\frac{1}{\varepsilon}\right)$, the expansion

$$\int_{t_2}^{\infty} \frac{e^{i\nu Brt}}{t} dt = -e^{i\nu Brt}\left(\frac{1}{i\nu Brt_2} + \frac{1}{(i\nu Brt_2)^2} + \ldots\right)$$

valid for large t_2, yields terms of order $\frac{\varepsilon}{\nu}$, $\frac{\varepsilon^2}{\nu^2}$ etc.

Similarly

$$\int_{t_2}^{\infty} \frac{e^{i\nu Brt}}{t^2} dt \text{ yields terms of order } \frac{\varepsilon^2}{\nu}, \frac{\varepsilon^3}{\nu^2} \text{ etc.};$$

$$\int_{t_2}^{\infty} e^{i\nu Brt} dt = 0\left(\frac{1}{\nu}\right).$$

$$\int_{t_2}^{\infty} e^{i\nu Brt}\, t\, dt \text{ yields terms of order } \frac{1}{\varepsilon\nu}, \frac{1}{\nu^2}.$$

Since n is always at least equal to k, careful examination shows that $K_{n_3}(r)$ contains terms of order

$$\varepsilon^2 e^{i\frac{\nu}{u\beta_1^2}\lambda}, \quad \frac{\varepsilon^3}{\nu} e^{i\frac{\nu}{u\beta_1^2}\lambda} \quad \text{etc.}$$

The integration to λ, to be performed according to eq. (A.3), makes that the error in I_m due to the neglect of $K_{n_3}(r)$ is order $\frac{\varepsilon^2}{\nu}$ (and further terms $\frac{\varepsilon^3}{\nu^2}$ etc.). A similar reasoning shows that neglect of $K_{n_2}(r)$ causes an error of the same order. If Y_0 is longer than Y_1, both t_1 and t_2 become $+\infty$ if $\varepsilon \to 0$. There is then no term similar to $K_{n_1}(r)$ and the whole result is $0\left(\frac{\varepsilon^2}{\nu}\right)$. This means that the final integration to X, given by eq. (4.2), is confined to the interval $-l(Y)$ to $l(Y)$.

A.3 *Calculation of* $J_n(r)$.

It has been shown in Sec. (A.2) that eq. (A.3) may be replaced by

$$I_n(r) = \lim_{z_0 \to 0} \frac{\partial^2}{\partial z_0^2} \int_{-\infty}^{X_0 - X} K_{n_1}(r)\, d\lambda + 0\left(\frac{\varepsilon^2}{\nu}\right) \qquad \text{(A.18)}$$

Substituting $\vartheta - \theta = \gamma$ into eq. (A.17) and using the formula

$$\int_0^{\infty} e^{-iz\cosh\gamma} \cosh n\gamma \, d\gamma = \frac{\pi}{2i} e^{-in\frac{\pi}{2}} H_n^{(2)}(z) \qquad \text{(A.19)}$$

one obtains

$$
\left.\begin{aligned}
K_0^{(2)} &= \frac{\pi}{i}\ \frac{\cos\varphi}{\beta_1} e^{i\frac{\nu}{u\beta_1^2}\lambda}\ H_0^{(2)}\left(\frac{\nu}{U}\ \frac{M_1}{\beta_1^2} r\right) \\
K_1^{(2)} &= \frac{\pi}{i}\,\varepsilon\left(\frac{\cos\varphi}{\beta_1}\right)^3 \tan\varphi\, e^{i\frac{\nu}{u\beta_1^2}\lambda} \left\{\lambda\, H_0^{(2)}\left(\frac{\nu}{U}\ \frac{M_1}{\beta_1^2} r\right) + irM_1 H_1^{(2)}\left(\frac{\nu}{U}\ \frac{M_1}{\beta_1^2} r\right)\right\} \\
K_2^{(2)} &= \frac{\pi}{i}\,\varepsilon^2\left(\frac{\cos\varphi}{\beta_1}\right)^5 e^{i\frac{\nu}{u\beta_1^2}\lambda} \left\{\left(\lambda^2\tan^2\varphi - \frac{\beta^2 r^2}{2}\right) H_0^{(2)}\left(\frac{\nu}{U}\ \frac{M_1}{\beta_1^2} r\right) + \right. \\
&\qquad \left. + 2\,i\lambda r M_1 \tan^2\varphi\, H_1^{(2)}\left(\frac{\nu}{U}\ \frac{M_1}{\beta_1^2} r\right) - r^2 M_1\beta_1 \tan\varphi\, H_2^{(2)}\left(\frac{\nu}{U}\ \frac{M_1}{\beta_1^2} r\right)\right\}
\end{aligned}\right\} \tag{A.20}
$$

It follows from the second equation (A.6) that

$$
\frac{\partial^2}{\partial z_0^2} = \left(\frac{dr}{dz_0}\right)^2 \frac{\partial^2}{\partial z^2} + \frac{d^2 r}{dz_0^2}\ \frac{\partial}{\partial r}
$$

and hence

$$
\lim_{z_0\to 0} \frac{\partial^2}{\partial z_0^2} = \frac{\beta_1^2}{\cos^2\varphi}\ \frac{1}{|\lambda|} \lim_{z\to|\lambda|} \frac{\partial}{\partial r} + \frac{\beta_1^4}{\cos^4\varphi} \lim_{z_0\to 0} \left\{\frac{z_0^2}{r^2}\ \frac{\partial^2}{\partial r^2} - \frac{z_0^2}{r^3}\ \frac{\partial}{\partial r}\right\}. \tag{A.21}
$$

If this equation is used, the operation $\lim\limits_{z_0\to 0} \dfrac{\partial^2}{\partial z_0^2}$ should first be brought under the integralsign in eq. (A.18).

The second term on the right hand side of eq. (A.21) will always lead to a contribution equal to 0 except possibly at the singular point $\lambda = 0$. This means that if we assume

$$
\lim_{z_0\to 0} \frac{\partial^2}{\partial z_0} = \frac{\beta_1^2}{\cos^1\varphi}\ \frac{1}{|\lambda|} \lim_{r\to|\lambda|} \frac{\partial}{\partial r} \tag{A.22}
$$

the results will be correct for $X_0 - X < 0$, but may be incorrect for $X_0 - X > 0$, viz. if the integral resulting from the omitted term is divergent.

It appears that this complication only occurs for the integral $I_0(r)$. However, as is shown in Sec. 3, the true result for $I_0(r)$ if $X_0 - X > 0$ is known and hence we will use for the moment eq. (A.22). Finaly, the result for $I_0(r)$ should be modified if $X_0 - X > 0$.

By aid of eqs. (A.18), (A.20) and (A.22), it is found that

$$
\begin{aligned}
I_0(r) &= -\pi i \frac{\beta_1}{\cos\varphi} \int_{-\infty}^{X_0-X} e^{i\frac{\nu}{u\beta_1^2}\lambda}\ \frac{1}{|\lambda|} \lim_{r\to|\lambda|} \frac{\partial}{\partial r}\ H_0^{(2)}\left(\frac{\nu}{U}\ \frac{M_1}{\beta_1^2} r\right) d\lambda \\
I_1(r) &= -\pi i\varepsilon \left(\frac{\sin\varphi}{\beta_1}\right) \int_{-\infty}^{X_0-X} e^{i\frac{\nu}{u\beta_1^2}\lambda}\ \frac{1}{|\lambda|} \lim_{r\to|\lambda|} \frac{\partial}{\partial r} \left\{\lambda H_0^{(2)}\left(\frac{\nu}{U}\ \frac{M_1}{\beta_1^2} r\right) + irM_1 H_1^{(2)}\left(\frac{\nu}{U}\ \frac{M_1}{\beta_1^2} r\right)\right\} d\lambda \\
I_2(r) &= -\pi i\varepsilon^2 \left(\frac{\cos\varphi}{\beta_1}\right)^3 \int_{-\infty}^{X_0-X} e^{i\frac{\nu}{u\beta_1^2}\lambda}\ \frac{1}{|\lambda|} \lim_{r\to|\lambda|} \frac{\partial}{\partial r} \left\{\left(\lambda^2\tan^2\varphi - \frac{\beta^2 r^2}{r}\right) H_0^{(2)}\left(\frac{\nu}{U}\ \frac{M_1}{\beta_1^2} r\right) + \right. \\
&\qquad \left. + 2\,i\lambda r M_1 \tan^2\varphi\, H_1^{(2)}\left(\frac{\nu}{U}\ \frac{M_1}{\beta_1^2} r\right) - r^2 M_1\beta_1 \tan\varphi\, H_2^{(2)}\left(\frac{\nu}{U}\ \frac{M_1}{\beta_1^2} r\right)\right\} d\lambda.
\end{aligned} \tag{A.23}
$$

Making use of the following relations, valid for any cylinder function,

$$
\left.\begin{aligned}
z\, C_n'(z) &= n\, C_n(z) - z\, C_{n+1}(z) \\
z\, C_n'(z) &= -n\, C_n(z) + z\, C_{n-1}(z)
\end{aligned}\right\} \tag{A.24}
$$

eqs. (A.23) may be simplified to

$$
\begin{aligned}
I_0(r) &= \pi i \frac{\nu M_1}{U\beta_1 \cos\varphi} \int_{-\infty}^{X_0-X} e^{i\frac{\nu}{u\beta_1^2}\lambda}\ H_1^{(2)}\left(\frac{\nu}{U}\ \frac{M_1}{\beta_1^2}|\lambda|\right) \frac{d\lambda}{|\lambda|} \\
I_1(r) &= \pi\varepsilon \frac{\nu M_1 \sin\varphi}{U\beta_1^3} \int_{-\infty}^{X_0-X} e^{i\frac{\nu}{u\beta_1^2}\lambda} \left\{M_1 H_0^{(2)}\left(\frac{\nu}{U}\ \frac{M_1}{\beta_1^2}|\lambda|\right) + i\frac{\lambda}{|\lambda|} H_1^{(2)}\left(\frac{\nu}{U}\ \frac{M_1}{\beta_1^2}|\lambda|\right)\right\} d\lambda
\end{aligned} \tag{A.25}
$$

$$I_2^{(r)} = \pi i \varepsilon^2 \left(\frac{\cos\varphi}{\beta_1}\right)^3 \int\limits_{-\infty}^{X_0-X} e^{i\frac{\nu}{u\beta_1^2}\lambda} \left[\left(\beta^2 - 2i\frac{\nu}{U}\frac{M_1^2}{\beta_1^2}\lambda\right) H_0^{(2)}\left(\frac{\nu}{U}\frac{M_1}{\beta_1^2}|\lambda|\right) + \right.$$

$$\left. + \frac{\nu}{U}\frac{M_1}{\beta_1^2}|\lambda| \left\{ \tan^2\varphi - \frac{\beta^2}{2} + M_1\beta_1 \tan\varphi \right\} H_1^{(2)}\left(\frac{\nu}{U}\frac{M_1}{\beta_1^2}|\lambda|\right)\right] d\lambda.$$

It follows from eq. (A.18) that if we use these expressions for $I_0^{(r)}$ and $I_1^{(r)}$ an error of order $\frac{\varepsilon^2}{\nu}$ is made. Hence, the approximation goes wrong for $\nu \to 0$ but holds for $\nu \to \infty$. We shall show now that if $I_2^{(r)}$ is neglected completely, the error which is made is again of order $\frac{\varepsilon^2}{\nu}$ if $\nu \to 0$, while it is of order $\frac{\varepsilon^2}{\sqrt{\nu}}$ if $\nu \to \infty$.

Putting

$$\frac{\nu}{U\beta_1^2}|\lambda| = t \tag{A.26}$$

it follows that

$$\left.\begin{aligned} I_2^{(r)} &= \pi i \frac{\varepsilon^2}{\nu} \frac{U\cos\varphi}{\beta_1^3} \left\{ \int\limits_0^{\nu\infty} f_1(t)dt - \int\limits_0^{T} f_1(t)dt \right\} \text{ if } X_0 - X < 0 \\ I_2^{(r)} &= \pi i \frac{\varepsilon^2}{\nu} \frac{U\cos\varphi}{\beta_1^3} \left\{ \int\limits_0^{\nu\infty} f_1(t)dt + \int\limits_0^{T} f_2(t)dt \right\} \text{ if } X_0 - X > 0 \end{aligned}\right\} \tag{A.27}$$

where

$$f_1(t) = e^{-it}\left\{(\beta^2 + 2iM_1^2t)H_0^{(2)}(M_1t) + M_1t(\tan^2\varphi - \frac{\beta^2}{2} + M_1\beta_1\tan\varphi)H_1^{(2)}(M_1t)\right\}$$

$$f_2(t) = e^{it}\left\{(\beta^2 - 2iM_1^2t)H_0^{(2)}(M_1t) + M_1t(\tan^2\varphi - \frac{\beta^2}{2} + M_1\beta_1\tan\varphi)H_1^{(2)}(M_1t)\right\}$$

and

$$T = \frac{\nu}{U\beta_1^2}|X_0 - X|. \tag{A.28}$$

For $\nu \to 0$ both cases yield

$$I_2^{(r)} = \pi i \frac{\varepsilon^2}{\nu} \frac{U\cos\varphi}{\beta_1^3} \int\limits_0^{\nu\infty} f_1(t)dt.$$

The condition $Im\,\nu < 0$ makes that the integral converges and that $I_2^{(r)} = 0\left(\frac{\varepsilon^2}{\nu}\right)$ if $\nu \to 0$.
For $\nu \to \infty$, one has to consider the three integrals

$$\int\limits_0^T e^{\pm it} H_0^{(2)}(M_1t)dt, \quad \int\limits_0^T e^{\pm it}\, t\, H_0^{(2)}(M_1t)dt, \quad \int\limits_0^T e^{\pm it}\, t\, H_1^{(2)}(M_1t)dt.$$

Using the asymptotic expansion of the Hankel function viz.

$$\frac{e^{-iM_1t}}{\sqrt{M_1t}},$$

it is seen that the first integral converges for $T \to \infty$, but the two other integrals diverge ($Im\,\nu$ remains small) like $\sqrt{T}$ or using eq. (A.1.28) like $\sqrt{\nu}$. Hence, $I_2^{(r)}$ is of order $\frac{\varepsilon^2}{\sqrt{\nu}}$ if $\nu \to \infty$.

A.4 The left semi-wing.

The left semi-wing shows the important simplification that the integrand never becomes singular since R_l' is always larger than 0.

Since

$$\frac{\partial}{\partial z_0} = \frac{dR_l'}{dz_0} \frac{\partial}{\partial R_l'} = \varepsilon^2\beta^2 \frac{z_0}{R_l'} \frac{\partial}{\partial R_l'}$$

and since $R_l' > 0$, one has

$$\lim_{z_0 \to 0} \frac{\partial^2}{\partial z_0^2} = \frac{\varepsilon^2\beta^2}{R_l'} \frac{\partial}{\partial R_l'}.$$

The expression for $I_n^{(l)}$, eq. (A.1), may then be written as

$$I_n^{(l)} = \varepsilon^2\beta^2 \int_{-y_1(X)}^{0} \int_{-\infty}^{X_0-X} \frac{1}{R_l'} \frac{\partial}{\partial R_l'} \left\{ e^{i\frac{\nu}{u\beta^2}\left[\lambda + \frac{M^2}{\varepsilon}(y_0+y)\tan\varphi - \frac{M}{\varepsilon}R'_l\right]} \frac{(y+y_0)^n}{R_l'} d\lambda\, dy \right\}$$

where

$$R_l' = \{(Y_0+Y)^2\tan^2\varphi + \beta^2(Y_0-Y)^2\}^{\frac{1}{2}}$$

Performing the differentiation to R_l' and interchanging the order of integration, the result is

$$I_n^{(l)} = -\varepsilon^2\beta^2 \int_{-\infty}^{X_0-X} e^{i\frac{\nu}{u\beta^2}\lambda} \int_{-y_1(X)}^{0} e^{i\frac{\nu}{u\beta^2}\left[\frac{M^2}{\varepsilon}(y_0+y)\tan\varphi - \frac{M}{\varepsilon}R'_l\right]} \left\{ i\frac{\nu}{U\beta^2}. \frac{M}{\varepsilon} \frac{1}{R_l'^2} + \frac{1}{R_l'^3} \right\} (y+y_0)^n\, dy\, d\lambda$$

Consider first the integration to Y. Due to the fact that

$$M^2(Y_0+Y)\tan\varphi - M R_l'$$

never vanishes, the integrand is highly oscillatory if $\frac{\varepsilon}{\nu}$ is small. Without the factor

$$i\frac{\nu}{U\beta^2} \frac{M}{\varepsilon} \frac{1}{R_l'^2} + \frac{1}{R_l'^3}$$

the integral would be of order $\frac{\varepsilon}{\nu}$. With this factor, the dominant term in the integral becomes of order 1. Performing also the integration to λ, it follows that $I_n^{(l)}$ is again of order $\frac{\varepsilon^2}{\nu}$. It is seen that this result holds also if $\frac{\varepsilon}{\nu}$ is not small, since the integral to Y then again is of order 1.

Completed: 14 Dec. 1954

C.C.L. Class. C 516-4; C 608-4

REPORT M. 1936.

Static Tests and Fatigue Tests on Redux-bonded Built-up and Solid Light-alloy Spar Booms

by

A. HARTMAN and J. H. RONDEEL.

Summary.

Three types of Redux-bonded spar booms were subjected to static tests and fatigue tests in compression and/or bending. For comparison, bending tests were also carried out on solid machined booms.

Angle-section booms were manufactured either by preforming the individual sheets before bonding or by bonding in the flat condition followed by rubber press forming. More complicated sections were bonded from preformed sheets.

The tests results are given in tables and diagrams and the conclusions are listed in section 4.

Contents.

This investigation has been performed by order of the Netherlands Aircraft Development Board (NIV).

1 Introduction.

The excellent experience of the Royal Dutch Aircraft Factories, Fokker, with bonded light-metal joints has led to the consideration of metal bonding as a procedure to build up aircraft spar booms. With this procedure booms with the desired change in section along the length of the booms can be realized in an easy manner by decreasing or increasing the number of glued metal sheets. The expensive milling operation of solid booms can be omitted and this gives a substantial saving in material and manufacturing expenses. Compared with riveted booms an increased strength can be expected because the bonding of the metal sheets over the whole area of contact prevents local buckling. Therefore, technically and economically the bonded boom promises to offer favourable prospects compared with the solid milled boom and booms built up with rivets or bolts.

The first static tests carried out by Fokker (ref. 1) gave encouraging results and it was decided to extend the investigation. In cooperation between Fokker and NLL a test programme was set up containing both static and fatigue tests, which was approved by the Structures Committee of the Netherlands Aircraft Development Board. The results of the investigation are given in this report.

2 Test pieces, test equipment and procedure.

Test pieces.

The bonded test pieces can be divided in 3 types, indicated in this report as type A, type B and type C. The dimensions of the *type A* specimens are given in fig. 1. The specimens were built up by Redux-bonding 2 to 6 preformed sheets of 26 S-T alclad, thickness 1.5 mm, the Redux-bonding being done after bending of the sheets to the correct angle shape.

The *type B* specimens were built up by Redux-bonding 4 or 5 sheets of 24 S-T alclad. The characteristic difference with the type A specimens is that the sheets of the B-specimens were bonded in a flat condition, indicated schematically in fig. 2a and were bent on the rubber press after bonding, as indicated schematically in fig. 2b. With this procedure the forming (of two specimens simultaneously) on the rubber press has to be executed on the heat-treated sheet, because heat-treating of the sheet material after bonding is impossible. Prevention of cracking during forming sets a limit to the plastic deformation to which the outer fibers may be exposed. Test specimens were chosen having a combination of overall thickness and radius of curvature such that cracking

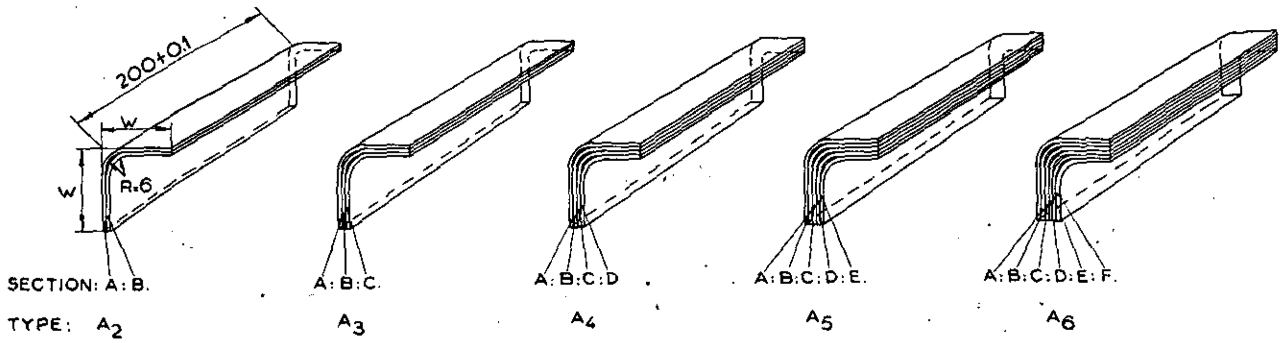

SECTION	WIDTH W
A	33.0
B	31.5
C	30.0
D	28.5
E	27.0
F	25.5

Fig. 1. Redux-bonded sparbooms type A.

did just not occur (fig. 2c). It is evident that from the fatigue point of view such nearly critical booms are the most interesting. Therefore, only these spar booms were tested. The shape and dimensions of the specimens type B are given in fig. 2a to c.

2a

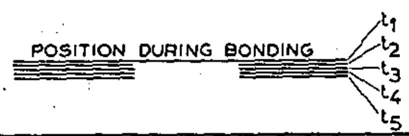

TYPE	t_1	t_2	t_3	t_4	t_5	SHEET THICKNESS	TOTAL THICKNESS
	IN mm						
B_1	1.0	1.0	1.0	0.4	—	3.4	4.0
B_2	1.0	0.8	0.8	0.8	—	3.4	4.0
B_3	1.2	1.2	0.6	0.4	—	3.4	4.0
B_4	1.2	0.6	0.6	0.4	0.4	3.2	4.0
B_5	1.5	1.0	0.5	0.4	—	3.4	4.0

2b

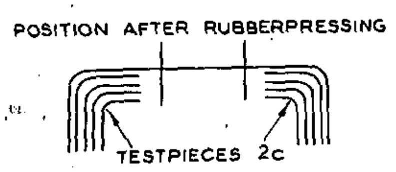

2c

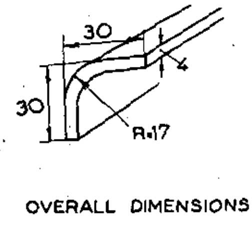

Fig. 2. Redux-bonded sparbooms type B.

The composition of the specimens *type C* is apparent from fig. 3, which gives a survey of the cross-sections of the specimens used in this investigation. Just like the specimens type A the specimens type C have been bonded after the bending of the sheets. They are more complicated and were built up of flat and curved 24 S-T alclad sheets; the length of each specimen was about 300 mm.

All specimens type A—C were bonded at the Royal Dutch Aircraft Factories, Fokker, according to the standard Fokker procedure with Redux, the well-known metal adhesive of Aero Research Ltd in England.

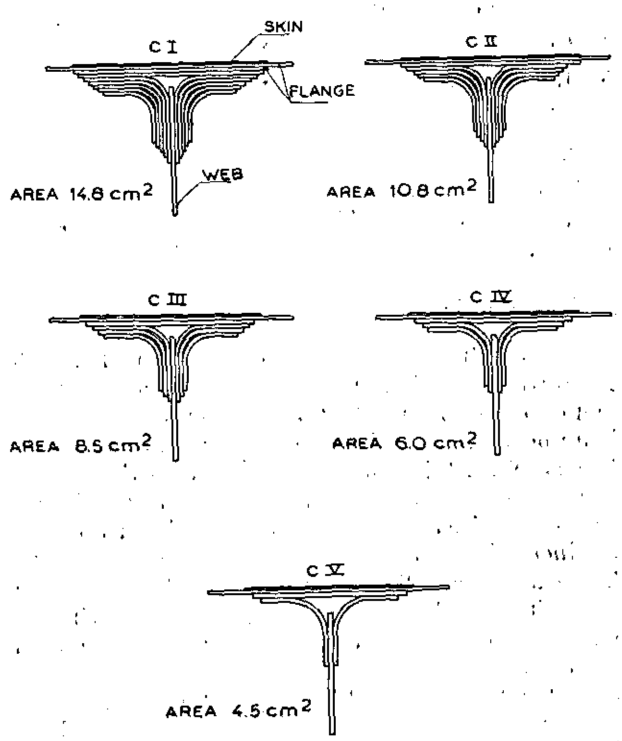

Fig. 3. Redux-bonded sparbooms type C.

TABLE 1.

Mechanical properties of the materials used for the fabrication of the different types of specimens.

Type of specimens	Type of Material	Thickness in mm	Yield Stress $\sigma_{0,2}$ in kg/mm²	U. T. S. σ_T in kg/mm²	Elongation in % $l = 50$ mm
			40.9	46.4	9
A	26 ST	1.5	41.6 mean	46.7	9 mean
	Alclad		40.3 40.4	46.7 46.4	9 9
			40.5	46.7	9
			39.7	45.9	9
			39.6	45.9	9
C(B)	24 ST	0.45	30.5	44.0	15
	Alclad		30.0 mean	44.6 mean	19 mean
		2.0	32.3 31.7	45.7 45.0	17 17
			32.4	45.7	17
D	Fliegw.	ø 41 mm	37.3 mean	52.2 mean	14 mean
	3115.5		38.7 38.0	51.4 51.8	12 13

The *solid specimens* were made in the workshop of the NLL. They were milled from a round bar (Fliegwerkstoff 3115.5) as indicated in fig. 4a. The dimensions of the specimens are given in fig. 4b.

The mechanical properties of the alloys are given in table 1.

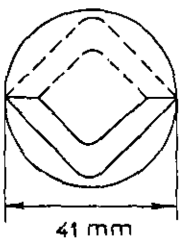

Fig. 4a. Position of the specimen in the bar.

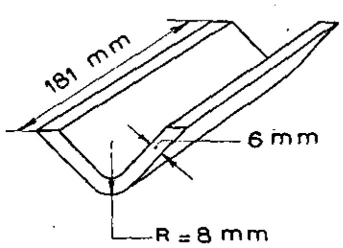

Fig. 4b. Solid specimen.

Test equipment.

The static compression tests were carried out dependent on the magnitude of the load on different machines. The 150 tons Avery Compression testing machine was used for the very high failing loads of the specimens type C 1, C 2 and C 3. This machine is specially suitable for compression tests on panels, stringers etc. because of its large rigidity. For the remaining specimens type C and the specimens type A and B, the 50 tons Amsler fatigue testing machine was used as a static compression testing machine. The static bending tests on the specimens type A and B were carried out on the Amsler 2 and 10 tons Vibraphore with a 2 and 10 tons dynamometer. These 2 Amsler Vibraphores were also used for the compression and the bending fatigue tests on the specimens type A and B. The compression fatigue tests on the specimens type C were carried out on the Amsler 50 tons low frequency fatigue-testing machine. Fig. 5 gives a photo of a specimen type C in the Amsler 50 tons machine during a compression test; fig. 6 gives a photo of a specimen type B in the Amsler Vibraphore during a bending test.

Procedure.

The table next page gives a survey of the tests.

For the *static compression tests* both ends of the specimens were milled flat and parallel. Then they were put in the machine between flat plates and the load was gradually increased till collapse of the specimens. The maximum load was read and particulars on the collapse were observed.

For the *static bending tests* the specimens were supported on the arm of a special fork which was mounted in the Amsler Vibraphore and gradually loaded in the centre with a die till collapse of the specimens. The maximum load was noted. The 3 point bending test set-up is given in fig. 7.

The *fluctuating compression tests* on the bonded specimens type A and B were carried out in the Amsler Vibraphore at a frequency of about 6000/min with a minimum load of 500 kg and a maximum load of 75 % of the static strength. The tests were stopped when after 10^7 cycles no failure had occurred. Because all the specimens investigated in this manner proved to be undamaged after the tests no other loads were tried. The fluctuating compression tests on the bonded specimens type C were carried out in the Amsler 50 tons fatigue testing machine at a frequency of about 525/min.,

Test	Type of specimen			
	A bonded	B bonded	C bonded	D solid
Static compression test to failure	yes	yes	yes	no
Static 3 point bending test (fig. 7)	,,	,,	no	yes
Fluctuating compressive load; max. load 75 % static strength	,,	,,	yes	no
Ditto 68 % static strength	no	no	,,	,,
,, 60 % ,, ,,	,,	,,	,,	,,
Fluctuating bending load 3 point bending test	yes	yes	no	yes

a minimum load of approximately 1 or 2 ton and a maximum load of 75 %, 68 % and 60 % of the static strength. The tests were stopped after an endurance of 5.10^6 cycles or by failure of the specimens.

From the heaviest specimens of this type (C_I) a flange plate of the boom loosened after a certain number of load cycles had been sustained, without collapse of the remaining part of the specimens. Then the tests were continued at a lower load, corresponding to about the same maximum compressive stress in the part left over.

When the specimen did not fail after 5.10^6 cycles the damage caused by the fatigue loading was determined by a static compression test to failure.

The testing arrangement and the machine used for the static bending tests were also used for the *fluctuating bending tests*. The S-N curve at fluctuating bending has been determined for the bonded specimens type A and B and the solid specimens at a ratio of minimum to maximum load of 0.1 and a frequency of about 4000/minute for endurances of 5.10^4 to 5.10^7 cycles. The first tests showed failure of some specimens by longitudinal cracks under the die, caused by bending outwards of the flanges of the specimens. These troubles were solved by fixing a steel clamp round the specimen as indicated in fig. 8. The maximum tensile stress in the bottom sheet was determined by means of strain gauges. As shown in figs 7 and 8, a resistance-wire strain gauge, type Philips nr GM 4473, was stuck in lengthwise direction on the bottom surface in the centre of the specimen on at least 2 specimens of each type. By repeated measuring, the load at which the strain in the outermost fibre reached the value of 0.002 was exactly determined and for every specimen of this type the tensile stress at this load was assumed to be 14 kg/mm². The stress at other loads was supposed to change proportionnally.

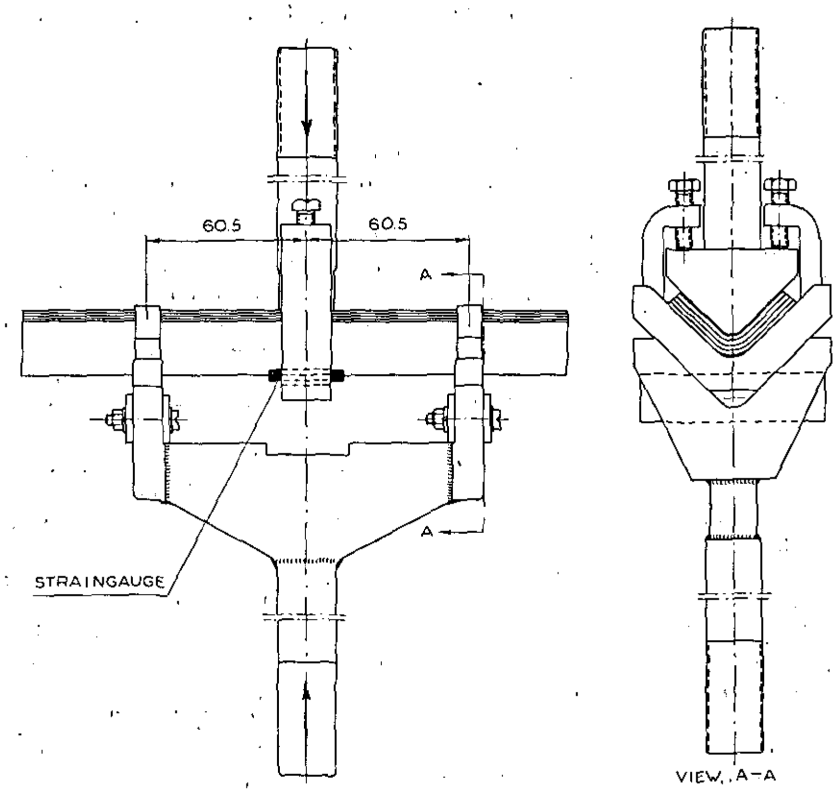

Fig. 7. Set-up for three point bending tests.

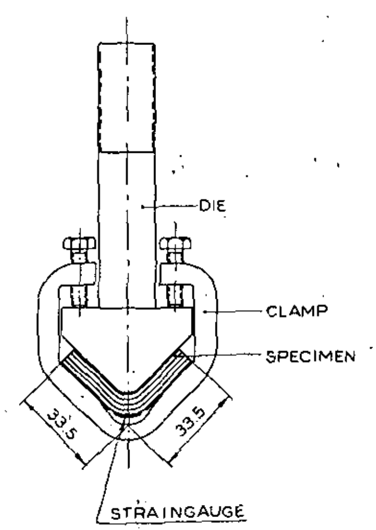

Fig. 8. Clamping of centre of specimens.

Specimen type-nr	Load in kg min	Load in kg max	Number of cycles	Max. load as % static strength	Remarks	Static strength after the fatigue loading in kg
A 2 — 1	—	5970	1	—	—	—
A 2 — 2	1000	4500	10.380.000	appr. 75 %	no failure	—
A 2 — 3	1000	4500	10.000.000	„ „	„ „	6010
A 6 — 1	—	21100	1	—	—	—
A 6 — 2	—	20800	1	—	—	—
A 6 — 3	1000	12600	10.147.000	appr. 60 %	no failure	—
A 6 — 4	1000	15800	10.017.000	„ 75 %	„ „	20900
B 1 — 1	—	5140	1	—	—	—
B 1 — 2	—	5130	1	—	—	—
B 1 — 3	200	3900	14.031.000	appr. 75 %	no failure	5120
B 4 — 1	—	4910	1	—	—	—
B 4 — 2	—	5060	1	—	—	—
B 4 — 3	250	3700	10.707.000	appr. 75 %	no failure	5040

3 Results.

3.1 *Results of the static and fatigue tests in compression on the Redux-bonded spar booms types A and B.*

The results of these tests are given in the table. All specimens tested proved to be undamaged after 10^7 cycles at a compression fatigue loading of 75 % of the static strength. Therefore the investigation was limited to the testing of some representative specimens of each type. For type A these were the thinnest and the thickest specimens and for type B specimens built up of 4 and 5 alclad sheets.

At static loading all the specimens failed by buckling with no loosening of the bonded joints. The compressive stress at maximum load determined from the gross area and neglecting the adhesive was for the A 2, B 1 and B 4 specimens nearly 33 kg/mm² and for the more rigid A 6 specimens 42,5 kg/mm².

3.2 *Results of the static and fatigue tests in 3-point bending on the Redux-bonded and solid spar booms.*

The results of the static bending tests on the bonded specimens type A and B of figs 1 and 2 and the solid specimens of fig. 4 are given in table 2. Included in this table are the mean values of the load, at which the strain in the outermost fibre was 0.002, and the section moduli calculated from the measurements. The table shows that after testing to failure no cracking of the sheet could be detected and with the exception of one specimen no tearing of the adhesive occurred. All B 1—B 5 specimens, having the same overall dimensions, have almost the same measured section modulus and the same calculated maximum bending stress in the outermost fibre independent of the construction. The solid specimens, having a section modulus between those of the A 2 and A 3 specimens but closer to the A 3 than to the A 2 specimen, withstood a calculated maximum bending stress in the outermost fibre between the values for the A 2 and A 3 specimens and near to the A 3 value. Thus, the results fit the hypothesis that a bonded spar boom behaves in bending like a solid spar boom of equal section modulus.

The results of the fatigue bending tests on the bonded specimens types A and B of figs 1 and 2 and the solid specimens of fig. 4 are given in table 3 and in figures 9—13. In figs 9—11 the endurance has been plotted as a function of the range of bending stress in the outermost fibre. From fig. 9 it is obvious that on this basis all results of the specimens type A lie in the same rather broad scatter band, independent of the number of alclad sheets. Likewise, all the results of the 5 types B-specimens lie in one scatter band (see fig. 10), somewhat narrower than that for the A-specimens and with a slightly higher endurance at low stresses. These small differences between the specimens type A and B may be attributed to small differences in bending fatigue strength between the 26 S-T and 24 S-T alclad materials, used respectively for the A and B specimens, and to small differences in shape. On the whole the results of the bending fatigue tests on the specimens type A and B fit the hypothesis that a bonded spar boom behaves like a solid spar boom of the same section modulus. Apparently this hypothesis is quite contradictory to the results of the solid specimens type D given in fig. 11. This figure shows, plotted on a bending stress-endurance basis, a large superiority for the solid spar booms compared to the bonded spar booms. This superiority of the bending fatigue strength of the solid spar boom should, however, not be attributed to the difference "solid" or "bonded", but to the difference in material composition of the outside of the specimens. The outside of the bonded specimens is pure aluminium as the specimens were built up of alclad sheets, the outside of the

TABLE 2.

Results of static bending tests.

Type of specimen	P ↓, span l	Mean Value of P_1 in kgs strain in outermost fibre 0.002	Measured Section modulus in mm³ $W = \frac{1/4\, P_1 l}{14}$	Value of P_{max} in kg	σ_{max} in kg/mm² calculated as M/W	Remarks
A 2	$l = 120$ mm	300	640	1450—1380	66	Buckling of the specimen, no cracking
A 3	,,	410	880	2250—2250	77	,, ,, ,, ,, ,, ,,
A 4	,,	530	1130	3000—3100	81	,, ,, ,, ,, ,, ,,
A 5	,,	630	1350	3950—4050	89	,, ,, ,, ,, ,, ,,
A 6	,,	730	1560	4750—4750	91	,, ,, ,, ,, ,, ,,
B 1	,,	230	495	960—970—1020	60	,, ,, ,, ,, ,, ,,
B 2	,,	240	515	960—1080—980	59	,, ,, ,, ,, ,, ,,
B 3	,,	230	495	1010—1080—1060	63	,, ,, ,, ,, ,, ,,
B 4	,,	220	450	920—650*—1000—990	64	,, ,, ,, ,, ,, ,,
B 5	,,	230	495	960	59	,, ,, ,, ,, ,, ,,
solid	,,	360	770	1900—1900	74	,, ,, ,, ,, ,, ,,

* one glue line torn.

TABLE 3.

Results of fatigue bending tests at $R = 0.1$.

Type and number of specimen	Outline		Load in kg		Range of stress kg/mm²	Endurance $\times 10^{-3}$	Remarks
	specimen	testing	min	max			
A 2—10	fig. 1	7 and 8	90	740	30.2	63	cracking in the bottom sheet
A 2—11	”	”	60	630	26.6	220	” ” ” ” ”
A 2—12	”	”	50	530	22.4	384	” ” ” ” ”
A 2—13	”	”	40	450	19.1	524	” ” ” ” ”
A 2— 6	”	”	30	360	15.4	1751	” ” ” ” ”
A 2— 5	”	”	30	330	14.0	28733	test piece did not fail
A 3—10	”	”	70	820	25.6	241	cracking in the bottom sheet
A 3— 1	”	”	30	650	21.2	149	” ” ” ” ”
A 3— 3	”	”	50	650	20.5	503	” ” ” ” ”
A 3— 6	”	”	50	550	17.1	1026	” ” ” ” ”
A 3— 7	”	”	40	440	13.7	3711	” ” ” ” ”
A 3— 4	”	”	40	440	13.7	1436	” ” ” ” ”
A 3— 5	”	”	40	380	11.6	24295	test piece did not fail
A 4—11	”	”	100	1000	23.8	360	cracking in the bottom sheet
A 4—10	”	”	80	880	21.2	224	” ” ” ” ”
A 4— 1	”	”	80	800	19.0	350	” ” ” ” ”
A 4— 2	”	”	70	700	16.7	371	” ” ” ” ”
A 4— 4	”	”	60	660	15.9	887	” ” ” ” ”
A 4— 5	”	”	60	630	15.1	882	” ” ” ” ”
A 4— 3	”	”	60	600	14.3	22545	” ” ” ” ”
A 4— 6	”	”	60	580	13.7	22114	test piece did not fail
A 5— 1	”	”	140	1420	28.5	100	cracking in the bottom sheet
A 5— 2	”	”	100	1000	20.0	503	” ” ” ” ”
A 5— 3	”	”	80	880	17.8	954	” ” ” ” ”
A 5— 4	”	”	70	770	15.6	4535	” ” ” ” ”
A 5— 6	”	”	70	740	14.9	1851	” ” ” ” ”
A 5— 5	”	”	70	700	14.0	20431	” ” ” ” ”
A 6—11	”	”	140	1400	24.2	434	” ” ” ” ”
A 6—12	”	”	100	1100	19.2	1406	” ” ” ” ”
A 6— 5	”	”	100	1100	19.2	807	” ” ” ” ”
A 6—10	”	”	140	1000	16.5	1990	” ” ” ” ”
A 6—13	”	”	70	840	14.8	2047	” ” ” ” ”
A 6—14	”	”	70	720	12.5	33672	” ” ” ” ”
B 1— 2	fig. 2	”	50	510	28.0	147	” ” ” ” ”
B 1— 1	”	”	60	490	26.2	281	” ” ” ” ”
B 1— 4	”	”	40	400	22.0	467	” ” ” ” ”
B 1— 5	”	”	30	330	18.3	2424	” ” ” ” ”
B 1— 7	”	”	30	310	17.0	6969	” ” ” ” ”
B 1— 6	”	”	20	260	14.6	20108	” ” ” ” ”
B 2—11	”	”	50	545	29.2	84	” ” ” ” ”
B 2—10	”	”	40	450	24.0	187	” ” ” ” ”
B 2—12	”	”	40	390	20.5	554	” ” ” ” ”
B 2— 1	”	”	40	360	18.7	587	” ” ” ” ”
B 2— 2	”	”	30	300	15.8	2888	” ” ” ” ”
B 2—13	”	”	20	265	14.5	6425	” ” ” ” ”
B 3—11	”	”	50	545	30.4	132	” ” ” ” ”
B 3—10	”	”	40	450	25.0	160	” ” ” ” ”
B 3—12	”	”	40	390	21.3	339	” ” ” ” ”
B 3— 2	”	”	30	320	17.6	7085	” ” ” ” ”
B 3—13	”	”	20	265	14.9	3700	” ” ” ” ”
B 3— 1	”	”	20	250	14.0	13983	” ” ” ” ”
B 4—11	”	”	50	545	31.8	93	” ” ” ” ”
B 4—10	”	”	40	450	26.0	234	” ” ” ” ”
B 4—12	”	”	40	390	22.2	346	” ” ” ” ”
B 4— 1	”	”	30	300	17.2	701	” ” ” ” ”
B 4— 2	”	”	20	260	15.2	21552	” ” ” ” ”
B 4— 3	”	”	20	260	15.2	5667	” ” ” ” ”
B 5—10	”	”	40	450	25.0	256	” ” ” ” ”
B 5— 2	”	”	30	340	18.9	3578	” ” ” ” ”
B 5— 1	”	”	30	300	16.4	8130	” ” ” ” ”
B 5— 3	”	”	20	270	15.2	27570	” ” ” ” ”
D — 4	fig. 4	”	90	1040	37.0	368	crack at the bottom
D — 2	”	”	90	980	34.6	879	” ” ” ”
D — 7	”	”	90	950	33.5	21253	test piece did not fail
D — 5	”	”	90	910	31.9	9696	crack at the bottom
D — 6	”	”	90	910	31.9	30982	test piece did not fail
D — 3	”	”	80	840	29.6	33459	” ” ” ” ”
D — 1	”	”	60	700	25.0	30669	” ” ” ” ”

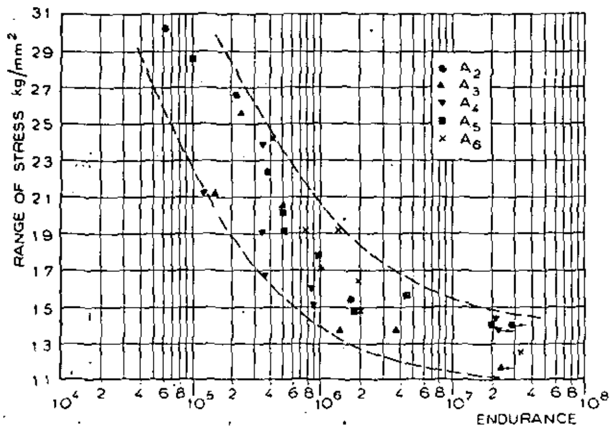

Fig. 9. Results of fluctuating bending fatigue tests at $R = 0.1$ on specimens type A (fig. 1).

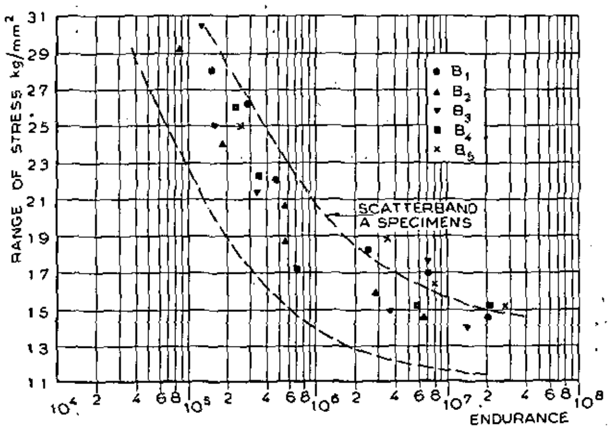

Fig. 10. Results of fluctuating bending fatigue tests at $R = 0.1$ on specimens type B.

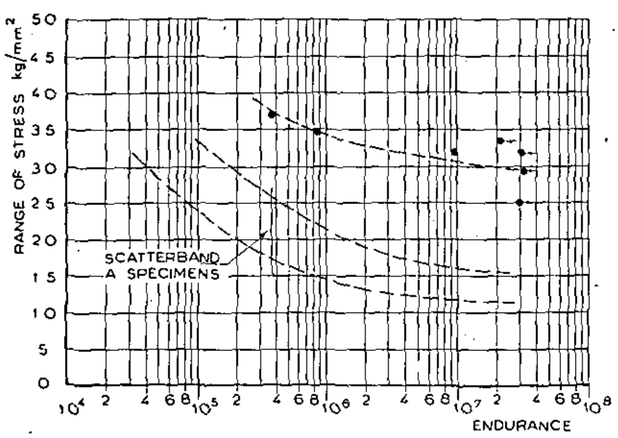

Fig. 11. Results of fluctuating bending fatigue tests at $R = 0.1$ on specimens type D.

solid specimens is an *Al-Cu-Mg alloy, Fliegwerkstoff* 3115.5. The unclad Al-Cu-Mg alloy has a much larger fatigue strength than the clad alloy. Ref. 2 gives for 24 S-T clad and unclad a fatigue limit at fluctuating tension ($R = 0$) of 15 and 28 kg/mm² respectively at an endurance of 10^7 cycles. The fatigue limit at fluctuating bending $R = 0.1$ and $n = 10^7$ cycles in fig. 11, respectively

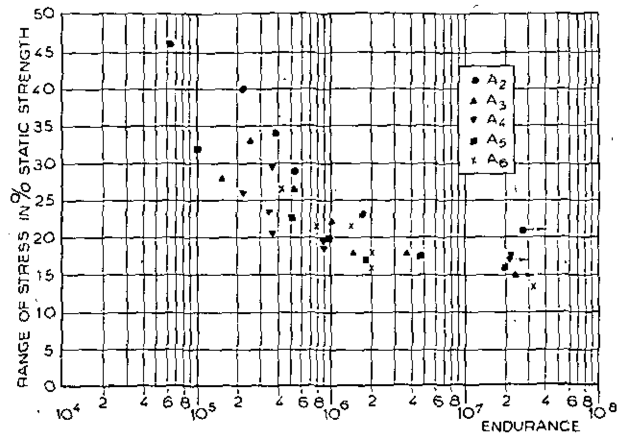

Fig. 12. Results of fluctuating bending fatigue tests at $R = 0.1$ on specimens type A.

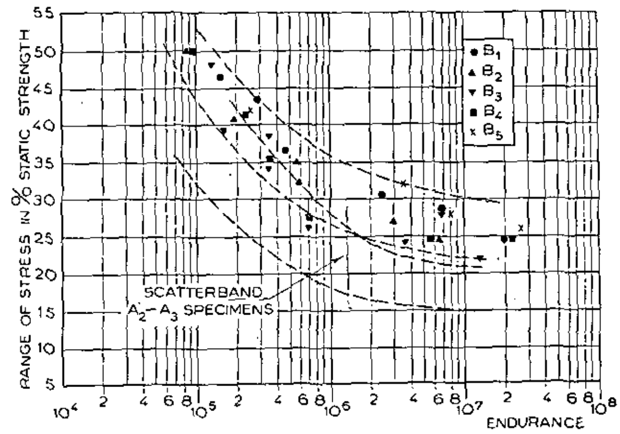

Fig. 13. Results of fluctuating bending fatigue tests at $R = 0.1$ on specimens type B.

14 and 30 kg/mm² for the bonded and solid spar booms, shows a reasonable agreement with the above mentioned values for clad and unclad 24 S-T. The differences in endurance between the bonded and the solid spar booms at the same bending stress may be explained by the difference in fatigue strength between clad and unclad Al-Cu-Mg alloy. If a high corrosion resistance is not required, it seems advisable to build up bonded spar booms of unclad material to increase the fatigue strength.

The figures 12 and 13 present the endurance of the bonded specimens type A and B as a percentage of the ultimate static strength. The figures 9 and 10 showed that all bonded specimens had equal endurance at equal range of stress in the outermost fibre and table 2 showed that the ultimate static strength calculated as bending stress in the outermost fibre by the simple formula $\frac{\text{Bending Moment}}{\text{Section modulus}}$ depended *on the section modulus. Consequently* the points of the specimens type B in fig. 13 lie rather dispersed in one scatter band, whereas after drawing one scatter band for the specimens type A the points in fig. 12 of the specimens type A 2 with the lowest section modulus all lie on the right side. The endurance of the specimens type B plotted in fig. 13 as a percentage of the static strength is superior to the endurance of the specimens type A plotted on the same basis. In view of the foregoing, this superiority has not been caused by superiority in the method of manufacturing the specimens type B — bending of the specimens after curing of the adhesive — but by differences in section modulus and shape.

3.3 *Results of the static and fatigue tests in compression on the composite Redux-bonded spar booms type C.*

The results of the compression tests on the bonded specimens type C (fig. 3) are given in table 4. In this table the phenomena occurring during the static and fatigue tests are likewise assembled.

The mean static compressive stress at failure of the specimens is about 39 km/mm², except for the lightest specimen C V where only a maximum stress of 32.4 kg/mm² was reached [1]). The material of the booms was 24 S-T alclad, the mechanical properties are given in table 1.

All specimens tested statically without prior fatigue loading failed by buckling of the whole specimen, only from specimen C IV-1 one flange plate with the skin loosened at the maximum load.

Fluctuating compressive loads of 60 % and 68 % of the ultimate were endured 5.10^6 cycles by all specimens type C II to C V incl. with only minor damage. Apart from some bladders in the skin due to local loosening of the glue joint, and consequently the forming of skin cracks, only in the case of specimen C III-4 cracks in the web occurred.

Of specimen C II-2 with a maximum fluctuating load of 75 % of the static load one flange plate with the skin loosened during a weekend between 0.79 and 2.23×10^6 load cycles. The maximum load dropped to 28.7 tons, but the maximum compressive stress was raised from 29.2 kg/mm² (75 %) to 32.7 kg/mm² (84 %). Then the test was stopped without loading the remainder of the specimen to collapse.

With specimen C III-2 (75 %) after 74.000 load cycles two small cracks in the web occurred, and the glue joint between web and stiffeners loosened a little bit. Then after 82 400 load reversals both flange plates with the skin sprang loose abruptly and the remainder of the specimen fell apart.

With specimen C IV-2 (75 %) the same probably happened overnight, after about 520 000 load cycles.

On specimen C V-2 (75 %) the same happened after 2.207.000 load reversals.

None of the heaviest specimens (C I) endured 5×10^6 load cycles without severe damage. Between 0.83 and 1.61×10^6 cycles two flange plates with the skin of specimen C I-2 loosened from the boom, also two fragments ruptured from the web. The maximum pulsating load was then relieved, until the compressive stress in the remaining part of the specimen again reached a value of 30.6 kg/mm² (75 % of the static compressive stress) and the test was continued until 5×10^6 load cycles were reached.

Nearly the same happened with specimen C I-3 (60 %) (see table 4).

With specimen C I-4 (68 %) firstly the skin with one flange plate loosened (932.000 load cycles), then the second flange plate (989.000 load cycles) and though some pieces of the web were loosened the remaining specimen withstood 5×10^6 load reversals at a maximum compressive stress of 68 % of the static stress.

A remarkable fact was that of all specimens, after being subjected to the fatigue test, during the final static test one or more flange plates loosened at or quite near the maximum load; this happened only once with the non-fatigued specimens (C IV-1).

Figs 14 to 18 incl. show the specimens type C after the tests.

The surface of the loosened glued flanges of the fatigued specimens all showed a network of small cracks, which could easily be detected at a small magnification. Such cracks did not occur in the glued surface of the statically tested specimens.

Figs 19 and 20 show the difference between these surfaces at a magnification of 50 ×. The cracks in the fatigued specimen can clearly be detected, and are still more evident on fig. 21 (150 ×).

Figs 22 and 23 each show two cross-sections of cladding layers of a fatigued specimen (150 ×).

Fig. 22 is unetched, fig. 23 is etched. From these figures it is evident that the cracks occur in the cladding only and do not progress into the 24 S crystallites.

The differences in the behaviour of the fatigued specimens at the maximum static load and the only statically tested specimens, viz. the abrupt loosening of the glue joint with the former, may be attributed to the cracks in the cladding.

That cracking of the clad layer during the fatigue loading does not require the presence of a glue layer between the sheets is further proved by the figures 24 and 25. Fig. 24 shows the external surface of a sparboom type C where no gluelayer is present, which failed by static loading; no cracks are visible. Fig. 25 shows the same surface of a fatigued specimen clearly indicating the presence of cracks on the surface.

It may be of interest to carry out fatigue tests on similar spar booms manufactured of unclad material.

4 Conclusions.

The methods of manufacturing of the bonded spar booms

a Rubber pressing of the sheets before bonding, type A

b *Rubber pressing of the sheets after bonding,* type B

had no influence on the compression fatigue strength.

[1]) This value probably is accidentally low, since higher stresses were reached in static tests on prior-fatigued specimens (see table 4).

The bonded spar booms type A, fig. 1 and type B, fig. 2 withstood a compression load fluctuating between 10 and 75 % of the ultimate static load for 10^7 cycles without deterioration in static strength.

All the bonded spar booms type A and B behaved like solid spar booms of equal section modulus.

The endurance of the bonded spar booms type A and B in the 3 point bending tests was determined by the range of bending stress in the outermost fibre. Equal range of stress gave equal endurance. The scatter in endurance was rather large.

The bending fatigue strength of the solid spar booms (type D — fig. 4) proved to be much superior to the fatigue strength of the bonded specimens type A and B. This superiority was caused by the superiority in fatigue strength of unclad to clad Al-Cu-Mg alloy.

With the exception of the specimens type C I all composite spar booms type C endured more than 5×10^6 load reversals at compressive stresses of 60 % and 68 % of the ultimate static stress. The specimens type C I suffered severe damage before 5×10^6 load cycles were endured. The damage consisted of complete loosening of one or more flange plates from the specimen, or of rupturing of fragments from the web. The remaining parts of the specimens endured nevertheless 5×10^6 load cycles at the same maximum compressive stress.

None of the specimens type C sustained 5×10^6 load cycles at a maximum fluctuating stress of 75 % of the ultimate static stress.
The ultimate compressive static stress of all type C specimens after the fatigue tests ranged from 93 to 110 % of the static stress of the specimens which were only tested statically. The collapse of the former specimens during the final static test was, however, quite different from that of the latter. Of the fatigued specimens some glue joints always loosened explosively at or near the maximum compressive load. This different behaviour may be attributed to small cracks formed in the clad layer of the fatigued specimens.

It is recommended to carry out some supplementary tests on similar specimens manufactured of unclad material.

5 References.

1. SCHLIEKELMANN, R. J. *The Application of Metal-to-Metal Adhesives in Composite Spar Booms.* Fokker Report R 16 (1951).

2. RUSSELL, H. W., JACKSON, L. R., BEAVER, W. W., GROVER, H. J. Fatigue Strength and Related Characteristics of Aircraft Joints. NACA T. N. 1485 (1948).

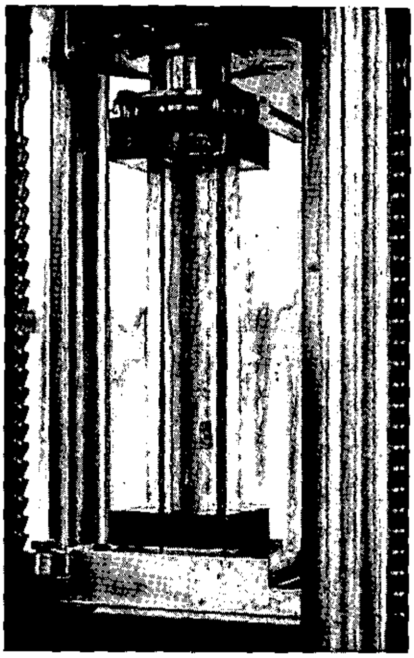

Fig. 5. Test set-up of the specimens type C for compressive fatigue tests.

Fig. 6. Test set-up for specimens type A and B for three point bending fatigue tests.

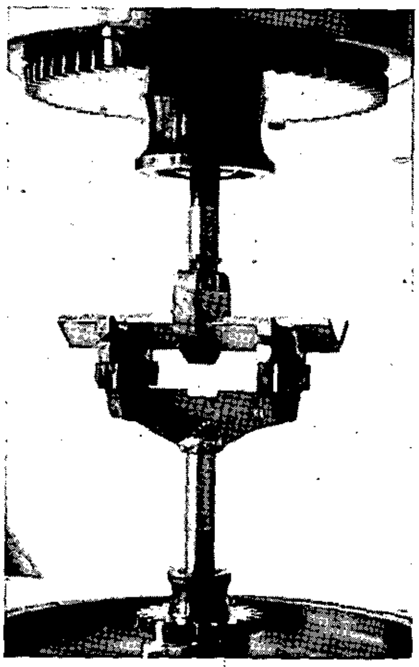

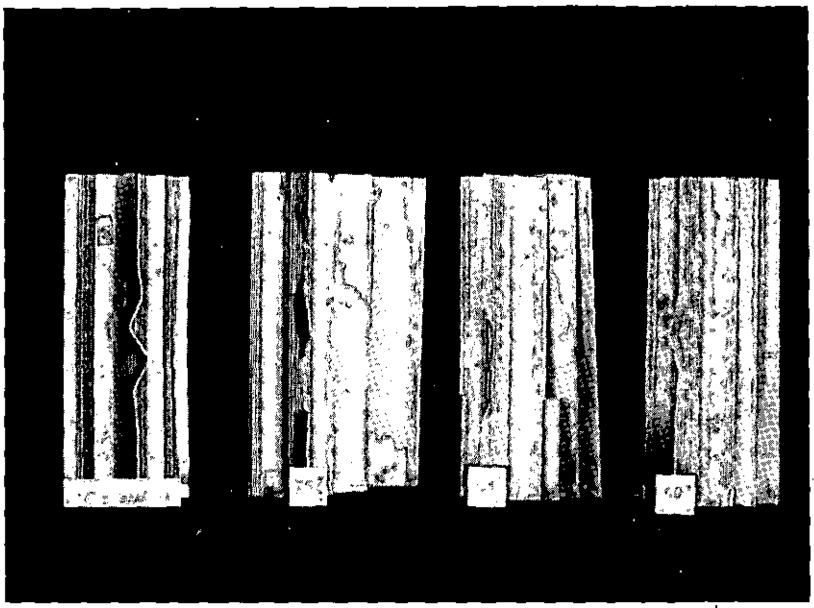

Fig. 14. Specimens type C I after the tests.

Fig. 15. Specimens type C II after the tests.

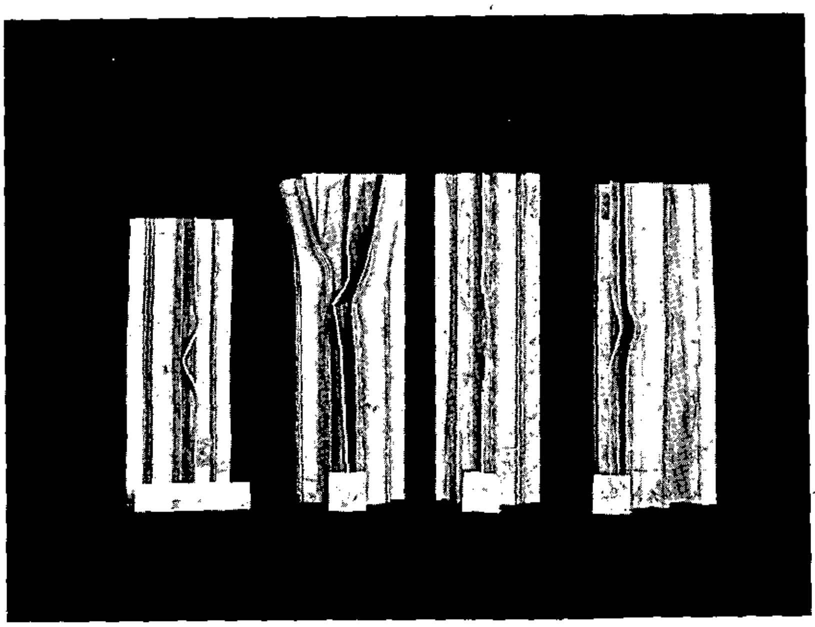

Fig. 16. Specimens type C III after the tests.

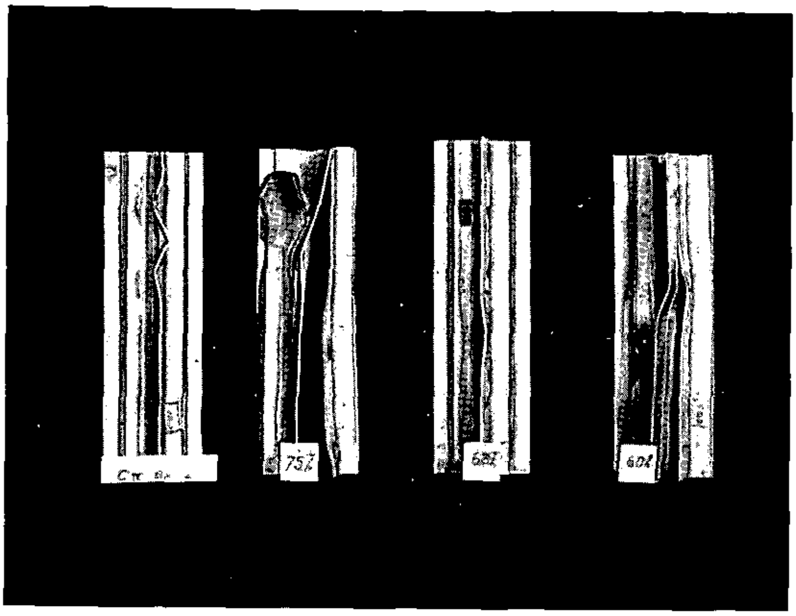

Fig. 17. Specimens type C IV after the tests.

Fig. 18. *Specimens* type C V after the tests.

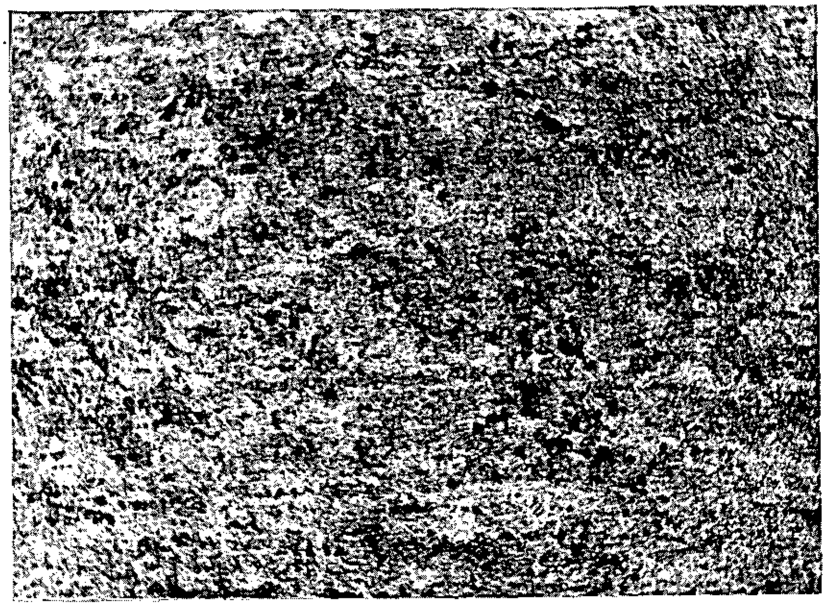

Fig. 19. Metal surface of statically failed specimen. 50 ×

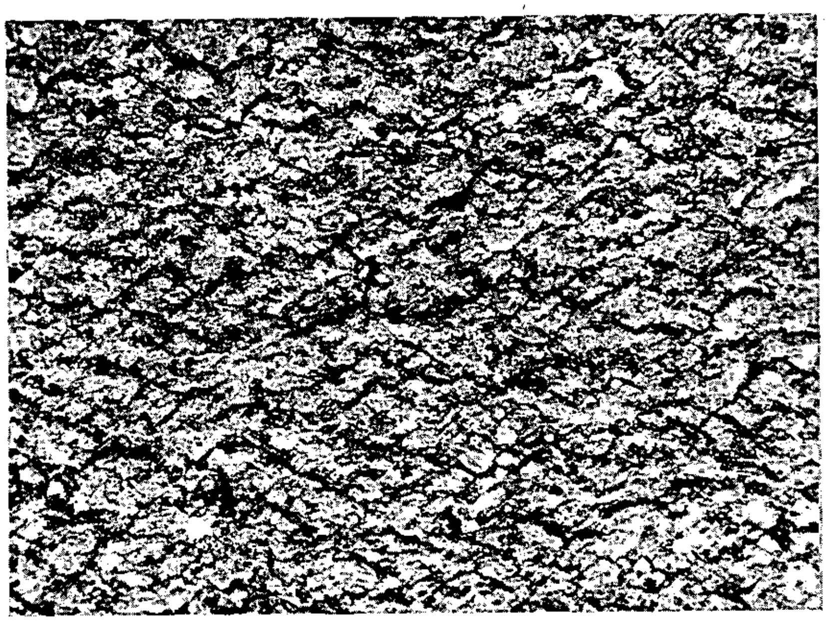

Fig. 20. Metal surface of fatigued and thereafter statically failed specimen. 50 ×

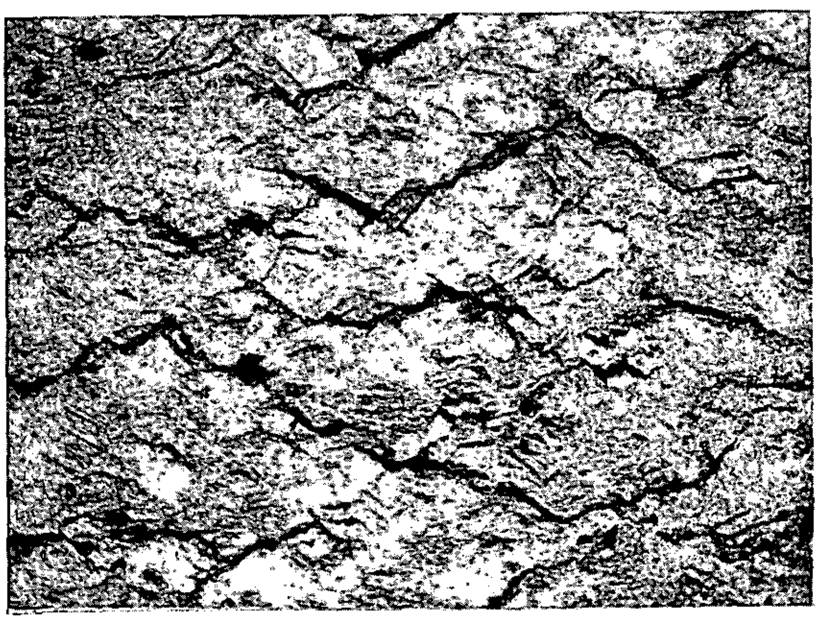

Fig. 21. Metal surface of fatigued and thereafter statically failed specimen. 150 ×

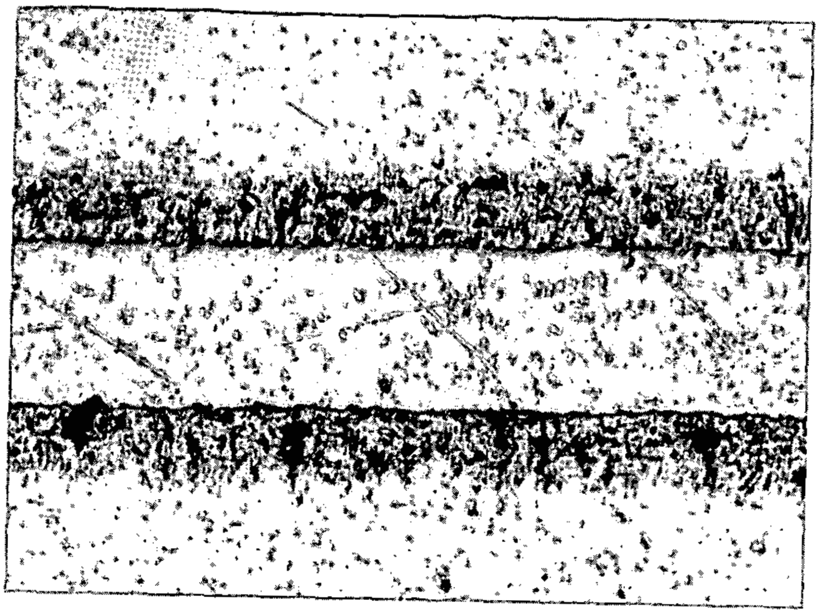

Fig. 22. Cross section of the fatigued clad layer, unetched. 150 ×

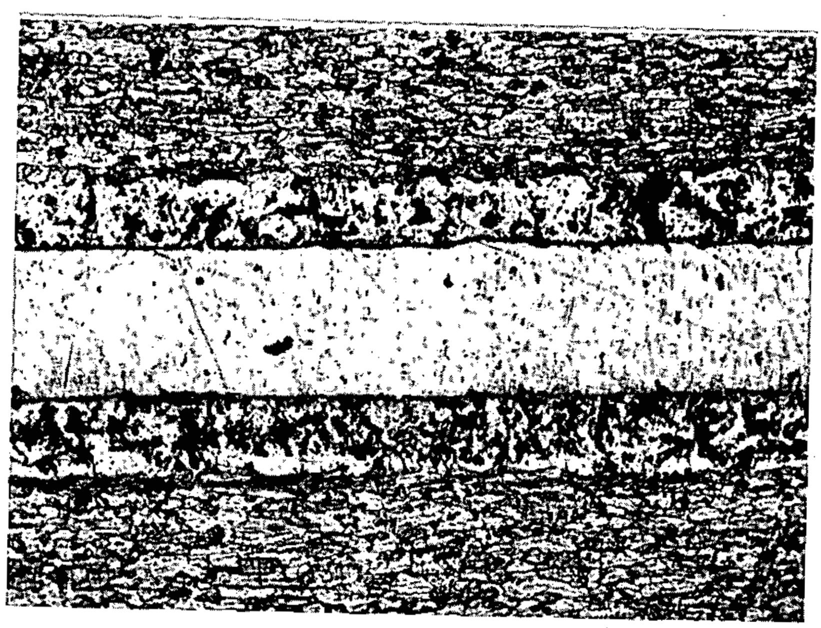

Fig. 23. Cross section of the fatigued clad layer, etched. 150 ×

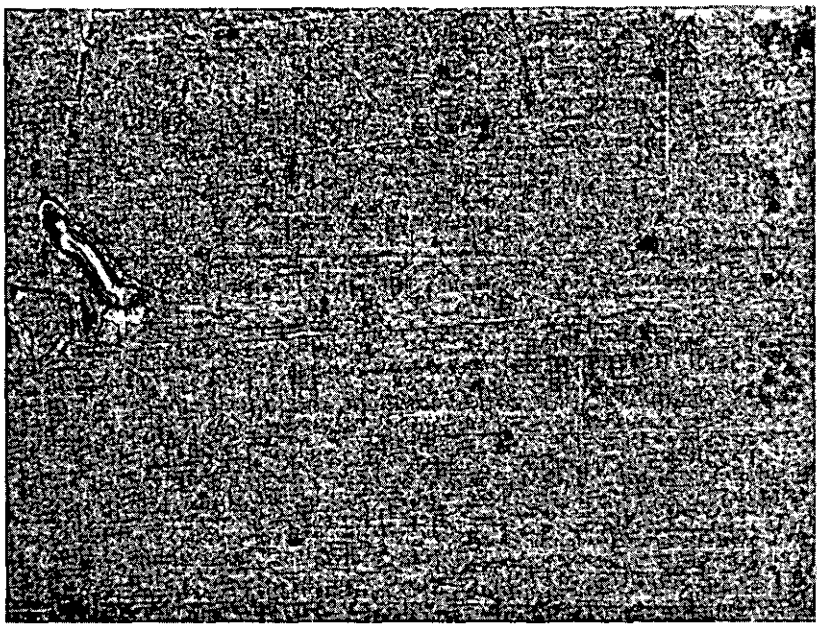

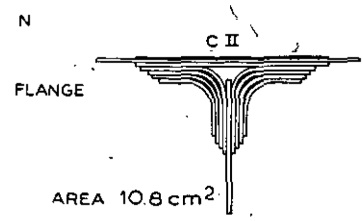

Fig. 24. Surface of statically failed specimen. 150 ×

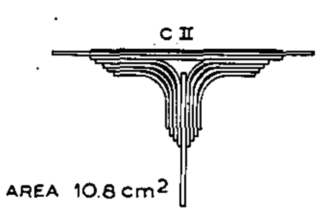

Fig. 25. Surface of fatigued and thereafter statically failed specimen. 150 ×

C.C.L.: Class. C 527-4

REPORT M. 1943.

A Comparative Investigation on the Influence of Sheet Tickness, Type of Rivet and Number of Rivet Rows on the Fatigue Strength at Fluctuating Tension of Riveted Single Lap Joints of 24 ST-Alclad Sheet and 17 S Rivets

by

A. HARTMAN.

Summary.

Fatigue tests at fluctuating tension were carried out on riveted single lap joints of 24 ST alclad sheet and 17 S rivets to determine the influence of sheet thickness, type of rivet and number of rivet rows. The results indicate that for the type of specimen used a change of sheet thickness has no influence on the fatigue limit (calculated as stress range in the sheet, $n = 50.10^6$), but that except for NACA rivets, at high loads thicknesses exceeding 1 mm give a decrease in endurance at the same stress amplitude. The type of rivet (snap rivet, countersunk V rivet, countersunk NACA rivet) too has no influence on the fatigue limit, but the NACA rivet is superior to the 2 other types of rivets at relatively high loads. Increase of the number of rivet rows from 2 to 3 at the same static strength of the joint has no influence on the S-N curve of joints with 0.8 mm and 1.2 mm sheets.

Contents.

This investigation has been performed by order of the Netherlands Aircraft Development Board (N.I.V.).

1 Introduction.

In reference 1 results are given of a comparative investigation carried out at the N.L.L. on the fatigue strength at fluctuating tension on several types of riveted lap joints. The tests showed:

1 snap and countersunk riveted lap joints of 0.8 mm 24 ST alclad had the same load-endurance curve,

2 plotted as a stress (in the sheet)-endurance curve (scatter band) there was no significant difference between the countersunk riveted lap joints of 1.2 and 0.8 mm 24 ST alclad, though the sheet in one type was sunk and in the other dimpled.

The Fatigue Committee of the Netherlands Aircraft Development Board (N.I.V.), when discussing the results of these tests, considered it desirable to extend the scope of the investigation and to determine in more detail the influence of the following factors on the fatigue strength

1 the influence of the sheet thickness,

2 the influence of the method of filling up the holes in the sheet by the method of riveting (type of rivet),

3 at the same static strength the influence of the rivet pattern (number of rows).

The supplementary tests to achieve these aims, the results of which are given in this report, comprised fatigue tests at fluctuating tension on:

1 snap riveted lap joints with sheets of various thicknesses,

2 lap joints with snap rivets, countersunk V rivets and countersunk NACA rivets,

3 snap riveted lap joints with 2 and 3 rivet rows.

2 Details of the test specimens and test procedure.

2.1 *Test specimens.*

The 24 ST alclad material used for the manufacture of the riveted lap joints was supplied by the Nederlandse Aluminiummaatschappij N.V. at Utrecht. The works specification gives as mechanical properties of this alloy.

$\sigma_{0.2}$ — tensile yield strength > 27 kg/mm², typical value 30 kg/mm².

σ_B — tensile ultimate strength > 41 kg/mm², typical value 45 kg/mm².

δ — elongation $l = 2'' > 12$ %, typical value 18 %.

Tensile tests on test pieces cut at random from riveted specimens with a sheet thickness of 1.6 mm gave the following values

$\sigma_{0.2} =$ 32.5 — 31.9 — 32.6 — 32.1; mean 32.3 kg/mm².

$\sigma_B =$ 45.5 — 45.0 — 45.3 — 44.8; mean 45.1 kg/mm².

The mechanical properties of the 0.8 and 1.2 mm sheet materials given in ref. 1 are 36.9 and 38.1 kg/mm² respectively for the tensile yield strength and 46.0 and 47.0 kg/mm² for the ultimate tensile strength. All rivets were 17 S, riveted cold in the solution heat treated temper.

The test pieces were single lap joints with 2 or 3 rows of rivets. The shape and dimensions of the two types of specimens are given in fig. 1. To

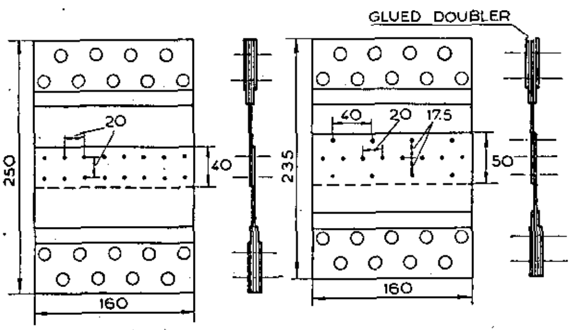

Fig. 1. Shape and dimensions of the specimens.

prevent failure of the specimen in the clamping head of the testing machine all the specimens were reinforced with a redux-bonded doubler as schematically drawn in fig. 1.

3 types of riveted joints were used in this investigation, schematically given in figs. 2a—2c incl.

fig. 2a — type Pb — both sheets flat — snap rivets,

fig. 2b — type V — front sheet sunk, rear sheet flat,
die head is countersunk part of the rivet.

fig. 2c — type NACA — front sheet sunk, rear sheet flat,
closing head is countersunk part of the rivet.

All specimens were made at the Royal Fokker Aircraft Co according to common practice.

2.2 *Test procedure.*

The static tensile testing of the specimens was carried out in an Amsler 20 tons universal testing machine; the fatigue testing in an Amsler Vibraphore of 10 tons. The clamping device used in

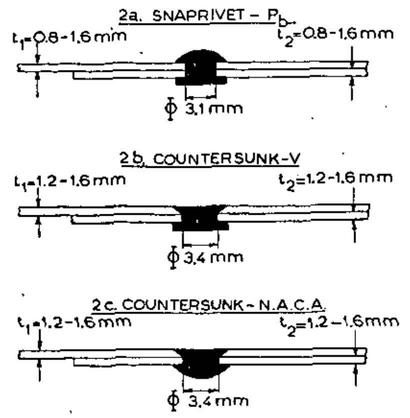

Fig. 2. Types of riveted joints.

the tests in ref. 1 was again used, both for the static and the fatigue tests. The 10 tons dynamometer of the Vibraphore was used for tests with max. loads > 2 and the 2 tons dynamometer for tests with max. loads < 2 tons.

The Wöhler curves (S-N curves) were determined for fluctuating tension with a minimum load of 100 kg. The frequency of the load reversals was about 8000/minute. If after about 50.10^6 load reversals the test piece had not cracked the test was stopped. Otherwise the end of the test was the cracking of the specimen in the joint. By adjusting the switch-off relay always in the same way it was achieved that the switching-off took place at approximately the same degree of crack formation. Complete failure of the specimen would have occurred soon afterwards. Specimens which had not failed in the fatigue testing, were loaded to failure in the static testing machine to determine whether the fatigue loading had caused any deterioration of the static strength of the joint.

3 Results of the static tests.

The results of the static tests are given in table 1 and in fig. 3. The points in fig. 3 do not indicate

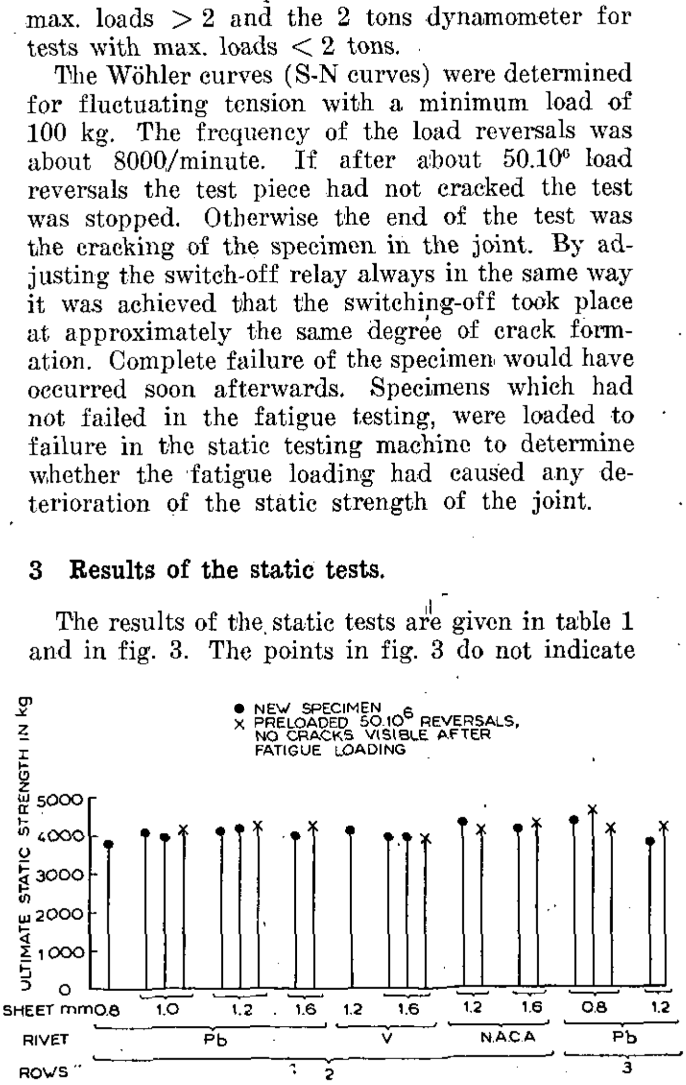

Fig. 3. Results of the static tests.

TABLE 1.

Results of the static tension tests.

Type of rivet		Test piece according to	Sheet thickness in mm	Load at failure in kg	Remarks	
Pb snap	fig. 2a	fig. 1a	0.8	3800	ref. 1	Type of failure I
,, ,,	,, ,,	,, ,,	1.0	4110		,, ,, ,,
,, ,,	,, ,,	,, ,,	1.0	3950		,, ,, ,,
,, ,,	,, ,,	,, ,,	1.0	4140	preloaded with 50 . 10^6 load reversals 100—600 kg	,, ,, ,,
,, ,,	,, ,,	,, ,,	1.2	4150		,, ,, ,,
,, ,,	,, ,,	,, ,,	1.2	4220		,, ,, ,,
,, ,,	,, ,,	,, ,,	1.2	4260	preloaded with 50 . 10^6 load reversals 100—640 kg	,, ,, ,,
,, ,,	,, ,,	,, ,,	1.6	4000		,, ,, ,,
,, ,,	,, ,,	,, ,,	1.6	4290	preloaded with 50 . 10^6 load reversals 100—860 kg	,, ,, ,,
V-countersunk	,, 2b	,, ,,	1.2	4125	ref. 1	,, ,, ,,
,, ,,	,, ,,	,, ,,	1.6	3970		,, ,, ,,
,, ,,	,, ,,	,, ,,	1.6	3980		,, ,, ,,
,, ,,	,, ,,	,, ,,	1.6	3930	preloaded with 50 . 10^6 load reversals 100—800 kg	,, ,, ,,
NACA ,,	,, 2c	,, ,,	1.2	4340		,, ,, ,,
,, ,,	,, ,,	,, ,,	1.2	4180	preloaded with 50 . 10^6 load reversals 100—700 kg	,, ,, ,,
,, ,,	,, ,,	,, ,,	1.6	4200		,, ,, ,,
,, ,,	,, ,,	,, ,,	1.6	4320	preloaded with 50 . 10^6 load reversals 100—860 kg	,, ,, ,,
Pb snap	,, 2a	,, 1b	0.8	4380		,, ,, II
,, ,,	,, ,,	,, ,,	0.8	4680	preloaded with 80 . 10^6 load reversals 100—420 kg	,, ,, ,,
,, ,,	,, ,,	,, ,,	0.8	4140	preloaded with 50 . 10^6 load reversals 100—500 kg	,, ,, I
,, ,,	,, ,,	,, ,,	1.2	3710		,, ,, ,,
,, ,,	,, ,,	,, ,,	1.2	4150	preloaded with 50 . 10^6 load reversals 100—600 kg	,, ,, ,,

Type of failure I. Failure by shearing of all rivets little distortion of rivet holes.
Type of failure II. Failure of the rivets distinct distortion of the rivet holes.

much variation in static strength between the different types of joint. As all the joints failed by shear of the rivets and had the same number of rivets of almost the same diameter this result is easily understood. The average static strength of all specimens is 4140 kg, which corresponds to an average shear stress in the snap rivets of 34. kg/mm² and in the V and NACA rivets of 29 kg/mm². The tensile stresses in the sheets corresponding to the average static strength have also been computed for comparison with the fatigue test results. Based on the gross cross section of the sheet they are 32.3, 25.9, 21.6 and 16.2 kg/mm² for 0.8, 1.0, 1.2 and 1.6 mm sheet respectively.

The situation of the points, indicated with crosses in fig. 3, 5 times over and 3 times under the points which indicate the static strength of a new specimen of the same type, proves that the static strength of a riveted lap joint is not influenced by fatigue loading at low stresses if this fatigue loading has not caused any visible cracking of the sheet.

4 Results of the fatigue tests.

4.1 *Tests on specimens with snap rivets.*

Table 2 gives the results of the fatigue tests with fluctuating tension on 24 ST alclad single lap joints riveted with 17 S *snap rivets. In these tests the* thickness of the sheet ranged from 0.8 to 1.6 mm.

The results for the specimens with 2 rows of rivets are plotted in figs. 4 and 5 in which also are given the results of the former tests given in ref. 1. The stresses of fig. 4 are calculated as stress range in the gross section, in fig. 5 as nominal stress range in the net section of the sheet. The situation of the points in these figures indicates that an increase in the sheet thickness from 0.8 to 1.6 mm had hardly any influence on the fatigue limit ($n = 50.10^6$) of the joint and a small deteriorating effect on the endurance at relatively high loads. The deteriorating effect at high loads was noticeable for sheet thicknesses exceeding 1 mm. With some specimens it was accompanied by a change in type of failure. For joints with thin sheet *the sheet was always critical* but with thick sheet at high loads (see table 2) some rivet heads bursted off, so in this case *the rivets became critical*. As the rivet heads bursted off and did not shear off like in the static tesst, the tensile stress in the rivet caused by the increased bending moments[3] of the joints with thick sheet may have made the rivets critical. On the other hand, the static stress in the sheet at failure decreases as the sheet thickness increases and this may cause a lowering of the S (stress in sheet) — N curve when the maximum fatigue load is nearing the ultimate static strength (also see section 4.3). Whatever the cause may be the results prove that for snap riveted lap joints the shape of the S-N curve below $n = 10^6$ approx. depends on the ratio between the maximum load of the fatigue cycle and the static strength of the joint.

The plotted points in fig. 6, giving the results of the tests on specimens with 2 and 3 rows of rivets and about the same static strength, indicate

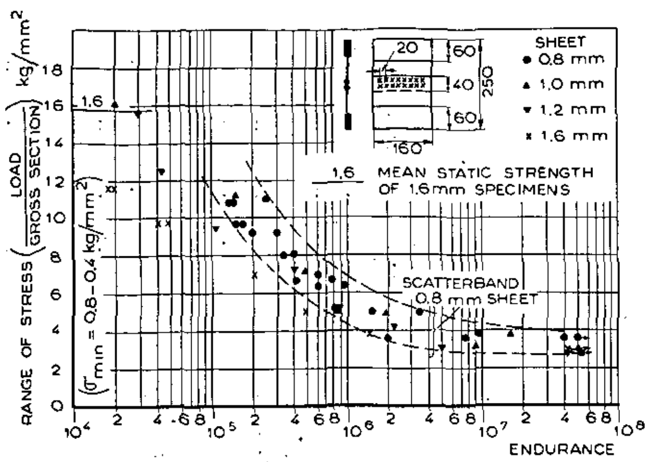

Fig. 4. Results of fatigue tests with fluctuating tension on 24 ST alclad single lap joints riveted with 17 S snap rivets.

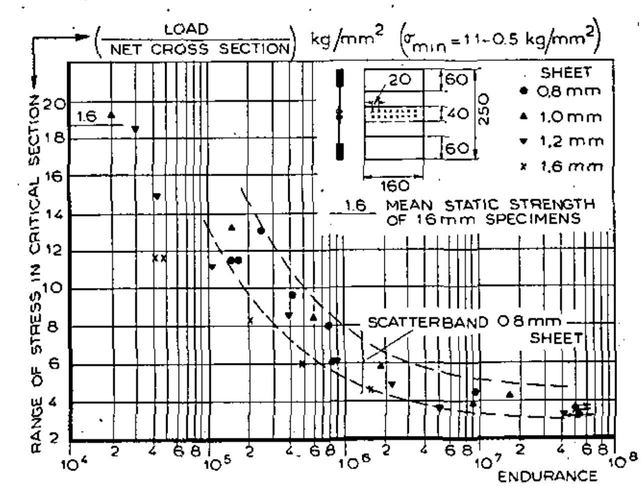

Fig. 5. Results of fatigue tests with fluctuating tension on 24 ST alclad single lap joints riveted with 17 S snap rivets.

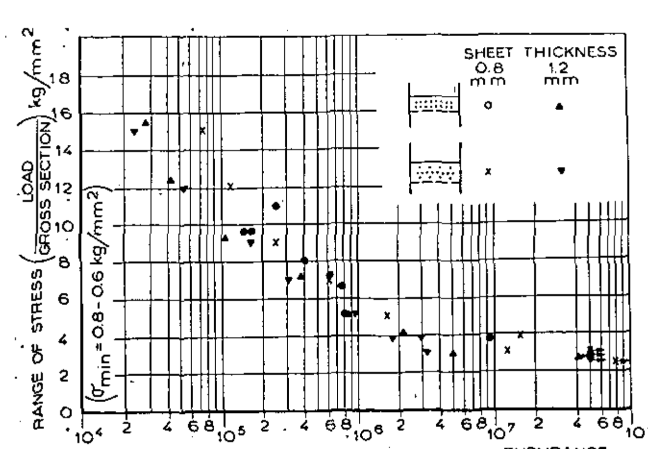

Fig. 6. Results of fatigue tests with fluctuating tension on 24 ST alclad single lap joints with 2 and 3 rows of snap rivets.

TABLE 2.

Results of fatigue tests with fluctuating tension on 24 ST alclad single lap joints riveted with 17 S snap rivets.

Sheet thickness mm	Specimens according to fig.		Load in kg min.	Load in kg max.	Stress range in plain sheet kg/mm²	Endurance $\times 10^{-3}$	Remarks
0.8	1a	2a	100	1520	11.1	243	type of failure I ref. 1
,,	,,	,,	,,	1340	9.7	151	,, ,, ,, II ,,
,,	,,	,,	,,	1340	9.7	169	,, ,, ,, I ,,
,,	,,	,,	,,	1140	8.1	410	,, ,, ,, ,, ,,
,,	,,	,,	,,	960	6.7	784	,, ,, ,, ,, ,,
,,	,,	,,	,,	760	5.2	812	,, ,, ,, II ,,
,,	,,	,,	,,	580	3.8	9488	,, ,, ,, I ,,
,,	,,	,,	,,	460	2.8	52518	test piece did not fail ,,
1.0	,,	,,	200	2800	16.2	20	type of failure I
,,	,,	,,	100	1900	11.3	150	,, ,, ,,
,,	,,	,,	,,	1900	11.3	429	,, ,, ,, ,, switching off relay did not function well
,,	,,	,,	,,	1250	7.2	493	type of failure I
,,	,,	,,	,,	900	5.0	1858	,, ,, ,, ,,
,,	,,	,,	,,	700	3.8	16674	,, ,, ,, ,,
,,	,,	,,	,,	620	3.2	9095	,, ,, ,, ,,
,,	,,	,,	,,	600	3.1	50242	test piece did not fail
1.2	,,	,,	,,	3100	15.6	29	type of failure I A
,,	,,	,,	,,	2500	12.5	43	,, ,, ,, ,,
,,	,,	,,	,,	1900	9.4	112	,, ,, ,, I
,,	,,	,,	,,	1500	7.3	399	,, ,, ,, ,,
,,	,,	,,	,,	1100	5.2	876	,, ,, ,, ,,
,,	,,	,,	,,	900	4.2	2248	,, ,, ,, ,,
,,	,,	,,	,,	700	3.1	5094	,, ,, ,, ,,
,,	,,	,,	,,	640	2.8	50884	test piece did not fail
1.6	,,	,,	,,	3100	11.7	20	type of failure I B
,,	,,	,,	,,	3100	11.7	20	,, ,, ,, ,,
,,	,,	,,	,,	2600	9.8	42	,, ,, ,, I A
,,	,,	,,	,,	2600	9.8	49	,, ,, ,, ,,
,,	,,	,,	,,	1900	7.0	208	,, ,, ,, I
,,	,,	,,	,,	1400	5.1	496	,, ,, ,, ,,
,,	,,	,,	,,	1100	3.9	1540	,, ,, ,, ,,
,,	,,	,,	,,	860	3.0	49469	test piece did not fail
0.8	1b	,,	,,	2050	15.2	77	type of failure I
,,	,,	,,	,,	1650	12.1	120	,, ,, ,, ,,
,,	,,	,,	,,	1250	9.0	259	,, ,, ,, ,,
,,	,,	,,	,,	1000	7.0	621	,, ,, ,, ,,
,,	,,	,,	,,	750	5.1	1670	,, ,, ,, ,,
,,	,,	,,	,,	600	3.9	15761	,, ,, ,, ,,
,,	,,	,,	,,	500	3.1	50320	test piece did not fail
,,	,,	,,	,,	500	3.1	13413	type of failure I
,,	,,	,,	,,	420	2.5	78882	test piece did not fail
1.2	,,	,,	,,	3000	15.1	25	type of failure I A
,,	,,	,,	,,	2400	12.0	53	,, ,, ,, I
,,	,,	,,	,,	1850	9.1	166	,, ,, ,, ,,
,,	,,	,,	,,	1450	7.0	310	,, ,, ,, ,,
,,	,,	,,	,,	1100	5.2	958	,, ,, ,, ,,
,,	,,	,,	,,	850	3.9	3052	,, ,, ,, ,,
,,	,,	,,	,,	850	3.9	1802	,, ,, ,, ,,
,,	,,	,,	,,	700	3.1	3271	,, ,, ,, ,,
,,	,,	,,	,,	600	2.6	49386	test piece did not fail

Type of failure I; fatigue crack in the sheet at the side of the diehead.
,, ,, ,, I A; *moreover some rivet heads broken out.*
,, ,, ,, I B; some rivet heads bursted off.
,, ,, ,, II; fatigue crack in the sheet at the side of the closing head.
,, ,, ,, II A; moreover some rivet heads broken out.

that both for the joints with 0.8 and 1.2 mm sheet the number of rivet rows had no influence on the endurance at low or high loads. Neither was the influence of the sheet thickness on the fatigue strength of single lap snap riveted joints, mentioned in the preceding paragraph, dependent upon the number of rivet rows.

The situation of the points in fig. 6 clearly shows that the endurance at the same range of stress, both for the joints with 2 and 3 rivet rows, was less for joints with 1.2 mm sheet than for joints with 0.8 mm sheet. The fatigue limit ($n = 50.10^6$) was hardly influenced by the sheet thickness.

4.2 *Tests on specimens with countersunk V rivets.*

The countersunk V-riveted joint with a sunk front sheet cannot be used for thin sheets. Therefore, the tests on this type of joint had to be restricted to sheet thicknesses of 1.2 and 1.6 mm. The results of the tests are given in table 3 and are plotted in figs 7—9 incl. The stresses in fig. 7 are calculated as stress range in the gross section and in figs 8 and 9 as stress range in the net section of the sheet. Here too, like with the snap riveted joint, larger thickness of the sheet at the same stress amplitude was accompanied by a decrease in endurance at high loads. The situation of the points even in some degree indicates that the fatigue limit was unfavourably influenced by an increase of sheet thickness from 1.2 to 1.6 mm. As this result is contradictory to the results for snap- or NACA riveted joints and the number of test specimens is rather small, it will require further tests before a definite conclusion can be reached.

4.3 *Tests on specimens with countersunk NACA rivets.*

The NACA rivets, like the V rivet, can be used only in relatively thick sheet. The tests, the results of which are given in table 3 and in the figs 7—9 incl., were restricted to sheet thicknesses of 1.2 and 1.6 mm. The stresses in fig. 7 are calculated as stress range in the gross section and in figs. 8 and 9 as stress range in the net section of the sheet.

The situation of the points in the figures clearly shows that the sheet thickness had no influence on the endurance, neither at high nor at low stress amplitude. Both for the joints with 1.6 and 1.2 mm sheet the points lie in the scatter band for thin (0.8 mm) snap riveted joints of ref. 1. Probably for NACA riveted joints, even with thick sheets of 1.6 mm the S-N curve is determined by the stress concentration in the sheet caused by the rivets and the shape between $n = 10^4$ and $n = 10^7$ is not influenced by the ratio between the maximum fatigue stress and the static strength of the joint.

An NACA riveted specimen (see fig. 9) of 1.6 mm sheet sustained a fluctuating tensile load equal to the mean static strength 16000 times; in this case the fatigue strength is apparently not affected whether the rivets are loaded far below or near to their static shearing strength. The better filling up of the countersunk hole in the front sheet by the NACA method of riveting, by which the hole

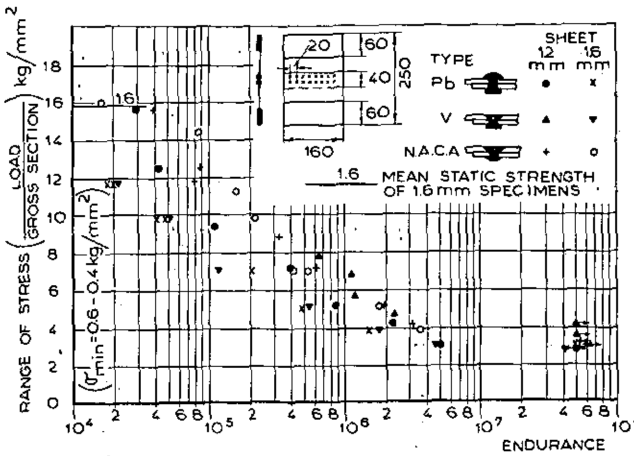

Fig. 7. Results of fatigue tests with fluctuating tension on 24 ST alclad single lap joints riveted with 3 types of rivets.

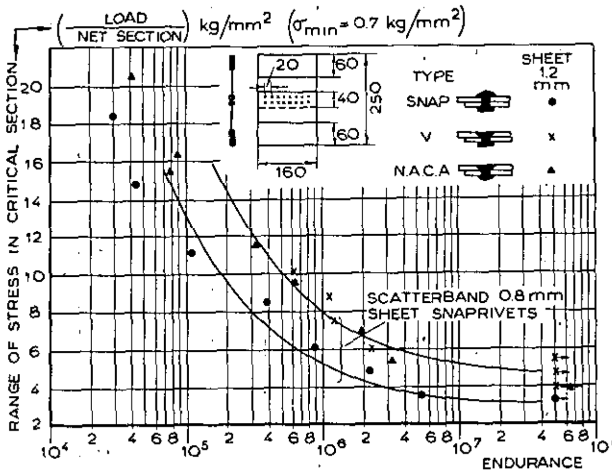

Fig. 8. Results of fatigue tests with fluctuating tension on 24 ST alclad single lap joints riveted with 3 types of rivets.

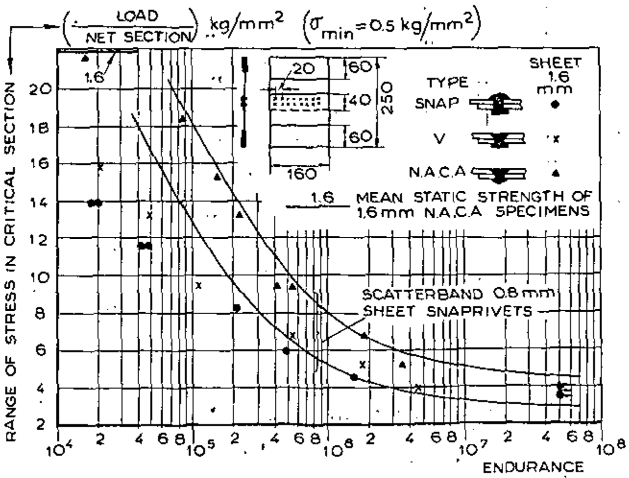

Fig. 9. Results of fatigue tests with fluctuating tension on 24 ST alclad single lap joints riveted with 3 types of rivets.

TABLE 3.

Results of fatigue tests with fluctuating tension on 24 ST alclad single lap joints riveted with 17 S *countersunk V or NACA rivets.*

Sheet thickness mm	Specimens according to fig.		Load in kg min.	Load in kg max.	Stress range in plain sheet kg/mm²	Endurance × 10⁻³	Remarks
1.2	1a	2b	100	1600	7.8	633	type of failure I ref. 1
,,	,,	,,	,,	1400	6.8	1158	,, ,, ,, II ,,
,,	,,	,,	,,	1200	5.7	1182	,, ,, ,, ,, ,,
,,	,,	,,	,,	1000	4.7	2346	,, ,, ,, ,, ,,
,,	,,	,,	,,	900	4.1	54979	test piece did not fail
,,	,,	,,	,,	900	4.1	55036	,, ,, ,, ,, ,,
,,	,,	,,	,,	800	3.6	57961	,, ,, ,, ,, ,,
,,	,,	,,	,,	700	3.1	58077	,, ,, ,, ,, ,,
1.6	,,	,,	,,	3100	11.7	21	type of failure I A
,,	,,	,,	,,	2600	9.8	49	,, ,, ,, I
,,	,,	,,	,,	1900	7.0	116	,, ,, ,, I A
,,	,,	,,	,,	1400	5.1	558	,, ,, ,, I
,,	,,	,,	,,	1100	3.9	1791	,, ,, ,, ,,
,,	,,	,,	,,	860	3.0	4643	,, ,, ,, ,,
,,	,,	,,	,,	800	2.7	46985	test piece did not fail
1.2	,,	2c	,,	3100	15.6	39	type of failure I and II
,,	,,	,,	,,	2500	12.5	88	,, ,, ,, II
,,	,,	,,	,,	2360	11.8	79	,, ,, ,, ,,
,,	,,	,,	,,	1800	8.9	318	,, ,, ,, ,,
,,	,,	,,	,,	1500	7.3	611	,, ,, ,, ,,
,,	,,	,,	,,	1100	5.2	1913	,, ,, ,, ,,
,,	,,	,,	,,	900	4.2	3188	,, ,, ,, ,,
,,	,,	,,	,,	700	3.1	54091	test piece did not fail
1.6	,,	,,	,,	4200	16.0	16	type of failure II
,,	,,	,,	,,	3800	14.5	85	,, ,, ,, II A
,,	,,	,,	,,	3000	11.3	158	,, ,, ,, II
,,	,,	,,	,,	2600	9.8	219	,, ,, ,, II A
,,	,,	,,	,,	1900	7.0	549	,, ,, ,, II
,,	,,	,,	,,	1900	7.0	413	,, ,, ,, ,,
,,	,,	,,	,,	1400	5.1	1837	,, ,, ,, ,,
,,	,,	,,	,,	1100	3.9	3517	,, ,, ,, ,,
,,	,,	,,	,,	860	3.0	52172	test piece did not fail

Type of failure I; fatigue crack in the sheet at the side of the diehead.
,, ,, ,, I A; moreover some rivet heads broken out.
,, ,, ,, I B; some rivet heads bursted off.
,, ,, ,, II; fatigue crack in the sheet at the side of the closing head.
,, ,, ,, II A; moreover some rivet heads broken out.

is filled up by the closing head of the rivet, possibly prevents premature loosening or failing of the rivets at high fatigue loads.

4.4 *Comparison of the results.*

A comparison of the results shows that the fatigue limits of the joints, calculated as stress range in the sheets, were hardly influenced by the type of rivets used, viz snap, countersunk V or NACA rivets. For the types of specimens used, sketched in figs 1 and 2, at $n = 50.10^6$ load reversals the mean stress range calculated as stress in the net section of the sheet in all cases was 3.8 kg/mm² at a min. stress ranging from 0.5 to 1 kg/mm², independent of sheet thickness variations between 0.8 and 1.6 mm. Differences between the various types of rivets appeared only at relatively high loads (and sheet thicknesses > 1 mm). In these circumstances the NACA riveted lap joint proved to be superior to the snap and countersunk V riveted lap joints and should be preferred in cases of a high ratio of stress amplitude to static strength. The situation of the points in fig. 8 indicates that with 1.2 mm sheet the V riveted joint is slightly superior to the snap riveted joint. In thick sheet the countersunk V riveted joint has no advantage over the snap riveted joint.

A change of the 2 row snap riveted joint sketched in fig. 1a to the 3 row snap riveted joint of about the same static strength of fig. 1b does not affect the fatigue strength.

In the technical literature much has been published on the behaviour of riveted lap joints under fatigue loading. A comparison of the results given in this report with results given in the literature, though desirable, is difficult to achieve. The dimensions of the specimens ,the loading cycle, the rivet pattern, etc., used by the various investigators differ considerably, which makes comparison of the results a difficult problem. In due course a search of the literature will be made to get a picture of our knowledge on the fatigue strength of riveted light-alloy lap joints. The results of this study will be reported in a separate paper.

5 Conclusions.

The sheet thickness, rivet type and number of rivet rows had no significant influence on the ultimate static strength of the joints, owing to the equal number of rivets in each specimen and the failure of all specimens by shearing of the rivets.

The ultimate static strength of the riveted lap joints was not influenced by fatigue loading at low stresses if this fatigue loading did not cause any visible cracking of the sheet.

The fatigue limit of the lap joints was hardly influenced by the type of rivet used, viz. snap-, countersunk V or countersunk NACA rivet (fig. 2a—2c) nor by the sheet thickness (0.8—1.6 mm) and the number of rivet rows at the same static strength (fig. 1a, 1b). At $n = 50.10^6$ the mean fatigue limit at fluctuating tension was 3.8 kg/mm² calculated as stress range in the net section of the sheet (min. stress 0.5—1 kg/mm²).

As regards fatigue strength both at sheet thicknesses of 0.8 and 1.2 mm and at high and low endurances the 2 row snap riveted lap joint of fig. 1a was equivalent to the 3 row snap riveted lap joint of the same static strength of fig. 1b.

The NACA riveted lap joint of fig. 2c proved to be superior to the snap- and countersunk V riveted lap joints of fig. 2a—b at loads above the fatigue limit and a relatively high ratio between the stress amplitude and the static strength. One NACA riveted specimen withstood 16000 cycles with a maximum fatigue load equal to the average static shearing strength of the rivets.

Between $n = 10^4$ and $n = 10^7$ the S-N curve for the NACA riveted joints, S calculated as tensile stress in the sheet, was not influenced by the sheet thickness, i. e. by the ratio between the maximum fatigue load and the static strength, as it was with the snap- and countersunk V riveted specimens.

The snap- and countersunk V riveted lap joints of 1.6 mm sheet were equivalent. In the thinner sheet of 1.2 mm the countersunk V riveted joint showed somewhat higher fatigue strengths.

6 References.

1 A. Hartman, G. C. Duyn. A Comparative Investigation on the Fatigue Strength at Fluctuating Tension of Several Types of Riveted Lap Joints, a Series of Bolted and some Series of Glued Lap Joints of 24 ST Alclad. N.L.L. Report M. 1857 (1952).

REPORT S. 427

Investigation of the Post-Buckling Effective Strain Distribution in Stiffened, Flat, Rectangular Plates Subjected to Shear and Normal Loads

by

W. K. G. FLOOR.

Summary.

In an earlier N.L.L.-Report (ref. 1) diagrams have been presented for the determination of the average stresses and strains in stiffened, initially flat, rectangular plates that have developed buckles under the influence of external longitudinal and lateral normal loads as well as shear loads. They are based upon the theory from ref. 2 because this is considered most reliable in general. This theory, and hence the diagrams, are strictly valid only when the stresses do not exceed the proportionality limit anywhere in the plate.

The present report contains a set of diagrams, by means of which the largest effective strain, according to the HUBER, VON MISES and HENCKY criterion, can be determined. These diagrams are also based upon the theory from ref. 2. Their practical application is demonstrated by some numerical examples. The effective strain at several stations in the plate can be read from the diagrams. The largest effective strain may occur at different stations, dependent upon the magnitude of the loads and the ratios between normal and shear loads.

In some cases the effective strain may have a maximum somewhere in the plate that exceeds the largest strain read from the diagrams. The difference between both strains, however, can only be a few percent of the strain.

In ref. 2 a waveform assumption for the buckles in the plate is also proposed that might give more reliable results when the angle between the general direction of the buckles and the longitudinal edges is small. The corrections that would be required in the diagrams from ref. 1 when choosing this waveform assumption are shown by some numerical examples to be practically negligible throughout the major parts of the ranges covered by the diagrams, and reasonably small in the remaining parts of these ranges.

Contents.

This investigation has been performed by order of the Netherlands Aircraft Development Board (N.I.V.).

1 Introduction.

In a previous publication the relations between the deformations and the stresses in stiffened flat rectangular plates loaded above the buckling load by shear stresses and normal stresses have been presented in the form of a number of diagrams (ref. 1). These diagrams are based upon KOITER's theory (ref. 2), because this theory is considered to yield accurate results for all ratios of load to buckling load from unity to infinity.

The theory from ref. 2, and hence the diagrams presented in ref. 1, are based upon the assumption of purely elastic behaviour of the material of the buckled plate. The stress distribution in a buckled plate is a complicated function of the coordinates in and normal to the plane of the plate. When for arbitrary external loading the stresses are known everywhere in the plate, the highest loads for which the theory and diagrams remain valid can be determined from the condition that the highest local stresses occurring anywhere in the plate reach the proportionality limit of the material.

The normal and shear stresses acting in the longitudinal and lateral directions of the rectangular plate and presented in the diagrams from ref. 1 are averages over the whole plate. It is hence impossible to determine the elastic limit loads from these diagrams without additional information being available on the distribution of these stresses throughout the plate, i. e. on their variation in the longitudinal and lateral directions as well as in the direction normal to the plane of the plate.

The stress or strain distribution throughout the plate can be determined from the external deformations of the plate as a whole (the edges remaining straight and opposite edges parallel), the expressions for the form of the buckles in the plate (i. e. for the displacements of an arbitrary point of the plate in the longitudinal, lateral and normal directions) and the parameters in these expressions.

The strains are reduced to an effective strain by means of the HUBER, VON MISES and HENCKY criterion (ref. 3). The diagrams from ref. 1 cannot be considered to yield reliable results once the effective stress, i. e. the product of the effective strain and the modulus of elasticity, exceeds the uniaxial stress at the proportionality limit.

The details of the stress distribution depend to a large extent upon the assumed waveform of the buckles. The waveform assumed in ref. 2 yields a good approximation of the elastic energy stored in the buckled plate and also of the average stresses presented in the diagrams from ref. 1. This does not necessarily imply, however, that the details of the stress distribution and the maximum stresses are obtained with equally good accuracy. It is considered that the maximum of the effective strain anywhere in the buckled plate will nevertheless provide a reasonable indication for determining whether the proportionality limit is exceeded. It should also be remembered in this respect that the proportionality limit itself is not usually known with great precision. In addition the deviations in the relations between stresses and strains averaged over the whole plate that occur when the load exceeds the proportionality limit load to a small extent are relatively small.

It was stated in ref. 1 that it would be desirable to investigate whether the accuracy of the diagrams in ref. 1 could be improved by assuming a waveform in which the nodal lines orthogonally intersect the longitudinal edges of the plate, such as waveform assumption no. 2 in ref. 2.

The aircraft industry showed much interest in the construction of a set of diagrams complementing the diagrams already presented in ref. 1. The new diagrams should contain curves for constant ratios of the effective strain to a critical strain defined in ref. 1. The coordinate system should be the same as in the original diagrams to enable a rapid determination of the effective strain.

The Netherlands Aircraft Development Board charged the National Aeronautical Research Institute with the construction of such diagrams and a concise investigation of the improvements obtainable with a more suitable assumed waveform. Results of the investigation are presented in this report, that should be read in conjunction with ref. 1.

Relations between the local strains in the plate as functions of longitudinal, lateral and normal coordinates on one hand and the average strains in the plate considered as a whole and the waveform parameters on the other hand are derived in sec. 3 from the expressions representing the assumed waveform.

Problems encountered in finding those points of a buckled plate where the effective strain is largest are discussed in sec. 4.

The numerical results are discussed in sec. 5 and presented in the form of a set of diagrams. It will in general be necessary to read the effective strains at different points of the plate in order to find the largest effective stress.

The application of the diagrams is demonstrated by some numerical examples in sec. 6.

In sec. 7 numerical results obtained by assuming waveform no. 2 from ref. 2 are compared with results calculated in the way described in ref. 1.

The conclusions that can be drawn from the investigations are presented in sec. 8.

2 Symbols.

b	width of the (infinitely long) plate (fig. 3.1)
f	maximum amplitude of the buckles in the plate (fig. 3.1)
h	thickness of the plate
m	cotangent of the angle φ between the nodal lines of the buckles and the X-direction (fig. 3.1)
u, v, w	displacements of an arbitrary point $(x, y, 0)$ of the median plane $(z=0)$ of the plate in the X-, Y- and Z-directions respectively during buckling (fig. 3.1)
x, y, z	coordinates in the X-, Y- and Z-directions respectively (fig. 3.1)
D	$=b^2/L^2$
E	modulus of elasticity
F	$=\pi^2 f^2/4b^2$
G	modulus of rigidity
L	half-wave length of the buckles in the plate (fig. 3.1)
X	longitudinal direction of the plate (fig. 3.1)
Y	lateral direction of the plate (fig. 3.1)
Z	direction normal to the plane of the plate (fig. 3.1)
α	ratio between the width of the edge regions and the total width of the plate (fig. 3.1)
γ	angle of shear of the plate considered as a whole (fig. 3.2)
γ_{xy}	local angle of shear, defined by (3.5)
$\varepsilon_1, \varepsilon_2$	compressive strains in the longitudinal (X-) and lateral (Y-) directions of the plate considered as a whole (fig. 3.2)
ε_e	effective strain, defined by (4.1)
ε_{xx}, ε_{yy}	local tensile strains in the longitudinal (X-) and lateral (Y-) directions respectively, defined by (3.5)
ε_p	uniaxial tensile strain at the proportionality limit

ε^* critical compressive strain for pure longitudinal compression, hinged edges, defined by (3.2)

ϑ $=\pi y/\alpha b$

$\bar{\vartheta}, \bar{\bar{\vartheta}}$ special values of ϑ (fig. 4.5), roots of (D. 11)

ν lateral contraction ratio

σ_1, σ_2 average tensile stresses in the longitudinal (X-) and lateral (Y-) directions respectively (fig. 3.2)

τ shear stress (fig. 3.2)

ψ $=\pi(x-my)/L$

$\bar{\psi}, \bar{\bar{\psi}}$ special values of ψ (fig. 4.3), roots of (D. 9)

Φ $=(1-\nu^2)^2\varepsilon_e^2$, sec. 4.2.

3 Local strains in the buckled plate.

3.1 *The assumed waveform of the buckles.*

In this investigation as well as in ref. 1 the waveform no. 1 from ref. 2 was assumed. The mathematical expressions for the displacements u, v and w of an arbitrary point (x, y) of the median plane $z=0$ of the plate in the X-, Y- and Z-directions respectively are presented in Appendix A of ref. 1. The X-, Y- and Z-directions, the dimensions of the infinitely long rectangular plate and the main parameters of the assumed waveform of the buckles, viz. the amplitude f, the half-wave length L, the cotangent m of the angle φ between the nodal lines and the longitudinal or X-direction and the ratio α are shown in fig. 3.1.

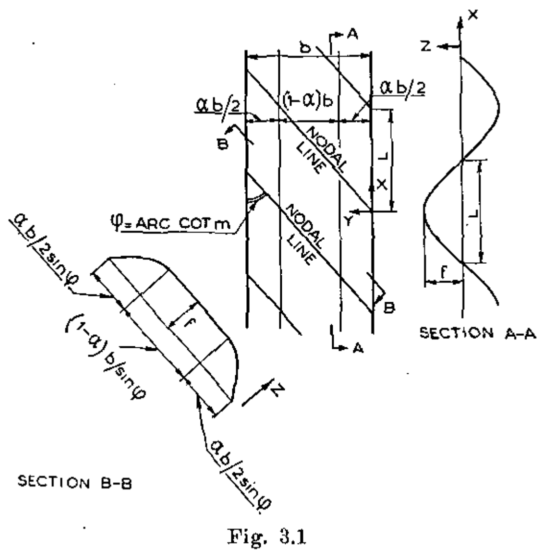

Fig. 3.1

It is observed that the nodal lines are straight and that they do not intersect the longitudinal edges of the plate orthogonally, except in the special case $\tau=0$. This is not in accordance with the assumption that the plate is hinged at the longitudinal edges, but the error introduced in this way is considered to be negligible unless m is large, say $m>2$ (ref. 1).

The edges remain straight and parallel. The average deformations ε_1, ε_2 and γ of the plate considered as a whole and the corresponding average external stresses σ_1, σ_2 and τ are shown in fig. 3.2. For convenience only a part of length L from the infinitely long plate is considered.

It is observed from fig. 3.1 that the buckled plate can be divided into three parts, viz. two edge regions, wide $\alpha b/2$ each, and a central region, wide $(1-\alpha)b$. The amplitude of the buckles is

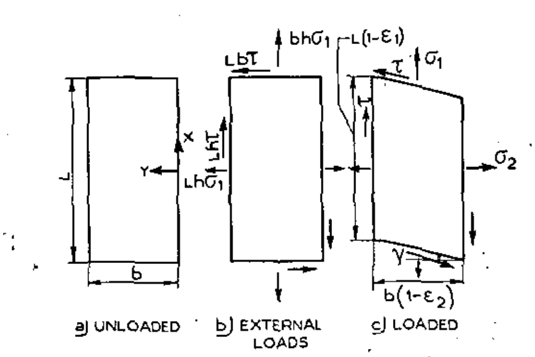

Fig. 3.2

of course zero at the edges and increases towards the central region according to a sine law. It remains constant in the central region. Finally, w is a periodic function of x, because the plate is infinitely long.

It is observed from fig. 3.2 that σ_1 and σ_2 are positive as tensile stresses, whereas ε_1 and ε_2 are positive as compressive strains.

3.2 *The local strains in the median plane of the plate.*

From the expressions for u, v and w as functions of x and y, presented in Appendix A of ref. 1, the tensile strains $\bar{\varepsilon}_{xx}$ in the X- and $\bar{\varepsilon}_{yy}$ in the Y-direction and the shear strain $\bar{\gamma}_{xy}$ in the median plane $z=0$ of the plate are calculated according to

$$\left.\begin{aligned}\bar{\varepsilon}_{xx}&=u_x+0.5\,w_x^2\,,\\ \bar{\varepsilon}_{yy}&=u_y+0.5\,w_y^2\,,\\ \bar{\gamma}_{xy}&=u_y+v_x+\;w_xw_y\,,\end{aligned}\right\}\qquad(3.1)$$

where u_x stands for $\partial u/\partial x$, etc.

It is found convenient to reduce the strains by dividing them by the critical compressive strain

$$\varepsilon^*=\pi^2h^2/3(1-\nu^2)b^2\qquad(3.2)$$

at which an infinitely long rectangular plate of width b and thickness h buckles when it is loaded in longitudinal compression only and when the edges are hinged and remain straight and parallel.

The strains $\bar{\varepsilon}_{xx}$, $\bar{\varepsilon}_{yy}$ and $\bar{\gamma}_{xy}$ are expressed in terms of the average strains ε_1, ε_2 and γ and the waveform parameters by evaluating eqs. (3.1). The results are presented in Appendix A. Instead of the parameters f and L indicated in fig. 3.1, more convenient parameters were introduced. They are defined by

$$\left.\begin{aligned}F&=\pi^2f^2/4b^2\,,\\ D&=b^2/L^2\,.\end{aligned}\right\}\qquad(3.3)$$

It is observed by comparing (A. 3) and (A. 4) that $\bar{\varepsilon}_{yy}$ has a discontinuity at $y = \alpha b/2$.

In the centre region, $\alpha b/2 \leqslant y \leqslant (1-\alpha/2)b$, the strains are constant, but in the edge regions, $0 \leqslant y \leqslant \alpha b/2$, the strains $\bar{\varepsilon}_{xx}$ and $\bar{\varepsilon}_{yy}$ are dependent on

$$\vartheta = \pi y/\alpha b$$

and hence on y, whereas $\bar{\varepsilon}_{yy}$ depends also upon

$$\psi = \pi(x - my)/L,$$

and hence upon both x and y.

3.3 *The bending strains.*

For arbitrary values of $-h/2 \leqslant z \leqslant h/2$ the tensile strains in the X- and Y-directions and the shear strain are in general different from the strains in the median plane ($z = 0$) for the same coordinates x and y.

The differences are caused by the curvatures assumed by the plate when it buckles.

These bending strains are proportional to z because the theory is based upon the assumption that straight lines normal to the median plane of the unbuckled plate are transformed into straight lines normal to the median plane of the buckled plate during buckling (ref. 2).

The tensile strains $\bar{\bar{\varepsilon}}_{xx}$ in the X- and $\bar{\bar{\varepsilon}}_{yy}$ in the Y-direction and the shear strain $\bar{\bar{\gamma}}_{xy}$ caused by bending of the plate during buckling can thus be expressed as

$$\left.\begin{aligned}
\bar{\bar{\varepsilon}}_{xx} &= -zw_{xx} = (2z/h)\bar{\bar{\varepsilon}}'_{xx}, \\
\bar{\bar{\varepsilon}}_{yy} &= -zw_{yy} = (2z/h)\bar{\bar{\varepsilon}}'_{yy}, \\
\bar{\bar{\gamma}}_{xy} &= -z\,w_{xy} = (2z/h)\bar{\bar{\gamma}}'_{xy}.
\end{aligned}\right\} \qquad (3.4)$$

The bending strains are extremal at the upper face $z = h/2$ and at the lower face $z = -h/2$ of the plate.

The bending strains $\bar{\bar{\varepsilon}}'_{xx}$, $\bar{\bar{\varepsilon}}'_{yy}$ and $\bar{\bar{\gamma}}'_{xy}$ for $z = h/2$ can be expressed as functions of the coordinates x and y in the median plane of the plate and the parameters for the waveform of the buckles. The results of these calculations are presented in Appendix B.

It is observed by comparing (B. 3) and (B. 4) that ε'_{yy} has a discontinuity at $y = \alpha b/2$. This was to be expected (ref. 2).

The bending strains are extremal for $\cos\psi = \pm 1$, i. e. at the nodal lines, at the edge $y = 0$ and for $\sin\psi = \pm 1$, i. e. at the crest lines, at $y = \alpha b/2$. In the central region they are extremal only at the crest lines, but zero at the nodal lines. The crest lines are running parallel to the nodal lines at a distance $L/2$, measured in the X-direction (fig. 3.1).

3.4 *The strains in the faces of the plate.*

The tensile strains ε_{xx} in the X- and ε_{yy} in the Y-directions and the shear strain γ_{xy} at the point (x, y, z) in the plate are defined by

$$\varepsilon_{xx}/\varepsilon^* = \bar{\varepsilon}_{xx}/\varepsilon^* + \bar{\bar{\varepsilon}}_{xx}/\varepsilon^*, \text{ etc.} \qquad (3.5)$$

At the upper face of the plate, $z = h/2$, they can thus be expressed as

$$\varepsilon_{xx}/\varepsilon^* = \bar{\varepsilon}_{xx}/\varepsilon^* + \bar{\bar{\varepsilon}}'_{xx}/\varepsilon^*, \text{ etc.} \qquad (3.6)$$

and at the lower face, $z = -h/2$, as

$$\varepsilon_{xx}/\varepsilon^* = \bar{\varepsilon}_{xx}/\varepsilon^* - \bar{\bar{\varepsilon}}'_{xx}/\varepsilon^*, \text{ etc.} \qquad (3.7)$$

4 **Determination of the largest effective strain in the plate.**

4.1 *The effective strain.*

The effective strain ε_e after the HUBER, VON MISES and HENCKY criterion (ref. 3) is related to the tensile strains ε_{xx} in the X- and ε_{yy} in the Y-direction and to the shear strain γ_{xy} by the expression

$$\begin{aligned}
(1-\nu^2)^2\varepsilon_e^2 &= (1-\nu+\nu^2)(\varepsilon_{xx}^2+\varepsilon_{yy}^2) + \\
&+(-1+4\nu-\nu^2)\varepsilon_{xx}\varepsilon_{yy} + 0.75(1-\nu)^2\gamma_{xy}^2. \quad (4.1)
\end{aligned}$$

In the numerical evaluation it is assumed that $\nu = 0.3$, in accordance with ref. 1.

Equation (4.1) can then be written as

$$\begin{aligned}
\Phi &= 0.8281(\varepsilon_e/\varepsilon^*)^2 = \\
&= 0.79[(\varepsilon_{xx}/\varepsilon^*)^2 + (\varepsilon_{yy}/\varepsilon^*)^2] + \\
&+ 0.11(\varepsilon_{xx}/\varepsilon^*)(\varepsilon_{yy}/\varepsilon^*) + 0.3675(\gamma_{xy}/\varepsilon^*)^2. \quad (4.2)
\end{aligned}$$

The quantity Φ can be expressed as a function of the coordinates x and y, or the angles ψ and ϑ,

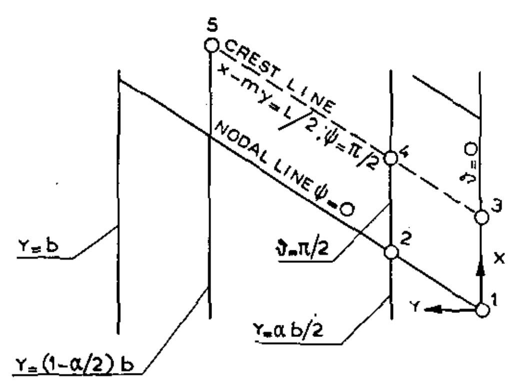

STATION Nº	ψ	ϑ	$2z/h$
1	0	0	-1
2	0	$\pi/2$	–
3	$\pi/2$	0	–
4	$\pi/2$	$\pi/2$	± 1
4-5	$\pi/2$	–	-1

Fig. 4.1

the strains ε_1, ε_2 and γ and the parameters of the waveform of the buckles.

The results of this calculation are presented in Appendix C.

It is observed from (C. 1) and (C. 4) that Φ, and hence $\varepsilon_e/\varepsilon^*$, varies always with ψ. In the edge regions, it varies also with ϑ.

4.2 *The extrema of the effective strain.*

For specified loading the values of the waveform parameters, i. e. of α, m, D and F/ε^*, are known from the investigation of ref. 1. The effective strain, and hence the quantity Φ after (4.2), depends either upon ψ alone, viz. (C. 4), or upon ψ and ϑ, viz. (C. 1).

The coordinates x and y, or the more convenient quantities ψ and ϑ, defining the points of the upper or lower faces of the plate where ε_e is extremal, should be solved from the equations

$$\left.\begin{aligned} \partial\Phi/\partial\psi &= 0, \\ \partial\Phi/\partial\vartheta &= 0. \end{aligned}\right\} \quad (4.3)$$

In the centre region, $\alpha b/2 \leqslant y \leqslant (1-\alpha/2)b$, only the first equation remains.

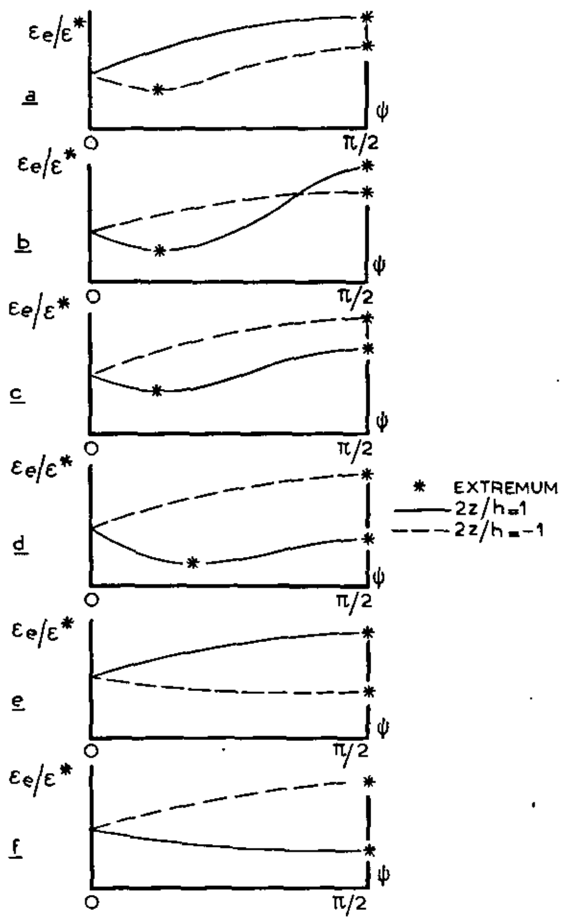

Fig. 4.2

4.3 *The centre region of the plate.*

The investigation presents no difficulties as far as the centre region $\alpha b/2 \leqslant y \leqslant (1-\alpha/2)b$ is concerned. It follows from (D. 3) that Φ reaches extremal values for $\cos\psi = 0$, i. e. for $\psi = \pi/2$. The case $\psi = -\pi/2$ need not be considered for reasons of symmetry. When $|\overline{B}_0| \leqq 2\,\overline{C}_0$, (D. 3) has also a solution

$$\sin\psi = \mp \overline{B}_0/2\,\overline{C}_0\,.$$

In this case, (D. 7) yields

$$\partial^2\Phi/\partial\psi^2 = 2\,\overline{C}_0(1-\overline{B}_0{}^2/4\,\overline{C}_0{}^2).$$

This expression is never negative since $\overline{C}_0 > 0$, i. e. Φ is a minimum. For $\psi = \pi/2$,

$$\partial^2\Phi/\partial\psi^2 = \mp\overline{B}_0 - 2\,\overline{C}_0\,.$$

This is never positive, i. e. Φ is a maximum both for $2z/h = 1$ and for $2z/h = -1$. The relations between $\varepsilon_e/\varepsilon^*$ and ψ for these cases are qualitatively represented in figs. 4.2*a* and 4.2*c*.

When $|\overline{B}_0| > 2\,\overline{C}_0$, (D. 3) yields only the solution $\psi = \pi/2$, and it follows from (D. 7) that

$$\partial^2\Phi/\partial\psi^2 = \mp\overline{B}_0 - 2\,\overline{C}_0\,.$$

Hence, Φ is a maximum for $2z/h = 1$, i. e. at the upper surface of the plate, and a minimum for $2z/h = -1$, i. e. at the lower surface, when $\overline{B}_0 > 0$.

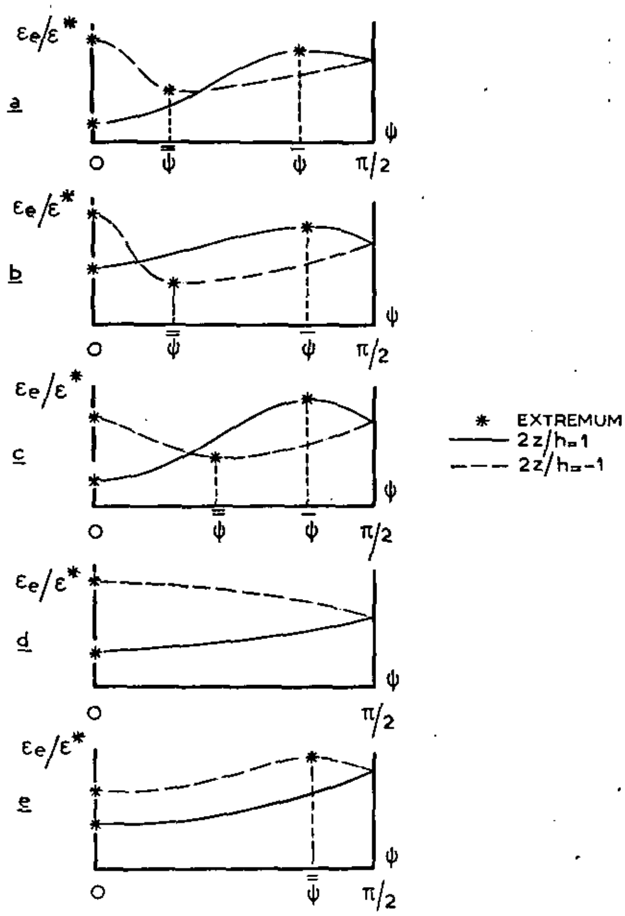

Fig. 4.3

The reverse is true when $\overline{B}_0 < 0$. The relations between $\varepsilon_e/\varepsilon^*$ and ψ for these cases are qualitatively represented in fig. 4.2*e* and 4.2*f* respectively.

In the numerical evaluation both cases $2z/h = 1$ and $2z/h = -1$ are investigated and the highest value of Φ is chosen for the calculation of the largest ε_e in the centre region of the plate, because neither the sign nor the magnitude of $\overline{B}_0$ is a priori known.

Throughout the range of the investigations $\varepsilon_e/\varepsilon^*$ was always larger for $2z/h = -1$, i. e. at the lower face of the plate, than at $2z/h = 1$ (fig. 4.2*c*, 4.2*f*).

TABLE 4.1. Numerical results for some representative cases where $\vartheta = 0$.

$\tau_1/E\varepsilon^*$	$\sigma_1/E\varepsilon^*$	$\sigma_2/E\varepsilon^*$	case (fig. 4.3)	$2z/h=1$: $\cos\bar{\psi}$	$2z/h=1$: $\varepsilon_e/\varepsilon^*$, $\psi=0$	$2z/h=1$: $\varepsilon_e/\varepsilon^*$, $\psi=\bar{\psi}$	$2z/h=1$: $\varepsilon_e/\varepsilon^*$, $\psi=\pi/2$	$2z/h=-1$: $\cos\bar{\bar{\psi}}$	$2z/h=-1$: $\varepsilon_e/\varepsilon$, $\psi=0$	$2z/h=-1$: $\varepsilon_e/\varepsilon$, $\psi=\bar{\bar{\psi}}$	$2z/h=-1$: $\varepsilon_e/\varepsilon$, $\psi=\pi/2$
50	—10	90	*c*	0.15594	225.53	246.96	246.36	0.62428	248.11	240.32	246.36
50	0	100	*d*	—	150.08	—	157.49	—	159.62	—	157.49
50	—5	60	*a*	0.28825	248.65	277.56	273.29	0.54993	289.76	258.89	273.29
50	10	70	*d*	—	122.48	—	130.63	—	136.15	—	130.63
30	—20	50	*a*	0.25235	233.96	255.54	252.83	0.59044	261.25	239.96	252.83
30	—20	100	*e*	—	186.37	—	198.62	0.0072162	195.18	198.92	198.62
30	—5	100	*d*	—	116.78	—	117.91	—	118.57	—	117.91
30	0	60	*d*	—	82.926	—	85.646	—	87.550	—	85.646
10	—25	100	*e*	—	174.15	—	182.55	0.015037	176.80	182.56	182.55
10	—15	20	*a*	0.28745	100.89	104.94	104.01	0.49953	111.31	101.18	104.01
10	—35	100	*c*	0.036055	275.44	295.05	295.01	0.97361	280.10	280.05	295.01
10	—35	10	*b*	0.23707	326.98	347.85	343.04	0.59889	362.57	314.36	343.04

TABLE 4.2. Numerical results for some representative cases where $\psi = \pi/2$.

$\tau_1/E\varepsilon^*$	$\sigma_1/E\varepsilon^*$	$\sigma_2/E\varepsilon^*$	case (fig. 4.5)	$2z/h=1$: $\sin\bar{\vartheta}$	$2z/h=1$: $\varepsilon_e/\varepsilon^*$, $\vartheta=0$	$2z/h=1$: $\varepsilon_e/\varepsilon^*$, $\vartheta=\bar{\vartheta}$	$2z/h=1$: $\varepsilon_e/\varepsilon^*$, $\vartheta=\pi/2$	$2z/h=-1$: $\sin\bar{\bar{\vartheta}}$	$2z/h=-1$: $\varepsilon_e/\varepsilon^*$, $\vartheta=0$	$2z/h=-1$: $\varepsilon_e/\varepsilon^*$, $\vartheta=\bar{\bar{\vartheta}}$	$2z/h=-1$: $\varepsilon_e/\varepsilon^*$, $\vartheta=\pi/2$
50	—10	90	*b*	0.75484	246.36	194.11	213.52	0.22133	246.36	251.62	194.22
50	0	100	*c*	0.81423	157.49	137.03	139.90	0.45670	157.49	163.35	155.84
50	—5	60	*a*	0.71647	273.29	220.00	253.69	0.14768	273.29	276.29	203.94
50	10	70	*e*	—	130.63	—	123.56	0.65012	130.63	138.25	137.60
30	—20	50	*a*	0.74686	252.83	192.66	220.01	0.15505	252.83	256.23	164.47
30	—20	100	*b*	0.81479	198.62	154.33	161.86	0.26148	198.62	203.87	159.77
30	—5	100	*e*	—	117.91	—	110.27	0.85032	117.91	121.08	120.98
30	0	60	*d*	0.86218	85.646	77.758	78.198	0.78313	85.646	90.225	89.897
10	—25	100	*b*	0.84261	182.55	140.70	145.41	0.26415	182.55	187.40	145.16
10	—15	20	*a*	0.71008	104.01	79.035	94.054	0.21577	104.01	106.67	72.90
10	—35	100	*a*	0.80851	295.01	213.20	230.26	0.18981	295.01	300.66	187.00
10	—35	10	*a*	0.76043	343.04	256.11	293.65	0.097344	343.04	345.15	165.20
0	—26.10	62.36	*a*	0.78594	182.5	133.24	146.3	0.21639	182.5	186.97	121.6
0	—19.33	5.06	*a*	0.72044	124.1	91.165	110.4	0.16809	124.1	126.40	69.01
0	—10.55	99.75	*f*	—	105.5	—	104.6	—	105.5	—	106.3
0	—5.86	2.37	*b*	0.63249	18.89	13.987	18.89	0.36243	18.89	20.267	15.97

4.4 *The edge regions of the plate.*

It is observed by inspection that $\varepsilon_e/\varepsilon^*$ is an extremum for either $\psi = 0$, $\vartheta = 0$ (station 1, fig. 4.1) or $\psi = \pi/2$, $\vartheta = \pi/2$ (station 4), (D. 1) and (D. 2) being satisfied. The condition for $\varepsilon_e/\varepsilon^*$ to be a maximum obtained by substitution of either (D. 4)′, (D. 5)′ and (D. 6)′ or (D. 4)″, (D. 5)″ and (D. 6)″ in (E. 1) turns out to be so complicated that no general conclusions, such as were obtained for the edge region (sec. 4.3), can be drawn from it.

Numerical evaluations lead to the conclusion that for $\vartheta = \pi/2$ (2—4, fig. 4.1) $\varepsilon_e/\varepsilon^*$ varies with ψ,

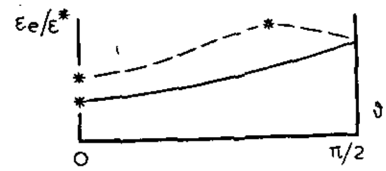

Fig. 4.4

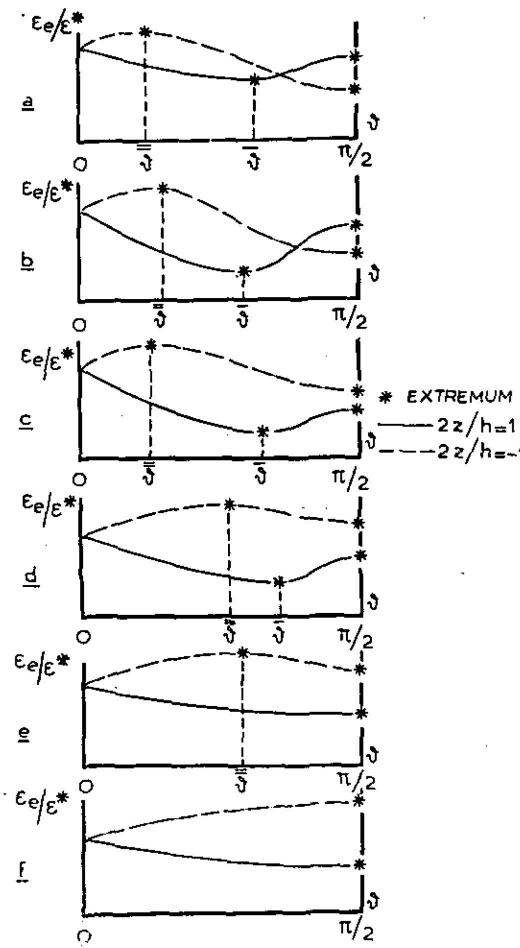

Fig. 4.5

i. e. in the longitudinal direction, as shown in fig. 4.2*b*, 4.2*c*, 4.2*d* or 4.2*f*. It is evident that in this case only $\psi = \pi/2$ (station 4, fig. 4.1) needs to be considered.

At the edge $\vartheta = 0$ (1—3, fig. 4.1) $\varepsilon_e/\varepsilon^*$ varies with ψ, i. e. in the longitudinal direction, as shown in fig. 4.3. In the cases of fig. 4.3*c* and 4.3*e* $\varepsilon_e/\varepsilon^*$ reaches a maximum at $\psi = \bar{\psi}$ and $\bar{\bar{\psi}}$ respectively exceeding $\varepsilon_e/\varepsilon^*$ at $\psi = 0$ (station 1, fig. 4.1) or at $\psi = \pi/2$ (station 3). It is observed from the numerical examples presented in table 4.1 that the differences are so small that it is considered allowable to restrict the evaluation to $\psi = 0$ and $\psi = \pi/2$.

At the nodal lines $\psi = 0$ (1—2, fig. 4.1) the largest $\varepsilon_e/\varepsilon^*$ occurs nearly always at $\vartheta = 0$ (station 1, fig. 4.1). In two cases considered $\varepsilon_e/\varepsilon^*$ varied with ϑ according to fig. 4.4. The largest $\varepsilon_e/\varepsilon^*$ proves to be always smaller than for $\psi = \pi/2$, $\vartheta = \pi/2$ (station 4). Hence, $\psi = 0$ need not be considered in the numerical evaluation.

At the crest lines $\psi = \pi/2$ (3—4, fig. 4.1) $\varepsilon_e/\varepsilon^*$ varies with ϑ as shown in fig. 4.5. It is observed from the numerical results presented in table 4.2 that the difference between $\varepsilon_e/\varepsilon^*$ at $\vartheta = \bar{\bar{\vartheta}}$ and at $\vartheta = 0$ (station 3, fig. 4.1) or $\vartheta = \pi/2$ (station 4) is not always negligible. It is nevertheless allowable to leave this case out of consideration in the numerical evaluation because $\varepsilon_e/\varepsilon^*$ is never found to exceed by more than 2.6 % the largest $\varepsilon_e/\varepsilon^*$ in any of the stations 1, 3 and 4 from fig. 4.1.

In the cases to which figs. 4.3*d* and 4.5*c*, 4.5*d* or 4.5*e* or to which figs. 4.3*e* and 4.5*b* apply $\varepsilon_e/\varepsilon^*$ has a maximum at some station $0 < \psi < \pi/2$, $0 < \vartheta < \pi/2$. It is the largest $\varepsilon_e/\varepsilon^*$ anywhere in the plate, but it is expected to exceed only slightly the largest $\varepsilon_e/\varepsilon^*$ in any of the stations indicated in fig. 4.1, considered in the numerical evaluation.

The calculation of the largest $\varepsilon_e/\varepsilon^*$ is omitted because it proves to be very cumbersome. This is no serious objection especially when it is realized that the details of the stress distribution throughout the buckled plate are approximated in the theory with probably much less accuracy than the elastic energy.

A more detailed discussion of the stresses in the edge regions of the plate is presented in Appendix E.

5 Numerical results.

5.1 *Presentation of the results.*

The results of the calculations are presented in the form of a set of diagrams, figs. 5.1 to 5.19 incl. The coordinates are $\varepsilon_1/\varepsilon^*$ and $\varepsilon_2/\varepsilon^*$, as in the diagrams of ref. 1. The present diagrams cover the same region of coordinates as those of ref. 1. They contain a set of curves of constant $\varepsilon_e/\varepsilon^*$.

When $\varepsilon_1/\varepsilon^*$ and $\varepsilon_2/\varepsilon^*$ are specified or have been determined by means of the diagrams of ref. 1, the corresponding $\varepsilon_e/\varepsilon^*$ can thus be determined by interpolation from the present diagrams. It will in general be necessary to read $\varepsilon_e/\varepsilon^*$ at all stations indicated in fig. 4.1. Obviously, the largest $\varepsilon_e/\varepsilon^*$ obtained in this way should then be considered in the computation of the largest effective strain anywhere in the buckled plate.

The strain ε^* is determined from (3.2) and the known dimensions of the construction. The tensile strain ε_p at the proportionality limit can be derived from the ordinary uniaxial tensile stress-strain diagram for the material of the construction considered.

The theory from ref. 2, and hence the diagrams from ref. 1 and the present diagrams, are strictly valid only if $\varepsilon_e \leqq \varepsilon_p$ throughout the buckled plate.

For some of the stations shown in fig. 4.1, $\varepsilon_e/\varepsilon^*$ will exceed $\varepsilon_e/\varepsilon^*$ at all other stations only in a restricted range of $\varepsilon_1/\varepsilon^*$ and $\varepsilon_2/\varepsilon^*$. This is curves of the important ranges could not be determined with great accuracy. The transition points between the heavy and the thin lines are probably well without these limiting curves.

It is observed that in constructing the present diagrams four values of $\tau/E\varepsilon^*$ only have been con-

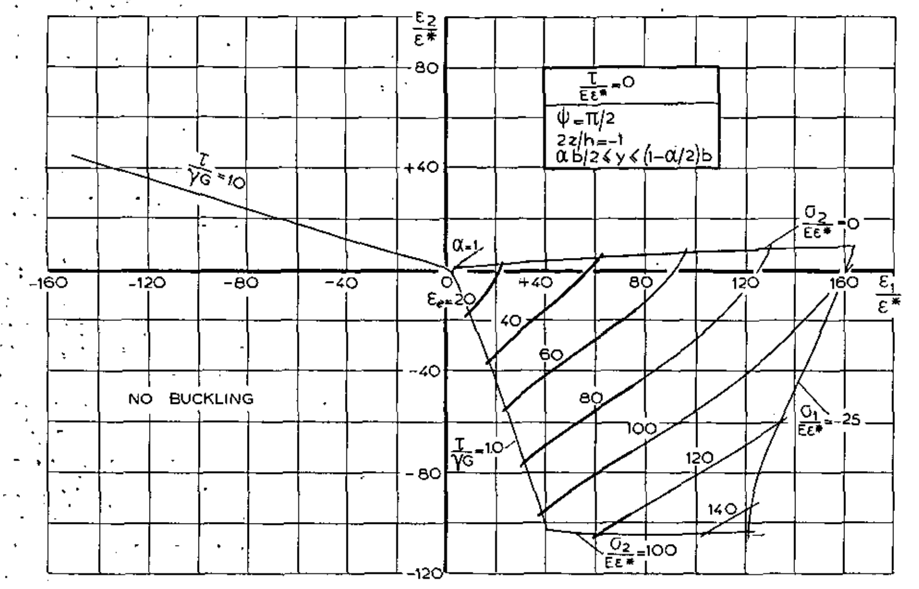

Fig. 5.1

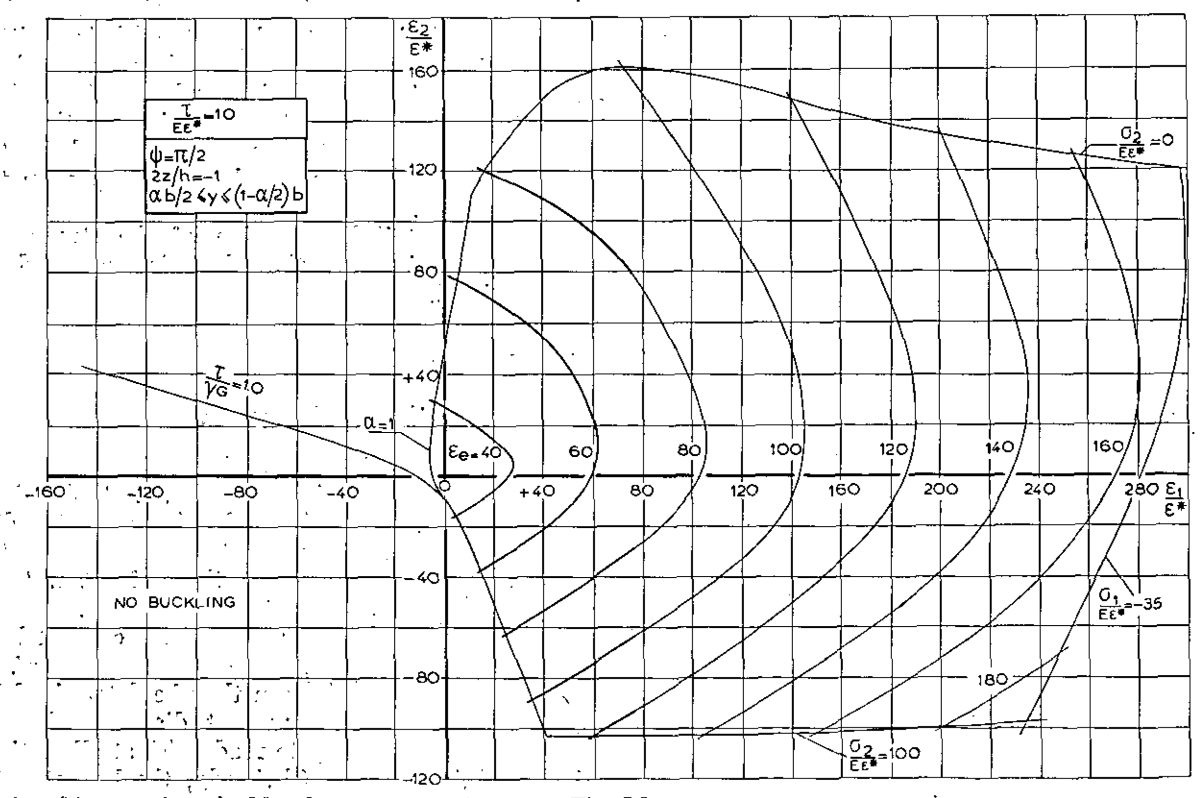

Fig. 5.2

indicated in the diagrams for convenience by drawing the curves as heavy lines within and as thin lines without this range. In the determination of $\varepsilon_e/\varepsilon^*$ for specified $\varepsilon_1/\varepsilon^*$ and $\varepsilon_2/\varepsilon^*$ all diagrams can be disregarded in which the point $(\varepsilon_1/\varepsilon^*, \varepsilon_2/\varepsilon^*)$ falls in the range of thin lines. The transitions were in general so gradual that the limiting sidered instead of eleven, as in ref. 1. This was considered justified in the first place because numerical examples have shown that $\varepsilon_e/\varepsilon^*$ can be obtained with reasonable accuracy for intermediate values of $\tau/E\varepsilon^*$ by interpolation.

In the second place, the diagrams for the effective strain cannot be considered to be as accurate

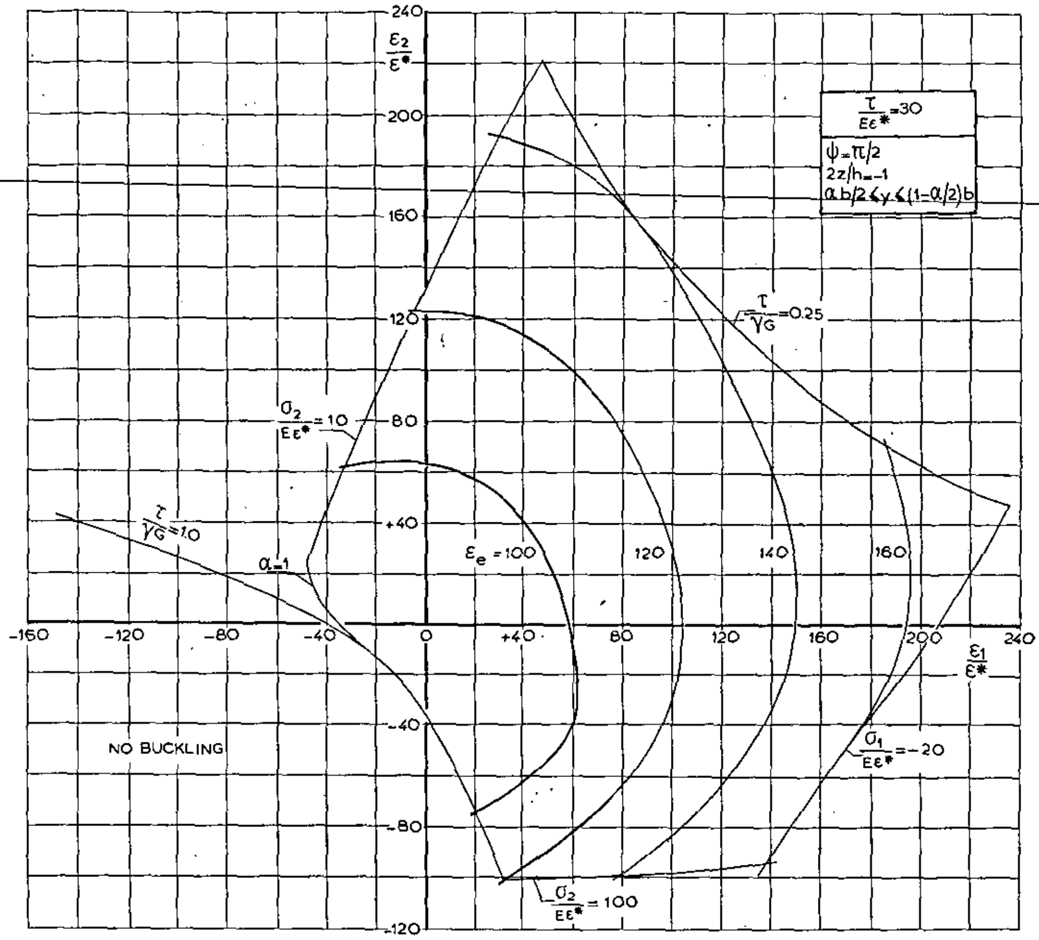
$\frac{\tau}{E\varepsilon^*}=30$
$\psi=\pi/2$
$2z/h=-1$
$\alpha b/2 \leq y \leq (1-\alpha/2)b$
$\frac{\varepsilon_2}{\varepsilon^*}$
$\frac{\varepsilon_1}{\varepsilon^*}$
$\frac{\tau}{\gamma_G}=0.25$
$\frac{\sigma_2}{E\varepsilon^*}=10$
$\frac{\tau}{\gamma_G}=1.0$
$\alpha=1$
$\varepsilon_e=100$
120
140
160
$\frac{\sigma_1}{E\varepsilon^*}=-20$
$\frac{\sigma_2}{E\varepsilon^*}=100$
NO BUCKLING

Fig. 5.3

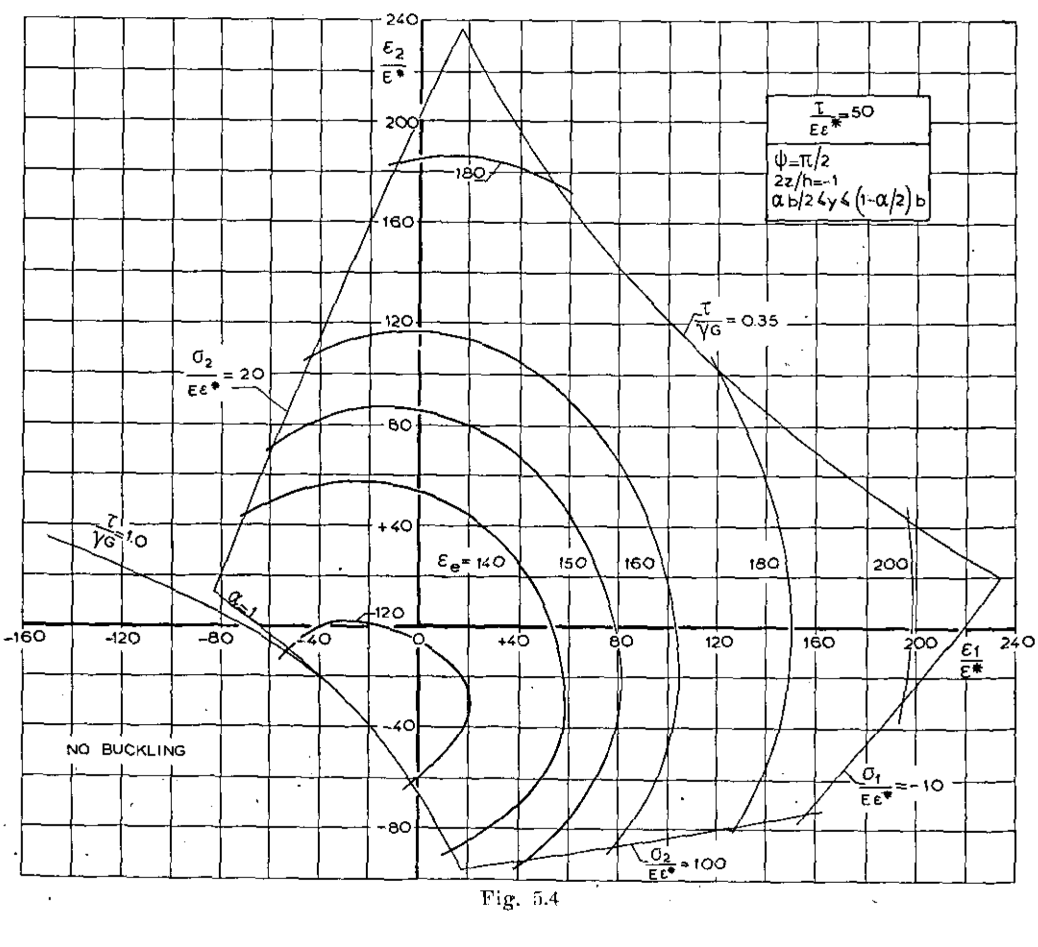
$\frac{\tau}{E\varepsilon^*}=50$
$\psi=\pi/2$
$2z/h=-1$
$\alpha b/2 \leq y \leq (1-\alpha/2)b$
$\frac{\varepsilon_2}{\varepsilon^*}$
$\frac{\varepsilon_1}{\varepsilon^*}$
180
$\frac{\tau}{\gamma_G}=0.35$
$\frac{\sigma_2}{E\varepsilon^*}=20$
$\frac{\tau}{\gamma_G}=1.0$
$\alpha=1$
$\varepsilon_e=140$
150
160
180
200
120
$\frac{\sigma_1}{E\varepsilon^*}=-10$
$\frac{\sigma_2}{E\varepsilon^*}=100$
NO BUCKLING

Fig. 5.4

as those for the average stresses presented in ref. 1 (sec. 4.4). An eventual small refinement obtainable by constructing diagrams for intermediate values of $\tau/E\varepsilon^*$ would thus result in a reduction of the relatively small interpolation errors much smaller than the errors already present as a consequence of the imperfect approxi-

and calculated strain will increase only slowly when ε_e exceeds ε_p to a slight extent.

5.2 *The centre region.*

In the centre region, i. e. for $\alpha b/2 \leqslant y \leqslant (1-\alpha/2)b$, (fig. 3.1), the largest effective strain is

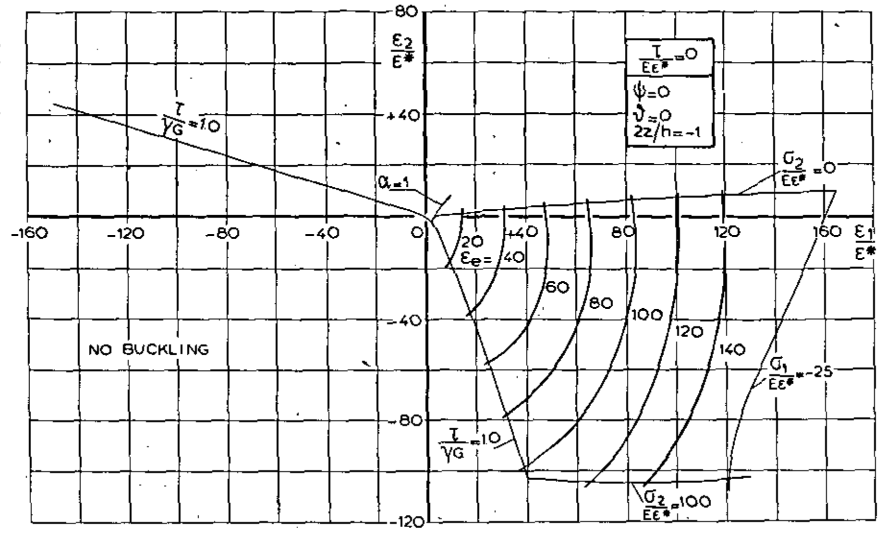

Fig. 5.5

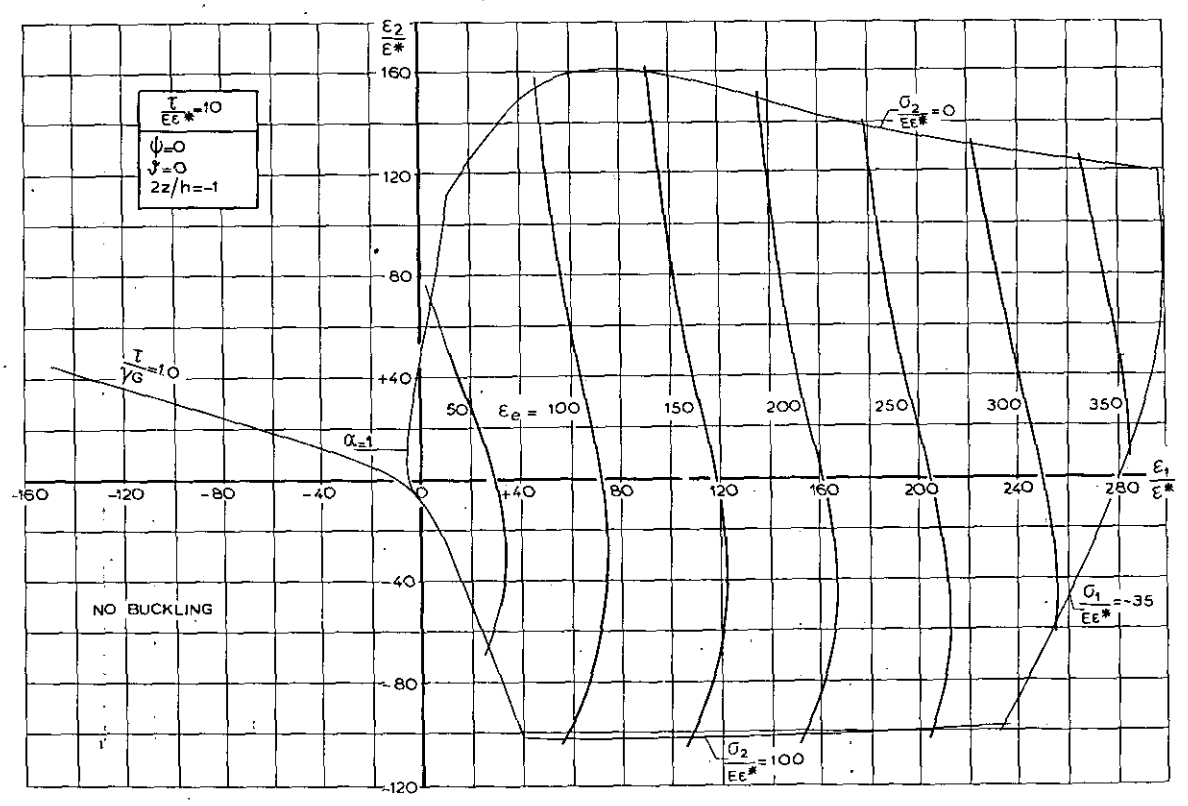

Fig. 5.6

mation of the details of the stress distribution in actual constructions by the theory from ref. 1.

Finally, it will be difficult to determine ε_p with great accuracy. It is not to be expected however that this will lead to large errors when ε_e exceeds ε_p only slightly since the difference between actual

observed at the crest line (sec. 4.3) at the lower face of the plate, $2z/h = -1$. It is constant along the line 4—5, or $\psi = \pi/2$, in fig. 4.1.

The results are shown in figs. 5.1 to 5.4 incl. It is observed that $\varepsilon_e/\varepsilon^*$ may be critical in this case only for small and moderate $\varepsilon_1/\varepsilon^*$.

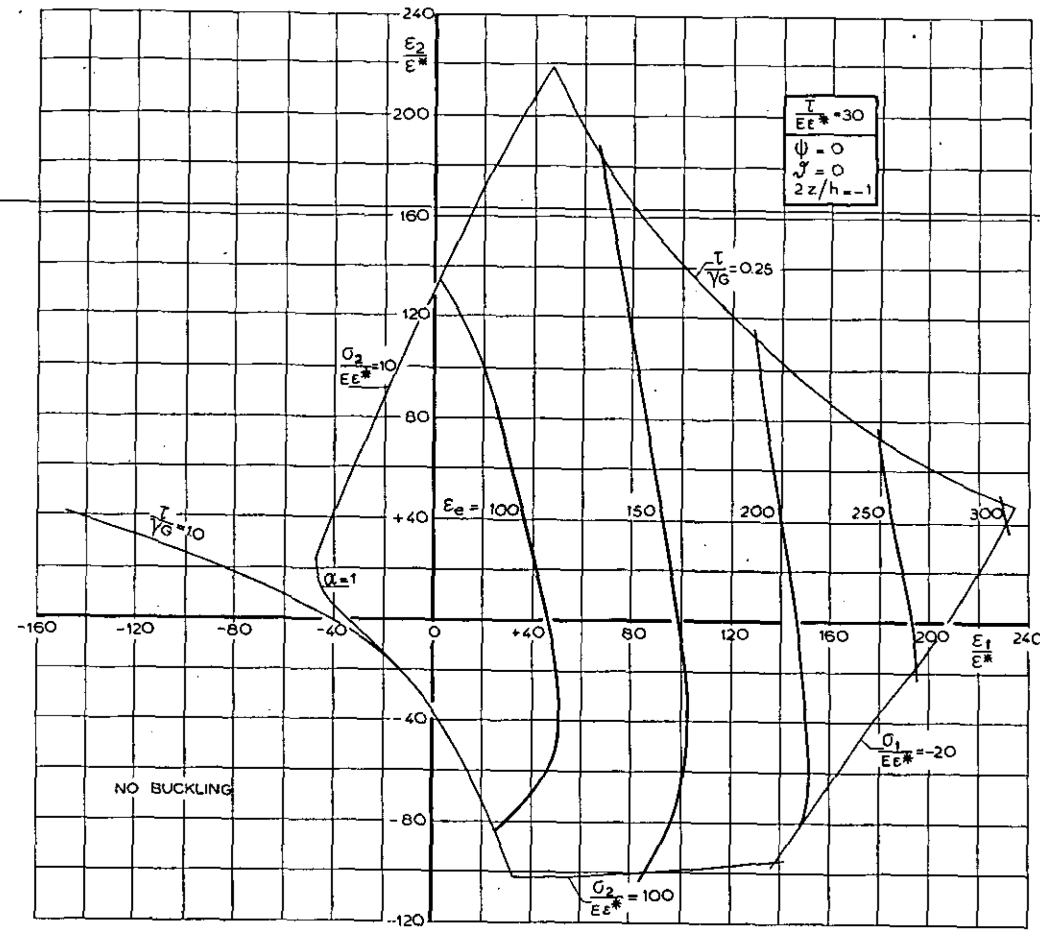

$\frac{\tau}{E\varepsilon^*}=30$
$\psi = 0$
$\vartheta = 0$
$2z/h = -1$
$\frac{\varepsilon_2}{\varepsilon^*}$
$\frac{\varepsilon_1}{\varepsilon^*}$
$\frac{\tau}{\sqrt{G}}=0.25$
$\frac{\sigma_2}{E\varepsilon^*}=10$
$\frac{\tau}{\sqrt{G}}=10$
$\alpha=1$
$\varepsilon_e = 100$
150
200
250
300
$\frac{\sigma_1}{E\varepsilon^*}=-20$
NO BUCKLING
$\frac{\sigma_2}{E\varepsilon^*}=100$

Fig. 5.7

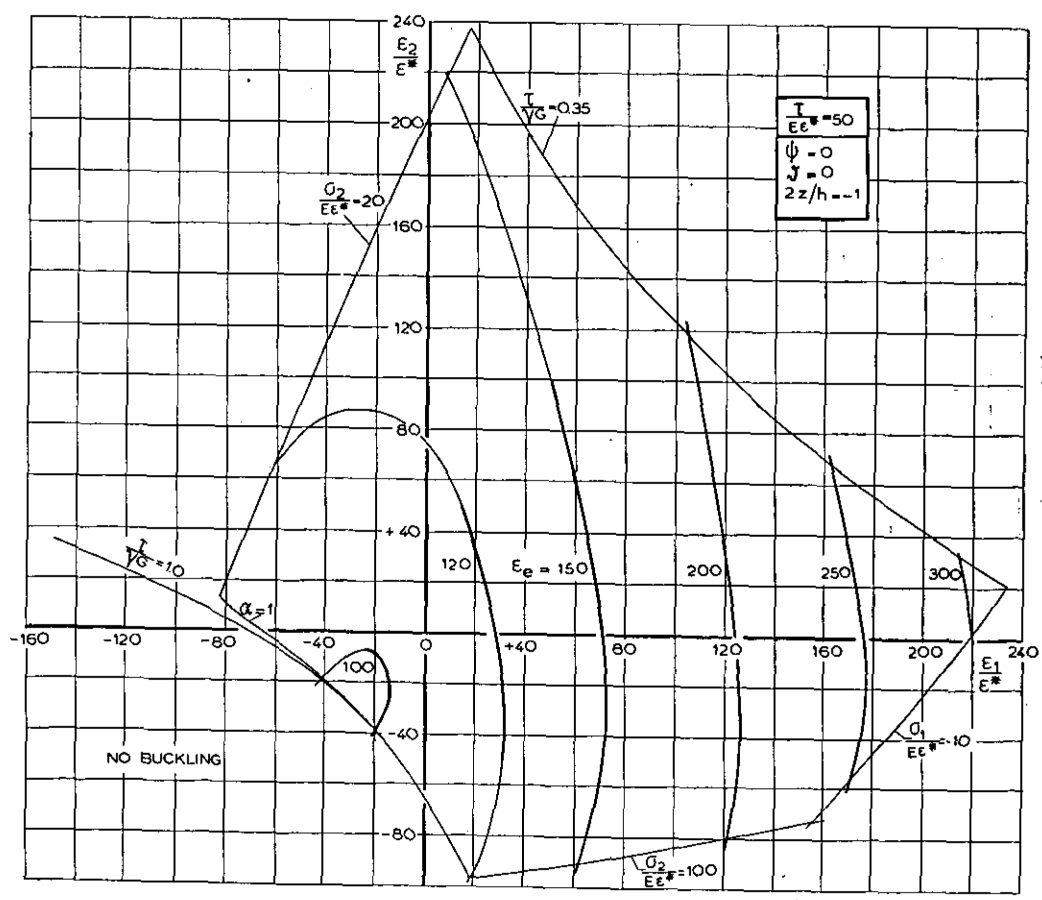

$\frac{\tau}{E\varepsilon^*}=50$
$\psi = 0$
$\vartheta = 0$
$2z/h = -1$
$\frac{\varepsilon_2}{\varepsilon^*}$
$\frac{\varepsilon_1}{\varepsilon^*}$
$\frac{\tau}{\sqrt{G}}=0.35$
$\frac{\sigma_2}{E\varepsilon^*}=20$
$\frac{\tau}{\sqrt{G}}=10$
$\alpha=1$
100
120
$\varepsilon_e = 150$
200
250
300
$\frac{\sigma_1}{E\varepsilon^*}=-10$
NO BUCKLING
$\frac{\sigma_2}{E\varepsilon^*}=100$

Fig. 5.8

5.3 The edge regions.

In the edge regions, i.e. for $0 \leqslant y \leqslant \alpha b/2$, (fig. 3.1), the effective strain was determined at several stations (sec. 4.4).

At the intersection of the nodal line and the edge of the plate, i.e. at $\psi = 0$, $\vartheta = 0$ or station 1 in fig. 4.1, $\varepsilon_e/\varepsilon^*$ is largest at the lower face of the plate, i.e. for $2z/h = -1$. The results are shown in figs. 5.5 to 5.8 incl. It is observed that in this case $\varepsilon_e/\varepsilon^*$ may be critical for most combinations of $\varepsilon_1/\varepsilon^*$ and $\varepsilon_2/\varepsilon^*$ except for small $\varepsilon_1/\varepsilon^*$ and for large $\varepsilon_2/\varepsilon^*$.

At the intersection of the crest line and the edge of the plate, i.e. at $\psi = \pi/2$, $\vartheta = 0$ or station 3 in fig. 4.1, $\varepsilon_1/\varepsilon^*$ is independent of z. The results for this case are shown in figs. 5.9 to 5.12 incl. It is observed that in this case $\varepsilon_e/\varepsilon^*$ may be critical for nearly all combinations of negative $\varepsilon_2/\varepsilon^*$ and positive $\varepsilon_1/\varepsilon^*$.

At *the transition point between the edge and* the centre regions on the crest line, just inside the edge region, i.e. at $\psi = \pi/2$, $\vartheta = \pi/2$ or station 4 in fig. 4.1, $\varepsilon_e/\varepsilon^*$ is either largest for $2z/h = 1$ or for $2z/h = -1$. The results for $2z/h = 1$, i.e. the upper face of the plate, are shown in figs. 5.13 to 5.15 incl. It is observed that in this case $\varepsilon_e/\varepsilon^*$ may be critical for combinations of small $\varepsilon_1/\varepsilon^*$ and positive $\varepsilon_2/\varepsilon^*$ and for combinations of moderate $\varepsilon_1/\varepsilon^*$ and large $\varepsilon_2/\varepsilon^*$.

The results for $2z/h = -1$, i.e. the lower face of the plate, are shown in figs. 5.16 to 5.19 incl.

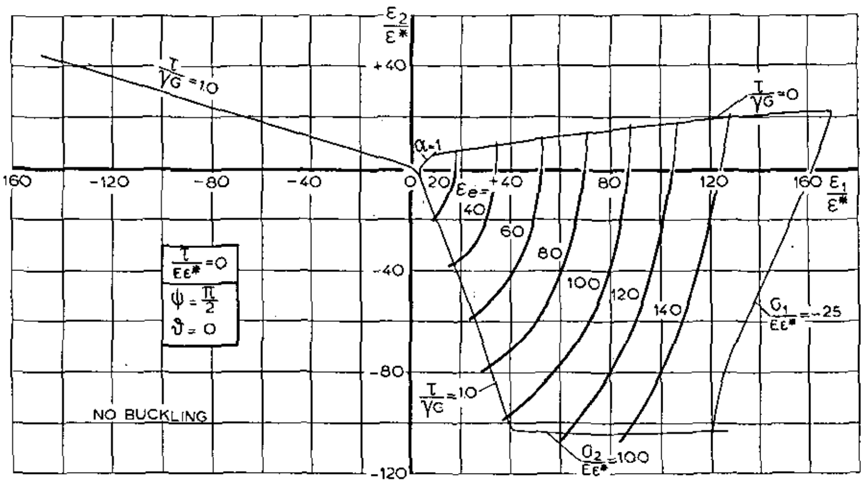

Fig. 5.9

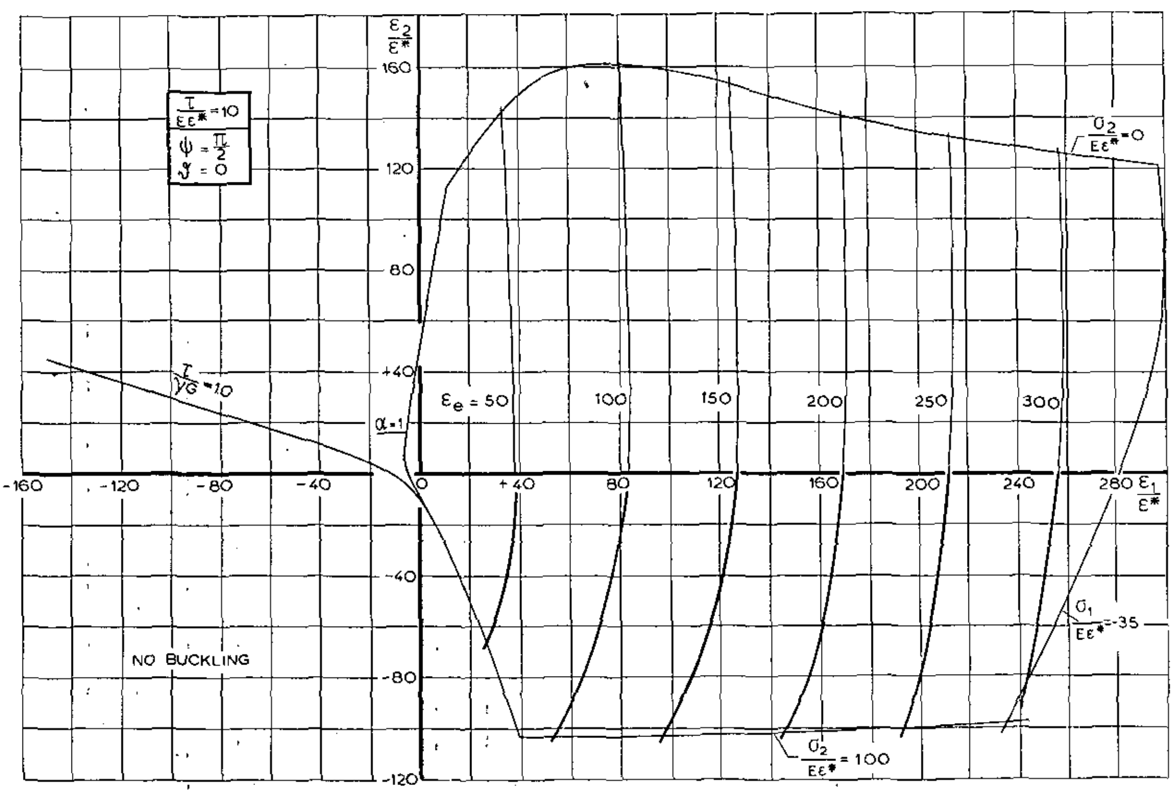

Fig. 5.10

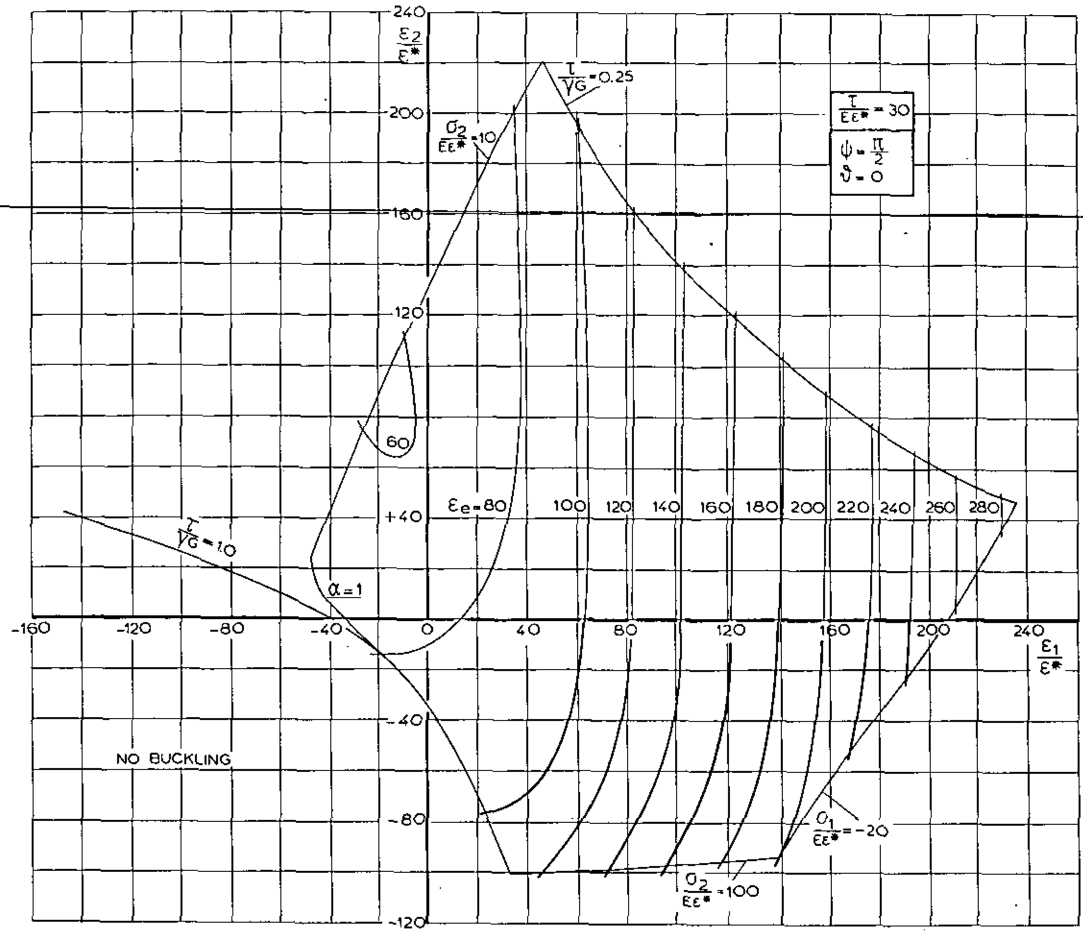

Fig. 5.11

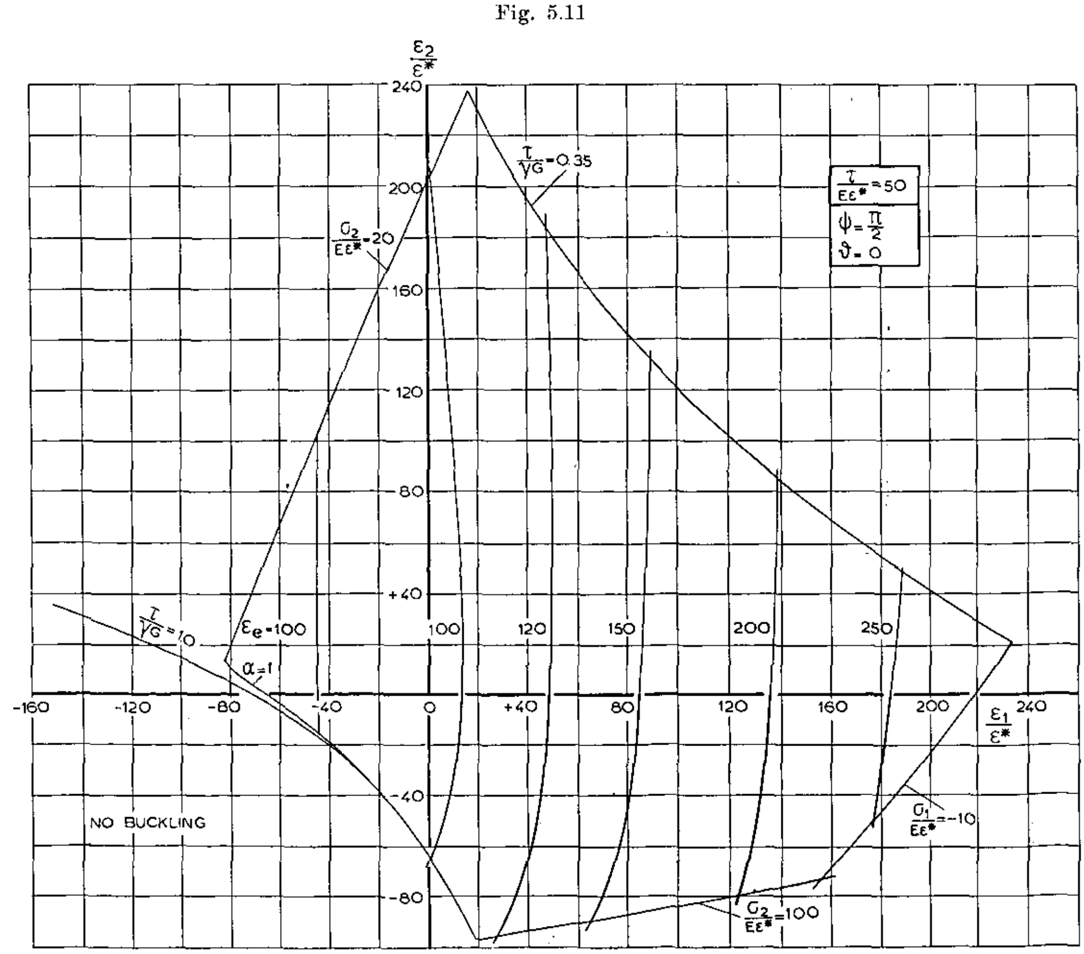

Fig. 5.12

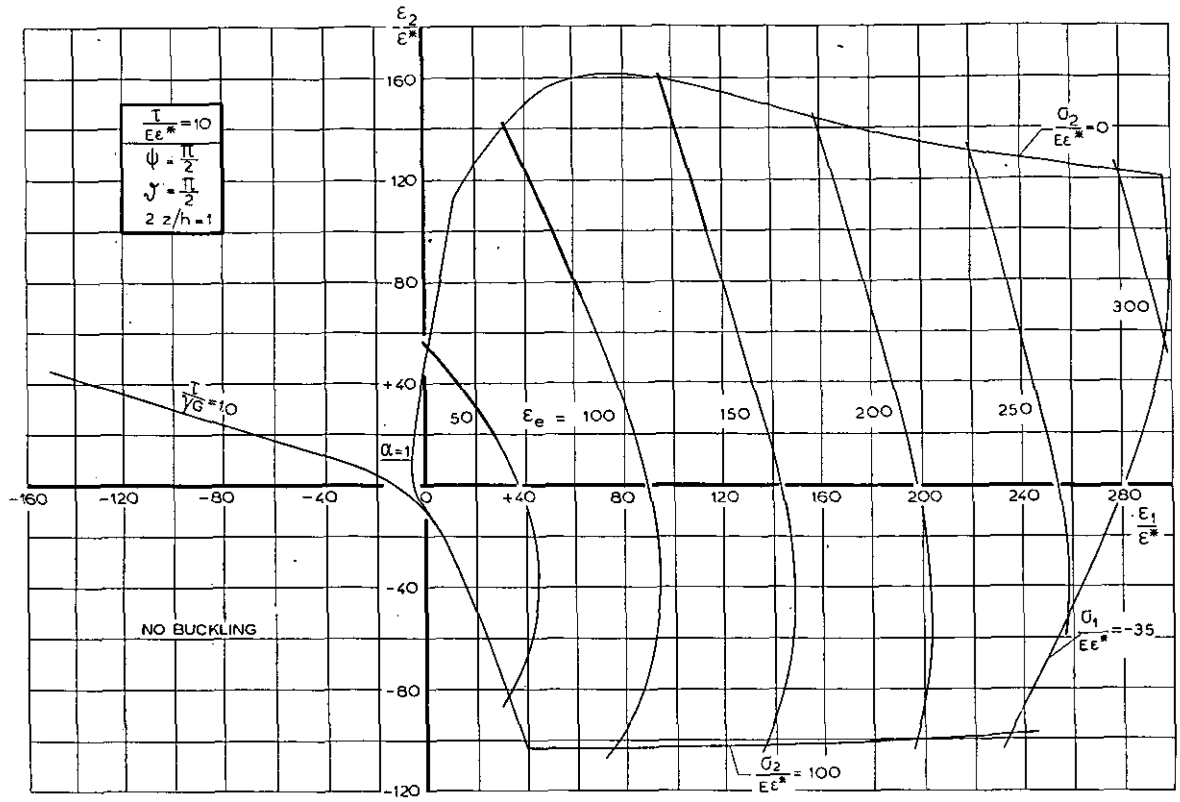

Fig. 5.13

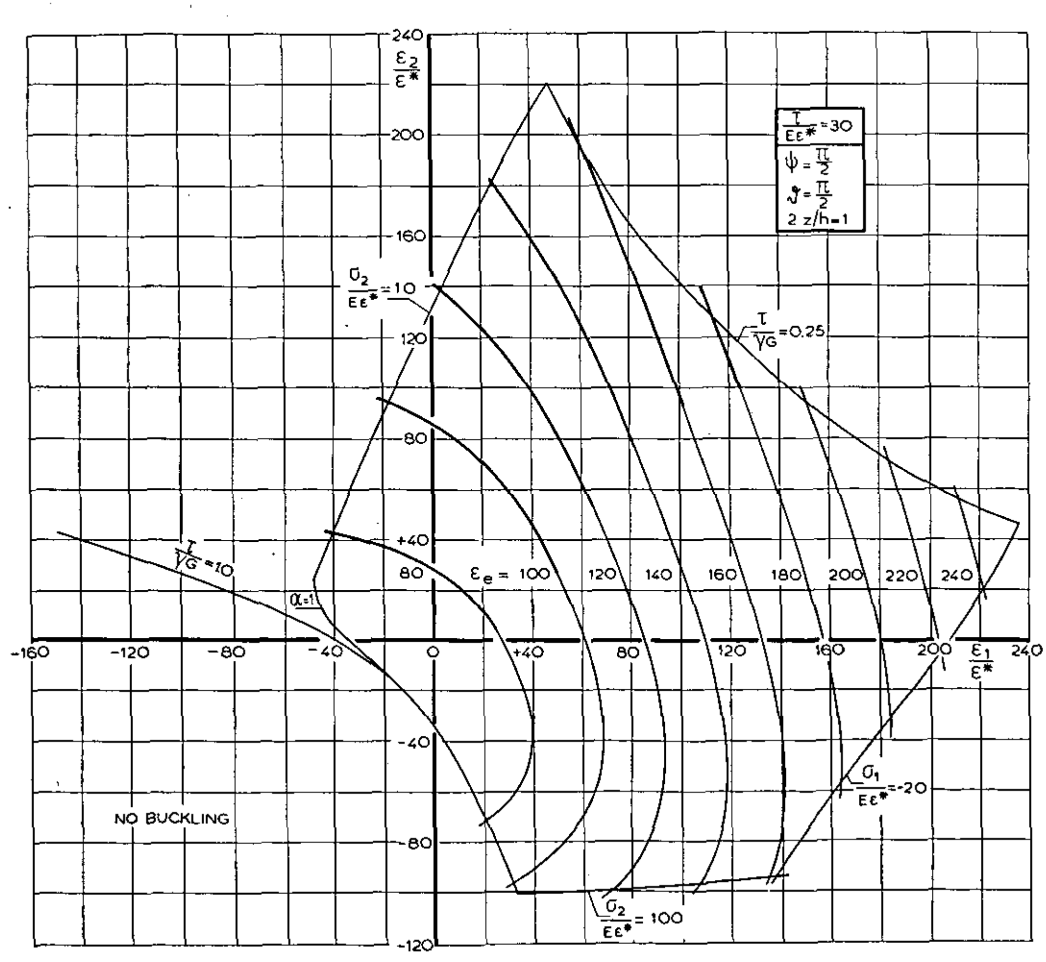

Fig. 5.14

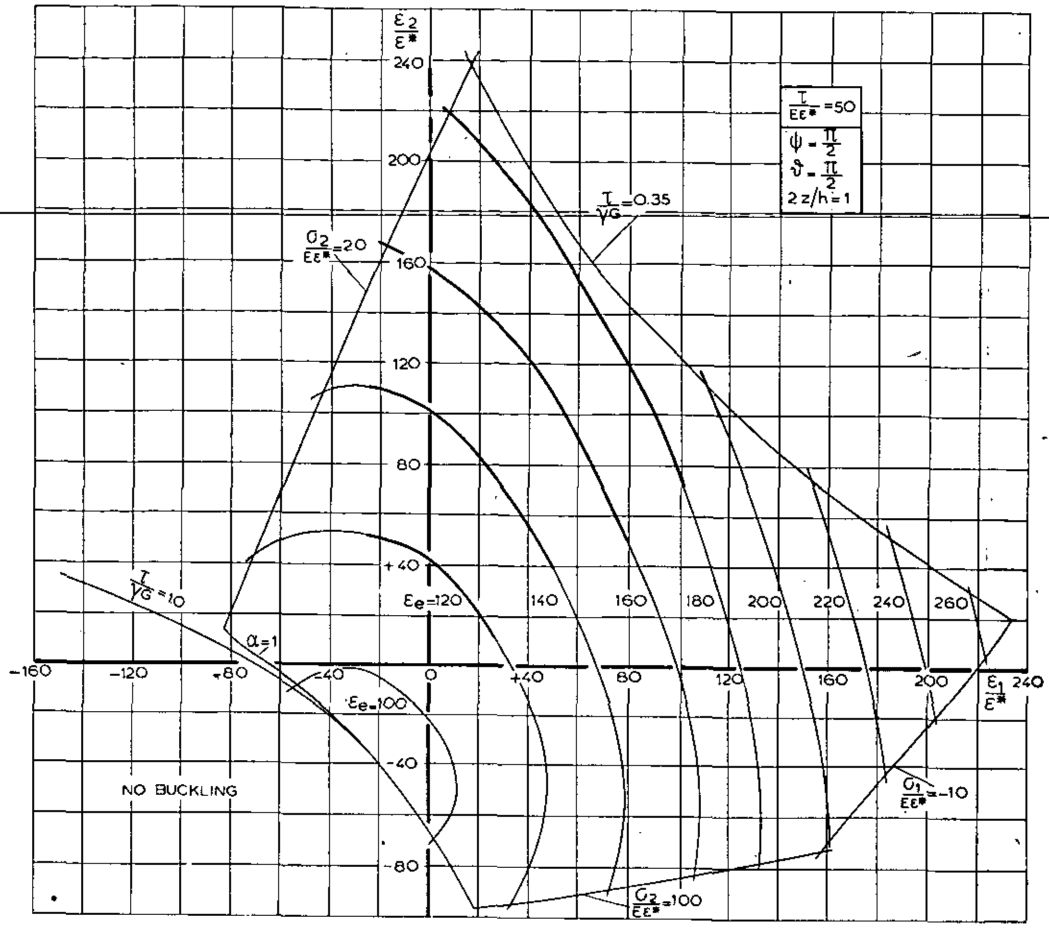

Fig. 5.15

It is observed that $\varepsilon_e/\varepsilon^*$ in this case may be critical only for small and moderate $\varepsilon_1/\varepsilon^*$ and $\varepsilon_2/\varepsilon^*$.

The differences between figs. 5.1 to 5.4 incl. and figs. 5.16 to 5.19 incl. are due to the discontinuity in ε_{yy} at $y = \alpha b/2$ (sec. 3.2). A comparison shows that they remain within reasonable limits, the general form of the curve being nearly identical in both cases.

The stress distribution in an actual construction does not show such discontinuities. Their presence in the results obtained from theory demonstrates that the approximation of the actual stress distribution by means of theory is not in general very accurate.

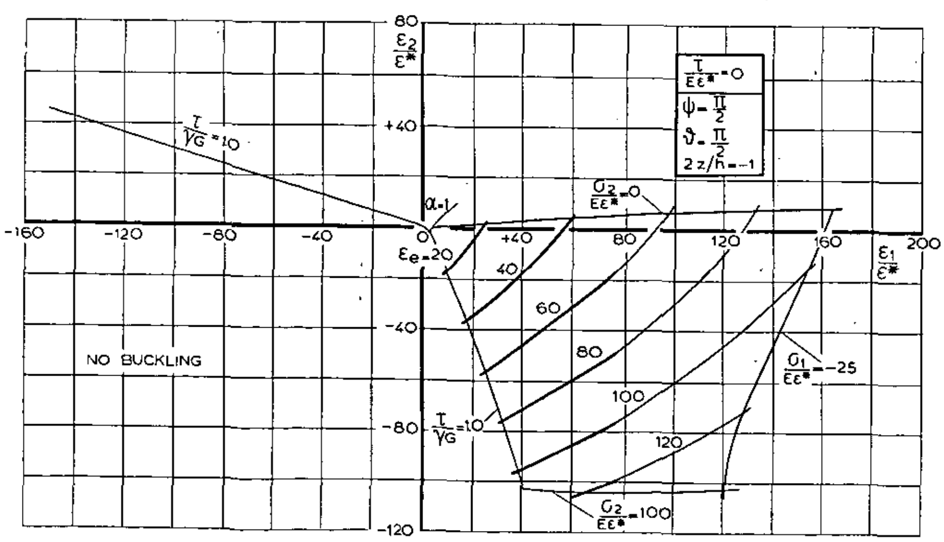

Fig. 5.16

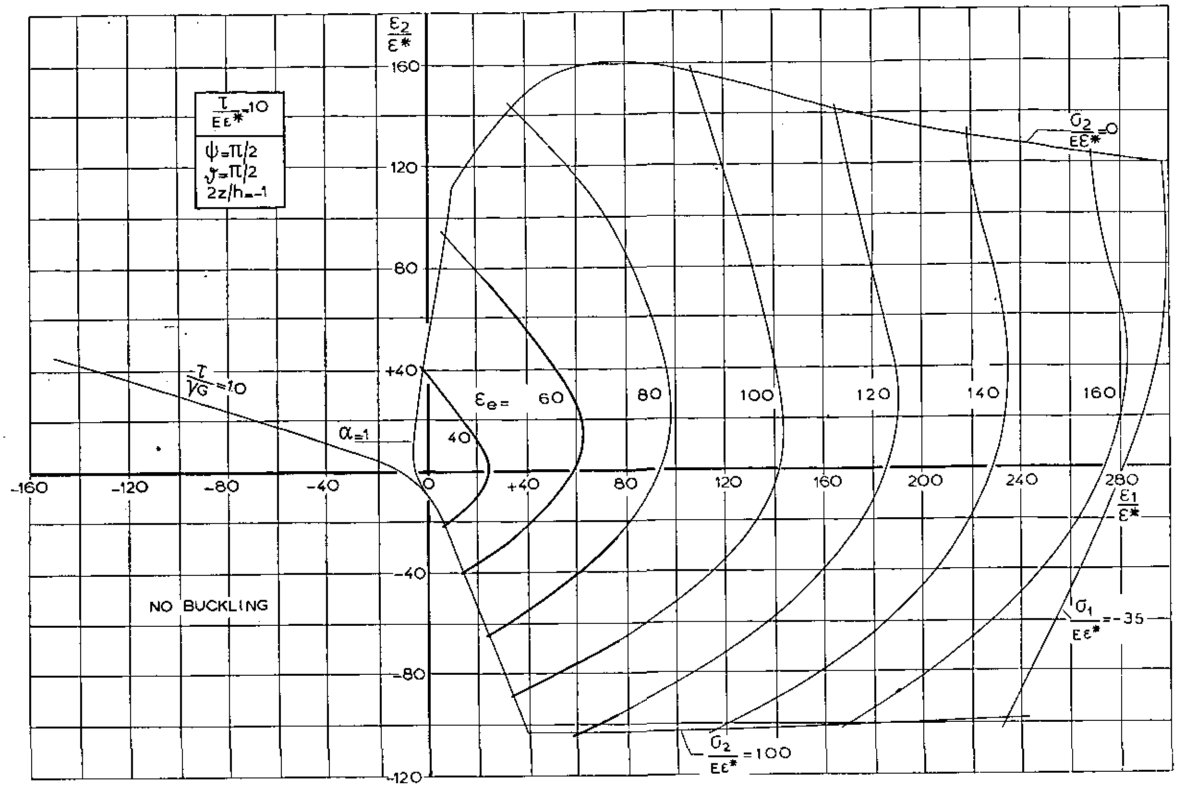

Fig. 5.17

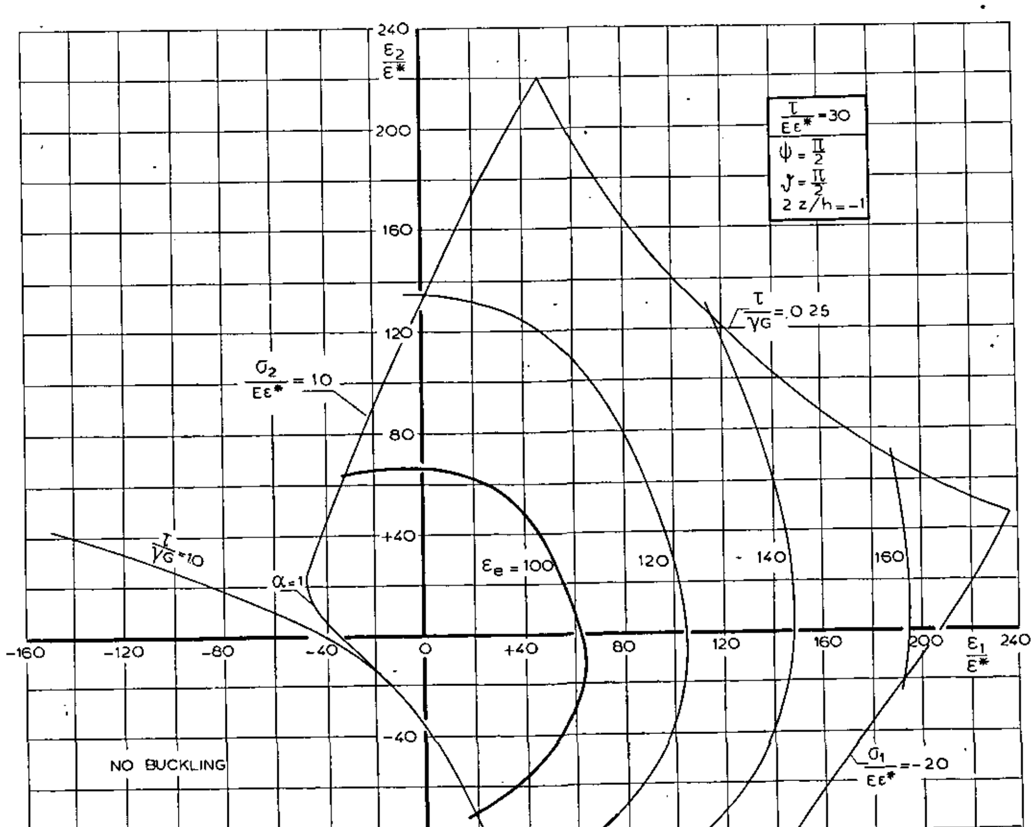

Fig. 5.18

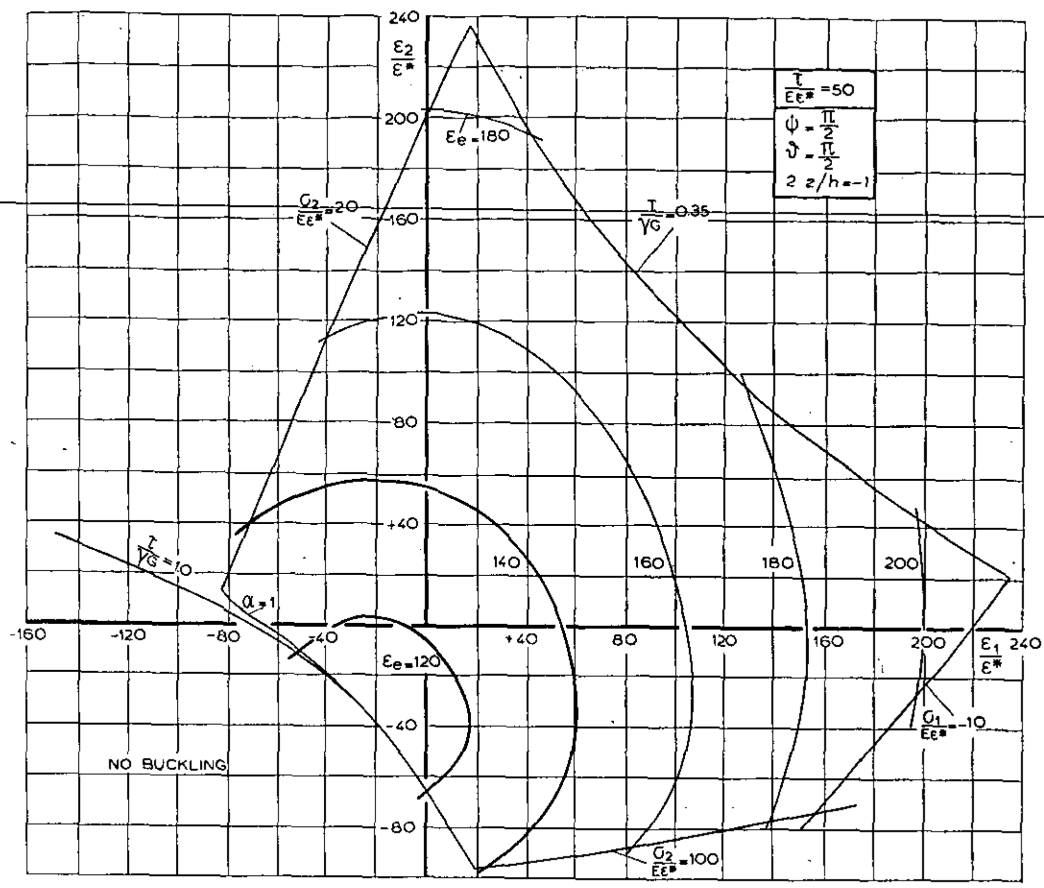

Fig. 5.19

6 Numerical examples.

To demonstrate the practical application of the diagrams figs. 5.1 to 5.19 incl. the effective strain is determined for the same constructions and loads considered as numerical examples in ref. 1. The effective strain ratios $\varepsilon_e/\varepsilon^*$ are presented as functions of the shear ratio $\tau/E\varepsilon^*$ for each of the stations shown in fig. 4.1 except those not covered by the diagrams because they are never critical throughout the range of the investigation (sec. 5.3).

The results for the first example are presented in table 6.1 and shown in fig. 6.1. The largest effective strain occurs at the intersections of the nodal line and the edge at the lower face of the plate.

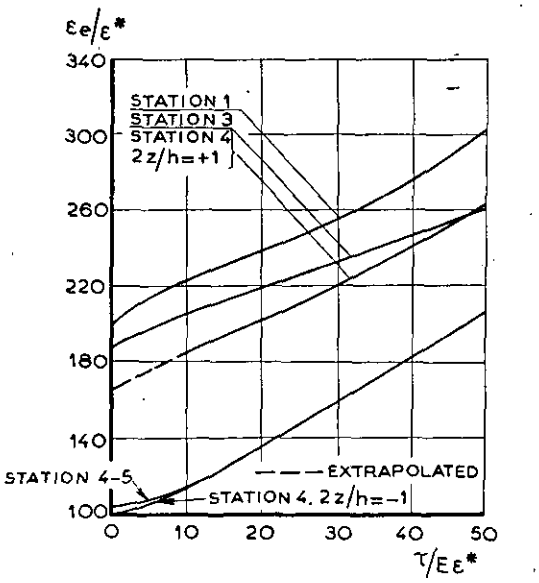

Fig. 6.1

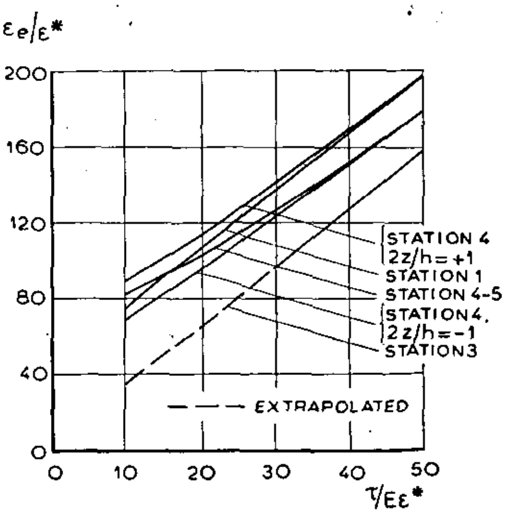

Fig. 6.2

The results for the second example are presented in table 6.2 and shown in fig. 6.2. The largest effective strain occurs in the edge region at the intersection of the crest line and the transition

TABLE 6.1.

Numerical results for the first example.

$\tau/E\varepsilon^*$	$\varepsilon_1/\varepsilon^*$	$\varepsilon_2/\varepsilon^*$		$\varepsilon_e/\varepsilon^*$				
			station [1]	4—5	1	3	4	4
			$2z/h$	—1	—1	—	1	—1
0	173	6		103	200	187	165 [3]	100
10	176	24		114	223	206	185	114
30	187	60.5		159	256	232	221	158
50	202	94		207 [2]	303 [2]	261 [2]	263 [2]	206 [2]

[1]) see fig. 4.1. [2]) extrapolated. [3]) see sec. 6.

TABLE 6.2.

Numerical results for the second example.

$\tau/E\varepsilon^*$	$\varepsilon_1/\varepsilon^*$	$\varepsilon_2/\varepsilon^*$		$\varepsilon_e/\varepsilon^*$				
			station [1]	4—5	1	3	4	4
			$2z/h$	—1	—1	—	1	—1
0	—	—		—	—	—	—	—
10	20	125		82	75	35 [2]	89	69
30	59	128.5		127	137	97	141	124
50	98	133		179	197	158	198	178

[1]) see fig. 4.1. [2]) extrapolated.

TABLE 6.3.

Numerical results for the third example.

$\tau/E\varepsilon^*$	$\varepsilon_1/\varepsilon^*$	$\varepsilon_2/\varepsilon^*$		$\varepsilon_e/\varepsilon^*$				
			station [1]	4—5	1	3	4	4
			$2z/h$	—1	—1	—	1	—1
0	100	4		64	119	115	103 [2]	62
10	100	19		78	134	118	114	81
30	100	52		123	160	137	147	123
50	100	80		169	189	161	182	169

[1]) see fig. 4.1. [2]) see sec. 6.

TABLE 6.4.

Numerical results for the fourth example.

$\tau/E\varepsilon^*$	$\varepsilon_1/\varepsilon^*$	$\varepsilon_2/\varepsilon^*$		$\varepsilon_e/\varepsilon^*$				
			station [1])	4—5	1	3	4	4
			$2z/h$	—1	—1	—	1	—1
0	—	—		—	—	—	—	—
10	12	100		71	64	28 [2])	75	60
30	38	100		116	114	80	120	113
50	61	100		163	160	128	164	162

[1]) see fig. 4.1. [2]) extrapolated.

TABLE 7.1.

Comparison between results obtained for waveform assumptions no. 1 and no. 2 from ref. 2.

Example	1	2	3	4	5	6
$\sigma_{11}/E\varepsilon^* = \sigma_{12}/E\varepsilon^*$	31.235	—24.522	—19.323	—34.889	41.406	7.7533
$\sigma_{21}/E\varepsilon^* = \sigma_{22}/E\varepsilon^*$	12.608	40.495	0.69824	10.230	12.557	4.0212
$\tau_1/E\varepsilon^* = \tau_2/E\varepsilon^*$	25.983	24.397	4.8417	4.7736	30.102	14.007
$\varepsilon_{11}/\varepsilon^*$	—24.035	229.01	118.37	273.35	—29.989	18.043
$\varepsilon_{12}/\varepsilon^*$	—22.629	227.92	117.88	273.20	—28.034	17.812
$\varepsilon_{21}/\varepsilon^*$	5.3018	6.0062	31.398	9.6251	24.294	62.386
$\varepsilon_{22}/\varepsilon^*$	8.9797	5.0237	28.585	9.0392	31.301	66.747
α_1	0.80373	0.25421	0.32283	0.21861	0.77747	0.70000
α_2	0.95773	0.24754	0.32368	0.21880	0.93383	0.80248
m_1	1.5788	0.43643	0.49054	0.18153	1.7943	1.57880
m_2	1.4548	0.42441	0.45152	0.17125	1.6707	1.5259
D_1	2.4480	23.357	11.966	26.508	2.1654	2.4480
D_2	2.4062	23.129	12.061	26.516	2.0858	2.1618
F_1/ε^*	2.3339	9.4340	9.8496	9.9679	5.7794	15.454
F_2/ε^*	3.8466	9.4911	9.7292	9.9617	8.6382	18.819

σ_{11}, σ_{21}, α_1 etc. means σ_1, σ_2, α etc. for waveform no. 1.

σ_{12}, σ_{22}, α_2 etc. means σ_1, σ_2, α etc. for waveform no. 2.

between the centre and edge regions at the upper face of the plate. At high loads it is nearly equal to the effective strain at the intersection of the nodal line and the edge at the lower face of the plate.

The results for the third example are presented

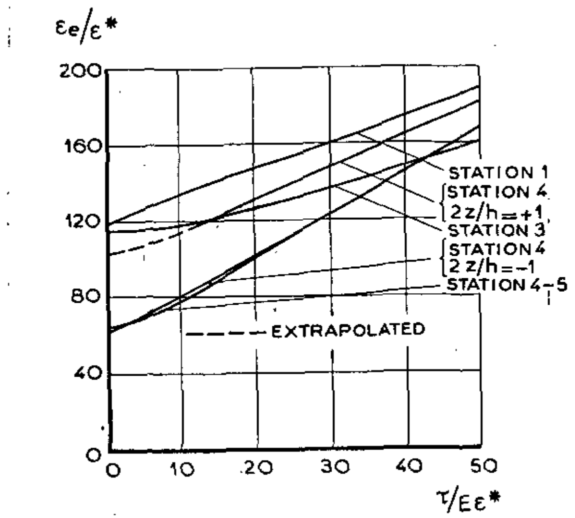

Fig. 6.3

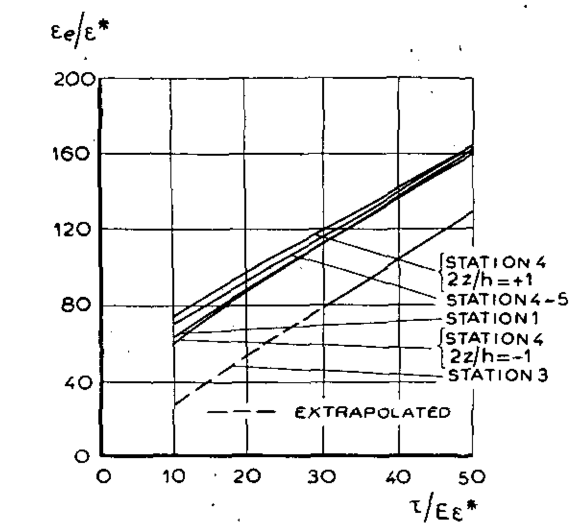

Fig. 6.4

in table 6.3 and shown in fig. 6.3. The largest effective strain occurs at the intersection of the nodal line and the edge at the lower face of the plate.

The results for the fourth example are presented in table 6.4 and shown in fig. 6.4. The largest effective strain occurs in the edge region at the intersection of the crest line and the transition between the centre and edge regions at the upper face of the plate. At high loads it is nearly equal to the effective strains at the same station and at the intersection between the nodal line and the edge both at the lower face of the plate.

In the first and third examples the effective strains at the intersection of the crest line and the transition between the centre and edges regions are practically identical in both regions. Small differences are observed only when $\tau/E\varepsilon^*$ is small. In the second and fourth examples the differences are more pronounced, especially when $\tau/E\varepsilon^*$ is small. No results could be obtained in these two cases for $\tau/E\varepsilon^* = 0$, and hence for $0 < \tau/E\varepsilon^* < 10$, the combinations of $\varepsilon_1/\varepsilon^*$ and $\varepsilon_2/\varepsilon^*$ falling outside the range covered by figs. 5.1, 5.5, 5.9 and fig. 5.16.

It appears from all diagrams that the effective strains for intermediate values of $\tau/E\varepsilon^*$ can be determined with good accuracy by interpolation. The restriction of the numerical evaluation to four values of $\tau/E\varepsilon^*$ only (sec. 5.1) is thus justified.

The effective strain at the proportionality limit, $\varepsilon = \varepsilon_p$, is derived from the tensile stress-strain curve for the plate material (sec. 5.1) and ε^* is calculated from (3.2). Figs. 6.1 to 6.4 yield the corresponding $\tau/E\varepsilon^*$, and hence the shear stress τ_p. The diagrams from ref. 1, figs. 5.1 to 5.19 incl. and hence also figs. 6.1 to 6.4 incl. cannot be expected to yield reliable results when τ exceeds τ_p (sec. 1, 5.1).

7 Investigation of improved waveform assumptions for the buckles in the plate.

It was suggested in ref. 1 that more reliable results would probably be obtained for combinations of $\tau/E\varepsilon^*$, $\varepsilon_1/\varepsilon^*$ and $\varepsilon_2/\varepsilon^*$ for which the angle between the direction of the nodal lines in the centre region of the plate and the X-axis (fig. 3.1) is much smaller than $\pi/4$, i. e. $m > 2$, by basing the calculation upon waveform assumption nr. 2 from ref. 2 instead of upon waveform assumption nr. 1.

For waveform assumption nr. 2 the nodal lines in the edge regions of the buckled plate intersect the edges orthogonally, in accordance with the assumption that the edges of the plate are hinged.

The nodal lines are curved in the edge regions and straight in the centre region of the plate. Their curvature changes discontinuously but their slope continuously at the transitions between the centre and the edge regions.

Determination of $\varepsilon_1/\varepsilon^*$, $\varepsilon_2/\varepsilon^*$ and $\tau/G\gamma$ for specified $\sigma_1/E\varepsilon^*$, $\sigma_2/E\varepsilon^*$ and $\tau/E\varepsilon^*$ and waveform assumption nr. 2 would require lengthy calculations and interpolations. Instead, the parameters α, m and D for waveform assumption nr. 1 were determined for specified $\sigma_1/E\varepsilon^*$, $\sigma_2/E\varepsilon^*$ and $\tau/E\varepsilon^*$.

Substituting these values, $\alpha_2 = \alpha$, $m_2 = m$ and $D_2 = D$ for the parameters in the adequate expressions derived for waveform assumption nr. 2 yielded a set of corresponding $\sigma_{12}/E\varepsilon^*$, $\sigma_{22}/E\varepsilon^*$, $\tau_2/E\varepsilon^*$, $\varepsilon_{12}/\varepsilon^*$, $\varepsilon_{22}/\varepsilon^*$ and also F_2/ε^*. The suffix 2 denotes that this set constitutes a solution valid for waveform assumption nr. 2.

Finally, assuming $\sigma_{11} = \sigma_{12}$, $\sigma_{21} = \sigma_{22}$, $\tau_1 = \tau_2$, the corresponding $\varepsilon_{11}/\varepsilon^*$ and $\varepsilon_{21}/\varepsilon^*$ as well as α_1, m_1, D_1 and F_1/ε^* are determined from the theory based upon waveform assumption nr. 1. The suffix 1 denotes that this set constitutes a solution valid for waveform assumption nr. 1.

The results of the calculations are presented in table 7.1. It is convenient to compare the results for both waveform assumptions, as far as ε_1 and ε_2 are concerned, in the diagrams presented in ref. 1

for $\tau/E\varepsilon^* = 25$ (examples 1 and 2), 5 (examples 3 and 4), 30 (example 5) and 15 (example 6), although the actual values $\tau/E\varepsilon^*$ are slightly different.

It is observed that the points $(\varepsilon_{11}/\varepsilon^*, \varepsilon_{21}/\varepsilon^*)$ and $(\varepsilon_{12}/\varepsilon^*, \varepsilon_{22}/\varepsilon^*)$ in the diagrams lie close together for examples 2 and 3 and very close for example 4, because m is small.

Their distance is slightly larger but yet reasonably small for examples 1, 5 and 6 where m is large. This is shown in fig. 7.1 for example 5,

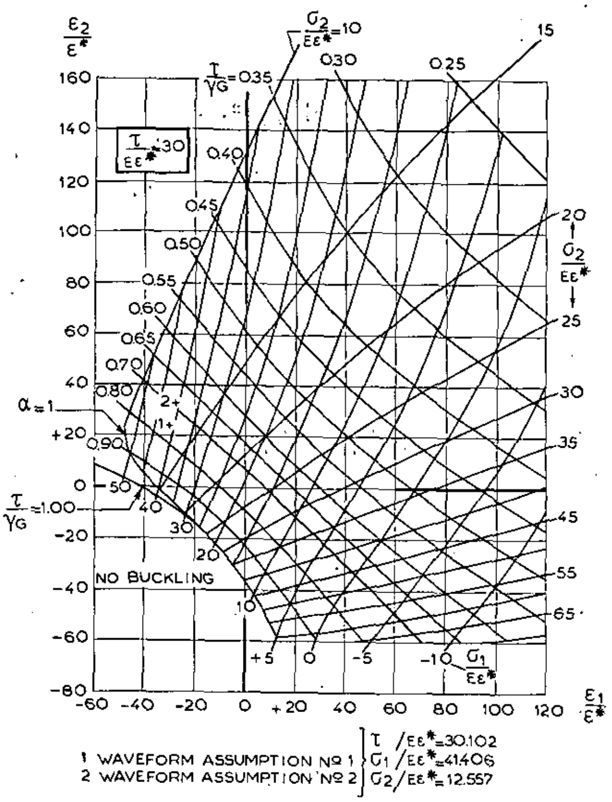

Fig. 7.1

where the differences in $\varepsilon_1/\varepsilon^*$ and $\varepsilon_2/\varepsilon^*$ are most pronounced.

The line connecting the points 1 and 2 in this figure represents the direction in which and the distance over which the intersections of the curves of constant $\sigma_1/E\varepsilon^*$ and $\sigma_2/E\varepsilon^*$ in the neighbourhood of point 1 have to be displaced when changing over from waveform nr. 1 to waveform nr. 2.

It can be concluded from the results gained for these examples that the improvements obtainable by basing the diagrams from ref. 1 upon waveform nr. 2 from ref. 2 instead of upon waveform nr. 1 are so small that it is fully justified to use the diagrams in their present form in all practical applications.

It is interesting to note that for example 1 the amplitude for waveform nr. 1 is only 78 % from the amplitude for waveform 2. In the other examples the differences are smaller. In example 6 the wavelength for waveform nr. 1 is 94 % from the wavelength for waveform nr. 2. In the other examples the differences are smaller. It is further noted from table 7.1 that the angle between the X-axis and the direction of the nodal lines in the centre region of the plate is slightly larger for waveform nr. 2 than for waveform nr. 1. In those cases where the differences between $\varepsilon_1/\varepsilon^*$, $\varepsilon_2/\varepsilon^*$ for both waveforms are most pronounced α is markedly larger for waveform nr. 2 than for nr. 1. In the remaining cases, however, the differences in α are very small.

8 Conclusions.

8.1 *The effective strain in the buckled plate.*

For the buckled plate shown in fig. 3.1 and loaded and strained according to fig. 3.2 the effective strain has been determined at the stations shown in fig. 4.1. The results of these calculations are presented in the form of the diagrams figs. 5.1 to 5.19 incl. These diagrams contain a set of curves for which the ratio between the effective strain ε_e after the criterion of HUBER, VON MISES and HENCKY and the critical strain ε^* defined by (3.2) is a constant. The diagrams should be used in conjunction with those published in ref. 1. Their practical application is demonstrated in sec. 6, tab. 6.1 to 6.4 incl. and figs. 6.1 to 6.4 incl.

For the present diagrams, as for those from ref. 1, waveform assumption nr. 1 from ref. 2, defined in Appendix A of ref. 1, was chosen. Expressions for the distributions of the local strains (sec. 3.2, 3.3 and 3.4) are presented in Appendix A and B.

The expression for the distribution of the effective strain (sec. 4.1) throughout the plate is presented in Appendix C.

8.2 *The maximum of the effective strain.*

It is proposed to consider as the maximum effective strain for specified $\varepsilon_1/\varepsilon^*$, $\varepsilon_2/\varepsilon^*$ and $\tau/E\varepsilon^*$ the largest effective strain ε_e obtained by reading or interpolation of the appropriate diagrams from figs. 5.1 to 5.19 incl. This infers that only the effective strains at the stations shown in fig. 4.1 have been considered.

Numerical evaluations have shown that for large $\sigma_2/E\varepsilon^*$ together with negative or, only for large $\tau/E\varepsilon^*$, small positive $\sigma_1/E\varepsilon^*$ (ref. 1, figs. 2.2, 2.3 and 2.4) the effective strain will have a maximum at some station in the parallelogram 1-2-3-4 from fig. 4.1 that exceeds the largest effective strain determined from the diagrams.

The conditions for an extremum of the effective strain (sec. 4.2) are derived in Appendix D. Excluding the stations 1 and 4 from fig. 4.1 for which it is obvious that (D.1) and (D.2) are satisfied the solution of these complicated equations for ψ and ϑ is rather laborious (sec. 4.4). Along the sides of the parallelogram either ψ or ϑ is a constant and a solution of the one remaining equation is readily obtained. Results of such calculations are shown qualitatively in figs. 4.2 to 4.5 incl. and numerical results are presented in tables 4.1 and 4.2.

It is observed that the largest effective strain anywhere along the sides of the parallelogram never exceeds the largest strain in the corners, i. e. according to figs. 5.1 to 5.19 incl., by more than 2.6 % (sec. 4.4). It is to be expected that the largest effective strain anywhere inside the parallelogram will exceed the largest strain along the sides only to a small extent.

In view of this and also in accordance with the fact that the stress distribution in the buckled plate is not approximated with the same degree of accuracy as the elastic energy (sec. 5.1) it is considered justified to restrict the numerical evaluation to those cases considered in the construction of figs. 5.1 to 5.19 incl.

Another argument in favour of this simplification is that, for the determination whether the diagrams from ref. 1 can yet be applied, the effective strain should be compared with the tensile strain at the proportionality limit, which is not known with great accuracy. The deviations from the diagrams as the proportionality limit is exceeded to a slight extent will also be rather small (sec. 5.1).

8.3 *Improved waveform assumptions for the buckled plate.*

For some combinations of specified $\sigma_1/E\varepsilon^*$, $\sigma_2/E\varepsilon^*$ and $\tau/E\varepsilon^*$ the strain ratios $\varepsilon_1/\varepsilon^*$ and $\varepsilon_2/\varepsilon^*$ have been determined for both waveform assumptions nr. 1 and nr. 2 from ref. 1 (sec. 7). The second assumption is considered more adequate than the first one in computing diagrams of the type presented in ref. 1, because the nodal lines of the buckles, according to this assumption, intersect the longitudinal edges of the plate perpendicularly.

Results of the calculations are presented in table 7.1. For the example in which the largest differences were observed they are also shown in fig. 7.1. It appears that the correction of the diagrams from ref. 1, required when substituting waveform nr. 2 for nr. 1, consists in principle of shifting the curves of constant $\sigma_1/E\varepsilon^*$ and $\sigma_2/E\varepsilon^*$ over a small distance. The correction is practically negligible except in the neighbourhood of the curve $\alpha = 1$ for positive $\varepsilon_2/\varepsilon^*$, where m approaches or exceeds 2. Even in these parts of the diagrams the corrections remain relatively small.

The diagrams from ref. 1 can thus be considered sufficiently reliable throughout the full range covered by them.

9 References.

1. Floor, W. K. G., Burgerhout, T. J. Evaluation of the Theory on the Post-Buckling Behaviour of Stiffened, Flat, Rectangular Plates Subjected to Shear- and Normal Loads. Report S. 370, National Luchtvaartlaboratorium, Amsterdam, 1952.
2. Koiter, W. T. Het schuifplooiveld bij groote overschrijdingen van de knikspanning. Rapport S 295, Nationaal Luchtvaartlaboratorium, Amsterdam, 1944. With an English abstract: Theoretical Investigation of the Diagonal Tension Field of Flat Plates. Amsterdam, 1946.
3. Nadaï, A., Wahl, A. M. Plasticity. Mc Graw-Hill Book Co Inc. New York, 1931.

Completed: July 1953.

APPENDIX A.

Expressions for the local strains in the median plane of the plate.

Substituting (A. 1) from ref. 1, (3.2) and (3.3) in (3.1) the following expressions for the tensile strains $\bar{\varepsilon}_{xx}$ and $\bar{\varepsilon}_{yy}$ in the longitudinal (X-) and lateral (Y-) directions respectively and the shear strain $\bar{\gamma}_{xy}$ in the median plane ($z = 0$) of the plate are obtained, valid in the edge regions, i. e. for $0 \leqslant y \leqslant \alpha b/2$.

$$\left.\begin{aligned}
\bar{\varepsilon}_{xx}/\varepsilon^* &= -\varepsilon_1/\varepsilon^* + (1-\cos^2\vartheta)DF/\varepsilon^*,\\
\bar{\varepsilon}_{yy}/\varepsilon^* &= -\varepsilon_2/\varepsilon^* + [\tfrac{1}{2}\,\alpha + \tfrac{1}{2}\,\alpha^2 -\\
&\quad -0.5\,\nu\alpha D + 0.5(2-\alpha)m^2D]F/\varepsilon^* +\\
&\quad + \nu D(F/\varepsilon^*)\cos^2\vartheta - (1/\alpha^2)(F/\varepsilon^*)\cos^2\psi,\\
\bar{\gamma}_{xy}/\varepsilon^* &= 2(1+\nu)\tau/E\varepsilon^*.
\end{aligned}\right\} \quad (\text{A. }1)$$

At the edge $y = 0$ these expressions can be simplified to the set

$$\left.\begin{aligned}
\bar{\varepsilon}_{xx}/\varepsilon^* &= -\varepsilon_1/\varepsilon^*,\\
\bar{\varepsilon}_{yy}/\varepsilon^* &= -\varepsilon_2/\varepsilon^* + [\tfrac{1}{2}\,\alpha + \tfrac{1}{2}\,\alpha^2 -\\
&\quad -(1/\alpha^2)\cos^2\psi + 0.5\,(2-\alpha)\\
&\quad (\nu + m^2)D]F/\varepsilon^*,\\
\bar{\gamma}_{xy}/\varepsilon^* &= 2(1+\nu)\tau/E\varepsilon^*.
\end{aligned}\right\} \quad (\text{A. }2)$$

At the transition to the central region, $y = \alpha b/2$, they can be simplified to

$$\left.\begin{aligned}
\bar{\varepsilon}_{xx}/\varepsilon^* &= -\varepsilon_1/\varepsilon^* + DF/\varepsilon^*,\\
\bar{\varepsilon}_{yy}/\varepsilon^* &= -\varepsilon_2/\varepsilon^* + [\tfrac{1}{2}\,\alpha + \tfrac{1}{2}\,\alpha^2 -\\
&\quad -(1/\alpha^2)\cos^2\psi - 0.5\,\nu\alpha D +\\
&\quad + 0.5\,(2-\alpha)m^2D]F/\varepsilon^*,\\
\bar{\gamma}_{xy}/\varepsilon^* &= 2(1+\nu)\tau/E\varepsilon^*.
\end{aligned}\right\} \quad (\text{A. }3)$$

Substituting (A. 2) from ref. 1, (3.2) and (3.3) in (3.1) the following expressions for the strains $\bar{\varepsilon}_{xx}$, $\bar{\varepsilon}_{yy}$ and $\bar{\gamma}_{xy}$ in the median plane ($z = 0$) of the plate are obtained, valid in the centre region, i. e. for $\alpha b/2 \leqslant y \leqslant (1-\alpha/2)b$.

$$\left.\begin{aligned}
\bar{\varepsilon}_{xx}/\varepsilon^* &= -\varepsilon_1/\varepsilon^* + DF/\varepsilon^*,\\
\bar{\varepsilon}_{yy}/\varepsilon^* &= -\varepsilon_2/\varepsilon^* + [\tfrac{1}{2}\,\alpha - 0.5\,\nu\alpha D +\\
&\quad + 0.5\,(2-\alpha)m^2D]F/\varepsilon^*,\\
\bar{\gamma}_{xy}/\varepsilon^* &= 2\,(1+\nu)\tau/E\varepsilon^*.
\end{aligned}\right\} \quad (\text{A. }4)$$

APPENDIX B.

Expressions for the local bending strains at the upper face ($z = h/2$) of the buckled plate.

Substituting (A. 1) from ref. 1, (3.2) and 3.3) in (3.4) the following expressions for the tensile strains $\bar{\bar{\varepsilon}}'_{xx}$ in the X- and $\bar{\bar{\varepsilon}}'_{yy}$ in the Y-directions and the shear strain $\bar{\bar{\gamma}}'_{xy}$ in the upper face of the plate, $z = h/2$, are obtained, valid in the edge regions, i. e. for $0 \leqslant y \leqslant \alpha b/2$.

$$\left.\begin{aligned}
\bar{\bar{\varepsilon}}'_{xx}/\varepsilon^* &= D\sqrt{3(1-\nu^2)F/\varepsilon^*}\ \sin\psi\sin\vartheta,\\
\bar{\bar{\varepsilon}}'_{yy}/\varepsilon^* &= (m^2D + 1/\alpha^2)\sqrt{3(1-\nu^2)F/\varepsilon^*}\\
&\qquad \sin\psi\sin\vartheta +\\
&+ (2\,m/\alpha)\sqrt{3(1-\nu^2)DF/\varepsilon^*}\cos\psi\cos\vartheta,\\
\bar{\bar{\gamma}}'_{xy}/\varepsilon^* &= -2\,mD\sqrt{3(1-\nu^2)F/\varepsilon^*}\\
&\qquad \sin\psi\sin\vartheta -\\
&- (2/\alpha)\sqrt{3(1-\nu^2)DF/\varepsilon^*}\ \cos\psi\cos\vartheta.
\end{aligned}\right\}\quad (B.\,1)$$

At the edge $y = 0$ these expressions can be simplified to the set

$$\left.\begin{aligned}
\bar{\bar{\varepsilon}}'_{xx}/\varepsilon^* &= 0,\\
\bar{\bar{\varepsilon}}'_{yy}/\varepsilon^* &= (2\,m/\alpha)\sqrt{3(1-\nu^2)DF/\varepsilon^*}\ \cos\psi,\\
\bar{\bar{\gamma}}'_{xy}/\varepsilon^* &= -(2/\alpha)\sqrt{3(1-\nu^2)DF/\varepsilon^*}\cos\psi.
\end{aligned}\right\}\quad (B.\,2)$$

At the transition to the central region, $y = \alpha b/2$, they can be simplified to

$$\left.\begin{aligned}
\bar{\bar{\varepsilon}}'_{xx}/\varepsilon^* &= D\sqrt{3(1-\nu^2)F/\varepsilon^*}\sin\psi,\\
\bar{\bar{\varepsilon}}'_{yy}/\varepsilon^* &= (m^2D + 1/\alpha^2)\sqrt{3(1-\nu^2)F/\varepsilon^*}\\
&\qquad \sin\psi,\\
\bar{\bar{\gamma}}'_{xy}/\varepsilon^* &= -2\,mD\sqrt{3(1-\nu^2)F/\varepsilon^*}\ \sin\psi.
\end{aligned}\right\}\quad (B.\,3)$$

Substituting (A. 2) from ref. 1, (3.2) and (3.3) in (3.4) the following expressions for the strains $\bar{\bar{\varepsilon}}'_{xx}$, $\bar{\bar{\varepsilon}}'_{yy}$ and $\bar{\bar{\gamma}}'_{xy}$ in the upper face ($z = h/2$) of the plate are obtained, valid in the centre region, i. e. for $\alpha b/2 \leqslant y \leqslant (1-\alpha/2)b$.

$$\left.\begin{aligned}
\bar{\bar{\varepsilon}}'_{xx}/\varepsilon^* &= D\sqrt{3(1-\nu^2)F/\varepsilon^*}\ \sin\psi,\\
\bar{\bar{\varepsilon}}'_{yy}/\varepsilon^* &= m^2D\sqrt{3(1-\nu^2)F/\varepsilon^*}\ \sin\psi,\\
\bar{\bar{\gamma}}'_{xy}/\varepsilon^* &= -2\,mD\sqrt{3(1-\nu^2)F/\varepsilon^*}\ \sin\psi.
\end{aligned}\right\}\quad (B.\,4)$$

APPENDIX C.

The expression for the effective strain.

Substituting (3.6) or (3.7), (A. 1) and (B. 1) in (4.2) the following expression for $\Phi = 0.8281(\varepsilon_e/\varepsilon^*)^2$ is obtained for the edge regions $0 \leqslant y \leqslant \alpha b/2$.

$$\begin{aligned}
\Phi = {} & (A_0 - A_1\cos^2\psi + A_2\cos^4\psi) \pm\\
& \pm (B_0 - B_1\cos^2\psi)\sin\psi\sin\vartheta +\\
& + C_0\sin^2\psi\sin^2\vartheta \pm (D_0 - D_1\cos^2\psi)\cos\psi\cos\vartheta +\\
& + (E_0 + E_1\cos^2\psi)\cos^2\vartheta \pm F_0\cos\psi\cos^3\vartheta +\\
& + G_0\cos^4\vartheta + H_0\sin\psi\cos\psi\sin\vartheta\cos\vartheta \pm\\
& \pm K_0\sin\psi\sin\vartheta\cos^2\vartheta.
\end{aligned}\qquad (C.\,1)$$

The upper signs are valid for the upper surface of the plate, i. e. for $2\,z/h = 1$, and the lower signs for the lower surface, i. e. for $2\,z/h = -1$.

The constants in (C. 1) are defined as follows:

$$\left.\begin{aligned}
A_0 &= 0.79\ (a_x^2 + a_y^2) + 0.11\,a_x a_y +\\
&\quad + 0.3675\,a^2,\\
A_1 &= (0.11\,a_x + 1.58\,a_y)c_y,\\
A_2 &= 0.79\,c_y^2,\\
B_0 &= 1.58\ (a_x d_x + a_y d_y) +\\
&\quad + 0.11\ (a_x d_y + a_y d_x) - 0.735\,ad,\\
B_1 &= (0.11\,d_x + 1.58\,d_y)c_y,\\
C_0 &= 0.79\ (d_x^2 + d_y^2) + 0.11\,d_x d_y + 0.3675\,d^2,\\
D_0 &= (0.11\,a_x + 1.58\,a_y)e_y - 0.735\,a\,e,\\
D_1 &= 1.58\,c_y e_y,\\
E_0 &= -1.58\ (a_x b_x - a_y b_y) +\\
&\quad + 0.11\ (a_x b_y - a_y b_x),\\
E_1 &= 0.79\ (e_y^2 - 2\,b_y c_y) +\\
&\quad + 0.11\,b_x c_y + 0.3675\,e^2,\\
F_0 &= -(0.11\,b_x - 1.58\,b_y)e_y,\\
G_0 &= 0.79\ (b_x^2 + b_y^2) - 0.11\,b_x b_y,\\
H_0 &= (0.11\,d_x + 1.58\,d_y)e_y + 0.735\,d\,e,\\
K_0 &= -1.58\ (b_x d_x - b_y d_y) -\\
&\quad - 0.11\ (b_x d_y - b_y d_x).
\end{aligned}\right\}\quad (C.\,2)$$

A_0, A_2, B_1, C_0, D_1, G_0 and H_0 are never negative.

The constants in (C. 2) are expressed by

$$\left.\begin{aligned}
a_x &= -\varepsilon_1/\varepsilon^* + DF/\varepsilon^*,\\
a_y &= -\varepsilon_2/\varepsilon^* + [1/2\,\alpha + 1/2\,\alpha^2 - 0.5\,\nu\alpha D +\\
&\quad + 0.5\ (2-\alpha)m^2D]F/\varepsilon^*,\\
a &= 2\ (1+\nu)\tau/E\varepsilon^*,\\
b_x &= DF/\varepsilon^*,\\
b_y &= \nu DF/\varepsilon^*,\\
c_y &= (1/\alpha^2)F/\varepsilon^*,\\
d_x &= D\sqrt{3(1-\nu^2)F/\varepsilon^*},\\
d_y &= (m^2D + 1/\alpha^2)\sqrt{3(1-\nu^2)F/\varepsilon^*},\\
d &= 2\,mD\sqrt{3(1-\nu^2)F/\varepsilon^*},\\
e_y &= (2\,m/\alpha)\sqrt{3(1-\nu^2)D\,F/\varepsilon^*},\\
e &= (2/\alpha)\sqrt{3(1-\nu^2)D\,F/\varepsilon^*}.
\end{aligned}\right\}\quad (C.\,3)$$

In these formulas $\nu = 0.3$ should be substituted (sec. 4.1); except for a_x and a_y they are never negative.

Substituting (3.6) or (3.7), (A. 4) and (B. 4) in (4.2), the following expression for Φ is obtained, valid in the centre region $\alpha b/2 \leqslant y \leqslant (1-\alpha/2)b$.

$$\Phi = \overline{A}_0 \pm \overline{B}_0 \sin\psi + \overline{C}_0 \sin^2\psi. \qquad \text{(C. 4)}$$

The upper sign is valid for $2z/h = 1$, the lower sign for $2z/h = -1$.

The constants in (C. 4) are defined as follows:

$$\left.\begin{aligned} \overline{A}_0 &= 0.79\,(a_x^2 + \overline{a}_y^2) + 0.11\,a_x\overline{a}_y + \\ &\quad + 0.3675\,a^2, \\ \overline{B}_0 &= 1.58\,(a_x d_x + \overline{a}_y\overline{d}_y) + 0.11\,(a_x\overline{d}_y + \\ &\quad + \overline{a}_y d_x) - 0.735\,ad, \\ \overline{C}_0 &= 0.79\,(d_x^2 + \overline{d}_y^2) + 0.11\,d_x\overline{d}_y + \\ &\quad + 0.3675\,d^2. \end{aligned}\right\} \qquad \text{(C. 5)}$$

The constants in (C.5) are expressed by (C.3) and by

$$\left.\begin{aligned} \overline{a}_y &= -\varepsilon_2/\varepsilon^* + [\tfrac{1}{2}\,_x - 0.5\,\nu\alpha D + \\ &\quad + 0.5\,(2-\alpha)m^2 D]F/\varepsilon, \\ \overline{d}_y &= m^2 D\sqrt{3\,(1-\nu^2)}F/\varepsilon^*, \end{aligned}\right\} \qquad \text{(C. 6)}$$

where $\nu = 0.3$. In (C. 6), $\overline{a}_y$ may be negative or positive, $\overline{d}_y$ is never negative.

APPENDIX D.

The extremum conditions for the effective strain.

Substituting (C. 1) in (4.3) the following equations are obtained, from which the quantities ψ and ϑ should be solved for the edge regions $0 \leqslant y \leqslant \alpha b/2$.

$$\begin{aligned} &2(A_1 - 2A_2\cos^2\psi)\sin\psi\cos\psi \pm \\ &\pm(B_0 - B_1\cos^2\psi + 2B_1\sin^2\psi)\cos\psi\sin\vartheta + \\ &+2C_0\sin\psi\cos\psi\sin^2\vartheta \mp \\ &\mp(D_0 - 3D_1\cos^2\psi)\sin\psi\cos\vartheta - \\ &-2E_1\sin\psi\cos\psi\cos^2\vartheta \mp F_0\sin\psi\cos^3\vartheta + \\ &+H_0(\cos^2\psi - \sin^2\psi)\sin\vartheta\cos\vartheta \pm \\ &\pm K_0\cos\psi\sin\vartheta\cos^2\vartheta = 0. \end{aligned} \qquad \text{(D. 1)}$$

$$\begin{aligned} &\pm(B_0 - B_1\cos^2\psi)\sin\psi\cos\vartheta + \\ &+2C_0\sin^2\psi\sin\vartheta\cos\vartheta \mp \\ &\mp(D_0 - D_1\cos^2\psi)\cos\psi\sin\vartheta - \\ &-2(E_0 + E_1\cos^2\psi)\sin\vartheta\cos\vartheta \mp \\ &\mp 3F_0\cos\psi\sin\vartheta\cos^2\vartheta - 4G_0\sin\vartheta\cos^3\vartheta + \\ &+H_0\sin\psi\cos\psi(\cos^2\vartheta - \sin^2\vartheta) \pm \\ &\pm K_0\sin\psi\cos\vartheta(\cos^2\vartheta - 2\sin^2\vartheta) = 0. \end{aligned} \qquad \text{(D. 2)}$$

The upper signs are valid at the upper face of the plate, viz. for $2z/h = 1$, and the lower signs should be used at the lower face, viz. for $2z/h = -1$.

The constants in (D. 1) and (D. 2) are defined by (C. 2).

Substituting (C. 4) in (4.3) the following equation is obtained, from which ψ should be solved for the centre region $\alpha b/2 \leqslant y \leqslant (1-\alpha/2)b$.

$$\pm\overline{B}_0\cos\psi + 2\,\overline{C}_0\sin\psi\cos\psi = 0. \qquad \text{(D. 3)}$$

The upper sign is valid for $2z/h = 1$, the lower sign for $2z/h = -1$. The constants in (D. 3) are defined by (C. 5).

The second derivatives of Φ are required for the determination whether Φ is a maximum or a minimum. For the edge regions they read

$$\begin{aligned} \partial^2\Phi/\partial\psi^2 &= 2A_1(\cos^2\psi - \sin^2\psi) - \\ &-4A_2(\cos^2\psi - 3\sin^2\psi)\cos^2\psi \mp \\ &\mp(B_0 + 2B_1\sin^2\psi - 5B_1\cos^2\psi)\sin\psi\sin\vartheta + \\ &+2C_0(\cos^2\psi - \sin^2\psi)\sin^2\vartheta \mp \\ &\mp(D_0 + 6D_1\sin^2\psi - 3D_1\cos^2\psi)\cos\psi\cos\vartheta - \\ &-2E_1(\cos^2\psi - \sin^2\psi)\cos^2\vartheta \mp \\ &\mp F_0\cos\psi\cos^3\vartheta - \\ &-2H_0\sin\psi\cos\psi\sin\vartheta\cos\vartheta \mp \\ &\mp K_0\sin\psi\sin\vartheta\cos^2\vartheta. \end{aligned} \qquad \text{(D. 4)}$$

$$\begin{aligned} \partial^2\Phi/\partial\psi\partial\vartheta &= \pm(B_0 + 2B_1\sin^2\psi - \\ &-B_1\cos^2\psi)\cos\psi\cos\vartheta + \\ &+4(C_0 + E_1)\sin\psi\cos\psi\sin\vartheta\cos\vartheta \pm \\ &\pm(D_0 - 3D_1\cos^2\psi)\sin\psi\sin\vartheta \pm \\ &\pm 3F_0\sin\psi\sin\vartheta\cos^2\vartheta + \\ &+H_0(\cos^2\psi - \sin^2\psi)(\cos^2\vartheta - \sin^2\vartheta) \pm \\ &\pm K_0\cos\psi(\cos^2\vartheta - 2\sin^2\vartheta)\cos\vartheta. \end{aligned} \qquad \text{(D. 5)}$$

$$\begin{aligned} \partial^2\Phi/\partial\vartheta^2 &= \mp(B_0 - B_1\cos^2\psi)\sin\psi\sin\vartheta + \\ &+2C_0\sin^2\psi(\cos^2\vartheta - \sin^2\vartheta) \mp \\ &\mp(D_0 - D_1\cos^2\psi)\cos\psi\cos\vartheta - \\ &-2(E_0 + E_1\cos^2\psi)(\cos^2\vartheta - \sin^2\vartheta) \mp \\ &\mp 3F_0\cos\psi(\cos^2\vartheta - 2\sin^2\vartheta)\cos\vartheta - \\ &-4G_0(\cos^2\vartheta - 3\sin^2\vartheta)\cos^2\vartheta - \\ &-4H_0\sin\psi\cos\psi\sin\vartheta\cos\vartheta \pm \\ &\pm K_0\sin\psi(2\sin^2\vartheta - 7\cos^2\vartheta)\sin\vartheta. \end{aligned} \qquad \text{(D. 6)}$$

For the centre region the second derivative of Φ reads

$$\partial^2\Phi/\partial\psi^2 = \mp\overline{B}_0\sin\psi + 2\overline{C}_0(\cos^2\psi - \sin^2\psi). \qquad \text{(D. 7)}$$

For $\psi = 0$, $\vartheta = 0$, (D. 4), (D. 5) and (D. 6) read respectively

$$\partial^2\Phi/\partial\psi^2 = 2A_1 - 4A_2 \mp (D_0 - 3D_1) - 2E_1 \mp F_0, \qquad \text{(D. 4)}'$$

$$\partial^2\Phi/\partial\psi\partial\vartheta = \pm(B_0 - B_1) + H_0 \pm K_0, \qquad \text{(D. 5)}'$$

$$\partial^2\Phi/\partial\vartheta^2 = \mp(D_0 - D_1) - 2(E_0 + E_1) \mp 3F_0 - 4G_0. \qquad \text{(D. 6)}'$$

For $\psi = \pi/2$, $\vartheta = \pi/2$ they read respectively

$$\partial^2\Phi/\partial\psi^2 = -2A_1 \mp (B_0 + 2B_1) - 2C_0, \qquad \text{(D. 4)}''$$

$$\partial^2\Phi/\partial\psi\partial\vartheta = \pm D_0 + H_0, \qquad \text{(D. 5)}''$$

$$\partial^2\Phi/\partial\vartheta^2 = \mp B_0 - 2C_0 + 2E_0 \pm 2K_0 \qquad \text{(D. 6)}''$$

For $\vartheta = 0$, (D. 1) yields $\sin\psi = 0$, i. e. $\psi = 0$, or

$$\begin{aligned} &-4A_2\cos^3\psi \pm 3D_1\cos^2\psi + 2(A_1 - E_1)\cos\psi \mp \\ &\mp(D_0 + F_0) = 0. \end{aligned} \qquad \text{(D. 8)}$$

For $\vartheta = \pi/2$, (D. 1) yields $\cos\psi = 0$, i. e. $\psi = \pi/2$, or

$$4A_2 \sin^3\psi \pm 3B_1 \sin^2\psi + 2(A_1 - 2A_2 + C_0) \sin\psi \pm \pm (B_0 - B_1) = 0. \qquad (D.9)$$

For $\psi = 0$, (D. 2) yields $\sin\vartheta = 0$, i. e. $\vartheta = 0$, or

$$-4G_0 \cos^3\psi \mp 3F_0 \cos^2\vartheta - 2(E_0 + E_1) \cos\vartheta \mp \mp (D_0 - D_1) = 0. \qquad (D.10)$$

For $\psi = \pi/2$, (D. 2) yields $\cos\vartheta = 0$, i. e. $\vartheta = \pi/2$, or

$$4G_0 \sin^3\vartheta \mp 3K_0 \sin^2\vartheta + 2(C_0 - E_0 - 2\,G_0) \sin\vartheta \pm \pm (B_0 + K_0) = 0. \qquad (D.11)$$

For $\psi = \pi/2$, (D. 1) yields

$$\partial\Phi/\partial\psi = (\mp D_0 \mp F_0 \cos^2\vartheta - H_0 \sin\vartheta) \cos\vartheta. \qquad (D.12)$$

For $\vartheta = 0$, (D. 2) yields

$$\partial\Phi/\partial\vartheta = (\pm B_0 \mp \mp B_1 \cos^2\psi + H_0 \cos\psi \pm K_0) \sin\psi. \qquad (D.13)$$

APPENDIX E.

The edge regions of the plate.

For the edge regions of the plate two solutions of (D. 1) and (D. 2) are evident at once, viz.

$$\psi = 0,\ \vartheta = 0$$

and

$$\psi = \pi/2,\ \vartheta = \pi/2.$$

Fig. 4.1 gives a survey of the combinations of ψ and ϑ considered in the investigation. The conditions that Φ is a maximum are obtained by substituting (D. 4)′, (D. 5)′ and (D. 6)′ in the first case and (D. 4)″, (D. 5)″ and (D. 6)″ in the second case in

$$\begin{aligned} \Phi_{\psi\psi}\Phi_{\vartheta\vartheta} - \Phi^2_{\psi\vartheta} &> 0, \\ \Phi_{\psi\psi} &< 0, \qquad (E.1) \\ \Phi_{\vartheta\vartheta} &< 0, \end{aligned}$$

where $\Phi_{\psi\psi}$ denotes $\partial^2\Phi/\partial\psi^2$, etc.

It is not possible to draw a general conclusion from the complicated expressions obtained whether Φ is a maximum or a minimum.

The equations (D. 1) and (D. 2) can be solved by a method of successive approximations. The method was not followed because it is rather laborious. (D. 1) can be expressed as an eighth order equation for $\sin\psi$ (or $\cos\psi$) whose coefficients depend upon ϑ. Similarly, (D. 2) can be expressed as an eighth order equation in $\sin\vartheta$ ($\cos\vartheta$), its coefficients depending upon ψ. Both equations have to be solved in each step in the computation procedure.

Numerical calculations carried out for $\vartheta = \pi/2$ have shown that Φ for $\psi = 0$ is practically always smaller than for $\psi = \pi/2$ and $2z/h = 1$ or $2z/h = -1$. In very few cases it is slightly larger than Φ for $\psi = \pi/2$ and $2z/h = 1$ but smaller than Φ for $\psi = \pi/2$ and $2z/h = -1$. It is observed from (D.1) and (D. 2) that Φ is not extremal for $\psi = 0$, $\vartheta = \pi/2$ unless $B_0 = B_1$ and $D_0 = D_1$. These conditions will not be fulfilled except perhaps for very special combinations of loads.

For $\vartheta = \pi/2$ the investigation hence leads to similar conclusions as for the centre region, as was to be expected.

Throughout the range covered by the investigation Φ is nearly always a minimum at the value of ψ that can be determined by solving (D. 9) and the character of the relation between $\varepsilon_e/\varepsilon^*$ and ψ is qualitatively represented by fig. 4.2*b*, 4.2*c* or 4.2*d*, i. e. $\varepsilon_e/\varepsilon^*$ is a maximum at $\psi = \pi/2$ both for $2z/h = 1$ and for $2z/h = -1$. This was even found to be the case when $\varepsilon_e/\varepsilon^*$ is larger for $\psi = 0$ than for $\psi = \pi/2$ and $2z/h = 1$ (fig. 4.2*d*).

In one case considered (D. 9) yielded no solution and the relationship between $\varepsilon_e/\varepsilon^*$ could be represented qualitatively by fig. 4.2*f*, i. e. $\varepsilon_e/\varepsilon^*$ is an extremum only for $\psi = \pi/2$. It can thus be concluded that for $\vartheta = \pi/2$ the numerical evaluations can be restricted to $\psi = \pi/2$, $2z/h = 1$ and $2z/h = -1$.

An entirely different situation exists at the edges, i. e. for $\vartheta = 0$. Here it was found from numerical calculations that in some cases Φ is larger for $\psi = \pi/2$ than for $\psi = 0$. The corresponding difference in $\varepsilon_e/\varepsilon^*$ was only in one case slightly more than 5.3 % but in most cases less than 2 %. It is observed from (D. 1) and (D. 2) that Φ is an extremum for $\psi = \pi/2$, $\vartheta = 0$ only when $D_0 = -F_0$ and $B_0 = -K_0$.

These conditions will not be fulfilled except perhaps for very special combinations of loads. It is thus to be expected that Φ, when it is larger for $\psi = \pi/2$ than for $\psi = 0$, will reach its maximum at some value of $0 < \psi < \pi/2$. This may also occur when Φ is slightly smaller for $\psi = \pi/2$ than for $\psi = 0$.

The values $\psi = \bar{\psi}$ and $\psi = \bar{\bar{\psi}}$ for which Φ reaches an extremum for $2z/h = 1$ and $2z/h = -1$ respectively are obtained by solving (D. 8). Substitution in (C. 1) yields the corresponding Φ. The results of such calculations for a number of representative cases, including those where the differences between Φ for $\psi = \pi/2$ and $\psi = 0$ are largest, are presented in table 4.1. In the part of the total range of the investigations falling outside the range covered by the examples from table 4.1, the largest $\varepsilon_e/\varepsilon^*$ for $\vartheta = 0$ is always found at $2z/h = -1$ and $\psi = 0$. The relationship between $\varepsilon_e/\varepsilon^*$ and ψ is shown qualitatively in fig. 4.3. It is observed that $\varepsilon_e/\varepsilon^*$ is always a maximum for $\psi = \bar{\psi}$ and $2z/h = 1$. This maximum is sometimes smaller (fig. 4.3*a*, 4.3*b*), sometimes larger (fig. 4.3*c*) than the maximum for $\psi = 0$ and $2z/h = -1$. For $2z/h = -1$ and $\psi = \bar{\bar{\psi}}$, $\varepsilon_e/\varepsilon^*$ is a minimum except in the case of fig. 4.3*e*, where it exceeds $\varepsilon_e/\varepsilon^*$ for $\psi = 0$ (which is a minimum only in this case) and also $\varepsilon_e/\varepsilon^*$ for $\psi = \pi/2$.

In the case of fig. 4.3*c*, the difference between $\varepsilon_e/\varepsilon^*$ for $2z/h = 1$, $\psi = \bar{\psi}$ and $\psi = \pi/2$ did not exceed 1.6 % but the difference between $\varepsilon_e/\varepsilon^*$ for $2z/h=1$, $\psi=\bar{\psi}$ and $\varepsilon_e/\varepsilon^*$ for $2z/h=-1$, $\psi=0$ was entirely negligible.

In the case of fig. 4.3*e*, the difference between $\varepsilon_e/\varepsilon^*$ for $2z/h=-1$, $\psi=\bar{\bar{\psi}}$ and $\psi=\pi/2$ was also entirely negligible. For $\tau/E\varepsilon^*=0$, $\bar{\psi}=\bar{\bar{\psi}}=\pi/2$.

It is thus justified to restrict the numerical evaluations for $\vartheta=0$ to $\psi=0$ and $\psi=\pi/2$, both for $2z/h=-1$, i. e. the lower surface of the plate.

In two cases investigated $\varepsilon_e/\varepsilon^*$ proved to be slightly larger for $\psi=0$, $\vartheta=\pi/2$ than for $\psi=0$, $\vartheta=0$, both for $2z/h=1$ and $2z/h=-1$. Although $\varepsilon_e/\varepsilon^*$ for $\vartheta=\pi/2$ was largest in these cases at $\psi=\pi/2$, it was considered of some interest to investigate the behaviour of $\varepsilon_e/\varepsilon^*$ at the nodal line $\psi=0$.

To this purpose, ϑ was solved from (D. 10) and substituted in (C. 1).

The relation between $\varepsilon_e/\varepsilon^*$ and ϑ is qualitatively represented in fig. 4.4.

For $2z/h=-1$, the maximum of $\varepsilon_e/\varepsilon^*$ did not exceed the minimum at $\vartheta=0$ by more than 3 %, but it remained markedly smaller than the largest $\varepsilon_e/\varepsilon^*$ at $\psi=\pi/2$, $\vartheta=\pi/2$. Hence, the case $\psi=0$, $\vartheta=\pi/2$ need to be considered in the numerical evaluations.

In several cases the numerical evaluation shows that for $\psi=\pi/2$, i. e. at the crest lines, $\varepsilon_e/\varepsilon^*$ is larger for $\vartheta=0$ than for $\vartheta=\pi/2$ and $2z/h=1$ or $2z/h=-1$. For a number of representative cases the values $\vartheta=\bar{\vartheta}$ and $\vartheta=\bar{\bar{\vartheta}}$ for which Φ reaches an extremum for $2z/h=1$ and $2z/h=-1$ respectively were solved from (D. 11) and substituted in (C. 1). The results of this investigation are presented in table 4.2. In the part of the total range of the evaluations falling outside the range covered by the examples from table 4.2, the largest $\varepsilon_e/\varepsilon^*$ for $\psi=\pi/2$ is always found at $\vartheta=\pi/2$.

The relations between $\varepsilon_e/\varepsilon^*$ and ϑ are qualitatively represented in fig. 4.5.

Excluding the case of fig. 4.5*f*, in which $\varepsilon_e/\varepsilon^*$ is largest at $\vartheta=\pi/2$, $2z/h=-1$, it is observed that $\varepsilon_e/\varepsilon^*$ is always a minimum for $2z/h=1$, $\vartheta=\bar{\vartheta}$ and for $2z/h=-1$, $\vartheta=\pi/2$. It is always a maximum for $2z/h=-1$, $\vartheta=\bar{\bar{\vartheta}}$ and, excluding the case of fig. 4.5*e*, also for $2z/h=1$, $\vartheta=\pi/2$.

The difference between $\varepsilon_e/\varepsilon^*$ for $2z/h=-1$ at $\vartheta=\bar{\bar{\vartheta}}$ and at $\vartheta=0$ never exceeded 3.8 % in the cases fig. 4.5a, 4.5*b* and 4.5*c* except in the last example from table 4.2 where this difference was 7.3 %. The difference between $\varepsilon_e/\varepsilon^*$ for $2z/h=-1$ at $\vartheta=\bar{\bar{\vartheta}}$ and at $\vartheta=\pi/2$ never exceeded 0.5 % in the cases of fig. 4.5*d* and 4.5*e*.

It is observed however that $\varepsilon_e/\varepsilon^*$ for $2z/h=-1$ is larger in several cases at $\psi=0$, $\vartheta=0$. In those cases in which $\varepsilon_e/\varepsilon^*$ is largest for $2z/h=-1$ and $\vartheta=\bar{\bar{\vartheta}}$ the differences between this maximum and $\varepsilon_e/\varepsilon^*$ for $2z/h=-1$ and $\psi=0$, $\vartheta=0$ or $\psi=\pi/2$, $\vartheta=0$ or, eventually, $\psi=\pi/2$, $\vartheta=\pi/2$, never exceeded 2.6 %.

This difference is considered sufficiently small to justify the restriction of the numerical evaluation for $\psi=\pi/2$ to the cases $\vartheta=0$ and $\vartheta=\pi/2$.

It follows from a closer examination of tables 4.1 and 4.2 and figs. 4.3 and 4.5 that in those cases in which the variation of $\varepsilon_e/\varepsilon^*$ along the edges ($\vartheta=0$) and the crest lines ($\psi=\pi/2$) can be represented qualitatively by figs. 4.3*d* and 4.5*c* or 4.5*d* or 4.5e respectively or by fig. 4.3*e* and fig. 4.5*b* respectively, $\varepsilon_e/\varepsilon^*$ will have a maximum exceeding the maximum at $2z/h=-1$, $\psi=\pi/2$ and $\vartheta=\bar{\bar{\vartheta}}$. The reason is that, except perhaps for very special combinations of loads, $\partial(\varepsilon_e/\varepsilon^*)/\partial\psi\neq 0$, as can be verified by substituting $\vartheta=\bar{\bar{\vartheta}}$ from table 4.2 in (D. 12) with the lower signs. It is to be expected however that the difference between the absolute maximum and the maximum at $\psi=\pi/2$, $\vartheta=\bar{\bar{\vartheta}}$ will be practically negligible. It is hence considered justified to restrict the numerical evaluation to $\psi=0$, $\vartheta=0$, $\psi=\pi/2$, $\vartheta=0$ and $\psi=\pi/2$, $\vartheta=\pi/2$, especially when it is considered that the details of the stress distribution in an actual construction are not approximated in the theory with an equal degree of accuracy as the elastic energy (sec. 1).

C.C.L. Class. C 470-3: C 705-3: C 708-3

REPORT S. 445.

The Effective Width in the Plastic Range of Flat Plates under Compression

by

M. BOTMAN and J. F. BESSELING.

Summary.

The effective width in the plastic range of 24 S-T clad and unclad flat plates was experimentally determined. A testing apparatus for flat-end tests was used, the longitudinal edges of the bays of the specimens (length to width ratio of bays: 4.67) being supported by knife-edges. Amplitude and wave-length measurements were taken with a mirror device. In the first series of 12 specimens with a thickness of 1.5 mm the necessary number of bays was established and in the second series of 14 plates different thicknesses, covering the range of the ratio $\sqrt{\frac{\varepsilon_{cr}}{\varepsilon_e}}$ between 0.2 and 0.8, were used. The results show a good agreement of the effective widths in the plastic range with the theoretical results of KOITER (ref. 3) for the effective width in the elastic range. No marked difference between clad and unclad plates could be observed.

An important result of the experiments is the fact that the maximum load of flat plates under compression can be calculated with very good accuracy from the stress-strain relation of the material of the plates and the theoretical curve for the effective width in the elastic range.

Contents.

This investigation, which has been performed by order of the Netherlands Aircraft Development Board (N. I. V.), is reported in full in the N.L.L.-Reports S. 414 and S. 438 (refs. 1 and 2). These reports are reproduced here in condensed form.

1 Introduction.

For the calculation of the allowable load in plate-stringer structures knowledge is required about the effective width of the plate under compressive loads exceeding the buckling loads. The effective width [1]) of a plate under axial compression is defined as the width of a plate with the same thickness and the same specific shortening

[1]) henceforth to be denoted as e. w.

as the original plate, carrying the same load in the unbuckled condition as the original plate in the buckled condition.

Satisfactory approximate solutions for the e. w. have been derived for cases in which in no single point of the plate the elastic limit of the material is exceeded. However, the calculation of the ultimate load of the structure will in many cases only be possible when the e. w. is also known in the plastic range. No theoretical studies about the magnitude of the e. w. in the plastic range being available, an experimental investigation concerning this problem was considered to be of importance.

To restrict the scope of the research only panels with rectangular bays and with simply supported longitudinal edges will be considered. These conditions are realised or form a somewhat conservative approximation in the majority of stiffened shell structures, consisting of plates stiffened in two directions by groups of stringers. The length of a bay of the panel is usually a multiple of the width. The longitudinal stiffeners bordering the bay carry part of the compressive load; besides this, one of their main functions is to stabilise the plate, i. e. displacements of the edges of the plate perpendicular to the plane of the plate are prevented. Hence, buckling of the plate will only occur between successive stringers, and in adjacent bays of the panel the buckles will develop in opposite directions. It follows from the foregoing that the stiffeners and the plate hardly exert any force on each other in the direction perpendicular to the plate, and that the edges of the plate will remain straight in the plane of the plate. Thus for loads sufficiently below the load at which general instability of the whole panel occurs and the load at which local buckling of the stiffeners takes place, it can be supposed that the edges of the bays, which are sufficiently remote from the edge bays and from the loaded edges, remain completely straight.

The torsional rigidity of the stringers will have some effect on the edge support of the plates. However, in the cases where open-section stiffeners are used the torsional rigidity is very small and the edges of the bay of the plate can be regarded as simply supported. The tests in this report only refer to specimens with simply supported edges.

In the present report the N.L.L.-Reports S. 414 and S. 438 (refs. 1 and 2) are reproduced in condensed form. All particulars not mentioned here can be found in these reports.

The results of the experiments will be compared with the theoretical results for the elastic range derived in ref. 3. The results of the tests described in ref. 4, which were executed at Bristol Aeroplane Co. Ltd., will also be considered.

2 List of symbols.

A $= (nb + 2\,d)h$. Cross sectional area of a specimen.
A_s Cross sectional area of a stiffener.
E Modulus of elasticity.
E_s Secant modulus of elasticity.
E_t Tangent modulus of elasticity.
J_2 Stress invariant (see ref. 25).
K $= \frac{\sigma_{cr}}{E}\left(\frac{b}{h}\right)^2$. Buckling stress coefficient used in ref. 4.
L Half wave length in x-direction.
P Compressive load.
P_{cr} Buckling load.
W Amplitude of wave form.
a Length of a bay.
b Width of a bay.
b_m Effective width of a bay.
b_m' Effective width of a bay in view of the compressive stiffness (see section 4.2 and the appendix).
d Width of outer edges.
h Thickness.
m, n Positive integers.
n Number of bays of a specimen.
r Radius of knife-edge.
s Total play at knife-edge.
w Transverse displacement.
x Coordinate in longitudinal direction.
y Coordinate in lateral direction.
ε Specific shortening in x-direction.
ε_{cr} Specific shortening at which buckling occurs.
ε_e Specific shortening at which the elastic limit of the material is exceeded.
φ Slope in y-direction of the wave form at the longitudinal edges.
ν Poisson's ratio.
$\bar{\sigma}$ Average compressive stress.
σ_{cr} Buckling stress.
σ_e $= E \,.\, \varepsilon_e$.
$\sigma_{0.2}$ Compressive stress at which in the material 0.2 per cent permanent strain occurs.

3 Mechanical and geometric properties affecting the effective width.

3.1 *Dimensions of specimens.*

For given edge conditions and a certain length-width ratio of a bay the e. w. in the elastic region is completely determined by the ratio $\frac{\varepsilon_{cr}}{\varepsilon}$ and the number of half waves in the longitudinal direction. The relation between the e. w. and $\frac{\varepsilon_{cr}}{\varepsilon}$ in the elastic range for different supports of the unloaded longitudinal edges and for bays with an infinite length was derived in ref. 3. The wavelength is in this case a continuous function of $\sqrt{\frac{\varepsilon_{cr}}{\varepsilon}}$, decreasing at increasing ε.

For a certain finite length of the bay, however, only a finite number of half waves can occur. Thus the wavelength cannot change continually, but the number of half waves will increase with one or two, each time the wave form becomes unstable at higher loads. The part of the accumulated energy in the plate, which exceeds the energy in the plate in the next wave form, will come free at the transition as a bang, if this part of the energy is large enough. The calculation of the influence of this abrupt change in wavelength on the magnitude of the e.w. by means of the theory of ref. 3, showed that this influence can be neglected for length-width ratios $\frac{a}{b} \geqslant 5$.

The buckling load of a long, simply-supported plate under axial compression is determined by the thickness to width ratio of the plate. The choice of this ratio depends on the range of values of ε, for which the e.w. must be determined.

The thickness of the plate may of course vary across the plate only within very small tolerances. This is one of the reasons why the use of plates with a thickness of less than 1 mm cannot be recommended. Another reason lies in the fact that relatively large initial eccentricities inherent to thin plates have a large influence on the results. Furthermore, it will be difficult to prevent the occurrence of local buckling at the edges.

3.2 *Longitudinal edges.*

As in the bays of a stiffened shell, the longitudinal edges of the specimen must be supported against displacements perpendicular to the plane of the plate. In actual constructions this is always done by means of stiffeners. The presence of stiffeners on the test specimens would, however, introduce the difficulty that the load measured on the compression machine acts on both the plate and the stiffeners. Thus the load acting on the plate can only be determined by subtracting the load in the stiffeners from the total measured load or by extensive strain measurements in the plate. The first method presupposes knowledge of the load in the stiffeners, which can be obtained by measurement or calculation. The accuracy with which the load in the stiffeners will be found is, however, not large owing to bending deformation caused by initial eccentricities of the stiffeners and the nearly always occurring inhomogeneity of the material. With heavy stringers, where initial eccentricities are relatively unimportant, the load in the panel must be determined as the difference between two large values, which will also affect the accuracy.

The determination of the load in the plate by strain measurements requires a large number of test points, e.g. in the tests described in ref. 5 about 600 measurements were made per specimen (see also refs. 6 and 7). An accurate determination of the stress distribution becomes nearly impossible as soon as somewhere in the plate plastic deformation occurs.

Specimens without longitudinal stiffeners form the most attractive solution, because the load in the plate can be measured directly. The edges of the specimen are to be supported against displacements perpendicular to the plane of the plate. Difficulties arising from this method are the possibility of play between the support and the plate, and friction. Very little play in the supports will have a negligible effect on the e.w., but with large play or with local interruptions of the supports local buckling of the plate can occur. On the other hand friction will be larger when the play between the support and the plate decreases.

In refs. 4, 8, 9, 10, and 11 supports are used, which give approximately hinged-edge conditions. The supports used in refs. 4, 6, 12 and 13 approximate clamped conditions. In some cases these supports can only be used at free ends of the specimen. When the specimen consists of more bays all longitudinal edges must have the same method of support. The application of knife-edges (ref. 10) for these specimens is regarded to be a very attractive method, because of the simplicity and the expected low friction with small amounts of play. Single knife-edges can of course be used only to represent hinged-edge conditions.

When the edges are unable to twist freely in planes perpendicular to the direction of the load, the edge is not simply supported, but more or less clamped and the buckling load of the plate will then be higher. According to the theoretical results of ref. 3 the e.w. as a function of $\frac{\varepsilon_{cr}}{\varepsilon}$ will in the elastic range remain the same. For a certain value of ε, however, the e.w. will be larger than in the case of simply supported longitudinal edges.

3.3 *Loaded edges.*

The loaded edges must be as straight as possible and they must be parallel to each other. These requirements hold especially during the tests and therefore the compression machine must come up to certain requirements as well.

The usual universal testing machines are as a rule not stiff enough, which results in the use of auxiliary constructions. In the tests of refs. 8, 12, 13, 14 and 15 special methods were used to locate the compressive load on the specimen. In the case of refs. 9, 10, 16 and 17 special rigs were made to ensure parallel displacements of the loaded edges.

The 150-tons Avery compression testing machine, present at the N.L.L., possesses qualities, making auxiliary constructions superfluous. The loading platens have a satisfactory flatness and stiffness and the whole machine is very rigid. The lower platen can be adjusted in planes under different angles with the upper platen, but it is more practical to finish the loaded edges sufficiently flat and parallel.

It is difficult to obtain the correct end constraint at the loaded edges. Attempts to realise perfectly hinged loaded edges may be regarded as unsuccesfull. In this case the edge corresponds with a nodal line of the wave form occurring after exceeding the buckling load, because no relative displacements and no moments are present in points of a nodal line. The slope of the buckled plate normal to the loaded edge will not be constant along the edge. This is the reason why constructions like those used in refs. 8, 10, 13 and 15 are not satisfactory.

Clamped loaded edges can in general be obtained with less difficulty, but in these cases the lateral expansion at the edges is also completely prevented, which is not the case in actual skin-stringer panels. The loaded edges of the specimens described in refs. 4, 6, 12 and 16 were imbedded in some material like Wood's metal. This method is, however, reported to be unsatisfactory, because temperature effects caused appreciable distortion in the plate and the edges did not remain straight after the load exceeded the buckling load due to yielding of the Wood's metal. In another method used in refs. 6, 18 and 19, the loaded edges were clamped between steel strips. In all these methods the shortening of the plate cannot be determined simply from the relative displacement of the loading platens, but a correction must be introduced for the end strips and the clamps.

This latter correction is not necessary with the results of so called flat-end tests, in which the compression load acts directly on the edge of the specimen. These edges must then be perfectly straight and parallel and the loading platens of the testing machine must satisfy the same requirements, especially during loading. An advantage of this method lies in its simplicity. Furthermore, the friction between the edge and the platen generates the only forces preventing the free lateral expansion at the loaded edges.

It is well known that friction at the loaded edges can have appreciable influence on the relation between the load and the deformation. The friction hampers the lateral expansion of the plate in the neighbourhood of these edges. In refs. 14, 20, 21 and 22 tests are described on several specimens, mostly solid and hollow cylinders made of different materials. The results show that especially for length-width ratios less than 1, differences of at least 20 % in the force occur at large deformations. With small deformations the differences can be several percents. Probably the force still is appreciably too large for length-width ratios of about 2. According to ref. 23 the influence of friction can be reduced considerably when suitable lubrication is provided.

It is recommended to use specimens with length-width ratios in excess of 1. In view of the most convenient length-width ratio for a bay of a panel, which according to section 3.1 should be at least 5, the number of adjacent bays may be equal to or less than this value.

Strain measurements on a specimen in order to obtain an impression about the amount of friction are recommended.

Prevention of the lateral expansion owing to the support at the loaded edge or to the friction between the edge and the platen of the compression machine may be regarded as transverse stiffening (see section 3.4).

3.4 *Transverse stiffening.*

In the unbuckled state compressive stresses in the plate in axial direction cause lateral expansion following from POISSON's ratio. If parallel displacement of the longitudinal edges is prevented due to the presence of transverse stiffeners, compressive stresses will also appear in the lateral direction. The plate is now being compressed in two mutually perpendicular directions, resulting in a decrease of the buckling load. This decrease amounts to maximum 30 % and 15.5 % for simply supported and clamped edges respectively, but for values of $\frac{A_s}{ah} < 1$ the decrease is smaller than 15 % and 8 % respectively.

According to ref. 24 the postbuckling stiffness of the plate is larger for panels with transverse stiffeners, e. g. for slender bays the post-buckling stiffness appears to be about 24 % larger for $\frac{A_s}{ah} = 1$ than for $\frac{A_s}{ah} = 0$. This can be explained by the fact that the transverse stiffeners carry most of the compressive stress, which in plates without transverse stiffeners is carried only by the plate at the nodal lines (see fig. 3.1). Hence the compressive stresses in the plate along the nodal line are smaller than in the case of plates without stiffeners and this counteracts the proceeding of buckling, resulting in larger post-buckling stiffness.

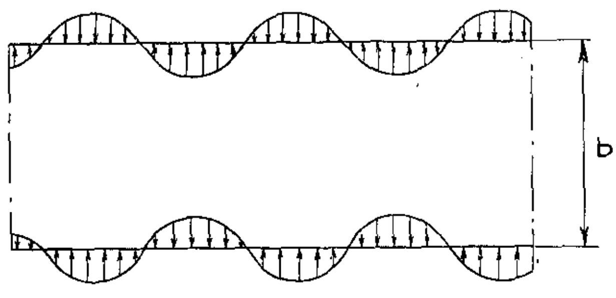

Fig. 3.1. Distribution of normal stresses after buckling at the simply supported longitudinal edges, which are kept straight.

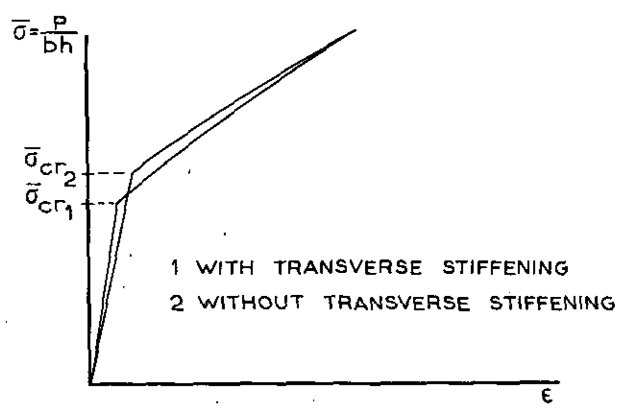

Fig. 3.2. The influence of transverse stiffening on the shape of the load-deformation curve of a plate.

In fig. 3.2 the load-deformation curves of plates with and without transverse stiffeners are compared. It can be seen that although the buckling load is lower for plates with transverse stiffeners, the larger post-buckling stiffness tends to reduce the differences in the e. w.

The influence of the transverse stiffening, represented by the (if necessary fictive) ratio $\frac{A_s}{ah}$, must in general be known in experiments in order to obtain reproducible results.

The bending rigidity of the longitudinal stiffeners in the plane of the plate is another important factor. When the edges remain straight, i. e. when they have an infinite stiffness against bending in the plane of the plate, tensile and compressive stresses will act on the plate in the buckled state as shown in fig. 3.1. For edges with a finite stiffness these stresses will decrease. This does not influence the magnitude of the buckling load, but the stiffness of the buckled plate will be appreciably smaller. For panels without transverse stiffening the decrease in stiffness can be, according to ref. 24, about 19 %. For panels with transverse stiffening the decrease is somewhat less.

The aim of the experiments will always be the determination of the c. w. of a bay of the plate with straight edges. Thus a correction on the results of the tests may be necessary allowing for the bending stiffness of the longitudinal edges. One can obtain almost perfectly straight edges when the test specimen consists of several equal adjacent bays. In that case corrections may be unnecessary.

3.5 *Transition from elastic to plastic range.*

The state of stress in a buckled plate is not homogeneous and the stress distribution for arbitrary loads in excess of the buckling load is not known exactly. Therefore it is in general not possible to determine the point on the plate where and the load at which in that point the elastic limit of the material is exceeded.

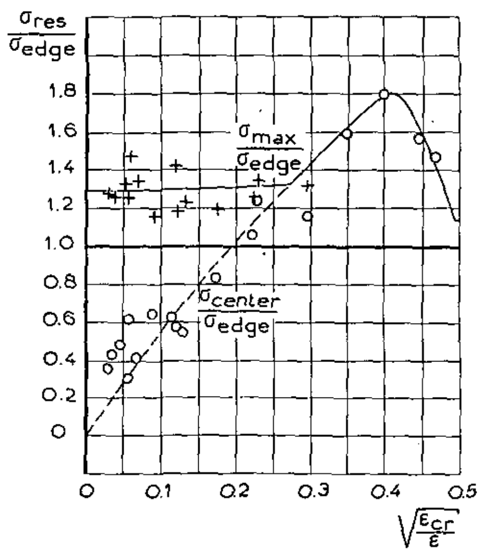

Fig. 3.3. The relation between $\sqrt{\frac{\sigma_{max}}{\sigma_{edge}}}$ and $\sqrt{\frac{\varepsilon_{cr}}{\varepsilon}}$ (from ref. 5).

The problem whether the elastic limit in the plate is exceeded, is treated in ref. 5. In fig. 3.3 the results are represented, showing the relation, determined from experiments, between the ratio of the maximum value of the axial stress and the compressive stress in the stringers, and $\sqrt{\frac{\varepsilon_{cr}}{\varepsilon}}$. The experiments, however, were conducted on specimens with clamped longitudinal edges. Furthermore not the maximum value of a principal stress determines whether the elastic limit is reached, but the value of the stress invariant J_2 (criterion of Von Mises — ref. 25), which is a measure for the distortion energy in an elementary part of a body. Hence, fig. 3.3 has little value for the determination of the point in which plastic deformation starts, for plates with simply supported longitudinal edges.

From ref. 26 it can be concluded, that calculations, from which the load can be accurately predicted, at which in a point of the plate the elastic limit of the material will be reached, are not practicable.

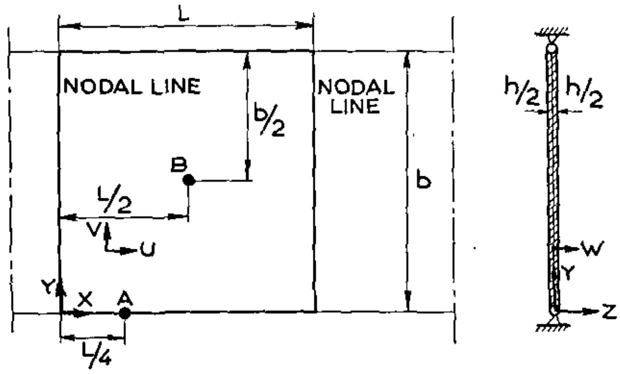

Fig. 3.4. Location of points A and B for which the magnitude of J_2 was determined.

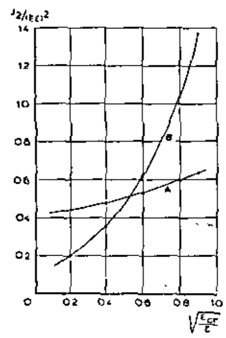

Fig. 3.5. The relation between J_2 and $\sqrt{\frac{\varepsilon_{cr}}{\varepsilon}}$ for the points A and B.

In order to get at least an impression whether the elastic limit first will be reached in the center of the plate or at the longitudinal edges, in ref. 1 the value of J_2 of a point on the longitudinal axis of the plate was compared with the value of J_2 of a point on the edge. A plate was considered without transverse stiffening and with simply supported edges, which remained straight. Approximate stress distributions were used, following from the displacement functions assumed in ref. 3. The points A and B (fig. 3.4) were chosen because of some advantages in the calculations, the point A being positioned on the longitudinal edge, and the point B being the point on the centerline of the plate with the largest bending stress. The result of the calculation is shown in fig. 3.5, giving the value of $\frac{J_2}{(E\varepsilon)^2}$ as a function of $\sqrt{\frac{\varepsilon_{cr}}{\varepsilon}}$.

It can be concluded from fig. 3.5, that the elastic limit is more probably reached first near the edge the larger $\varepsilon/\varepsilon_{cr}$ is when this occurs.

Furthermore the shape of the curve for point B as compared with the curve for point A suggests strongly, that for stresses little in excess of the buckling stress, the critical point will lie in the center of the plate.

It can be expected that the influence of plasticity on the e. w. will depend on the position of the critical point, in which the first plastic deformation occurs. With thin plates (ε_{cr} small) this point will probably lie on the edge and with thick plates in the center of the plate.

4 · Test programme and equipment.

4.1 *Loading arrangement.*

The 150-tons Avery compression testing machine comes up to the requirements specified in section 3.3. The combination of flat-end tests and longitudinal edges of the bays of the specimens supported by knife-edges was considered to possess the most advantages. From the point of view of the simplicity of the loading arrangement it was decided to use only specimens with bays of equal width. The values of $\sqrt{\frac{\varepsilon_{cr}}{\varepsilon_e}}$ at which for the different specimens the elastic limit will be exceeded, will then be determined only by the thickness of the plate. Because of the possibility of local buckling of the plate at the edges and the influence of initial eccentricities the thickness of the plate was chosen to be larger than 1 mm. The width of the bays of 150 mm seemed to be suitable in view of the values of $\sqrt{\frac{\varepsilon_{cr}}{\varepsilon_e}}$ to be attained. The dimensions of the loading platens enable the use of specimens consisting of up to 5 such bays. For the length of the specimens 700 mm was taken, being the most economical length in connection with the available commercial dimensions. Hence the overall length-width ratio of the specimen is but little smaller than 1, and for the bays of the specimen this ratio amounts to 4.67.

In figs. 4.1 and 4.2 the general arrangement of the test rig is shown, fig. 4.1 giving the half of the rig, which is rigidly connected to the lower platen of the machine, and fig. 4.2 giving the complete test rig. The connection of the other half of the rig to the lower platen is adjustable. Each half of the rig carries 5 single knife-edges. The load is applied to the plate via two compression strips, connected to the upper and lower platens. These strips contain slots with a depth of about 2 mm, in which the plates are fitted with some lateral play. The width of the slots is adapted to the thickness of the plates. Before the tests the slots are filled with graphite grease in order to reduce the friction as much as possible.

Especially with thin plates it was considered necessary to support the longitudinal edges of the bays along the whole length of the specimen. Therefore in the upper compression strip a number of transverse grooves were made in which the top ends of the knife-edges can move freely during shortening of the specimen. Because of undesirable local deformations of the unsupported parts of the loaded edges near these grooves in the first test, small bridge pieces were inserted in the grooves in the subsequent tests (see fig. 4.3).

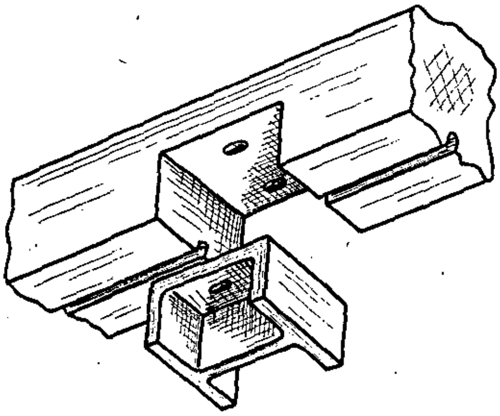

Fig. 4.3. Bridge piece in upper compression strip.

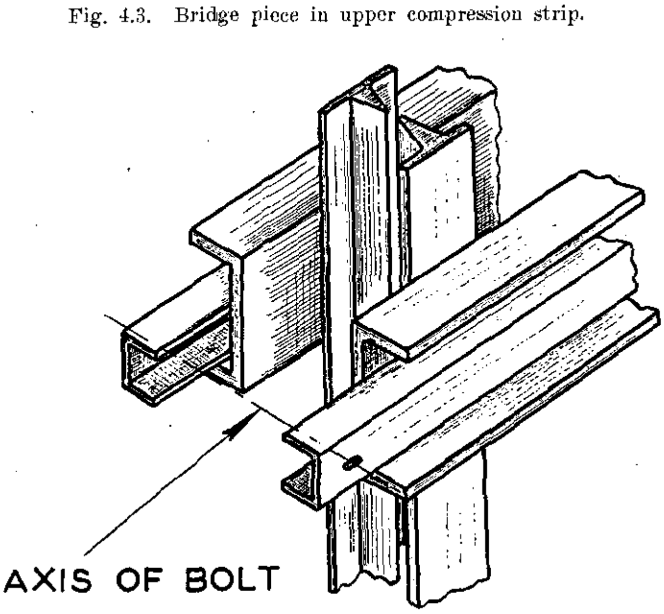

Fig. 4.4. Bolted connection of channel beams.

Another improvement in the test rig, introduced after the first tests, concerns the rigidity of the connection of both halves of the rig to the lower platen. It appeared that both groups of knife-edges were pushed apart when with irregular wave forms the load was largely in excess of the buckling load. Satisfactory rigidity of both halves of the test rig was obtained by the construction shown in fig. 4.4. In the channel beams supporting the knife-edges, smaller beams were inserted, which were connected at the ends with bolts.

Fig. 4.5 shows different forms of knife-edges, which were used successively. These changes in the form of the knife-edges were introduced in order to reduce the friction. The sliding pieces in form *c* were made of perspex and red copper with a length of 50 mm each and interspaced about 2 mm. The disadvantage of this form was the appreciably larger external radius of about 5 mm as compared with the radius of the initial knife-edge of 1.5 mm. This is not the case with shape *d*, which was adopted for the ultimate tests.

Fig. 4.1. Half of test rig with dial gauge in position *a*.

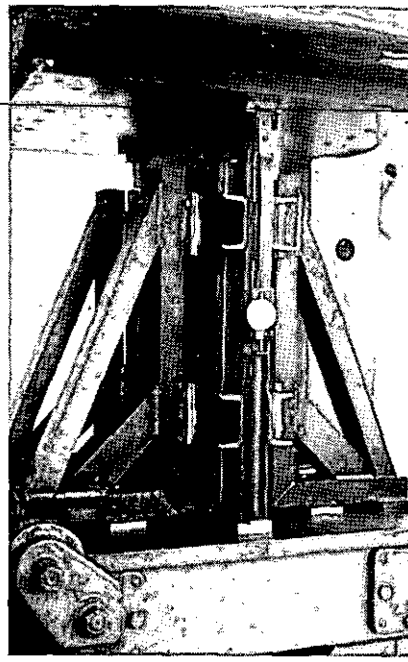

Fig. 4.2. Complete test rig with dial gauge in position *b*.

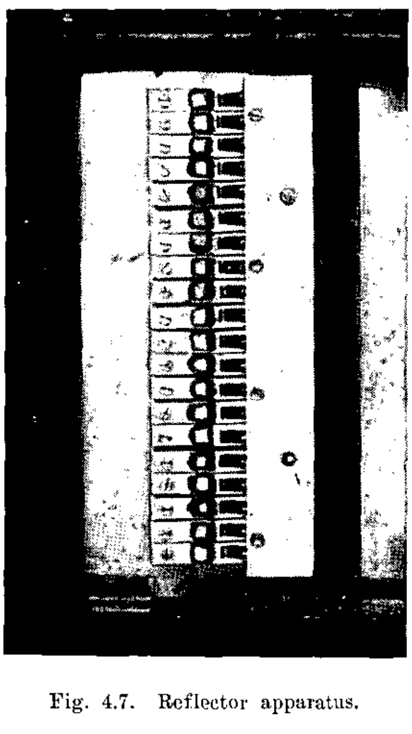

Fig. 4.7. Reflector apparatus.

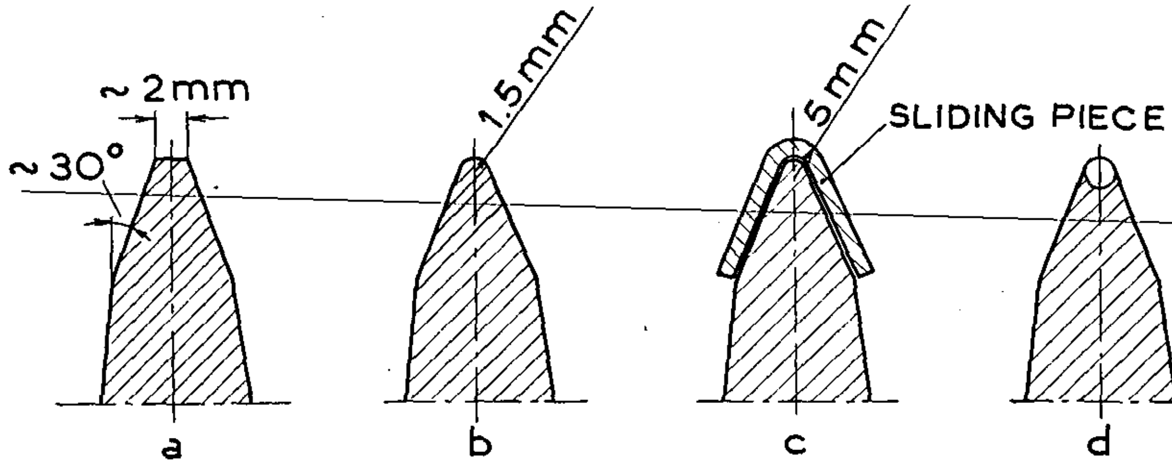

Fig. 4.5. Different forms of knife edges.

Here the extremities of the knife-edges are formed by pieces of brass wire with a length of 5 cm and a diameter of 2 mm. These pieces are inserted with interspaces of 2 mm in a slot, machined in the original knife-edge, and filled with graphite grease.

4.2 *The amount of play between plate and knife-edge supports.*

In order to obtain simply supported longitudinal edges of the specimen, some play must exist between the plate and the knife-edges. Otherwise the edges will be clamped when heavy buckling takes place. The necessary amount of play depends on the shape of the knife-edges, the thickness of the plate, and the greatest slope of the wave form

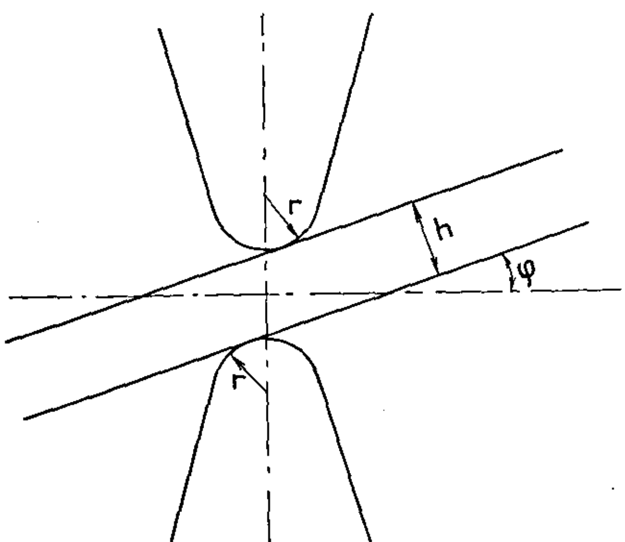

Fig. 4.6. The play at the knife edges.

at the longitudinal edges (see fig. 4.6). The transverse expansion following from Poisson's ratio will be neglected. The amount of play can be calculated from

$$s = (2\,r + h)\,\left(\frac{1}{\cos \varphi_{\max}} - 1\right), \qquad (4.1)$$

if the magnitude of $\varphi_{\max}$ is known. In general it will not be possible to predict $\varphi_{\max}$ with sufficient accuracy. Therefore the necessary amount of play should be determined experimentally.

The influence of the play between the plate and the longitudinal supports can be demonstrated as follows.

It is supposed that the longitudinal edges of the plate can take a form, given by

$$w = 0.5\, s \sin \frac{n\,\pi\,x}{a}. \qquad (4.2)$$

This results in an extra specific shortening of the plate

$$\Delta\varepsilon = \frac{1}{a} \int_0^a dx \sqrt{1 + \left(\frac{\partial w}{\partial x}\right)^2} - 1$$

or

$$\Delta\varepsilon = \frac{1}{a} \int_0^a \frac{1}{2} \left(\frac{\partial w}{\partial x}\right)^2 dx = \frac{n^2\,\pi^2\,s^2}{16\,a^2}. \qquad (4.3)$$

Now $s \ll \frac{a}{n}$, thus $\Delta\varepsilon$ is very small. Hence the necessary amount of play for a given thickness of the plate (according to (4.1)), will in general result in an extra specific shortening, which is negligible compared with the shortenings in the range of values of $\sqrt{\frac{\varepsilon_{cr}}{\varepsilon}}$ were the elastic limit is exceeded. For the determination of the e. w. in the plastic range $\Delta\varepsilon$ will, therefore, not be of importance.

4.3 *Measuring equipment.*

The magnitude of the load is indicated directly on the loading machine. The accuracy in the loading range to be considered for these tests amounts to about 15 kg. In order to avoid errors due to friction in the machine the desired load must always be approached from the side of smaller loads.

The shortening of the specimen under loading is derived from the displacement of the loading platens with respect to each other. The displacement is measured with two dial gauges rigidly connected to the upper platen (figs. 4.1 and 4.2) on either side of the specimen. In the first tests both dial gauges were mounted in position "a", but in the subsequent tests both gauges were used in position "b". The accuracy of the measurements with the dial gauges is about 0.01 mm.

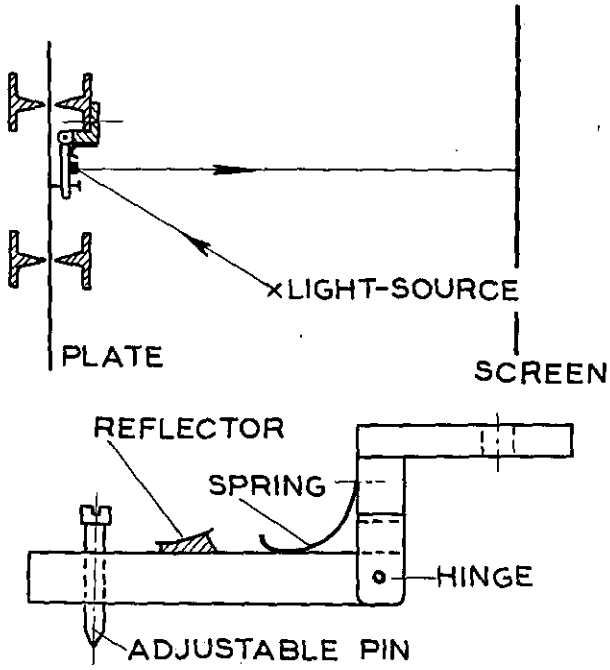

Fig. 4.8. Principle of reflector apparatus.

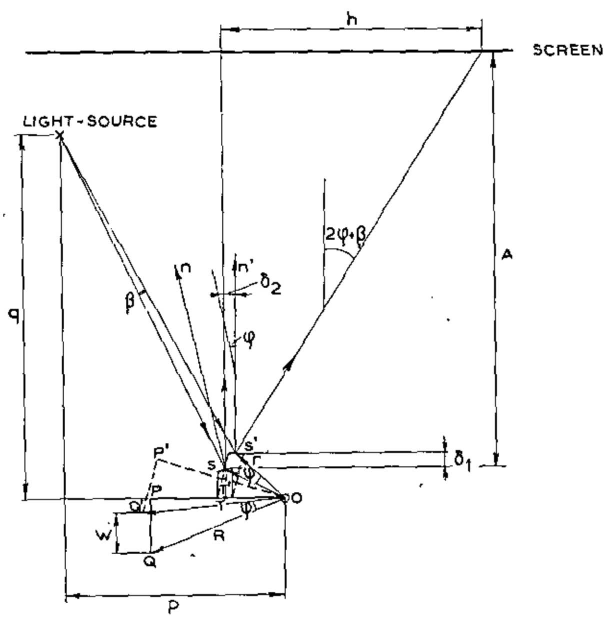

$$h = (A - \delta_1)\,\mathrm{tg}\,(2\varphi + \beta) + \delta_2$$

$$\varphi = \mathrm{bg}\,\sin\frac{PQ}{R} - \mathrm{bg}\,\sin\left(\frac{PQ}{R} - \frac{w}{R}\right)$$

$$\beta = \mathrm{bg}\,\mathrm{tg}\,\frac{p - r\cos(\varphi_0 + \varphi)}{q - r\sin(\varphi_0 + \varphi)} - \mathrm{bg}\,\mathrm{tg}\,\frac{p - r\cos\varphi_0}{q - r\sin\varphi_0}$$

$$\varphi_0 = \mathrm{bg}\,\mathrm{tg}\,\frac{ST}{OT}$$

$$\delta_1 = r\sin(\varphi_0 + \varphi) - r\sin\varphi_0$$

$$\delta_2 = r\cos\varphi - r\cos(\varphi_0 + \varphi)$$

Fig. 4.9. Geometry of the reflector apparatus.

The amplitude of the waves, the wave length and the wave form are determined on the longitudinal axis of the center bay of the specimen with devices especially developed for these tests (see fig. 4.7). The principle is shown in fig. 4.8. Against one of the knife-edge supports near the center of the specimen a system of small levers is attached, on which small hollow-ground reflectors are fitted. These reflectors throw a sharp image of a light source upon a screen. An adjustable pin at the end of each lever is in contact with the plate of which the transverse displacements

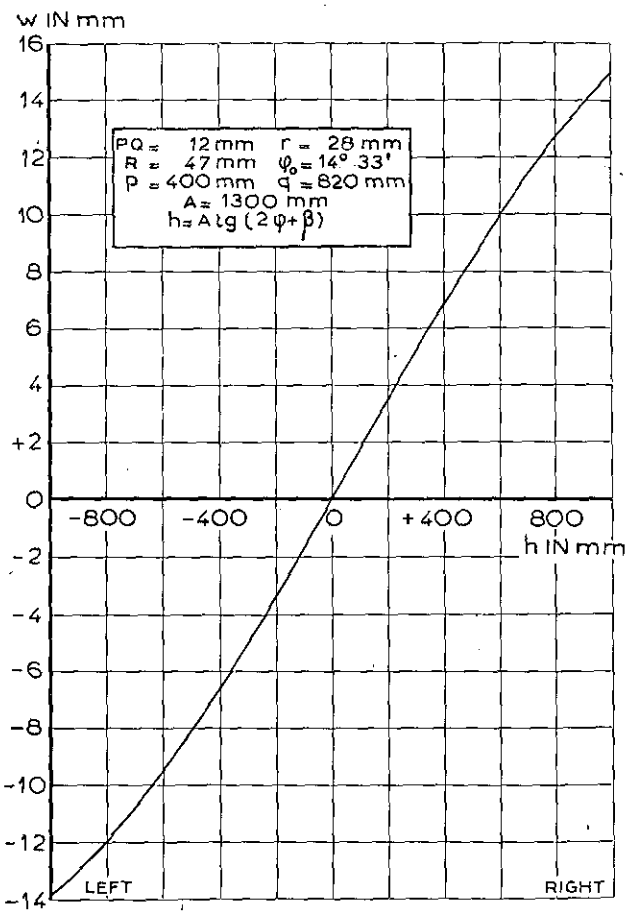

Fig. 4.10. Calculated relation between measured displacement h of the image on the screen and the displacement w of the adjustable pin on the plate.

must be measured. The pressure of a small spring against the lever causes the pin to remain in contact with the plate. Fig. 4.9 gives the necessary dimensions for the calculation of the displacements. The displacement of the pin as a function of the measured displacement of the image on the screen can easily be determined. For the dimensions chosen in the tests the result is given in fig. 4.10. The enlargement is about 58 times and the displacements of the image on the screen can be read with an accuracy of about 2 mm.

In the preliminary tests some measurements with electrical resistance strain-gauges were carried out, mainly in order to determine the effect of friction at the loaded edges. To this end a Baldwin recorder

TABLE 4.1

Characteristic values of the specimens.

Group	Spec. no.	Number of bays	Total width mm	Mean thickness mm	$\sigma - \varepsilon$ curve	E kg/mm²	$10^6 \frac{\sigma_{0.2}}{E}$	$10^6 \varepsilon_e = 10^6 \frac{\sigma_e}{E}$	$10^6 \varepsilon_{cr}$	$\sqrt{\frac{\varepsilon_{cr} E}{\sigma_{0.2}}}$	$\sqrt{\frac{\varepsilon_{cr}}{\varepsilon_e}}$
Preliminary tests.	B 5-1	5	765	1.56	B 1	7400	4860	2700	396	0.285	0.383
	B 5-2	5	765	1.555	B 2	7425	4780	2900	395	0.287	0.368
	B 5-3	5	765	1.525	B 3	7500	5290	3070	379	0.267	0.351
	B 4-1	4	612	1.53	B 3	7500	5290	3070	382	0.268	0.353
	B 3-1	3	459	1.58	B 1	7400	4860	2700	407	0.290	0.388
	B 3-2	3	459	1.56	B 2	7425	4780	2900	399	0.289	0.370
	B 3-3	3	459	1.565	B 2	7425	4780	2900	399	0.289	0.370
	B 2-1	2	306	1.58	B 1	7400	4860	2700	407	0.289	0.388
	B 2-2	2	306	1.54	B 3	7500	5290	3070	386	0.270	0.354
	B 1-1	1	153	1.57	B 1	7400	4860	2700	402	0.287	0.385
	B 1-3	1	153	1.545	B 2	7425	4780	2900	389	0.285	0.366
	B 1-5	1	153	1.56	B 3	7500	5290	3070	396	0.274	0.359
Definitive tests.	A 3-1	3	459	1.24	A 1	7260	4920	3100	250	0.225	0.284
	A 3-2	3	459	1.25	A 1	7260	4920	3100	254	0.227	0.286
	A 3-3	3	459	1.24	A 1	7260	4920	3100	250	0.225	0.284
	A 3-4	3	459	1.26	A 1	7260	4920	3100	258	0.229	0.289
	AC 3-1	3	459	1.20	AC 1	6950	4560	2880	234	0.227	0.285
	AC 3-2	3	459	1.20	AC 1	6950	4560	2880	235	0.227	0.286
	BC 3-1	3	459	1.515	BC 1	6815	4920	2760	373	0.275	0.368
	BC 3-2	3	456	1.515	BC 1	6815	4920	2760	373	0.275	0.368
	C 3-1	3	459	2.05	C 1	7290	4830	2850	682	0.376	0.489
	C 3-2	3	459	2.05	C 1	7290	4830	2850	682	0.376	0.489
	CC 3-1	3	459	2.035	CC 1	6800	5160	2940	674	0.362	0.479
	CC 3-2	3	459	2.015	CC 1	6800	5160	2940	662	0.358	0.474
	D 3-1	3	459	2.99	D 1	7420	4360	2590	1460	0.579	0.750
	D 3-2	3	459	2.995	D 1	7420	4360	2590	1460	0.579	0.750

was used, having an accuracy of about 10 μ strain at a gauge factor of 2.00.

Strain-gauge measurements were also conducted on plate CC3 — 2 on the outer bays near the upper loaded edge in order to determine the influence of a possible non-parallelism of the loaded edges on the stress distribution in the plate. The same strain-gauge recorder was used.

4.4 *Dimensions of specimens.*

The length and the width of the bays and the possible number of bays were already established in section 4.1, the length being 700 mm, the width of the bays 150 mm, and the number of bays 5. Beyond the outer longitudinal supports small plate strips are necessary, thus giving the specimens a total width a small amount in excess of a multiple of the width of a bay. These plate strips must be taken as small as possible, otherwise appreciable errors can be introduced in the effective width.

The tests can be divided into two groups, the first containing specimens with different numbers of bays and the same thickness, and the second group consisting of specimens with the same number of bays and different thicknesses. The first group of tests (reported in ref. 1) was conducted to investigate the influence of the number of bays on the magnitude of the effective width. The second group (reported in ref. 2) covered a range of values of $\sqrt{\varepsilon_{cr}/\varepsilon_e}$ and was arranged only after the minimum number of bays was established from the former tests. This number of bays appeared to be three (see section 5.3).

The thicknesses of the specimens must be varied in such a way that the desired range of values of $\sqrt{\frac{\varepsilon_{cr}}{\varepsilon_e}}$ will be covered. With the known theoretical value of ε_{cr} for the case of the axially compressed plate with simply supported longitudinal edges, neglecting the influence of the finite length of the bays, the value of $\sqrt{\frac{\varepsilon_{cr}}{\varepsilon_e}}$ becomes

$$\sqrt{\frac{\varepsilon_{cr}}{\varepsilon_e}} = \frac{h}{b}\sqrt{\frac{\pi^2}{3(1-\nu^2)\,.\,\varepsilon_e}} \quad \text{for } \varepsilon_{cr} < \varepsilon_e\,. \tag{4.4}$$

With $\nu = 0.32$ and $b = 150$ mm it follows from (4.4) that

$$\sqrt{\frac{\varepsilon_{cr}}{\varepsilon_e}} = 0.0128\,\frac{h}{\sqrt{\varepsilon_e}}\,. \tag{4.5}$$

Table 4.1 contains the dimensions and some characteristic values of the specimens. It can be seen that the value of $\sqrt{\frac{\varepsilon_{cr}}{\varepsilon_e}}$ for the specimens of the first group ranges from 0.35 — 0.39. For the specimens of the second group the range of values of $\sqrt{\frac{\varepsilon_{cr}}{\varepsilon_e}}$ covered, lies between 0.28 and 0.75.

4.5 *Material of specimens.*

The material of the specimens will be either unclad or clad 24 S-T or 75 S-T.

The shape of the transition curve from the elastic to the plastic range in the $\sigma - \varepsilon$ graph is important in view of the influence of the plasticity on the e. w. Therefore it might be advantageous to compare the behaviour of specimens made from two materials which have a pronounced difference in this respect. This is the case with 24 S-T and 75 S-T. In fig. 4.11 two examples are given of curves for pure compression, the curve for 75 S-T being derived from ref. 27. The curvature in the graph for 24 S-T is smaller than for 75 S-T; with the latter material the value of $\frac{\sigma_{0.2}}{\sigma_e}$ is smaller than with the former. It can be expected therefore, that the transition from the elastic to the plastic region in the specimens will be most pronounced with 75 S-T.

The difference between unclad and clad sheet will also be a point of investigation. In clad sheet the basis material and the cladding material have about the same modulus of elasticity, but the elastic limit σ_e of the basis material is about 2—2.5 times the elastic limit of the cladding material.

The influence of the difference in the moduli of both materials on the buckling stress of a specimen was investigated in ref. 2, and this influence proved to be negligibly small. The influence of the difference in the elastic limits of both materials can be estimated in the same way. Consider the case that the buckling stress exceeds the elastic limit $\sigma_{e_{cl}}$. It is now assumed that during buckling the ratio of the bending stress in the cladding and the maximum bending stress of the basis material is equal to the ratio $\sigma_{e_{cl}}/\sigma_{e_{basis}}$, and if for the ratio of these stresses the minimum value $\frac{1}{2.3}$ is taken, then the difference in the buckling stress appears to be maximum 16 %. Hence the buckling stress of clad sheet can be up to 16 % smaller than the buckling stress of unclad sheet of the same thickness, if at the buckling stress the elastic limit of the cladding is exceeded.

In the first group of tests all specimens were made of unclad 24 S-T sheet. Most of the specimens of the second group were also made of 24 S-T, but for comparison some specimens were made of clad 24 S-T sheet. It is intended to investigate the behaviour of specimens made of 75 S-T sheet material in future tests.

The stress-strain curves for the material of each specimen in pure compression were determined with the solid-guide fixture described in ref. 28. These curves are plotted in fig. 4.12. The points on the stress-strain curves for the material of the cladded specimens at which the elastic limit of the cladding material is exceeded, could not be determined with good accuracy. These points lie for all curves at approximately $\varepsilon = 7\,.\,10^{-4}$. The decrease in slope of the curves beyond these points was too small to be drawn.

The first letter of the indication of the speci-

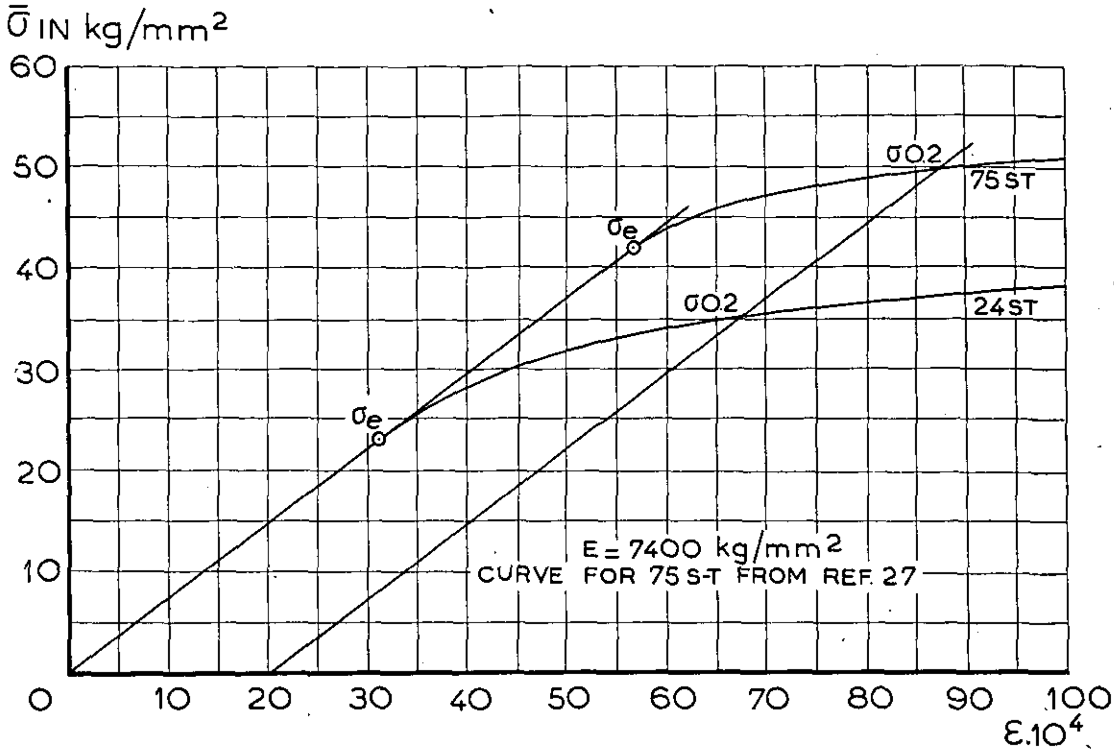

Fig. 4.11. Stress-strain curves for 24 S-T and 75 S-T in pure compression.

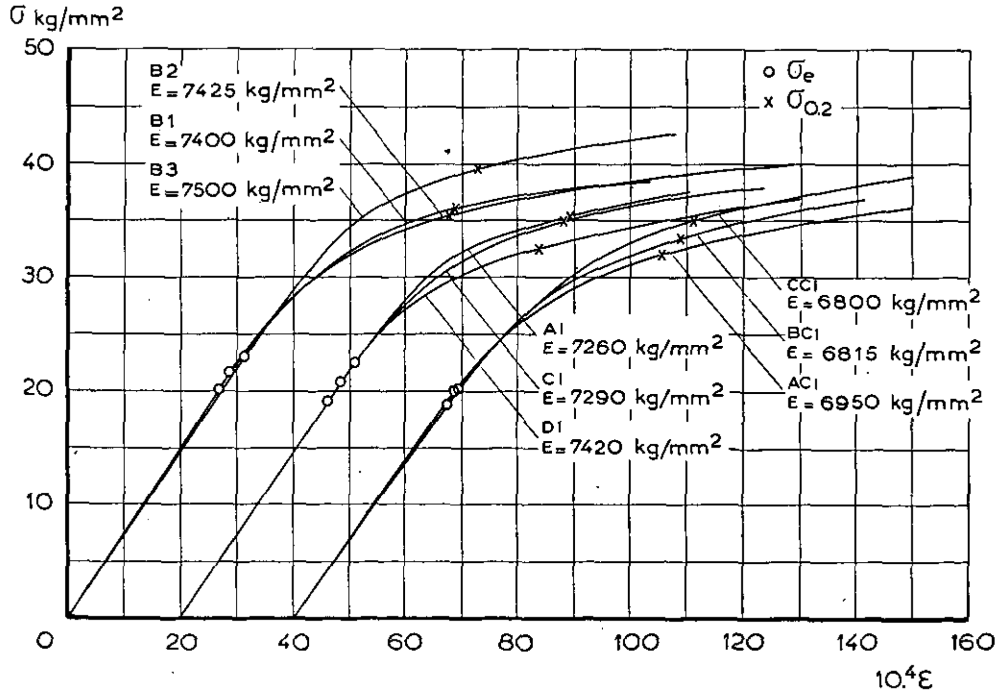

Fig. 4.12. Stress-strain relations of the material used in the tests.

mens refers to the nominal thickness of the plate: A = 1 mm, B = 1.5 mm, C = 2 mm, D = 3 mm. When the letter C is added, the specimen is made of clad sheet material. The first figure stands for the number of bays and the last figure for the number of the specimen, all tests except one being executed at least in duplicate.

5 Tests.

5.1 *Description of tests.*

The test programme has been divided into two groups, the first group referring to the preliminary tests, with which the possibilities of the test arrangement and the number of bays of the specimens were determined, and the second group referring to the definitive tests (see also sections 4.4 and 4.5). The tests from both groups will be described successively.

5.1.1 *Preliminary tests.*

According to table 4.1 the value of $\sqrt{\dfrac{\varepsilon_{cr}}{\varepsilon_e}}$ for these specimens ranges from 0.35 to 0.39. On account of the results of section 3.5 it can be expected that the elastic limit first will be exceeded *at the longitudinal edges of the bays.* In view of the possibility of local buckling at the edges, the thickness chosen will, therefore, be unfavourable for the determination of the e. w. in the plastic range. For the appreciation of the loading arrangement, however, this can be regarded as an advantage.

In general all specimens showed, before buckling, irregular waves with a very small amplitude, possibly because of the play at the knife-edge supports. For load in excess of the buckling load the waves were generally regular. In most of the tests, the buckle amplitudes at top and bottom of the test specimen were approximately equal up to the maximum load, indicating that friction between the plate and the knife-edges was small. Buckling always occurred suddenly, but only with specimen B 3-3 this was attended with bangs. With all specimens, except those consisting of one bay, sudden changes in wave form occurred at high loads in excess of the buckling load. This jump to smaller wave lengths was also often accompanied by bangs. With long delayed changes in wave length, as with specimen B 5-2, the bang was very loud and the change in wave length was attended with a sudden drop in the load. With the sliding pieces on the knife-edges (fig. 4.5 - *c*) applied in the later tests, a more gradual transition to a smaller wavelength was obtained, resulting in less heavy bangs.

In some tests irregular waves appeared in adjacent bays of the specimen. These waves, pointing to the same side in adajcent bays, exerted large forces on the knife-edges and caused permanent deformation of the loading frame.

Figs. 5.1—5.3 incl. show the permanent deformation of some of the specimens after unloading. It is seen that in general the permanent deformations were most severe near the upper loaded edge of the test specimen.

5.1.2 *Definitive tests.*

It was decided to use in the definitive tests specimens with three bays only. Thus the parts at the outer bays of the frame supporting the knife-edges were not required any more. These parts were used, therefore, for a direct connection of both halves of the frame with bolts, making the extra construction shown in fig. 4.4 superfluous. A more rigid frame was obtained in this way.

Before the tests the knife-edges were straightened again. For the knife-edges the construction shown in fig. 4.5 - *d* was used. These knife-edges performed more satisfactorily. Large loads on the knife-edges and local buckling in the plates at the edges could, however, not be prevented completely. Permanent buckles after unloading were in general present over a larger part of the plate length than in the preliminary tests and during the tests the same phenomena were observed.

In figs. 5.4—5.8 incl. photographs of some specimens after the tests are shown. Some points, in which local buckling occurred, are encircled and buckles pointing towards the same side are indicated with crosses.

5.2 *Evaluation of test results.*

By representing the relation between the average stress $\bar{\sigma}$ in a bay and the specific shortening ε in the way developed in ref. 3, the results of the tests can be compared with the results of the theory for the elastic range.

The e. w. b_m is defined by the expressions for the load P in a bay.

$$P = \bar{\sigma} \,.\, bh = \sigma_{\text{edge}} \,.\, b_m \,.\, h. \tag{5.1}$$

Hence

$$\frac{b_m}{b} = \frac{\bar{\sigma}}{\sigma_{\text{edge}}}. \tag{5.2}$$

The edge stress σ_{edge} can be calculated from the specific shortening of the plate

$$\sigma_{\text{edge}} = E_s \,.\, \varepsilon\,, \tag{5.3}$$

while the average stress $\bar{\sigma}$ follows from P with (5.1). Thus the ratio $\dfrac{b_m}{b}$ can be calculated from the measured $P - \varepsilon$ curve. The result will be plotted against $\sqrt{\dfrac{\varepsilon_{cr}}{\varepsilon}}$, instead of ε, then being comparable with the theoretical result for the elastic range from ref. 3.

The presence of the small plate strips beyond the outer longitudinal edges introduces an error in the average stress, which can be approximated by

$$\Delta\bar{\sigma} = \frac{P}{A} - \frac{P - 2\, dh \,.\, \sigma_{\text{edge}}}{nbh} \approx \frac{2\, d}{nb}\, \sigma_{\text{edge}}\,, \tag{5.4}$$

in which n represents the number of complete bays, and d is the width of the edge strips. The width d can be chosen such, that this error can be neglected.

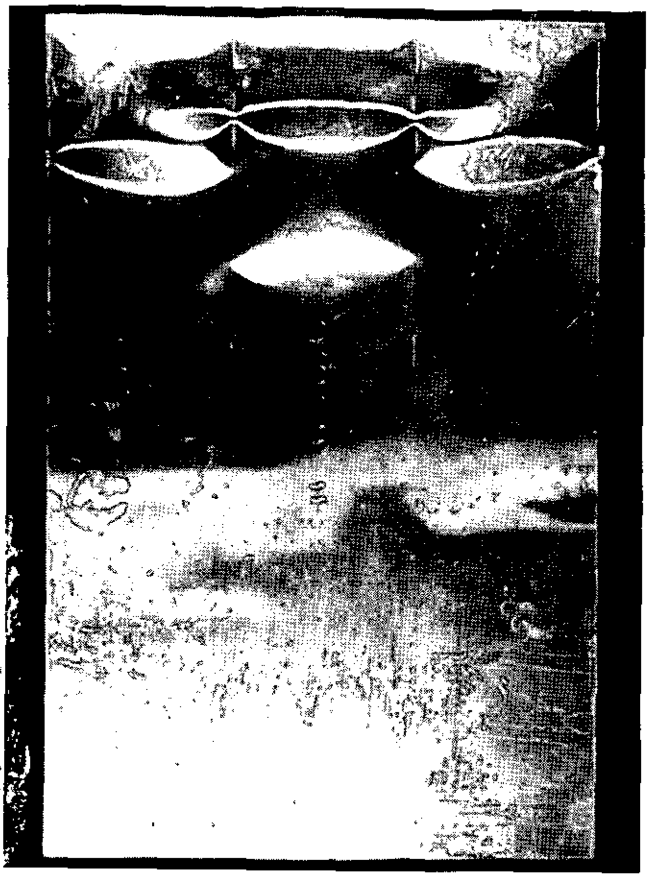

Fig. 5.1. Permanent deformation of specimen B 3-3.

Fig. 5.3. Permanent deformation of specimen B 3-2.

Fig. 5.2. Permanent deformation of specimen B 5-2.

Fig. 5.4. Permanent deformation of specimen A 3-1.

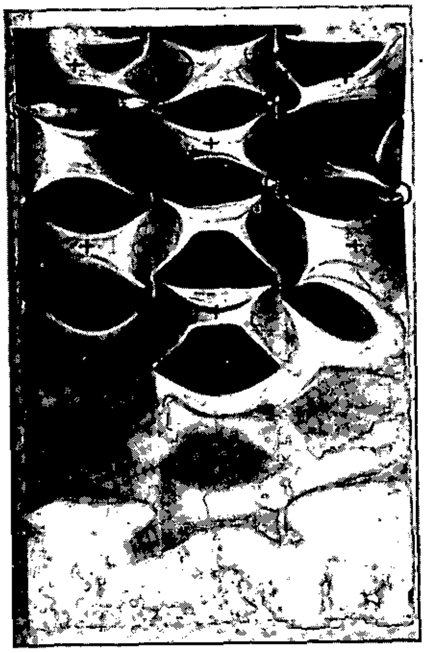

Fig. 5.5 Permanent deformation of specimen AC 3-2.

Fig. 5.6. Permanent deformation of specimen BC 3-2.

Fig. 5.7. Permanent deformation of specimen C 3-1.

Fig. 5.8. Permanent deformation of specimen D 3-1.

The edge stress is determined from the stress-strain curve of the material at the specific shortening of the edges. This stress does not occur in reality, for the state of stress near the longitudinal edges is not uniaxial.

The average specific shortening of the plate follows from the measured displacement of the loaded edges with respect to each other, divided by the plate length. When friction is present between the knife-edges and the plate, the load in lower sections of the plate will be smaller than in upper sections. However, with sufficiently low friction this difference can be regarded as negligible, and thus the specific shortening at the edges will be equal to the average specific shortening of the specimen.

The theoretical value of the buckling strain ε_{cr} will be calculated from the well-known formula (see ref. 3)

$$\varepsilon_{cr} = \frac{\pi^2}{3(1-\nu^2)} \cdot \left(\frac{h}{b}\right)^2. \qquad (5.5)$$

Strictly, this formula holds good only when no transverse stiffening is present, when all edges of the plate are simply supported, when the elastic limit of the material is not exceeded, and for $a = nb$ in which n represents an integer. For the chosen length-width ratio of the bays $\frac{a}{b} = 4.67$ the departure from formula (5.5) is, however, very small, even when the loaded edges are not simply supported but clamped.

The theoretical buckling stress follows from (5.5) with

$$\sigma_{cr} = E \,.\, \varepsilon_{cr}\,. \qquad (5.6)$$

Like (5.5) this formula holds good only in the elastic range of the material.

An experimental buckling load can be derived from the amplitude measurements. For loads in excess of the buckling load the only parameter governing the behaviour of the plate is the ratio $\frac{W}{L}$. Because the load in the plate must be independent from the sign of W, the load in the plate can be expressed by

$$P = P_{cr}\left[1 + a_1\left(\frac{W}{L}\right)^2 + \right.$$
$$\left. + a_2\left(\frac{W}{L}\right)^4 + \ldots\right] \text{ for } P > P_{cr}. \qquad (5.7)$$

For loads in small excess of the buckling load the graph showing the relation between P and $\left(\frac{W}{L}\right)^2$ will be substantially linear and the intersection with the load axis will give the experimental buckling load. Instead of P the average stress $\bar{\sigma}$ can be plotted, thus giving directly the experimental buckling stress.

The relation between $\frac{b_m}{b}$ and $\sqrt{\frac{\varepsilon_{cr}}{\varepsilon}}$ in the plastic range may be dependent of the value of $\sqrt{\frac{\varepsilon_{cr}}{\varepsilon_e}}$ and of the general form of the stress-strain curve of the material. For values of $\sqrt{\frac{\varepsilon_{cr}}{\varepsilon}}$ larger than $\sqrt{\frac{\varepsilon_{cr}}{\varepsilon_e}}$ the experimental results must correspond with the theoretical curve for the elastic range shown in fig. 5.9.

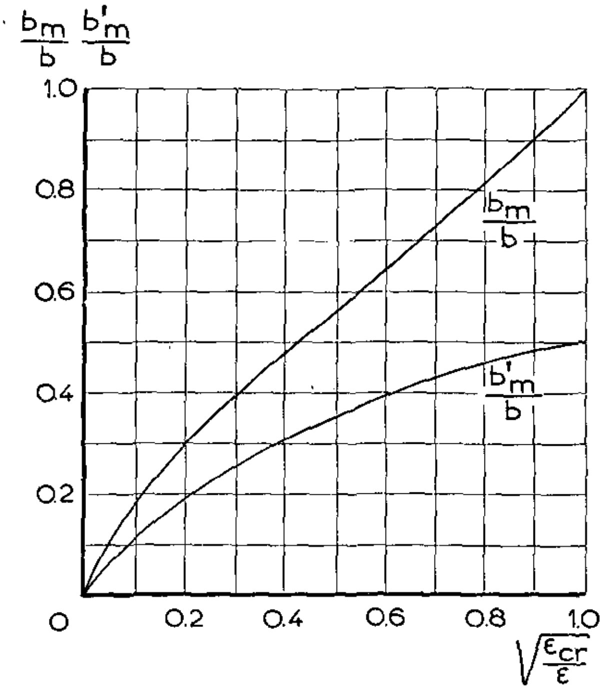

Fig. 5.9. Theoretical curve for the effective width in the elastic range (form ref. 3).

The theoretical curve for the e. w. b_m' in the elastic range is also given in fig. 5.9. The e. w. b_m' in view of the compressive stiffness of the plate is defined in the elastic range by

$$\frac{dP}{d\varepsilon} = E \,.\, hb_m'. \qquad (5.8)$$

For readers not familiar with the effective width b_m' a more detailed description of this quantity is given in Appendix A.

The relation between b_m' and b_m can be derived by differentiation of (5.1).

$$\frac{dP}{d\varepsilon} = h\left(\frac{d\sigma_{\text{edge}}}{d\varepsilon}\, b_m + \sigma_{\text{edge}}\, \frac{db_m}{d\varepsilon}\right) =$$
$$= Eh\left(b_m + \varepsilon\, \frac{db_m}{d\varepsilon}\right). \qquad (5.9)$$

Equating (5.8) and (5.9) gives

$$\frac{b_m'}{b} = \frac{b_m}{b} + \varepsilon \frac{d\frac{b_m}{b}}{d\varepsilon}. \qquad (5.10)$$

These equations hold, however, only for the elastic range.

In the plastic range equation (5.9) becomes

$$\frac{dP}{d\varepsilon} = h\left(E_t \,.\, b_m + E_s \,.\, \varepsilon\, \frac{db_m}{d\varepsilon}\right) =$$
$$= E_t\, h\left(b_m + \frac{E_s}{E_t}\, \varepsilon\, \frac{db_m}{d\varepsilon}\right). \qquad (5.11)$$

Defining now b_m' by replacing E in eq. (5.8) by the tangent modulus E_t, equation (5.10) becomes.

$$\frac{b_m'}{b} = \frac{b_m}{b} + \frac{E_s}{E_t}\,\varepsilon\,\frac{d\dfrac{b_m}{b}}{d\varepsilon}. \qquad (5.12)$$

The relation between $\frac{b_m'}{b}$ and ε or $\sqrt{\frac{\varepsilon_{cr}}{\varepsilon}}$ can be calculated from the $\frac{b_m}{b} - \sqrt{\frac{\varepsilon_{cr}}{\varepsilon}}$ curve with formula (5.10) or (5.12). Since this calculation requires a differentiation of the empirical curve for b_m/b and of the stress-strain curve of the material, the accuracy of b_m'/b may not be expected to be high.,

The ultimate results of the tests will be given in graphs showing the relation between the ratios $\frac{b_m}{b}$ and $\frac{b_m'}{b}$ and the ratio $\sqrt{\frac{\varepsilon_{cr}}{\varepsilon}}$. These graphs are applicable only for the specific material, and the values of $\sqrt{\frac{\varepsilon_{cr}}{\varepsilon_e}}$ used in the tests. Thus $\sqrt{\frac{\varepsilon_{cr}}{\varepsilon_e}}$ will appear in these graphs as a parameter. Because it is difficult to determine the value of ε_e with good accuracy, the ratio $\sqrt{\frac{\varepsilon_{cr}E}{\sigma_{0\cdot2}}}$ has also been given for each specimen (see table 4.1) as a characteristic parameter.

It would not be very useful to continue the tests above a certain value of the strain, because in compressed panels the strain will also be restricted to the maximum strain at which the stiffeners fail. For this maximum value of the strain $9000\,\mu$ strain was chosen, this being the strain at which $\sigma_{0.2}$ will be reached in 75 S-T (see fig. 4.11). The stress $\sigma_{0\cdot2}$ in 24 S-T will then be exceeded considerably, and this strain will certainly not be reached in panels with stiffeners and plate made of 24 S-T. The tests on specimens of 24 S-T will, however, be continued up to a strain of $9000\,\mu$, in view of constructions in which the stiffeners are made of 75 S-T and the plates of 24 S-T.

5.3 *Results of measurements.*

The results of the wave form measurements for some of the specimens are shown in figs. 5.10—5.13 incl. The results of the amplitude and deformation measurements for some of the specimens are given in figs. 5.14, 5.15, and 5.16. The strain gauge measurements will be dealt with in section 5.4.

On closer inspection of the wave-form measurements it appears that large differences in the wave length and the location of the nodes can occur in different specimens for loads in small excess of the buckling load. From ref. 29 it is known that with clamped edges the transition from m to $m+1$ half waves will take place at a length-width ratio of

$$\frac{a}{b} = \sqrt{m(m+2)}\ . \qquad (5.13)$$

In the present tests $\frac{a}{b} = 4.67$ (see section 4.1). Thus for loads in small excess of the buckling load 4 half waves should be present, because $\sqrt{4(4+2)} = 4.90$. In the experiments, however, nearly always 5 half waves appeared.

With simply supported loaded edges the transition from 4 to 5 half waves takes place at $\frac{a}{b} = 4.47$. From this it can, however, not be concluded, that the loaded edges in the flat-end tests were not completely clamped, because the theoretical wave form was not fully realised. Some irregular differences in wave length occurred along the length of the bay. The magnitude of the slope of the waves next to the loaded edges does suggest, however, that at least for loads far in excess of

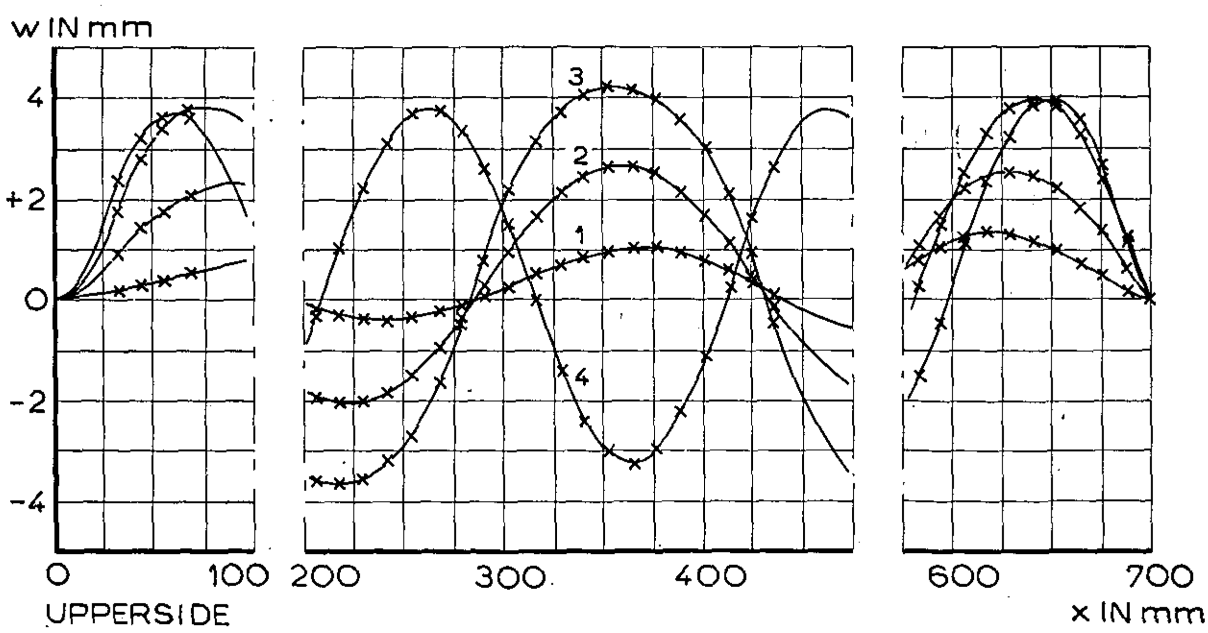

Fig. 5.10. Wave-form measurements for specimen B 5-2.

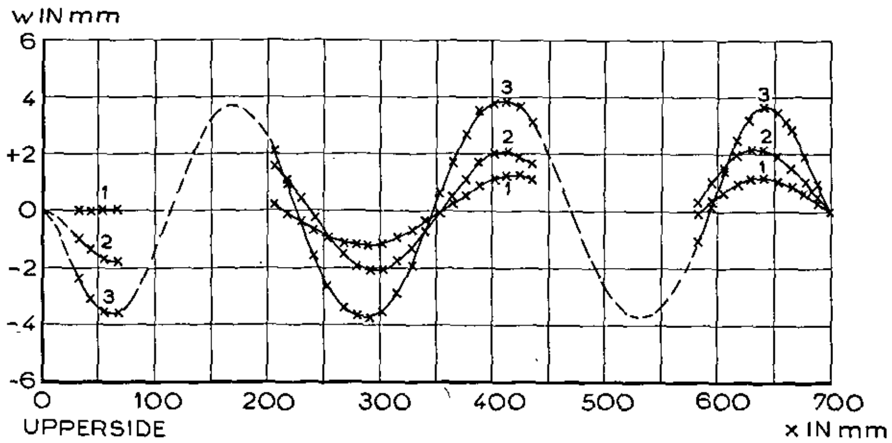

Fig. 5.11. Wave-form measurements for specimen A 3-1.

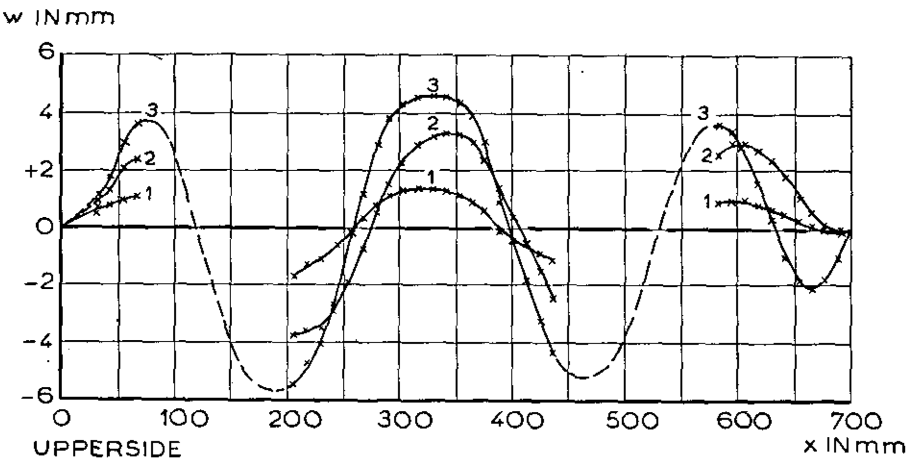

Fig. 5.12. Wave-form measurements for specimen BC 3-2.

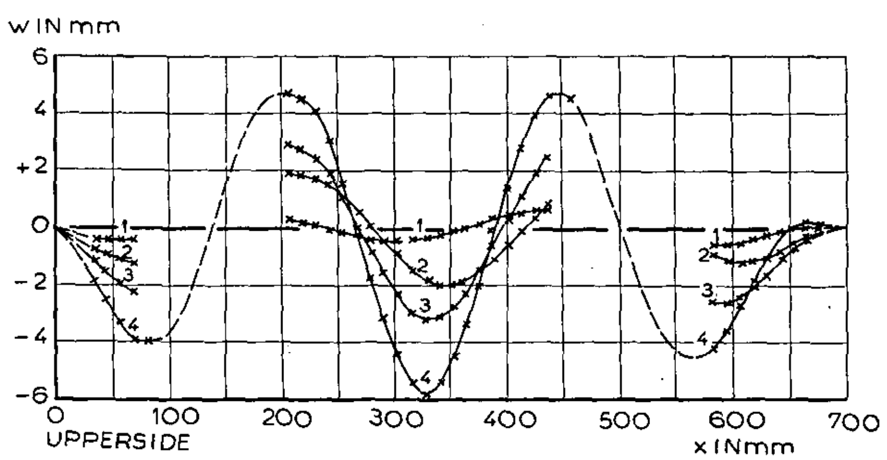

Fig. 5.13. Wave-form measurements for specimen D 3-1.

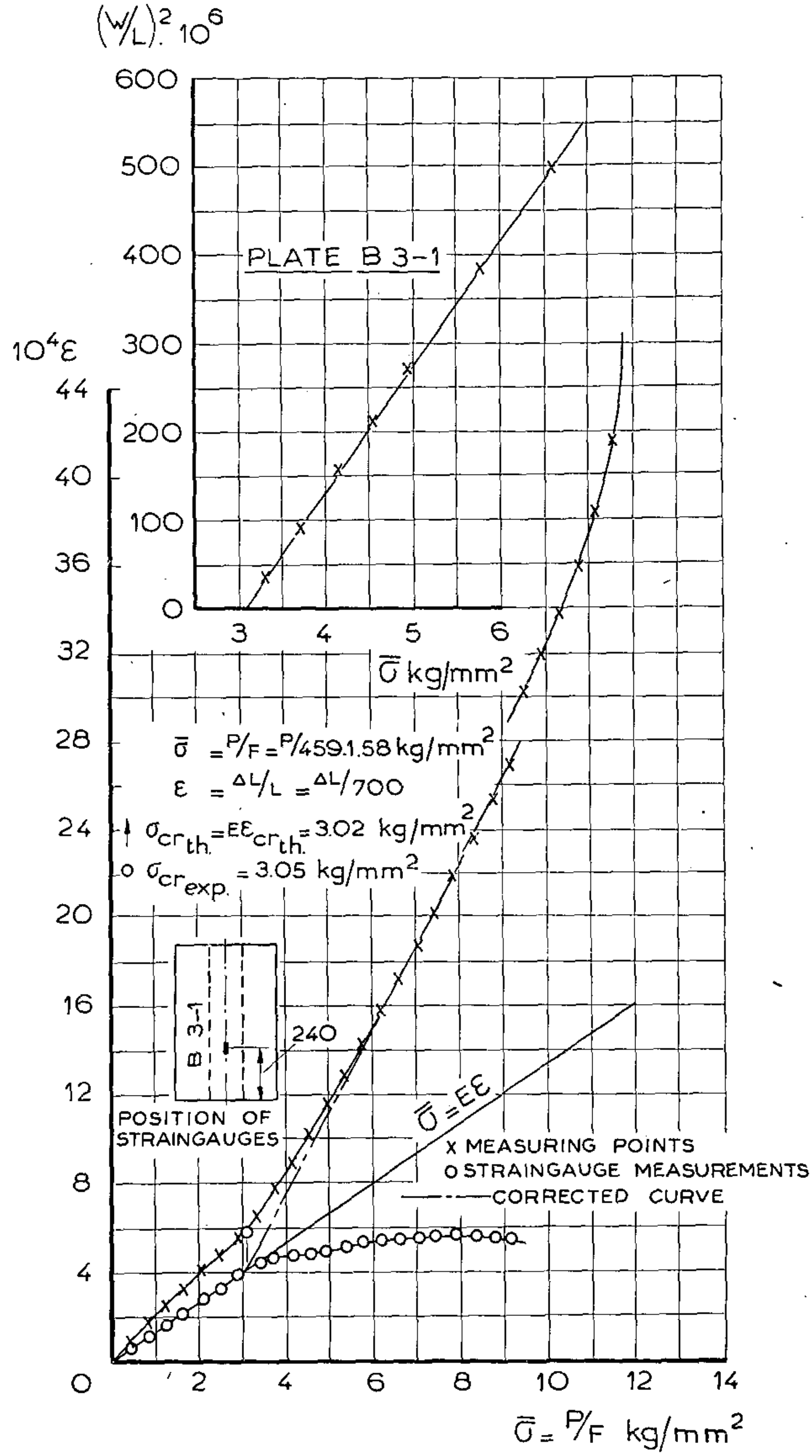

Fig. 5.14. Results of amplitude- and deformation measurements for specimen B 3-1.

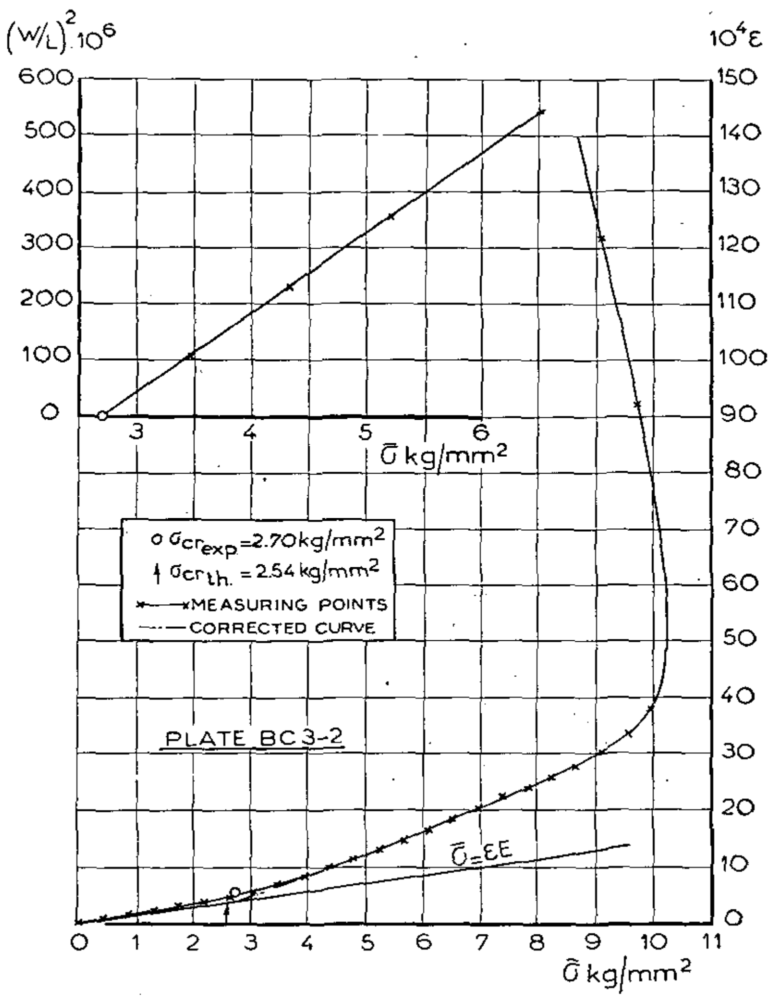

Fig. 5.15. Results of amplitude- and deformation measurements for specimen BC 3-2.

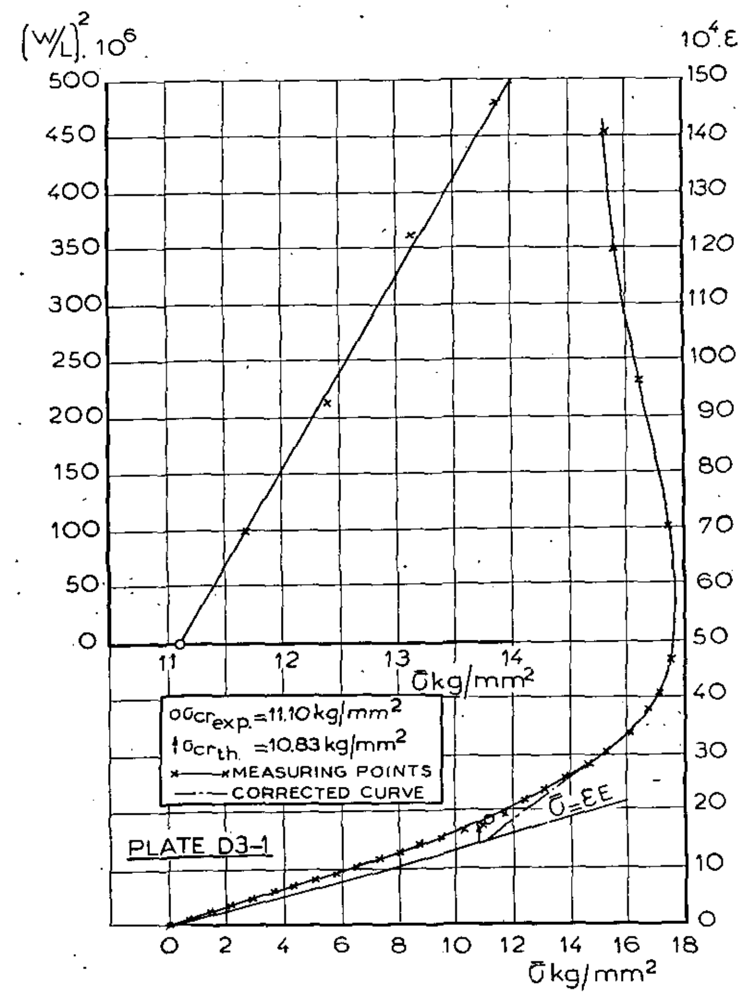

Fig. 5.16. Results of amplitude- and deformation measurements for specimen D 3-1.

the buckling load the loaded edges were not completely clamped.

For specimens B 3-1, B 5-1, B 3-3 and B 5-2 of the preliminary tests and for all specimens of the definitive tests the experimental buckling stress was determined from the $\bar{\sigma} - \left(\frac{W}{L}\right)^2$ graphs. These graphs proved to be straight lines in nearly all cases. In general the experimental buckling stresses were somewhat higher than the theoretical values derived from formulas (5.5) and (5.6). Except in the cases of specimens B 3-3, A 3-2, and AC 3-1, this difference was always less than 10 %. Probably the cause will lie mainly in the small number of values of $\frac{W}{L}$ for small loads, and in the inaccuracy with which the wave length has been determined. Some measuring results at low loads were omitted from the graphs, because they were regarded as unreliable.

The relation between the average stress and the shortening of the specimen does not equal the stress-strain relation of the material for loads below the buckling load (see also the results of the strain gauge tests discussed in section 5.4.3). The prebuckling stiffness of the plate was smaller than the theoretical stiffness of a completely flat plate. Part of this decrease in stiffness is caused by the play at the knife-edge supports. Irregularities in the stress-strain curves in the neighbourhood of the origin are also caused by the fact that the loaded edges are not perfectly parallel. Hence before the $\bar{\sigma} - \varepsilon$ curves were used for the evaluation of the e. w., some corrections had to be introduced. These corrections will be discussed in section 5.4.

A sudden change in wave-form will appear in the $\bar{\sigma} - \varepsilon$ curve as a discontinuity (see fig. 5.14). These changes did not occur with specimens consisting of one bay, probably because no stresses were present along the longitudinal edges in the lateral direction.

The area of the plate strips beyond the outer longitudinal supports was such, that the difference between the average stress across the whole specimen and the average stress after correction for the load in the plate strips (see section 4.3) could be neglected. For example, for plate B 3-2 at the maximum load this difference amounts to $\Delta \bar{\sigma} = 0.42$ kg/mm², according to (5.4).

The measurements in the range of loads in excess of the maximum load appeared in the preliminary tests to be irregular, and they were, except in the case of specimen B 3-2, regarded as unreliable. In the definitive tests the measurements in this range were more satisfactory, probably because of less friction at the edges.

From the corrected $\bar{\sigma} - \varepsilon$ curves and the stress-strain relations of the material the ratio $\frac{b_m}{b}$ was calculated for a number of values of $\frac{\varepsilon_{cr}}{\varepsilon}$. The experimentally determined value of ε_{cr} was used when available, except for the specimens A 3-2, A 3-4, and AC 3-1, for which the experimental values were regarded as unreliable. The results of these calculations are shown together with the theoretical curves for $\frac{b_m}{b}$ in the elastic range (from ref. 3) in figs. 5.17—5.23 incl.

From the obtained relation between $\frac{b_m}{b}$ and $\sqrt{\frac{\varepsilon_{cr}}{\varepsilon}}$ the ratio $\frac{b_m'}{b}$ was calculated with formula (5.12). These curves are also given in the figs. 5.18—5.23 incl., together with the theoretical curve for $\frac{b_m'}{b}$ in the elastic range. The value of the parameter $\sqrt{\frac{\varepsilon_{cr}}{\varepsilon_e}}$ has been given in the figures for each curve of $\frac{b_m'}{b}$, these curves appearing to be dependent on this parameter.

The curves in figs. 5.18—5.23 incl. differ from those given in ref. 2. In that report the curves for $\frac{b_m'}{b}$ were calculated with formula (5.10), which gave erroneous results in the plastic range. These errors were corrected here.

The differences between the experimental results of $\frac{b_m}{b}$ in the figs. 5.17—5.23 incl. and the theoretical curves from ref. 3, appear to be small for the plastic range when the specimens had 3 or more bays. The differences are generally larger in the elastic range, which can be easily explained by supposing that the correction of the $\bar{\sigma} - \varepsilon$ curves for stresses in excess of the buckling stress is not exactly true. This holds especially for stresses in small excess of the buckling stress. A small change in $\bar{\sigma}$ will then cause a large change in the e. w.

The deviation of the experimental results for $\frac{b_m'}{b}$ from the theoretical curve in the elastic range is sometimes considerable. For values of $\sqrt{\frac{\varepsilon_{cr}}{\varepsilon}}$ smaller than $\sqrt{\frac{\varepsilon_{cr}}{\varepsilon_e}}$ this is not surprising, because the $\frac{b_m'}{b}$ curve must have an intersection with the $\sqrt{\frac{\varepsilon_{cr}}{\varepsilon}}$ axis in this region, as will be explained in section 5.5. Thus the experimental results for $\frac{b_m'}{b}$ in this region cannot be compared with the theoretical curve for $\frac{b_m'}{b}$ in the elastic range. For values of $\sqrt{\frac{\varepsilon_{cr}}{\varepsilon}}$ larger than $\sqrt{\frac{\varepsilon_{cr}}{\varepsilon_e}}$ the results for $\frac{b_m'}{b}$ show the irregularities in the results for $\frac{b_m}{b}$, these irregularities being especially in this region more prominent than in the remain-

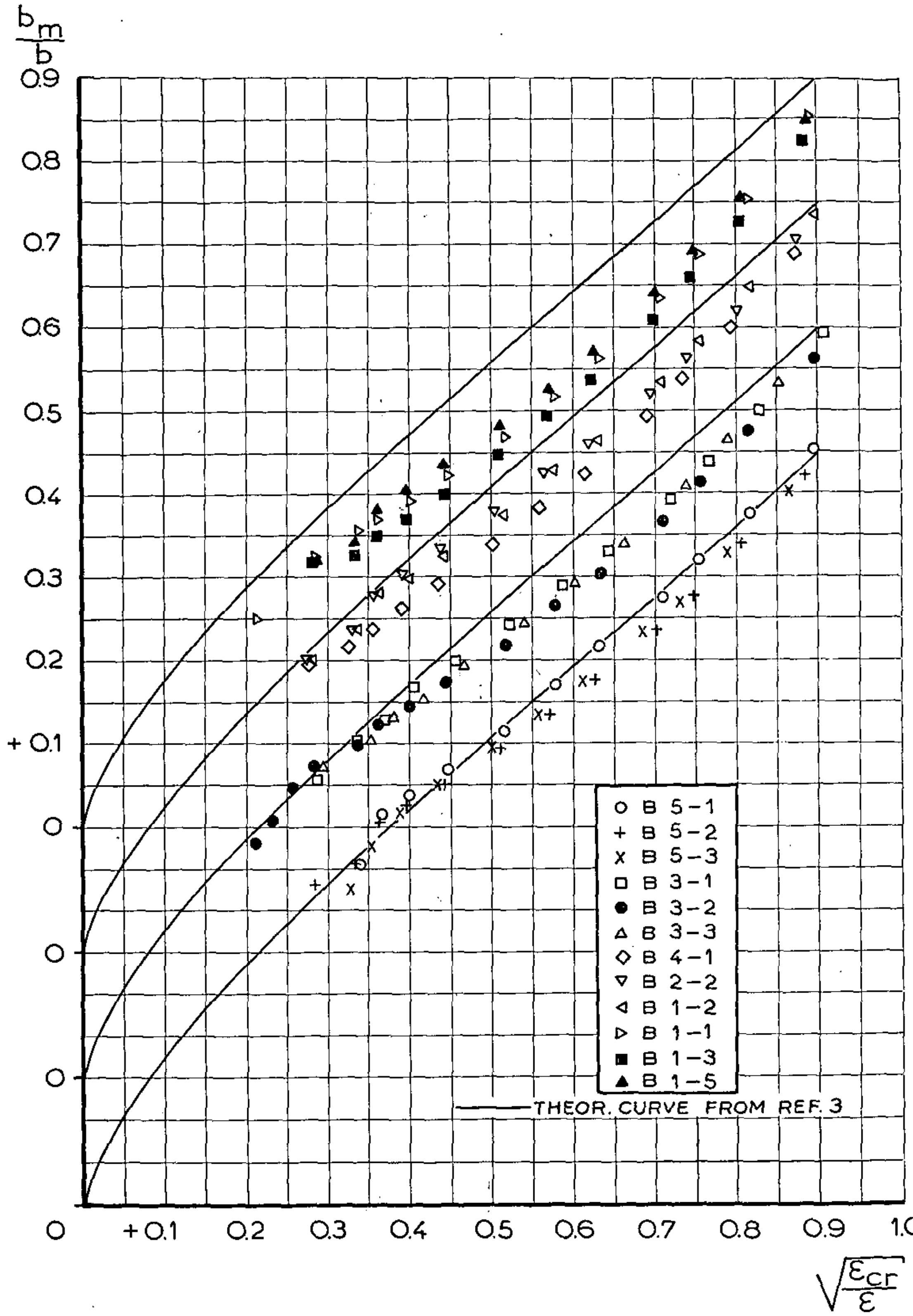

Fig. 5.17. Comparison of the results for the effective width from the preliminary tests with the theoretical curve for the effective width in the elastic range.

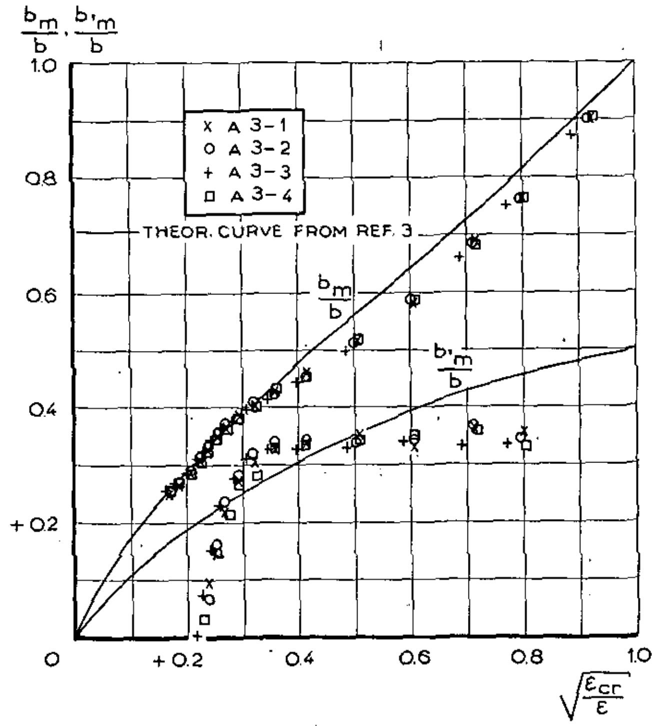

Fig. 5.18. Comparison of the results for the effective width for the specimens A 3-1 to A 3-4 incl. with the theoretical curve for the effective width in the elastic range.

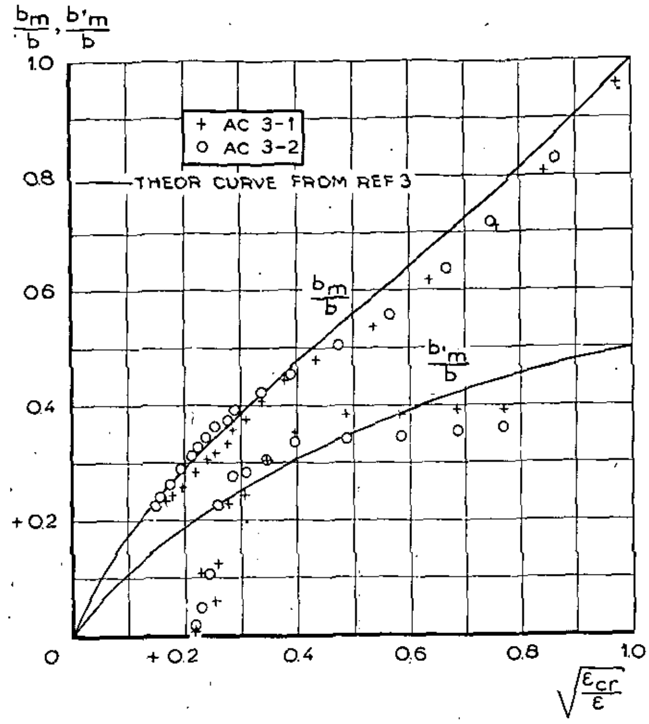

Fig. 5.19. Comparison of the results for the effective width for the specimens AC 3-1 and AC 3-2 with the theoretical curve for the effective width in the elastic range.

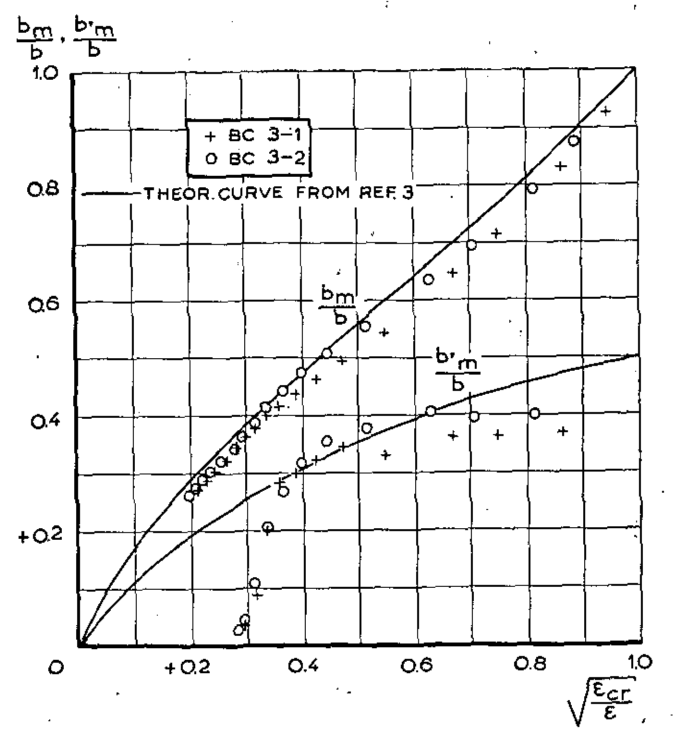

Fig. 5.20. Comparison of the results for the effective width for the specimens BC 3-1 and BC 3-2 with the theoretical curve for the effective width in the elastic range.

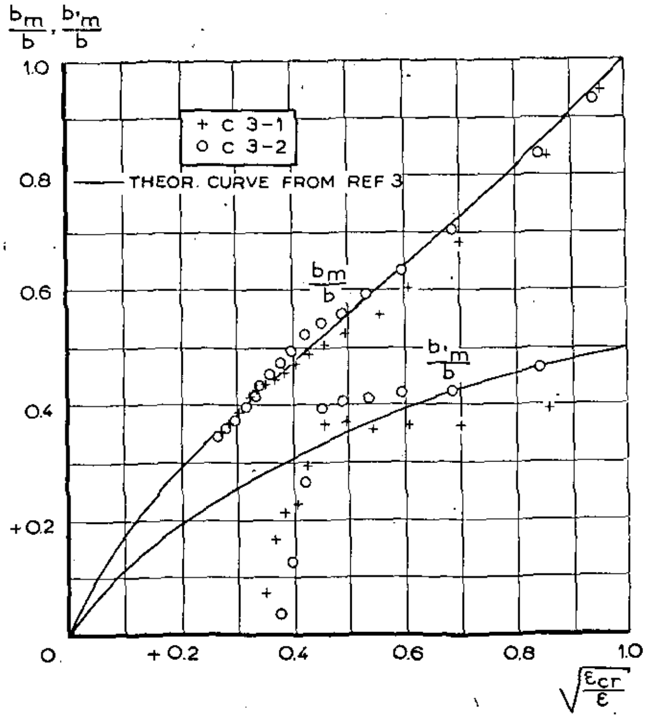

Fig. 5.21. Comparison of the results for the effective width for the specimens C 3-1 and C 3-2 with the theoretical curve for the effective width in the elastic range.

ing part of the $\frac{b_m}{b}$ curve. Errors in the results of $\frac{b_m'}{b}$ will also be introduced due to the numerical approximation of the differentiation in (5.12).

The influence of the accuracy of the buckling stress, and with that of the buckling strain, on the measuring results can be considerable. The inaccuracy of $\sqrt{\frac{\varepsilon_{cr}}{\varepsilon}}$ will be about twice the inaccuracy of ε_{cr}. When the experimental values of $\sqrt{\frac{\varepsilon_{cr}}{\varepsilon}}$ for a certain specimen appear to deviate for all values of $\frac{b_m}{b}$ with a constant percentage from the theoretical values of $\sqrt{\frac{\varepsilon_{cr}}{\varepsilon}}$, the reason for this difference may lie in a wrong value of ε_{cr}. It was doubtful whether the edge conditions for the determination of the buckling stress of a plate which is simply supported on 4 edges, were satisfied in the tests. Thus the theoretical buckling stress cannot be regarded as completely reliable, and therefore the experimentally derived buckling stress was used as much as possible for the evaluation of the results. Nevertheless with some specimens, of which the accuracy of the experimental buckling stress appeared to be good (e. d. D 3-2), this tendency of the experimental values of $\sqrt{\frac{\varepsilon_{cr}}{\varepsilon}}$ to deviate from the theoretical values of $\sqrt{\frac{\varepsilon_{cr}}{\varepsilon}}$ with a constant percentage, was still observed. Hence, it is probable that the experimental buckling stress was somewhat in error. For specimen D 3-2, for example, $\sigma_{cr_{exp}}$ was found to be about 2 % larger than $\sigma_{cr_{th}}$. If the values of $\sqrt{\frac{\varepsilon_{cr}}{\varepsilon}}$ for specimen D 3-2 in fig. 5.23 had been taken about 4 % smaller, the experimental result would have been closer to the theoretical curve. It seemed, however, to be more correct not to work towards this goal.

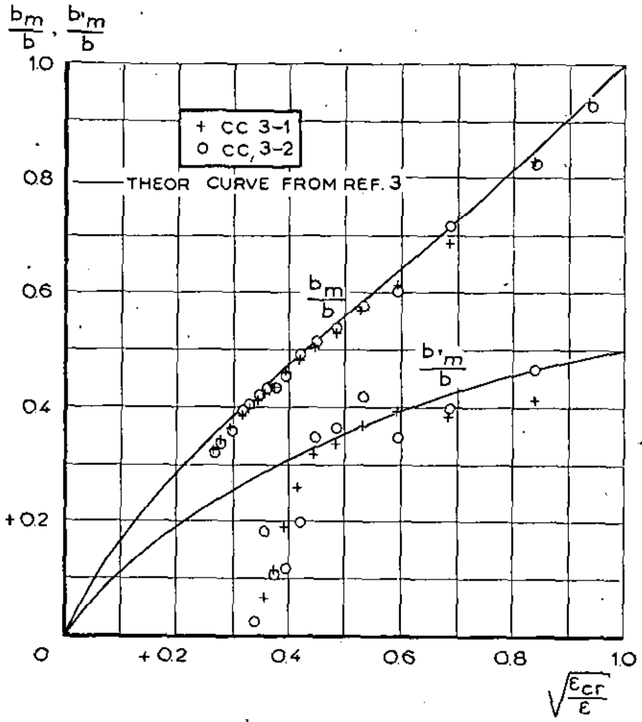

Fig. 5.22. Comparison of the results for the effective width for the specimens CC 3-1 and CC 3-2 with the theoretical curve for the effective width in the elastic range.

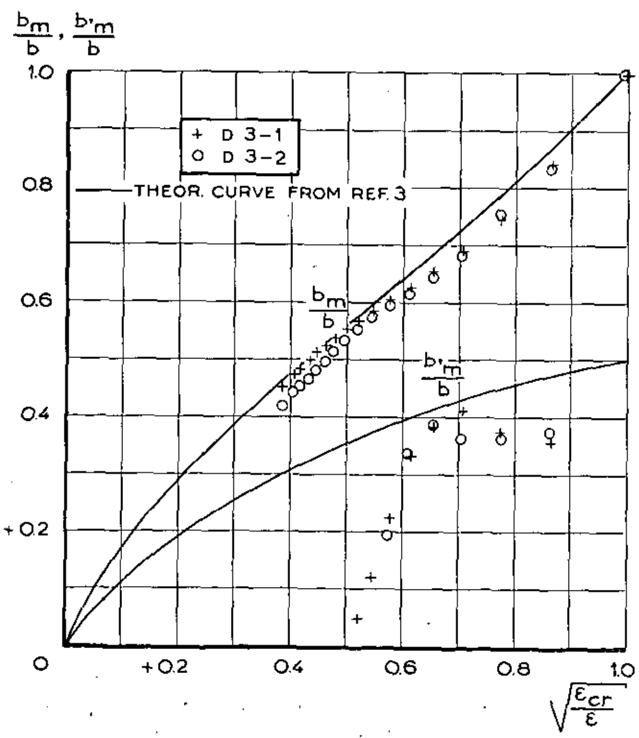

Fig. 5.23. Comparison of the results for the effective width for the specimens D 3-1 and D 3-2 with the theoretical curve for the effective width in the elastic range.

The agreement of the results from the preliminary tests with the theoretical curve for the elastic range proves to be good especially for the specimens with 5 and 3 bays. The influence of the number of bays is shown clearly. The exception of specimen B 4-1 in this respect will be due to the unfavourable circumstances in which the test was carried out. From the small difference between the results of specimens with 3 and 5 bays the conclusion was drawn, that for the specimens of the definitive tests 3 bays were sufficient.

5.4 *Considerations and secondary measurements concerning the behaviour of the specimens.*

5.4.1 *Friction at loaded edges.*

In order to determine the influence of the friction at the loaded edges of the specimens, and whether this friction could be reduced sufficiently by means of lubrication with graphite grease, a number of strain-gauge tests were conducted on specimen B 5-1. On both sides of the plate 4 resistance wire strain-gauges were glued in lateral direction on 4 stations of the center line of the middle bay (see fig. 5.24). Opposite strain-gauges were connected in series, hence the average strain in the lateral direction was measured only. The strain gauge pairs 1—4 incl. were connected successively to the indicator by means of the circuit shown in fig. 5.24.

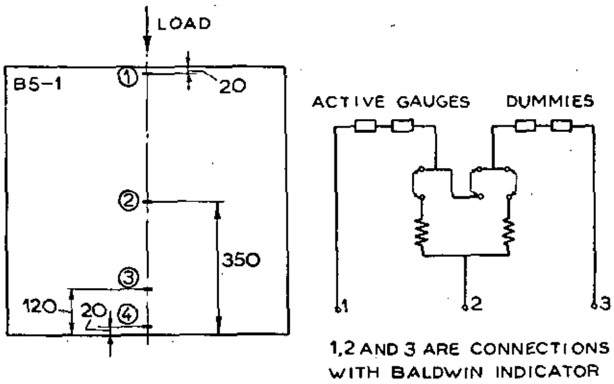

Fig. 5.24. Position of strain gauges on specimen B 5-1 and the circuit used in the tests.

load, because otherwise irregularities in the strain would appear, which would mostly be determined by the local wave form. Furthermore the strains in the lateral direction are very small. Therefore, and because of the limited accuracy of the measuring equipment, but a rough picture of the magnitude of the strains can be obtained.

The results of some measurements are presented in fig. 5.25. The increase of the lateral strain, indicated with $\Delta\varepsilon_y$, is shown as a function of the strain in the longitudinal direction ε_x. Measurements were started at $\varepsilon_x = 100.10^{-6}$ strain. The decrease of friction after lubrication of one or both of the loaded edges can be seen clearly. The straight lines drawn in the figures represent the relation between $\Delta\varepsilon_y$ and ε_x in the case that the specimen remains flat and that no transverse stiffening is present. The measuring results for specimens with both loaded edges lubricated lie sufficiently close to this line to regard the influence of friction as unimportant. Thus $\left(\frac{A_s}{ah}\right)_{\text{frict.}} = 0.$

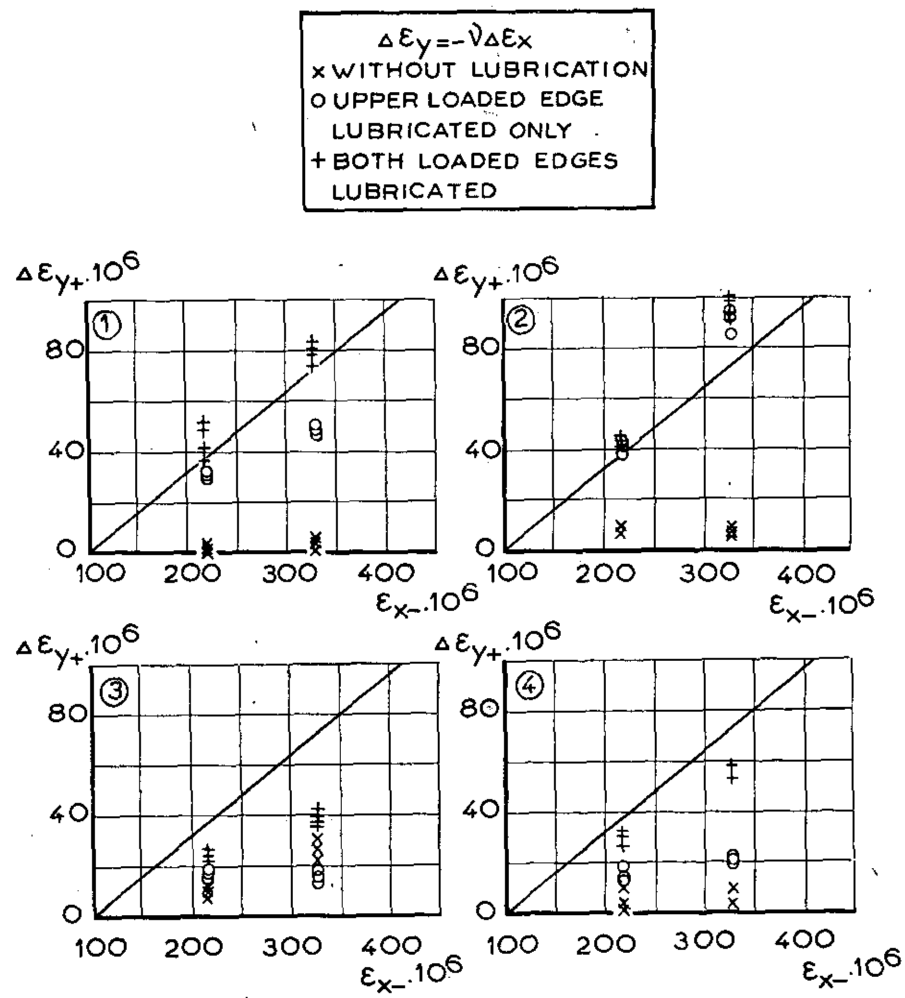

Fig. 5.25. Results of strain gauge measurements on specimen B 5-1.

Strains were measured with and without lubrication of the loaded edges and with lubrication of the upper loaded edge only.

The range in which measurements can be carried out, is restricted to loads lower than the buckling

For a more accurate determination of the influence of the friction at the loaded edges on the stress distribution in the plate four pairs of strain gauges are not sufficient.

5.4.2 *Parallelism of loaded edges.*

The $\bar{\sigma} - \varepsilon$ curves of the specimens showed in the neighbourhood of the origin a departure of the expected straight line (see fig. 5.26). This departure appears to be caused by irregularities in the compressive stresses on the loaded edges.

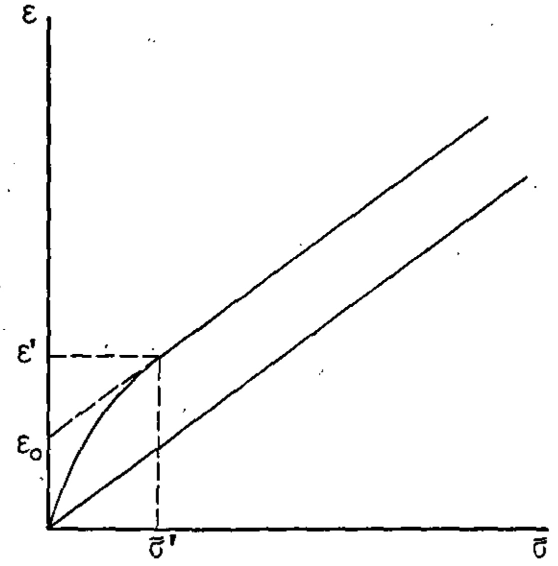

Fig. 5.26. The departure from the straight line of the $\bar{\sigma}-\varepsilon$ curve near the origin.

Suppose that the upper loaded edge is not parallel to the upper loading platen of the machine. In the beginning of the test the plate will now be unloaded over the width a (fig. 5.27). If it is assumed that the distribution of the stress and strain along the loaded edge is linear, as shown in fig. 5.27, the relation can be derived between

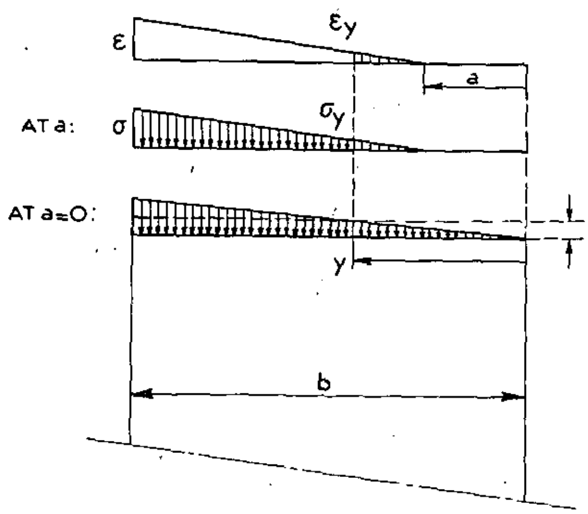

Fig. 5.27. *Assumed stress distribution at low loads.*

the strain ε (for $y = b$) and the average stress $\bar{\sigma}$ for the region $0 < \bar{\sigma} < \bar{\sigma}'$, in which $\bar{\sigma}'$ represents the average stress occurring when $a = 0$.

For values of $\bar{\sigma} > \bar{\sigma}'$ the average stress will increase linearly with ε (see fig. 5.26).

$$\bar{\sigma} = E(\varepsilon - \varepsilon_0). \tag{5.14}$$

At a distance y $(a < y < b)$ the stress is

$$\sigma_y = \sigma \cdot \frac{y-a}{b-a}, \tag{5.15}$$

and the strain

$$\varepsilon_y = \varepsilon \cdot \frac{y-a}{b-a}. \tag{5.16}$$

Now the average stress is

$$\bar{\sigma} = \tfrac{1}{2}\,\sigma \cdot \frac{b-a}{b}. \tag{5.17}$$

From $\sigma_y = \varepsilon_y \cdot E$ and the formulas (5.15), (5.16), and (5.17) it follows that

$$\varepsilon = 2\,\frac{b}{b-a} \cdot \frac{\bar{\sigma}}{E}, \tag{5.18}$$

giving for $a = 0$

$$\varepsilon' = 2\,\frac{\bar{\sigma}'}{E}. \tag{5.19}$$

According to (5.14)

$$\varepsilon' - \varepsilon_0 = \frac{\bar{\sigma}'}{E},$$

hence

$$\varepsilon_0 = \frac{\bar{\sigma}'}{E}. \tag{5.20}$$

The relation represented by (5.18) corresponds with the curve of fig. 5.26. With this the departure from the straight line of the $\bar{\sigma} - \varepsilon$ curve in *the neighbourhood of the origin has been explained.* For an exact description of the behaviour of the plate a correction of the $\bar{\sigma} - \varepsilon$ curve must be carried out. Instead of the strain ε the value $(\varepsilon - \varepsilon_0)$ must be taken as the ordinate of the figures. Therefore the point $(\bar{\sigma} = 0, \varepsilon = \varepsilon_0)$ must be chosen as a new origin. This correction has already been carried out in the figures.

The occurrence of an uneven stress distribution across the width of the plate for small loads was

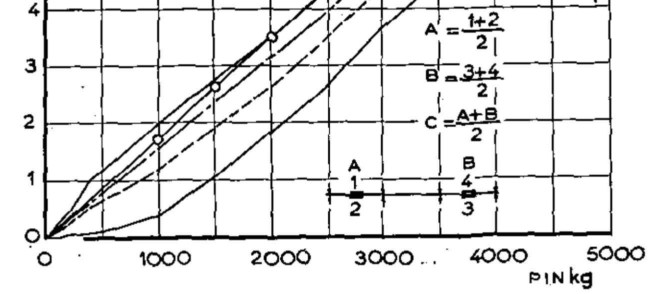

Fig. 5.28. Results of strain gauge measurements on specimen CC 3-2.

experimentally demonstrated with strain-gauge measurements on specimen CC 3-2. The position of the gauges 1, 2, 3, and 4 in axial direction on the center line of the two outer bays of the specimen, and 50 mm below the upper loaded edge, is shown in fig. 5.28, which also contains the results of the measurements.

Curves A and B, representing the average strain in the left and right gauges, show clearly that both sides of the plate are not equally loaded. The curve C, giving the average value of A and B, is in general parallel to the curve $\bar{\sigma} = E\,\varepsilon$ and the measured $\bar{\sigma} - \varepsilon$ curve. The nearly constant difference between the curve C and the $\bar{\sigma} - \varepsilon$ curve has probably been caused by zero-drift of the gauges, which could not be determined, because the specimen was not unloaded before the buckling load was reached. In general strain gauges give no accurate indications at low loads. Hence the curves must be regarded more as qualitative results.

5.4.3 *Influence of play at knife-edge supports.*

The diagram representing the relation between the average compressive stress $\bar{\sigma}$ and the average strain ε of the specimens, showed that for loads smaller than the buckling load the strain ε is larger than the value $\frac{\bar{\sigma}}{E}$. Strain-gauge measurements on specimen B 3-1 showed, however, an accurate accordance between the average strain and the value $\frac{\bar{\sigma}}{E}$. Two strain gauges, one on each side of the plate, were attached at a point of the center line of the middle bay of the specimen (see fig. 5.14). The results of the measurements are presented in fig. 5.14. It follows that the difference between ε and $\frac{\bar{\sigma}}{E}$ cannot be explained by supposing that the decrease in stiffness has been caused by initial eccentricities in the same way as this occurs with normal plate buckling. For, in that case the local strain in a point on the center line of the bay should be smaller than $\frac{\bar{\sigma}}{E}$, and the compressive stress at the edges of the bay should be larger than in the middle.

The difference between ε and $\frac{\bar{\sigma}}{E}$ can partly be explained by supposing that Euler-buckling occurs in the complete specimen. This is possible because of the play between the knife-edge supports. In the following this phenomenon will be investigated.

In the case of Euler-buckling of the plate the displacement w of a point of the plate normal to the plane of the plate can be represented by

$$w = W_B \cos \frac{\pi x}{L_B}, \tag{5.21}$$

in which W_B is the amplitude and L_B is the half wave length of the buckling form. Now approximately

$$W_B = 0.5\, s\,. \tag{5.22}$$

This can only be approximately true, because W_B will not be constant, but will be a function of y in consequence of the normal forces exerted by the knife-edges on the plate.

The buckling stress of the plate is

$$\sigma_B = \frac{\pi^2 E}{12(1-\nu^2)} \left(\frac{h}{L_B}\right)^2. \tag{5.23}$$

If it is supposed that L_B can change continually when the load on the specimen changes, than L_B will always take such a value that σ_B equals the average stress $\bar{\sigma}$ in the plate, at least before local buckling of the plate starts.

Thus

$$L_B = \frac{\pi h}{2\sqrt{3(1-\nu^2)}} \sqrt{\frac{E}{\bar{\sigma}}}. \tag{5.24}$$

With $h = 1.5$ mm and $\nu = 0.32$ this becomes

$$L_B = 1.436 \sqrt{\frac{E}{\bar{\sigma}}} \text{ mm.} \tag{5.25}$$

The average shortening of the specimen in the case of Euler-buckling follows from

$$\varepsilon = \frac{\bar{\sigma}}{E} + \frac{1}{L_B} \int_0^{L_B} \frac{1}{2} \left(\frac{\partial w}{\partial x}\right)^2 dx,$$

or with (5.15)

$$\varepsilon = \frac{\bar{\sigma}}{E} + \frac{\pi^2 W_B^2}{4 L_B^2}. \tag{5.26}$$

Substitution of (5.22) and (5.25) gives

$$\varepsilon = (1 + 0.299\,.\,s^2)\frac{\bar{\sigma}}{E}\,. \tag{5.27}$$

This relation between ε and $\bar{\sigma}$ has been represented in fig. 5.29, together with the experimental $\bar{\sigma} - \varepsilon$ curve for specimen B 3-1, and the stress-strain curve for the material of this specimen. Fig. 5.29 shows clearly that the difference between ε and $\frac{\bar{\sigma}}{E}$ can only be explained completely when relatively large plays are present. In fact the largest play, which was necessary with knife-edge form c (fig. 4.5 - c), amounted to 0.74 mm, according to (4.1), in which $\varphi = 20°$ was taken. Thus the deviation of the $\bar{\sigma} - \varepsilon$ curve from the stress-strain curve of the material cannot be explained completely with the actual plays. The theoretical derivation of the influence of the play, given here, is however approximative. Furthermore the play at the inner knife-edges can be appreciably larger than the play at the outer knife-edges, due to the deformation of the frames supporting the knife-edges. This deformation was observed after later tests (e. g. after the test of specimen B 4-1). Therefore the above explanation is thought to be sufficient.

It can be expected that the influence of the play will decrease for loads in excess of the buckling load, because in that case the shortening will be large compared with the extra shortening due to the play at the supports. It is necessary to introduce a correction of the $\bar{\sigma} - \varepsilon$ curves of the specimens for loads just in excess of the buckling load, in order to obtain satisfactory results also for this range. This correction is shown in all $\bar{\sigma} - \varepsilon$ graphs.

For stresses lower than the buckling stress $\sigma_{cr} = E\,\varepsilon_{cr}$ the experimentally derived curve has been replaced by the straight line $\varepsilon = \dfrac{\bar{\sigma}}{E}$. From the point $\bar{\sigma} = \sigma_{cr}$, $\varepsilon = \varepsilon_{cr}$ a tangent has been drawn to the original curve. This tangent forms the corrected curve for the range of stresses in excess of the buckling stress. From the point of tangency onwards the original curve will be used. Theoretically the influence of the play between the knife-edges cannot be neglected completely past the point of tangency with the original curve. Therefore the corrected curve will be somewhat on the safe side in the neighbourhood of and beyond this point.

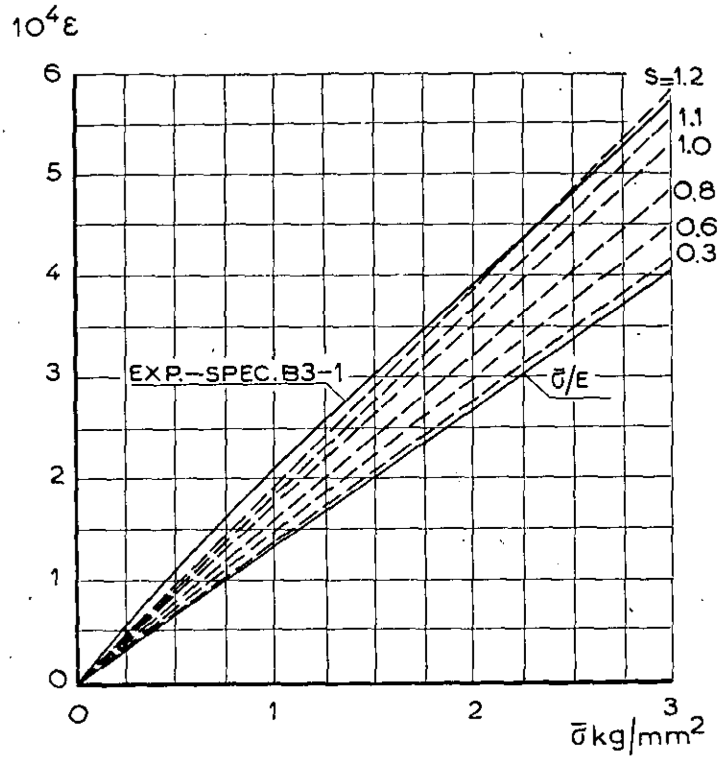

Fig. 5.29. Decrease of stiffness of a specimen caused by overall instability due to the play between the knife-edge supports and the plate.

5.5 *Determination of maximum load of specimens.*

The maximum load in a panel will occur when $\dfrac{dP}{d\varepsilon} = 0$ or according to (5.8) when $b_m' = 0$. This condition can be written as

$$\frac{b_m}{b} + \frac{E_s}{E_t}\,\varepsilon\,\frac{d\dfrac{b_m}{b}}{d\varepsilon} = 0 \qquad \text{(see 5.12)},$$

or after introducing $\sqrt{\dfrac{\varepsilon_{cr}}{\varepsilon}}$ instead of ε as

$$\frac{b_m}{b} - \frac{E_s}{E_t}\cdot\frac{1}{2}\sqrt{\frac{\varepsilon_{cr}}{\varepsilon}}\;\frac{d\dfrac{b_m}{b}}{d\sqrt{\dfrac{\varepsilon_{cr}}{\varepsilon}}} = 0. \quad (5.28)$$

From (5.28) it follows that the value of $\sqrt{\dfrac{\varepsilon_{cr}}{\varepsilon}}$ for which $\dfrac{b_m'}{b} = 0$, is given by

$$\sqrt{\frac{\varepsilon_{cr}}{\varepsilon}} = \frac{E_t}{E_s}\;\frac{2\,\dfrac{b_m}{b}}{d\dfrac{b_m}{b}\Big/ d\sqrt{\dfrac{\varepsilon_{cr}}{\varepsilon}}}. \quad (5.29)$$

Hence the maximum load could be computed from (5.1) with the value of b_m belonging to the value of $\sqrt{\dfrac{\varepsilon_{cr}}{\varepsilon}}$ for which $b_m' = 0$. These values of $\sqrt{\dfrac{\varepsilon_{cr}}{\varepsilon}}$ depend on the material and the dimensions of the specimens, and they have not yet been determined theoretically. Thus this method can only be used when sufficient experimental data are available.

In fig. 5.30 the values of $\sqrt{\frac{\varepsilon_{cr}}{\varepsilon}}$ at which $\frac{b_m'}{b}$ vanished are plotted for the tests considered in this report against the values of $\sqrt{\frac{\varepsilon_{cr}}{\varepsilon_e}}$ for each specimen. The values of $\sqrt{\frac{\varepsilon_{cr}}{\varepsilon}}$ at which $\frac{b_m'}{b} = 0$

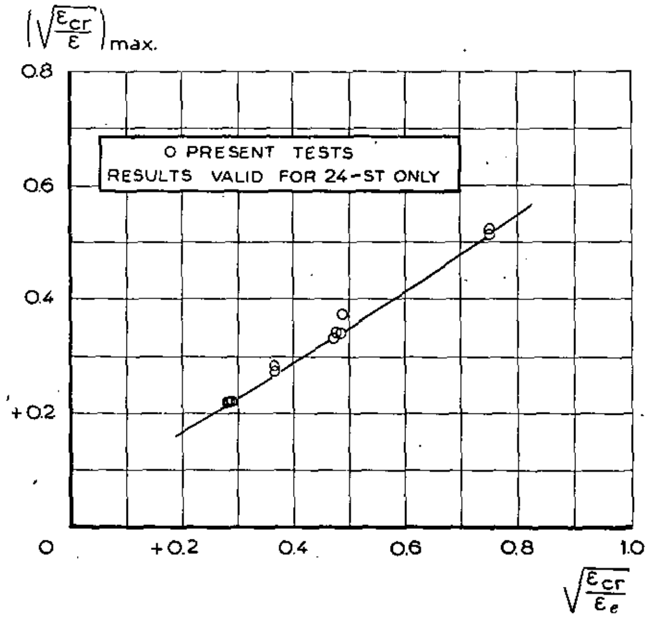

Fig. 5.30. The relation between the parameter $\left(\sqrt{\frac{\varepsilon_{cr}}{\varepsilon}}\right)_{max}$ at which the maximum load is reached and the parameter $\sqrt{\frac{\varepsilon_{cr}}{\varepsilon_e}}$.

were determined from the $\frac{b_m'}{b} - \sqrt{\frac{\varepsilon_{cr}}{\varepsilon}}$ curves, if necessary by extrapolation. The values of $\sqrt{\frac{\varepsilon_{cr}}{\varepsilon}}$ at which the maximum load was reached in the actual tests agree with the values of $\sqrt{\frac{\varepsilon_{cr}}{\varepsilon}}$ at which $\frac{b_m'}{b} = 0$. It must be realised that this graph is valid only for the material used in the tests (i. e. 24 S-T). For other materials the graph may be different.

When the value of $\sqrt{\frac{\varepsilon_{cr}}{\varepsilon}}$ at which the maximum load is reached is known, the value of $\frac{b_m}{b}$ at which the maximum load is reached can be derived directly from the theoretical $\frac{b_m}{b} - \sqrt{\frac{\varepsilon_{cr}}{\varepsilon}}$ curve (fig. 5.9). For convenience the results of fig. 5.30 are plotted in fig. 5.31 in terms of $\frac{b_m}{b}$. From this figure the value of $\frac{b_m}{b}$ at which the maximum load is reached can be read for each value of $\sqrt{\frac{\varepsilon_{cr}}{\varepsilon_e}}$. Because of the relatively small number of test points on which the curve is based the use of this figure can, however, not yet be recommended. Furthermore the results are applicable only in constructions made of 24 S-T.

The maximum load could, of course, be determined by solving eq. (5.29) by trial and error,

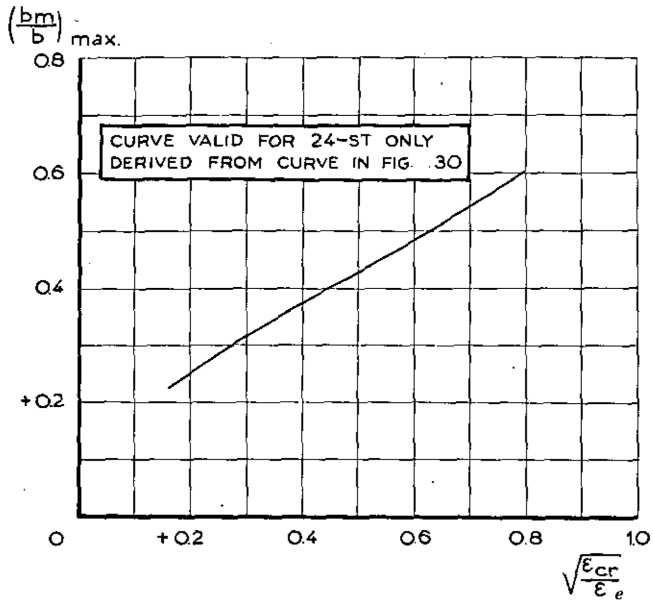

Fig. 5.31. The relation between the parameter $\left(\frac{b_m}{b}\right)_{max}$ at which the maximum load is reached and the parameter $\sqrt{\frac{\varepsilon_{cr}}{\varepsilon_e}}$.

but this method seems to be less accurate.

The excellent agreement between the results for the e. w. in the plastic range and the theoretical curve for the elastic range offers an opportunity to predict with good accuracy from the latter and the stress-strain curve of the specific material the maximum loads of plates. This can be done as follows.

At a point A in the plastic range of the stress-strain curve of the material the stress σ_A and the strain ε_A are determined. With the theoretical buckling strain ε_{cr} the ratio $\sqrt{\frac{\varepsilon_{cr}}{\varepsilon_A}}$ is calculated and from the theoretical curve for the e. w. in the elastic range (fig. 5.9) the ratio $\frac{b_m}{b}$ can be found. The average stress $\bar{\sigma}_A$ in the plate at the strain ε_A can be derived from $\bar{\sigma}_A = \frac{b_m}{b} \cdot \sigma_A$. By repeating this calculation of $\bar{\sigma}_A$ for some values of ε_A in the neighbourhood of the expected maximum strain the value $\bar{\sigma}_{max}$ can be determined.

This procedure has been carried out for all specimens of the definitive tests. The maximum load appeared to lie in the region of $40 < 10^4 \cdot \varepsilon_A < 70$ for all specimens. The value of $\bar{\sigma}_A$ was therefore calculated only for the values $10^4 \cdot \varepsilon_A = 40$, 50, 60, TABEL 6.1

Characteristic values of the specimens of ref. 4.

Edge support	Spec. no. [1]	Width in	Mean thickness in	$10^{-6} E$ lbs/in²	$10^6 \frac{\sigma_{0.2}}{E}$	$10^6 \varepsilon_e = 10^6 \frac{\sigma_e}{E}$	$10^6 \varepsilon_{cr}$	$\sqrt{\frac{\varepsilon_{cr} E}{\sigma_{0.2}}}$	$\sqrt{\frac{\varepsilon_{cr}}{\varepsilon_e}}$
Ball-edged	1A	2.160	0.0618	10.09	5680	4260	2960	0.721	0.833
	2A	2.550	0.0637	10.09	5680	4260	2250	0.630	0.727
	3A	2.910	0.0647	10.09	5680	4260	1790	0.561	0.648
	4A	3.600	0.0656	10.09	5680	4260	1200	0.459	0.530
	5A	4.290	0.0660	10.09	5680	4260	854	0.388	0.448
	6A	5.270	0.0659	10.09	5680	4260	564	0.315	0.364
	7A	6.520	0.0652	10.09	5680	4260	361	0.252	0.291
	8A	7.900	0.0634	10.09	5680	4260	183	0.179	0.207
	19A	3.730	0.0677	10.09	5680	4260	1190	0.457	0.528
	20A	4.460	0.0687	10.09	5680	4260	857	0.388	0.448
	1B	2.240	0.0641	10.82	5820	4470	2950	0.712	0.812
	2B	2.630	0.0658	10.82	5820	4470	2260	0.623	0.711
	3B	2.880	0.0639	10.82	5820	4470	1780	0.553	0.631
	4B	3.630	0.0660	10.82	5820	4470	1195	0.453	0.517
	5B	4.350	0.0669	10.82	5820	4470	854	0.383	0.437
	6B	5.550	0.0693	10.82	5820	4470	563	0.311	0.355
	7B	6.870	0.0687	10.82	5820	4470	361	0.249	0.284
	8B	8.010	0.0668	10.82	5820	4470	251	0.208	0.237
Roller-edged	9A	0	0.0661	—	—	—	—	—	—
	10A	2.18	0.0624	10.09	5680	4260	5170	0.954	1.102
	11A	2.57	0.0643	10.09	5680	4260	3950	0.833	0.963
	12A	2.94	0.0654	10.09	5680	4260	3130	0.742	0.857
	13A	3.645	0.0663	10.09	5680	4260	2090	0.606	0.700
	14A	4.335	0.0667	10.09	5680	4260	1490	0.512	0.591
	15A	5.265	0.0659	10.09	5680	4260	990	0.418	0.482
	16A	6.388	0.0639	10.09	5680	4260	631	0.333	0.385
	17A	7.600	0.0633	10.09	5680	4260	438	0.278	0.321
	18A	0	0.0665	—	—	—	—	—	—
	21A	3.086	0.0687	10.09	5680	4260	3130	0.742	0.857
	9B	0	0.0696	—	—	—	—	—	—
	10B	2.207	0.0631	10.82	5820	4470	5160	0.942	1.074
	11B	2.627	0.0657	10.82	5820	4470	3950	0.824	0.940
	12B	3.062	0.0674	10.82	5820	4470	3060	0.725	0.827
	13B	3.590	0.0653	10.82	5820	4470	2090	0.599	0.683
	14B	4.260	0.0656	10.82	5820	4470	1500	0.507	0.579
	15B	5.180	0.0647	10.82	5820	4470	985	0.411	0.469
	16B	6.300	0.0630	10.82	5820	4470	631	0.329	0.376
	17B	7.320	0.0610	10.82	5820	4470	438	0.274	0.313
	18B	0	0.0655	—	—	—	—	—	—
Stringer-edged	B1A	5	0.10605	11.11	5810	4400	2840	0.699	0.803
	B1B	5	0.10585	11.11	5810	4400	2830	0.697	0.802
	B2A	5	0.08345	11.11	5810	4400	1760	0.550	0.632
	B2B	5	0.08420	11.11	5810	4400	1790	0.555	0.637
	B3A	5	0.06814	11.11	5810	4400	1170	0.448	0.515
	B3B	5	0.06865	11.11	5810	4400	1190	0.452	0.520
	B4A	5	0.04918	11.11	5810	4400	610	0.324	0.372
	B4B	5	0.05001	11.11	5810	4400	631	0.329	0.379

[1]) In the numbers of the ball- and roller-edged specimens the letter A is given to clad panels (D.T.D. 546) and the letter B to unclad panels (D.T.D. 646). All stringer-edged panels are made from unclad material (D.T.D. 646).

and 70. The agreement with the measured maximum loads proved to be very good. The error in the calculated value, averaged over all specimens, was smaller than $\pm$ 2.2 % of the measured value. The largest errors (smaller than $\pm$ 5 %) appeared with the specimens BC 3-2, C 3-1, C 3-2, and D 3-2, these being the specimens with the largest thickness of the plate.

6 Results of ref. 4.

6.1 *Description of tests.*

The experiments described in ref. 4 agree with the present tests to a large extent. There are, however, some significant differences.

The specimens consisted of only one bay with a length of 35 in. and a varying width between the longitudinal supports of 35—120 times the plate thickness. All plates had the same thickness, nominally 16 s.w.g., and were made of clad (D.T.D. 546) or unclad (D.T.D. 646) material. The specimens with stiffeners, however, all had the same width (5 in.), and varying thicknesses (from 12—18 s.w.g.).

Three different longitudinal edge supports were used: rows of steel balls in vee-grooved blocks, intended to imitate hinged-edge conditions, rows of steel rollers in recessed blocks, intended to imitate clamped-edge conditions, and a single Z-section stringer on one side of the specimen at both edges.

Flat-end tests were carried out in the case of the hinged-edged and the clamped-edged conditions, the loaded edges of the stiffened specimens were cast in Wood's metal.

The plate load and mean strain were measured. The shape of the skin buckles was determined with a dial indicator. The indicator was arranged to be free to slide laterally on a cross-frame, which was itself free to slide vertically on edge runners attached to the edge support rig. The weight of the cross-frame and indicator was balanced by lead weights. Amplitudes were measured at the nodes of grid lines, which were marked on the plates symmetrically about the center and extending over a length of 3 times the width. In some cases amplitudes were measured over the whole length of the panel.

Table 6.1 contains some dimensions and characteristic values of the specimens. The buckling strain ε_{cr} has been calculated for ideal simply supported and clamped longitudinal edges. It can be seen that the values of $\sqrt{\dfrac{\varepsilon_{cr}}{\varepsilon_e}}$ for the specimens are in general smaller than 1, as was the case with the present tests.

6.2 *Results of tests.*

The influence of friction at the supports of the longitudinal edges was determined in separate tests for each type of support. In the ball-edged panels the friction proved to be negligible, contrary to the roller-edged panels for which corrections of the load-strain curves due to friction were necessary.

From the measured buckling shape $\left(\dfrac{W}{L}\right)^2 - P$ curves were determined and from these an experimental value of the buckling stress was established. A second experimental value of the buckling stress was determined from the load-strain curve, taking the value of the strain at which a sudden reduction in slope occurs.

The experimental buckling stresses were compared with the theoretical value. For the ball-edged panels a fair agreement appeared between both experimental values and the theoretical value, except in the case of the clad specimens which buckled at loads in excess of the yield load of the cladding. In these cases the experimental values were about 15 % smaller than the experimental values for similar unclad panels. This agrees very well with the results described in section 4.5.

For the roller-edged panels the experimental values appeared to be smaller than the theoretical value, the clamping effect of the roller supports being too small. Here again clad panels exhibit experimental values smaller than the experimental values for unclad panels. The experimental buckling stresses of the stringer-edged panels showed a good mutual agreement for plates with large thicknesses, but the agreement was not good for plates with small thicknesses. The clamping effect of the stringers approximated ideal clamping better in panels with smaller thicknesses.

In the tests the elastic limit of the material was not exceeded very far, the results being given only for strains up to $5 \cdot 10^{-3}$. The elastic limit in the material is reached at a strain of about $4 \cdot 10^{-3}$.

The results are presented in the form of load-strain curves, from which $\bar{\sigma} - \sigma_{edge}$ curves, and $\dfrac{d\,\bar{\sigma}}{d\,\sigma_{edge}} - \sigma_{edge}$ curves were deduced, using the panel E in the elastic region. These curves are already corrected for the friction occurring at the longitudinal support.

The results of some specimens are used here for the evaluation of the e. w. as a function of $\sqrt{\dfrac{\varepsilon_{cr}}{\varepsilon}}$. For ε_{cr} the experimental value derived from the amplitude measurements was chosen.

The ratio $\dfrac{b_m}{b}$ was calculated with formulas (5.2) and (5.3) for some values of ε from the $\bar{\sigma} - \sigma_{edge}$ curves given in the original reports on which ref. 4 is based, and shown in figs. 6.1—6.4 incl.

The ratio $\dfrac{b_m'}{b}$ could be derived from the given $\dfrac{d\,\bar{\sigma}}{d\,\sigma_{edge}} - \sigma_{edge}$ curves, and is also shown in figs. 6.1—6.4 incl. Substituting (5.2) in (5.10) and taking $\sigma_{edge} = E\,\varepsilon$, we find for the elastic region

$$\frac{b_m'}{b} = \frac{d\,\bar{\sigma}}{d\,\sigma_{edge}} \quad (6.1)$$

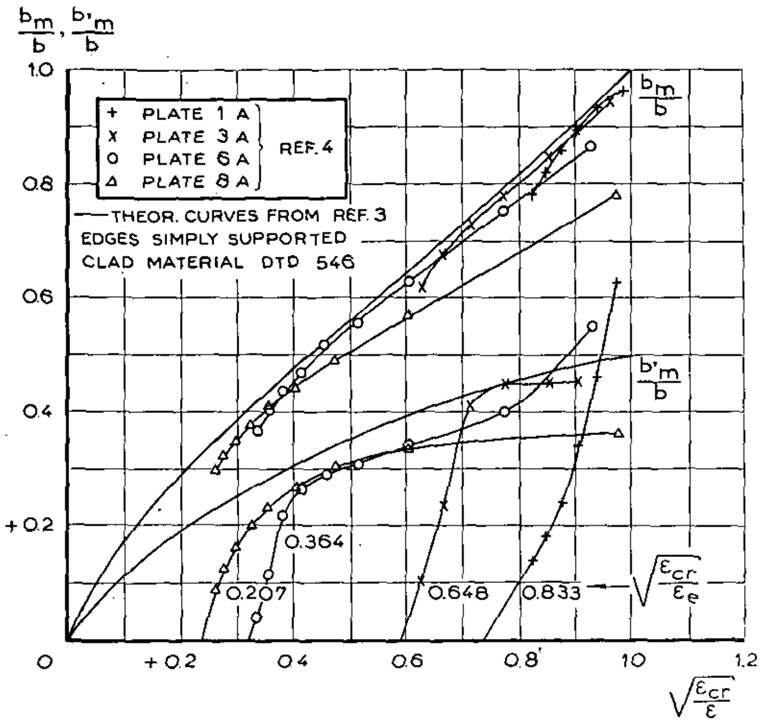

Fig. 6.1. Comparison of the results for the effective width of some specimens from ref. 4 with the theoretical curves for the effective width in the elastic range from ref. 3.

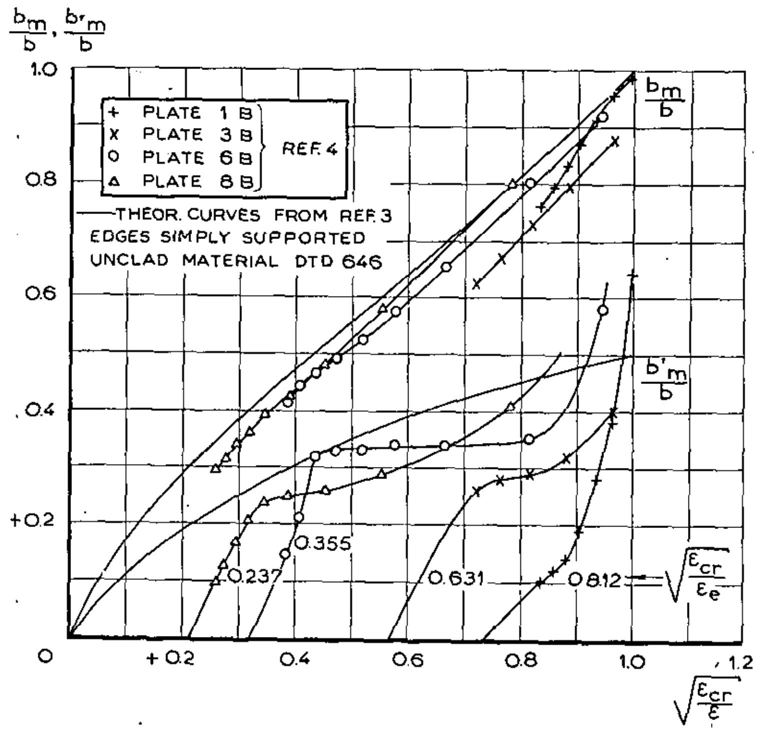

Fig. 6.2. Comparison of the results for the effective width of some specimens from ref. 4 with the theoretical curves for the effective width in the elastic range from ref. 3.

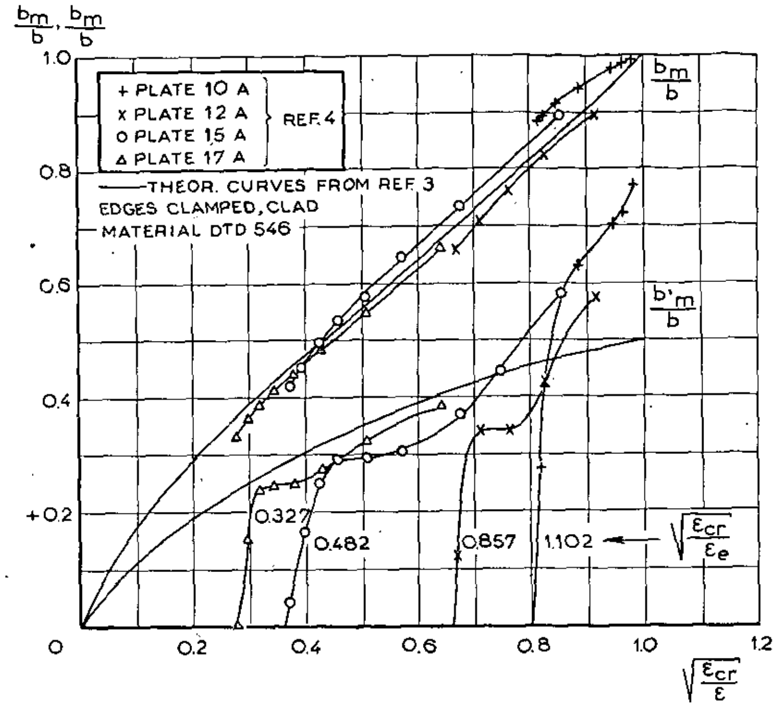

Fig. 6.3. Comparison of the results for the effective width of some specimens from ref. 4 with the theoretical curves for the effective width in the elastic range from ref. 3.

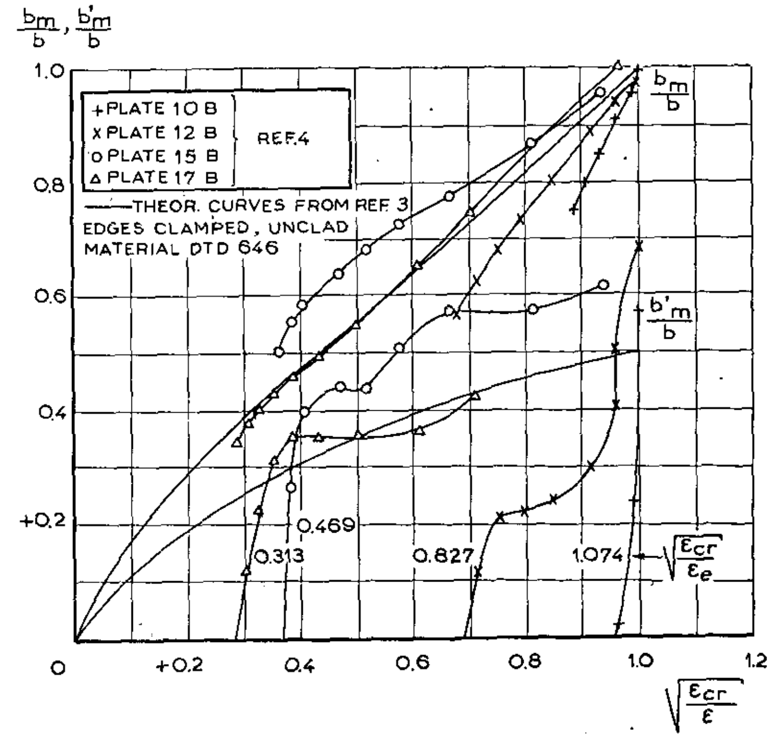

Fig. 6.4. Comparison of the results for the effective width of some specimens from ref. 4 with the theoretical curves for the effective width in the elastic range from ref. 3.

This equation holds also for the plastic region, which can be shown by substituting (5.2) in (5.12) and taking $\sigma_{edge} = E_s \cdot \varepsilon$ and $\frac{d\,\sigma_{edge}}{d\varepsilon} = E_t$.

In ref. 4 the value of $\frac{d\,\bar{\sigma}}{d\,\sigma_{edge}}$ has been calculated using the panel E in the elastic region. Hence this ratio does not represent $\frac{b_m'}{b}$ in the plastic region. For accurate results in the plastic region the values of $\frac{d\,\bar{\sigma}}{d\,\sigma_{edge}}$ derived in ref. 4 must be multiplied with the factor $\frac{E}{E_t}$ belonging to the same value of ε. This factor is always larger than one, hence $\frac{d\,\bar{\sigma}}{d\,\sigma_{edge}}$ was underestimated in the plastic region.

The maximum load in the panel will be found at the value of $\sqrt{\frac{\varepsilon_{cr}}{\varepsilon}}$ given by (5.29), for which $b_m' = 0$. This value of $\sqrt{\frac{\varepsilon_{cr}}{\varepsilon}}$ will be too large when the plasticity of the material is not taken into account. Hence the intersection of the $\frac{b_m'}{b}$ curves with the $\sqrt{\frac{\varepsilon_{cr}}{\varepsilon}}$-axis must be displaced to lower values of $\sqrt{\frac{\varepsilon_{cr}}{\varepsilon}}$.

The $\frac{b_m'}{b}$ curves shown in figs. 6.1—6.4 incl. are not corrected for the effect of plasticity, because sufficient stress-strain curves for the material of the specimens were not available for all specimens. Hence the curves for $\frac{b_m'}{b}$ in figs. 6.1—6.4 incl. show too small values of $\frac{b_m'}{b}$ in the plastic region. The values of $\sqrt{\frac{\varepsilon_{cr}}{\varepsilon_e}}$ for which the $\frac{b_m'}{b}$ curves are valid, are given in figs. 6.1—6.4 incl.

Because of the error in the curve for $\frac{b_m'}{b}$ in the plastic region the values of $\sqrt{\frac{\varepsilon_{cr}}{\varepsilon}}$ for which $b_m' = 0$ are not plotted in fig. 5.30. Comparison of these values of $\sqrt{\frac{\varepsilon_{cr}}{\varepsilon}}$ derived from figs. 6.1—6.4 incl. with the results of the present tests in fig. 5.30 shows, however, that the values of $\sqrt{\frac{\varepsilon_{cr}}{\varepsilon}}$ from ref. 4 are too large, which was expected.

6.3 *Discussion of results.*

The tests with ball- and roller edge supports did not imitate hinged-edge and clamped-edge conditions. They were, however, representative of slight and heavy edge fixation. In the first case the plate material outside the supports had an important influence on the results and in the second case the flexibility of the rollers caused the difference with the clamped-edge conditions. The results had to be corrected for initial errors due to friction and contact deformation.

The departure of the results for $\frac{b_m}{b}$ in figs. 6.1—6.4 incl. from the theoretical curve is in general larger than in the present tests. This can be caused by the fact that the specimens consist of but one bay, and by the friction at the supports.

According to the results of the present tests the e. w. of a specimen with one bay will be smaller than the e. w. of a specimen with more bays (e. g. compare the results for the specimens B 5-1 and B 1-1 in fig. 5.17).

Probably the large departure from the theoretical curve in the case of the hinged-edged condition will mainly be due to this effect. In the tests with the roller edge supports, however, this effect will be much smaller, but now the friction at the supports will play a more important role.

Suppose that the friction has not been taken into account. Then the measured load at a certain average strain of the whole specimen will be too large and this results in a too large ratio $\frac{b_m}{b}$. Therefore, when the test results are not corrected sufficiently (or not at all) for initial errors due to friction the resulting effective width will be too large.

The agreement of the measuring results for $\frac{b_m}{b}$, shown in figs. 6.1—6.4 incl., with the theoretical curves is, in view of the possible errors mentioned above, quite fair. It is clear that in some cases the departure of the test points from the theoretical curves will be smaller when a more suitable value of ε_{cr} is used. Obviously in these cases the experimental buckling strain ε_{cr} was wrong (see section 5.3).

No marked difference in the results for clad and unclad specimens and for hinged-edged and clamped-edge conditions could be found.

7 **Conclusions.**

7.1 The test arrangement, designed for the preliminary tests and used with little modifications in the definitive tests, proved to be satisfactory for the proposed test programme. The longitudinal supports carried out as knife-edges required careful attention, because the amount of play between the knife-edges and the panel had to be fixed between narrow limits. Too much play will give rise to local buckling near the supports. Furthermore the possibility exists that the plate does not remain plane at low loads. Too little play, however, will cause friction along the knife-edges, resulting in large errors in the results. Nevertheless errors in the results could not be avoided. They were compensated by suitable corrections.

The frames carrying the knife-edge supports were not rigid enough, which appeared especially after some tests in which irregular wave forms caused large forces in the supports.

It has been shown that the fact, that the loaded *edges of the specimens are not eaxctly parallel,* has some influence on the stress distribution in the plate. This influence is important only in the neighbourhood of the origin of the load-deformation curve. A correction for this error at low loads was introduced.

7.2 A value for the buckling stress could be determined experimentally from the amplitude measurements. In some cases, however, this value was not accurate because the number of amplitude measurements in the neighbourhood of the buckling stress was too small. It can be recommended, therefore, to take in future tests more amplitude measurements at loads in small excess of the buckling load. Irregularities in the wave form occurred at loads in small excess of the buckling load.

7.3 From the preliminary tests it can be concluded, that the scatter in the results of similar specimens is very low, and that the difference in effective width between corresponding specimens with three or more bays is negligible. There appeared, however, a marked difference with specimens having less than three bays. Hence the definitive tests could be conducted on specimens with three bays.

For the range of $\sqrt{\frac{\varepsilon_{cr}}{\varepsilon_e}}$ covered in the preliminary tests the theoretical effective width in the elastic region can be used safely in the plastic region.

7.4 The specimens of the definitive tests, all consisting of three bays, covered the range of $\sqrt{\frac{\varepsilon_{cr}}{\varepsilon_e}}$ between 0.284 and 0.750. The difference between the effective width in the plastic region and the theoretical effective width in the elastic region appeared to be small for all values of the parameter $\sqrt{\frac{\varepsilon_{cr}}{\varepsilon_e}}$ used in the tests, and therefore the theoretical value for the effective width in the elastic region can be used safely throughout this range of $\sqrt{\frac{\varepsilon_{cr}}{\varepsilon_e}}$. The results for the effective width in view of the compressive stiffness showed in the elastic range (thus for values of $\sqrt{\frac{\varepsilon_{cr}}{\varepsilon}}$ larger than the value of the parameter $\sqrt{\frac{\varepsilon_{cr}}{\varepsilon_e}}$ for each specimen) a larger difference with the corresponding theoretical curve, but it must be realised that these points are derived by calculation from the measuring points for the effective width, so that these points contain all errors present in the original points plus the errors due to the not exact calculation. The values of the effective width in view of the compressive stiffness in the plastic range $\left(\sqrt{\frac{\varepsilon_{cr}}{\varepsilon}} < \sqrt{\frac{\varepsilon_{cr}}{\varepsilon_e}}\right)$ appeared not to be comparable with the curve for the elastic range, these curves being in the plastic range dependent of the parameter $\sqrt{\frac{\varepsilon_{cr}}{\varepsilon_e}}$, of the shape of the stress-strain curve of the material in the plastic region, and of the dimensions of the specimen. These curves are therefore valid only for the material and the shape of the specimens investigated.

It can be concluded from the tests that the presence of cladding does not influence the effective width in the plastic region.

It is possible that the agreement between the effective widths in the plastic and elastic regions would not be so good for materials having a different form of stress-strain curve. It is therefore recommended to extend these tests to specimens made of materials like 75 S-T and 2 S or 3 S.

7.5 A point of further research is formed by the edge conditions at the longitudinal supports. All present tests were conducted on specimens with simply supported edges. Tests on specimens with *fully clamped edges will, however, be difficult to* realise, as is shown in ref. 4. Furthermore, the results of ref. 4 give no indication that the e. w. for specimens wiht clamped edges will be different from the e. w. for specimens with simply supported edges at the same value of $\varepsilon/\varepsilon_{cr}$; this agrees with the theoretical results of ref. 3.

7.6 The excellent agreement between the results for the effective width in the plastic range and the theoretical curve for the elastic range makes it possible to predict with good accuracy the maximum load of plates under compression from the stress-strain relation of the material and the theoretical curve of the effective width in the elastic range. For all specimens of the definitive tests the maximum load was calculated and the error in the calculated value as compared with the measured maximum load, averaged over all specimens appeared to be smaller than ± 2.2 % of the measured value.

8 References.

1 Besseling, J. F. De experimentele bepaling van de meedragende breedte van vlakke platen in het elastische en het plastische gebied. N.L.L.-rapport S. 414, Amsterdam 1953.

2 Botman, M. De experimentele bepaling van de meedragende breedte van vlakke platen in het elastische en het plastische gebied (deel II). N.L.L.-rapport S. 438, Amsterdam 1954.

3 Koiter, W. T. De meedragende breedte bij groote overschrijding der knikspanning voor verschillende inklemming der plaatranden. N.L.L.-rapport S. 287, Amsterdam 1943.

4 Farrar, D. J. Investigation of skin buckling. R. and M. no. 2652, London 1953.

5 Lahde, R. und Wagner, H. Versuche zur Ermittlung der mittragenden Breite von verbeulten Blechen. Luftfahrtforschung, Bd. 13, 1936, p. 214—223.

6 Jackson, K. B. and Hall, A. H. Curved plates in compression. Nat. Res. Council Canada. Aero. Rep. AR - 1, 1947.

7 Neut, A. van der and Floor, W. K. G. Experimental investigation of the postbuckling behaviour of flat plates loaded in shear and compression. N.L.L.-report S. 341, Amsterdam 1949.

8 ANON. Methods of conducting buckling tests of plywood panels in compression. Forest Prod. Lab. Rep. no. 1554, 1946.

9 HOFF, N. J. and MAUTNER, S. E. The buckling of sandwich-type panels. Aero. Sci., Vol. 12, 1945, p. 285—297.

10 HOFF, N. J., BOLEY, B. A. and COAN, J. M. The development of a technique for testing stiff panels in edge-wise compression. Proc. S.E.S.A., Vol. 5, no. 2, 1948, p. 14—24.

11 FRUBERGER, W., SHAW, F. S., SILBERSTEIN, J. P. O., and SMITH, R. C. T. Plywood panels in compression. Flat panels with grain and various angles to direction of loading. Australian Council for Aeronautics, Report ACA-30, 1947.

12 COX, H. L. c. s. Compression tests on seven panels of monocoque construction. R. and M. nr. 2042, 1945.

13 BOLLER, K. H. Buckling loads of flat sandwich panels in compression. Buckling of flat sandwich panels with loaded edges simply supported and the remaining edges clamped. Forest Prod. Lab., Rep. no. 1525-B, 1947.

14 SIEBEL, E. c. s. Handbuch der Werkstoffprüfung, Bd. II. Die Prüfung der metallischen Werkstoffe. J. Springer, Berlin, 1939, p. 85—97.

15 BOLLER, K. H. Buckling loads of flat sandwich panels in compression. The buckling of flat sandwich panels with edges simply supported. Forest Prod. Lab., Rep. no. 1525-A, 1947.

16 WELTER, G. Curved aluminium alloy sheets in compression for monocoque constructions. J. Aero. Sci., Vol. 12, 1945, p. 357—369.

17 ROSSMANN, C. A., BARTONE, L. M. and DOBROWSKI, C. V. Compression strength of flat panels with Z-section stiffeners. Naca W.R. — L 499, 1947.

18 EBNER, H. Theorie und Versuche zur Festigkeit von Schalenrümpfen. Luftfahrtforschung, Bd. 14, 1937, p. 93—115.

19 KROMM, A. Einfluss der Nietteilung auf die Druckfestigkeit versteifter Schalen aus Duralumin. Luftfahrtforschung, Bd. 14, 1937, p. 116—120.

20 MEYER, H. und NEHL, F. Die grundlegenden Vorgänge der bildsamen Verformung. Stahl und Eisen, Bd. 45, 1925, p. 1961—1972.

21 PRANDTL, L. Anwendungsbeispiele zu einem Henckyschen Satz über das plastische Gleichgewicht. Zamm, Bd. 3, 1923, p. 401—406.

22 NADAI, A. Beobachtungen der Gleichflächenbildung an plastischen Stoffen. Proc. 1st Int. Congress Appl. Mech., Delft, 1924, p. 318—325.

23 HÜBERS, K. Das Verhalten einiger technischen Eisenarten beim Druckversuch. Bericht des Walzwerkausschusses des Vereins Deutscher Eisenhüttenleute, No. 32, Verlag Stahleisen, Düsseldorf, 1923.

24 COX, H. L. The buckling of a flat rectangular plate under axial compression and its behaviour after buckling. R. and M., no. 2041, 1945.

25 BESSELING, J. F. Over het knikvraagstuk in het plastische gebied bij staven en platen. N.L.L.-rapport S. 407, Amsterdam 1952.

26 COX, H. L. The buckling of a flat rectangular plate under axial compression and its behaviour after buckling (II). Condiitons for permanent buckles. R. and M., no. 2175, 1945.

27 MILLER, J. A. Stress-strain and elongation graphs for aluminium alloy 75 S-T 6 Sheet. Naca TN 2085, April 1950.

28 RONDEEL, J. H. en DUYN, G. E. A "solid-guide" fixture for determining the properties of thin sheet material in compression. N.L.L.-report S. 368, Amsterdam, 1950.

29 TIMOSHENKO, S. Theory of elastic stability. First ed., Mc. Graw-Hill Book Cy. New York, 1936.

APPENDIX.

Calculation of the ultimate compression load with respect to general instability of a panel with stringers in the direction of the load.

A panel, loaded in compression and consisting of a plate with stringers in the direction of the load, will ultimately collapse by local failure of the stringers or by general instability. In most cases general instability will occur after the buckling stress of the plate has been exceeded. For panels with relatively heavy stringers the critical load may even lie beyond the elasticity limit. The load, at which general instability will occur, can be computed from the formule

$$P_{cr} = k\,\frac{\pi^2 B}{l^2}\,, \tag{A.1}$$

where k is determined by the clamping conditions of the loaded edges and where B represents the bending stiffness of the cross-section. In case the elasticity limit has been exceeded the bending stiffness has to be calculated for increasing compression strain over the whole cross-section (Shanley-effect). The bending stiffness is defined by

$$\delta M = B\,\delta w''. \tag{A.2}$$

Consider a cross-sectional element of a panel (fig. A.1). Let z be the transverse coordinate with reference to the neutral axis in bending. Then δM is given by

$$\delta M = \int_S \delta\sigma\, z\, dS. \tag{A. 3}$$

If $\delta\varepsilon$ denotes the increment of specific shortening due to bending and if the subscript 1 refers to one bay of the plate and the subscript 2 to the adjacent stringer, then

$$\delta M = \frac{dP_1}{d\varepsilon}\,\delta\varepsilon_1\,.\,z_1 + E_{t_2}\int_{S_2} \delta\varepsilon\, z\, dS$$

or

$$\delta M = \left(\frac{dP_1}{d\varepsilon}\,z_1{}^2 + E_{t_2} I_2\right)\delta w''. \tag{A. 4}$$

Thus for the bending stiffness of one cross-sectional element is found

$$B = \frac{dP_1}{d\varepsilon}\,z_1{}^2 + E_{t_2} I_2\,. \tag{A. 5}$$

Now

$$P_1 = \sigma_1\, h b_m\,, \tag{A. 6}$$

where σ_1 is the stress in the plate at the stiffener attachment line.

It follows

$$\frac{dP_1}{d\varepsilon} = h\left(\frac{d\sigma_1}{d\varepsilon}\,b_m + \sigma_1\,\frac{db_m}{d\varepsilon}\right)$$

or

$$\frac{dP_1}{d\varepsilon} = hE_{t_1}\left(b_m + \frac{E_{s_1}}{E_{t_1}}\,\varepsilon\,\frac{db_m}{d\varepsilon}\right). \tag{A. 7}$$

In terms of e.w. the stiffness of the plate can be expressed by

$$\frac{dP}{d\varepsilon} = E_{t_1} h\, b_m', \tag{A. 8}$$

where

$$\frac{b_m'}{b} = \frac{b_m}{b} + \frac{E_{s_1}}{E_{t_1}} \varepsilon \frac{d \frac{b_m}{b}}{d\varepsilon}. \tag{A. 9}$$

Now (A. 5) can be written as follows

$$B = E_{t_1} h\, b_m' z_1^2 + E_{t_2} I_2. \tag{A. 10}$$

In case the materials of the stringers and of the plate have an identical compressive stress-strain curve, formula (A. 10) assumes the simple form

$$B = E_t I', \tag{A. 11}$$

in which I' is the moment of inertia of one cross-sectional element about the neutral axis in bending, including the contribution of the plate by means of the e.w. b_m', defined by (A. 9).

$\frac{b_m'}{b}$ may have a negative value in the plastic range, as E_t will soon become much smaller than E_s.

The determination of the neutral axis in bending can easily be given in terms of the e.w. b_m'. Let the distance from the center of gravity of the

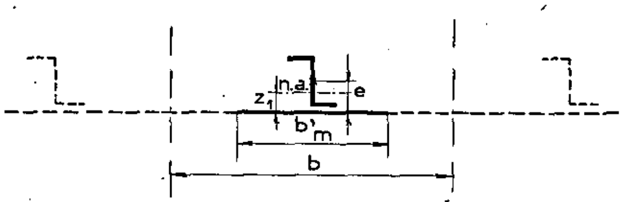

Fig. A 1. Geometry of one cross-sectional element of panel.

stringer cross-section to the plate be denoted by e (fig. A. 1), then it follows

$$Z_1 = \frac{E_{t_2} S_2 e}{E_{t_2} S_2 + E_{t_1} b_m' k}. \tag{A. 12}$$

As b_m' may be < 0, z_1 may be $> e$.

Further for I_2 can be written

$$I_2 = S_2 i^2 + S_2 (e - z_1)^2, \tag{A. 13}$$

if i represents the radius of inertia of the stringer cross-section.

In each particular case the value of P_{cr} has to be determined by graphical means. For some values of ε, corresponding with definite values of

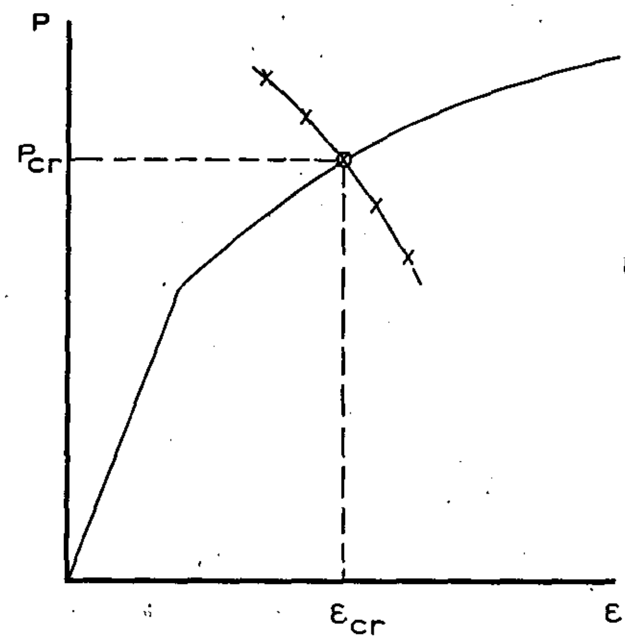

Fig. A 2. Graphical determination of P_{cr}.

P, P_{cr} is computed from (A. 1) and (A.10). The intersection of the $P - \varepsilon$ curve and the $P_{cr} - \varepsilon$ curve gives the value of the critical load and the critical specific shortening (fig. A. 2).